UNIVERSITÀ DI PARMA

UNIVERSITA' DEGLI STUDI DI PARMA

DOTTORATO DI RICERCA IN

"SCIENZE CHIMICHE"

CICLO XXXII

DEVELOPMENT OF NEW MONO- AND MULTIVALENT LIGANDS FOR MEDICALLY RELEVANT PROTEINS AND PEPTIDES

Coordinatore:

Prof. Roberto Corradini

Tutor:

Prof. Francesco Sansone

Dottorando: Davide Sbravati

Anni 2016/2019

To my beloved family

and Pegasino

“Non sono le persone a fare i viaggi,

ma i viaggi a fare le persone”

John Steinbeck

Contents

Abstract

Among all biomolecules, proteins are the main effectors of biological functions in living organisms. Thanks to their high diversity in term of structure, shape and composition, proteins have been exploited by Nature for a wide range of purposes acting as enzymes, receptors, messengers, structural fibres and transporters. Unfortunately, when genes codifying for them are mutated, their expression might lead to afunctional proteins or to unusual concentration levels for those proteins. For this reason, proteins can be used as convenient targets for limiting or even stopping the incoming disease. In this context, this PhD project has dealt with the development of new synthetic molecules for the targeting of medically relevant peptides/proteins, in particular Carbonic Anhydrases, Transthyretin, $A\beta_{16-22}$, Mcl-1 and p300 .

Looking for selectivity and efficiency in Carbonic Anhydrases (CAs) inhibition, a wide set of monovalent and multivalent potential inhibitors bearing ammonium and sulfonamide moieties were designed, synthetized and tested in stopped-flow assay towards a small library of CA isoforms. Monovalent sulfonamide-bearing molecules showed to be very potent and selective inhibitors (Ki in low-nanomolar range) towards human CAs (in particular, hCAI and hCAII), whereas dimeric analogues were pretty inactive towards all tested isoforms. On the contrary, almost all the series of calixarene-based derivatives exposing ammonium or benzensulfonamide units showed very good selectivity towards fungine Can2 CA, and significant efficiency (Ki in micromolar range) towards fungine MgCA, even better than the reference compound acetazolamide (nowadays, used for the topic treatment of glaucoma). Remarkably, the structure at the solid state of the complexes between hCAII and four ligands were determined by X-Ray diffraction. Even if no multivalent effect was observed with the calixarene-based inhibitors, however, for some of them, the efficiency shown suggests the involvement of the macrocyclic cavity in establishing additional interactions with the protein. This aspect is currently still under investigation.

Transthyretin (TTR), when mutated, is prone to unfold its tetrameric structure and produce amyloidogenic fibrils responsible of Alzeheimer's disease. In order to find molecules able to prevent the tetramer disaggregation, we synthetized new "kinetic stabilizers" based on well-known Tolcapone and Biochanin A structures with the aim to improve their binding affinities. By Western Blot assays in plasma samples it turned out in particular that 3-deoxytolcapone is more selective towards Wild-Type TTR with respect to Tafamidis and Diflunisal, but less than Tolcapone. By the way since metabolic transformations modify Tolcapone at 3-OH group impairing its activity, the synthetized 3-deoxytolcapone represents a promising alternative in the treatment of amyloidogenic diseases.

Another project of this PhD work has dealt with the study of polarity and aggregation of $A\beta_{16-22}$, the smallest model peptide fragment of β-amyloid ($A\beta_{42}$), which is another etiological factor of the formation of amyloidogenic fibrils. In this context, during a secondment at University of Leeds two classes of more hydrophobic $A\beta_{16-22}$ sequences were synthetized with iodo-, chloro- and methoxy-phenylalanine in position 19 and 20, one capped at N-terminus with acetyl moiety, one capped with TAMRA-AhX moiety The former was employed for the study of morphology and topology of fibrils and nanotubes with Electron Microscopy (TEM), the latter was employed for kinetic aggregation studies in Fluorescence Quenching Assay (FQA). From these studies it came out that these new peptides are still able to make fibrils and nanotubes and that increasing the apolarity, in particular in position 19, the aggregation is slightly enhanced.

In the same period at University of Leeds, the attention was focused also on the inhibition of protein-protein interactions (PPIs) in systems like p300/HIF1α and Mcl-1/Noxa, often involved in tumour development. Since their reciprocal recognition passes through interactions involving either Leu or Val side chains, a library was synthetized of calix[4]arenes with isopropyl or isobutyl groups at the upper rim for the recognition and ethoxyethyl or methylencarboxy moieties at the lower rim to increase the solubility in water. Mainly for solubility issues, in Fluorescence Anisotropy assays only the derivative with methylencarboxy groups at lower rim showed to be active towards Mcl-1 and p300 (low micromolar Ki). To understand more about the binding of this molecule with biological counterparts, NMR and cocrystallization assays are currently in progress.

Chapter 1

Introduction

1.1 Biological background

Proteins and in general peptides perform a vast array of functions in organisms, including catalysis, DNA replication, transport across membranes, mediators or initiators in transferring information and triggering stimuli, tools for the communication between cells and biological structures[1–4]. Their correct functioning allows cells and organisms to regularly develop, grow, contrast adverse events and, if necessary, also recruit death-inducing factors to protect the subject, when fatal irreversible genetic translational errors occur. On the contrary, their alteration and dysfunction are responsible for the activation of cascades of pathological pathways and correlated diseases[5–7]. For this reason, it is very important to develop molecules able to interact with proteins and peptides in case of misregulation to be used as therapy for affected subjects.

1.2 PhD summary

In this context, this PhD project has dealt with the development of new synthetic molecules for the targeting of medically relevant proteins, such as Carbonic Anhydrases, Transthyretin, Mcl-1, p300 and $A\beta_{16\text{-}22}$.

Since CO_2 is a gas widely produced by living organisms in cell respiration, toxic by accumulation in cells, Nature exploits Carbonic Anhydrases (CAs) to solubilize this hydrophobic gas giving the possibility to organisms to dispose of it by hematic circulation. CAs essentially catalyse the CO_2 hydratation reaction transforming it in a bicarbonate ion (much more soluble in aqueous environment) with a simultaneous proton release. Besides the role in CO_2 stabilization, this reaction is at the base of different physiological functions such as bone resorption, gastric acidic secretion and renal tissue acidification[4,8–14]. Unfortunately, when a mutation occurs in the gene encoding for CAs, misregulation or uncontrolled overexpression is triggered leading to a various plethora of dysfunctions, such as tumorigenesis, glaucoma, mountain sickness, epilepsy, oedema, obesity, sterility and cariogenesis[5,6,15]. This high number of diseases is caused not only by the basal role of this class of enzymes in biologic systems but also by their ubiquity. In fact, for example, CA isoforms in humans are distributed in almost all tissues and subcellular compartments[16]. Considering, moreover, that other isoforms are present in pathogenic microorganisms[17–19], CAs are being, since some years, a relevant target for medicinal research with the aim to synthesize systems able to block their catalytic activity. Nowadays the main strategies employed exploit the use of sulfonamide-bearing molecules, which binds to zinc ion present in the active site and directly involved in the catalytic activity of the enzyme replacing the activated water-bound molecule, and ammonium-bearing molecules, which, instead, binds to water-bound molecule interrupting the dense hydrogen bond network established by conserved water molecules and wall residues used by the enzyme to release the proton by-product[16] in the bulk solution. In this context, one of the goals of this doctorate work (**Chapter 2**) was to synthesize sulfonamide-/ammonium-bearing phenols and dimeric analogues (for the exploration of formation of chimera-like or intercrossing systems) as new potential inhibitors (examples in **Figure 1.1**). In collaboration with prof. C. Supuran and his team at University of Florence, these derivatives were tested towards a set of CAs in stopped-flow assays. From this analysis turned out that sulfonamide-bearing phenols showed to be very potent and selective inhibitors (low-nanomolar range) towards human carbonic anhydrases (in particular, hCAI and hCAII), whereas dimeric analogues were pretty inactive towards all tested isoforms.

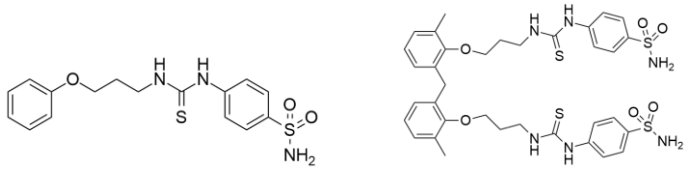

Figure 1.1. Examples of inhibitors synthesized in our laboratories: on the left, a monomeric analogue; on the right, a divalent analogue.

Even if enzymes are usually in monomeric form with single active sites, in recent years some researchers are indeed exploring the use of multivalent ligands to inhibit enzyme activity with improved efficiency (with respect to more classical monovalent ligands), mainly on the basis of a binding-rebinding process supported by the proximity of multiple copies of ligand, which guarantees an high local pharmacophore concentration[20–24]. In our project (**Chapter 3**), for our perspectives and experience, taking into account its versatility and potentiality, multivalent calixarene scaffold was chosen to realize sulfonamide-/ammonium-functionalized inhibitors (examples in **Figure 1.2**). Moreover, beyond the potential multivalent effect, the calixarene scaffold can participate to the binding exploiting the aromatic cavity for the inclusion of proper residues when blocked in the cone geometry or using the hydrophobic surface of its phenolic components for contacts with lipophilic regions of the proteins. In collaboration with prof. C. Supuran and his team at University of Florence, our derivatives were tested towards different human (hCAI, hCAII, hCAIX) and non-human isoforms (VchCAβ, Can2, MgCA). From this analysis almost all calixarene derivatives showed good selectivity towards Can2, whereas towards MgCA they showed to very efficient (micromolar range), even more than the reference acetazolamide (nowadays, used for the topic treatment of glaucoma). Interestingly, these data were supported by the determination of the solid structure by X-Ray diffraction of the complex between some of our derivatives and hCAII.

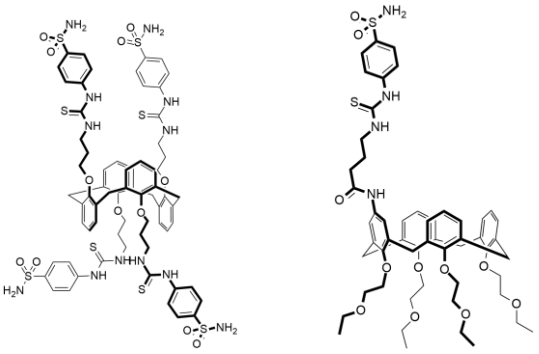

Figure 1.2. Examples of inhibitors synthesized in our laboratories: on the left, a tetrafunctionalized calix[4]arene in 1,3 alternated conformation with benzenesolfonamide moieties; on the right, a monofunctionalized calix[4]arene at the upper rim with benzenesolfonamide moiety in cone geometry.

Transthyretin (TTR) is another target protein addressed during this PhD research. It is a tetrameric protein, in which one of the two channels present has the task of recognition and transport of retinol and thyroxine-based hormones (T4/T3)[25]. This protein, unfortunately, is involved in amyloidogenic diseases, since TTR itself and some mutant versions with time tend to unfold generating in nerves (FAP) or heart (FAC) very hydrophobic fibrils, which are cause of severe symptoms[26,27]. One of the most important inhibition strategies exploited nowadays is the one that uses the so-called “kinetic stabilizers” (e.g. Tafamidis, Diflunisal, Tolcapone, Biochanin A)[28–31], which essentially binds into thyroxine-based hormone pockets stabilizing the

tetrameric structure and preventing its disassembly. In this context (**Chapter 4**), in collaboration with prof. Berni of University of Parma, on the basis of previous computational studies (Molecular Dynamics) aimed at evaluating the effect of modifications in the structure of well established TTR ligands, different modifications were introduced by chemical synthesis on Tolcapone (**Figure 1.3**) and Biochanin A molecules, known to have very good TTR stabilizing properties. In particular, according to computational data, a Tolcapone analogue lacking OH in 3 position and Biochanin A sulphated in 7 position were synthesized and tested in serum samples towards WT-TTR through Western Blots in slightly denaturating conditions to favour the dissociation of the tetramer into monomers. What came out is that 3-deoxytolcapone is more selective than Tafamidis and Diflunisal, but less than Tolcapone and methyltolcapone, while 7-sulphate-Biochanin A seems to be not selective at all towards TTR and so not exploitable as therapeutic agent. The binding interactions of methyltolcapone (**Figure 1.3**), tolcapone (**Figure 1.3**) and 3-deoxytolcapone (**Figure 1.3**) with TTR were rationalized by cocrystals obtained by Berni's co-workers. Because of the difficult synthesis of methyltolcapone and risk of liver failure with Tolcapone treatment, due to its fast metabolism, the synthetized 3-deoxytolcapone represents a promising alternative in the treatment of amyloidogenic diseases.

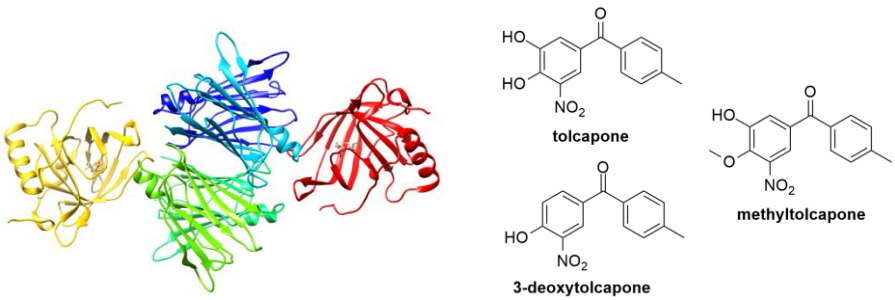

Figure 1.3. On the left, WT-TTR tetramer representation with Chimera software; on the right, derivatives used as kinetic stabilizers in biological tests.

Another protein responsible for amyloidogenesis is APP (Amyloid Precursor Protein). Besides its physiological functions, this transmembrane protein is very important since involved in etiopathology of Alzheimer's disease[32–36]. The subsequent action of α- and γ-secretases cuts APP releasing the so-called β-amyloid ($A\beta_{42}$) responsible for the formation of the harmful fibrils[36]. Since this process is mostly driven by the hydrophobic core of $A\beta_{16-22}$ (**Figure 1.4**)[37,38], during my secondment at University of Leeds in the group of Prof. A. J. Wilson (**Chapter 5**), I carried out the synthesis of peptidic variants more hydrophobic than WT-$A\beta_{16-22}$ (Ac-KLVFI(19)F(20)AE-$CONH_2$, Ac-KLVF(19)FI(20)AE-$CONH_2$, Ac-KLVFI(19)FI(20)AE-$CONH_2$ and chloro- and methoxy-analogues) in order to test their aggregation properties with the perspective of coupling them to calix[4]arene scaffolds as tools for amyloid fibrils disassembly. Peptides were synthesized on automatic synthesizer and purified by preparative C18-HPLC. All synthesized peptides have been aggregates into fibrils and nanotubes and their morphologies were studied by Electron Microscopy (TEM). In order to determine the aggregation kinetics for all the variants (included the WT), the peptides were synthesized again with AhX-TAMRA cap at N-terminus. Due to high complexity of these crudes, probably related to the stability of precursor peptides, just TAMRA-AhX-KLVFI(19)F(20)AE-$CONH_2$ and TAMRA-AhX-KLVFI(19)FI(20)AE-$CONH_2$ were not purified with success. Pure TAMRA-labelled peptides were tested in Fluorescence Quenching Assay (FQA). Comparing all kinetic results, an increase in the initial aggregation rate was observed passing from methoxy-, chloro- to iodo-derivatives, in particular with variants with substitutions at position 19, which seems to confirm the dominant role for F19 in self-assembly. At this point, taking into account that coupling of these peptides onto preorganized scaffolds

might lead to new sequestrating devices, we decided to synthesize two different difunctionalized calix[4]arenes with terminal amine functionalities (**Figure 1.4**) and the respective fully-protected WT-$A\beta_{16-22}$ with C-terminus as carboxylic acid. In future, on these scaffolds will be coupled WT-$A\beta_{16-22}$ and the sequestrating properties of these new molecules will be studied.

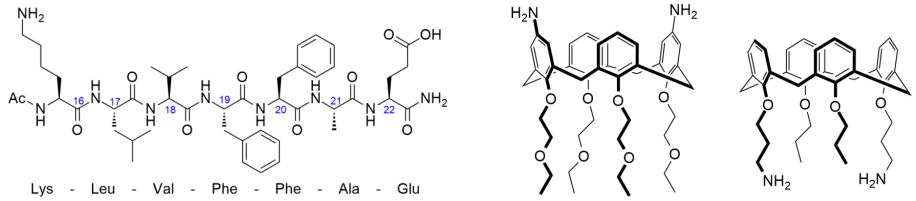

Figure 1.4. On the left, chemical structure of WT-$A\beta_{16-22}$; on the right, difunctionalized calix[4]arenes with amine moieties for the synthesis of WT-$A\beta_{16-22}$ sequestrating agents.

Many other proteins are involved in activation, communication and regulation processes by protein-protein interactions (PPIs)[39] or by peptide contacts through the recognition of particular secondary structure, localized in high-energy binding patch called "hot spots"[40,41]. Some proteins (e.g. p53/mdm2[42], p300/HIF1α[43,44], Mcl-1/Noxa[45]) are involved in cell growth and when some mutations occur in related genes, they are responsible for tumour development. Then, recently, new α-helix and β-sheet mimetics have been developed in many groups as small molecules for the contact inhibition[46–54]. In this context (**Chapter 6**), since by preliminary computational studies upper-rim trifunctionalized calix[4]arenes were shown able to locate the three substituents in analogous positions i, i+3-4, i+7 of classical α-helices, calix[4]arenes in cone conformation with proper functionalization were designed as potential inhibitors in α-helix-mediated contact between Mcl-1/Noxa-Bid (**Figure 1.5**) and p300/HIF1α[55–58]. In particular, were synthesized calix[4]arenes functionalized at the upper rim with three units either of isobutyl or methylene-O-isobutyl or methylene-O-isopropyl (**Figure 1.5**) in order to mimic Leu690-Leu693-Leu694 and Leu819-Leu822-Val825 hot spots, localized respectively on Noxa/BID and HIF1α. During my secondment at University of Leeds, I carried out some binding studies of our derivatives with the biological counterparts with Fluorescence Anisotropy assays. For one of the synthesized macrocycles Fluorescence Anisotropy assays gave interesting IC50 values towards the interaction process of proteins p300 and Noxa with their biological counterparts, which showed to be a promising inhibitor for PPI.

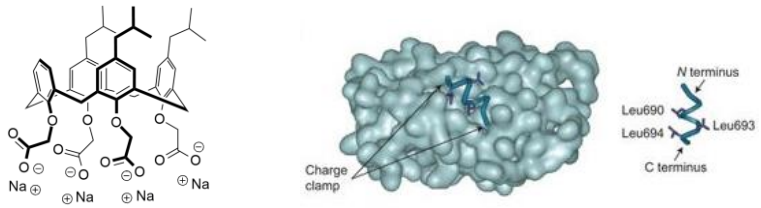

Figure 1.5. On the left, chemical structure Mcl-1/NoxaB and p300/HIF1α inhibitor synthetised in our laboratories; on the right, Mcl-1/NOXA B interaction (PDB code: 2JM6) along with NOXA B structure and the side-chains involved in binding.

1.3 References

1. Rodger P. McEver. Selectins: lectins that initiate cell adhesion under flow. *Curr. Opin. Cell Biol.* **14**, 581–586 (2002).

2. Leckband, D. & Sivasankar, S. Mechanism of homophilic cadherin adhesion. *Curr. Opin. Cell Biol.* **12**, 587–92 (2000).

3. Lutz, R. J. Role of the BH3 (Bcl-2 homology 3) domain in the regulation of apoptosis and Bcl-2-related proteins. in *Biochemical Society Transactions* **28**, 51–56 (Portland Press Ltd, 2000).

4. Supuran, C. T. Structure and function of carbonic anhydrases. *Biochemical Journal* **473**, 2023–2032 (2016).

5. Waheed, A. & Sly, W. S. Carbonic anhydrase XII functions in health and disease. *Gene* **623**, 33–40 (2017).

6. Supuran, C. T. Carbonic anhydrase inhibition and the management of hypoxic tumors. *Metabolites* **7**, (2017).

7. Campbell, K. J. & Tait, S. W. G. Targeting BCL-2 regulated apoptosis in cancer. *Open Biology* **8**, (2018).

8. Magid, E. & Turbeck, B. O. The rates of the spontaneous hydration of CO2 and the reciprocal reaction in neutral aqueous solutions between 0° and 38°. *BBA - Gen. Subj.* **165**, 515–524 (1968).

9. Aggarwal, M., Boone, C. D., Kondeti, B. & McKenna, R. Structural annotation of human carbonic anhydrases. *Journal of Enzyme Inhibition and Medicinal Chemistry* **28**, 267–277 (2012).

10. Rajachar, R. M., Tung, E., Truong, A. Q., Look, A. & Giachelli, C. M. Role of carbonic anhydrase II in ectopic calcification. *Cardiovasc. Pathol.* **18**, 77–82 (2009).

11. Langella, E., De Simone, G., Esposito, D., Alterio, V. & Monti, S. M. ζ-Carbonic anhydrases. in *Carbonic Anhydrases* 131–137 (Elsevier, 2019). doi:10.1016/B978-0-12-816476-1.00006-X

12. Capasso, C. δ-Carbonic anhydrases. in *Carbonic Anhydrases* 107–129 (Elsevier, 2019). doi:10.1016/B978-0-12-816476-1.00005-8

13. BENESCH, R. Carbonic Anhydrase and Calcification. *Ann. N. Y. Acad. Sci.* **429**, 457–458 (1984).

14. Ismail, I. S. The Role of Carbonic Anhydrase in Hepatic Glucose Production. *Curr. Diabetes Rev.* **14**, 108–112 (2018).

15. Mboge, M. Y., Mahon, B. P., McKenna, R. & Frost, S. C. Carbonic anhydrases: Role in pH control and cancer. *Metabolites* **8**, (2018).

16. Alterio, V., Di Fiore, A., D'Ambrosio, K., Supuran, C. T. & De Simone, G. Multiple binding modes of inhibitors to carbonic anhydrases: How to design specific drugs targeting 15 different isoforms? *Chem. Rev.* **112**, 4421–4468 (2012).

17. Supuran, C. T. Bacterial carbonic anhydrases as drug targets: Toward novel antibiotics? *Front. Pharmacol.* **JUL**, (2011).

18. Crystal structure and kinetic studies of a tetrameric type II β-carbonic anhydrase from the pathogenic bacterium Vibrio cholerae. Available at: https://reference.medscape.com/medline/abstract/26627652. (Accessed: 11th November 2019)

19. Zimmerman, S. A., Tomb, J. F. & Ferry, J. G. Characterization of CamH from Methanosarcina

thermophila, founding member of a subclass of the γ class of carbonic anhydrases. *J. Bacteriol.* **192**, 1353–1360 (2010).

20. Compain, P. *et al.* Glycosidase inhibition with fullerene iminosugar balls: A dramatic multivalent effect. *Angew. Chemie - Int. Ed.* **49**, 5753–5756 (2010).

21. Baldini, L., Casnati, A., Sansone, F. & Ungaro, R. Calixarene-based multivalent ligands. *Chem. Soc. Rev.* **36**, 254–266 (2007).

22. Abellán-Flos, M., Tanç, M., Supuran, C. T. & Vincent, S. P. Organic & Biomolecular Chemistry Exploring carbonic anhydrase inhibition with multimeric coumarins displayed on a fullerene scaffold †. *Org. Biomol. Chem.* **13**, 7445 (2015).

23. Fasting, C. *et al.* Multivalency as a chemical organization and action principle. *Angew. Chemie - Int. Ed.* **51**, 10472–10498 (2012).

24. Kanfar, N. *et al.* Effective Access to Multivalent Inhibitors of Carbonic Anhydrases Promoted by Peptide Bioconjugation. *Chem. - A Eur. J.* **23**, 6788–6794 (2017).

25. Wojtczak, A., Cody, V., Luft, J. R. & Pangborn, W. Structures of human transthyretin complexed with thyroxine at 2.0 A resolution and 3',5'-dinitro-N-acetyl-L-thyronine at 2.2 A resolution. *Acta Crystallogr. D. Biol. Crystallogr.* **52**, 758–65 (1996).

26. Ando, Y. & Suhr, O. B. Autonomic dysfunction in familial amyloidotic polyneuropathy (FAP). *Amyloid* **5**, 288–300 (1998).

27. Sousa, M. M., Cardoso, I., Fernandes, R., Guimarães, A. & Saraiva, M. J. Deposition of transthyretin in early stages of familial amyloidotic polyneuropathy: evidence for toxicity of nonfibrillar aggregates. *Am. J. Pathol.* **159**, 1993–2000 (2001).

28. Bulawa, C. E. *et al.* Tafamidis, a potent and selective transthyretin kinetic stabilizer that inhibits the amyloid cascade. *Proc. Natl. Acad. Sci. U. S. A.* **109**, 9629–9634 (2012).

29. Castaño, A., Helmke, S., Alvarez, J., Delisle, S. & Maurer, M. S. Diflunisal for ATTR cardiac amyloidosis. *Congest. Heart Fail.* **18**, 315–9

30. Sant'Anna, R. *et al.* Repositioning tolcapone as a potent inhibitor of transthyretin amyloidogenesis and associated cellular toxicity. *Nat. Commun.* **7**, (2016).

31. Yokoyama, T. & Mizuguchi, M. Inhibition of the amyloidogenesis of transthyretin by natural products and synthetic compounds. *Biol. Pharm. Bull.* **41**, 979–984 (2018).

32. Hellstrand, E., Boland, B., Walsh, D. M. & Linse, S. Amyloid β-protein aggregation produces highly reproducible kinetic data and occurs by a two-phase process. *ACS Chem. Neurosci.* **1**, 13–18 (2010).

33. Makin, O. S. & Serpell, L. C. Structures for amyloid fibrils. *FEBS Journal* **272**, 5950–5961 (2005).

34. Chiti, F. & Dobson, C. M. Protein Misfolding, Amyloid Formation, and Human Disease: A Summary of Progress Over the Last Decade. *Annu. Rev. Biochem.* **86**, 27–68 (2017).

35. Knowles, T. P. J., Vendruscolo, M. & Dobson, C. M. The amyloid state and its association with protein misfolding diseases. *Nat. Rev. Mol. Cell Biol.* **15**, 384–96 (2014).

36. Marina, G. B. *et al.* Amyloid β-protein (Aβ) assembly: Aβ40 and Aβ42 oligomerize through distinct pathways. *Proc. Natl. Acad. Sci. U. S. A.* **100**, 330–335 (2003).

37. Senguen, F. T., Doran, T. M., Anderson, E. A. & Nilsson, B. L. Clarifying the influence of core amino acid hydrophobicity, secondary structure propensity, and molecular volume on amyloid-β 16-22

self-assembly. *Mol. Biosyst.* **7**, 497–510 (2011).

38. Balbach, J. J. *et al.* Amyloid fibril formation by Aβ16-22, a seven-residue fragment of the Alzheimer's β-amyloid peptide, and structural characterization by solid state NMR. *Biochemistry* **39**, 13748–13759 (2000).

39. Jones, S. & Thornton, J. M. Principles of protein-protein interactions. *Proceedings of the National Academy of Sciences of the United States of America* **93**, 13–20 (1996).

40. Keskin, O., Ma, B. & Nussinov, R. Hot regions in protein-protein interactions: The organization and contribution of structurally conserved hot spot residues. *J. Mol. Biol.* **345**, 1281–1294 (2005).

41. Li, J. & Liu, Q. 'Double water exclusion': A hypothesis refining the O-ring theory for the hot spots at protein interfaces. *Bioinformatics* **25**, 743–750 (2009).

42. Brooks, C. L. & Gu, W. New insights into p53 activation. *Cell Research* **20**, 614–621 (2010).

43. Iyer, N. G., Özdag, H. & Caldas, C. p300/CBP and cancer. *Oncogene* **23**, 4225–4231 (2004).

44. Gu, J., Milligan, J. & Huang, L. E. Molecular mechanism of hypoxia-inducible factor 1α-p300 interaction. A leucine-rich interface regulated by a single cysteine. *J. Biol. Chem.* **276**, 3550–3554 (2001).

45. Guikema, J. E., Amiot, M. & Eldering, E. Exploiting the pro-apoptotic function of NOXA as a therapeutic modality in cancer. *Expert Opin. Ther. Targets* **21**, 767–779 (2017).

46. Xiang, W., Yang, C. Y. & Bai, L. MCL-1 inhibition in cancer treatment. *OncoTargets and Therapy* **11**, 7301–7314 (2018).

47. Hird, A. W. & Tron, A. E. Recent advances in the development of Mcl-1 inhibitors for cancer therapy. *Pharmacol. Ther.* **198**, 59–67 (2019).

48. Saraogi, I. *et al.* Synthetic α-helix mimetics as agonists and antagonists of islet amyloid polypeptide aggregation. *Angew. Chemie - Int. Ed.* **49**, 736–739 (2010).

49. Biros, S. M. *et al.* Heterocyclic α-helix mimetics for targeting protein-protein interactions. *Bioorganic Med. Chem. Lett.* **17**, 4641–4645 (2007).

50. Ernst, J. T., Becerril, J., Park, H. S., Yin, H. & Hamilton, A. D. Design and application of an α-helix-mimetic scaffold based on an oligoamide-foldamer strategy: Antagonism of the Bak BH3/Bcl-xL complex. *Angew. Chemie - Int. Ed.* **42**, 535–539 (2003).

51. Saraogi, I., Incarvito, C. D. & Hamilton, A. D. Controlling curvature in a family of oligoamide α-helix mimetics. *Angew. Chemie - Int. Ed.* **47**, 9691–9694 (2008).

52. Cummings, C. G., Ross, N. T., Katt, W. P. & Hamilton, A. D. Synthesis and biological evaluation of a 5-6-5 imidazole-phenyl-thiazole based α-helix mimetic. *Org. Lett.* **11**, 25–28 (2009).

53. Yin, H. *et al.* Terephthalamide derivatives as mimetics of helical peptides: Disruption of the Bcl-xL/Bak interaction. *J. Am. Chem. Soc.* **127**, 5463–5468 (2005).

54. Shaginian, A. *et al.* Design, Synthesis, and Evaluation of an α-Helix Mimetic Library Targeting Protein−Protein Interactions. *J. Am. Chem. Soc.* **131**, 5564–5572 (2009).

55. Yin, H., Frederick, K. K., Liu, D., Wand, A. J. & DeGrado, W. F. Arylamide derivatives as peptidomimetic inhibitors of calmodulin. *Org. Lett.* **8**, 223–225 (2006).

56. Walensky, L. D. *et al.* A Stapled BID BH3 Helix Directly Binds and Activates BAX. *Mol. Cell* **24**, 199–210 (2006).

57. Rodriguez, J. M. & Hamilton, A. D. Benzoylurea oligomers: Synthetic foldamers that mimic extended α helices. *Angew. Chemie - Int. Ed.* **46**, 8614–8617 (2007).

58. Ahn, J.-M. & Han, S.-Y. Facile synthesis of benzamides to mimic an α-helix. *Tetrahedron Lett.* **48**, 3543–3547 (2007).

Chapter 2

Small sulfonamide/ammonium-bearing inhibitors for Carbonic Anhydrases

2.1 Introduction

2.1.1 General background

Most organisms to live produce CO_2, which is the major by-product of the cellular respiration in aerobic metabolism. This suggests that Nature has been evolved in order to avoid the harmful accumulation of this gas preventing several damages to cells[1–5]. Over ages, evolution tackled this hazardous threat exploiting one of the most efficient, easiest and trivial reaction ever known on earth: CO_2 hydratation reaction (**Figure 2.1.1.1**). In this way, CO_2 is easily solubilized in biological fluids as bicarbonate anion and moved in and out the cells preventing possible back-pressure damages to membranes due to its accumulation. Bicarbonate ion is therefore a fast carbon source exploitable in catabolic reactions. Moreover, considering the high CO_2 hydratation reversibility, it is also used by Nature as buffering[6] and purging system[7,8]. Indeed, in humans, when bicarbonate anions get in bloodstream and reach lungs, there the CO_2 pressure is so high that CO_2 release is thermodynamically favoured.

$$CO_2 + H_2O \rightleftharpoons HCO_3^- + H^+$$

Figure 2.1.1.1. Reaction of solubilization of CO_2 in water.

Even if CO_2 hydration is very fast at physiologic pH, it is not fast enough to satisfy as such biological needs[9,10]. So, for this reason, Nature developed interesting tools, called Carbonic Anhydrases (CAs), which are metalloenzymes able to catalyze this reaction accelerating it 10^4-10^6 times with respect to the uncatalyzed one and leading carbon metabolism to a very competitive level[11]. For its rapidity, efficiency and reversibility, this catalyzed process has widely spread over and Nature has been using it for a huge number of physiological processes such as cellular respiration[12], pH regulation[6,13], bone resorption[14,15], biosynthetic reactions (gluconeogenesis[16], lipogenesis[17] and ureagenesis[18,19]), electrolyte secretion in tissues and organs[20], calcification[21–23]. For their ubiquitous character, these enzymes are basilar for life and hence they are getting a central place in research in order to fully understand their mechanisms, structures, functional roles and how to modulate their activity, in particular when responsible of or associated to pathological states.

2.1.2 Carbonic Anhydrases: classification

CAs belong to a metalloprotein superfamily present both in eukaryotes and in prokaryotes, codified by six different families of uncorrelated genes. They are classified in α, β, γ, δ, η, ζ CAs:

- α-CAs are the most studied family since represents the most abundant group in Nature. Vertebrates, but also some bacteria and green algae, own this type of CAs. They are mainly monomers (just few examples of homodimers are reported in literature[24–28]) and the active site is made of a zinc ion tetracoordinated to three imidazole units (His94, His96, His119) and a water molecule into a tetrahedral geometry.
- β-CAs are another highly-studied family, since it is owned mostly by prokaryotic organisms responsible of several diseases as Haemophilius influenza[29], Escherichia coli[30], M. tuberculosis[31], Vibrio cholera[32] and Cryptococcus neoformans[33] and also by plant chloroplasts[34]. They are in the form of dimers, tetramers (dimers of dimers) or multiples of these homodimers. Each dimer has an αβ fold, specifically made of an N-terminal

chain, which extends away from the protein core and makes additional stabilizing contacts with the adjacent monomer, a conserved zinc-binding core and a C-terminal domain rich in α-helices. The conserved zinc-binding region is essentially a β sheet, made of four parallel strands flanked on both sides by α-helices, derived from C-terminal domain. The active site is very peculiar since the zinc ion is surrounded by two cysteines (Cys42 and Cys 102), one histidine (His98) and a fourth ligand (generally a hydroxide ion or Asp44) that determines the nature of the complex conformation. In fact, when this is an aspartate (Type II), the active site assumes the so-called "close conformation" due to saturation of the first coordination sphere, which inactivates the catalytic site. When, on the contrary, pH is >8.3, a β-conserved Arg (included in the so-called catalytic dyad Asp-Arg) starts making new ionic interactions with the coordinated aspartate residue (Asp44). This event weakens the coordination bond, which allows more easily the replacement of the side chain of this amino acid by a water molecule (Type I). Consequently, the catalytic site state is changed into an "open conformation", which makes indeed the enzyme ready to work[24].

- γ-CAs were characterized for the first time from the methanogenic archeon Methanosarcina thermophila[35]. The enzyme, called Cam[36], is a single-stranded polypeptide, that adopts a left-handed parallel β-helix fold, in which only left-handed crossover connections among an untwisted parallel β-stands were observed. It is a trimer where three zinc-containing catalytic sites are located at the interface between two monomers. Over times, it has been discovered that in this family geometry and metal centre can be different from the common ones. Indeed, it has been demonstrated by XRD that, in some cases, according to biodisponibility, Zn(II) can be substituted by either Fe (II) or Co (II). Here the side chain imidazoles of three histidines (His81, His117 and His122) can be arranged mainly in a tetrahedral or bipyramidal trigonal geometry with Fe(II) or Zn(II), and in an octahedral geometry with Co(II). Right through this CA type, it has been discovered that the catalytic activity does not only come from a pure zinc-mediated increase of water-bound acidity, but it is a result of cooperation with other surrounding amino acids. In fact in Co(II)-dependent CA, Asn73 and Gln75 help pre-orienting the cobalt ion for the interaction with the carbon dioxide, while Asn202 prepares the carbon dioxide, by polarization, for coordination to cobalt hydroxide-bound moiety.
- δ-CAs. In this class are present some examples of CAs of some rare diatoms. Since just few differences compared to the other families have been discovered, this group is at the centre of a scientific debate for the actual existence of this family[37]. η-CAs were recently found in organisms of the genus *Plasmodium* (i.e. *P. falciparum*). At the beginning of their discovery, they were supposed to belong to α-CAs like γ-CAs and δ-CAs, given the superimposable composition and the similar structure of the active site. Though, studying more deeply the primary structure of this protein, it was shown that the His positions in polypeptide chains are different in these three families. In fact, if in α-CAs His are positioned in x, x+2, x+25, in η-CAs they are shifted to positions x, x+2 and x+24. Moreover this type is generally bigger in dimensions (>400 aa) with respect to α-type (250-280 aa). Contrarily, the differences with δ-CAs reside mainly in mutation of particular amino acids. In fact, the dyad Glu106-Thr199 and His64, are respectively replaced by Ser106-Ser199 and Phe64, dramatically altering the activity of the enzyme itself.
- ζ-CAs were found exclusively in bacteria and, in particular, in few chemolithotrophs and marine cyanobacteria that contain carboxysomes such as *T. weissflogii*, a species of phytoplankton[38]. The interesting feature of this type of CAs is that, even if the catalytic site is equal to Type I (open conformation) β-CAs, here the metal centre is consists of Cd(II), which represents an evolutionary adaption to low zinc levels in marine habitat. Also here, as well as for γ-CA, the only difference from α-type is the positions of the three catalytic histidines: if in α-type they are located in x, x+3 and x+112, in γ-CA are positioned in x, x+36 and x+41. These modifications are effective proof of divergent evolution.

2.1.3 Human Carbonic Anhydrases

Vertebrate α-CAs (and human's too) are divided, in turn, in 16 sub-classes, called isoforms, which differ one another for catalytic activity, tissue and subcellular distribution, oligomeric arrangement, expression levels and for response to different classes of inhibitors[39]. Due to these high number of features, these can be classified in several ways, but the most common is that related to subcellular distribution (**Figure 2.1.3.1A**). They are subdivided in:

- cytosolic CAs (CA I, II, III, VII, XIII)
- membrane CAs (CA IV, IX, XII, XIV, XV)
- mitochondrial CAs (CA VA, VB)
- saliva- and milk-secreted CAs (CA VI)

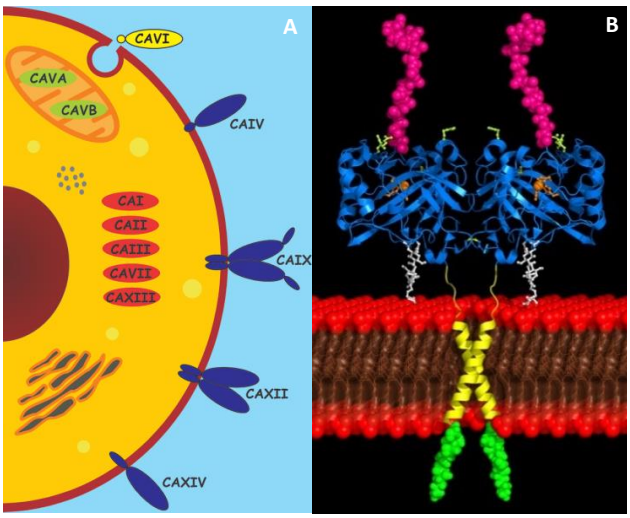

Figure 2.1.3.1. A) Subcellular distribution of CA isoforms. Adapted from reference[39]; B) Proposed model showing the structural arrangement of the CA IX dimer on the cellular membrane. The X-ray structure of the dimeric catalytic domain is reported in cyan, with Arg-58, Arg-60, and Arg-130 in green and the glycan moieties in white. The hypothetical arrangements of the PG domains, the transmembrane helices and the cytoplasmic portions are schematically reported in magenta, yellow, and green, respectively. Adapted from reference[40].

Actually, there is one more class we should pay attention to, i.e. the Carbonic Anhydrase Related Proteins-CARP (CA VIII, X, XI). By XRD and physiological experiments, it has been understood that this class is made of globular proteins that are completely acatalytic. For this reason they cannot be considered enzymes and their biological roles are still under investigation[39]. The most important human carbonic anhydrases due to their excellent catalytic activity properties are the cytosolic ones, which retain the same globular structure observed with CARPs. Also the saliva- and milk-secreted CA VI has the same structure of cytosolic ones, but this, instead, is provided with an internal disulphide bond and two N-linked oligosaccharides, which are essential for its stabilization and secretion[41]. The monomeric plasma membrane CA IV (monomeric), differently to CAVI, exploits a phosphatidylinositol glycan chain (GPI tail), not for stabilization purposes, but to link itself to the cell surface. This linkage is possible thanks to the presence of highly positively charged amino acids (Lys37, Lys39,

Lys42, Lys43, Arg46, Lys187, Lys188, Arg189A, His190, Arg213, and Lys258) in the GPI tail, which are responsible of tight interactions with phosphate or carbohydrate groups in lipids[42].

CA IX (dimers)[43] (**Figure 1.1.3.1B**), XII (dimers)[44] and XIV (monomers)[45] are the most complex ones, in fact, they are made of four domains:

- a topological extracellular domain is 377 amino acids long (Gln38-Asp414)
- a helical transmembrane domain is 21 amino acids long (Ile415-Met435)
- a cytoplasmic domain is 24 amino acids long (Arg436-Ala459)
- a proteoglycan-like (PG) domain is 75 amino acids long (Gln38-Asp112).

Differently to other ones, these last membrane-bound isoforms are mainly involved in cell communication and in tumour progression[46]. In particular, for this important biological role they are deeply investigated.

2.1.4 hCAII: structure and mechanism

hCAII represents one of the most studied CAs for its high bioavailability, its stability and the ease of expression, purification and crystallization. Thanks to their highly-conserved structures, hCAII can be taken as a structural model for all cytosolic isoforms[47]. It is an ellipsoidal-shaped protein with approximate dimensions of 50 x 40 x 40 $Å^3$ and it contains six right-handed α-helices, all located on the surface of the molecule, which enclose a large twisted β-structure formed by 2 parallel β-strands and 8 antiparallel β-strands. Zinc ion is located at the bottom of a 15 Å-deep funnel, which is coordinated by three conserved histidines (His94, His96, His119) in the classical α-fashion x, x+2, x+25 and a water molecule/hydroxyl ion with a distorted tetrahedral geometry. Analysing the composition of funnel walls, the active site has been considered a "bipolar" cavity. In fact, half of it is lined with hydrophobic amino acids (Ala121, Ala135, Val207, Phe91, Leu131, Leu138, Leu146, Leu109, Pro201 and Pro202), while the opposite half is lined with hydrophilic residues (His64, His67, His200, Asn69, Gln92, Thr199, Tyr7 and Val62). The actual reason of this "bipolarity" is related to the opposite polarity that needs to deal with. In fact, the enzyme must orient simultaneously either polar entities, such as water or bicarbonate, or hydrophobic molecules, like CO_2.

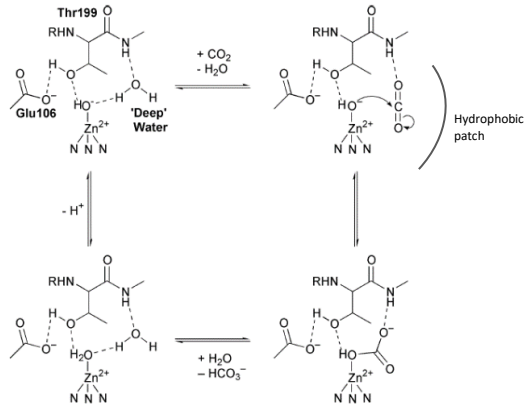

Figure 2.1.4.1. Mechanism of action of hCAs. Adapted from reference[48].

As matter of fact, when CO_2 goes through the funnel to reach the active site, it is trapped by some residues onto a hydrophobic patch (Val121, Val143, Leu198 and Trp209), which allows the molecule to be oriented in a favourable way next to zinc ion (**Figure 2.1.4.1**). At this point, CO_2, nearby zinc-bound hydroxide ion too, is close enough to trigger the synthesis of bicarbonate ion and rapidly to be replaced by an incoming water molecule. The next deprotonation step represents the rate-determining step of all mechanism since the proton shuffle through the funnel is not so trivial considering the high rigidity of the enzyme. This proton expulsion is guaranteed by a dense hydrogen-bonding network created by side chains of amino acids located onto the hydrophilic patch. In fact, zinc-bound hydroxide ion is directly connected by hydrogen bond to the so-called "deep water" (highly conserved water in crystal structures) and to Thr199, which, in turn, is bridged to carboxylic moiety of Glu106 and then to His64. This last amino acid is the so-called "gate-keeper", which, shifting its conformation between an "in" (pointing to the active site) and an "out" conformation (pointing to the outer buffer), represents a sort of mobile bridge that completes the proton shuffling giving H^+ to the last proton transporters (His3, His4, His10, His15 and His17) located on the rim of the funnel[49]. This very efficient and dense proton shuffle is what allows CAs overcome the RDS step and make them the fastest enzymes in Nature.

2.1.5 Etiology and pathologies

Due to the high number of isoforms and ubiquity characterizing these enzymes (**Table 2.1.5.1**), several types of diseases can arise from their dysregulation. In particular, when it is observed their overexpression or malfunctioning, for instance because of genetic mutations in conserved region, occur different cascade processes, which can activate several pathway leading to the outbreak of multiple diseases.

Table 2.1.5.1. Organ/Tissue distribution, CO_2 hydration activity, CO_2 affinity and off-targets for the 15Humanα-CA Isozymes. Adapted from reference[50].

	organ/tissue distribution	catalytic activity (CO_2 hydration)	affinity for sulfonamides	disease in which is involved	possible off-targets among other hCAs
CA I	erythrocytes, gastrointestinal tract, eye	low	medium	retinal/cerebral oedema	Unknown
CA II	erythrocytes, eye, gastrointestinal tract, bone osteoclasts, kidney, lung, testis, brain	high	very high	Glaucoma Edema Epilepsy altitude sickness	hCAI Unknown Unknown Unknown
CA III	skeletal muscle, adipocytes	very low	very low	oxidative stress	Unknown
CA IV	kidney, lung, pancreas, brain capillaries, colon, heart	medium	high	glaucoma retinitis pigmentosa stroke	hCAI Unknown Unknown
CA VA	muscle, eye liver	low	high	obesity	hCAI/hCAII
CA VB	heart and skeletal muscle, pancreas, kidney, spinal cord, gastrointestinal tract	high	high	obesity	hCAI/hCAII
CA VI	salivary and mammary glands	low	very high	cariogenesis	hCAII
CA VII	central nervous system	high	very high	epilepsy	Unknown
CA VIII	central nervous system	acatalytic	ND[a]	neurodegeneration cancer	Unknown Unknown
CA IX	tumours, gastrointestinal mucosa	high	high	cancer	hCAI/hCAII
CA X	central nervous system	acatalytic	ND[a]		
CA XI	central nervous system	acatalytic	ND[a]		
CA XII	kidney, intestine, reproductive epithelia, eye, tumors	low	very high	cancer glaucoma	hCAI/hCAII Unknown
CA XIII	kidney, brain, lung, gut, reproductive tract	low	high	sterility	Unknown
CA XIV	kidney, brain, liver, eye	low	high	epilepsy neuropathy	Unknown Unknown

[a]ND = not determined. No data are available in the literature on CA X and XI involvement in diseases.

Therefore, the tough ongoing challenge is to find out new innovative molecules able to work as selective inhibitors preventing a simultaneous, wide and indistinct activity against different isoforms and then limiting side effects, but also to maximize the therapeutic effect onto the specific disorder-correlated isoform. Unfortunately, the issue of selectivity among isoforms is very hard to realize since these enzymes are mostly conserved making very challenging finding amino acids accessible as specific targets. Because of these issues, medicinal chemists are still

focused onto the easier realization of systems selective to membrane-bound CAs (generally involved in hypoxic tumours) tuning the polarity of this inhibitors in order to prevent the cell uptake.

2.1.6 Inhibitors classification

All the inhibitors proposed and studied so far, can be divided into two classes: out-of-active-site binding inhibitors and in-active-site binding inhibitors. The former class was discovered by Vu and co-workers[51] during an ESI-FTICR-MS screening onwards a large library of natural compounds, tested as inhibitors against hCAII. Testing these molecules, it was observed that a coumarin derivative, in particular 6-(1S-hydroxy-3-methylbutyl)-7-methoxy-2H-chromen-2-one **I** (**Figure 2.1.6.1A**), shows a nanomolar-range inhibitor activity after an incubation time of around 6h. After this amazing discovery, Supuran studied more deeply this type of molecules synthesizing and testing new structural analogues. By X-Ray diffraction obtained from hCAII-**I** cocrystal[52], just the hydrolized form of compound **I**, namely cis-2-hydroxy-4-(1S-3-methylbutyl)-3-methoxy-cinnamic acid (compound **II** in **Figure 2.1.6.1A**), was observed. In particular these acid carboxylic products were observed at the entrance of the active site away from zinc ion. This means that for long incubation times CA is able to act as an esterase hydrolyzing lactones (in this case coumarins) into carboxylic acids, which the real active inhibitors. An interesting work of D'Ambrosio and co-workers[53], carried out onto acid carboxylic derivatives, shows why products of coumarin hydrolysis are so efficient (**Figure 2.1.6.1B**). It can be seen that one O atom of the carboxylate moiety of inhibitor **II** is involved in a hydrogen bond with the backbone nitrogen atom of Tyr7, whereas the other one interacts with ND2 atom of Asn11. Moreover, simultaneously, the same carboxylate is involved in two strong hydrogen bonds with water molecules, which, in turn, interact with the backbone oxygen of Trp5 and the ND1 atom of His64, the so-called "gate-keeper". The high number of stabilizing interactions and the "gate-keeper" frozen in out-conformation makes coumarin-based derivatives interesting suicide inhibitors, which stick at a distance of about 14Å from the active site, occluding the entrance to substrates. This efficient allosteric behaviour is the reason why this class can easily reach nanomolar inhibition constant.

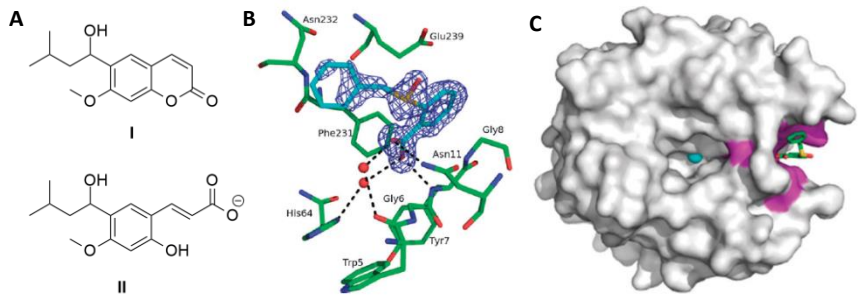

Figure 2.1.6.1. A) Chemical structures of 6-(1S-hydroxy-3-methylbutyl)-7-methoxy-2H-chromen-2-one **I** and cis-2-hydroxy-4-(1S-3-methylbutyl)-3-methoxy-cinnamic acid **II**; **B**) Electron density of 2-benzylsulfynilbenzoic acid and relative contacts with hCAII; **C**) hCAII/2-benzylsulfynilbenzoic acid complex. The inhibitor recognition site is highlighted in magenta, whereas zinc ion is highlighted in cyan. Figures adapted from reference[53].

For the in-active-site binding inhibitors, another classification can be made according to the different inhibition mechanisms. Indeed, they can be subdivided in: zinc-binders inhibitors (ZBI) and zinc-bound water binder inhibitors (WBI). Besides the easy and small inorganic anions[26,54–

[56] (e.g. cyanide, trithiocarbonate, hydrogen sulphide and azide), which have shown very weak inhibition constants in millimolar-submillimolar range because of the few interactions established in the active site, N-hydroxyureates and acetohydroxamates have shown very good properties as zinc binders inhibitors. These compounds were developed in response to accurate studies on hCAII cocrystals with carbamic acid and urea, obtained by monitoring the CA esterase activity respectively on cyanate and cyanamide. Here, strong binding between urea and zinc can be seen and this drove Temperini et al.[57,58] to the introduction of an additional OH group to increase the affinity of these molecules (**Figure 2.1.1.6A**). In fact, in his work he showed that NHOH moiety in N-hydroxyureates and acetohydroxamates adds more stabilizing hydrogen-bonds with Thr199 bringing these molecules to a micromolar-range inhibition.

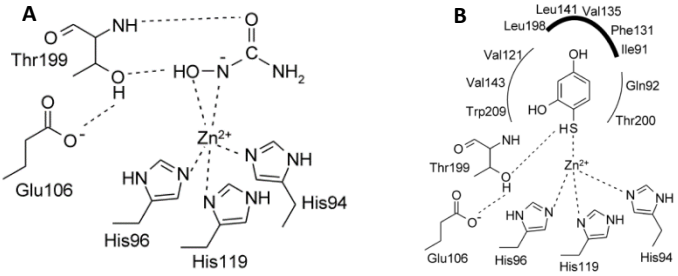

Figure 2.1.6.2. A) Schematic representation of N-hydroxyurea (PDB code: 2GEH) in hCAII active site; **B**) Schematic representation of 4-mercaptobenzene-1,3-diol (PDB code:2OSF) in hCAII active site. Figures adapted from reference[39].

A small class of ZBIs is represented by mercaptophenols. In these compounds, the efficiency strongly depends on the OH position. It has been demonstrated that in p-hydroxythiophenol, as SH moiety binds to zinc ion, the OH group is projected in the opposite direction towards the hydrophobic patch destabilizing the complex as a consequence (**Figure 2.1.6.2B**). On the contrary, locating OH group in ortho position or deleting it up, inhibition constants decrease from 148 μM to 0.631 μM[39].

Apart from these compounds, which are limited by very little flexibility in chemical space modification and small structures, sulfonamides represent the most versatile and potent inhibitors still used for clinical purposes[59,60]. Through a rationale studies based on cocrystals comparison made by Alterio in collaboration with Supuran[61], it has been demonstrated that two are the major factors that justify the high efficiency of these inhibitors: on one hand, they combine the negatively-charged nitrogen atom of sulfonamide, involved in the binding, and the positively-charged zinc ion; on the other hand, the binding with zinc ion pre-orients the sulfonamide NH moiety close by Thr199OG1 atom in order to make a further hydrogen bond which stabilizes the structure. From this preliminary study on, medicinal chemistry has been carrying on the so-called “tail approach”, which consists in adding a wide plethora of new functional groups in the back of pharmacophore (the “head”) to find new stabilizing interactions with residues in the upper part of the funnel. The first and the most famous compounds synthesized with this concept in mind are benzenesulfonamides. These compounds maximize their potentialities if substituted in para position by thioureido-, methylamino, ureido-, carboxy- and hydrazido- moieties.

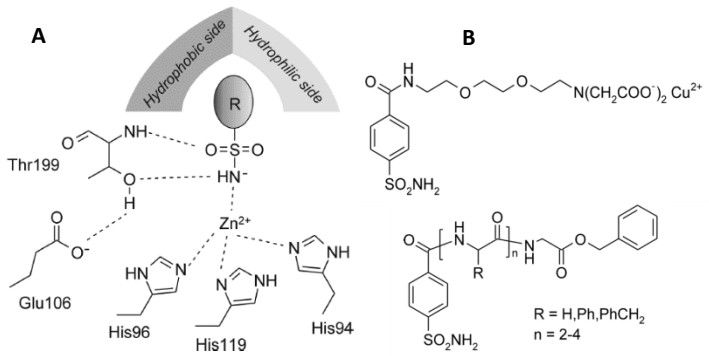

Figure 2.1.6.3. A) Schematic representation of sulphonamide binding mode in hCAII active site; **B**) Inhibitors towards hCAII used in the "two-prong" approach. Figure adapted from reference[50].

Besides the classical coordination to zinc ion, it has been demonstrated that these groups can orient phenyl ring in order to establish several Van Der Waals interaction with Phe131, Gln92, Leu198, Val121 and Thr200. The major advantage is that changing para substituents in length and nature, it allows us to increase pre-existing interactions or create new contacts at different distances. For instance, if halogen substituents increase just the sulfonamide deprotonation strengthening the pre-existing zinc-sulfonamide bond, sulfamoyl-benzenecarboxamides can be easily functionalized in order to create further distant multiple interactions. First attempts were made by Supuran et al.[62,63], functionalizing them with oligo-peptide chains, and by Srivastava et al.[64], functionalizing them with bis(ethoxyethyl) chains, provided at their end with iminodiacetate-Cu(II) ligand (**Figure 2.1.6.3**). It has been shown that these are very good inhibitors playing in nanomolar-range affinity, but actually the reasons are totally different: the former is involved in an intensive network of hydrophobic interactions with the protein (Pro201, Phe131, Leu198 and Pro202), which strongly stabilize the complex; the latter combines the effect of primary inhibition (sulphonamide-zinc ion) with the chelation of catalytic His64 in "in" conformation, which, once blocked, cannot ultimate the proton shuffling. Design of difunctional inhibitors, like the ones show in **Figure 2.1.6.3B**, is called "two-prong" approach.

Recently these compounds have been tested changing in different ways the linker used to couple benzenesulfonamide moiety to the tail scaffold. Among all, ureido and thioureido linkers are clearly remarkable to be quoted since they exploit different principles in the binding, not used by the common inhibition strategies[65–68]. They, in fact, exploit the high flexibility of ureido or thioureido linker, that give the chance to the molecule to find the conformation, which best fits the funnel minimizing the system energy. Moreover thioureido linker increases the water solubility and tends to inhibit selectively hCAI, hCAII and hCAIX, representing interesting compounds for the design of antiglaucoma/antitumor agents. The few cocrystal structures obtained show all the canonical sulphonamide binding mode and very variable tail interactions (**Figure 2.1.6.4**). Since there are just few examples in literature, these compounds must be investigated more deeply given the high number of potentialities.

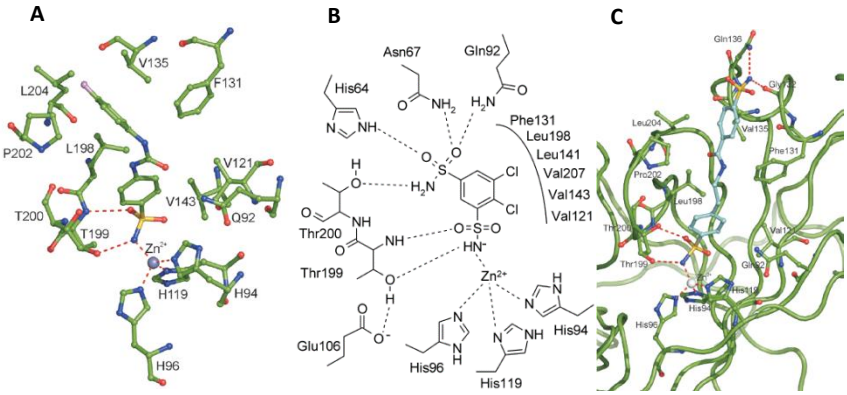

Figure 2.1.6.4. A) Interactions of a thioureidic-based sulfonamide inhibitor with the active site of hCAII; B) Interactions of dichlorophenamide inhibitor with the active site of hCAII; C) Interactions of a disulfonamide inhibitor with the active site of hCAII. Figures adapted from reference[50].

Another interesting class is the one related to benzenedisulfonamides. Up to now, just two different types of molecules were characterized: those with the two sulfonamide moieties on the same aromatic ring[69] and those with the sulfonamide moieties onto different aromatic rings, separated by an appropriate linker[59]. Both of them are nanomolar inhibitors of hCAII, whose efficiency is explained by the simultaneous binding of zinc ion with one sulfonamide in anionic form and by a stereo-electronic complementary amino acid, which enhances stability of the other sulfonamide. Many of these inhibitors clinically have been widely used for the treatment of glaucoma and different neurological disorders (e.g. dichlorophenamide[26,70,71], **III** in **Figure 2.1.6.6**), due to their high affinity for hCAII. The only difference between these two subclasses is the different amino acids recognized due to the different length of the inhibitor core. Indeed, in the work of Alterio et al.[69] beyond the canonical sulphonamide binding to zinc ion, dichlorophenamide (**Figure 2.1.6.4B**) clearly establishes further interactions with Thr200, His64, Asn67, Gln92 and the hydrophobic patch (Phe131, Leu198, Leu141, Val207, Val143 and Val121), while 4-(4-sulfamoylphenylcarboxamidoethyl)benzenesolfonamide, which resembles to a difunctionalized divalent bisphenol, loses every additional interaction seen in the previous case, but gains two H-bonds between the distal sulphonamide moiety and the out-of-active-site Gln136 and Gly132 because of its longer core (**Figure 2.1.6.4C**)[72]. Obviously, in this very last example the inhibitor efficiency depends, not just on the linker between the two aromatic rings, but on the nature and the degree of aromatic substitution as well. Right modifying the nature of sulfonamide-bearing aromatic ring were discovered several compounds with better affinity than the previous ones. Since the aromatic ring is in a bipolar cavity, it may be used for making contacts, not just with hydrophobic residues, but also with hydrophilic residues. Having this thought in mind, medicinal chemists were led to exploit as active unit a heterocyclic sulfonamide giving birth at the most famous class of CAIs, known so far. Several are the compounds belonging to this heterocycle class. Comparing almost all the results obtained in literature, some rules can be outlined:

- sulfonamides with five-membered ring are usually more efficient than those with six-membered rings.
- sulfonamides with nitrogen or sulfur atoms in the heterocycle ring are associated to better CA inhibitory properties (e.g. thiophene, thiadiazole and thiadiazoline derivatives)[50].

One of the most important molecules is acetazolamide (AAZ), which, other than the treatment of oedema, gastroduodenal ulcers and mountain sickness, is still clinically used for the topic

treatment of glaucoma thanks to its very good affinity and pharmacological properties. Differently from the classical thiophene derivatives, thiadiazolidine and thiadiazole derivatives, AAZ among them, through the endocyclic nitrogen atoms can establish two additional interactions with Thr200, whereas thiophene derivatives do not (**Figure 2.1.6.5**). Some studies about thiadiazolidine and thiadiazole derivatives have demonstrated that their pharmacological properties can be easily improved adding fluorinated tails, which make the correct balance in hydrophobicity/hydrophilicity ratio for cellular uptake[73].

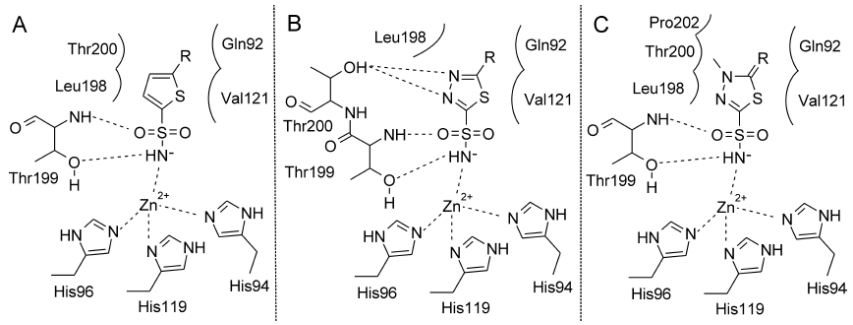

Figure 2.1.6.5. Inhibition mode of A) thiophene, B) thiadiazole and C) thiadiazoline derivatives. Figures adapted from reference[50].

However, thiophene derivatives get good properties just if included in thienothiopyran ring. They, in fact, binding zinc ion, orient thiopyran ring in a way that block His64 by its normal job of proton shuffler. Among all the molecules belonging to this class, dorzolamide opened a new interesting subclass of inhibitors. In fact, dorzolamide **IV** has recently been used for the synthesis of bifunctional compounds containing an additional (NO)-releasing moiety **V**[74] (**Figure 2.1.6.6**). Although the presence of NO target in eye, these compounds haven't been explored for the treatment of glaucoma. In fact, it has been demonstrated that once given these drugs to hypertensive glaucoma patients, which develop a decreased NO/cGMP content[75] in the aqueous humour, intraocular pressure can lowered to normal conditions[76–78]. This represents a case of the so-called Multi-Target-Directed Ligands approach (MTDL): the design of hybrid molecules containing moieties and pendants able to interact with different targets in order to reduce issues related to multiple drugs administration, pharmacokinetics and low patient compliance[79].

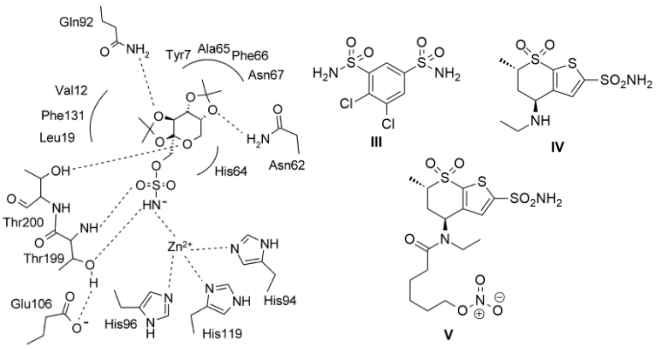

Figure 1.1.6.6. On the left, inhibition mode of topiramate in the active site of hCAII (PDB code: 3HKU; figure adapted from reference[50]); on the right, dichlorphenamide (**III**), dorzolamide (**IV**) and dorzolamide functionalized with (NO)-releasing moiety (**V**).

Another case of MTDL is that of sugar-containing sulfonamide/sulfamates/sulfamides. Even if with no sugar moiety they would still have inhibitory activity, they gain extraordinary properties in multifactorial inhibition. From Shank's work[80,81], one of these molecules (Topiramate) (**Figure 2.1.6.6**) has been defined a potent anticonvulsant, since it is responsible of multiple target inhibition (enhancement of GABA-ergic transmission, CO_2 retention as a consequence of inhibition of the red cell and brain CAs and blockade of sodium channels and kainate/AMPA receptors).

Beside ZBIs that we have largely talked about, there is the group of WBIs, which over the years have been used for several applications as antimutagenic, antiviral, anticancer, anti-inflammatory, antioxidant or antibacterial. Two are the classes related to this group: phenols and polyamines. Phenols as hCAII inhibitors were discovered in 1982 by Lindskog and co-workers[82,83], who by cocrystals, obtained from phenol and hCAII, rationalized the kinetic behaviour of these compounds. It was found that phenolic OH is bound in the active site in a new binding mode. In fact, along with all the hydrophobic interactions with the hydrophobic pocket delimited by Val121, Val143, Leu198 and Trp209, phenolic OH is engaged in two stabilizing hydrogen bonds: one with the zinc-bound water/hydroxide ion and one with NH amide of Thr199 (**Figure 2.1.6.7A**). After this first evidence, two different structural studies[25,84] were carried out during which it has been discovered that the binding in the hydrophobic patch phenol occupies the CO_2 recognition site. This was the first proof that phenol molecules inhibit by a competitive mechanism. For these interesting findings, phenols are getting more and more studied and used as lead compounds for the development of new inhibitors.

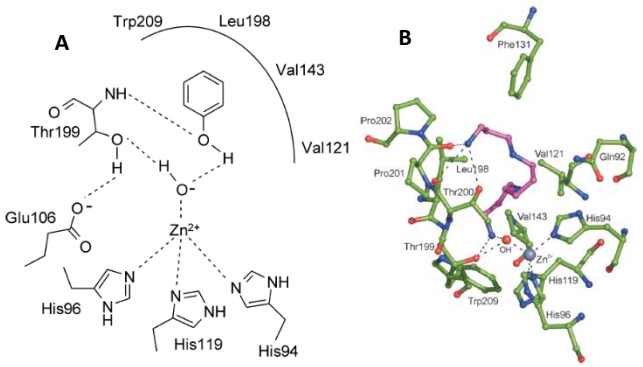

Figure 2.1.6.7. A) Inhibition mode of phenol in the active site of hCAII, **B**) Inhibition mode of a polyamine derivative in the active site of hCAII (PDB code: 3KWA). Figures adapted from reference[50].

The polyamines as CA inhibitors were discovered by chance during a work on CA activators, in particular histamine and L-adrenaline[85]. X-ray crystallographic studies showed that these molecules, bound at the entrance of CA active site, facilitate the in-out shuffling of the proton coming from the zinc-bound water, which limits the catalytic cycle. With this in mind, polyamines, like spermine or spermidine, were thought as potential very strong candidates for CA activation. Though, this was experimentally confutated. In fact, in cocrystals obtained with hCAII (**Figure 2.1.6.7B**)[86], it can be seen that spermine is present in coiled tetracation conformation and binds to zinc-bound hydroxide with the ending-ammonium tail in the same fashion as phenols. Differently from phenols, here the primary binding is reinforced by an electrostatic attraction between positively-charged nitrogen atom and negatively-charged oxygen atom. Also here a dense network is present of stabilizing interactions like hydrogen bonds between hydroxide-bound spermine terminal ammonium and Thr199OG1, hydrogen

bonds with Thr200 and Pro201 and several Van Der Waals interactions with enzyme residues, as Phe131, Thr199, Pro202, Gln92, Val143, Thr200, Val121, Leu198 and Pro201.

2.1.7 Inhibitor selectivity

As it can be understood from this brief review, CAs are well-studied enzymes and their properties can be modulated by a wide plethora of inhibitors. As already highlighted, unfortunately, all CAs within a type own a very small amount of not-conserved residues and so this makes difficult to target just one particular isoform. Beside some examples, in which some inhibitors showed up to be selective towards an isoform over another one, the only way to make selective molecules seems to be the playing around the hydrophobicity/hydrophilicity ratio or the CA types involved in the disease. In this context, in fact, it is possible to target out easily just the membrane-bound ones without interacting with the cytosolic ones. In doing this, it must be taken into account that cytosolic isoforms are inside the cell and so their inhibition should require molecules able to cross the membrane, whereas for membrane isoforms do not, given their extracellular catalytic domains that protrude outside the cell. Working with polar molecules represents the best solution to reduce the off-target CA side effects generally encountered with the classical inhibitors.

Pyridinium-based sulphonamides are examples of these types of molecules. From different experiments, it has been demonstrated that 1-N-(4-sulfamoylphenyl-ethyl)-2,4,6-trimethylpyridinium perchlorate[87], even if it is able to inhibit in vitro some cytosolic isoforms in the nanomolar range like CAI and CAII, in vivo it is completely inactive towards them preferring the pharmacokinetically easy-accessible CAIX. This is just an example but several are the molecules present in literature engineered with charges to avoid the membrane permeation[88]. An alternative to this is the functionalization of already validated inhibitors with peptide or sugar moieties. This “sugar approach” guarantees, as well as the “charge approach”, the synthesis of water-soluble adducts that cannot be uptaken by cells, since unable to cross the lipophilic plasmatic membrane[89,90].

Also bacteria own their CAs and some of these have just η, α or β types. This is a huge advantage in the design of new potential antibacterial. In fact in Nature are present several microbes which have different isoforms only from α-type. If we were able to find some significant differences in these non-human CAs or transporters that can mediate a selective uptake in bacteria cells, this could be an exploitable strategy to defeat some important infections caused by these organisms. Unfortunately, up to now, there are not enough data to assess that microbial CAs could be innovative bio-targets even if so much central in life cycle of these pathogenic organisms[91]. This innovative forefront is surely limited by the crystallizability of several microbial types, which cannot let us determine the substantial differences with α-type CAs and surely by the constant interest of pharmaceutical company in investing in the profitable classic targets (cell wall biosynthesis, protein biosynthesis, DNA and RNA biosynthesis and folate biosynthesis). It is also true that in antibacterial field we got at a point in which the antibiotic resistance is a rising problem more and more serious[92]. So these CAs must be studied since might represent a worthy and valid alternative in therapeutic treatments of infections.

2.1.8 Disulphide prodrugs and fluorescent probes

Among all human isoforms, the most interesting one for selectivity purposes is CAIX, which is the main isoform involved in many cancers. The acidic extracellular pH is demonstrated to be

one of the main factors responsible of tumour diffusion[93]. In fact, acidic pH activates several pathological pathways that nourish the tumour itself such as impaired immune functions, increased invasion and upregulation of proteases and angiogenic factors[94,95]. Over years, this acidic microenvironment was associated to a significant accumulation of lactic acid produced by glycolysis, weakly disposed by tumour cells[96]. The proton extrusion, obtained by lactic acid, is reinforced by CA activity, in particular by CAIX[13,43,46]. Due to its high activity, its extracellular domain and its ease to be transcriptionally activated by hypoxia-inducible factor-1 HIF-1 (CA9 gene), CAIX is exploited by Nature to create a microenvironment favourable to tumour diffusion[40]. A very interesting class of inhibitors in this context is that of the hypoxia-activable prodrugs, which smartly exploit this pathological mechanism to work. They are essentially dimers of canonical aromatic sulfonamide by means of disulphide bonds[93,97]. These disulphide bonds can be easily broken in the typical acidic reducing conditions of tumour extracellular space generating two smaller molecules, which are more active towards CAIX rather than the buky dimer. N,N-(2,2-dithiodibenzoyl)bis-sulfonamide[97] is one of these forefront bioreductive compounds. It has been demonstrated that this molecule in the oxidized form is a weak inhibitor (micromolar affinity), whereas in the reduced form it becomes a good inhibitor for CAI (K_I= 276 nM) and very good inhibitor for CAII and CAIX (K_I=16nM and 9.1 nM respectively). From hCAII cocrystals (**Figure 2.1.8.1A**) it was seen that aminocarbonylbenzenesulfonamide moiety establishes strong van der Waals interactions with residues Gln92, Val121, Phe131, Leu198, Thr199, Thr200, Pro201, Pro202 and Asn67, while the aromatic thiol substituent interacts weakly with the protein. Supporting these data, some modelling experiments were conducted on hCAIX. It was discovered that the slightly-higher affinity towards CAIX with respect to CAII, could be rationalized to a possible additional polar interaction between Gln67 and the thiol moiety of the inhibitor (**Figure 2.1.8.1B**). Considering the highly lipophilic plasmatic membrane and overexpression of membrane-associated isoforms in cancer (in particular CAIX), these inhibitors represent smart devices to selectively inhibit hCAIX in tumors.

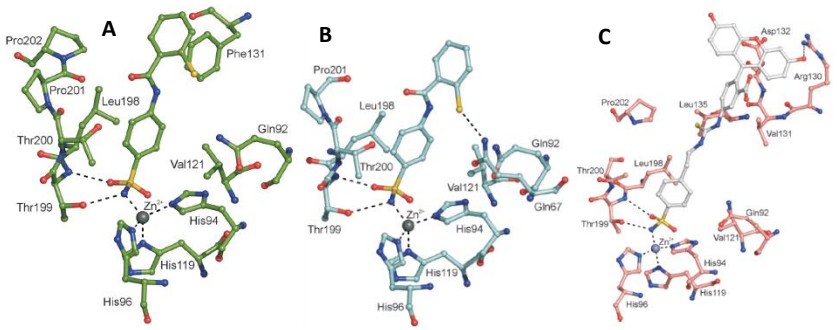

Figure 2.1.8.1. A) Inhibition mode of reduced N,N-(2,2-dithiodibenzoyl)bis-sulfonamide in the active site of hCAII, **B**) Inhibition mode of reduced N,N-(2,2-dithiodibenzoyl)bis-sulfonamide in the active site of hCAIX, **C**) Inhibition mode of (4-sulfamoylphenylethylthioureido)-fluorescein in the active site of hCAIX. Figure adapted from reference[50].

Starting from the Švastová's preliminary work[87,93] on pyridinium-based inhibitors, which, given their high polar properties, showed up selective to membrane-bound CAs and good lead for hCAIX specific targeting, in 1996 Christianson's group[98] started to synthesize fluorescent-labelled inhibitors to better study the selectivity issue. The studied inhibitor is an aromatic sulphonamide labelled with fluorescein, which represents the best fluorophore in biological field, since the excitation and the emission wavelength (495 nm and 519 nm respectively) are within the so-called "biological window". Over years, this preliminary probe was improved by Supuran's group[99], essentially shortening its linker, since the fluorophore, too far from the active site, was not able to create new additional interactions. The new (4-

sulfamoylphenylethylthioureido)-fluorescein has reached K_d= 0.30 nM towards tumour-associated CAIX, and its affinity makes it the favourite probe in clinical studies as imaging device for severe hypoxic tumours (**Figure 2.1.1.12C**). Such a high affinity, it can be explained by established interactions between:

- the thioureidic moiety and residues Val121, Phe131, Val135, Leu198, Thr199, Thr200, Pro202 and Gln92.
- the bulky fluorophore and the dyad Val135-Asp130 in the small α-helix at the rim of the funnel.
- the carboxy fluorophore group and Arg130 (characteristic aminoacid of hCAIX active site).

Over years, new probes were developed such as spin-labelled (e.g.TEMPO) inhibitors for EPR applications[100] or ^{129}Xe-Cryptophane inhibitors for MRI applications[101], but just for bio-imaging and not for theranostic purpose.

2.1.9 CAIX as bio-target in angiogenesis

Angiogenesis is a physiological process involving several beneficial pathways such as wound healing and reproduction. On the other hand, angiogenesis can be exploited by cancer cells in a starving state to recruit oxygen and nutrient supplies. In 1971, Folkman[102,103] suggested that angiogenesis inhibition is a promising tool to stop cancer proliferation, in particular, developing molecules able to target angiogenetic-based processes like vascular endothelial growth factor (VEGF)[104] or stop the extracellular matrix degradation[105].

Photodynamic therapy (PDT) is one of the techniques for clinical purposes to kill cancer cells. PDT[106] essentially uses singlet oxygen ($^1O_2$) made from molecular oxygen by irradiation of a photosensitizer (PS) to induce apoptosis, tumour vasculature shutdown and subsequent recruitment of immune mediators[107]. PDT has different advantages such minimal invasiveness compared to other techniques, improved localization of therapeutical effect by using a PS and light and applicability for repeated cycles without limited side effects, but unfortunately in the most current one an oxygen-dependent type II mechanism is exploited, which helps the tumour to spread itself. In fact, the PDT-induced hypoxia, generated by oxygen consumption through directly PS or indirectly vasculature degradation, triggers in hypoxic cells a signalling cascade that ends with the realising of pro-angiogenic growth factors such as angiopoietin (ANGPT), epidermal growth factor (EGF) and vascular endothelial growth factor (VEGF). Analogously to this, PDT-induced hypoxia activates hypoxia-inducing factor (HIF) in the upregulation of many regulatory genes switching the transcription of angiogenic factors, among which resides gene encoding for CAIX. CAIX is therefore used by tumour cells as a tool to reinforce the acidic extracellular pH, which was triggered in the first place by the therapy itself. Since the most common angiogenesis inhibitors are fusion proteins or antibodies, the research is moving towards non-protein inhibitors to overcome administration and metabolism limits related to protein stability. Considering the tumour-specific overexpression of CAIX (biomarker in breast cancer) and its high-restricted expression in normal cells, Jung and co-workers[108] synthetized a PS-labelled CAIX inhibitor in order to combine the advantages of CAIX knockdown and targeting with those derived from PDT.

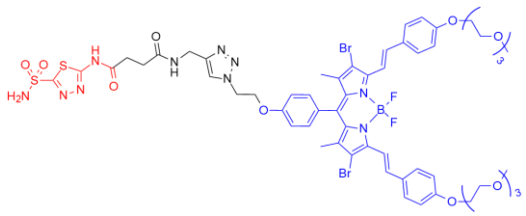

Figure 2.1.9.1. AAZ-BODIPY used by Jung for the selective inhibition of CAIX. In red AAZ and in blue BODIPY.

The molecule in question is essentially a BODIPY-labelled AAZ (**Figure 2.1.9.1**), which joins the spectrochemical properties of the fluorophore widely-spread in biological applications with acetazolamide (AAZ), which represents one of the most important CA sulphonamide-based inhibitors clinically used. Upon irradiation at 660 nm, cancer cell mitochondrial structures are selectively disrupted by singlet oxygen reducing moreover the gene expression of several angiogenetic factors (e.g. VEGFA and ANGPT2). These devices sound very promising tools for theranostic applications, since AAZ provides an efficient tumor-targeting tool associated to a good CAIX inhibition and the fluorophore provides good properties as PS and tracking probe for cellular distribution and uptake.

2.2 Aim of the work

The aim of this work was to synthesize small molecules to be used as new CA inhibitors. As we already reviewed, the inhibitors used for CA applications known up to now have completely different structures. The huge quantity of examples present in literature shows that, changing their heads and tails, their properties can be easily tuned so they can be smartly exploited in several mechanisms. Among these, the most famous ones are sulphonamide-based inhibitors, which, bind to zinc ion replacing zinc-bound hydroxide ion and displacing CO_2 from its binding pocket in a competitive way. Studying deeply this case, we found an interesting cocrystal structure, which represents the starting point of our work[99].

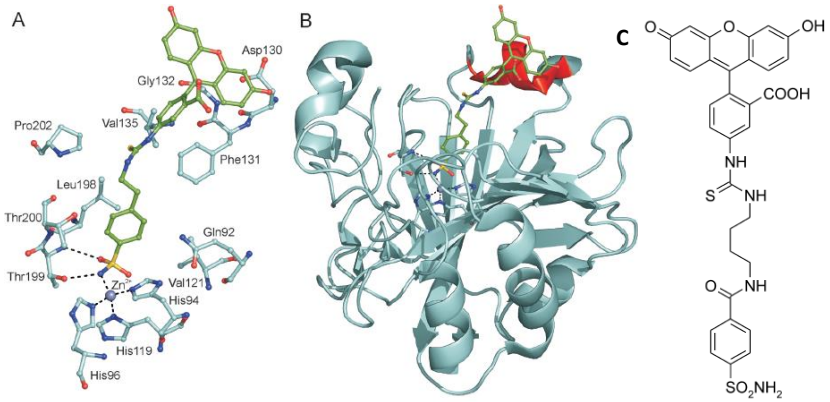

Figure 2.2.1. A) Inhibition mode of fluorescein-based inhibitor into the active site of hCAII (PDB code: 2F14); **B**) Schematic representation of hCAII/fluorescein-based inhibitor complex. In red is highlighted the Asp130-Val135 α-helix, with which fluorescein makes contacts; **C**) Chemical structure of fluorescein-based inhibitor observed in previous cocrystals. Figures adapted from reference[50].

In the complex structure, it can be seen that sulfonamide moiety interacts with zinc ion in the canonical way and how the whole molecule is stabilized by just few hydrophobic interactions, in

particular with Leu198, Pro202 and Phe131 (**Figure 2.2.1A**). Actually if we look more carefully at the structure, the hydrophobic interaction between the lower ring of fluorescein and aromatic ring of Phe131 is a kind of edge-to-face CH-π, which generally is less stable than π-π stacking. Because of the high rigidity of fluorescein group and the contacts with the upper part of fluorescein with Asp130-Val135 α-helix (**Figure 2.2.1B**), probably, in this case, the edge-to-face CH-π configuration represents the most stable one. For this reasons, we planned to synthesize compound **4b** and **4c** (**Figure 2.3.1.1**), which represent a sort of label-free monomers, which, lacking the fluorescent probe and being, as consequence, more flexible, hopefully could stack on Phe131 in the classical parallel fashion. At the same time, molecules **4b** and **4c** immediately resulted of interested for us because, for the presence of the phenolic unit, well represent monomeric models of calix[n]arenes functionalized at the lower rim with the same sulfonamide unit that we already had in mind as potential multivalent ligands for CAs. We will discuss about these compounds in chapter 3 using in fact derivatives **4a** and **4b** as monovalent reference compounds to investigate the occurring of a multivalent effect and/or the involvement of the calixarene macrocyclic arrangement in the CAs inhibition.

In the design of **4a** and **4b** we decided to use an amidic or a thioureidic linker to connect the benzenesulfonamide unit to the phenol because they are easy to generate and able to establish additional stabilizing contacts. Moreover, thioureidic linker should give to the molecule the required flexibility to optimize interactions with the enzymes.

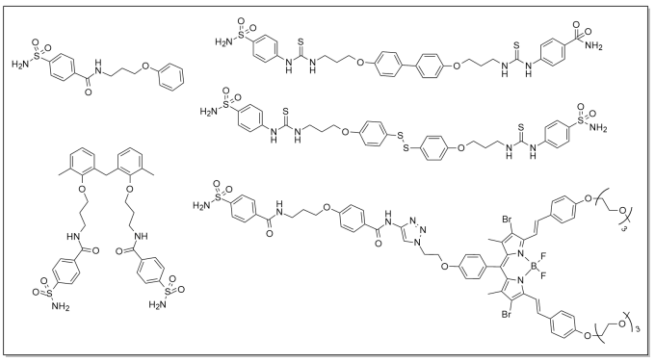

Figure 2.2.2. Examples of inhibitors synthetized in our laboratory.

Considering the very interesting and in part unexpected results obtained by these simple molecules (see below), in order to increase the selectivity and efficiency towards the tumour-correlated CAIX, we synthesized also bisphenol-based dimers with two different geometries to explore the possibility of a simultaneous binding to two CA units. In this context to increase the selectivity towards the extracellular CAIX, disulphide dimeric prodrugs were developed with the goal to create devices cleavable in typical acidic pH around cancer cells. In future, moreover, starting from Jung's work[108] (**Paragraph 2.1.9**), we will end up the synthesis of a derivative based on compound **4c** labelled with BODYPY. We expect that this system can maintain its excellent inhibition properties joining the advantages gained by the easy tracking of the fluorophore in tissues and its efficiency in contrasting the drawbacks of PDT for a general innovative theranostic application.

2.3 Results and discussion

2.3.1 Synthesis of phenol-based sulfonamides

The synthesis of the monomeric sulfonamides **4a** and **4b** is rather simple (**Figure 1.3.1.1**). The phenolic OH was deprotonated with K_2CO_3 and then to the resulting anion N-(3-bromopropyl)phthalimide was added in dry DMF in order to have the protected aminopropyl arm. The achievement of compound **2** was determined by ^{1}H-NMR spectroscopy through the presence in the spectrum (parameters: $CDCl_3$, 400MHz, 25 °C) of phthalimidic aromatic signals at 7.87 and 7.74 ppm along with those at 4.06, 3.94 and 2.21 ppm relative to propylic arm. The deprotection of amine moiety was realized heating up to reflux compound **2** in EtOH with $NH_2NH_2 \cdot H_2O$. The loss of phthalimidic aromatic signals in ^{1}H-NMR spectrum was considered diagnostic for compound **3**. These two steps are characterized by yields higher than 80% thanks to the well-validated reactions used and the easiness of work-up. In particular compound **2** was just precipitate in acidic water, whereas compound **3** was purified through an acid extraction with subsequent precipitation in basic water. The compounds were then vacuum filtered by Buchner, dried and used as themselves for the next steps. Compound **4b** was synthesized by reaction between 4-isothiocyanatobenzenesulfonamide and compound **3**. To synthesize the amidic derivative **4c**, 4-sulfamoylbenzoic acid was firstly deprotonated with DIPEA and immediately preactivated for 10 minutes with EDC as active ester and finally coupled to amine derivative **3**. Even these two compounds are isolated by easy work-up: for the former, basic extraction and subsequent precipitation in 1N HCl; for the latter, simple acidic quenching and re-extraction with AcOEt. For both compounds the presence of aromatic protons of sulfonamide-bearing ring at about 8-7.5 ppm in ^{1}H-NMR spectrum and the presence of C=O (in the case of **4c**) and C=S (in the case of **4b**) signals at 165.7 and 180.9 ppm in ^{13}C-NMR spectrum were considered as diagnostic for the conjugation reactions. In part, amine derivative **3** was treated with a methanol solution of 1N HCl to achieve the corresponding ammonium salt to test as inhibitor as such.

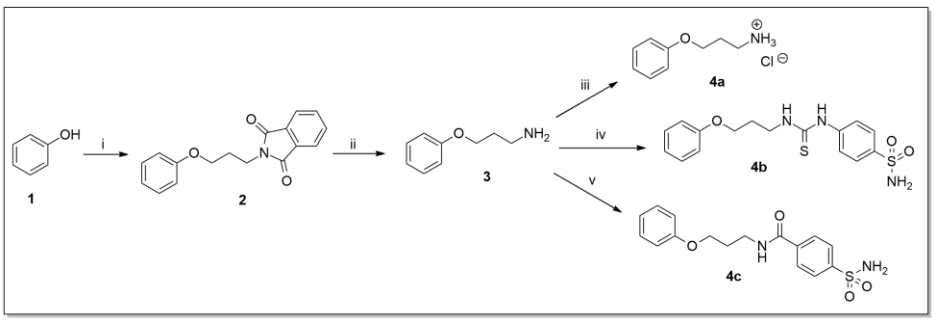

Figure 2.3.1.1. Synthesis of sulphonamide-bearing and ammonium-bearing monomers. Reactions conditions: i) K_2CO_3 (4 eq), N-(3-bromopropyl)phthalimide (1 eq), dry DMF, 65 °C, 1 day (87% yield); ii) $NH_2NH_2 \cdot H_2O$ (9.6 eq), EtOH, reflux, on (88% yield); iii) 1N HCl (1 ml), MeOH, rt, 1h (quantitative yield); iv) 4-isothiocyanatobenzenesulfonamide (1 eq), dry DMF, rt, 1 day (80% yield); v) 4-sulfamoylbenzoic acid (1 eq), DIPEA (2.5 eq), EDC (1.2 eq), HOBt (1.2 eq), dry DCM, rt, 1 day (83% yield).

Acquiring ^{1}H-NMR spectra of compound **4b** in solvents at increasing polarity, it has been observed that aliphatic protons in propyl chain are poorly perturbated, whereas aromatic protons close to sulfonamide undergo a significant change in chemical shift, in particular when the sulfonamide is deprotonated. In fact, aromatic protons in ortho to sulfamoyl moiety shift

from 7.60 to 6.75 ppm, meaning that, when deprotonated, sulfamoyl acts as a strong shielding group. This is confirmed by spectra acquired in MeOD and DMSO-d_6 (**2** and **3** in **Figure 2.3.1.2**), in which the same signals undergo change in chemical shifts significantly smaller. Passing from a polar solvent to the apolar $CDCl_3$, aggregates are clearly formed as confirmed in the ^{1}H-NMR spectrum **1** (**Figure 2.3.1.2**), characterized by multiple broad signals.

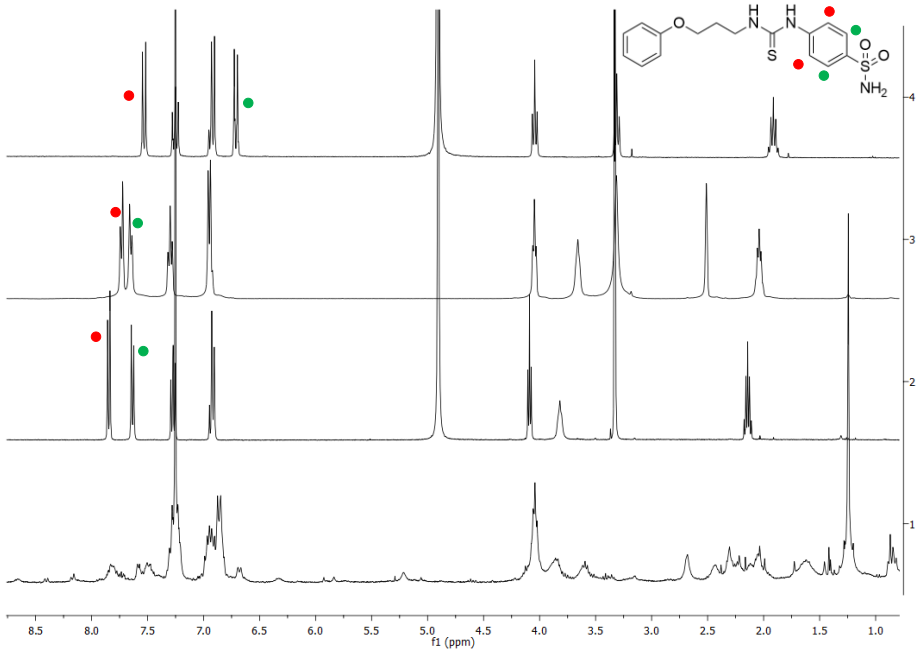

Figure 2.3.1.2. ^{1}H-NMR (400MHz, 298K) spectra of compound **4b**, respectively in (**4**) D_2O/NaOD 1:1, (**3**) DMSO-d_6, (**2**) MeOD and (**1**) $CDCl_3$.

2.3.2 Synthesis of bisphenol-based dimers

The synthesis of bisphenol-based dimers followed the same steps as for monomers (**Figure 2.3.2.1**), The achievement of compound **6** was determined by ^{1}H-NMR with the presence of phthalimidic proton signals at 7.87 and 7.73 ppm along with those related to the propylic arms at 4.08, 3.95 and 2.23 ppm, whereas for compound **7** was monitored the loss of phthalimidic proton signals at 7.87 and 7.73 ppm.

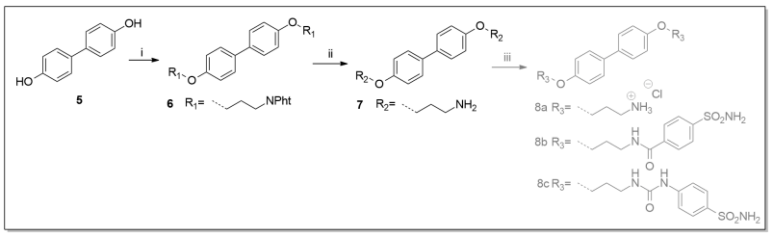

Figure 2.3.2.1. Synthesis of amine bisphenol-based derivative. Reactions conditions: i) K_2CO_3 (3 eq), N-(3-bromopropyl)phthalimide (2.1 eq), dry DMF, 65°C, 1 night (88% yield); ii) $NH_2NH_2{\cdot}H_2O$ (20 eq), EtOH, reflux, 16h (quantitative yield).

The synthesis of compound **8a** was carried out in the same way as for compound **4a**, but surprisingly, in this case, a degradation occurs. In **Figure 2.3.2.2** is reported the ^{1}H-NMR spectrum of the crude obtained after the treatment with the acidic methanolic solution to generate the ammonium salt

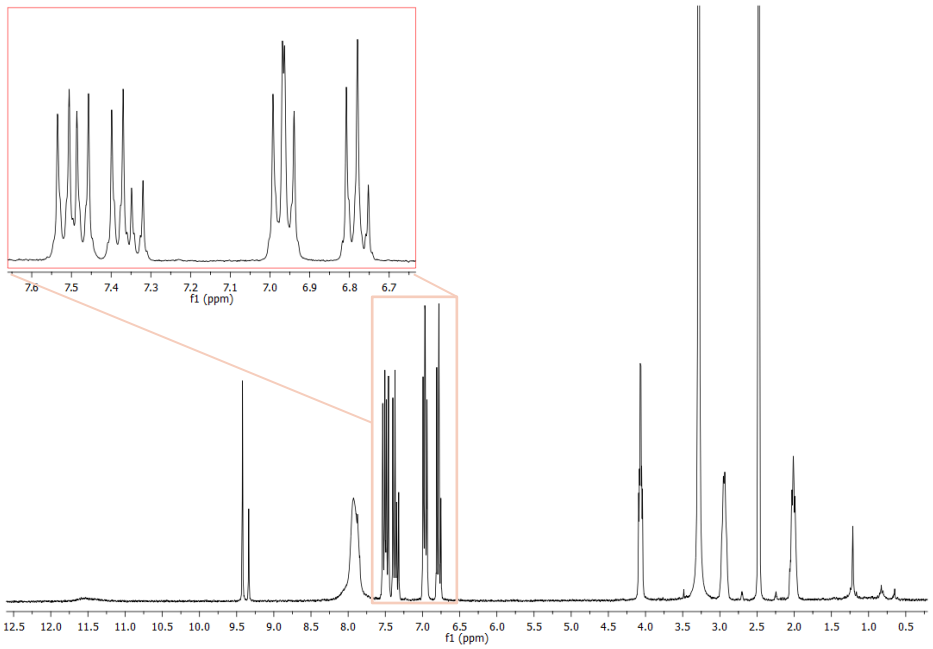

Figure 2.3.2.2. ^{1}H-NMR spectrum of compound **8** after evaporation of acidic methanolic solution in DMSO-d_6.

Differently from compound **7**, in the range 7.51-6.50 ppm, within which the aromatic protons of the molecule resonate, more signals are present than those expected, even in deuterated aprotic polar solvents as DMSO-d_6, generally used for excluding aggregate formation due to possible intermolecular interactions. Moreover, these aromatic signals integrate for more protons than those expected with respect to propylic protons integral calibration. This evidence, along with the two singlets at 9.42 and 9.34 ppm, likely related to different free phenolic OH, led us to think that for this compound an acidic treatment causes a cleavage of propyl chains from bis-phenol scaffold. Some attempts to obtain the desired salt **4a** with softer treatments failed bringing to the same decomposition. However, considering the weak acidic pH used in stopped-flow analysis and the high ammonium pKa (10.5), the buffer might be a good environment for amine protonation without cleavage of propyl chains. For these reasons, in this case, the potential ligand was provided for the inhibition test in the amine form as compound **7**.

To synthesize compound **8b** were made a couple of attempts. The first one, analogue to the synthesis of amidic derivative **4c**, consisted in the reaction between amine **7** and 4-sulfamoylbenzoic acid using EDC as stoichiometric coupling agent. The crude was analysed by ^{1}H-NMR and the related spectrum showed only the presence of reactants (two doublets at 8.10 and 7.95 ppm for aromatic protons of 4-sulfamoylbenzoic acid and two doublets at 7.50 and 7.10 ppm for aromatic protons of compound **7**). Small signals at 7.42 and 6.80 ppm could be a trace of the target compound, but, due to its high insolubility in most common solvents, the crude could not be purified. The reaction was tried again in dry DMF either in round-bottom

flask or in a microwave reactor (200 W, 200 psi) at 100 °C to fasten kinetics and increase solubility, but even in these cases reactants were not converted at all. Even worse it happened in the synthesis of derivative **8c**. Using the same protocol adopted for the synthesis of compound **4b**, the target molecule underwent a degradation that remembers the one seen for the synthesis of compound **8a**. The ^{1}H-NMR spectrum shows the coexistence of different species of propyl degradation, presumably obtained by acidic quenching, but it cannot be excluded the presence of compound **8c** (**Figure 2.3.2.3**). Repeating the reaction in dry DMF in a microwave reactor (200 W, 200 psi, 100 °C) did not improve the situation.

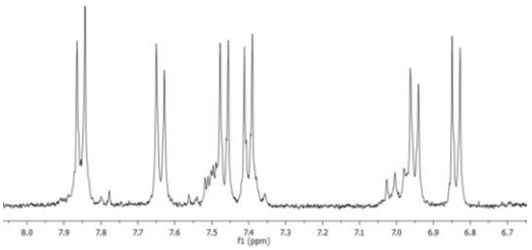

Figure 2.3.2.3. ^{1}H NMR (300 MHz, MeOD) of crude of compound **8c**.

2.3.3 Synthesis of gemini dimers

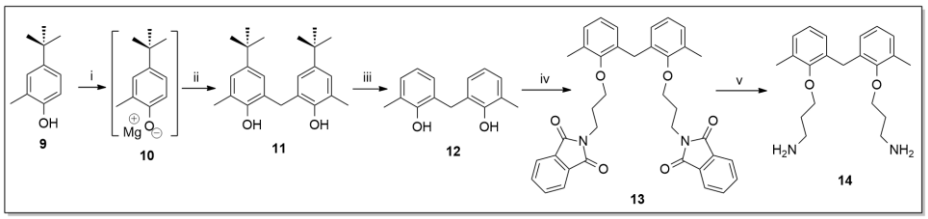

Figure 2.3.3.1. Synthesis of gemini intermediates. Reactions conditions: i) Mg (1.0 eq), I_2 (catalytic amount), EtBr (1.2 eq), dry THF, 4 h + 1 h, reflux; ii) paraformaldehyde (0.5 eq), toluene, 7h, reflux (25% yield); iii) $AlCl_3$ (2.5 eq), dry toluene, rt, 16h (69% yield); iv) K_2CO_3 (3 eq), N-(3-bromopropyl)phthalimide (2 eq), dry DMF, 65°C, 16h (66% yield); v) NH_2NH_2·H2O (22 eq), abs EtOH, reflux, 16h (92% yield).

To obtain the gemini analogues of compounds **4a**-**c**, the bis-phenolic intermediate **12** was necessary. Starting then from phenol **9**, derivative **11** was synthesised in a two-step process, in which the anionic phenolate **10**, obtained by reaction of 4-tert-butyl-O-cresol (**9**) with Grignard reagent EtMgBr, was not characterized but used directly for the next step. The methylene bridge between two units of **10** was made exploiting a double aromatic electrophilic substitution realized dropping the Grignard solution into a formaldehyde solution. After recrystallization in DCM/Hex, compound **11** was obtained in low yield (25%), probably due to the degradation of Grignard reagent. The successful outcome of reaction was determined by ^{1}H-NMR observing in the spectrum of **12** the singlets at 3.93 ppm related to methylene bridge protons, the singlet at 5.96 ppm related to two phenolic OH and the absence of signals relative to aromatic protons in ortho position to phenolic OH. Subsequently, to maintain a structural analogy with monomers and to generate gemini not too hydrophobic, compound **11** was subjected to a retro Friedel-Craft alkylation with $AlCl_3$ as a Lewis acid. The ^{1}H-NMR spectrum of the relative final product **12** showed the presence of a triplet at 6.82 ppm (para aromatic proton) and the absence of the singlet at 1.26 ppm (tert-butyl protons) which confirmed the

success of reaction. The synthesis for compounds **13**-**14**-**15a** is not described and discussed since identical to those for compounds **6**-**7**-**4a**.

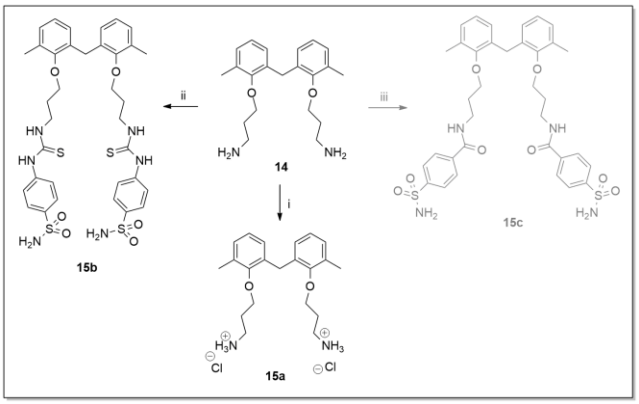

Figure 2.3.3.2. Synthesis of gemini derivatives. Reactions conditions: i) 1N HCl, MeOH, rt, 40 minutes (quantitative yield); ii) 4-isothiocyanate-benzenesulfonamide (2.2 eq), dry DMF, rt, 4 h (52% yield).

For the synthesis of compound **15b**, the same protocol employed for compound **4b** was used with **14**. Even if the reaction belongs to the click-chemistry reactions and then should be characterized by high yield, high reactivity and high atom economy, in this case, after chromatography purification, the desired product was isolated in 57% yield, rather low for this type of reaction. TLC analysis evidenced the presence of a spot reactive to ninhydrin likely related to compounds with at least one free amine moiety, which suggests that this reaction cannot be pushed over because of the bulky molecule scaffold.

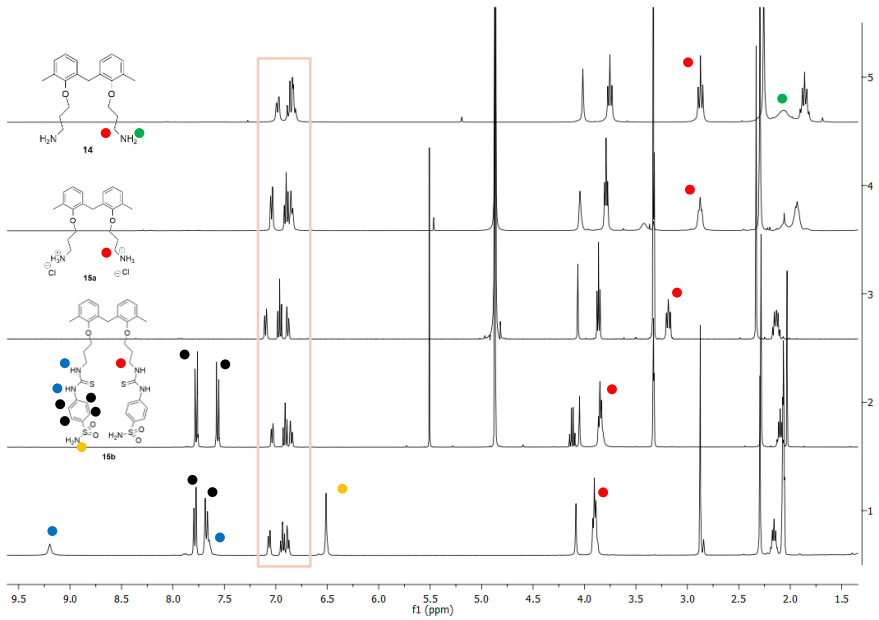

Figure 2.3.3.3. ^{1}H NMR spectra of compound **15b** in **1**) acetone-d_6 (400 MHz) and **2**) MeOD (400 MHz); **3**) of compound **15a** (MeOD, 400 MHz); of compound **14** in **4**) MeOD (400 MHz) and **5**) in $CDCl_3$ (300 MHz).

As shown in **Figure 2.3.3.3**, passing from amine derivative **14** to ammonium **15a** and to thioureido derivative **15b**, the signal of methylene directly attached to nitrogen atom is progressively deshielded (respectively 2.80, 3.20 and 3.80 ppm), thanks to the increasing electron-withdrawing features of terminal moieties. This shift, considered diagnostic for compound **15a**, along with the presence of two doublets at 7.75 and 7.53 ppm, related to benzenesulfonamide aromatic protons, were defined indicative for the obtaining of compound **15b**. Moving to an aprotic polar solvent (acetone-d_6), it was possible to identify thoureidic protons (9.23 and 7.65 ppm) and sulfamic protons (6.50 ppm). Comparing all the spectra together, it is possible to understand how polarity of the solvent poorly influences aromatic protons of the scaffold.

2.3.4 Synthesis of disulphide-based dimers

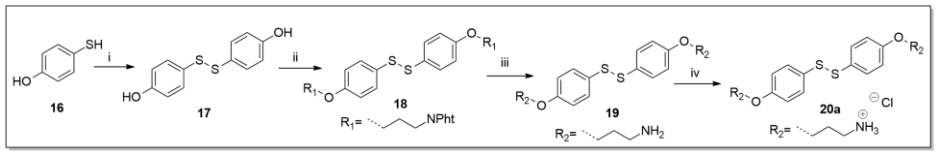

Figure 2.3.4.1. Synthesis of disulfide derivatives. Reactions conditions: i) NaI (0.2 eq), H_2O_2 (1.1 eq), AcOEt rt, 1h (98% yield); ii) NaH (2.1 eq), N-(3-bromopropyl)phthalimide (2.1 eq), dry DMF, rt, 3 h (25% yield); iii) $NH_2NH_2 \cdot H_2O$ (19.9 eq), abs EtOH, reflux, 16h (98% yield); iv) 1N HCl, MeOH, rt, 40 minutes (quantitative yield).

The first step is the dimerization of 4-mercaptophenol **16** was realized in presence of H_2O_2, as oxidizing agent, and NaI, as catalyst. The successful outcome of the reaction was confirmed by TLC and by ^{1}H NMR, monitoring the disappear of the classical thiol proton signal in an aprotic apolar solvent. The synthesis of compounds **18**, **19** and **20a** are analogous to those used for compounds **6**, **7** and **8a** and so this reason, they are not described and discussed.

2.3.5 Inhibition studies

Figure 2.3.5.1. A) Typical laboratory set-up; **B**) Schematic functioning of stopped-flow technique.

For slow reactions (seconds range), relaxation techniques are usually used. Essentially the system is taken to equilibrium and it is monitored after a perturbation. Since CA catalysed reaction rates are in the millisecond range, these classical techniques are pretty useless. In these cases we need to rely on rapid-reaction techniques, such as UV-vis-assisted stopped-flow assays (**Figure 2.3.5.1A**), in which reaction rates are determined after 2-3 ms, before the steady-state is established.The instrument actually is very simple (**Figure 2.3.5.1B**). It is made of two syringes, prefilled with two different solutions, which are simultaneously plunged through a high-fast mixer in an optical cell. As long as the reaction goes on, a light source irradiates the cell and the beam coming off is captured by detector, which is then elaborated as an absorbance or fluorescence signal. As the syringes push the solutions in, a third syringe is pulled

back till a block is hit, causing the sudden flow stopping. If this third syringe run is calibrated in order to locate the solution mix in the optical cell, the "stopped-flow" is realized and very fast reaction (ms range) can be monitored. In CA applications generally solution 1 is pre-filled with red phenol and a mix solution of CA/inhibitor, previously pre-equilibrated each other enough time to let the E-I complex formation, while solution 2 is pre-filled with an aqueous saturated solution of CO_2, that mimics physiological conditions. The experiment is reiterated generally 4 times using inhibitor solutions (for equilibration) 10 times more concentrated each time. In this way, as the inhibitor concentration increases, the phenol red protonation is slowed down and so is the formation of its yellow protonated form, whereas the absorbance-time curves monitored at 557 nm (deprotonated red form) gets less steep. The instrument gives us IC50, the inhibitor concentration required to reduce of 50% the catalytic activity, and inhibition constant Ki, calculated by the following formula:

$$Ki = \frac{IC_{50} - \frac{[E]}{2}}{\frac{S}{K_m} + 1}$$

Figure 2.3.5.2. Formula for the calculation of Ki, where IC50 is the inhibitor concentration required to reduce of 50% the catalytic activity, E is the enzyme concentration, S is the substrate concentration and Km is the substrate concentration at which the reaction rate is half of the maximum velocity for the enzyme in question).

Inhibition studies were carried out in Claudiu Supuran's lab at the Department of Neurosciences, Psychology, Drug and Child Health Neurofarba of University of Florence. All the final compounds described above were tested towards six different CA isoforms (hCAI, hCAII, hCAIX, VchCAβ, Can2, MgCA) and compared to AAZ.

Table 2.3.5.3. Inhibition data of monomeric and dimeric compounds towards the selected isoforms, obtained from stopped-flow technique. Each value is an average from 3 different assays (errors were in the range of ± 5-10 % of the reported values).

	K_i (nM)					
Compound	hCAI	hCAII	hCAIX	VchCAβ	Can2	MgCA
4c *(amide monomer)*	8.4	4.1	21.8	4143.8	>10000	>10000
4b *(thioureido monomer)*	8.2	8.1	28.8	4801.7	122	>10000
4a *(ammonium monomer)*	>10000	>10000	>10000	>10000	>10000	>10000
8a *(diammonium bisphenol)*	>10000	>10000	>10000	6354.4	297	2100
15a *(diammonium gemini)*	>10000	>10000	>10000	>10000	>10000	>10000
15b *(dithioureidic gemini)*	421.6	89.1	674.3	>10000	80.4	>10000
20a *(diammonium disulfide)*	>10000	>10000	>10000	>10000	>10000	>10000
AAZ	250	12	25	451	10	74000

From this screening, some interesting data were obtained. Amide monomer **4c** and thioureido monomer **4b** are clearly very efficient inhibitors towards the three investigated hCAs with K_i values in the low nanomolar range, that are even lower than those of AAZ for hCAI and hCAII. This high affinity, along with the high selectivity showed towards the tested hCAs with respect to non-human isoforms, makes these compounds very interesting tools to inhibits these enzymes. In particular, considering the data in **Table 2.3.5.3**, compounds **4b-c** are promising molecules for the hCAI inhibition in retinal/cerebral oedema.

Also dithioureido gemini **15b** is rather active towards hCAs with K_i in the nanomolar range, but, unfortunately, even if divalent, it is less active than AAZ and **4a**-**b** as well. Evidently, the residual conformational freedom of the two arms goes against the binding weakening it.

Diamine bisphenol **8a** is an inhibitor showing a low-micromolar K_i for MgCA resulting in that case more active than AAZ, but is inactive towards the other isoforms tested. Moreover, the ammonium monomer **4a** is totally inactive towards the same isoforms. This interesting evidence suggests that the second propylammonium arm in **8a** cooperates with the first propylammonium arm in a way that helps stabilizing the complex. Furthermore, comparing this rigid molecule with diammonium disulfide **20a** and diammonium gemini **15a**, it is clear that conformational mobility of S-S bond and methylene bridge between the two aromatic rings of the scaffold inactivates the inhibitor: probably if a binding occurs, it is easily broken by the rotation of the molecule.

Unfortunately, the idea of exploiting a multivalent effect through the adoption of dimeric ligands did not result successfully. The affinity found for these compounds in comparison to their monovalent analogues is always lower.

2.3.6 X-Ray diffraction on hCAII/**4b** cocrystal

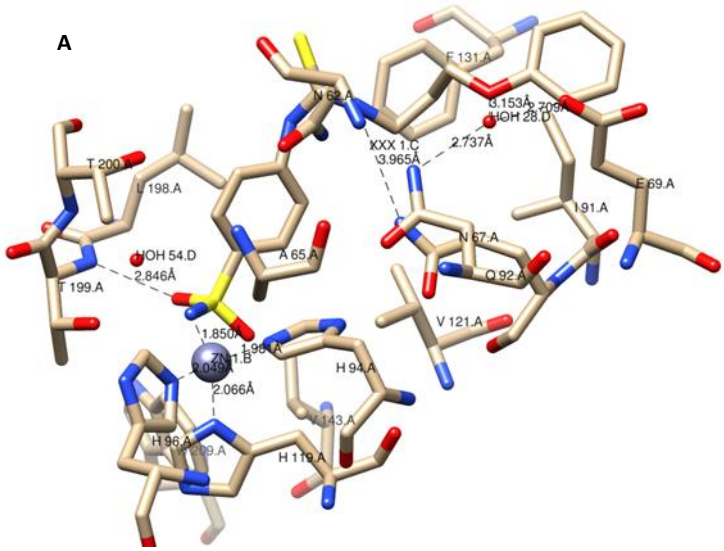

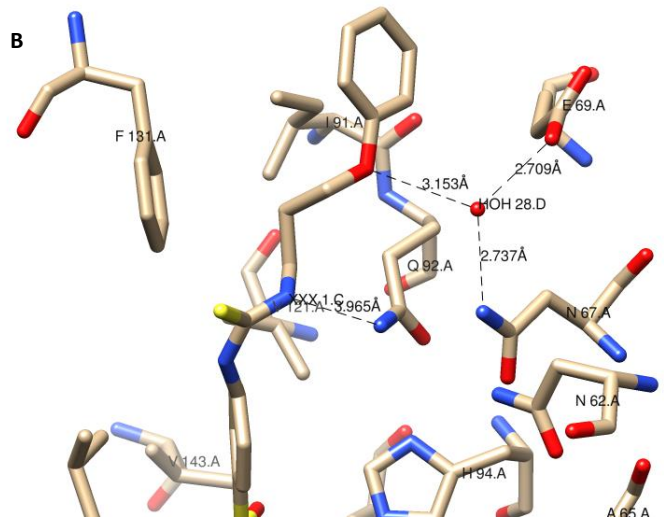

Figure 2.3.6.1. Head (**A**) and tail (**B**) contacts in hCAII/**4b** cocrystal between **4b** and enzyme active site.

According to inhibition data, monomeric compounds **4c** and **4b** were shown to be very interesting molecules for the inhibition of hCAs. An important element of knowledge about their mode of action came from the achievement of cocrystals suitable for XRay diffraction of the complex between hCAII and **4b**. and The structure at the solid state was resolved at Electra synchrotron in Trieste by PhD student Andrea Angeli of Supuran's group. It can be seen (**Figure 2.3.6.1A**) that the sulfonamide moiety, as designed, reaches the bottom of the funnel, where it binds to the catalytic zinc ion. Moreover, the sulfuryl group of sulfonamide head is engaged in a hydrogen bond with NH of Thr199, whereas benzenesulfonamide is stabilized by hydrophobic contacts with Leu198 and Val121. These are the classical interactions used by benzenesulfonamide moiety to anchor rigidly its head in the active site and could not be enough to justify the high efficiency of compound **4b**. Checking more carefully the structure, few additional interactions involving the tail of the inhibitor can be seen (**Figure 2.3.6.1B**). In fact, there are additional hydrophobic interactions between the propyl spacer and Phe131, between Glu69/Ile91 and the phenolic ring along with a hydrogen bond among the phenolic O atom and a conserved water molecule stabilized by Asn67 and Glu69. Aligning hCAII in cocrystal structures with compound **4b** and N-4-Methyl-1-piperazinyl-N'-(p-sulfonamide)phenylthiourea, a new inhibitor of which just the crystal structure is known, it can be seen (**Figure 2.3.6.2**) how in both cases thioureido linker does not make any kind of interactions with enzyme, but just gives to the molecules the flexibility required to maximize the hydrophobic and polar contacts in the tail. Probably, an additional contribution to the high efficiency of compound **4b** can be attributed to the hydrogen bond between phenolic oxygen atom and the conserved water, not observed in the complex with N-4-Methyl-1-piperazinyl-N'-(p-sulfonamide)phenylthiourea.

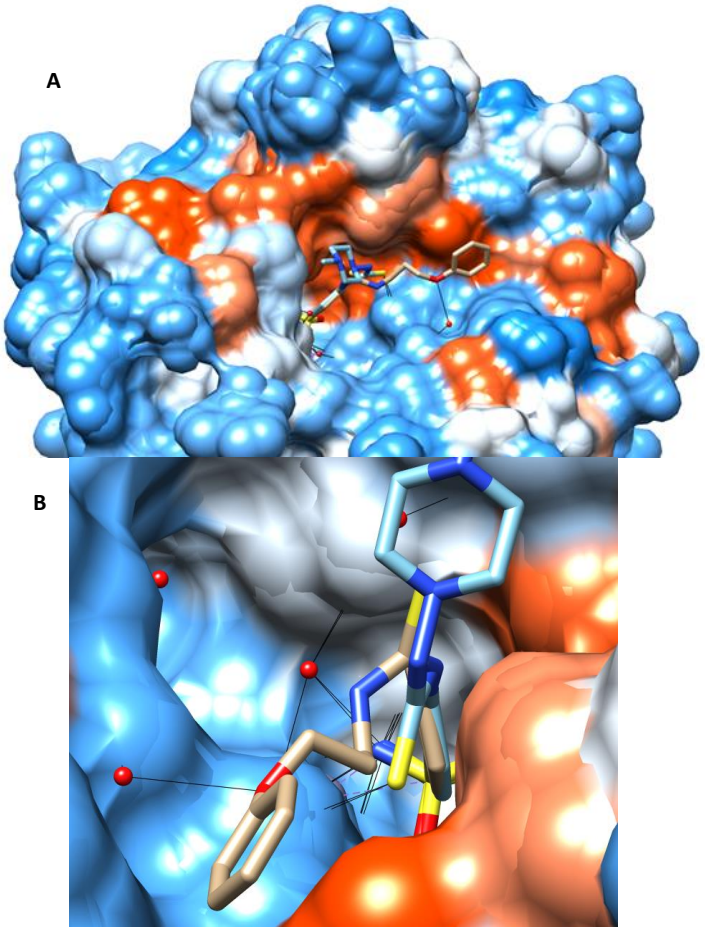

Figure 2.3.6.2: Alignment of hCAII in cocrystals with compound **4b** and N-4-Methyl-1-piperazinyl-N'-(p-sulfonamide)phenylthiourea.

2.3.7 Perspectives: theranostic applications

Given the good inhibitory properties for compound **4b** and **4c**, even better than AAZ, we propose the synthesis for the corresponding BODIPY-labelled monomers. The starting point of this idea comes from the work of Jung and coworkers[108], who reported on the synthesis and properties of a BODIPY-labelled AAZ as tracking and therapeutic tool for CAIX-correlated cancer cells. The synthesis of the fluorophore moiety was realized by following the classical synthesis of BODIPY core, namely aldolic condensation between aldehyde **21a** and imidazole **22**, subsequent oxidation to C-C double bond and final quenching with $BF_3 \cdot OEt_2$. Following, appropriate modifications were made to get the final compound suitable for biological applications. Hence, the precursor **23** was subjected sequentially to a nucleophilic substitution of bromine atom to azide **24**, a bromination of imidazole rings in order to shift absorption/emission wavelength in the "biological window" and a Knoevenagel reaction between the core and an aldehyde functionalized with triethoxyethyl chains **21b** in order to get the final molecule soluble in water.

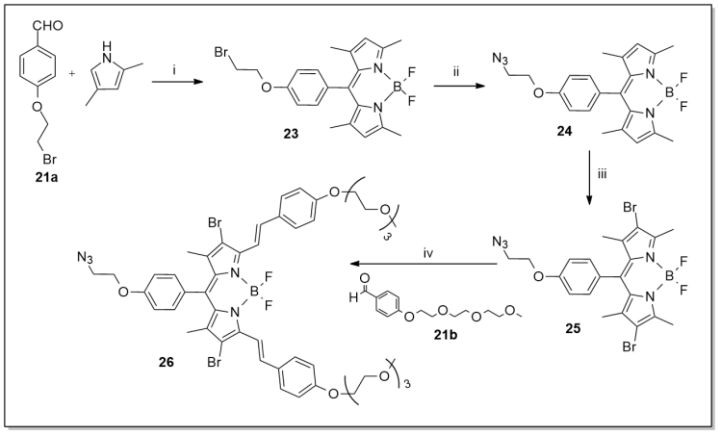

Figure 2.3.7.1. Synthesis of BODIPY part. Reactions conditions: ia) 2,4-dimethylpyrrole (2.2 eq), compound **21a** (1.0 eq), TFA (catalytic amount), dry DCM, rt, 5 h, ib) p-chloranil (10.1 eq), 1h, rt, ic) NEt_3 (20.1 eq), 30 minutes, rt, id) $BF_3{\cdot}OEt_2$ (21.5 eq), 30 minutes, rt (40% overall yield); ii) NaN_3 (3.0 eq), dry DMF, reflux, 16h (73% yield); iii) NBS (2.0 eq), dry DCM/dry DMF 4:1, rt, 1 h (99% yield); iv) compound **21c** (2.4 eq), glacial CH_3COOH (26.8 eq), piperidine (15.5 eq), $Mg(ClO_4)_2$ (catalytic amount), 4Å molecular sieves, dry toluene, reflux, 7 h (4% yield).

As far as the modification of the monomer is concerned, we have designed a new synthetic strategy able to grow on one side the sulfonamidic arm and on the other an alkyne moiety required for triazole synthesis. Unfortunately for lack of time, the synthesis is still on and no inhibition and spectroscopic data were collected yet. The first steps consisted in the introduction of 3-azidopropyl arm on phenolic OH of compound **27** by nucleophilic substitution, oxidation to carboxylic acid of aldehyde moiety and protection of this group as methyl ester to avoid the inconvenient formation of zwitterionic species in the next steps. All the steps performed so far resulted easy and with good yields and all intermediates were characterized by NMR and ESI-MS. From here, the synthesis is totally unexplored, but, since the reactions thought are employed in different works in good yields, this strategy seems to be very promising. In future compound **30** will be then reduced through a catalytic hydrogenation using 10% Pd/C as catalyst, coupled with 4-sulfamoylbenzoic acid by EDC, deprotected by LiOH to give carboxylic acid and finally coupled again by EDC with propargylamine in order to have a free alkyne ready for a "click" conjugation with compound **26**.

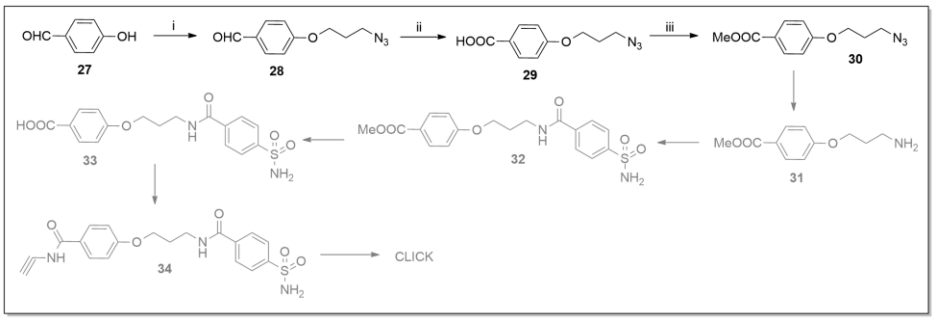

Figure 2.3.6.2. Synthesis of BODIPY part. Reactions conditions: i) K_2CO_3 (1.2 eq), compound **22b** (1.8 eq), dry DMF, rt, on (76% yield); ii) 0.7 M NaH_2PO_4 (pH=7), 30% H_2O_2 (1.5 eq), $NaClO_2$ (1.4 eq), $CHCl_3$/ACN, rt, 1 day (88% yield); iii) H_2SO_4 (catalytic amount), MeOH, reflux, 6h (quantitative yield).

2.4 Conclusions

As widely discussed in **Paragraph 2.1.1**, Carbonic Anhydrases (CAs) are very important enzymes, which catalyse a myriad of physiological functions, such CO_2 solubilization, gastric acid secretion, bone resorption, buffering and so on. In order to exploit such different and numerous functions, Nature has developed several families and isoforms of these proteins, which differ each other by catalytic activity, organism, cellular and tissue distribution and expression. Mutations associated to genes encoding for CAs frequently result, in affected patients, in severe pathologies. For this reason, a lot of inhibitors functionalized with sulphonamide and ammonium moieties have been developed so far in order to target out the isoforms responsible of the disease.

In this project a small library of monovalent phenol-based inhibitors and divalent para-bisphenol-, ortho-methylenbisphenol- and disulfanedylbisphenol-based inhibitors with sulphonamide and ammonium arms were designed and synthetised successfully. In all the ammonium derivatives the ammonium group was outdistanced from aromatic scaffold through a propyl spacer. Sulfonamide derivatives were realized conjugating the benzenesulfonamide active unit to previous ammonium derivatives via amide or thioureido linkers, which in literature showed to establish further stabilizing interaction with enzyme walls. All the synthesis were easy and characterized by good yields, in particular for monomeric **4a**,**b**,**c** (yield>80% for each single step). All derivatives were tested in Supuran's laboratories via stopped-flow inhibition assays towards a selected number of isoforms (hCAI, hCAII, hCAIX, VchβCA, Can2 and MgCA). Compounds **4c** and **4b** showed to be selective towards tested hCAs, in particular towards hCAI and hCAII (Ki=4-8nM), for which the lowest inhibition constants were reached. Moreover, towards these isoforms they showed to be clearly more active than the reference Acetazolamide (AAZ), which is the drug nowadays used in the topic treatment of glaucoma. So the high efficiency-selectivity towards hCAI and hCAII along with the easy synthesis make this new monomers very interesting tools as therapy against hCAI-II-correlated diseases (e.g. glaucoma and retinal/cerebral oedema). Of compound **4b**, in addition, was obtained a cocrystal with hCAII, in which is seen that the inhibitor is bound to zinc ion via sulphonamide moiety in the canonical way. Moreover, the hydrogen bond between the phenolic oxygen atom and a water conserved molecule could be the reason of the excellent inhibition properties of **4b**. As far as divalent compounds are concerned just compound **8a** showed a slight selectivity for Can2 (Ki=297nM), even if, unfortunately, less active than AAZ. Moving to MgCA, the same compound is one order of magnitude (Ki=2100nM) more active than AAZ, which makes it an interesting tool as antibacterial drug. For compound **15b**, instead, it is observed a partial selectivity towards Can2. In fact, even if with **15b** is reached the lowest inhibition constant, the compound shows a partial activity towards tested hCAs too. In order to understand more about the binding of this inhibitor, cocrystallization assays will be set up towards hCAII.

Taking into account the low selectivity of **4c** and **4b** towards hCAIX (generally involved in progression of hypoxic tumours), in future of these monomers will be synthetised disulphide-based dimers, which are known in literature to be activated just in hypoxic conditions. Moreover, in our laboratories we will conclude the functionalization of **4c** with BODIPY to realize a theranostic fluorescent inhibitor for Photodynamic Therapy (PDT) in the treatment of CAIX-related cancer.

2.5 Experimental part

General information. All moisture-sensitive reactions were carried out under a nitrogen atmosphere. All dry solvents were prepared according to standard procedures and stored over 3 or 4 Å molecular sieves. All other reagents were commercial samples and used without further purification. TLC were performed using prepared plates of silica gel (Merck 60 F_{254} on aluminium) and revealed using UV light or staining reagents: $FeCl_3$ (1% in H_2O/MeOH 1:1), ninhydrin (5% in EtOH), basic solution of $KMnO_4$ (0.75% in H_2O). Flash chromatography was performed on 32-63 µm on 60 Å Merck silica gel. Melting points were determined on an electrothermal apparatus Gallenkamp, in capillaries sealed under nitrogen. ^{1}H NMR (300 or 400 MHz) and ^{13}C NMR spectra (75 or 100 MHz) were recorded on Bruker AV300 and AV400 spectrometers using partially deuterated solvents as internal standards. All ^{13}C NMR were performed with proton decoupling. Mass spectra were recorded in Electrospray Ionization (ESI) mode using a SQ Detector, Waters (capillary voltage = 2.40-3.50 kV, cone voltage = 40-100 V, extractor voltage = 2 V, source block temperature = 150 °C, desolvation temperature = 300 °C, cone gas (N_2) flow rates = 95 L/hr, desolvation gas (N_2) flow rates = 480 L/hr) in MeOH.

Synthesis.

1-phenoxy-3-phthalimidopropane (2). In a 2-necked round-bottom flask, K_2CO_3 (12.76 mmol, 1.76 g) was stirred in a phenol (3.19 mmol, 0.3 g) solution in dry DMF (15 ml) for 30 minutes at 65°C. Then N-(3-bromopropyl)phthalimide (3.19 mmol, 0.86 g) was added in and the mixture was left reacting for 1 day at 65°C, monitoring the reaction by TLC (AcOEt/Hex 1:9, R_f=0.17). Hence the reaction mixture was poured into a flask pre-filled with 1N HCl/ice (35 ml + 35 ml) under vigorous stirring. Once the effervescence was over and the pH of the solution was acidic, the suspension was filtered to get compound **2** as a white powder (0.78 g, 2.19 mmol, 87% yield). **^{1}H NMR** (400 MHz, $CDCl_3$) δ (ppm): 7.87 (dd, *J* = 5.5, 3.1 Hz, 2H, Pht*H*), 7.74 (dd, *J* = 5.5, 3.1 Hz, 2H, Pht*H*), 7.27 – 7.23 (m, 2H, m-Ar*H*), 6.94 (bt, *J* = 7.5 Hz, 1H, p-Ar*H*), 6.83 (bd, *J* = 7.5 Hz, 2H, o-Ar*H*), 4.06 (t, *J* = 6.3 Hz, 2H, NC*H*$_2$CH$_2$CH$_2$O), 3.94 (t, *J* = 6.3 Hz, 2H, NCH$_2$CH$_2$C*H*$_2$Or), 2.21 (q, *J* = 6.3 Hz, 2H, NCH$_2$C*H*$_2$CH$_2$O). The spectroscopic data obtained are in agreement with those ones reported in literature[109].

1-phenoxy-3-aminopropane (3). In a 2-necked round-bottom flask, compound **2** (11.44 mmol, 3.22 g) and $NH_2NH_2 \cdot H_2O$ (0.11 mol, 3.562 ml) were stirred in EtOH (60 ml) for 4 h at reflux, monitoring the reaction by TLC (AcOEt/MeOH 9:1, R_f=0.00). The solvent was removed under reduced pressure and hence the crude was suspended in 1M NaOH (60 ml), which in turn was extracted with DCM (4 x 40 ml). The combined organic phases were dried with anhydrous Na_2SO_4 and then filtered. The solvent was removed by reduced pressure to get compound **3** as a white powder (1.52 g, 10.06 mmol, 88% yield). **^{1}H NMR** (300 MHz, $CDCl_3$) δ (ppm): 7.35 – 7.20 (m, 2H, m-Ar*H*), 6.98 – 6.86 (m, 3H, o-,p-Ar*H*), 4.04 (dt, *J* = 6.6 Hz, *J* = 1.2 Hz, 2H, NCH$_2$CH$_2$C*H*$_2$O), 2.90 (dt, *J* = 6.6 Hz, *J* = 1.2 Hz, 2H, NC*H*$_2$CH$_2$CH$_2$O), 1.91 (dp, *J* = 6.6 Hz, *J* = 1.2 Hz, 2H, NCH$_2$C*H*$_2$CH$_2$O), 1.25 (s, 2H, N*H*$_2$). The spectroscopic data obtained are in agreement with those ones reported in literature[110].

1-phenoxy-3-aminopropane hydrochloride (4a). In a 1-necked round-bottom flask, compound **3** (4.22 mmol, 0.64 g) was dissolved in MeOH (20 ml) and under magnetic stirring, 1N HCl (1 ml) was dropped in as long as pH=1 was reached. The methanolic solution was evaporated by reduced pressure and the resulting aqueous phase was lyophilized to get compound **4a** as a light yellow powder (0.79 g, 4.23 mmol, quantitative yield). **^{1}H NMR** (400 MHz, MeOD) δ (ppm): 7.32 – 7.28 (m, 2H, m-Ar*H*), 6.98 – 6.94 (m, 3H, o-,p-Ar*H*), 4.13 (t, *J* = 6.6 Hz, 2H, OC*H*$_2$CH$_2$CH$_2$N), 3.18 (t, *J* = 6.6 Hz, 2H, OCH$_2$CH$_2$C*H*$_2$N), 2.20-2.13 (m, 2H, OCH$_2$C*H*$_2$CH$_2$N). **^{13}C NMR** (100 MHz, MeOD) δ (ppm): 158.5 (i-*C*ArO), 129.2 (m-*C*ArO), 120.8 (p-*C*ArO), 114.1 (o-*C*ArO), 64.7

(O*C*$H_2CH_2CH_2N$), 37.2 (OCH_2CH_2*C*H_2N), 27.0 (OCH_2*C*H_2CH_2N). **ESI-MS (+)**: calcd. for $C_9H_{14}NO$ [(M-Cl)$^+$]: m/z 152.10, found m/z 152.17 (100%). **Mp**: 148°C-153°C

4-(3-(3-phenoxypropyl)thioureido)benzenesulfonamide (4b). In a 2-necked round-bottom flask, a solution of 4-isothiocyanatobenzenesulfonamide (0.69 mmol, 0.14 g) in dry DCM (5 ml) was added dropwise to compound **3** (0.69 mmol, 0.11 g) under magnetic stirring. The mixture was left reacting for 1 day at room temperature, whereas the next morning the reaction was monitored by TLC (AcOEt/MeOH 8:2, R_f=0.07). Upon completion, the organic phase was washed with 1N HCl (5 ml) and in turn the acidic aqueous phase was re-extracted with AcOEt (4 x 5 ml). The solvent was removed under reduced pressure to get compound **4b** as a light yellow powder (0.18 g, 0.50 mmol, 80% yield). **^{1}H NMR** (400 MHz, DMSO-d_6) δ (ppm): 7.73 (d, *J* = 8.3 Hz, 2H, m-Ar*H*SO_2NH_2), 7.65 (d, *J* = 8.3 Hz, 2H, m-Ar*H*NH), 7.30 (t, *J* = 7.5 Hz, 2H, m-Ar*H*O), 6.94 (t, *J* = 7.5 Hz, 3H, o-,p-Ar*H*O), 4.05 (t, *J* = 7.0 Hz, 2H, O*C*$H_2CH_2CH_2N$), 3.66 (s, 2H, OCH_2CH_2*C*H_2N), 2.04 (p, *J* = 7 Hz, 2H, OCH_2*C*H_2CH_2N). **^{13}C NMR** (100 MHz, DMSO-d_6) δ (ppm): 180.9 (*C*SNH_2), 159.0 (i-*C*ArO), 138.9 (i-*C*ArNH), 129.9 (i-*C*ArSO_2NH_2), 126.7 (o-*C*ArSO_2NH_2), 122.1 (m-*C*ArO), 121.0 (o-*C*ArNH), 114.9 (p-/o-*C*ArO), 65.8 (O*C*$H_2CH_2CH_2N$), 41.6 (OCH_2CH_2*C*H_2N) 28.6 (OCH_2*C*H_2CH_2N). **ESI-MS (-)**: calcd. for $C_{16}H_{18}N_3O_3S_2$ [(M-H)$^-$]: m/z 364.09, m/z 364.02 (38%); calcd. for $C_{16}H_{19}N_3O_3S_2Cl$ [(M+Cl)$^-$]: m/z 400.06, found m/z 400.06 (15%).

N-(3-phenoxypropyl)-4-sulfamoylbenzamide (4c). In a 2-necked round-bottom flask, 4-sulfamoylbenzoic acid (0.69 mmol, 0.15 g) and DIPEA (1.73 mmol, 0.302 ml) were stirred in dry DCM (20 ml) for 10 minutes at room temperature. Then EDC (0.83 mmol, 0.16 g) was added and the resulting mixture was stirred for 10 minutes. This fresh-made solution was hence dropped in another solution of compound **3** (0.69 mmol, 0.11 g) in dry DCM (10 ml) and eventually stirred for 1 day at room temperature, monitoring the reaction by TLC (AcOEt/MeOH 8:2, R_f=0.71). The reaction mixture was diluted with EtOAc (20 ml) and extracted with 1M NaOH (4 x 15 ml). The basic aqueous solution was therefore taken to pH=1 with 1N HCl (70 ml) and the suspension was filtered out to get compound (?) as a white powder (0.19 g, 0.58 mmol, 83% yield). **^{1}H NMR** (400 MHz, DMSO-d_6) δ (ppm): 8.74 (t, *J* = 6.1 Hz, 1H, $OCH_2CH_2CH_2N$*H*CO), 8.00 (d, *J* = 8.4 Hz, 2H, o-Ar*H*CONH), 7.90 (d, *J* = 8.4 Hz, 2H, o-Ar*H*SO_2NH_2), 7.48 (s, 2H, SO_2NH_2), 7.29 (dt, *J* = 7.3 Hz, 1.6 Hz, 2H, m-Ar*H*O), 6.93 (t, *J* = 7.3 Hz, 3H, o-,p-Ar*H*O), 4.05 (t, *J* = 6.1 Hz, 2H, O*C*$H_2CH_2CH_2$NHCO), 3.45 (q, *J* = 6.1 Hz, 2H, OCH_2CH_2*C*H_2NHCO), 2.00 (p, *J* = 6.5 Hz, 2H, OCH_2*C*H_2CH_2NHCO). **^{13}C NMR** (100 MHz, DMSO-d_6) δ (ppm): 165.7 (ArH*C*ONH), 159.0 (i-*C*Ar$OCH_2CH_2CH_2$NH), 146.6 (i-*C*ArSO_2NH_2), 137.9 (i-*C*Ar$CONH_2$), 129.9 (m-*C*Ar$OCH_2CH_2CH_2$NH), 128.3 (o-*C*Ar$OCH_2CH_2CH_2$NH), 126.1 (o-*C*ArSO_2NH_2), 120.9 (p-*C*Ar$OCH_2CH_2CH_2$NH), 114.9 (o-*C*Ar$OCH_2CH_2CH_2$NH), 65.6 (ArCO*C*$H_2CH_2CH_2$NH), 37.0 (Ar$COCH_2CH_2$*C*H_2NH), 29.3 (Ar$COCH_2$*C*H_2CH_2NH). **ESI-MS (-)**: calcd. for $C_{16}H_{17}N_2O_4S$ [(M-H)$^-$]: m/z 333.09, found m/z 333.10 (100%), calcd. for $C_{16}H_{18}N_2O_4SCl$ [(M+Cl)$^-$]: m/z 369.14, found m/z 369.07 (30%).

4,4'-(3-N-phthalimido)propyl-bisphenol (6). In a 2-necked round-bottom flask, 4-4'-bisphenol (2.64 mmol, 0.50 g) was dissolved in dry DMF (15 ml). Then K_2CO_3 (7.92 mmol, 1.09 g) was added and the resulting green suspension was stirred for 30 minutes at room temperature. Therefore N-(3-Bromopropyl)phthalimide (5.54 mmol, 1.48 g) was added and the mixture was stirred for 1 night at 65°C, monitoring it by TLC (AcOEt/Hex 1:1, R_f=0.35). The reaction was quenched pouring it into a mixture of H_2O/ice (100 ml + 100 ml) under vigorous magnetic stirring. Upon filtration, compound **6** was obtained as a green powder (1.29 g, 2.30 mmol, 88% yield). **^{1}H-NMR** (400 MHz, $CDCl_3$) δ (ppm): 7.87 (dd, J=5.4, 3.1 Hz, 4H, C*H*CCON), 7.73 (dd, *J* = 5.4, 3.1 Hz, 4H, C*H*CHCCON), 7.42 (d, *J* = 8.7 Hz, 4H, OCCHC*H*), 6.87 (d, *J* = 8.7 Hz, 4H, OCC*H*), 4.08 (t, *J* = 6.4 Hz, 4H, O*C*$H_2CH_2CH_2N$), 3.95 (t, *J* = 6.4 Hz, 4H, OCH_2CH_2*C*H_2N), 2.23 (p, *J* = 6.4 Hz, 4H, OCH_2*C*H_2CH_2N). The spectroscopic data obtained are in agreement with those ones reported in literature[111].

4,4'-(3-amino)propyl-bisphenol (7). In a 1-necked round-bottom flask, compound **6** (2.27 mmol, 1.27 g) and $NH_2NH_2 \cdot H_2O$ (45.40 mmol, 1.414 ml) were stirred in 96% EtOH (25 ml) for 1 night at reflux, monitoring the reaction by TLC (AcOEt/MeOH 9:1). The reaction was quenched adding H_2O (100 ml) to get compound (?) by filtration as a white powder (0.78 g, 2.60 mmol, 99% yield). **^{1}H-NMR** (400 MHz, $CDCl_3$) δ (ppm): 7.48 (d, *J* = 8.7 Hz, 4H, OCCHC*H*), 6.97 (d, *J* = 8.7 Hz, 4H, OCC*H*), 4.11 (t, *J* = 6.4 Hz, 4H, O$CH_2CH_2CH_2$N), 2.96 (t, *J* = 6.4 Hz, 4H, O$CH_2CH_2CH_2$N), 1.97 (t, *J* = 6.4 Hz, 4H, O$CH_2CH_2CH_2$N), 1.54 (s, 4H, NH_2). The spectroscopic data obtained are in agreement with those ones reported in literature[111].

bis[(2-hydroxy-3-methyl-5-tert-butyl)phenyl]methane (11). In a 3-necked round-bottom flask, Mg (60.00 mmol, 1.44 g) and dry THF (60 ml) were stirred at reflux. A small crystal of I_2 was added and subsequently, a solution of EtBr (70.00 mmol, 5.240 ml) in dry THF (40 ml) was slowly dropped in over a period of 4 h. Once the mixture turned grey-brown and cloudy, a solution of 4-tertbutyl-O-cresol (60.00 mmol, 9.84 g) in dry THF (60 ml) was added in the same way over a period of 1 h. The solvent was hence removed by reduced pressure and the powder was dissolved in toluene (200 ml). Then paraformaldehyde (30.00 mmol, 0.90 g) was added and the mixture was stirred for 7 h at reflux, monitoring it by TLC (DCM). The orange mixture was, therefore, cooled down at room temperature and then 1N HCl (100 ml) was added in. The aqueous phase was extracted with Et_2O (3 x 50 ml) and all the organic phases (toluene one included) were combined, dried out at rotavapor and precipitated in DCM/Hex to get compound **11** as a pure white powder (4.98 g, 14.64 mmol, 25% yield). **^{1}H NMR** (400 MHz, $CDCl_3$) δ (ppm): 7.19 (d, *J* = 2.3 Hz, 2H, m-Ar*H*OH), 7.01 (d, *J* = 2.3 Hz, 2H, m-Ar*H*OH), 5.96 (s, 2H, O*H*), 3.93 (s, 2H, ArCH_2Ar), 2.25 (s, 6H, ArCH_3), 1.29 (s, 18H, tBu). The spectroscopic data obtained are in agreement with those ones reported in literature[112].

bis[(2-hydroxy-3-methyl)phenyl]methane (12). In a 2-necked round-bottom flask, compound **11** (3.24 mmol, 1.10 g) was dissolved in dry toluene (25 ml) and upon vigorous stirring, $AlCl_3$ (8.09 mmol, 1.08 g) was added in. The mixture was left reacting for 1 night, monitoring it by TLC (AcOEt/Hex 2:8). The reaction was quenched adding 1N HCl/ice 1:1 (25 ml + 25 ml) and the aqueous phase was re-extracted with AcOEt (2 x 50 ml). The organic phases were combined and the solvent was removed by reduced pressure. The crude was then purified by recrystallization in DCM/Hex to get compound **12** as white crystals (0.51 g, 2.24 mmol, 69% yield). **^{1}H NMR** (400 MHz, $CDCl_3$) δ (ppm): 7.15 (d, *J* = 7.4 Hz, 2H, m-Ar*H*OH), 7.01 (d, *J* = 7.4 Hz, 2H, m-Ar*H*OH), 6.82 (t, *J* = 7.4 Hz, 2H, p-Ar*H*OH), 5.97 (s, 2H, O*H*), 3.95 (s, 2H, ArCH_2Ar), 2.26 (s, 6H, ArCH_3). The spectroscopic data obtained are in agreement with those ones reported in literature[112].

bis[(2-(3'-phthalimidopropoxy)-3-methyl)phenyl]methane (13). In a 2-necked round-bottom flask, compound **12** (0.44 mmol, 0.10 g) and K_2CO_3 (1.32 mmol, 0.18 g) were stirred in dry DMF (5 ml) for 30 minutes at room temperature. Then N-(3-bromopropyl)phthalimide (0.88 mmol, 0.24 g) was added in and the mixture was left reacting at 65°C for 1 night monitoring it by TLC (AcOEt/Hex 1:1). The reaction was quenched with 1N HCl (5 ml) and the mixture was extracted with DCM (3 x 20 ml). The organic phases were combined together and washed with brine (3 x 20 ml) and eventually H_2O (3 x 20 ml). The product was finally purified by a flash chromatography column (AcOEt/Hex 4:6) to get compound **13** as a white powder (0.17 g, 0.29 mmol, 66% yield). **^{1}H NMR** (300 MHz, $CDCl_3$) δ (ppm): 7.83 (dd, *J* = 5.4, 3.0 Hz, 4H, Pht*H*), 7.71 (dd, *J* = 5.4, 3.0 Hz, 4H, Pht*H*), 6.96 (d, *J* = 6.9 Hz, 2H, p-Ar*H*O), 6.91-6.79 (m, 4H, m-Ar*H*O), 4.04 (s, 2H, ArCH_2Ar), 3.91 (t, *J* = 6.5 Hz, 4H, O$CH_2CH_2CH_2$N), 3.81 (t, *J* = 6.5 Hz, 4H, O$CH_2CH_2CH_2$N), 2.29 (s, 6H, ArCH_3), 2.17 (p, *J* = 6.5 Hz, 4H, O$CH_2CH_2CH_2$N). The spectroscopic data obtained are in agreement with those ones reported in literature[112].

bis[(2-(3'-aminopropoxy)-3-methyl)phenyl]methane (14). In a 1-necked round-bottom flask, compound **13** (0.94 mmol, 0.57 g) and $NH_2NH_2 \cdot H_2O$ (21.00 mmol, 1.000 ml) were suspended in absolute EtOH (36 ml). Upon stirring, the suspension was taken to reflux and left reacting for 1 night, monitoring it by TLC (AcOEt/Hex 6:4). The solvent was removed by reduced pressure and the resulting crude was stirred in DCM for 30 minutes. The suspension was filtered off and the collected organic phase was dried out by rotavapor to get compound **14** as a colourless oil (0.30 g, 0.87 mmol, 92% yield). **^{1}H NMR** (300 MHz, $CDCl_3$) δ (ppm): 6.98 (dd, *J* = 7.1, 1.6 Hz, 2H, p-Ar*H*O), 6.94 – 6.76 (m, 4H, m-Ar*H*O), 4.02 (s, 2H, $ArCH_2Ar$), 3.75 (t, *J* = 6.4 Hz, 4H, $OCH_2CH_2CH_2N$), 2.87 (t, *J* = 6.4 Hz, 4H, $OCH_2CH_2CH_2N$), 2.26 (s, 6H, CH_3), 2.06 (s, 4H, NH_2), 1.86 (p, *J* = 6.4 Hz, 4H, $OCH_2CH_2CH_2N$). **ESI-MS (+):** calcd. for $C_{21}H_{31}N_2O_2$ [$(M+H)^+$]: m/z 343.33, found m/z 343.23 (100%), calcd. for $C_{21}H_{32}N_2O_2Na$ [$(M+Na)^+$]: m/z 365.30, found m/z 365.22 (50%). The spectroscopic data obtained are in agreement with those ones reported in literature[112].

bis[(2-(3'-aminopropoxy)-3-methyl)phenyl]methane dihydrochloride (15a). In a 1-necked round-bottom flask, compound **14** (0.26 mmol, 88.00 mg) was dissolved in MeOH (2 ml) and upon stirring, 1N HCl was added in till a pH=2 was reached. After 40 minutes, the solvent was removed by reduced pressure to get compound **15a** as a white powder (97.00 mg, 0.28 mmol, 99% yield). **^{1}H NMR** (400 MHz, CD_3OD) δ (ppm): 7.10 (d, *J* = 7.0 Hz, 2H, m-Ar*H*O), 6.96 (t, *J* = 7.0 Hz, 2H, p-Ar*H*O), 6.88 (d, *J* = 7.0 Hz, 2H, m-Ar*H*O), 4.06 (s, 2H, $ArCH_2Ar$), 3.86 (t, *J* = 6.0 Hz, 4H, $OCH_2CH_2CH_2N$), 3.18 (t, *J* = 6.0 Hz, 4H, $OCH_2CH_2CH_2N$), 2.33 (s, 6H, $ArCH_3$), 2.13 (p, *J* = 6.0 Hz 4H, $OCH_2CH_2CH_2N$). **^{13}C NMR** (100 MHz, CD_3OD) δ 155.1 (i-*C*ArO), 133.5 ($CArCH_2CAr$), 130.7 ($CArCH_3$), 129.3 (m-*C*ArO), 128.33 (m-*C*ArO), 124.0 (p-*C*ArO), 69.4 ($OCH_2CH_2CH_2N$), 37.4 ($OCH_2CH_2CH_2N$), 29.6 ($ArCH_2Ar$), 28 ($OCH_2CH_2CH_2N$), 15.2 ($ArCH_3$).

bis[(2-(3'-(p-benzensolfonamidyl)thioureido)propoxy-3-methyl)phenyl]methane (15b). In a 1-necked round-bottom flask, compound **14** (0.30 mmol, 0.10 g) was dissolved in dry DMF (2 ml). Upon stirring, 4-isothiocyanate-benzensolfonamide (0.66 mmol, 0.14 g) was added in and the mixture was left reacting for 4 h, monitoring it by TLC (AcOEt). The solvent was removed by reduced pressure and the resulting crude was purified by a flash chromatography column (AcOEt/Hex 9:1) to get compound **15b** as a light yellow powder (0.12 g, 0.16 mmol, 52% yield). **^{1}H NMR** (400 MHz, Acetone-d_6) δ (ppm): 9.20 (bs, 2H, CSN*H*Ar), 7.79 (d, *J* = 8.7 Hz, 4H, o-Ar*H*SO_2NH_2), 7.67 (d, *J* = 8.7 Hz, 4H, m-Ar*H*SO_2NH_2), 7.66-7.65 (m, 2H, $OCH_2CH_2CH_2NHCS$), 7.06 (d, *J* = 7.3 Hz, 2H, m-Ar*H*O), 6.94 (t, *J* = 7.3 Hz, 2H, p-Ar*H*O), 6.88 (d, *J* = 7.3 Hz, 2H, m-Ar*H*O), 6.51 (s, 4H, SO_2NH_2), 4.08 (s, 2H, $ArCH_2Ar$), 3.94-3.86 (m, 8H, $OCH_2CH_2CH_2N$, $OCH_2CH_2CH_2N$), 2.29 (s, 6H, $ArCH_3$), 2.16 (p, *J* = 6.4 Hz, 4H, $OCH_2CH_2CH_2N$). **^{13}C NMR** (100 MHz, CD_3OD) δ 180.7 (NH*C*SNH), 155.4 (i-*C*ArO), 142.5 (i-*C*ArN), 138.7 (i-*C*ArS), 133.7 ($CArCH_2$), 130.8 ($CArCH_3$), 129.1 (m-*C*ArO), 128.3 (m-*C*ArO), 126.6 (m-*C*ArSO_2NH_2), 123.7 (p-*C*ArO), 122.2 (o-*C*ArSO_2NH_2), 70.8 ($OCH_2CH_2CH_2N$), 42.5 ($OCH_2CH_2CH_2N$), 29.5 ($ArCH_2Ar$), 29.1 ($OCH_2CH_2CH_2N$), 15.2 ($ArCH_3$). **ESI-MS (-):** calcd. for $C_{35}H_{41}N_6O_6S_4$ [$(M-H)^-$]: m/z 769.42, found m/z 769.20 (100%), calcd. for $C_{35}H_{42}N_6O_6S_4Cl$ [$(M+Cl)^-$]: m/z 805.17, found m/z 805.37 (38%). **Mp:** 130-134°C.

4,4'-disulfanedyldiphenol (17). In a 2-necked round-bottom flask, 4-mercaptophenol (1.58 mmol, 0.20 g) was dissolved in AcOEt (50 ml). Once dissolved, NaI (33.36 umol, 5.00 mg) and H_2O_2 (1.74 mmol, 0.135 ml) were added in and stirred together for 1 h at room temperature, monitoring the reaction by TLC (AcOEt/Hex 1:1). The mixture was washed with sat. $NaHCO_3$ (3 x 20 ml) and the combined aqueous phases were re-extracted with AcOEt (3 x 20 ml). The organic phases were combined and dried out by reduced pressure to get compound **17** as a light yellow powder (0.39 g, 1.56 mmol, 98% yield). **^{1}H NMR** (300 MHz, $CDCl_3$) δ (ppm): 7.26 (dt, *J* = 8.7, 3.0 Hz, 4H, o-Ar*H*S), 6.74 (dt, *J* = 8.7, 3.0 Hz, 4H, o-Ar*H*O). The spectroscopic data obtained are in agreement with those ones reported in literature[113].

4,4'-(3-N-phthalimido)propyl-disulfanedyldiphenol (18). In a 2-necked round-bottom flask, compound **17** (0.89 mmol, 0.22 g) was stirred in dry DMF (6 ml) for 30 minutes at room temperature along with 55% NaH (1.87 mmol, 81.70 mg). Then N-(3-bromopropyl)phthalimide (1.87 mmol, 0.50 g) was added in and the mixture was left reacting for 3 h at room temperature, monitoring it by TLC (AcOEt/Hex 1:1). The reaction was hence quenched with H_2O (50 ml) and then, once adjusted at pH=7 with 1N HCl, it was re-extracted in AcOEt (3 x 30 ml). The combined organic phases were washed with brine (3 x 50 ml), H_2O (3 x 20 ml) and eventually dried out by reduced pressure. The crude was recrystallized in hot AcOEt to get compound **18** as a white powder (0.51 g, 0.83 mmol, quantitative yield). **^{1}H NMR** (300 MHz, $CDCl_3$) δ (ppm): 7.83 (dd, *J* = 5.4, 3.1 Hz, 4H, C*H*CCON), 7.71 (dd, *J* = 5.4, 3.1 Hz, 4H, C*H*CHCCON), 7.32 (d, *J* = 8.7 Hz, 4H, m-Ar*H*S), 6.72 (d, *J* = 8.7 Hz, 4H, o-Ar*H*S), 4.00 (t, *J* = 6.4 Hz, 4H, OC*H*$_2$CH$_2$CH$_2$N), 3.89 (t, *J* = 6.4 Hz, 4H, OCH$_2$CH$_2$C*H*$_2$N), 2.17 (p, *J* = 6.4 Hz, 4H, OCH$_2$C*H*$_2$CH$_2$N). **^{13}C NMR** (100 MHz, $CDCl_3$) δ (ppm): 168.4 (*C*ON), 159.0 (i-*C*ArOCH$_2$), 134.0 (o-*C*ArS), 132.6 (*C*HCHCCON), 132.1 (*C*CON), 128.5 (i-*C*ArS), 123.3 (*C*HCCON), 115.1 (m-*C*ArS), 65.8 (O*C*H$_2$CH$_2$CH$_2$N), 35.4 (OCH$_2$CH$_2$*C*H$_2$N), 28.3 (OCH$_2$*C*H$_2$CH$_2$N).

4,4'-(3-amino)propyl-disulfanedyldiphenol (19). In a 1-necked round-bottom flask, compound **18** (0.36 mmol, 0.13 g) and $NH_2NH_2 \cdot H_2O$ (7.17 mmol, 0.348 ml) were stirred in absolute EtOH (10 ml) for 1 night at reflux, monitoring the reaction by TLC (AcOEt/Hex 1:1). The solvent was removed by reduced pressure and the residue was re-dissolved in DCM (50 ml). The organic phase was hence washed with 1N NaOH (3 x 20 ml) and eventually dried out by reduced pressure to get compound **19** as a white powder (12.80 mg, 0.35 mmol, 98% yield). **^{1}H NMR** (300 MHz, MeOD) δ (ppm): 7.36 (dt, *J* = 8.7, 1.8 Hz, 4H, m-Ar*H*S), 6.89 (dt, *J* = 8.7, 1.8 Hz, 4H, o-Ar*H*S), 4.04 (t, *J* = 6.4 Hz, 4H, OC*H*$_2$CH$_2$CH$_2$N), 2.84 (t, *J* = 6.4 Hz, 4H, OCH$_2$CH$_2$C*H*$_2$N), 1.93 (p, *J* = 6.4 Hz, 4H, OCH$_2$C*H*$_2$CH$_2$N). **^{13}C NMR** (100 MHz, MeOD) δ (ppm): 160.1 (i-*C*ArO), 159.2 (i-*C*ArO), 132.3 (m-*C*ArS), 131.4 (o-*C*ArS), 129.6 (i-*C*ArS), 128.3 (i-*C*ArS), 125.6 (o-*C*ArS), 114.9 (m-*C*ArS), 65.3 (O*C*H$_2$CH$_2$CH$_2$N), 37.5 (OCH$_2$CH$_2$*C*H$_2$N), 29.0 (OCH$_2$*C*H$_2$CH$_2$N).

4,4'-(3-amino)propyl-disulfanedyldiphenol dihydrochloride (20a). In a 1-necked round-bottom flask, compound **19** (19.22 umol, 7.00 mg) was dissolved in MeOH (1 ml) and upon stirring, it was acidified with 1N HCl (300 ul) till pH=5 was reached. The solvent was removed by reduced pressure to get compound **20a** as a white powder (8.38 mg, 19.22 umol, 99% yield). **^{1}H NMR** (300 MHz, MeOD) δ (ppm): 7.41 (dt, *J* = 9.0, 2.1 Hz, 4H, m-Ar*H*S), 6.94 (dt, *J* = 9.0, 2.1 Hz, 4H, o-Ar*H*S), 4.14 (t, *J* = 6.8 Hz, 4H, OC*H*$_2$CH$_2$CH$_2$N), 3.17 (t, *J* = 6.8 Hz, 4H, OCH$_2$CH$_2$C*H*$_2$N), 2.16 (p, *J* = 6.8 Hz, 4H, OCH$_2$C*H*$_2$CH$_2$N).

4-(2-bromoethoxy)benzaldehyde (21a). In a 2-necked round-bottom flask, 4-hydroxybenzaldehyde (20.49 mmol, 2.5 g), K_2CO_3 (40.97 mmol, 5.66 g) and 1,2-dibromoethane (85.94 mmol, 7.44 ml) were stirred in dry DMF (10 ml) for 4 h at 70 °C, monitoring the reaction by TLC (AcOEt/Hex 1:1, R_f=0.58). The mixture was then diluted in DCM (100 ml), washed with H_2O (3 x 20 ml) and eventually with brine (3 x 50 ml). The organic phase was dried with anhydrous Na_2SO_4, filtered and the solvent was finally removed by reduced pressure. The crude was purified by a flash chromatography column (DCM/Hex 2:1) to get compound **21a** as a scented yellow powder (5.43 g, 23.80 mmol, 99% yield). **^{1}H NMR** (300 MHz, $CDCl_3$) δ (ppm): 9.91 (s, 1H, C*H*O), 7.87 (dt, *J* = 8.7, 2.7 Hz, 2H, m-CAr*H*O), 7.04 (dt, *J* = 8.7, 2.7 Hz, 2H, o-CAr*H*O), 4.39 (t, *J* = 6.2 Hz, 2H, OC*H*$_2$CH$_2$Br), 3.69 (t, *J* = 6.2 Hz, 2H, OCH$_2$C*H*$_2$Br). The spectroscopic data obtained are in agreement with those ones reported in literature[114].

2-(2-(2-methoxyethoxy)ethoxy)ethyl-4-methylbenzenesulfonate (21b). In a 2-necked round-bottom flask, 2-(2-(2-methoxyethoxy)ethoxy)ethanol (15.23 mmol, 2.440 ml) and NEt_3 (30.45 mmol, 4.230 ml) were stirred together in DCM (200 ml) for 10 minutes at 0°C. Then tosyl

chloride (15.99 mmol, 3.05 g) was added in and the mixture was kept stirring for 1 night at room temperature, monitoring it by TLC (AcOEt/Hex 7:3). The mixture was washed with H_2O (3 x 100 ml) and the organic phase was dried with anhydrous Mg_2SO_4. Upon filtration, the solvent was removed by reduced pressure and the crude was purified by a flash chromatography column (DCM→AcOEt) to get compound **21b** as a yellowish oil (3.34 g, 10.50 mmol, 69% yield). **^{1}H NMR** (300 MHz, $CDCl_3$) δ (ppm): 7.79 (d, *J* = 8.2 Hz, 2H, o-Ar*H*SO_2), 7.33 (d, *J* = 8.2 Hz, 2H, m-Ar*H*SO_2), 4.15 (t, *J* = 4.8 Hz, 2H, OCH_2CH_2OTs), 3.67 (7, *J* = 4.8 Hz, 2H, OCH_2CH_2OTs), 3.63 – 3.55 (m, 6H, $OCH_2CH_2OCH_2CH_2OCH_2CH_2$OTs), 3.52 (m, 2H, CH_3OCH_2), 3.36 (s, 3H, CH_3OCH_2), 2.43 (s, 3H, ArCH_3). The spectroscopic data obtained are in agreement with those ones reported in literature[115].

4-(2-(2-(2-methoxyethoxy)ethoxy)ethoxy)benzaldehyde (21c). In a 2-necked round-bottom flask, 4-hydroxybenzaldehyde (1.57 mmol, 0.19 g) and K_2CO_3 (1.65 mmol, 0.23 g) were stirred in dry DMF (5 ml) for 30 minutes at room temperature. The mixture was heated up at 100°C and compound **21b** (3.14 mmol, 1.00 g) was added in. The mixture was kept stirring for 2 h, monitoring it by TLC (AcOEt/Hex 7:3). The mixture was hence diluted with DCM (50 ml), washed with H_2O (2 x 30 ml), brine (2 x 30 ml) and eventually dried with anhydrous Mg_2SO_4. Upon filtration, solvent was removed by reduced pressure and the crude was therefore purified by a flash chromatography column (AcOEt/Hex 7:3) to get compound **21c** as a colourless oil (0.39 g, 1.23 mmol, 78% yield). **^{1}H-NMR** (400 MHz, $CDCl_3$): 10.52 (s, 1H), 7.83 (dd, 1H, *J* = 8.0, 2.0 Hz), 7.53 (dt, 1H, *J* = 8.0, 2.0 Hz), 7.03 (t, 1H, J = 8.0 Hz), 7.00 (d, 1H, J = 8.0 Hz), 4.25 (t, 2H, J = 5.0 Hz), 3.92 (t, 2H, J = 5.0 Hz), 3.78 - 3.61 (m, 6H), 3.58 - 3.52 (m, 2H), 3.37 (s, 3H). The spectroscopic data obtained are in agreement with those ones reported in literature[116].

3-chloro-1-azidopropane (22a). In a 2-necked round-bottom flask, 1-bromo-3-chloropropane (20.32 mmol, 2.000 ml) and NaN_3 (20.32 mmol, 1.32 g) were stirred in dry DMF (75 ml) for 1 night at room temperature, monitoring the reaction by TLC (Hex/DCM 9:1). The mixture was diluted with Et_2O (100 ml) and then washed with H_2O (3 x 200 ml) and brine (100 ml). The organic phase was dried with anhydrous Na_2SO_4 and the solvent was removed by reduced pressure to get compound **22a** as a colourless oil (2.18 g, 18.24 mmol, 90% yield). **^{1}H NMR** (400 MHz, $CDCl_3$) δ (ppm): 3.66 (t, *J* = 6.3 Hz, 2H, $ClCH_2CH_2CH_2N$), 3.53 (t, *J* = 6.3 Hz, 2H, $ClCH_2CH_2CH_2N$), 2.04 (p, *J* = 6.3 Hz, 2H, $ClCH_2CH_2CH_2N$). **IR** (cm-1): 2100 (N_3 asymmetric stretching). The spectroscopic data obtained are in agreement with those ones reported in literature[117].

3-iodo-1-azidopropane (22b). In a 2-necked round-bottom flask, compound **22a** (18.26 mmol, 2.18 g) and NaI (36.51 mmol, 5.47 g) were stirred in acetone (20 ml) for 1 day at reflux, monitoring the reaction by TLC (Hex/AcOEt 7:3). The reaction was quenched with H_2O (20 ml) and the mixture was extracted with EtOAc (3 x 100 ml). Then the combined organic phases were washed with $Na_2S_2O_3$ (100 ml), H_2O (100 ml) and dried with anhydrous Na_2SO_4. Upon filtration, the solvent was removed by reduced pressure to get compound **22b** as yellow oil (5.08 g, 24.08 mmol, 99% yield). **^{1}H NMR** (300 MHz, $CDCl_3$) δ (ppm): 3.43 (t, *J* = 6.4 Hz, 2H, $ICH_2CH_2CH_2N$), 3.24 (t, *J* = 6.4 Hz, 2H, $ICH_2CH_2CH_2N$), 2.03 (p, *J* = 6.4 Hz, 2H, $ICH_2CH_2CH_2N$). The spectroscopic data obtained are in agreement with those ones reported in literature[117].

1,3,5,7-tetramethyl-8-(2-bromoethoxy)benzene-BODIPY (23). In a Schlenk tube, 2,4-dimethylpyrrole (2.41 mmol, 0.248 ml), compound **21a** (1.10 mmol, 0.25 g), TFA (catalytic amount) and dry DCM (5 ml) were stirred together for 5 h at room temperature, monitoring the formation of the intermediate by TLC (AcOEt/Hex 3:7). So p-chloranil (1.10 mmol, 0.27 g) was added in, checking the presence of the new oxidised intermediate by TLC (AcOEt/Hex 4:6). After 1h, firstly, NEt_3 (22.12 mmol, 3 ml) and then secondly, $BF_3{\cdot}OEt_2$ (23.67 mmol, 3 ml) were

added in, monitoring the presence of the final product by TLC (AcOEt/Hex 2:8). After an overall reaction time for this last step of 1 h (30 minutes x 2), the mixture was diluted with DCM (50 ml), washed with H_2O (2 x 25 ml), brine (25 ml) and eventually it was dried out at rotavapor. The crude was purified twice by flash chromatography columns (Hex/AcOEt 8:2) to get compound **23** as an orange-brown powder (0.18 g, 0.40 mmol, 40% yield). **^{1}H NMR** (300 MHz, $CDCl_3$) δ (ppm): 7.20 (d, *J* = 8.7 Hz, 2H, m-Ar*H*O), 7.04 (d, *J* = 8.7 Hz, 2H, o-Ar*H*O), 6.00 (s, 2H, $CH_3CCHCCH_3$), 4.37 (t, *J* = 6.2 Hz, 2H, $BrCH_2CH_2O$), 3.70 (t, *J* = 6.2 Hz, 2H, $BrCH_2CH_2O$), 2.57 (s, 6H, CH_3), 1.44 (s, 6H, CH_3). The spectroscopic data obtained are in agreement with those ones reported in literature[108].

1,3,5,7-tetramethyl-8-(2-azidoethoxy)benzene-BODIPY (24). In a 2-necked round-bottom flask, compound **23** (0.40 mmol, 0.18 g) and NaN_3 (1.20 mmol, 78.00 mg) were stirred in dry DMF (10 ml) for 1 night at reflux, monitoring the reaction by TLC (Hex/AcOEt 7:1). The mixture was diluted with Et_2O (100 ml), washed with H_2O (2 x 50 ml) and eventually the solvent was removed by reduced pressure to get compound **24** as orange-brown powder (0.12 g, 0.29 mmol, 73% yield). **^{1}H NMR** (300 MHz, $CDCl_3$) δ (ppm): 7.21 (d, *J* = 8.6 Hz, 2H, m-Ar*H*O), 7.05 (d, *J* = 8.6 Hz, 2H, o-Ar*H*O), 6.00 (s, 2H, $CH_3CCHCCH_3$), 4.22 (t, *J* = 4.9 Hz, 2H, NCH_2CH_2O), 3.68 (t, *J* = 4.9 Hz, 2H, NCH_2CH_2O), 2.57 (s, 6H, CH_3), 1.45 (s, 6H, CH_3). The spectroscopic data obtained are in agreement with those ones reported in literature[108].

1,3,5,7-tetramethyl-2,6-bromo-8-(2-azidoethoxy)benzene-BODIPY (25). In a 2-necked round-bottom flask, compound **24** (0.26 mmol, 0.11 g) and a solution of NBS (0.51 mmol, 91.17 mg) in dry DCM (5 ml) were stirred in dry DCM/dry DMF 4:1 (4 ml + 1 ml) for 1 h at room temperature, monitoring the reaction by TLC (Hex/AcOEt 8:2). The reaction was quenched with H_2O (20 ml) and the aqueous phase was re-extracted with DCM (3 x 20 ml). The combined organic phases were dried with anhydrous Na_2SO_4 and upon filtration, the solvent was removed by reduced pressure to get compound **25** as a pink-orange powder (0.17 g, 0.31 mmol, 99% yield). **^{1}H NMR** (600 MHz, $CDCl_3$) δ (ppm): 7.16 – 7.13 (m, 2H, m-Ar*H*O), 7.07 – 7.03 (m, 2H, o-Ar*H*O), 4.20 (t, *J* = 4.9 Hz, 2H, NCH_2CH_2O), 3.64 (t, *J* = 4.9 Hz, 2H, NCH_2CH_2O), 2.57 (s, 6H, CH_3), 1.39 (s, 6H, CH_3). The spectroscopic data obtained are in agreement with those ones reported in literature[108].

3,5-(4-vinyl(2-(2-(2-methoxyethoxy)ethoxy)ethoxy)benzen)-1,7-dimethyl-2,6-bromo-8-(2-azidoethoxy)benzene-BODIPY (26). In a 2-necked round-bottom flask, compound **25** (0.13 mmol, 71. 90 mg), compound **21c** (0.31 mmol, 83.70 mg), glacial CH_3COOH (3.48 mmol, 0.199 ml), piperidine (2.01 mmol, 0.199 ml), $Mg(ClO_4)_2$ (catalytic amount) and 4Å molecular sieves were stirred together in dry toluene (12 ml) for 7 h at reflux, monitoring the reaction by TLC (DCM/MeOH 97:3). The sieves were filtered off and washed with DCM (50 ml) and MeOH (50 ml) and eventually the solvent was removed by reduced pressure. The crude was purified on semipreparative TLC (DCM/MeOH 97:3) to get compound **26** as a dark green powder (59.95 mg, 56.21 umol, 44% yield). **^{1}H NMR** (600 MHz, $CDCl_3$) δ (ppm): 8.10 (d, *J* = 16.6 Hz, 2H), 7.64 - 7.58 (m, 6H), 7.17 (d, *J* = 8.5 Hz, 2H), 7.04 (d, *J* = 8.5 Hz, 2H), 6.96 (d, *J* = 9.0 Hz, 4H), 4.25 - 4.18 (m, 6H), 3.91 - 3.87 (m, 4H), 3.78 - 3.76 (m, 4H), 3.72 - 3.66 (m, 10H), 3.58 - 3.54 (m, 4H), 3.39 (s, 6H), 1.46 (s, 6H). The spectroscopic data obtained are in agreement with those ones reported in literature[108].

4-(3-azidopropoxy)benzaldehyde (28). In a 2-necked round-bottom flask, 4-hydroxybenzaldehyde (8.19 mmol, 1.00 g) and K_2CO_3 (9.83 mmol, 1.36 g) were stirred in dry DMF (20 ml) for 30 minutes at room temperature. Then compound **22b** (14.75 mmol, 3.11 g) was added in and the mixture was kept stirring for 1 night at room temperature, monitoring the reaction by TLC (AcOEt/Hex 1:1). The reaction was quenched with H_2O (20 ml) which was in turn extracted with EtOAc (3 x 40 ml). The combined organic phases were washed with sat. K_2CO_3

(50 ml), H_2O (2 x 20 ml) and eventually dried with anhydrous Na_2SO_4. Upon filtration, the solvent was removed by reduced pressure and the crude was purified with a flash chromatography column (Hex/ AcOEt 8:2) to get compound **28** as colourless oil (1.28 g, 6.24 mmol, 76% yield). **^{1}H NMR** (300 MHz, $CDCl_3$) δ (ppm): 9.91 (s, 1H, p-C*H*OArO), 7.86 (d, *J* = 8.7 Hz, 2H, m-Ar*H*O), 7.02 (d, *J* = 8.7 Hz, 2H, o-Ar*H*O), 4.16 (t, *J* = 6.4 Hz, 2H, OC*H*$_2$CH$_2$CH$_2$N), 3.56 (t, *J* = 6.4 Hz, 2H, OCH$_2$CH$_2$C*H*$_2$N), 2.11 (p, *J* = 6.4 Hz, 2H, OCH$_2$C*H*$_2$CH$_2$N). The spectroscopic data obtained are in agreement with those ones reported in literature[118].

4-(3-azidopropoxy)benzoic acid (29). In a 1-necked round-bottom flask, compound **28** (6.25 mmol, 1.28 g) was firstly dissolved in $CHCl_3$/ACN (20 ml + 20 ml) and as soon as the pH was adjusted at 7 with 10 ml of an aqueous solution of 0.7 M NaH_2PO_4, 30% H_2O_2 (9.37 mmol, 0.871 ml) and $NaClO_2$ (8.75 mmol, 0.79 g) were added in. The mixture was hence stirred for 1 day at room temperature, monitoring the reaction by TLC (AcOEt/Hex 7:3). The solution was diluted with DCM (100 ml) and then it was extracted with sat. $NaHCO_3$ (3 x 50 ml). The basic aqueous phases were combined and then acidified to pH=2 with 37% HCl (20 ml). The precipitate was filtered to get compound **29** as a white powder (1.22 g, 5.50 mmol, 88% yield). **^{1}H NMR** (600 MHz, $CDCl_3$) δ (ppm): 8.05 (dt, *J* = 9.0, 2.4 Hz, 2H, o-Ar*H*COOH), 6.93 (dt, *J* = 9.0, 2.4 Hz, 2H, m-Ar*H*COOH), 4.12 (t, *J* = 6.3 Hz, 2H, OC*H*$_2$CH$_2$CH$_2$N), 3.53 (t, *J* = 6.3 Hz, 2H, OCH$_2$CH$_2$C*H*$_2$N), 2.08 (p, *J* = 6.3 Hz, 2H, OCH$_2$C*H*$_2$CH$_2$N). **^{13}C NMR** (150 MHz, $CDCl_3$) δ (ppm): 171.3 (Ar*C*OOH), 163.2 (i-*C*ArO), 132.5 (o-*C*ArCOOH), 121.9 (i-*C*ArCOOH), 114.3 (m-*C*ArCOOH), 64.8 (O*C*H$_2$CH$_2$CH$_2$N), 48.2 (OCH$_2$CH$_2$*C*H$_2$N), 28.7 (OCH$_2$*C*H$_2$CH$_2$N).

Methyl 4-(3-azidopropoxy)benzoate (30). In a 1-necked round-bottom flask, compound **29** (0.90 mmol, 0.20 g), H_2SO_4 (catalytic amount) were stirred together in MeOH (30 ml) for 6h at reflux, monitoring the reaction by TLC (AcOEt/Hex 7:3). The solvent was removed by reduced pressure to get compound **30** as a yellowish oil (quantitative yield). **^{1}H NMR** (600 MHz, $CDCl_3$) δ (ppm): 7.92 (m, o-Ar*H*O), 6.90 (m, m-Ar*H*O), 4.09 (t, *J* = 6.2 Hz, OC*H*$_2$CH$_2$CH$_2$N), 3.87 (s, C*H*$_3$, OCH$_2$CH$_2$C*H*$_2$N), 3.52 (t, *J* = 6.2 Hz, OCH$_2$C*H*$_2$CH$_2$N), 2.12 (p, *J* = 6.2 Hz, OCH$_2$C*H*$_2$CH$_2$N). **^{13}C NMR** (151 MHz, $CDCl_3$) δ (ppm): 166.9, 162.5, 131.7, 122.9, 114.1, 64.8, 51.9, 48.2, 28.7.

Inhibition experiments.

Protocol. An Applied Photophysics stopped-flow instrument was used for assaying the CA catalyzed CO_2 hydration activity. Phenol red (at a concentration of 0.2 mM) was used as indicator, working at the absorbance maximum of 557 nm, with 20 mM Hepes (pH 7.5) as buffer, and 20 mM Na_2SO_4 (for maintaining a constant ionic strength), following the initial rates of the CA-catalyzed CO_2 hydration reaction for a period of 10-100 s. The CO_2 concentrations ranged from 1.7 to 17 mM for the determination of the kinetic parameters and inhibition constants. For each inhibitor, at least six traces of the initial 5-10% of the reaction were used for determining the initial velocity. The uncatalyzed rates were determined in the same manner and subtracted from the total observed rates. Stock solutions of inhibitor (0.1 mM) were prepared in distilled-deionized water, and dilutions up to 1 nM were done thereafter with distilled deionized water. Experiments were done using four different inhibitor concentrations, varying from 0.1 μM to 1 nM. Inhibitor and enzyme solutions were preincubated together for 6 h at room temperature (15 min just for AAZ) prior to assay, in order to allow for the formation of the E-I complex. The inhibition constants were obtained by nonlinear least-squares methods using PRISM 3, as reported earlier and represent the mean from at least three different determinations.

Cocrystallization.

Crystallization and X-ray data collection. Crystals were obtained using the hanging drop vapor diffusion method using 24 well Linbro plate. 2 µl of 0.8 mM solution of hCA II in Tris-HCl pH=8.0 were mixed with of a solution of 1.5, 1.6 and 1.7 M sodium citrate, 50 mM Tris pH 8.0 and were equilibrated against 500 µl of the same solution at 296 K. Crystals of the protein grew in a few days. hCAII crystals were soaked in 5mM inhibitor solution for 2 days. The crystals were flash-frozen at 100K using a solution obtained by adding 25% (v/v) glycerol to the mother liquor solution as cryoprotectant. Data on crystals of the complexes hCAII/**4b** were collected using synchrotron radiation at the ID-11.2C beamline at Elettra (Trieste, Italy) with a wavelength of 1.000 Å and a Pilatus3_6M Dectris CCD detector. Data were integrated and scaled using the program XDS[119].

Structure determination. The crystal structure of hCA II (PDB accession code: 4FIK) without solvent molecules and other heteroatoms was used to obtain initial phases of the structures using Refmac5[120]. 5% of the unique reflections were selected randomly and excluded from the refinement data set for the purpose of Rfree calculations. The initial |Fo - Fc| difference electron density maps unambiguously showed the inhibitor molecules. Atomic models for inhibitors were calculated and energy minimized using the program JLigand 1.0.40[121]. Refinements proceeded using normal protocols of positional, anisotropic atomic displacement parameters alternating with manual building of the models using COOT[122]. Solvent molecules were introduced automatically using the program ARP[123]. The quality of the final models were assessed with COOT. Graphical representations were generated with Chimera[124].

2.6 References

1. Permentier, K., Vercammen, S., Soetaert, S. & Schellemans, C. Carbon dioxide poisoning: a literature review of an often forgotten cause of intoxication in the emergency department. *International Journal of Emergency Medicine* **10**, (2017).

2. Langford, N. J. Carbon dioxide poisoning. *Toxicological Reviews* **24**, 229–235 (2005).

3. Ikeda, N., Takahashi, H., Umetsu, K. & Suzuki, T. The course of respiration and circulation in death by carbon dioxide poisoning. *Forensic Sci. Int.* **41**, 93–99 (1989).

4. Hill, L. & Flack, M. The effect of excess of carbon dioxide and of want of oxygen upon the respiration and the circulation. *J. Physiol.* **37**, 77–111 (1908).

5. Niu, Y. M. *et al.* Study on the effect of different oxygen therapies on rats with acute carbon dioxide poisoning. *Hum. Exp. Toxicol.* **31**, 126–133 (2012).

6. 26.4 Acid-Base Balance – Anatomy and Physiology. Available at: https://opentextbc.ca/anatomyandphysiology/chapter/26-4-acid-base-balance/. (Accessed: 7th November 2019)

7. Doyle, J. & Cooper, J. S. *Physiology, Carbon Dioxide Transport*. *StatPearls* (StatPearls Publishing, 2019).

8. Cordat, E. & Casey, J. R. Bicarbonate transport in cell physiology and disease. *Biochemical Journal* **417**, 423–439 (2009).

9. Hot, C. & Sturtevant, J. M. *The Kinetics of the Hydration of Carbon Dioxide at 25"*. THE JOURNAL OF BIOLOGICAL CHEMISTRY* **238**, (1963).

10. Magid, E. & Turbeck, B. O. The rates of the spontaneous hydration of CO2 and the reciprocal reaction in neutral aqueous solutions between 0° and 38°. *BBA - Gen. Subj.* **165**, 515–524 (1968).

11. Making a Fast Reaction Faster: Carbonic Anhydrases - Biochemistry - NCBI Bookshelf. Available at: https://www.ncbi.nlm.nih.gov/books/NBK22599/. (Accessed: 7th November 2019)

12. Henry, R. P. *MULTIPLE ROLES OF CARBONIC ANHYDRASE IN CELLULAR TRANSPORT A N D METABOLISM*. *PhysioL* (1996).

13. Mboge, M. Y., Mahon, B. P., McKenna, R. & Frost, S. C. Carbonic anhydrases: Role in pH control and cancer. *Metabolites* **8**, (2018).

14. Lehenkari, P., Hentunen, T. A., Laitala-Leinonen, T., Tuukkanen, J. & Väänänen, H. K. Carbonic anhydrase II plays a major role in osteoclast differentiation and bone resorption by effecting the steady state intracellular pH and Ca2+. *Exp. Cell Res.* **242**, 128–137 (1998).

15. Waite, L. C., Volkert, W. A. & Kenny, A. D. Inhibition of bone resorption by acetazolamide in the rat. *Endocrinology* **87**, 1129–1139 (1970).

16. Ismail, I. S. The Role of Carbonic Anhydrase in Hepatic Glucose Production. *Curr. Diabetes Rev.* **14**, 108–112 (2018).

17. Lynch, C. J. *et al.* Role of hepatic carbonic anhydrase in de nova lipogenesis. *Biochem. J.* **310**, 197–202 (1995).

18. Dodgson, S. J. Liver Mitochondrial Carbonic Anhydrase (CA V), Gluconeogenesis, and Ureagenesis in the Hepatocyte. in *The Carbonic Anhydrases* 297–306 (Springer US, 1991). doi:10.1007/978-1-4899-0750-9_25

19. HÄUSSINGER, D. & GEROK, W. Hepatic urea synthesis and pH regulation: Role of CO2, HCO−3, pH and the activity of carbonic anhydrase. *Eur. J. Biochem.* **152**, 381–386 (1985).

20. Hong, J. H. *et al.* Essential role of carbonic anhydrase XII in secretory gland fluid and HCO3-secretion revealed by disease causing human mutation. *J. Physiol.* **593**, 5299–5312 (2015).

21. BENESCH, R. Carbonic Anhydrase and Calcification. *Ann. N. Y. Acad. Sci.* **429**, 457–458 (1984).

22. Speer, M. Y. & Giachelli, C. M. Regulation of cardiovascular calcification. *Cardiovasc. Pathol.* **13**, 63–70 (2004).

23. Rajachar, R. M., Tung, E., Truong, A. Q., Look, A. & Giachelli, C. M. Role of carbonic anhydrase II in ectopic calcification. *Cardiovasc. Pathol.* **18**, 77–82 (2009).

24. Supuran, C. T. Structure and function of carbonic anhydrases. *Biochemical Journal* **473**, 2023–2032 (2016).

25. Domsic, J. F. *et al.* Entrapment of carbon dioxide in the active site of carbonic anhydrase II. *J. Biol. Chem.* **283**, 30766–30771 (2008).

26. Supuran, C. T. Carbonic anhydrases: Novel therapeutic applications for inhibitors and activators. *Nature Reviews Drug Discovery* **7**, 168–181 (2008).

27. Supuran, C. T. Journal of Enzyme Inhibition and Medicinal Chemistry Structure-based drug discovery of carbonic anhydrase inhibitors. (2012). doi:10.3109/14756366.2012.672983

28. Aggarwal, M., Boone, C. D., Kondeti, B. & McKenna, R. Structural annotation of human carbonic anhydrases. *Journal of Enzyme Inhibition and Medicinal Chemistry* **28**, 267–277 (2012).

29. Cronk, J. D. *et al.* Identification of a Novel Noncatalytic Bicarbonate Binding Site in Eubacterial

beta-Carbonic Anhydrase. *Biochemistry* **45**, 4351–4361 (2006).

30. Cronk, J. D., Endrizzi, J. A., Cronk, M. R., O'neill, J. W. & Zhang, K. Y. J. Crystal structure of E. coli β-carbonic anhydrase, an enzyme with an unusual pH-dependent activity. *Protein Sci.* **10**, 911–922 (2001).

31. Covarrubias, A. S. *et al.* Structure and function of carbonic anhydrases from Mycobacterium tuberculosis. *J. Biol. Chem.* **280**, 18782–18789 (2005).

32. Crystal structure and kinetic studies of a tetrameric type II β-carbonic anhydrase from the pathogenic bacterium Vibrio cholerae. Available at: https://reference.medscape.com/medline/abstract/26627652. (Accessed: 11th November 2019)

33. Mogensen, E. G. *et al.* Cryptococcus neoformans senses CO2 through the carbonic anhydrase Can2 and the adenylyl cyclase Cac1. *Eukaryot. Cell* **5**, 103–111 (2006).

34. DiMario, R. J., Clayton, H., Mukherjee, A., Ludwig, M. & Moroney, J. V. Plant Carbonic Anhydrases: Structures, Locations, Evolution, and Physiological Roles. *Molecular Plant* **10**, 30–46 (2017).

35. Alber, B. E. & Ferry, J. G. A carbonic anhydrase from the archaeon Methanosarcina thermophila. *Proc. Natl. Acad. Sci. U. S. A.* **91**, 6909–6913 (1994).

36. Zimmerman, S. A., Tomb, J. F. & Ferry, J. G. Characterization of CamH from Methanosarcina thermophila, founding member of a subclass of the γ class of carbonic anhydrases. *J. Bacteriol.* **192**, 1353–1360 (2010).

37. Capasso, C. δ-Carbonic anhydrases. in *Carbonic Anhydrases* 107–129 (Elsevier, 2019). doi:10.1016/B978-0-12-816476-1.00005-8

38. Langella, E., De Simone, G., Esposito, D., Alterio, V. & Monti, S. M. ζ-Carbonic anhydrases. in *Carbonic Anhydrases* 131–137 (Elsevier, 2019). doi:10.1016/B978-0-12-816476-1.00006-X

39. Alterio, V., Di Fiore, A., D'Ambrosio, K., Supuran, C. T. & De Simone, G. Multiple binding modes of inhibitors to carbonic anhydrases: How to design specific drugs targeting 15 different isoforms? *Chemical Reviews* **112**, 4421–4468 (2012).

40. Supuran, C. T. Carbonic anhydrase inhibition and the management of hypoxic tumors. *Metabolites* **7**, (2017).

41. Kivelä, J., Parkkila, S., Parkkila, A. K., Leinonen, J. & Rajaniemi, H. Salivary carbonic anhydrase isoenzyme VI. *Journal of Physiology* **520**, 315–320 (1999).

42. Waheed, A. & Sly, W. S. Membrane associated carbonic anhydrase IV (CA IV): A personal and historical perspective. *Subcell. Biochem.* **75**, 157–179 (2014).

43. Mahon, B. P. *et al.* The Structure of Carbonic Anhydrase IX Is Adapted for Low-pH Catalysis. *Biochemistry* **55**, 4642–4653 (2016).

44. Waheed, A. & Sly, W. S. Carbonic anhydrase XII functions in health and disease. *Gene* **623**, 33–40 (2017).

45. Whittington, D. A. *et al.* Expression, assay, and structure of the extracellular domain of murine carbonic anhydrase XIV: Implications for selective inhibition of membrane-associated isozymes. *J. Biol. Chem.* **279**, 7223–7228 (2004).

46. Benej, M., Pastorekova, S. & Pastorek, J. Carbonic anhydrase IX: Regulation and role in cancer. *Subcell. Biochem.* **75**, 199–219 (2014).

47. Eriksson, A. E., Jones, T. A. & Liljas, A. Refined structure of human carbonic anhydrase II at 2.0 Å

resolution. *Proteins Struct. Funct. Genet.* **4**, 274–282 (1988).

48. Sprigings, T. G. & Hall, C. D. A simple carbonic anhydrase model which achieves catalytic hydrolysis by the formation of an â€˜enzymeâ€“substrateâ€™™-like complexElectronic supplementary information (ESI) available: experimental data. See http://www.rsc.org/suppdata/p2/b1/b107683n/. *J. Chem. Soc. Perkin Trans. 2* 2063–2067 (2001). doi:10.1039/b107683n

49. De Simone, G. *et al.* Exploration of the residues modulating the catalytic features of human carbonic anhydrase XIII by a site-specific mutagenesis approach. *J. Enzyme Inhib. Med. Chem.* **34**, 1506–1510 (2019).

50. Alterio, V., Di Fiore, A., D'Ambrosio, K., Supuran, C. T. & De Simone, G. Multiple binding modes of inhibitors to carbonic anhydrases: How to design specific drugs targeting 15 different isoforms? *Chem. Rev.* **112**, 4421–4468 (2012).

51. Vu, H., Pham, N. B. & Quinn, R. J. Direct Screening of Natural Product Extracts Using Mass Spectrometry. *J. Biomol. Screen.* **13**, 265–275 (2008).

52. Maresca, A. *et al.* Erratum: Deciphering the Mechanism of Carbonic Anhydrase Inhibition with Coumarins and Thiocoumarins(Journal of Medicinal Chemistry (2010) 53(335?344) 10.1021/jm901287j). *Journal of Medicinal Chemistry* **58**, 5689 (2015).

53. D'Ambrosio, K. *et al.* Out of the active site binding pocket for carbonic anhydrase inhibitors. *Chem. Commun.* **51**, 302–305 (2015).

54. Lindskog, S. Structure and mechanism of Carbonic Anhydrase. *Pharmacology and Therapeutics* **74**, 1–20 (1997).

55. Maresca, A., Carta, F., Vullo, D. & Supuran, C. T. Dithiocarbamates strongly inhibit the β-class carbonic anhydrases from *Mycobacterium tuberculosis*. *J. Enzyme Inhib. Med. Chem.* **28**, 407–411 (2013).

56. Temperini, C., Scozzafava, A. & Supuran, C. T. Carbonic anhydrase inhibitors. X-ray crystal studies of the carbonic anhydrase II-trithiocarbonate adduct-An inhibitor mimicking the sulfonamide and urea binding to the enzyme. *Bioorganic Med. Chem. Lett.* **20**, 474–478 (2010).

57. Scozzafava, A. & Supuran, C. T. Hydroxyurea is a carbonic anhydrase inhibitor. *Bioorganic Med. Chem.* **11**, 2241–2246 (2003).

58. Temperini, C., Innocenti, A., Scozzafava, A. & Supuran, C. T. N-Hydroxyurea-A versatile zinc binding function in the design of metalloenzyme inhibitors. *Bioorganic Med. Chem. Lett.* **16**, 4316–4320 (2006).

59. Abbate, F., Casini, A., Owa, T., Scozzafava, A. & Supuran, C. T. Carbonic anhydrase inhibitors: E7070, a sulfonamide anticancer agent, potently inhibits cytosolic isozymes I and II, and transmembrane, tumor-associated isozyme IX. *Bioorganic Med. Chem. Lett.* **14**, 217–223 (2004).

60. Supuran, C. Diuretics: From Classical Carbonic Anhydrase Inhibitors to Novel Applications of the Sulfonamides. *Curr. Pharm. Des.* **14**, 641–648 (2008).

61. Supuran, C. T., Winum, J.-Y. Alterio, V.; Di Fiore, A.; D'Ambrosio, K.; Supuran, C. T.; De Simone, G. In Drug Design of Zinc-Enzyme Inhibitors: Functional, Structural, and Disease Applications. *Wiley Hoboken, NJ,* 73 (2009).

62. Abdoli, M., Bozdag, M., Angeli, A. & Supuran, C. T. Benzamide-4-sulfonamides are effective human carbonic anhydrase I, II, VII, and IX inhibitors. *Metabolites* **8**, (2018).

63. Chiaramonte, N., Romanelli, M. N., Teodori, E. & Supuran, C. T. Amino acids as building blocks for

carbonic anhydrase inhibitors. *Metabolites* **8**, (2018).

64. Banerjee, A. L. *et al.* Spacer-Based Selectivity in the Binding of "Two-Prong" Ligands to Recombinant Human Carbonic Anhydrase I †. *Biochemistry* **44**, 3211–3224 (2005).

65. Casini, A. *et al.* Carbonic anhydrase inhibitors: water-soluble 4-sulfamoylphenylthioureas as topical intraocular pressure-lowering agents with long-lasting effects. *J. Med. Chem.* **43**, 4884–92 (2000).

66. (PDF) QSAR study on para-substituted aromatic sulfonamides as carbonic anhydrase II inhibitors using topological information indices | A Afantitis - Academia.edu. Available at: https://www.academia.edu/5199950/QSAR_study_on_para-substituted_aromatic_sulfonamides_as_carbonic_anhydrase_II_inhibitors_using_topological_information_indices. (Accessed: 11th November 2019)

67. Pacchiano, F. *et al.* Selective hydrophobic pocket binding observed within the carbonic anhydrase II active site accommodate different 4-substituted-ureido-benzenesulfonamides and correlate to inhibitor potency. *Chem. Commun.* **46**, 8371–8373 (2010).

68. Cecchi, A. *et al.* Carbonic anhydrase inhibitors: Synthesis and inhibition of cytosolic/tumor-associated carbonic anhydrase isozymes I, II, and IX with sulfonamides derived from 4-isothiocyanato-benzolamide. *Bioorganic Med. Chem. Lett.* **14**, 5775–5780 (2004).

69. Alterio, V., De Simone, G., Monti, S. M., Scozzafava, A. & Supuran, C. T. Carbonic anhydrase inhibitors: Inhibition of human, bacterial, and archaeal isozymes with benzene-1,3-disulfonamides-Solution and crystallographic studies. *Bioorganic Med. Chem. Lett.* **17**, 4201–4207 (2007).

70. Tawil, R. *et al.* Randomized trials of dichlorphenamide in the periodic paralyses. Working Group on Periodic Paralysis. *Ann. Neurol.* **47**, 46–53 (2000).

71. Pastorekova, S., Parkkila, S., Pastorek, J. & Supuran, C. T. Carbonic anhydrases: Current state of the art, therapeutic applications and future prospects. *Journal of Enzyme Inhibition and Medicinal Chemistry* **19**, 199–229 (2004).

72. Casini, A., Abbate, F., Scozzafava, A. & Supuran, C. T. Carbonic anhydrase inhibitors: X-ray crystallographic structure of the adduct of human isozyme II with a bis-sulfonamide-two heads are better than one? *Bioorg. Med. Chem. Lett.* **13**, 2759–63 (2003).

73. Scozzafava, A. *et al.* Carbonic anhydrase inhibitors: Perfluoroalkyl/aryl-substituted derivatives of aromatic/heterocyclic sulfonamides as topical intraocular pressure-lowering agents with prolonged duration of action. *J. Med. Chem.* **43**, 4542–4551 (2000).

74. Steele, R. M. *et al.* Nitric oxide-donating carbonic anhydrase inhibitors for the treatment of open-angle glaucoma. *Bioorganic Med. Chem. Lett.* **19**, 6565–6570 (2009).

75. Galassi, F. *et al.* Nitric oxide proxies and ocular perfusion pressure in primary open angle glaucoma. *Br. J. Ophthalmol.* **88**, 757–760 (2004).

76. Kotikoski, H., Vapaatalo, H. & Oksala, O. Nitric oxide and cyclic GMP enhance aqueous humor outflow facility in rabbits. *Curr. Eye Res.* **26**, 119–123 (2003).

77. Becquet, F., Courtois, Y. & Goureau, O. Nitric oxide in the eye: Multifaceted roles and diverse outcomes. *Surv. Ophthalmol.* **42**, 71–82 (1997).

78. Nathanson, J. A. Nitrovasodilators as a new class of ocular hypotensive agents. *J. Pharmacol. Exp. Ther.* **260**, 956–65 (1992).

79. Carradori, S., Mollica, A., De Monte, C., Granese, A. & Supuran, C. Nitric Oxide Donors and

Selective Carbonic Anhydrase Inhibitors: A Dual Pharmacological Approach for the Treatment of Glaucoma, Cancer and Osteoporosis. *Molecules* **20**, 5667–5679 (2015).

80. Stringer, J. L. A comparison of topiramate and acetazolamide on seizure duration and paired-pulse inhibition in the dentate gyrus of the rat. *Epilepsy Res.* **40**, 147–53 (2000).

81. Shank, R. P. *et al.* Topiramate: Preclinical Evaluation of a Structurally Novel Anticonvulsant. *Epilepsia* **35**, 450–460 (1994).

82. Tibell, L., Forsman, C., Simonsson, I. & Lindskog, S. The inhibition of human carbonic anhydrase II by some organic compounds. *Biochim. Biophys. Acta* **829**, 202–8 (1985).

83. Simonsson, I., Jonsson, B. H. & Lindskog, S. Phenol, a competitive inhibitor of CO2 hydration catalyzed by carbonic anhydrase. *Biochem. Biophys. Res. Commun.* **108**, 1406–12 (1982).

84. Liang, J. Y. & Lipscomb, W. N. Binding of substrate CO2 to the active site of human carbonic anhydrase II: A molecular dynamics study. *Proc. Natl. Acad. Sci. U. S. A.* **87**, 3675–3679 (1990).

85. Temperini, C., Innocenti, A., Scozzafava, A. & Supuran, C. T. Carbonic anhydrase activators: Kinetic and X-ray crystallographic study for the interaction of d- and l-tryptophan with the mammalian isoforms I-XIV. *Bioorganic Med. Chem.* **16**, 8373–8378 (2008).

86. Carta, F. *et al.* Polyamines inhibit carbonic anhydrases by anchoring to the zinc-coordinated water molecule. *J. Med. Chem.* **53**, 5511–5522 (2010).

87. Pastorekova, S. *et al.* Carbonic anhydrase inhibitors: The first selective, membrane-impermeant inhibitors targeting the tumor-associated isozyme IX. *Bioorg. Med. Chem. Lett.* **14**, 869–873 (2004).

88. Supuran, C. T. & Scozzafava, A. Carbonic Anhydrase Inhibitors: Aromatic Sulfonamides and Disulfonamides Act as Efficient Tumor Growth Inhibitors. *J. Enzyme Inhib.* **15**, 597–610 (2000).

89. Wilkinson, B. L. *et al.* Inhibition of membrane-associated carbonic anhydrase isozymes IX, XII and XIV with a library of glycoconjugate benzenesulfonamides. *Bioorganic Med. Chem. Lett.* **17**, 987–992 (2007).

90. Wilkinson, B. L., Innocenti, A., Vullo, D., Supuran, C. T. & Poulsen, S. A. Inhibition of carbonic anhydrases with glycosyltriazole benzene sulfonamides. *J. Med. Chem.* **51**, 1945–1953 (2008).

91. Supuran, C. T. Bacterial carbonic anhydrases as drug targets: Toward novel antibiotics? *Front. Pharmacol.* **JUL**, (2011).

92. Brown, E. D. *et al.* Model for Synthetic Biology To Accelerate the Evolution of. *Trends Pharmacol. Sci.* **1354**, 336–343 (2015).

93. Švastová, E. *et al.* Hypoxia activates the capacity of tumor-associated carbonic anhydrase IX to acidify extracellular pH. *FEBS Lett.* **577**, 439–445 (2004).

94. Folkman, J. Angiogenesis: An organizing principle for drug discovery? *Nat. Rev. Drug Discov.* **6**, 273–286 (2007).

95. Carmeliet, P. & Jain, R. K. Angiogenesis in cancer and other diseases. *Nature* **407**, 249–257 (2000).

96. Turkcan, S., Kiru, L., Naczynski, D. J., Sasportas, L. S. & Pratx, G. Lactic acid accumulation in the tumor microenvironment suppresses 18 F-FDG uptake. *Cancer Res.* **79**, 410–419 (2019).

97. De Simone, G. *et al.* Carbonic Anhydrase Inhibitors: Hypoxia-Activatable Sulfonamides Incorporating Disulfide Bonds that Target the Tumor-Associated Isoform IX †. *J. Med. Chem.* **49**, 5544–5551 (2006).

98. Elbaum, D., Nair, S. K., Patchan, M. W., Thompson, R. B. & Christianson, D. W. Structure-Based Design of a Sulfonamide Probe for Fluorescence Anisotropy Detection of Zinc with a Carbonic Anhydrase-Based Biosensor. *J. Am. Chem. Soc.* **118**, 8381–8387 (1996).

99. Alterio, V. *et al.* Carbonic anhydrase inhibitors: X-ray and molecular modeling study for the interaction of a fluorescent antitumor sulfonamide with isozyme II and IX. *J. Am. Chem. Soc.* **128**, 8329–8335 (2006).

100. Cecchi, A. *et al.* Carbonic anhydrase inhibitors: Design of spin-labeled sulfonamides incorporating TEMPO moieties as probes for cytosolic or transmembrane isozymes. *Bioorganic Med. Chem. Lett.* **18**, 3475–3480 (2008).

101. Chambers, J. M. *et al.* Cryptophane xenon-129 nuclear magnetic resonance biosensors targeting human carbonic anhydrase. *J. Am. Chem. Soc.* **131**, 563–569 (2009).

102. Sherwood, L. M., Parris, E. E. & Folkman, J. Tumor Angiogenesis: Therapeutic Implications. *New England Journal of Medicine* **285**, 1182–1186 (1971).

103. Carmeliet, P. & Jain, R. K. Molecular mechanisms and clinical applications of angiogenesis. *Nature* **473**, 298–307 (2011).

104. Simons, M., Gordon, E. & Claesson-Welsh, L. Mechanisms and regulation of endothelial VEGF receptor signalling. *Nature Reviews Molecular Cell Biology* **17**, 611–625 (2016).

105. Alexander, C. M. & Werb, Z. Extracellular Matrix Degradation. in *Cell Biology of Extracellular Matrix* 255–302 (Springer US, 1991). doi:10.1007/978-1-4615-3770-0_9

106. Dolmans, D. E. J. G. J., Fukumura, D. & Jain, R. K. Photodynamic therapy for cancer. *Nat. Rev. Cancer* **3**, 380–387 (2003).

107. Henderson, B. W. & Dougherty, T. J. HOW DOES PHOTODYNAMIC THERAPY WORK? *Photochem. Photobiol.* **55**, 145–157 (1992).

108. Jung, H. S. *et al.* Overcoming the Limits of Hypoxia in Photodynamic Therapy: A Carbonic Anhydrase IX-Targeted Approach. *J. Am. Chem. Soc.* **139**, 7595–7602 (2017).

109. Zhao, W., Wurz, R. P., Peters, J. C. & Fu, G. C. Photoinduced, Copper-Catalyzed Decarboxylative C-N Coupling to Generate Protected Amines: An Alternative to the Curtius Rearrangement. *J. Am. Chem. Soc.* **139**, 12153–12156 (2017).

110. Behnke, N. E., Kielawa, R., Kwon, D.-H., Ess, D. H. & Kürti, L. Direct Primary Amination of Alkylmetals with *NH* -Oxaziridine. *Org. Lett.* **20**, 8064–8068 (2018).

111. *Self-Assembly of a Threaded Molecular Loop*.

112. Bagnacani, V. *et al.* Lower rim guanidinocalix[4]arenes: Macrocyclic nonviral vectors for cell transfection. *Bioconjug. Chem.* **23**, 993–1002 (2012).

113. Dou, Y. *et al.* Reusable cobalt-phthalocyanine in water: Efficient catalytic aerobic oxidative coupling of thiols to construct S-N/S-S bonds. *Green Chem.* **19**, 2491–2495 (2017).

114. Sundriyal, S., Viswanad, B., Ramarao, P., Chakraborti, A. K. & Bharatam, P. V. New PPARγ ligands based on barbituric acid: Virtual screening, synthesis and receptor binding studies. *Bioorganic Med. Chem. Lett.* **18**, 4959–4962 (2008).

115. *Supplementary Information Experimental*. (2013).

116. Nielsen, C. B. *et al.* Synthesis and characterization of water-soluble phenylene-vinylene-based singlet oxygen sensitizers for two-photon excitation. *J. Org. Chem.* **70**, 7065–7079 (2005).

117. Yao, L., Smith, B. T. & Aubé, J. Base-Promoted Reactions of Bridged Ketones and 1,3- and 1,4-Haloalkyl Azides: Competitive Alkylation vs Azidation Reactions of Ketone Enolates. *J. Org. Chem.* **69**, 1720–1722 (2004).

118. Tron, A. *et al.* Photodriven [2]rotaxane-[2]catenane interconversion. *Chem. Commun.* **51**, 2810–2813 (2015).

119. Kabsch, W. <title>\n *XDS*\n</title>. *Acta Crystallogr. Sect. D Biol. Crystallogr.* **66**, 125–132 (2010).

120. Murshudov, G. N. *et al.* REFMAC5 for the refinement of macromolecular crystal structures. *Acta Crystallogr. Sect. D Biol. Crystallogr.* **67**, 355–367 (2011).

121. Lebedev, A. A. *et al.* JLigand: A graphical tool for the CCP4 template-restraint library. *Acta Crystallogr. Sect. D Biol. Crystallogr.* **68**, 431–440 (2012).

122. Emsley, P., Lohkamp, B., Scott, W. G. & Cowtan, K. Features and development of Coot. *Acta Crystallogr. Sect. D Biol. Crystallogr.* **66**, 486–501 (2010).

123. Langer, G., Cohen, S. X., Lamzin, V. S. & Perrakis, A. Automated macromolecular model building for X-ray crystallography using ARP/wARP version 7. *Nat. Protoc.* **3**, 1171–1179 (2008).

124. Pettersen, E. F. *et al.* UCSF Chimera - A visualization system for exploratory research and analysis. *J. Comput. Chem.* **25**, 1605–1612 (2004).

Chapter 3

Calixarene-based inhibitors for carbonic anhydrases

3.1 Introduction

3.1.1 General: multivalent effect

As already said in **Chapter1**, proteins are the actual effector machines in cells and more in general in biological systems. They, in fact, are expressed to carry out several physiological functions such as structural, communicative or catalytic functions. In doing this, proteins interact with small molecules or other proteins via non-covalent bonds (ion-dipole, electrostatic, CH-π interactions and hydrogen bonds as well as hydrophobic effects, π-π stacking and van der Waals forces) to establish the formation of complexes[1], which trigger the activation response pathway in the cell. In order to increase the efficiency of binding with biological counterparts, Nature did not limit to use single interactions, but developed the so-called "multivalency strategy" (**Figure 3.1.1.1**) to make more tight bonds exploiting multiple interactions. A multivalency effect essentially occurs when an entity is capable to bind another entity via simultaneous identical interactions. This results in the formation of multiple identical ligand-protein or protein-protein complexes (host-guest complexes) in "1:1" stoichiometry or higher such as in large intermolecular aggregates. The driving advantage of multivalent effect, which explains why it has been over ages a largely-employed strategy by Nature, is that the final total binding energy is higher than the arithmetic sum of the energies of the single monovalent events. For the high number of factors we have to care about in the multivalent process it is rather complicated to describe it. First of all, all the binding units are located on a single platform and the initial intramolecular interactions are in competition with intermolecular ones, which should lead to multivalent complexes. Obviously, if a stereo-electronic match is observed between binding units on guest species and those on host species, the multivalent complexes formation is possible due to the subsequent enthalpic stabilization. As we well know, any binding process is not driven just by negative enthalpy (high absolute value), but also by positive entropy.

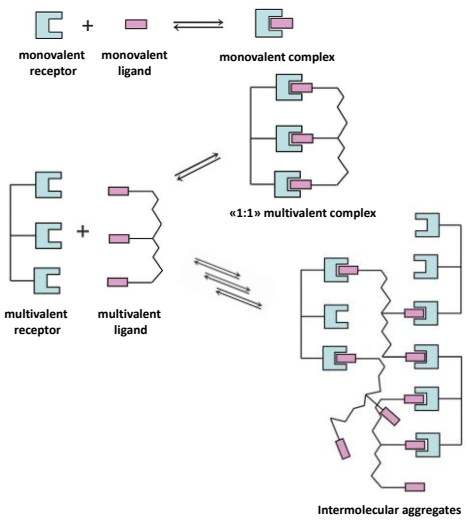

Figure 3.1.1.1. Schematic representation of multivalent bindings. Figure taken from reference[2].

Unfortunately, in almost all binding processes the final complex is usually more rigid than pre-binding states and this leads to a loss of conformation freedom in the ligand or protein (positive entropy), which goes against the overall process. To counter this disadvantageous phenomenon, Nature developed pre-organized and rigid ligands simultaneously able to lower the entropic loss and to increase binding and specificity during the binding.

The most common simple model to explain multivalent effect is the one proposed by Jencks[3]. The binding Gibbs energy for a multivalent system (ΔG°_{multi}) is defined as

$$\Delta G^\circ_{multi} = n\Delta G^\circ_{mono} + \Delta G^\circ_{interaction}$$

namely as the sum of the binding energies of the single monovalent binding (ΔG°_{mono}) and of the factor $\Delta G^\circ_{interaction}$ which takes into account the balance of unfavourable and favourable effects of tethering.

Interesting ways to define the goodness of multivalent effect in a particular binding process are the relative potency rp and the enhancement factor β, which can be employed respectively when we are dealing with half-maximal inhibitory concentrations (IC_{50}) or binding/dissociation constants.

The relative potency

$$rp = \frac{IC_{50}^{mono}}{IC_{50}^{multi}}$$

is calculated as the ratio between the IC_{50} value of the monovalent and of the multivalent entity, respectively.

The enhancement factor

$$\beta = \frac{K_{multi}}{K_{mono}}$$

is defined, instead, as the ratio between the binding constant related to the multivalent binding (K_{multi}) of a multivalent entity and the binding constant related to the monovalent binding (K_{mono}) of a monovalent entity to the same multivalent ligand[1].

The same rp and β factors can be expressed as normalized values rp/n and β/n, with n the valency of the complex. These new factors, being valency independent, are useful tools for direct comparison among multivalent ligands with different features, such as topology, valency and linker. A negative multivalent effect occurs when β/n and rp/n are <<1, meaning that the ligating unit shows less affinity for the receptor when coupled onto that multivalent scaffold, while a positive multivalent effect occurs when β/n and rp/n are >>1, where the multivalent ligand is more efficient than the monovalent correspondent system.

In biologic systems, several are the examples, in which multivalent effect is effectively exploited[4–7]. Cadherins (**Figure 3.1.1.2**) are integral proteins involved in homophilic trans-binding with other cells. This process (at the basis of adhesion among cells in organ and tissues)

passes through the X-dimerization of extracellular domains in presence of calcium ions to rearrange into trans dimer[8–10]. Once formed these trans-dimers tend to pair each other in a cis fashion to make strong linking structures. Considering the high K_d (mM scale) for either trans or cis single bonds, the formation of these structures is clearly stabilized by multivalency[11].

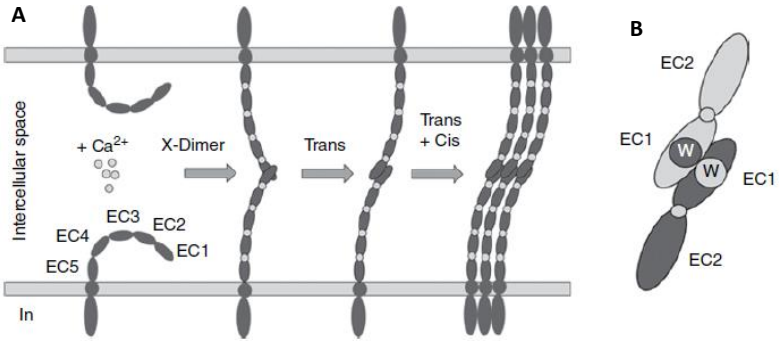

Figure 3.1.1.2. A) Formation of homophilic cadherin interactions in physiological pathways; **B**) Representation of EC1-EC1 domain recognition via tryptophan pairing. Figure adapted from reference[12].

Another example of multivalency in Biology is the selectin-tetrasaccharide sialyl Lewis X (sLeX) interaction observed in leukocyte–endothelial cell recognition during inflammation (**Figure 3.1.1.3**)[13,14]. Selectins are membrane-bound protrusions specialized in coordinating C-type lectins and are localized onto either leukocytes (L-selectin) or activated endothelial cells (P- and E-selectin). Individual selectin–sLeX interactions are characterized by low affinity (high µM-mM range[15]), but multiple interactions allow the extravasation of leukocytes from the bloodstream via a strong multivalent binding.

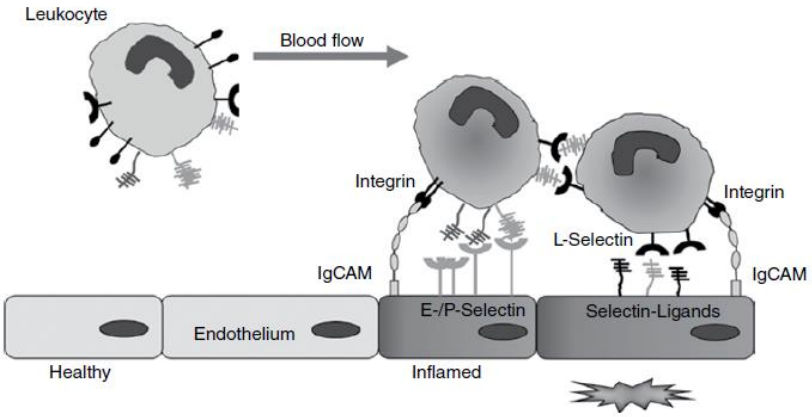

Figure 3.1.1.3. Leukocyte recruitment by inflamed endothelium cells. Upon blockage of leukocytes via Integrin/IgCAM interaction, multivalent interactions between selectins and sLeX trigger leukocytes extravasation. Figure adapted from reference[12].

3.1.2 Calix[n]arenes: features and uses in biology

Calix[n]arenes, together with, cucurbiturils, cyclodextrins, crown ethers and cyclopeptides, are macrocycles largely employed in supramolecular chemistry. Their easy functionalization and synthesis (even in large scale) along with the possibility of blocking them in different isomers make these molecules suitable tools for several applications[16]. Their standard hydrophobic scaffolds have been historically used for selective complexation of cations, but over times experimental studies on their functionalization with polar moieties moved the application field to biorecognition, biosensing, biotechnology and drug discovery thanks to the improved solubility properties in water.

The term calixarene derives from “calix”, because of the shape of the macrocycle which resembles to the Greek vase called calix crater (**Figure 3.1.2.1**), and “arene”, due to the aromatic composition of the scaffold.

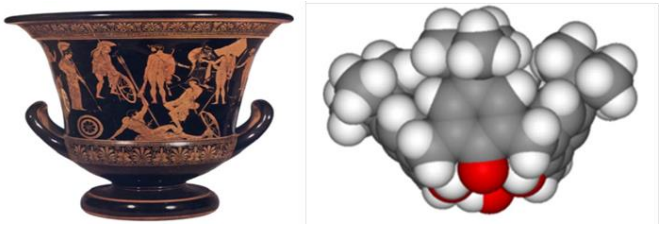

Figure 3.1.2.1. The CPK-model of the p-tert-butylcalix[4]arene and the calix krater from which its name derives.

The synthesis (**Figure 3.1.2.2**) essentially is a one-pot condensation between phenol and formaldehyde under basic conditions[17], which has been scaled up even to kilo-scale. Macrocycles with different number of phenolic groups and hence with different valency and size can be selected varying experimental parameters, such as the solvent, the base and the temperature. In particular, the odd-numbered calix[n]arenes (n = 5,7,9) are less affordable than the even-numbered ones (n = 4,6,8), which are obtained in much higher yields.

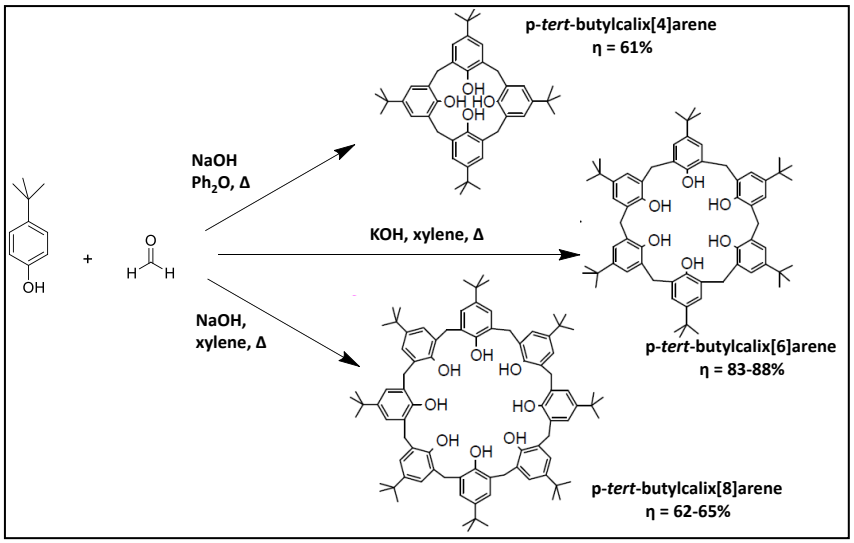

Figure 3.1.2.2. Synthesis of even-numbered calix[n]arenes.

In addition, calixarenes differentiate from other macrocycles for their versatile conformational properties. In fact, calix[n]arenes (n = 4,5,6,8) with methyl or ethyl groups at lower rim are conformationally mobile and in solution present a mixture of conformers, which can interconvert each other, whereas calix[4]arenes with alkyl chains longer than the ethyl group at lower rim can be blocked in 4 different conformations: 1,3-alternate, partial cone, cone and 1,2-alternate (**Figure 3.1.2.3b**)[18,19]. In the optic of multivalent ligands the possibility to have scaffolds able to orient active units towards different directions is an interesting way to study how simultaneous binding affects recognition of biological counterpart. In doing this, sometimes a rigid and preorganized structure increases the binding efficiency due to the less loss of degrees of freedom, whereas sometimes, instead, mobile conformation can help in adapting the ligand itself to the receptor geometry.

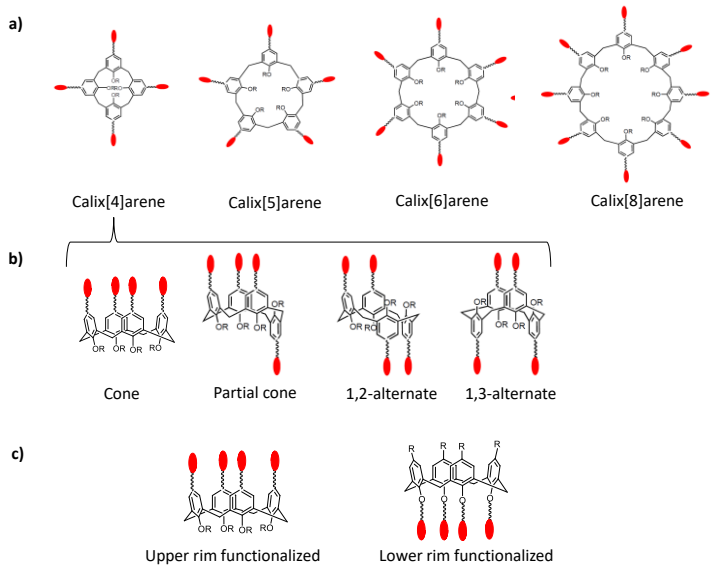

Figure 3.1.2.3. Schematic representation of the a) valencies, b) geometries and c) functionalizations of calix[n]arenes.

Eventually, calixarenes are characterized by two different rims: the lower rim, identified by hydroxyl groups, and the upper rim, determined by the para positions of the phenolic rings. A large variety of groups can be added to these two rims directly or via linker in a selective way (**Figure 3.1.2.3c**). The length, the nature and the mobility of the spacer must be opportunely modulated, since either take active units at proper distance or participate to the binding. Due to their numerous properties, calix[n]arenes allow to synthesize a library with different conformations, size and type of functionalization exploring a wide chemical space, which could help us more easily find the perfect ligand-protein match.

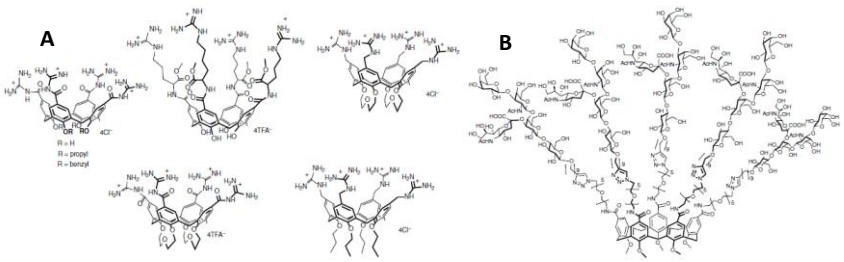

Figure 3.1.2.4. A) guanidine calixarenes for Shaker potassium channels stoppering and p53 stabilization; **B**) glycocalix[5]arene for multivalent inhibition of Cholera toxin.

This versatility could be exploited towards proteins to increase efficiency and specificity of binding phenomena allowing us to modulate or even stop pathological pathways. Several are the examples present in literature about the employment of functionalized calixarenes as multivalent ligands. A library of tetraguanidinium cone calix[4]arenes (**Figure 3.1.2.4A**) was synthesized to inhibit voltage-dependent potassium channels[20], mainly Shaker potassium channels, which are involved in different pathologies. It has been demonstrated that some

compounds can reach even an inhibition constant of 50μM, whereas the monomeric analogue is not active. The mechanism of action is still under investigation, but it is clear that it is supported by a multivalent effect. Similar compounds were used also in the stabilization of p53 tetramer required for activation of repair machinery and apoptosis process[21]. In fact, R337H mutation substitutes a permanently positive charged arginine with a histidine, which at physiological pH is half protonated and so physiological interactions with E336 and E339 are obviously weakened. Some of the compounds showed in **Figure 3.1.2.4A** have been shown selective to the mutated form and efficient binders at 400 μM. Supporting molecular studies demonstrated that guanidine calixarenes can bind to both sides of the protein complex via multiple Arg-Glu interactions, which implies that multivalency is exploited[22]. The best multivalent effect has been obtained with glycocalixarenes for the Cholera toxin (CT) inhibition[23]. CT is characterized by AB_5 structure, in which B units present epitopes selective to pentasaccharide GM_{10}, localized on cell surface. In order to stop the relative infection, in Sansone's laboratories was developed calix[5]arene derivative decorated at the upper rim with 5 units of GM10 in order to mimic the B_5 substructure of CT (**Figure 3.1.2.4B**). Through ELISA tests was determined an IC50=450pM and in comparison to the monovalent molecule, an amazing multivalent effect of 20000.

3.1.3 Multivalency in CA inhibition

As already largely discussed in **Chapter 2**, a wide plethora of small molecules with different scaffolds, tails and heads have been proposed and studied for CA inhibition. They are designed to make contacts inside the catalytic active site of the enzyme forming a 1:1 complex. However, as more widely anticipated previously, in recent years some research groups started to explore the possibility of exploiting multivalent ligands also for the inhibition of enzymes although these are mostly characterized by the presence of a single active site. The idea is to obtain an enhancement of the inhibition activity on the basis of a binding-rebinding process favoured by an increased local concentration of the ligand. In this context one of the most important class of enzymes tested for the inhibition by multimeric molecules is that of glycosidases. Towards them, some particular scaffolds showed to be able to exploit multivalency (even reaching rp/n=4800), in which the multiple exposition of the same active unit on a preorganized scaffold significantly increases dramatically their affinity for the biological counterpart with respect to the monovalent analogue.

Moreover, in Nature some CA isoforms are present in a multimeric assembly (e.g. dimeric VchCAβ). Therefore, towards these particular cases, multivalent ligands could put into play a real multivalent effect as that possible with oligomeric carbohydrate recognition proteins (e.g. lectins). If many examples are indeed known of high-efficiency multivalent ligands for non-enzymatic proteins, only a few preliminary examples are reported towards enzymatic proteins. In the attempts of multivalent inhibition of CAs, some preliminary studies have been carried out exploiting well-known multimeric scaffolds. Up to now, in this avant-garde idea PAMAM dendrimers and fullerenes were tested.

In Carta's work[24], has been shown how PAMAM derivatives can be very versatile scaffolds for the development of multivalent inhibition of CAs. Three generations of PAMAM derivatives were synthesized, which expose up to 32 benzenesolfonamide units *per* PAMAM core. Besides

their exceptional inhibition properties towards hCAI, hCAII, hCAIX and hCAXII, they have been shown as potent multivalent inhibitors. In particular, PAMAM G3 (**Figure 3.1.3.1A**) towards hCAII showed a relative potency normalized to the number of sulphonamide units (rp/n) of 285.7 nM, which shows a significant multivalent effect. Some of these derivatives, moreover, showed interesting properties in lowering intraocular pressure in glaucomatous animal models by inhibiting the hCAII and hCAXII enzymes present within the eye.

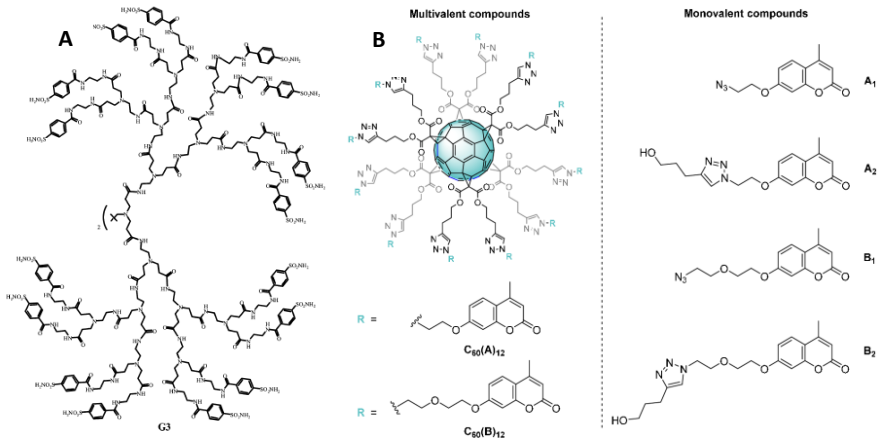

Figure 3.1.3.1. A) PAMAM G3 derivative functionalized with benzenesolfonamides, figure adapted from reference[24], **B**) fullerene derivatives functionalized with coumarins, figure adapted from reference[25].

Since fullerene-based multivalent molecules were shown in the past to be very efficient multivalent inhibitors towards α-mannosidases, Abellan-Flos and al.[25] tried to use multivalent coumarin-functionalized fullerenes as potential multivalent inhibitors towards CAs. They synthesized and studied different C60 fullerenes, in which twelve coumarin units were grafted on them by different spacers (**Figure 3.1.3.1B**). What turned out is that these structures are able to inhibit very efficiently CAs (in particular the extracellular ones), but without exploiting a clear significant multivalent effect.

Supuran and co-workers[26], as well, tried to decorate AuNPs with benzenesolfonamide moieties, but also in this case, despite their high efficiencies, they did not show a significant multivalent effect. Probably the high bulk of these systems and the crucial nature of spacers are responsible for a non-exploitable multivalent effect.

3.2 Aim of the work

As described in **Chapter 2**, compounds **4b** and **4c** are very efficient inhibitors of human CAI, CAII and CAIX with K_i in the nanomolar range, even slightly better than AAZ. Starting from this evidence, we thought that structures exposing multiple copies of these derivatives might have been interesting devices for further increasing the inhibition potency. Since made of multiple active units, if they were able either to bind simultaneously different molecules of enzymes or to put into play a binding-rebinding process, they could increase dramatically the affinity for those showing a multivalent effect, which would amplify the inhibition activity. Recently, in the group where this doctoral work has been performed and in collaboration with Supuran's group,

the use of calix[n]arenes as scaffold was proposed to generate a new class of potential CA inhibitors. Calixarenes, in fact, gave in past very interesting results when used to build multivalent ligands for non-enzymatic proteins like, for instance, lectins. For the design of proper calix[n]arene derivatives, the work started with the analysis of the XRD structure of the complex between hCAII and a benzensulfonamide containing ^{129}Xe-cryptophane ligand reported by Chamber's and co-workers[27] (**Figure 3.2.1**). The most relevant information for us resulted the length of the linker between the bulky macrocycle and sulfonamide head. In fact it can be seen how a spacer of 7 atoms between benzosulfonamide unit and cryptophane moiety is suitable to outdistance, in the bound state, the latter one enough away from enzyme walls. In the case of compounds **4b** and **4c**, the number of atoms between the phenolic benzene ring, considered as a model of the single aromatic unit in the calixarene scaffold, and benzosulfonamide is indeed 7 and 6, respectively. This, along with the low K_d (20 – 100 nM) observed for the ^{129}Xe-cryptophane ligand, seems to rule out repulsive interactions due to steric hindrance and turns this inhibitor a proper model for our purposes. Moreover, it represents an example of host-guest complex targeting the CA, an option that could result exploitable with calixarenes not only for sensor applications, but also to increase inhibition efficiency by inclusion in or external contact with the macrocyclic cavity of a complementary enzyme residue like a lipophilic side-chain.

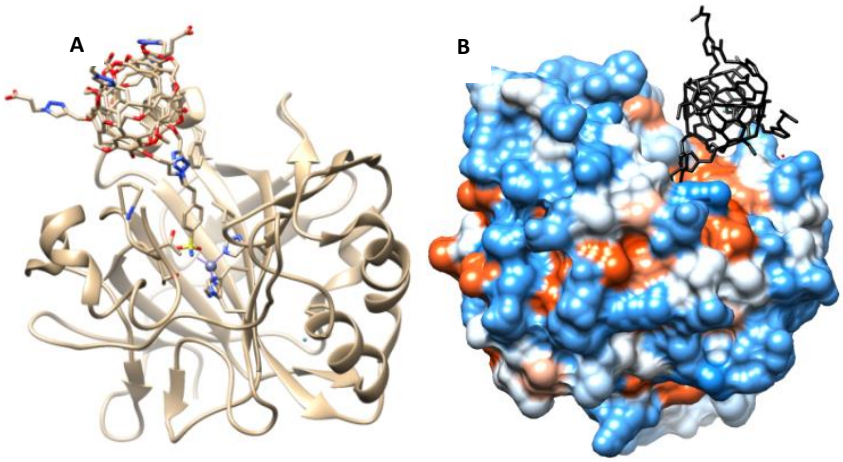

Figure 3.2.1. ^{129}Xe-cryptophane/hCAII (PDB code: 3CYU)[27] in ribbon (**A**) and hydrophobic surface representation (**B**). In **A** carbon atoms are white, oxygen atoms are red and nitrogen atoms are blue, whereas in **B** blue patches are polar side chains and red patches are apolar side chains (in black, ^{129}Xe-cryptophane). Figures were elaborated with Chimera software.

In this context, some calix[4]- and -[6]arenes functionalized with ammonium and benzensulfonamide moieties (**Figure 3.2.2**) had been already synthesized in our laboratory and accordingly to the first collected inhibition data at University of Florence, they all showed interesting efficiency and selectivity as inhibitors towards MgCA (previously seen in Chapter 2).

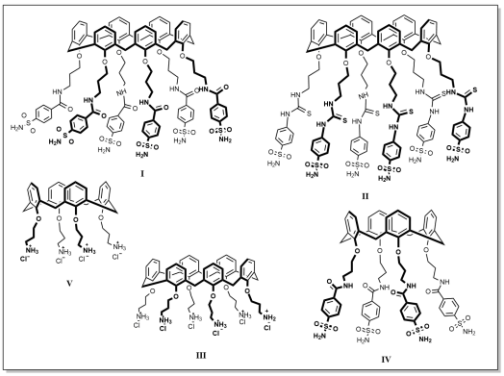

Figure 3.2.2. Calix[4]- and –[6]arene-based inhibitors already present in our laboratories.

The research was further developed during this doctoral work. Other lower rim functionalized calix[4]arenes (**Figure 3.2.3**), characterized by a variable number of active units and different conformational features, were designed to more deeply investigate the possible occurring of a multivalent effect and the contribution of the macrocycle in the binding. Moreover, upper-rim monofunctionalized calix[4]arenes were prepared to possibly exploit the presence of a preorganized cavity for the inclusion of hydrophobic residues in order to further stabilize the whole complex.

Starting from lower-rim functionalization, we decided to synthesize mono- and di-functionalized calix[4]arenes with ammonium/benzenesulfonamide moieties in cone conformation keeping the propyl spacer used for previous calix[4]- and -[6]arenes (**Figure 3.2.2**), meanwhile for upper-rim functionalization a Gaba spacer was used to connect the active unit to the calixarene scaffold. For a possible simultaneous interaction with more than a single enzyme unit, we decided to synthesize calix[4]arenes in 1,3-alternated conformation, which, projecting the active units in opposite directions, have the right geometry for simultaneous multiple binding.

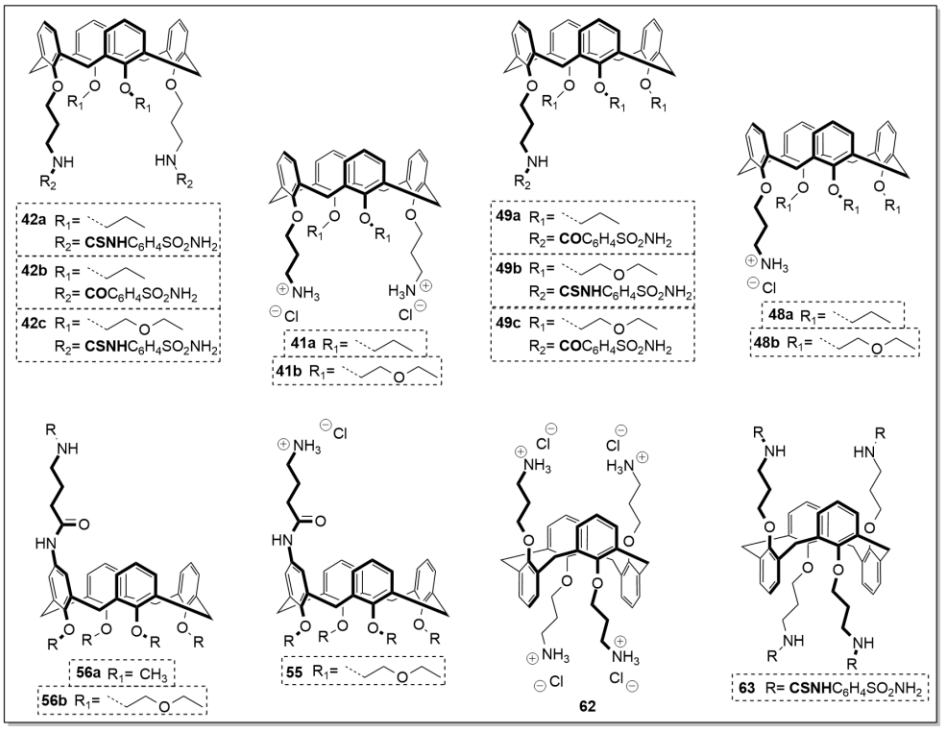

Figure 3.2.3. Library of partially functionalized calix[4]arenes, synthesized in our laboratories, bearing either sulphonamide or ammonium moieties.

3.3 Results and discussion

3.3.1 Synthesis of the lower-rim 26,28-difunctionalized calixarenes

The synthesis begun with the preparation of the calixarene scaffold **36** subsequently detertbutylated to **37** following the well established procedures since long time reported in literature[17]. To obtain the lower-rim difunctionalized ligands (**Figure 3.3.1.1**), compounds **38a-b** were synthesized using the respective alkylating agent and K_2CO_3 as base, which, as well known, determines the formation of the diametral difunctionalized derivatives. The choice of the two different type of chains is to obtain final ligands with a different degree of polarity.

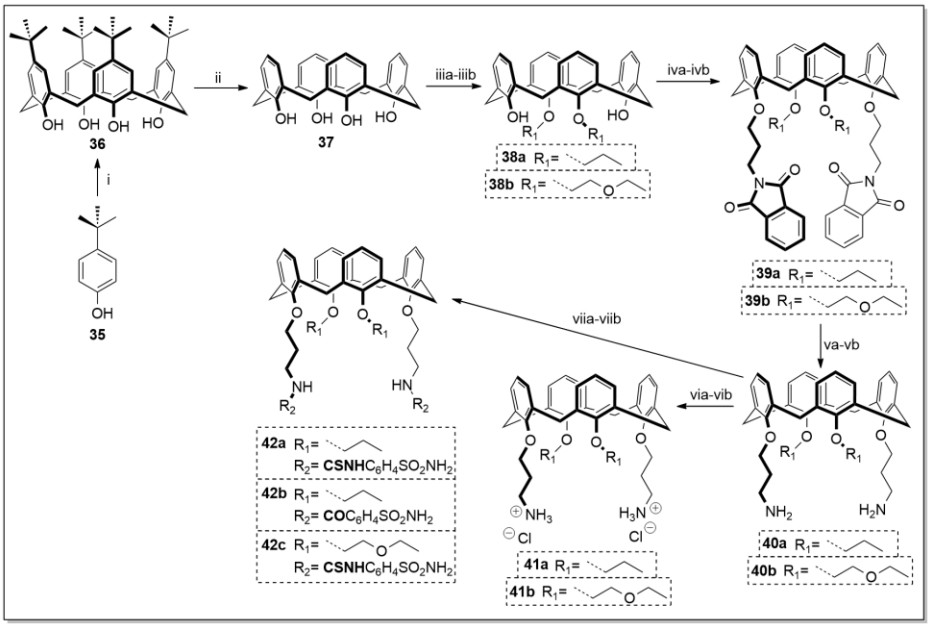

Figure 3.3.1.1. Synthesis of lower rim 26,28-difunctionalized derivatives. *Reactions conditions*: i) p-tert-butylphenol (1eq), 37% formaldehyde aqueous solution (1.3 eq), 10M NaOH (0.1 eq), 120 °C, 1h; diphenyl ether, reflux, 6 h (60% yield as complex 1:1 toluene: calixarene); ii) phenol (1.2 eq), $AlCl_3$ (5.5 eq), toluene, rt, 1h (71% yield); iiia) K_2CO_3 (4.2 eq), 3-iodopropane (4.2 eq), dry ACN, reflux, 4 days (99% yield); iiib) K_2CO_3 (4.2 eq), 2-bromo-ethoxyethylether (4.2 eq), KI (1.0 eq), dry ACN, reflux, 2 days (22% yield); iva) 55% NaH (4.0 eq), N-3-bromopropylphthalimide (4.0 eq), dry DMF, rt, 1 day (34% yield); ivb) 55% NaH (4.0 eq), N-3-bromopropylphthalimide (4.0 eq), dry DMF, rt, 15h (32% yield); va) $NH_2NH_2 \cdot H_2O$ (20.1 eq), abs EtOH, reflux, 15h (99% yield); vb) $NH_2NH_2 \cdot H_2O$ (20.3 eq), abs EtOH, reflux, 1 day (87% yield); via-b) 1N HCl (1 ml), MeOH (99% yield); viia) NEt_3 (9.7 eq), 4-isothiocyanatebenzensolfonamide (2.1 eq), dry DMF/dry DCM, 1 night, rt (91% yield); viib) 4-sulfamoylbenzoic acid (2.3 eq x 2), DIPEA (5.2 eq x 2), EDC (2.5 eq x 2), dry DMF, T = 80 °C, rampe time = 3 minutes, P = 200 psi, potency = 200 W, hold time = 2 h (8% yield); viic) NEt_3 (3 drops), 4-isothiocyanatebenzensolfonamide (2.2 eq), dry DMF/dry DCM, 1 night, rt (23% yield).

For compound **38a**, yield is quantitative, whereas for compound **38b** yield is much lower (22%) because of low reactivity of alkylating agent 2-bromo-ethoxyethylether. Even repeating the reaction in presence of KI as catalyst, a mixture of mono- and di-functionalized calix[4]arene was obtained, but fortunately, the two regioisomers could be easily purified either by chromatography column or repetitive recrystallization from DCM/MeOH. In ^{1}H-NMR spectrum of compound **38b** the presence of a singlet at 7.86 ppm related to 26,28-OH and the two doublets at 4.46 and 3.80 ppm related to methylene bridges in classical cone rigid 26,28-disubstituted calix[4]arene were considered diagnostic for the molecule. Compounds **39a**-**b**, **40a**-**b** and **41ab** were synthesized accordingly to the protocols used for the monomeric analogues **13**, **14** and **15a** (see **Chapter 2**).

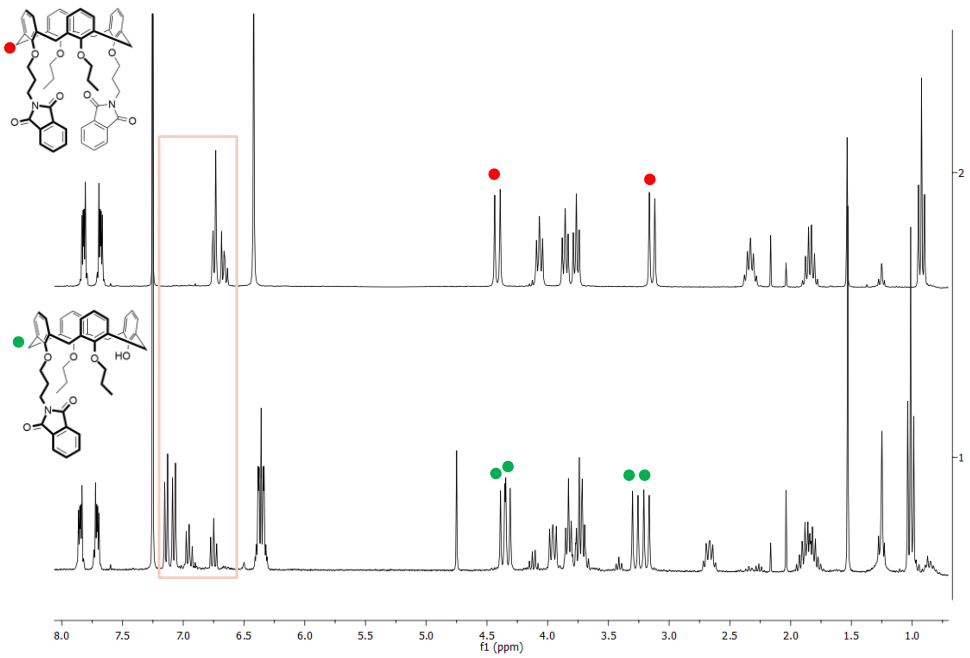

Figure 3.3.1.2. ^{1}H NMR ($CDCl_3$, 300MHz, 298K) spectra of compound **39a** (**2**) and monofunctionalized analogue (**1**).

In the synthesis of compound **39a** also its monofunctionalized precursor was isolated in 19% yield. As it can be seen in **Figure 3.3.1.2**, ^{1}H-NMR spectrum reflects the absence in the molecule of a C_2 axis of symmetry due to the missing of a phthalimido containing arm. In fact, if in the difunctionalized compound axial protons of methylene bridges are all chemically equivalent as the equatorial ones, in the monofunctionalized derivative they are pairwise equal because of the different chemical space. The same effect is seen for the aromatic protons as highlighted in the pink box in **Figure 3.3.1.2**.

From protected intermediates **39a**-**b** the corresponding diamino **40a**-**b** were easily obtained by removal of phtalimido groups. These were in turn transformed in the ammonium containing ligands **41a**-**b** by simple treatment with 1N HCl in methanol and in the two ligands **42a**,**c** by condensation with 4-isothiocyanatebenzensolfonamide. On the contrary, the reaction of both with 4-sulfamoylbenzoic acid to connect the benzensulfonamide units to the calixarene through an amide bond resulted unexpectedly difficult. Doing, in fact, the coupling, as previously done for compound **4c**, the target molecule **42b** was not isolated, obtaining only the monofunctionalized one in 20% yield. Then the reaction was repeated in a microwave reactor, and just after two microwave cycle at 80 °C (2 h each), although in a small amount, compound **42b** was finally obtained in 8% yield.

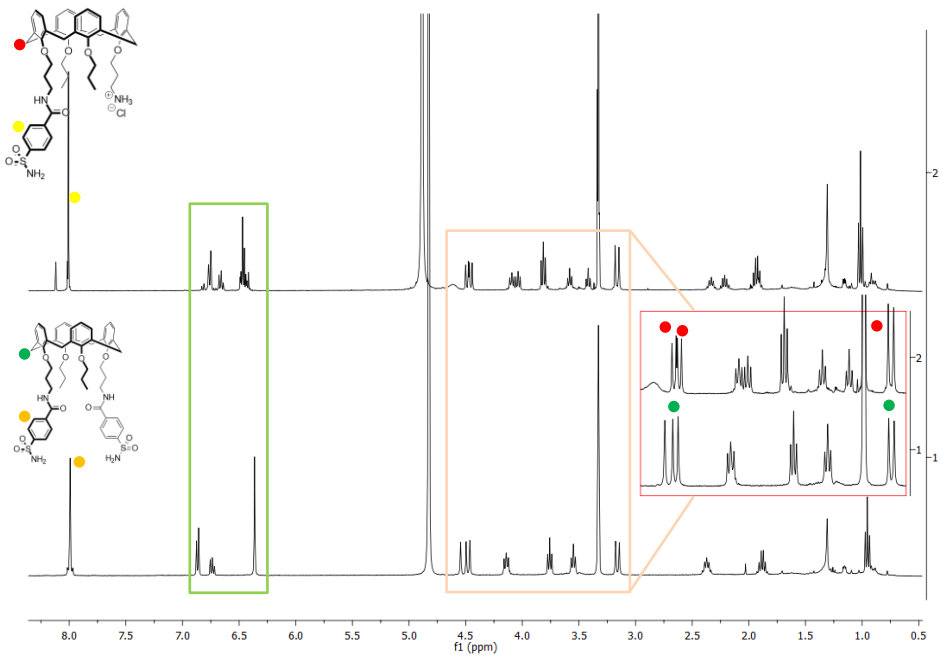

Figure 3.3.1.3. ^{1}H NMR (MeOD, 400MHz, 298K) spectra of (**1**) compound **42b** and (**2**) the monofunctionalized anologue.

In the ^{1}H NMR spectrum (**Figure 3.3.1.3-2**) the signal at 7.98 ppm related to protons of benzenesulfonamide ring was considered diagnostic for compound **42b**. The identification of monofunctionalized intermediate was driven by integration of protons of benzenesolfonamide ring and by the desymmetrization observed both in bridge protons and in propylic arm, which resembles that observed for compound **39a**.

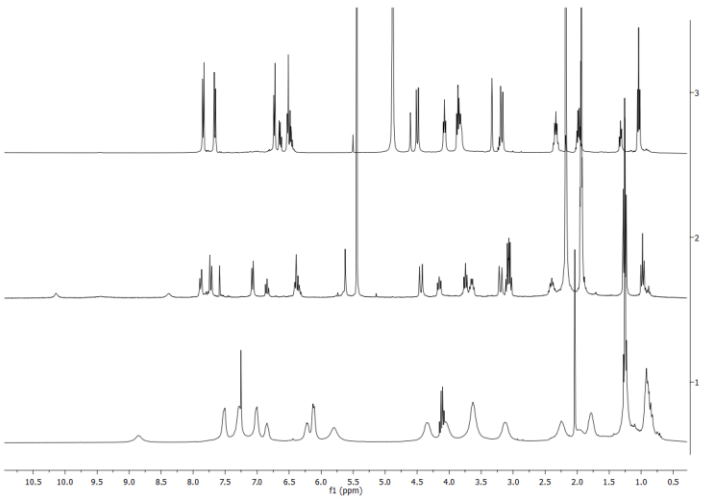

Figure 3.3.1.4. ^{1}H-NMR spectra (400 MHz, 298K) of compound **42c**, respectively in (**1**) $CDCl_3$, (**2**) CD_3CN and MeOD-d4 (**3**).

In **Figure 3.3.1.4** it can be observed that disulfonamide calix[4]arene **42c** aggregates in apolar solvents, in fact in respective ^{1}H-NMR spectrum in $CDCl_3$ all signals are broad as typically observed upon aggregation phenomena. The presence of groups giving hydrogen bonding can determine for this derivative intermolecular interactions.

3.3.2 Synthesis of the lower-rim monofunctionalized calixarenes

The synthesis of lower-rim monofunctionalized calix[4]arenes was realized following the strategy reported in **Figure 3.3.2.1**. going through the key monohydroxy compounds **45a**,**b**. For the synthesis of **45b,** it was carried out a direct trialkylation on **37** using BaO, $Ba(OH)_2 \cdot 8H_2O$ as bases and 2-bromo-ethoxyethylether, as alkylating agent. A mixture of triprotected and tetraprotected compounds was actually obtained after purification. However, this did not turn out as a problem since the tetrafunctionalized compound is totally unreactive in the subsequent step, after which was then easily separated from the desired product. The same direct protocol with 1-iodopropane has led to a mixture of unreacted compound **37**, monofunctionalized and difunctionalized derivatives. Even extending the reaction time or rising up the temperature, the target molecule **45a** was not obtained. For this reason, we decided to use a monobenzylation/debenzylation strategy, which consisted, in sequence, in the introduction of a benzyl group to protect a single hydroxyl group, functionalization of free OHs with iodopropane and removal by hydrogenation of benzyl unit. In step **i**, first of this sequence, (**Figure 3.3.2.1**) different bases were tested such as CsF (1.2 eq), K_2CO_3 (0.5 eq) and MeONa (1.2 eq). Differently from CsF and K_2CO_3, which gave lower yield of the desired product or crudes more difficult to purify, MeONa gave a crude with just compound **36** and **43**, which were easy separated through a percolation in toluene/Hex 7:3 with isolation of the monobenzylated calixarene **43** and complete recovery of unreacted compound **36**. The successful outcome of the reaction was assessed by ^{1}H-NMR observing in the spectrum the singlets at 9.55 and 9.20 ppm related to one and two free phenolic OH, respectively. These were classically alkylated with 1-iodopropane using NaH as base to obtain full functionalization and cone geometry (**44a**). Finally tripropoxy-calix[4]arene **45a** was obtained by catalytic hydrogenation in presence of Pd/C, monitoring in the ^{1}H-NMR spectrum the disappearing of signal at 4.92 ppm related to benzylic methylene and the signals related to benzyl group at 7.48 and 6.79 ppm.

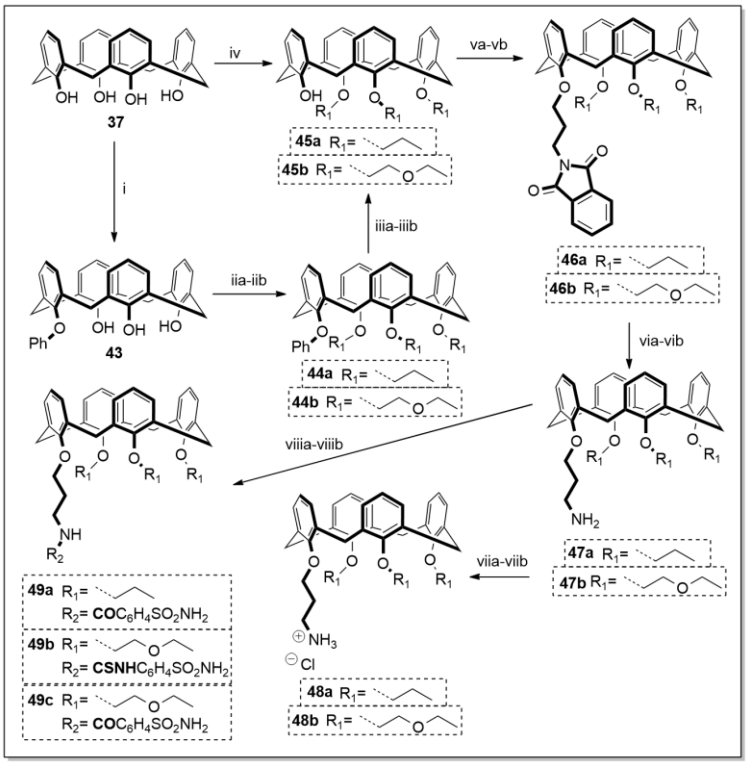

Figure 3.3.2.1. Synthesis of lower-rim monofunctionalized derivatives. *Reactions conditions*: i) NaOMe (1.2 eq), benzyl bromide (2.4 eq), dry ACN, reflux, 1 night (65% yield); iia) 55% NaH (5.0 eq), 1-iodopropane (5.0 eq), dry DMF, rt, 1 night (62% yield); iib) 55% NaH (5.0 eq), 2-bromo-ethoxyethylether (5.0 eq), dry DMF, rt, 5h (97% yield); iiia) H_2 (3.0 bar), 10% Pd/C (catalytic amount), AcOEt, rt, on (83% yield); iiib) H_2 (2.5 bar), 10% Pd/C (catalytic amount), AcOEt/EtOH, rt, 15h (91% yield); iv) BaO (4.7 eq), $Ba(OH)_2 \cdot 8H_2O$ (3.0 eq), 2-bromo-ethoxyethylether (20.0 eq), dry DMF, 80°C, on (62% yield); va) 55% NaH (2.3 eq), N-3-bromopropylphthalimide (2.3 eq), dry DMF, rt, 15h (36% yield); vb) 55% NaH (1.8 eq), NaI (catalytic amount), N-3-bromopropylphthalimide (1.8 eq), dry DMF, 80 °C, 2 days (75% yield); via) $NH_2NH_2 \cdot H_2O$ (15.3 eq), abs EtOH, reflux, 15h (54% yield); vib) $NH_2NH_2 \cdot H_2O$ (20.0 eq), abs EtOH, reflux, 15h (95% yield); viia-b) 1N HCl (1 ml), MeOH (99% yield); viiia) 4-sulfamoylbenzoic acid (9.7 eq), DIPEA (2.5 eq), EDC (11.9 eq), dry DMF, rt, on (41% yield); viiib) 4-isothiocyanatebenzensolfonamide (4.0 eq), dry DMF/dry DCM, 1 day, rt (78% yield); viiic) 4-sulfamoylbenzoic acid (2.3 eq x 2), DIPEA (5.1 eq x 2), EDC (2.4 eq x 2), dry DMF, T = 80°C, rampe time = 3 minutes, P = 200 psi, potency = 200 W, hold time = 1 h 30 minutes (48% yield).

The same protocol was tested also to obtain the triethoxyethyl derivative **45b** as well, and thanks to the good yields and the absence of the tetra functionalized macrocycle as impurity it represents indeed a feasible alternative to direct trifunctionalization. The synthesis of the subsequent compounds **46a**-**b, 47a**-**b**, **48a**-**b** and **49a-c** is not discussed since realized following the same procedures used for monomers **2**, **3** and-**4a**-**c**.

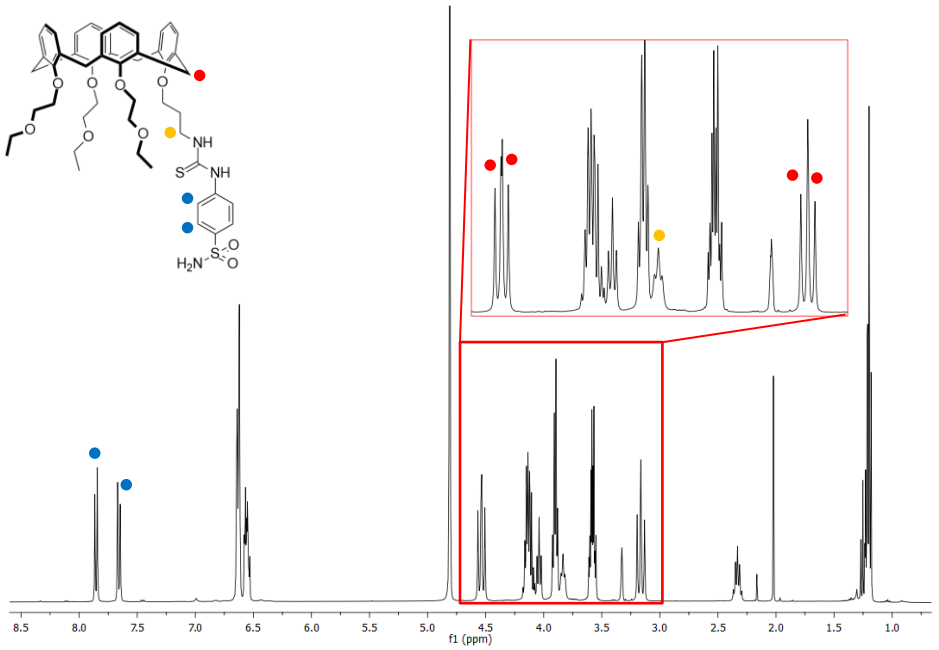

Figure 3.3.2.2. ^{1}H NMR (MeOD-d_4, 400MHz, 298K) spectrum of compound **49b**.

As example, ^{1}H NMR spectrum of final ligand **49b** is reported in **Figure 3.3.2.2**. Here, besides all proton signals of chains in the range 4.5-1.0 ppm, are present four distinct doublets for methylene bridges (typical for monosubstituted compounds) and at 7.86 and 7.66 ppm the classical pattern of the para-disubstituted aromatic ring related to the benzenesulfonamide moiety linked to calixarene scaffold. Comparing ^{1}H NMR spectrum of compound **47b** with this one, it has been possible to assign the broad triplet at 3.83 ppm to methylene group directly attached to nitrogen atom, which shifts from 3.06 to 3.83 ppm thanks to electron-withdraw property of thioureido group.

3.3.3 Synthesis of the upper-rim monofunctionalized calixarenes

Compounds **55** and **56b** (**Figure 3.3.3.1**) bearing the active unit at the upper rim were designed to have potential CA ligands with a relatively preorganized cavity oriented towards the active site and available for possible additional interactions with the border of the funnel. For them, we decided to introduce ethoxyethyl chains at the lower rim to improve the solubility in aqueous environment. Their conformationally mobile analogues **54** and **56a** were prepared in order to evidence possible advantages due either to the presence of the cavity or, in alternative, to the possibility for the ligand of conformational rearrangements during the complexation process.

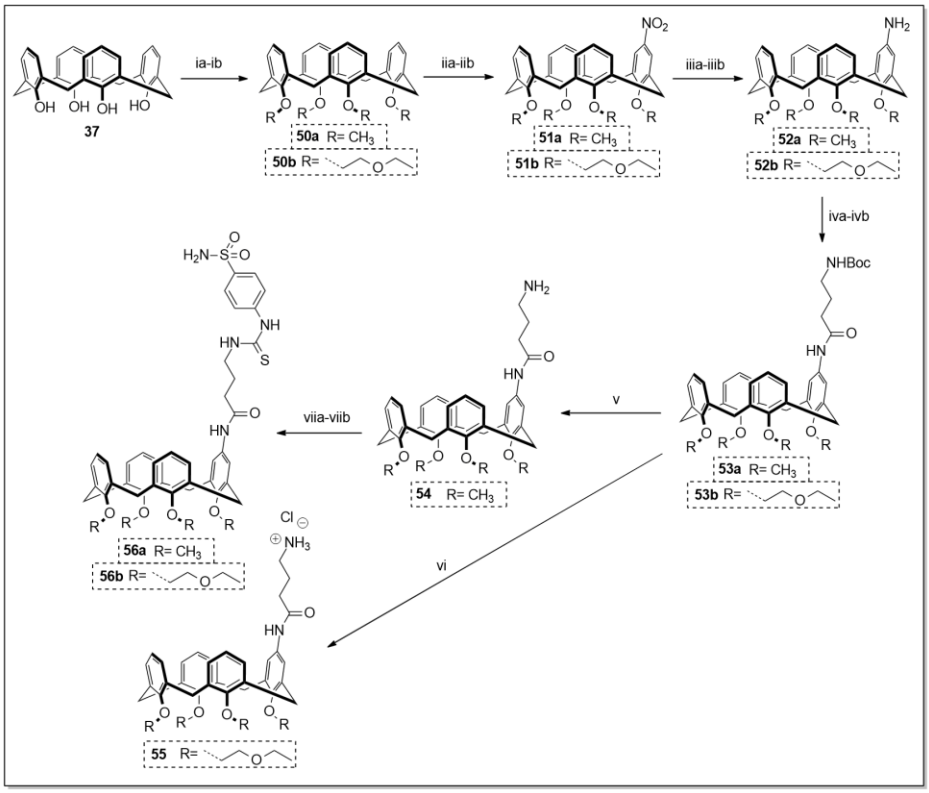

Figure 3.3.3.1. Synthesis of upper-rim monofunctionalized derivatives **51**-**56**. Reactions conditions: ia) 55% NaH (7.0 eq), CH_3I (7.0 eq), dry DMF, rt, 3 days (79% yield); ib) 55% NaH (4.2 eq), 2-bromo-ethoxyethylether (4.0 eq), dry DMF, 40 °C, 4 days (99% yield); iia) 65% HNO_3 (13.3 eq), glacial CH_3COOH (44.0 eq), DCM, rt, 40 minutes (10% yield); iib) 65% HNO_3 (9.0 eq), glacial CH_3COOH (44.0 eq), DCM, rt, 1 h 30 (16% yield); iiia) $NH_2NH_2 \cdot H_2O$ (19.8 eq), 10% Pd/C (catalytic amount), absolute EtOH, DCM, reflux, on; iiib) $NH_2NH_2 \cdot H_2O$ (10.1 eq), absolute EtOH, reflux, 5 h (90% yield); iva) EDC (1.2 eq), Boc-Gaba-OH (1.1 eq) , dry DMF, rt, 3 days (23% yield); ivb) EDC (1.1 eq), Boc-Gaba-OH (1.0 eq), dry DMF, 50 °C, 15h (26% yield); v) TES (19.7 eq), TFA (39.4 eq), dry DCM, rt, 4 h (72% yield); vi) TES (19.4 eq), TFA (40.2 eq), dry DCM, rt, 15h + EtOH/37%HCl 10:1, 30 minutes (99% yield); viia) DIPEA (5.0 eq), 4-isothiocyanatebenzensolfonamide (1.0 eq), dry DCM/dry DMF, rt, 4 days (26% yield); viib) DIPEA (0.2 eq), 4-isothiocyanatebenzensolfonamide (1.0 eq), dry DMF, rt, 15h (8% yield).

The first step was the full functionalization of the calix[4]arene lower rim with iodomethane or 2-bromo-ethoxyethylether, as alkylating agents, and NaH, as base, in dry DMF. Despite the long reaction time (4-5 days), compounds **50a** and **50b**, respectively, were obtained with high yields (>79%). The complete functionalization of phenolic OHs was confirmed for both compounds by ^{1}H NMR spectra in $CDCl_3$ which show the absence of the singlet related to free phenolic OHs. Differently from compound **50b**, for which is present a single pattern of sharp signals like the two doublets at 4.52 and 3.17 ppm for protons of methylene bridges indicating the cone geometry, for compound **50a** are evident two patterns of signals (**Figure 3.3.3.2**), both rather broad. One of them is composed of markedly broad signals because of the conformational mobility and the low exchange among different conformers, while the second one, constituted of sharper signals like the doublets at 4.39 and 3.22 ppm, corresponds to the cone one, the

most kinetically stable. The singlet at 1.52 ppm related to methyl protons confirms the successful outcome of reaction.

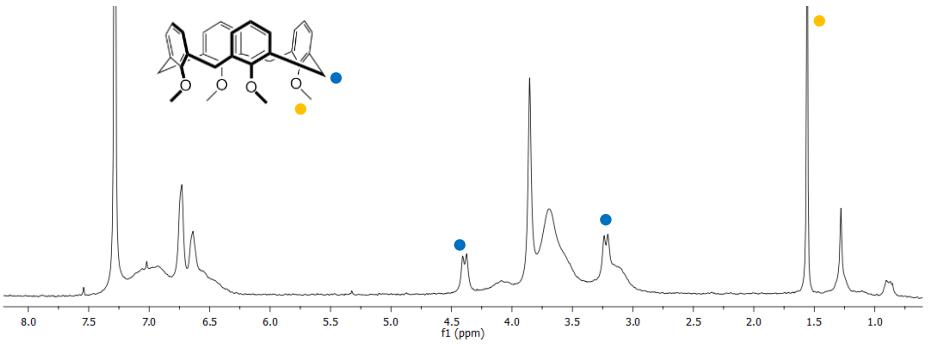

Figure 3.3.3.2. ^{1}H NMR (400 MHz, $CDCl_3$, 298K) spectrum of compound **50a**.

To obtain the nitro derivatives **51a**-**b**, compounds **50a-b** were stirred with 95% HNO_3 in glacial CH_3COOH (1/4, v/v) at room temperature quenching the reaction as soon as in TLC appeared dinitro derivative spot. Purification on silica flash chromatography column was in both cases difficult because of the similar polarity of by-products, which is the major reason of low yields for the isolated products (<20%).

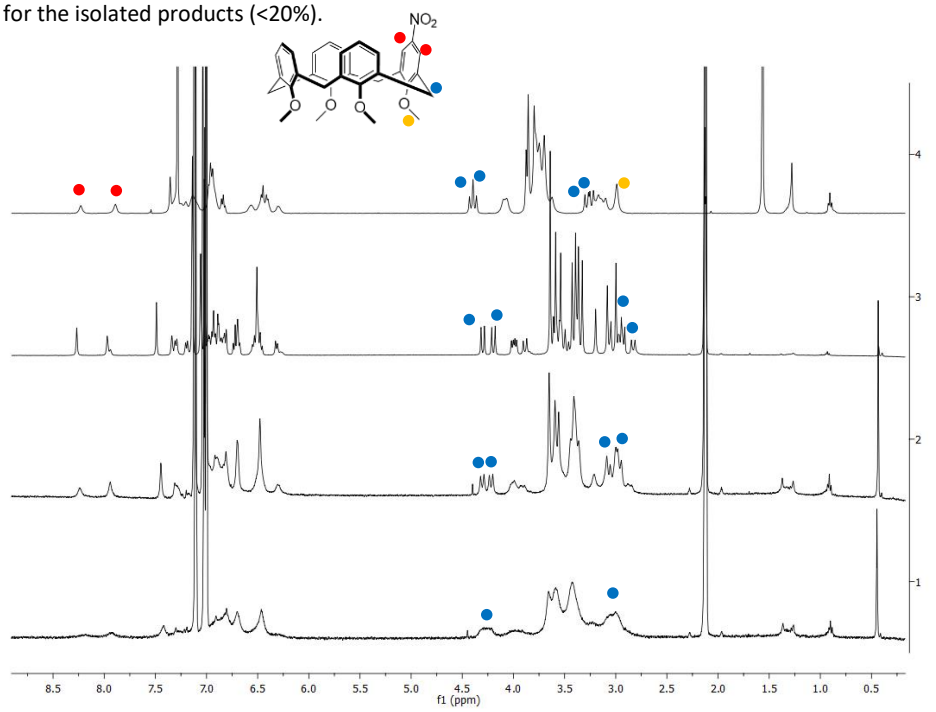

Figure 3.3.3.3. Series of ^{1}H NMR (400 MHz) spectra of compound **51a** in: **1**) toluene at 75 °C; **2**) toluene at 50 °C; **3**) toluene at 25 °C; **4**) $CDCl_3$ at 25 °C.

The spectrum ^{1}H NMR in $CDCl_3$ at room temperature (**Figure 3.3.3.3-4**) of compound **51a** turned out pretty complicated because of the compresence of several conformers, similarly to its

precursor **50a**. Singlets at 8.23 and 7.89 ppm, because of their deshielded positions, can be assigned to aromatic protons in ortho position to nitro group, while singlet at 2.99 ppm can be related to methyl protons of either partial cone or 1,3-alternate conformation being in both cases located in the shielding zone of the vicinal aromatic rings. Doublets at 4.41, 4.38, 3.28 and 3.23 ppm, clearly sharper than the other signals, represent methylenic bridges in the cone conformation, which are, in turn, more resolved in deuterated toluene (**Figure 3.3.3.3-3**). In this solvent, according to signal integration, it can be determined just on the basis of those four doublets that cone conformation is approximately 30% abundant over all the other possible conformations. To explore more deeply the conformational features of this macrocycle, ^{1}H NMR spectra in toluene were acquired at different temperatures (**Figure 3.3.3.3-1,2,3**). Raising up the temperature it can be seen that doublets of bridge methylene protons in cone conformation, well-resolved at 25°C, tend progressively to come close each other till at 70°C where signals are melted into two broad singlets. Unfortunately the highest temperature reached, 70 °C, was not enough to get coalescence and due to instrument limitations, we could not go further. The ^{1}H NMR analysis was supported by ESI-MS, which confirmed the nature of the mono nitration with the signal corresponding to the molecular ion $[M+Na]^+$ at m/z = 548. By chance, crystals of this derivative suitable for XRD were obtained, which showed that in solid-state the molecule packs itself in partial cone conformation maximizing contacts, where, in particular, the aromatic ring bearing nitro group is turned upside down in opposite orientation with respect to other aromatic rings. The reason why this conformation is favoured is related to a putative CH-π interaction between the electron-poor nitro aromatic ring and the methyl group on the opposite aromatic ring. Actually we do not know if compound **51a** is present in different conformations in crystallization solution as in $CDCl_3$ e toluene-d_8, but it is clear that if it was in dynamic equilibrium with different conformers, the partial cone geometry would be the one, which leads to the most stable packing.

The synthesis was kept on reducing quantitatively compounds **51a**-**b** with $NH_2NH_2{\cdot}H_2O$ into respective amine derivatives. The successful achievement of compound **51a** was conclusively demonstrated by ESI-MS, which showed the desired molecular peak at m/z=496 and by the absence, in ^{1}H NMR spectrum, of deshielded signals of aromatic protons in ortho position to nitro group (**Figure 3.3.3.4-1**).

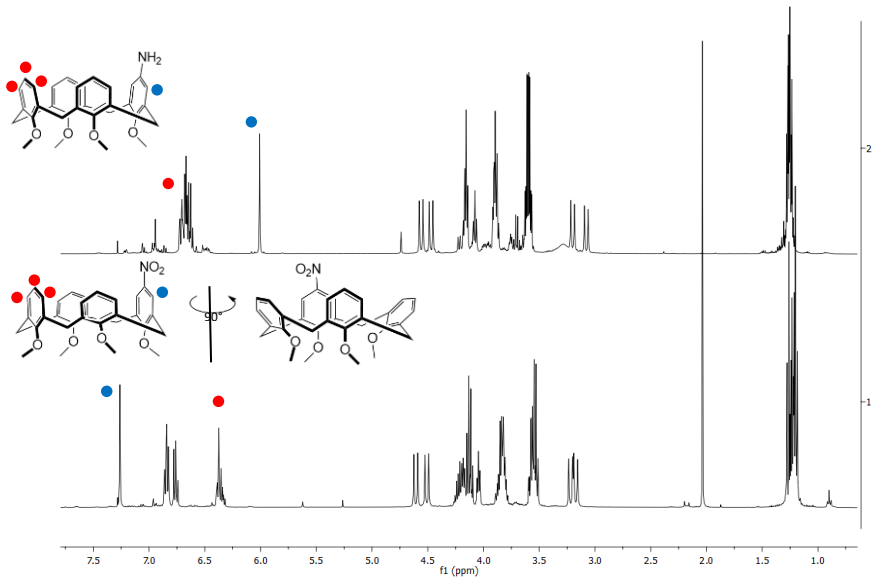

Figure 3.3.3.4. ^{1}H NMR (400MHz, $CDCl_3$, 25 °C) of compounds (**1**) **51a** and (**2**) **52a**.

It is to note the change of conformation in the cone geometry ascertained by ^{1}H NMR spectroscopy going from **51a** to **52a**. In the ^{1}H NMR spectrum in $CDCl_3$ of the former (**Figure 3.3.3.4-1**) aromatic protons on aromatic ring opposite to nitro-bearing ring are unusually shielded at 6.36 ppm. On the other hand, the protons in ortho position to NO_2 are deshielded much weaker than expected. These two effects are consequences of the tendency of the aromatic ring with NO_2 unit to stay parallel respect to the opposite ring because of CH-π interaction between NO_2-bearing ring and the opposite one forcing their protons in the shielding cone of the other two vicinal rings that, on the contrary, are forced to diverge. The calixarene assumes a conformation called flattened cone.

Compounds **52a**-**b** were then coupled using EDC with γ-aminobutyric acid protected on nitrogen atom with Boc group (GABA-Boc), which represents a proper spacer to outdistance sulfonamide or ammonium group from calixarene scaffold avoiding the establishment of destabilizing clashes with the enzyme walls. Once purified, the compounds were subjected to Boc removal in DCM with TFA and TES as scavenger for tert-butylic carbocation. Both compounds in these two steps were identified by ESI-MS and confirmed by ^{1}H NMR in particular for the loss of tert-butyl singlet at 1.48 ppm. For compound **54**, ^{1}H NMR was used to exclude the presence of unreacted Boc-GABA and TES, which were removed with a washing with solution of 1N NaOH and a trituration in n-hexane. The synthesis of compounds **55** and **56a**-**b** are not discussed since analogous to those used for compounds **4a-b**. All these last derivatives were characterized by ESI-MS, ^{1}H NMR and ^{13}C NMR. In **Figure 3.3.3.5**, ^{1}H NMR spectra of compound **56b**, acquired in different solvents, are reported.

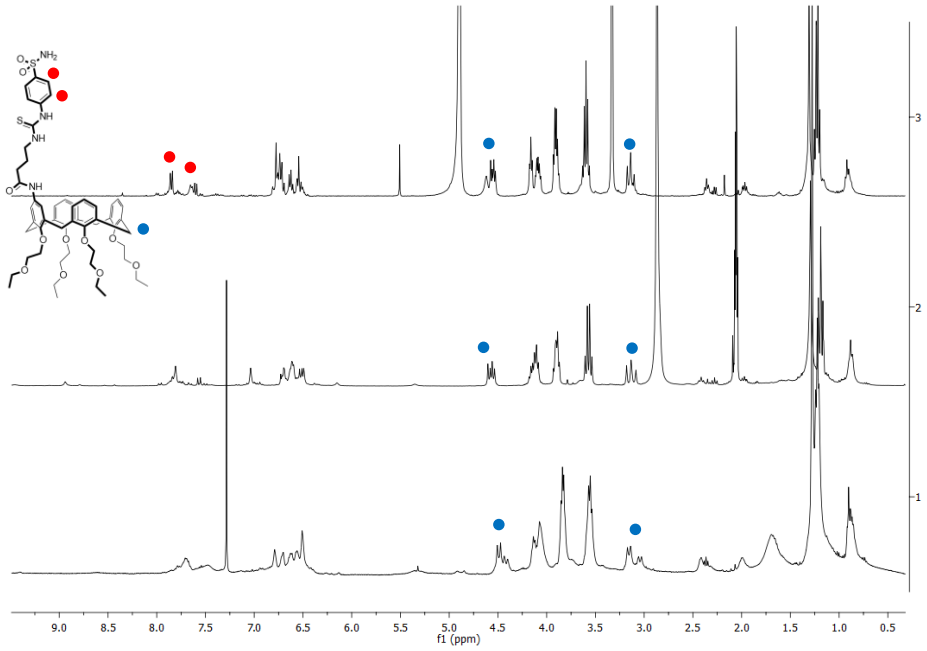

Figure 3.3.3.5: ^{1}H NMR spectra of compound **56b** in **1**) $CDCl_3$ at 25 °C (400 MHz); **2**) acetone-d_6 at 25 °C (300 MHz); **3**) MeOD at 25 °C (400 MHz).

As it can be seen, thanks to broad signals observed in $CDCl_3$ we can say that this compound tends to aggregate in apolar solvents, whereas it does not in polar ones.

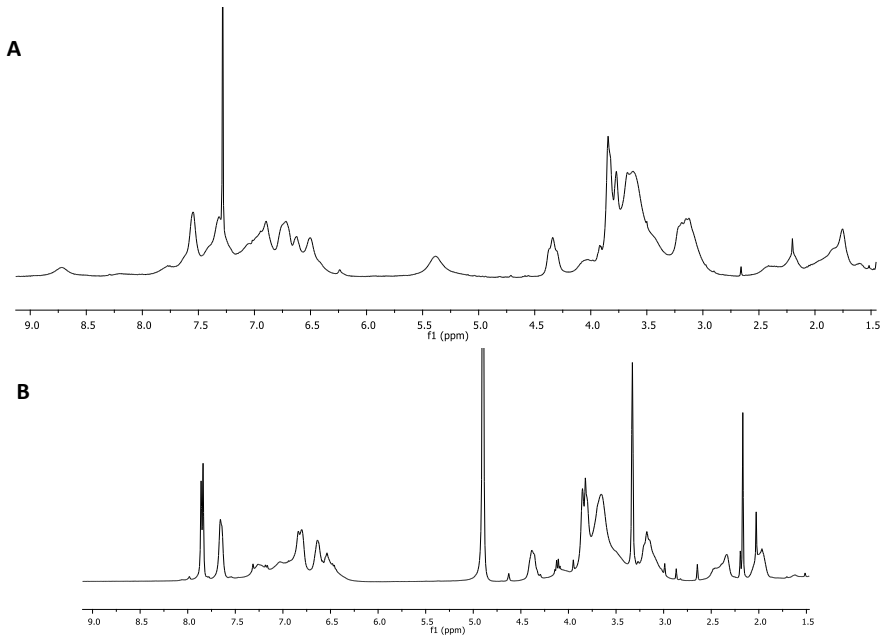

Figure 3.3.3.6. ^{1}H NMR spectra (400MHz, 25°C) of compound **56a** in: **A**) $CDCl_3$; **B**) MeOD-d_4.

The ^{1}H NMR spectrum in $CDCl_3$ of compound **56a** (**Figure 3.3.3.6A**) is not resolved and clear since it is a sum of broad peaks due to intermolecular interactions among calixarene units. Despite the difficult reading, it is observed at 8.72 ppm a signal related to thioureidic protons nearby the benzenesulfonamide aromatic ring and at 5.38 ppm a broad singlet of two sulfonamidic protons. These signals are totally suppressed in MeOD-d_4, as seen in **Figure 3.3.3.6B**.

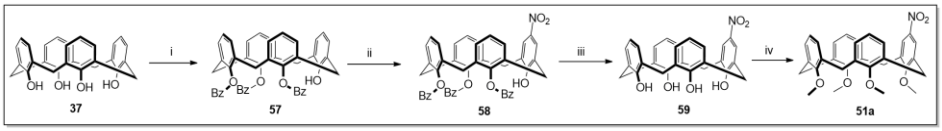

Figure 3.3.3.7: Alternative synthesis for compound **51a**. *Reactions conditions*: i) benzoyl chloride (8.1 eq), dry pyridine, 0 °C then at rt, 1 h (76% yield); ii) 90% HNO_3 (2.9 eq), glacial CH_3COOH (123.7 eq), DCM, rt, 40 minutes; iii) 1N NaOH (22 ml), THF/EtOH/H_2O , 85 °C, 15h (37% yield); iv) 55% NaH (10.5 eq), CH_3I (10.5 eq) , dry DMF, rt, 7 days (crude yield 71%).

Because of purification issues for the lack of regioselectivity in upper-rim mononitration, another synthetic strategy was explored for the synthesis of compound **51a**. This exploits the higher reactivity of the only unfunctionalized phenol ring upon tribenzylation at lower rim, which after hydrolysis and permethylation leads to the desired molecule. According to the higher number of steps, the longer reaction times and the similar yields, this strategy was considered not advantageous with respect to the previous one.

3.3.4 Synthesis of the 1,3-alternate tetrafunctionalized calixarenes

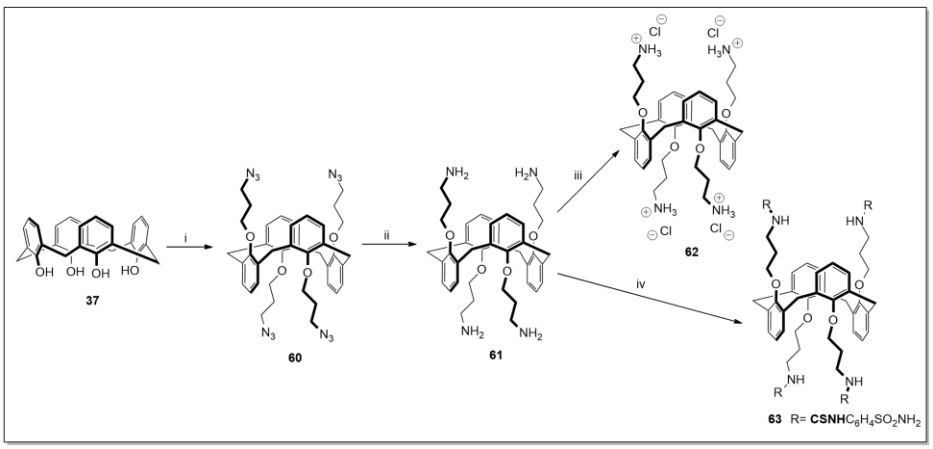

Figure 3.3.4.1. i) Cs_2CO_3 (10.0 eq), 1-iodo-3-azidopropane (5.0 eq), dry DMF, rt, 3 days (33% yield); ii) H_2 (3.0 bar), 10% Pd/C (catalytic amount), AcOEt, rt, 7h (57% yield); iii) 1N HCl (1 ml), MeOH (99% yield); iv) DIPEA (10.0 eq), 4-isothiocyanatebenzensolfonamide (4.4 eq), dry DMF, rt, 1 day (50% yield).

For the preparation of potential ligands in 1,3-alternate geometry, calixarene **60** was synthesized by a tetrafunctionalization in dry DMF with 1-bromo-3-azidopropane[28] using Cs_2CO_3

as base, whose cation is used to stabilize the 1,3-alternate conformation in which blocking the macrocycle. The compound was purified by recrystallization in DCM/Et_2O, giving nice cubic crystals appropriate for XRD analysis. The structure at the solid state indeed suggests that the propyl chains introduced at the lower rim are, probably, not long enough to project the sulfonamide units sufficiently away from calix[4]arene scaffold to allow the simultaneous interaction of the ligand with two different enzyme molecules located at opposite faces of the macrocyclic ligand. It is curious to note that in solid-state calix[4]arene **60** arranges generating holes (diameter 7 Å) occupied by solvent molecules (**Figure 3.3.4.2**).

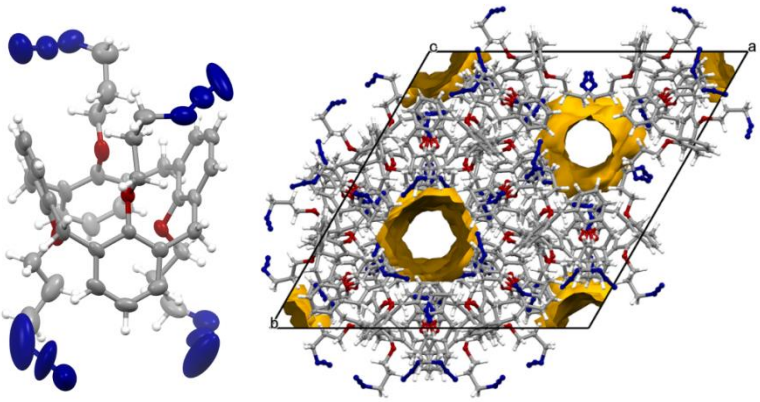

Figure 3.3.4.2. XRD structure of compound **60**.

From ^{1}H-NMR analysis, mainly the singlet at 3.85 ppm of bridge methylenes and signals at 3.57, 2.99 and 1.50 ppm of propyl arm corresponding to eight protons are evidence of the target molecule identity. Some attempts were made to introduce at the lower rim other functions to transform in amine units, in particular using as alkylating agents N-3-bromopropylphthalimide and 2-Tosyl-1-nitrile-ethane, but the reactions failed. Compound **60** was easily reduced by catalytic hydrogenation in AcOEt with 10% Pd/C. Alternatively to this, it was reduced by Staudinger reaction, but because of the high difficulty of purification from phosphinic species, this strategy was rapidly abandoned. The successful outcome of click reaction to make compound **63** was confirmed by ESI-MS through the absence of starting material **61** (positive ionization) and the presence of only compound **63** (negative ionization), even if TLC showed several spots. The filtered brownish solid was then analysed by ^{1}H-NMR, which showed, besides the characteristic signals of the target molecule, some impurities signals at 7.92 – 7.89 ppm. So the crude was prepurified by a reverse phase chromatography column (RP-18) with H_2O/Acetone in gradient from 2:1 to 1:2 and then by a recrystallization with acetone/Et_2O. By ^{1}H-NMR analysis, the brownish precipitate was rich in target molecule, whereas the yellow mother liquids were rich in impurities. Multiple attempts were made to get a solid more pure, but no further improvement was observed.

3.3.5 Inhibition studies

Also for these calixarene-based compounds inhibition studies were carried out by Supuran's coworkers at University of Florence. All the mentioned compounds were tested towards the six different isoforms (hCAI, hCAII, hCAIX, VchCAβ, Can2, MgCA) already used for the two

monovalent compounds described in the previous **Chapter2**. Also, in this case, AAZ was used as reference compound.

As it can be seen in **Table 3.3.5.1**, almost all tested calixarenes appear mainly selective for Can2 CA for which they show their lowest K_i values although higher with respect to AAZ. Analogously, most of them show a K_i towards MgCA lower than AAZ.
Towards Can2, almost all calixarenes showed to be high-nanomolar inhibitors, except for compounds **63**, **42bx**, **56b** and **56a**, with which even low-nanomolar Ki similar to AAZ are reached. In this context, if we compare compound **42bx** with compound **42b**, we notice that introducing a further propyl-benzenesulfonamide arm, the inhibition constant increases of one order of magnitude, whose behaviour, by the way, is kept in MgCA. This suggests that the thinner propyl-ammonium arm makes no significant clashes with enzyme without excluding its possibility to bind negative-charged moieties or electron-donating atoms, which would justify this interesting gain. Moving to ammonium analogues, it can be seen that tetra-ammonium derivative **V** in cone conformation is a nanomolar-range inhibitor towards Can2 and MgCA, meanwhile the same molecule in 1,3-alternated conformation **62** is totally inactive. As already commented in XRD structure of intermediate **60**, amidic nitrogen (and so sulfonamidic nitrogen as well) is just few far away from calixarene scaffold and so in order to reduce steric clashes, it would be better lengthen more the aliphatic chain. With this idea in mind, maybe, the molecule in this conformation would be able to simultaneously chelate multiple copies of enzyme boosting its affinity. Among these, it is significant underline which type of contribute make either propyl or ethoxyethyl chains to inhibition. Paying attention to monofunctionalized and difunctionalized calixarenes, it is clear how propyl chains are favourite to ethoxyethyl chains. In fact passing from dipropyl to diethoxyethyl derivatives, in particular from **42a** to **42c**, and from tripropyl to triethoxyethyl derivatives, in particular from **49a** to **49c** and from **48a** to **48b**, K_i increase due to expected clashes between ethoxyethyl chains and enzyme walls. This effect is mainly enhanced in the ammonium derivative **48a**-**48b**. Here, probably, the chain length is a very discriminating factor for inhibition. The reason underneath this evidence is not still clear. Further studies will be carried out to understand, which factor, among steric hindrance and polarity, is predominant in the binding. Particularly interesting is compound **56b**, which shows remarkable inhibition properties also towards two out of the three hCAs. In fact, towards hCAI (K_i= 84.9 nM) this upper rim monofunctionalized compound is more active than AAZ and towards hCAII (K_i= 48.1 nM) is very close to the efficiency of the drug. In this context it is significant to compare this ligand with the analogue lower rim monofunctionalized **49b**, as **56b** blocked in the cone geometry, and the analogue upper rim monofunctionalized **56a**, conformationally mobile. All three are equipped with a sulfonamide moiety linked to the calixarene through a thiourea unit, but only **56b** presents a defined cavity oriented to the same part of the space as the binding unit. Apart the case of hCAIX and Can2 for which there are no substantial differences, both **49b** and **56a** result less active than **56b** with an increase of K_i of one or two orders of magnitude and being completely inactive towards VchCAβ. The possible absence in **56b** of steric hindrance due to the ethoxyethylchains that on the contrary in **49b** are directing towards the active site funnel together with the sulfonamide unit, wh and the presence of the macrocyclic cavity in **56b** potentially oriented together with the binding unit towards the funnel and then available for additional interactions with lipophilic side chains of the enzyme seem to be important factors in the binding.

Table 3.3.5.1. Inhibition data of calixarene derivatives towards the selected isoforms, obtained from stopped-flow technique. Each value is a mean from 3 different assays (errors were in the range of ± 5-10 % of the reported values). All data are separated by a straight line when the degree of functionalization changes (in green, thioureidic derivatives; in red, amide derivatives; in black, ammonium derivatives).

	K_I (nM)					
Compound	hCAI	hCAII	hCAIX	VchCAβ	Can2	MgCA
I *(cone-calix[6]-hexa-amide)*	3349.1	497.2	872.5	5950	138	>100000
II *(cone-calix[6]-hexa-thiourea)*	5953.8	2397.4	817.8	7370.1	>100000	>100000
III *(cone-calix[6]-hexa-ammonium)*	>100000	>100000	>100000	6812.5	107	7500
IV *(cone-calix[4]-tetra-amide)*	8565.7	3878.9	4026.3	757.1	125	7100
V *(cone-calix[4]-tetra-ammonium)*	>100000	>100000	>100000	3144.9	136	7600
62 *(1,3-alternated-calix[4]-ammonium)*	>100000	>100000	>100000	>100000	>100000	>100000
63 *(1,3-alternated-calix[4]-thiourea)*	542.3	401.4	1795	>100000	63.4	>100000
42b *(cone-calix[4]-dipropyl-diamide)*	5521	533.6	1107	8555.1	270	8800
42bx *(cone-calix[4]-dipropyl-monoamide-monoammonium)*	>100000	4466	>100000	>100000	92.1	2585
42a *(cone-calix[4]-dipropyl-dithiourea)*	8286.6	1214.2	246.4	8163.3	>100000	3900
41a *(cone-calix[4]-dipropyl-diammonium)*	>100000	>100000	>100000	9411.6	267	7800
42c *(cone-calix[4]-diethoxyethyl-dithiourea)*	2692.3	342.7	2180.3	7488.4	260	8900
49a *(cone-calix[4]-tripropyl-monoamide)*	>100000	7377.6	1979.8	8151.8	253	5600
48a *(cone-calix[4]-tripropyl-monoammonium)*	>100000	>100000	>100000	7322.3	290	937
49c *(cone-calix[4]-triethoxyethyl-monoamide)*	5909.4	3090.2	1487.1	8819.2	247	8800
49b *(cone-calix[4]-triethoxyethyl-monothiourea)*	5567.9	894.7	1772.2	>100000	170	6700
56b *(cone-calix[4]-GABA-thiourea)*	84.9	48.1	1937	6745	50.4	931
56a *(mobile-calix[4]-GABA-thiourea)*	3751	859.7	1657	>100000	45.1	5325
48b *(cone-calix[4]-triethoxyethyl-monoammonium)*	>100000	>100000	>100000	>100000	237	>100000
55 *(cone-calix[4]-GABA-ammonium)*	>100000	>100000	>100000	>100000	>100000	>100000
acetazolamide (AAZ)	250	12	25	451	10	74000

As far as linker nature is concerned, thioureidic linker shows a little stabilizing effect with respect to the amide one. Keeping constant the nature of permanent protecting chains, if we pass from compound **42b** to **42a** and from compound **49c** to **49b**, inhibition constants get lower, which is probably imputable to additional interactions between S atom and enzyme aminoacid side-chains.

Since compounds **4a**, **4b** and **4c** represent the exact monomeric acyclic model of all synthesized calixarenes, we analysed the inhibition data also in view of verifying the possible occurrence of a multivalent effect. In the case of hCAs, not only this is not the case, but the calixarene derivatives are even worse inhibitors than the monovalent ligands. Moreover, also in the cases where the calixarene-based ligands are better than the monovalent, i.e. against MgCA, it is clear that no multivalent effect occurs in the binding. In fact, calixarenes with a different number of the same active unit show very close K_i values, like for instance compounds **IV**, **42b** and **49a** bearing 4, 2 and 1 sulfonamide units, respectively, or compounds **48a** and **41a** exposing 1 and 2 ammonium heads, respectively. However, towards this CA isoform, the data suggest that the insertion of the active unit, both ammonium and sulfonamide, in the macrocyclic structure improves its biological activity.

Table 3.3.5.2. Inhibition data of calixarene derivatives towards the selected isoforms, obtained from stopped-flow technique. Each value is a mean from 3 different assays (errors were in the range of ± 5-10 % of the reported values). All data are separated by a straight line when the linker or binding unit changes (in red, amide derivatives; in black, ammonium derivatives).

	K_I (nM)					
Compound	hCAI	hCAII	hCAIX	VchCAβ	Can2	MgCA
IV *(cone-calix[4]-tetra-amide)*	8565.7	3878.9	4026.3	757.1	125	7100
42b *(cone-calix[4]-dipropyl-diamide)*	5521	533.6	1107	8555.1	270	8800
49a *(cone-calix[4]-tripropyl-monoamide)*	>100000	7377.6	1979.8	8151.8	253	5600
4c *(amide monomer)*	8.4	4.1	21.8	4143.8	>10000	>10000
41a *(cone-calix[4]-dipropyl-diammonium)*	>100000	>100000	>100000	9411.6	267	7800
48a *(cone-calix[4]-tripropyl-monoammonium)*	>100000	>100000	>100000	7322.3	290	937
4a (ammonium monomer)	>10000	>10000	>10000	>10000	>10000	>10000
acetazolamide (AAZ)	250	12	25	451	10	74000

3.3.6 Solid state structure of hCAII/**49b**, hCAII/**56b** and hCAII/**63** complexes

In parallel with the evaluation of the inhibition ability of the compounds, suitable crystals for XRD analysis were collected at the group of Prof. Supuran of the complexes between hCAII and ligands **49b**, **56b** and **63**. The diffraction experiments, as in the case of the monomer **4b**, were performed at Synchrotron in Trieste and the structures solved by Andrea Angeli of Supuran's group.

The first fundamental information came from the structure of hCAII/**49b** complex. The predicted inhibition mode was in fact confirmed with the evidence of the sulfonamide arm located into the funnel (**Figure 3.3.6.1**). This resulted in the proof that these sulfonamide calixarenes indeed inhibit the enzyme exploiting the active units and targeting the active site and not interacting with other portions of the protein inducing rearrangement in the folding in turn responsible of a decreased enzymatic activity. Due to the novelty of these systems as potential inhibitors of CAs, this could not be taken for granted.

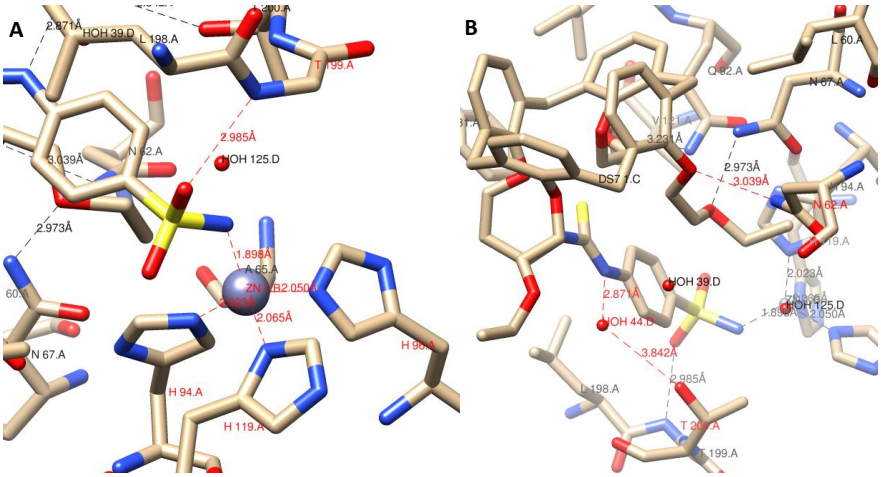

Figure 3.3.6.1. Stick representation of hCAII/**49b** cocrystal. In **A** catalytic active site is illustrated, in which zinc ion is tetracoordinated by three histidines (His94, His96 and His119) and nitrogen atom of benzenesulfonamide (highlighted in red). In **A** it is shown also how sulfamoyl moiety is furthermore stabilized through a hydrogen bond among S=O and amidic nitrogen of Thr199 (highlighted in red). In **B** it is shown the complex how it is seen out of the funnel. Besides the non-reliable polar interactions between ethoxyethylic oxygen atoms and enzyme wall, it is highlighted in red the bridge polar contacts that HOH 44 makes with hydroxyl group of Thr200 and nitrogen atom of thioureidic linker.

Benzenesolfonamide head binds in the canonical way with the nitrogen atom coordinating the zinc ion, which, in turn, is chelated by His94, His96 and His119. Moreover, in this case, benzenesulfonamide moiety is stabilized by a hydrogen bond among oxygen atom of sulfamoyl group and nitrogen atom of Thr199 and by a hydrophobic interaction among Leu198 and the aromatic ring of benzenesulfonamide. Besides these classical interactions, water molecule 44 carries out an interesting role. It essentially acts as bridge for hydrogen bonds with thioureidic nitrogen atom and hydroxyl group of Thr200, which as a consequence stabilizes furthermore the anchoring of pharmacophore in the active site.

Since the electronic density of the calixarene scaffold, together with that of the ethoxyethyl chains were not univocally determined, its structure was reconstructed starting from the constrains imposed by the phenolic ring bearing the sulfonamide and knowing the cone geometry of the calixarene. For this reason we cannot assess the exact localization of non-covalent interactions between the enzyme and this part of the ligand, since calixarene conformation was not resolved. However, considering the imposed cone conformation, on the whole, it has been calculated that hydrophobic stabilization of macrocyclic part might be mainly mediated by His4, Asn11, Leu60, Ala65, Asn67, Glu69, Ile91, Gln92, Val121 and Phe131. In addition to this, have been calculated additional hydrogen bonds between phenolic oxygen atom and side-chain nitrogen atom of Asn62 and between oxygen atom of terminal ethoxy in ethoxyethyl chain and side-chain nitrogen atom of Asn97. The actual existence of these last bonds cannot be confirmed for the same previous reasons.

The position of the sulfonamidic group respect to the macrocyclic cavity imposes that the latter one is oriented towards the bulk of the solvent.

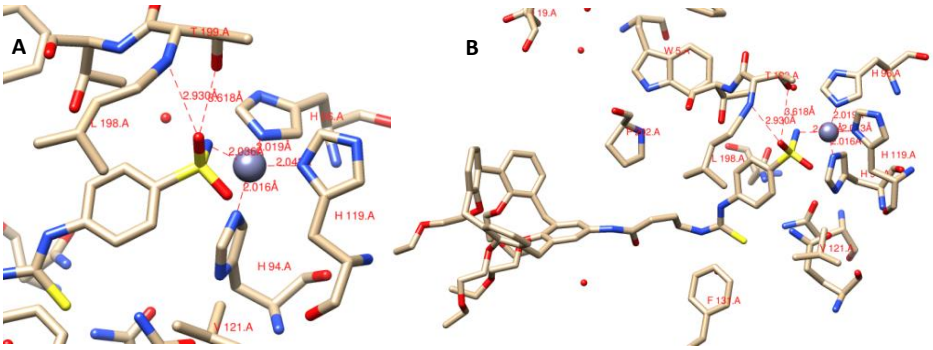

Figure 3.3.6.2. Stick representation of hCAII/**56b** cocrystal. In **A** apart from the classical binding fashion (His94, His96, His119 and sulfonamide), no particular new interactions are found (highlighted in red). In **B** it is shown the complex how it is seen from out of the funnel. The calixarene macrocycle is totally exposed in a solvent accessible area away from enzyme walls, whereas cysoid propyl spacer in engaged in hydrophobic interactions with Pro202 and Phe131.

As far as hCAII/**56b** XRD is concerned, it is again observed the same classical binding mode for sulfonamide. In **Figure 3.3.6.2B** it is shown how Pro202 and Phe 131 force propyl arm to stay in a cysoid conformation through hydrophobic interactions. Also, in this case, the structure of the macrocycle was not resolved except for the aromatic ring which bears the sulfonamide moiety. After its reconstruction and minimization, the macrocycle results reasonably located at the opening of the funnel in a solvent accessible area (**Figure 3.3.6.2B**). As can be seen in **Figure 3.3.6.2B**, calixarene cavity of compound **56b** is not able to include any side chain moiety. In future detailed studies will be carried out to understand the factors contributing to its excellent binding (K_i=48.1nM)

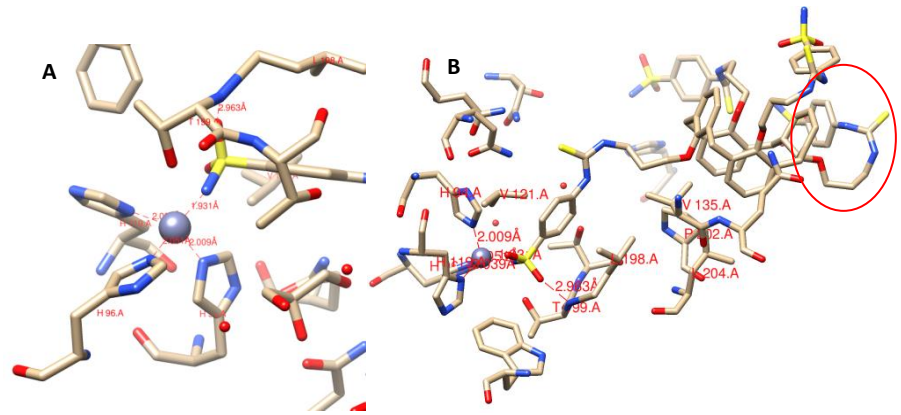

Figure 3.3.6.3. Stick representation of hCAII/**63** cocrystal. In red are highlighted the polar interaction within the cocrystal, whereas the red circle shows the bent conformation of benzenesulfonamide arm, which avoids steric clashes with enzyme funnel (**B**). In **A** the active site is represented.

Also in hCAII/**63** XRD (**Figure 3.3.6.3**) no particular differences in terms of contacts are observed. Even in this case, just the phenolic ring bearing the sulphonamide moiety was resolved, meanwhile the rest of the calix[4]arene was reconstructed and minimized. Unfortunately, it was not evidenced the existence of a multivalent complex between the calixarene and at least two enzyme molecules.

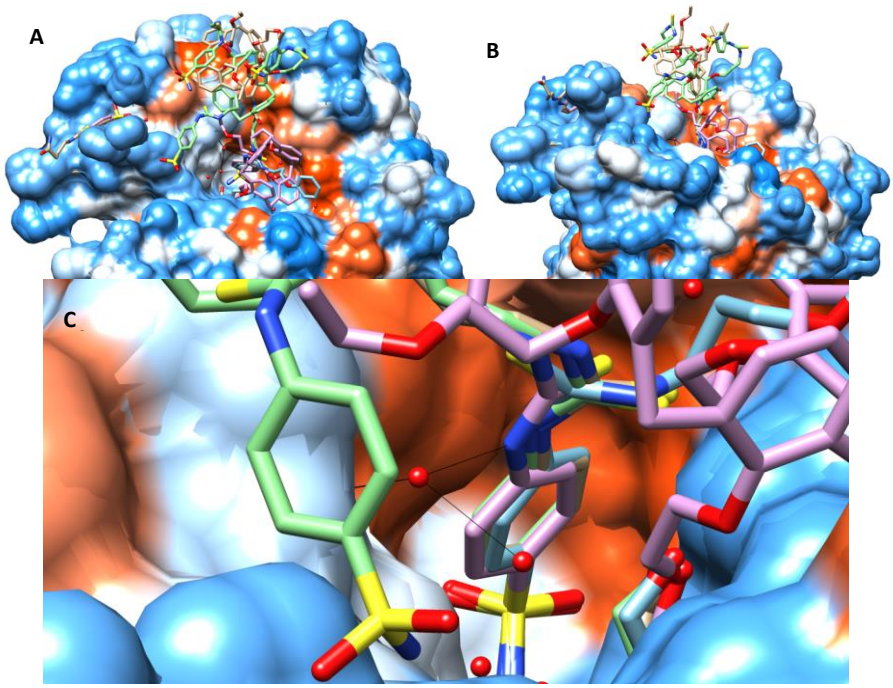

Figure 3.3.6.4. Superimposition of hCAII in cocrystals with compound **49b**, **56b**, **63** and **4b**. The superimposition was obtained aligning hCAII structures of all complexes and showing them as hydrophobic surfaces through Chimera software. Out-of-active-site (**A**-**B**) and in-active-site (**C**) viewings are proposed. In light blue, compound **4b**; in purple, compound **49b**; in green, compound **63**; in light brown, compound **56b**.

In **Figure 3.3.6.4C**, it can be seen how benzenesulfonamide moieties belonging to ligands **49b**, **56b**, **63** and **4b** are almost totally superimposable. Moreover, it is clear that thioureidic units are not establishing any kind of polar interactions, which thing is confirmed by random orientations kept in the considered compounds. It seems that they guarantee flexibility to molecules due to the different orientations of the relative tails.

3.4 Conclusions

As already said in **Chapter2**, misregulation or malfunctioning of Carbonic Anhydrases (CAs) lead to a myriad of diseases and so for this reason, these particular enzymes are getting very important biotargets of medical relevance. So, besides the classical small inhibitors currently used nowadays, have been developed few multivalent inhibitors based on scaffolds able to expose multiple copies of the same ligand unit in order to increase the local concentration of active units. Up to now, multivalent scaffolds explored in multivalent inhibition of CAs are fullerenes and PAMAMs, which showed interesting results of rp/n.

Considering that, in past, calixarenes showed very high efficiency in multivalent inhibition towards non-enzymatic proteins, in this project, we proposed the use of calixarene as scaffold for potential multivalent inhibition towards CAs. Starting from tetra- and hexa-functionalized caix[4-6]arenes with ammonium and benzenesulfonamide units, already present in our laboratories, which interesting inhibition results towards MgCA, we decided to synthetise a

large library of calix[4]arenes functionalized at the upper rim or at the lower rim with 1 or 2 active units. In the lower-rim-functionalized calixarenes in cone conformation free OHs were functionalized with propyl or ethoxyethyl chains to make derivatives with different polarity able to interact differently with enzyme walls. Tetrafunctionalized compounds with both actives units (ammonium and sulfonamides) were also synthetised in 1,3–alternated conformation with the idea to create inhibitors able to coordinate more enzyme molecules simultaneously. In addition to these inhibitors, also upper-functionalized calix[4]arenes were realized conjugating monoaminocalix[4]arenes with the benzenesulfonamide unit through a GABA-thioureidic spacer. Differently from lower-rim functionalized calixarene, which expose the cavity in the bulk solution, upper-rim functionalized calixarenes were meant to exploit the cavity for inclusion of lipophilic or ammonium side chains (e.g. lysines), since oriented towards enzyme walls. These types of compounds were fully functionalized at lower rim with either ethoxyethyl chains to increase water solubility or methyl groups to confer adaptability to the calixarene cavity inside the active site, due to the gained mobility. All the compounds were tested in Supuran's laboratories in stopped-flow assays towards hCAI, hCAII, hCAIX, VchβCA, Can2 and MgCA. As a first sight, even if less active than AAZ, we can say that almost all calixarene derivatives (except for the inactive **II**, **62**, **42a** and **55**) are selective towards Can2, since for this type of isoforms are reached the lowest inhibition constants. The highest efficiencies were obtained, instead, towards MgCA. In fact, here almost all calixarenes are more efficient than the reference AAZ with the lowest inhibition constants observed for compounds **56b** and **48a** (respectively, K_i=931nM and K_i=937nM). Paying attention to these active calixarenes it seems that no multivalent effect occurs in the binding. In fact, keeping constant the linker used to couple benzenesulfonamide moiety to calixarene scaffold, passing from difunctionalized (Ki=8800nM) to monofunctionalized (Ki=5600nM) derivative (as well as passing from hexafunctionalized to tetrafunctionalized derivative), the inhibition constants get lower, which means that monofunctionalized derivative is better than the difunctionalized one, totally opposite to a multivalent effect. Also compounds **49b**, **56b** and **56a** showed very interesting data towards hCAII. In fact, passing from the cone sulphonamide-calixarene monofunctionalized at the lower rim (**49b**) to cone sulphonamide-calixarene monofunctionalized at the upper rim (**56b**), we observe a drastic increase in efficiency (Ki=894.7nM→48.1nM), whereas we go back to worse efficiency (Ki=859.7nM) passing to the anologue calixarene in mobile conformation, which suggests that a cavity effect occurs in the binding. From relative cocrystal with hCAII, it can be seen that sulphonamide can enter the funnel binding the active site, but no cavity inclusion is observed. By the way, considering the comparison between **49b**, **56b** and **56a**, a macrocyclic effect surely occurs in stabilizing the complex maybe through a multivalent effect. The actual mechanism of how this macrocyclic effect works in this system is still under investigation.

In future will be setup new cocrystallization assays, in particular with MgCA with which calixarenes showed to be very efficient inhibitors, in order to have more information about our derivatives.

3.5 Experimental part

General information. All moisture-sensitive reactions were carried out under a nitrogen atmosphere. All dry solvents were prepared according to standard procedures and stored over 3 or 4 Å molecular sieves. All other reagents were commercial samples and used without further purification. TLCs were performed using prepared plates of silica gel (Merck 60 F_{254} on aluminium) and revealed using UV light or staining reagents: $FeCl_3$ (1% in H_2O/MeOH 1:1), ninhydrin (5% in EtOH), basic solution of $KMnO_4$ (0.75% in H_2O). Flash chromatography was performed on 32-63 µm on 60 Å Merck silica gel. Melting points were determined on an electrothermal apparatus Gallenkamp, in capillaries sealed under nitrogen. ^{1}H NMR (300 or 400 MHz) and ^{13}C NMR spectra (75 or 100 MHz) were recorded on Bruker AV300 and AV400 spectrometers using partially deuterated solvents as internal standards. All ^{13}C NMR were performed with proton decoupling. Mass spectra were recorded in Electrospray Ionization (ESI) mode using a SQ Detector, Waters (capillary voltage = 2.40-3.50 kV, cone voltage = 40-100 V, extractor voltage = 2 V, source block temperature = 150 °C, desolvation temperature = 300 °C, cone gas (N_2) flow rates = 95 L/hr, desolvation gas (N_2) flow rates = 480 L/hr) in MeOH.

Synthesis

5,11,17,23-tetra-tert-butyl-calix[4]arene-25,26,27,28-tetraol (36): In a 3-necked round-bottom flask, p-tert-butylphenol **35** (2.00 mol, 300 g), 37% formaldehyde aqueous solution (2.49 mol, 186 ml) and 10M NaOH aqueous solution (90 mmol, 3.6 g) were mixed together with a mechanical mixer. Through a mantle heater, the reaction was heated up until the colour mixture turned straw yellow (100°C-120°C). During the heating, the system was left under a low nitrogen flow with an open neck in order to remove water. After 1h the reaction turned turbid yellow and suddenly a viscous yellow foam was produced. Immediately the mechanical agitation was stopped and the mixture was let cool down at room temperature. Consequently, diphenyl ether (3 l) was added and using condensers and a Dean-Stark trap, the solution was taken to reflux (225°C) upon stirring. The mixture was distilled until the solution turned dark brown (6 h) and subsequently was cooled down at room temperature. The reaction was monitored by TLC (DCM/Hex 1:1, R_f=0.41). AcOEt (3 l) was added in and the mixture was kept stirring for 30 minutes. The suspension was therefore filtered out and the white-brownish solid was washed with AcOEt (2 x 300 ml), AcOH (500 ml), H_2O (2 x 300 ml) and eventually with acetone (2 x 150 ml). The recrystallization was carried out with the same experimental initial set-up using toluene (3 l) and upon stirring, it was heated up to 120°C in order to distil out the remaining water and to reduce the solution volume. As soon as the volume of toluene was halved, the heating was stopped and the compound (?) was let recrystallized at room temperature. The solid was filtered out and washed with further toluene (100 ml) to get compound **36** as bright white plate crystals (212.93 g, 287.30 mmol, 60% yield as complex 1:1 toluene: calixarene). **^{1}H-NMR** (400 MHz, tetrachloroethane-d_2) δ (ppm): 10.60 (s, 4H, O*H*), 7.13 (s, 8H, Ar*H*), 4.28 (d, *J* = 13.6 Hz, 4H, axial ArCH_2Ar), 3.58 (d, *J* = 13.6 Hz, 4H, equatorial ArCH_2Ar), 1.29 (d, *J* = 6.4 Hz, 36H, ArC(CH_3)$_3$). The spectroscopic data obtained are in agreement with those ones reported in literature[17].

calix[4]arene-25,26,27,28-tetraol (37): In a 3-necked round-bottom flask, compound **36** (15.40 mmol, 10.00 g) was suspended in toluene (100 ml) along with phenol (18.60 mmol, 1.75 g)

through a mechanical stirrer. $AlCl_3$ (84.6 mmol, 11.28 g) was added in and the mixture was left reacting for 1h at room temperature leading to a very viscous and red solution. Once assessed the completion of the reaction by TLC (Hex/AcOEt 7:3, R_f=0.65), 1N HCl (200 ml) and ice (200 ml) were added and the solution was stirred for 1 h. The collected organic phase was washed again with water (2 x 200 ml), whereas this last aqueous phase was re-extracted with toluene (250 ml). The organic phases were combined together, dried with anhydrous Na_2SO_4 and then filtered. After having evaporated all the solvent, the product was precipitated in $CHCl_3$/MeOH 1:1 at 0°C for 1h to get compound **37** as a light yellow solid (4.65 g, 10.95 mmol, 71% yield). **^{1}H NMR** (300 MHz, $CDCl_3$) δ (ppm): 10.20 (s, 4H, ArO*H*), 7.05 (d, *J* = 7.6 Hz, 8H, p-Ar*H*), 6.73 (t, *J* = 7.6 Hz, 4H, m-Ar*H*), 4.26 (bs, 4H, axial ArC*H*$_2$Ar), 3.55 (bs, 4H, equatorial ArC*H*$_2$Ar). The spectroscopic data obtained are in agreement with those ones reported in literature[17].

cone-25,27-bis(propoxy)-calix[4]arene-26,28-diolo (38a): In a 2-necked round-bottom flask, compound **37** (4.71 mmol, 2.00 g) and K_2CO_3 (19.79 mmol, 2.74 g) were stirred in dry ACN (80 ml) at room temperature for 30 minutes. Then at reflux 3-iodopropane (19.79 mmol, 1.930 ml) was added in and it was left reacting for 4 days, monitoring the reaction by TLC (Hex/AcOEt 8:2). The reaction was quenched with 1N HCl (20 ml) and the precipitate formed was filtered and recrystallized in DCM/Hex to get compound **38a** as white crystals (2.40 g, 4.72 mmol, 99% yield). **^{1}H NMR** (300 MHz, $CDCl_3$) δ (ppm): 8.30 (s, 2H, O*H*), 7.05 (d, *J* = 7.5 Hz, 4H, m-Ar*H*OCH$_2$CH$_2$CH$_3$), 6.92 (d, *J* = 7.5 Hz, 4H, m-Ar*H*OH), 6.74 (t, *J* = 7.5 Hz, 2H, p-Ar*H*OCH$_2$CH$_2$CH$_3$), 6.64 (t, *J* = 7.5 Hz, 2H, p-Ar*H*OH), 4.32 (d, *J* = 12.9 Hz, 4H, ArC*H*$_{ax}$HAr), 3.98 (t, *J* = 6.9 Hz, 4H, OC*H*$_2$CH$_2$CH$_3$), 3.38 (d, *J* = 12.9 Hz, 4H, ArC*H*$_{eq}$HAr), 2.07 (hex, *J* = 6.9 Hz, 4H, OCH$_2$C*H*$_2$CH$_3$), 1.32 (t, *J* = 6.9 Hz, 6H, OCH$_2$CH$_2$C*H*$_3$). The spectroscopic data obtained are in agreement with those ones reported in literature[29].

25,27-(2-ethoxyethylether)-calix[4]arene-26,28-olo (38b): in a 2-necked round-bottom flask compound **37** (3.53 mmol, 1.50 g) and K_2CO_3 (14.80 mmol, 2.05 g) were stirred in dry ACN (40 ml) for 30 minutes at reflux. Then 2-bromo-ethoxyethylether (14.80 mmol, 1.669 ml) and KI (3.53 mmol, 0.59 g) were added in and the mixture was left reacting for 2 days at reflux, monitoring it by TLC (Hex/AcOEt 8:2). The reaction was quenched with 1N HCl (50 ml) and the mixture was re-extracted with DCM (3 x 75 ml). The organic phases were combined, dried by reduced pressure and the crude was recrystallized three consecutive times with DCM/MeOH taking care of disposing each time the surnatant. The precipitate was filtered to get compound **38b** as yellow needle crystals (0.43 g, 0.76 mmol, 22% yield). **^{1}H NMR** (400 MHz, $CDCl_3$) δ (ppm): 7.86 (s, 2H, O*H*), 7.09 (d, *J* = 7.5 Hz, 4H, m-Ar*H*OCH$_2$CH$_2$OCH$_2$CH$_3$), 6.92 (d, *J* = 7.5 Hz, 4H, m-Ar*H*OH), 6.75 (t, *J* = 7.5 Hz, 2H, p-Ar*H*OCH$_2$CH$_2$OCH$_2$CH$_3$), 6.68 (t, *J* = 7.5 Hz, 2H, p-Ar*H*OH), 4.46 (d, *J* = 13.0 Hz, 4H, ArC*H*$_{ax}$HAr), 4.27 – 4.16 (m, 4H, OC*H*$_2$CH$_2$OCH$_2$CH$_3$), 4.02 – 3.95 (m, 4H, OCH$_2$C*H*$_2$OCH$_2$CH$_3$), 3.75 (q, *J* = 7.0 Hz, 4H, OCH$_2$CH$_2$OC*H*$_2$CH$_3$), 3.39 (d, *J* = 13.0 Hz, 4H, ArC*H*$_{eq}$HAr), 1.32 (t, *J* = 7.0 Hz, 6H, OCH$_2$CH$_2$OCH$_2$C*H*$_3$). The spectroscopic data obtained are in agreement with those ones reported in literature[30].

cone-25,27-(2-propoxy)-26,28-(3-N-phthalimido)propoxy-calix[4]arene (39a): In a 2-necked round-bottom flask, compound **38a** (2.10 mmol, 1.06 g) and 55% NaH (8.34 mmol, 0.36 g) were stirred in dry DMF (30 ml) for 15 minutes at 0°C. Then N-3-bromopropylphthalimide (8.34 mmol, 2.24 g) was added in and it was kept stirring for 1 day at room temperature, monitoring the reaction by TLC (Hex/AcOEt 8:2, R_f=0.10). The reaction was quenched with 1N HCl (20 ml)

and the precipitate formed was filtered. This solid was precipitated again in DCM/MeOH and again titrated in MeOH. The final crude was purified by a flash chromatography column (Hex/AcOEt 2:8→1:1) to get compound **39a** as a yellow foam (0.62 g, 0.70 mmol, 34% yield). **^{1}H NMR** (300 MHz, $CDCl_3$) δ (ppm): 7.88 – 7.76 (m, 4H, Pht*H*), 7.73 – 7.64 (m, 4H, Pht*H*), 6.74 (d, *J* = 6.5 Hz, 4H, m-Ar*H*O), 6.66 (dd, *J* = 8.4, 6.5 Hz, 2H, p-Ar*H*O), 6.42 (s, 6H, Ar*H*O), 4.41 (d, *J* = 13.4 Hz, 4H, ArCH_{ax}HAr), 4.07 (t, *J* = 7.4 Hz, 4H, NCH_2CH$_2$CH$_2$O), 3.86 (t, *J* = 7.4 Hz, 4H, NCH$_2$CH$_2$CH_2O), 3.76 (t, *J* = 7.4 Hz, 4H, OCH_2CH$_2$CH$_3$), 3.14 (d, *J* = 13.4 Hz, 4H, ArCH_{eq}HAr), 2.33 (p, *J* = 7.4 Hz, 4H, NCH$_2$CH_2CH$_2$O), 1.84 (hex, *J* = 7.4 Hz, 4H, OCH$_2$CH_2CH$_3$), 0.92 (t, *J* = 7.4 Hz, 6H, OCH$_2$CH$_2$CH_3). The spectroscopic data obtained are in agreement with those ones reported in literature[31].

cone-25,27-(2-ethoxyethylether)-26,28-(3-N-phthalimido)propoxy-calix[4]arene (39b): in a 2-necked round-bottom flask compound **38b** (0.64 mmol, 0.36 g) and 55% NaH (2.56 mmol, 0.11 g) were stirred in dry DMF (10 ml) for 30 minutes at 0°C. Then N-bromopropylphthalimide (2.56 mmol, 0.69 g) was added in and the mixture was kept stirring for 1 night at room temperature, monitoring it by TLC (Hex/AcOEt 6:4). The reaction was quenched with 1N HCl (5 ml) and the mixture was extracted with DCM (3 x 30 ml). The combined organic phase were washed with H_2O (3 x 30 ml), brine (3 x 30 ml) and eventually dried by reduced pressure. The crude was purified by a flash chromatography column (AcOEt/Hex 4:6) to get compound **39b** as a white powder (0.19 g, 0.20 mmol, 32% yield). **^{1}H NMR** (400 MHz, $CDCl_3$) δ 7.86 (dd, *J* = 5.3, 3.1 Hz, 4H, Pht*H*), 7.71 (dd, *J* = 5.4, 3.0 Hz, 4H, Pht*H*), 6.74 (d, *J* = 7.2 Hz, 4H, m-Ar*H*O), 6.67 (dd, *J* = 7.2, 7.0 Hz, 2H, p-Ar*H*O), 6.59 – 6.52 (m, 6H, Ar*H*), 4.53 (d, *J* = 13.4 Hz, 4H, axial ArCH_2Ar), 4.13 (t, *J* = 7.2 Hz, 4H, OCH$_2$CH$_2$CH_2NH$_2$), 4.11 (t, *J* = 5.5 Hz, 4H, OCH_2CH$_2$OCH$_2$CH$_3$), 3.91 (t, *J* = 7.2 Hz, 4H, OCH_2CH$_2$CH$_2$NH$_2$), 3.85 (t, *J* = 5.5 Hz, 4H, OCH$_2$CH_2OCH$_2$CH$_3$), 3.52 (q, *J* = 7.0 Hz, 4H, OCH$_2$CH$_2$OCH_2CH$_3$), 3.20 (d, *J* = 13.4 Hz, 4H, equatorial ArCH_2Ar), 2.40 (p, *J* = 7.2 Hz, 4H, OCH$_2$CH_2CH$_2$NH$_2$), 1.17 (t, *J* = 7.0 Hz, 6H, OCH$_2$CH$_2$OCH$_2$CH_3). **^{13}C NMR** (100 MHz, $CDCl_3$) δ (ppm): 168.2 (*C*=O), 156.6 (C_qAr), 156.0 (C_qAr), 135.4 (C_qAr), 134.7 (C_qAr), 133.9 (C_{Pht}), 132.3 (C_qAr), 128.5 (m-*C*Ar), 128.1 (C_qAr), 123.2 (C_{Pht}), 122.3 (p-*C*Ar), 122.2 (p-*C*Ar), 73.3 (O*C*H$_2$CH$_2$OCH$_2$CH$_3$), 72.6 (OCH$_2$*C*H$_2$NH$_2$), 69.7 (OCH$_2$*C*H$_2$OCH$_2$CH$_3$), 66.2 (OCH$_2$CH$_2$O*C*H$_2$CH$_3$), 35.5 (O*C*H$_2$CH$_2$CH$_2$NH$_2$), 31.0 (Ar*C*H$_2$Ar), 29.7 (OCH$_2$*C*H$_2$CH$_2$NH$_2$), 15.3 (OCH$_2$CH$_2$OCH$_2$C*H*$_3$). **ESI-MS (+)**: calcd. for $C_{58}H_{58}N_2O_{10}Na$ [(M+Na)$^+$] m/z 965.40, found m/z 965.89 (50%), calcd. for $C_{58}H_{58}N_2O_{10}K$ [(M+K)$^+$] m/z 981.37, found m/z 981.65 (20%).

cone-25,27-di(propoxy)-26,28-bis(3-aminopropoxy)-calix[4]arene (40a): In a 1-necked round-bottom flask, compound **39a** (0.70 mmol, 0.62 g) and $NH_2NH_2 \cdot H_2O$ (14.08 mmol, 0.439 ml) were stirred in absolute EtOH (20 ml) for 1 night at reflux, monitoring the reaction by TLC (AcOEt/MeOH 9:1). The solvent was removed by reduced pressure and the crude was suspended in H_2O (20 ml). The acqueous phase was extracted with DCM (4 x 20 ml) and finally the solvent was removed by reduced pressure to get compound **40a** as a white solid (0.44 g, 0.71 mmol, 99% yield). **^{1}H NMR** (300 MHz, $CDCl_3$) δ (ppm): 6.70 – 6.55 (m, 6H, Ar*H*), 6.52 (s, 6H, Ar*H*), 4.42 (d, *J* = 13.3 Hz, 4H, ArCH_{ax}HAr), 3.94 (t, *J* = 7.1 Hz, 4H, OCH_2CH$_2$CH$_3$), 3.85 (t, t, *J* = 7.1 Hz, 4H, NCH$_2$CH$_2$CH_2O), 3.15 (d, *J* = 13.3 Hz, 4H, ArCH_{eq}HAr), 2.89 (t, *J* = 7.1 Hz, 4H, NCH_2CH$_2$CH$_2$O), 2.03 (p, *J* = 7.1 Hz, 4H, NCH$_2$CH_2CH$_2$O), 1.92 (hex, *J* = 7.1 Hz, 4H, OCH$_2$CH_2CH$_3$), 1.50 (s, 4H, NH_2), 0.97 (t, *J* = 7.1 Hz, 6H, OCH$_2$CH$_2$CH_3). The spectroscopic data obtained are in agreement with those ones reported in literature[31].

cone-25,27-(2-ethoxyethylether)-26,28-(3-amino)propoxy-calix[4]arene (40b): In a 1-necked round-bottom flask, compound **39b** (0.20 mmol, 0.19 g) and $NH_2NH_2 \cdot H_2O$ (4.05 mmol, 0.126 ml) were stirred in absolute EtOH (20 ml) for 1 day at reflux, monitoring the reaction by TLC (AcOEt). The solvent was removed by reduced pressure and the crude was suspended in 1N NaOH (20 ml). The aqueous phase was extracted with DCM (4 x 20 ml) and finally the solvent was removed by reduced pressure. The crude was suspended in the minimum amount of DCM (1 ml) and it was left at 0°C for at least 2 h. Then the precipitate was filtered off and the solvent was removed by reduced pressure to get compound **40b** as a yellow oil (0.12 g, 0.18 mmol, 87% yield). **^{1}H NMR** (300 MHz, MeOD) δ (ppm): 6.85 - 6.75 (m, 4H, m-Ar*H*O), 6.73 – 6.60 (m, 2H, p-Ar*H*O), 6.38 (s, 6H, Ar*H*), 4.46 (d, *J* = 13.3 Hz, 4H, axial ArC*H*$_2$Ar), 4.15 (t, *J* = 5.6 Hz, 4H, OC*H*$_2$CH$_2$OCH$_2$CH$_3$), 3.91 (t, *J* = 6.9 Hz, 4H, OC*H*$_2$CH$_2$CH$_2$NH$_2$), 3.86 (t, *J* = 5.6 Hz, 4H, OCH$_2$C*H*$_2$OCH$_2$CH$_3$), 3.52 (q, *J* = 6.9 Hz, 4H, OCH$_2$CH$_2$OC*H*$_2$CH$_3$), 3.14 (d, *J* = 13.3 Hz, 4H, equatorial ArC*H*$_2$Ar), 2.84 (t, *J* = 6.9 Hz, 4H, OCH$_2$CH$_2$C*H*$_2$NH$_2$), 2.09 (p, *J* = 6.9 Hz, 4H, OCH$_2$C*H*$_2$CH$_2$NH$_2$), 1.18 (t, *J* = 6.9 Hz, 6H, OCH$_2$CH$_2$OCH$_2$C*H*$_3$).

cone-25,27-dipropoxy-26,28-bis(3-aminopropoxy)-calix[4]arene dihydrochloride (41a): In a 1-necked round-bottom flask, compound **40a** (24.10 umol, 15.00 mg) was dissolved in MeOH (2 ml) and under magnetic stirring 1N HCl (2 ml) was dropped in as long as pH=1 was reached. The methanolic solution was evaporated under reduced pressure and the resulting aqueous phase was lyophilized to get compound **41a** as a white powder (16.57 mg, 23.86 umol, 99% yield). **^{1}H NMR** (400 MHz, MeOD) δ (ppm): 6.81 (d, *J* = 7.5 Hz, 4H, m-Ar*H*O), 6.70 (t, *J* = 7.5 Hz, 2H, p-Ar*H*O), 6.45 (s, 6H, Ar*H*), 4.45 (d, *J* = 13.3 Hz, 4H, axial ArC*H*$_2$Ar), 4.00 (t, *J* = 7.2 Hz, 4H, OC*H*$_2$CH$_2$CH$_2$NH$_3$), 3.96 (t, *J* = 7.2 Hz, 4H, OC*H*$_2$CH$_2$CH$_3$), 3.22 (d, *J* = 13.3 Hz, 4H, equatorial ArC*H*$_2$Ar), 3.18 (t, *J* = 7.2 Hz, 4H, OCH$_2$CH$_2$C*H*$_2$NH$_3$), 2.27 (p, *J* = 7.2 Hz, 4H, OCH$_2$C*H*$_2$CH$_2$NH$_3$), 1.97 (hex, *J* = 7.2 Hz, 4H, OCH$_2$C*H*$_2$CH$_3$), 1.02 (t, *J* = 7.5 Hz, 6H, OCH$_2$CH$_2$C*H*$_3$).

cone-25,27-(2-ethoxyethylether)-26,28-bis(3-amino)propoxy-calix[4]arene dihydrochloride (41b): In a 1-necked round-bottom flask, compound **40b** (77.81 umol, 53.10 mg) was dissolved in MeOH (2 ml) and under magnetic stirring 1N HCl (2 ml) was dropped in as long as pH=1 was reached. The methanolic solution was evaporated under reduced pressure and the resulting aqueous phase was lyophilized. Finally it was reprecipitated in DCM/diethyl ether to get compound **41b** as a white powder (56.5 mg, 74.90 umol, 97% yield). **^{1}H NMR** (400 MHz, MeOD) δ (ppm): 6.72 (t, *J* = 7.8 Hz, 6H, Ar*H*), 6.62 (t, *J* = 7.8 Hz, 4H, Ar*H*), 6.57 – 6.37 (m, 2H, Ar*H*), 4.50 (d, *J* = 13.0 Hz, 4H, axial ArC*H*$_2$Ar), 4.19 (t, *J* = 4.6 Hz, 4H, OC*H*$_2$CH$_2$OCH$_2$CH$_3$), 4.09 (t, *J* = 6.8 Hz, 4H, OC*H*$_2$CH$_2$CH$_2$NH$_3$), 3.85 (t, *J* = 4.6 Hz, 4H, OCH$_2$C*H*$_2$OCH$_2$CH$_3$), 3.61 (q, *J* = 7.0 Hz, 4H, OCH$_2$CH$_2$OC*H*$_2$CH$_3$), 3.27 – 3.21 (m, 4H, OCH$_2$CH$_2$C*H*$_2$NH$_3$), 3.26 (d, *J* = 13.0 Hz, 4H, equatorial ArC*H*$_2$Ar), 2.34 (p, *J* = 6.8 Hz, 4H, OCH$_2$C*H*$_2$CH$_2$NH$_3$), 1.25 (t, *J* = 7.0 Hz, 6H, OCH$_2$CH$_2$OCH$_2$C*H*$_3$).

cone-25,27-dipropoxy-26,28-bis(3-((4-benzensulfanamidyl)thioureido)propoxy)-calix[4]arene (42a): In a 2-necked round-bottom flask compound **40a** (0.14 mmol, 85.00 mg) and NEt_3 (1.36 mmol, 0.190 ml) were stirred in dry DMF/dry DCM (1 ml + 1 ml) for 30 minutes at room temperature. Then 4-isothiocyanatebenzensolfonamide (0.30 mmol, 64.33 mg) was added in and the mixture was kept stirring for 1 night at room temperature, monitoring it by TLC (AcOEt/MeOH 9:1 + 1% NEt_3). The reaction was quenched with 1N HCl (5 ml) and the mixture was extracted with DCM (3 x 30 ml). The combined organic phases were dried at rotavapor and the crude was purified by semipreparative TLC (AcOEt + 1% NEt_3). The solid collected was hence

triturated in Et_2O and upon filtration, compound **42a** was obtained as a white powder (90.00 mg, 85.69 umol, 91% yield). **^{1}H NMR** (400 MHz, MeOD) δ (ppm): 7.84 (d, *J* = 8.7 Hz, 4H, m-Ar*H*SO_2), 7.66 (d, *J* = 8.7 Hz, 4H, o-Ar*H*SO_2), 6.73 (d, *J* = 7.4 Hz, 4H, m-Ar*H*O), 6.64 (t, *J* = 7.4 Hz, 2H, p-Ar*H*O), 6.56 – 6.44 (m, 6H, Ar*H*), 4.50 (d, *J* = 13.2 Hz, 4H, axial ArCH_2Ar), 4.07 (t, *J* = 7.2 Hz, 4H, O$CH_2CH_2CH_2$NH), 3.86 (t, *J* = 7.2 Hz, 4H, O$CH_2CH_2CH_3$), 3.82 (t, *J* = 7.2 Hz, 4H, $OCH_2CH_2CH_2$NH), 3.17 (d, *J* = 13.2 Hz, 4H, equatorial ArCH_2Ar), 2.33 (p, *J* = 7.2 Hz, 4H, $OCH_2CH_2CH_2$NH), 1.97 (hex, *J* = 7.2 Hz, 4H, $OCH_2CH_2CH_3$), 1.04 (t, *J* = 7.2 Hz, 6H, $OCH_2CH_2CH_3$). **^{13}C NMR** (100 MHz, MeOD) δ (ppm): 181.0 (*C*=S), 156.5 (C_qAr), 156.1 (C_qAr), 142.8 (C_qAr), 138.9 (C_qAr), 135.3 (C_qAr), 134.4 (C_qAr), 128.2 (*C*ArH), 127.8 (*C*ArH), 126.6 (m-*C*ArHSO_2), 122.5 (o-*C*ArHSO_2), 121.9 (*C*ArH), 121.6 (*C*ArH), 76.8 (O$CH_2CH_2CH_3$), 72.4 (O$CH_2CH_2CH_2$N), 41.6 ($OCH_2CH_2CH_2$N), 30.6 (ArCH_2Ar), 29.6 ($OCH_2CH_2CH_2$N), 23.3 ($OCH_2CH_2CH_3$), 9.8 ($OCH_2CH_2CH_3$). **ESI-MS (-)**: calcd. for $C_{54}H_{61}N_6O_8S_4$ [(M-H)$^-$] m/z 1049.35, found m/z 1049.28 (45%), calcd. for $C_{54}H_{61}N_6O_8S_4Cl$ [(M+Cl)$^+$] m/z 1085.32, found m/z 1085.84 (100%).

cone-25,27-dipropoxy-26,28-bis(3-(4-sulfamoylbenzamido)propoxy)-calix[4]arene (42b) and cone-25,27-dipropoxy-26- (3-(4-sulfamoylbenzamido))-28-(3-aminopropoxy)-calix[4]arene hydrochloride (42bx): In a 10 ml microwave tube equipped with a magnetic stir bar, compound **40a** (0.10 mmol, 64.50 mg), 4-sulfamoylbenzoic acid (0.23 mmol, 47.80 mg), DIPEA (0.52 mmol, 0.090 ml) and EDC (0.25 mmol, 47.00 mg) were dissolved in dry DMF (6 ml). The mixture was subjected to a first microwave cycle (T = 80°C, rampe time = 3 minutes, hold time = 2, P = 200 psi, potency = 200 W) at end of which it was monitored by TLC (AcOEt). Due to incomplete conversion of compound (?), another portion of 4-sulfamoylbenzoic acid (0.23 mmol, 47.80 mg) and EDC (0.25 mmol, 47.00 mg) were added in and the mixture was subjected to a second microwave cycle with the same experimental parameters. Once assessed the reaction was completed, it was quenched with 1N HCl (5 ml). The mixture was extracted with DCM (4 x 20 ml), washed with brine (2 x 20 ml) and then the solvent was removed by reduced pressure. The crude was purified by semipreparative TLC (AcOEt/Hex 7:3) to get compound **42b** as a white powder (7.90 mg, 7.99 umol, 8% yield). [**a**] **^{1}H-NMR** (400 MHz, MeOD) δ (ppm): 7.98 (s, 8H, CH*CH*CSO_2NH_2, *CH*$CHCSO_2NH_2$), 6.85 (d, J = 7.5 Hz, 4H, Ar*H*), 6.74 (dd, 2H, J = 6.8, 7.5 Hz, Ar*H*), 6.37 (s, 6H, Ar*H*), 4.49 (d, J = 13.2 Hz, 4H, axial ArCH_2Ar), 4.13 (t, J = 7.2 Hz, 4H, $OCH_2CH_2CH_2NH_2$), 3.77 (t, J = 7.2 Hz, 4H, O$CH_2CH_2CH_3$), 3.55 (t, J = 7.2 Hz, 4H, O$CH_2CH_2CH_2NH_2$), 3.16 (d, J = 13.2 Hz, 4H, equatorial ArCH_2Ar), 2.36 (p, J = 7.2 Hz, 4H, $OCH_2CH_2CH_2NH_2$), 1.89 (hex, J = 7.2 Hz, 4H, $OCH_2CH_2CH_3$), 0.96 (t, J = 7.5 Hz, 6H, $OCH_2CH_2CH_3$). [**a**] **^{13}C- NMR** (100 MHz, MeOD) δ (ppm): 225.0 (*Cq* Ar), 197.1 (*Cq* Ar), 167.3 (*C*ONH), 155.6 (*Cq* Ar), 146.3 (*Cq* Ar), 138.0 (*Cq* Ar), 135.9 (*Cq* Ar solf), 133.9 (*Cq* Ar solf), 128.3 (*C*H Ar), 127.6 (*C*H solf), 127.5 (*C*H Ar), 125.9 (*C*H Ar solf), 121.9 (*C*H Ar), 121.7 (*C*H Ar), 121.6 (*C*H Ar), 76.6 (O$CH_2CH_2CH_2NH_2$), 72.5 ($OCH_2CH_2CH_2NH_2$), 37.1 (O$CH_2CH_2CH_3$), 30.5 (ArCH_2Ar), 30.1 ($OCH_2CH_2CH_2NH_2$), 23.1 ($OCH_2CH_2CH_3$), 9.7 ($OCH_2CH_2CH_3$). [a] **ESI-MS (-)**: calcd. for $C_{54}H_{59}N_4O_{10}S_2$ [(M-H)$^-$] m/z 987.38, found m/z 987.18 (40%), calcd. for $C_{54}H_{60}N_4O_{10}S_2Cl$ [(M+Cl)$^+$] m/z 1023.34, found m/z 1023.51 (70%). [**b**] **^{1}H NMR** (400 MHz, MeOD) δ (ppm): 8.01 (s, 4H, solfonamide Ar*H*), 6.76 (d, *J* = 7.2 Hz, 4H, Ar*H*), 6.66 (t, *J* = 7.2 Hz, 2H, Ar*H*), 6.50 – 6.41 (m, 6H, Ar*H*), 4.48 (d, *J* = 13.2 Hz, 4H, ArCH_{ax}HAr), 4.46 (d, *J* = 13.2 Hz, 4H, ArCHH_{ax}Ar), 4.09 (t, *J* = 7.2 Hz, 2H, $OCH_2CH_2CH_2NH_3$), 4.04 (t, *J* = 7.2 Hz, 2H, $OCH_2CH_2CH_2NCO$), 3.82 (t, *J* = 7.4 Hz, 4H, O$CH_2CH_2CH_3$), 3.58 (t, *J* = 7.2 Hz, 2H, O$CH_2CH_2CH_2NH_3$), 3.42 (t, *J* = 7.2 Hz, 2H, O$CH_2CH_2CH_2NCO$), 3.16 (d, *J* = 13.2 Hz, 4H, ArCHH_{eq}Ar), 2.34 (p, *J* = 7.2 Hz, 2H, $OCH_2CH_2CH_2NH_3$), 2.22 (p, *J* = 7.2 Hz, 2H, $OCH_2CH_2CH_2NCO$), 1.92 (hex, *J* = 7.4 Hz, 4H, $OCH_2CH_2CH_3$), 1.01 (t, *J* = 7.4 Hz, 6H, $OCH_2CH_2CH_3$). [**b**] **^{13}C NMR** (100 MHz, MeOD) δ

(ppm): 162.4, 157.0, 155.9, 135.4, 134.3, 128.2, 127.7, 127.6, 125.9, 121.9, 121.6, 102.4, 76.7, 72.6, 35.0, 33.4, 30.5, 30.0, 29.3, 23.2, 9.7. [**b**] **ESI-MS (-)**: calcd. for $C_{54}H_{59}N_4O_{10}S_2$ [$(M-H)^-$] m/z 987.38, found m/z 987.48 (55%), calcd. for $C_{54}H_{60}N_4O_{10}S_2Cl$ [$(M+Cl)^+$] m/z 1023.34, found m/z 1023.66 (100%).

cone-25,27-(2-ethoxyethylether)-26,28-bis(3-((4-benzensulfanamidyl)thioureido)propoxy)-calix[4]arene (42c): In a 2-necked round-bottom compound **40b** (43.96 umol, 30.00 mg) and NEt_3 (3 drops from Pasteur pipette) were stirred in dry DMF/dry DCM (1 ml + 2 ml) for 30 minutes at room temperature. Then 4-isothiocyanatebenzensolfonamide (96.72 mmol, 20.70 mg) was added in and the mixture was kept stirring for 1 night at room temperature, monitoring it by TLC (AcOEt/Hex 8:2). The reaction was quenched with 1N HCl (5 ml) and the mixture was extracted with DCM (3 x 30 ml). The combined organic phases were dried at rotavapor and the crude was purified by semipreparative TLC (AcOEt/Hex 8:2) to get compound **42c** as a white powder (11.10 mg, 10.00 umol, 23% yield). **^{1}H NMR** (400 MHz, MeOD) δ (ppm): 7.85 (d, *J* = 8.7 Hz, 4H, m-Ar*H*SO_2), 7.65 (d, *J* = 8.7 Hz, 4H, o-Ar*H*SO_2), 6.69 – 6.51 (m, 12H, ArH_{calix}), 4.53 (d, *J* = 13.3 Hz, 4H, axial ArCH_2Ar), 4.13 (t, *J* = 5.2 Hz, 4H, OC$H_2$$CH_2OCH_2CH_3$), 4.07 (t, *J* = 7.2 Hz, 4H, OC$H_2$$CH_2CH_2N$), 3.89 (t, *J* = 5.2 Hz, 4H, OCH_2C$H_2$$OCH_2CH_3$), 3.85 (bt, *J* = 7.2 Hz, 4H, OCH_2CH_2CH_2N), 3.56 (q, *J* = 7.0 Hz, 4H, $OCH_2CH_2OCH_2CH_3$), 3.18 (d, *J* = 13.3 Hz, 4H, equatorial ArCH_2Ar), 2.34 (p, *J* = 7.2 Hz, 4H, OCH_2C$H_2$$CH_2N$), 1.18 (t, *J* = 7.0 Hz, 6H, $OCH_2CH_2OCH_2$CH_3). **^{13}C NMR** (100 MHz, MeOD) δ (ppm): 181.0 (*C*=S), 156.3 (*C*$_q$Ar), 156.1 (*C*$_q$Ar), 142.8 (*C*$_q$Ar), 134.9 (*C*$_q$Ar), 134.8 (*C*$_q$Ar), 128.1 (*C*ArH), 128.0 (*C*ArH), 126.7 (m-*C*ArSO_2), 122.0 (o-*C*ArSO_2), 121.9 (*C*ArH), 73.0 (O*C*$H_2CH_2OCH_2CH_3$), 72.6 (O*C*$H_2CH_2CH_2N$), 69.9 (OCH_2*C*$H_2OCH_2CH_3$), 66.1 (OCH_2CH_2O*C*H_2CH_3), 41.9 (OCH_2CH_2*C*H_2N), 30.6 (Ar*C*H_2Ar), 29.3 (OCH_2*C*H_2CH_2N), 14.4 ($OCH_2CH_2OCH_2$*C*H_3).

cone-25-(benzyloxy)-26,27,28-trihydroxycalix[4]arene (43): In a 2-necked round-bottom flask compound **37** (7.06 mmol, 3.0 g) and NaOMe (8.48 mmol, 0.45 g) were stirred in dry ACN (40 ml) for 30 minutes at reflux. Then benzyl bromide (17.00 mmol, 2.100 ml) was added in and the mixture was kept stirring for 1 night, monitoring the reaction by TLC (toluene/Hex 7:3, Rf=0.29). The reaction was quenched with 1N HCl (5 ml), ACN was removed by reduced pressure and then the aqueous phase was re-extracted with DCM (3 x 30 ml). The combined organic phases were dried with anhydrous Na_2SO_4 and upon filtration, the solvent was removed by reduced pressure. The crude was finally purified by a flash chromatography column (toluene/Hex 7:3) to get compound **43** as a white powder (1.94 g, 3.77 mmol, 65% yield). **^{1}H-NMR** (300 MHz, $CDCl_3$) δ (ppm): 9.57 (s, 1H, 27-O*H*), 9.23 (s, 2H, 26,28-O*H*), 7.71- 6.66 (m, 17H, Ar*H*), 5.22 (s, 2H, OCH_2Ar), 4.37 (d, *J* = 13.4 Hz, 2H, ArCH_{ax}HAr), 4.24 (d, *J* = 13.4 Hz, 2H, ArCHH_{ax}Ar), 3.46 (d, *J* = 13.4 Hz, 4H, equatorial ArCH_2Ar). The spectroscopic data obtained are in agreement with those ones reported in literature[32].

cone-25-benzyloxy-26,27,28-tripropoxy-calix[4]arene (44a): In a 2-necked round bottom flask compound **43** (1.94 mmol, 1.00 g) and 55% NaH (9.71 mmol, 0.42 g) were stirred in dry DMF (10 ml) for 30 minutes at 0°C. Then 1-iodopropane (9.71 mmol, 0.940 ml) was added in and the mixture was left reacting for 1 night at room temperature monitoring it by TLC (toluene/Hex 7:3). The reaction was quenched with 1N HCl (10 ml) and the mixture was extracted with AcOEt (4 x 50 ml). The combined organic phases were then dried with anhydrous Na_2SO_4 and upon filtration, the solvent was removed by reduced pressure. The crude was therefore purified by a

flash chromatography column (Hex/AcOEt 9:1) to get compound **44a** as a yellow oil (0.77 g, 1.20 mmol, 62% yield). **^{1}H NMR** (400 MHz, $CDCl_3$) δ (ppm): 7.48 (bd, *J* = 4.6 Hz, 2H, m-Ar*H*CH_2), 7.38 (bd, *J* = 4.6 Hz, 3H, o,p-Ar*H*CH_2), 6.79 (d, *J* = 8.0 Hz, 4H, m-ArH_{calix}), 6.73 – 6.67 (t, *J* = 8.0 Hz, 2H, p-ArH_{calix}), 6.51 (d, *J* = 8.0 Hz, 6H, ArH_{calix}), 4.92 (s, 2H, CH_2Ar), 4.49 (d, *J* = 13.4 Hz, 2H, ArCH_{ax}HAr), 4.42 (d, *J* = 13.4 Hz, 2H, ArCHH_{ax}Ar), 3.86 (t, *J* = 7.2 Hz, 6H, OC$H_2$$CH_2CH_3$), 3.18 (d, *J* = 13.4 Hz, 2H, ArCH_{eq}HAr), 3.13 (d, *J* = 13.4 Hz, 2H, ArCHH_{eq}Ar), 1.97 (hex, *J* = 7.2 Hz, 2H, 27-OCH_2CH_2CH_3), 1.87 (hex, *J* = 7.2 Hz, 4H, 26,28-OCH_2CH_2CH_3), 1.07 (t, *J* = 7.2 Hz, 3H, 27-OCH_2CH_2CH_3), 0.88 (t, *J* = 7.2 Hz, 6H, 26,28-OCH_2CH_2CH_3). **^{13}C-NMR** (100 MHz, $CDCl_3$) δ (ppm): 157.0, 156.1, 155.1, 137.9, 135.8, 135.6, 134.8, 134.6, 129.4 (*C*Bn), 128.4 (*C*Ar), 128.4 (*C*Ar), 128.1 (*C*Ar), 128.0 (*C*Ar), 127.9 (*C*Bn), 127.9 (*C*Ar), 121.9 (*C*Ar), 121.9 (*C*Ar), 76.8 (*C*H_2Bn), 76.6 (O*C*$H_2CH_2CH_3$), 31.1 (Ar*C*H_2Ar), 31.0 (Ar*C*H_2Ar), 23.4 (27-OCH_2*C*H_2CH_3), 23.1 (26,28-OCH_2CH_2*C*H_3), 10.6 (27-OCH_2CH_2*C*H_3), 10.0 (26,28-OCH_2CH_2*C*H_3). **ESI-MS (+)**: calcd. for $C_{44}H_{48}O_4(H_2O)$ [(M+H+H_2O)$^+$] m/z 658.37, found m/z 658.52 (20%), calcd. for $C_{44}H_{47}O_4Na$ [(M+Na)$^+$] m/z 663.35, found m/z 663.42 (100%), calcd. for $C_{44}H_{47}O_4K$ [(M+K)$^+$] m/z 679.32, found m/z 679.47 (30%). The spectroscopic data obtained are in agreement with those ones reported in literature[33].

cone-25,26,27-tris(2-ethoxyethylether)-28-(benzyloxy)-calix[4]arene (44b): in a 2-necked round bottom flask compound **43** (1.94 mmol, 1.00 g) and 55% NaH (9.71 mmol, 0.42 g) were stirred in dry DMF (10 ml) for 30 minutes at 0°C. Then 2-bromo-ethoxyethylether (9.71 mmol, 1.096 ml) was added in and the mixture was kept stirring for 5 h at room temperature, monitoring it by TLC (AcOEt/Hex 2:8). The reaction was quenched with 1N HCl (20 ml) and the mixture was extracted with AcOEt (3 x 70 ml) and dried with anhydrous Na_2SO_4. Upon filtration, The solvent was removed by reduced pressure to get compound **44b** as a yellow oil (1.37 g, 1.88 mmol, 97% yield). **^{1}H NMR** (300 MHz, CD_3CN) δ (ppm): 7.59 – 7.52 (m, 2H, m-Ar*H*O_{benz}), 7.48 – 7.37 (m, 3H, o,p-Ar*H*O_{benz}), 6.90 – 6.82 (m, 4H, Ar*H*), 6.72 (t, *J* = 7.5 Hz, 2H, p-Ar*H*O), 6.67 – 6.48 (m, 6H, Ar*H*), 4.99 (s, 2H, CH_2Ar), 4.58 (d, *J* = 13.2 Hz, 2H, ArCH_{ax}HAr), 4.48 (d, *J* = 13.2 Hz, 2H, ArCHH_{ax}Ar), 4.25 – 4.03 (m, 6H, OC$H_2CH_2OCH_2CH_3$), 3.91 (t, *J* = 5.1 Hz, 2H, 26-OCH_2C$H_2OCH_2CH_3$), 3.85 – 3.78 (m, 4H, 25,27-OCH_2C$H_2OCH_2CH_3$), 3.59 (q, *J* = 7.0 Hz, 2H, 26-$OCH_2CH_2OCH_2$CH_3), 3.50 – 3.38 (m, 4H, 25,27-$OCH_2CH_2OCH_2$CH_3), 3.21 (d, *J* = 13.2 Hz, 2H, ArCHH_{eq}Ar), 3.15 (d, *J* = 13.2 Hz, 2H, ArCH_{eq}HAr), 1.22 (t, *J* = 7.0 Hz, 3H, 26-$OCH_2CH_2OCH_2$CH_3), 1.16 (t, *J* = 7.0 Hz, 6H, 25,27-$OCH_2CH_2OCH_2$CH_3). **ESI-MS (+)**: calcd. for $C_{47}H_{54}O_7Na$ [(M+Na)$^+$] m/z 753.38, found m/z 753.49 (100%), calcd. for $C_{47}H_{54}O_7K$ [(M+K)$^+$] m/z 769.35, found m/z 769.55 (18%).

cone-26,27,28-tripropoxy-calix[4]arene-25-olo (45a): In a Parr reactor 10% Pd/C (catalytic amount) was suspended into a solution of compound **44a** (1.20 mmol, 0.77 g) in AcOEt (100 ml). H_2 was added in at 3.0 bar of pressure through a Parr apparatus and the mixture was left reacting for 1 night at room temperature, monitoring the reaction by TLC (Hex/AcOEt 8:2). The catalyst was filtered off with celite and the solvent was removed by reduced pressure to get compound **45a** as a white powder (0.55 g, 1.00 mmol, 83% yield). **^{1}H-NMR** (400 MHz, acetone-d6) δ (ppm): 7.26 (d, *J* = 7.5 Hz, 2H, m-Ar*H*), 7.16 (d, *J* = 7.5 Hz, 2H, m-Ar*H*), 7.05 – 6.98 (m, 1H, Ar*H)*, 6.79 (t, *J* = 7.5 Hz, 1H, p-Ar*H),* 6.49 (d, *J* = 7.5 Hz, 4H, Ar*H*), 6.42 (t, *J* = 7.5 Hz, 2H, p-Ar*H*), 5.23 (s, 1H, O*H*), 4.48 (d, *J* = 13.2 Hz, 2H, ArCH_{ax}HAr), 4.41 (d, *J* = 13.2 Hz, 2H, ArCHH_{ax}Ar), 3.93 – 3.87 (m, 2H, 27-CH_3CH_2CH_2O), 3.83 – 3.75 (m, 4H, 26,28-CH_3CH_2CH_2O), 3.35 (d, *J* = 13.2 Hz, 2H, ArCH_{eq}HAr), 3.29 (d, *J* = 13.2 Hz, 2H, ArCHH_{eq}Ar), 2.44 (hex, *J* = 7.0 Hz, 2H, 27-CH_3CH_2CH_2O),

2.10-1.85 (m, 4H, 26,28-$CH_3CH_2CH_2O$), 1.21 (t, *J* = 7.0 Hz, 6H, 26,28-$CH_3CH_2CH_2O$), 1.03 (t, *J* = 7.0 Hz, 3H, 27-$CH_3CH_2CH_2O$).

cone-25,26,27-tris(2-ethoxyethylether)-calix[4]arene-28-olo (45b) [hydrogenation]: In a Parr reactor 10% Pd/C (catalytic amount) was suspended into a solution of compound **44b** (1.69 mmol, 1.23 g) in AcOEt/EtOH (150 ml + 150 ml). H_2 was added in at 2.5 bar of pressure through a Parr apparatus and the mixture was left reacting for 1 night at room temperature, monitoring the reaction by TLC (Hex/AcOEt 8:2). The catalyst was filtered off and the solvent was removed by reduced pressure to get compound **45b** as a yellow oil (0.98 g, 1.54 mmol, 91% yield). **^{1}H NMR** (400 MHz, Acetone) δ (ppm): 7.24 (d, *J* = 7.5 Hz, 2H, m-Ar*H*O), 7.15 (d, *J* = 7.5 Hz, 2H, m-Ar*H*O), 6.98 (t, *J* = 7.5 Hz, 1H, p-Ar*H*O), 6.76 (t, *J* = 7.5 Hz, 1H, p-Ar*H*O), 6.58 (dd, *J* = 7.6, 2.1 Hz, 4H, m-Ar*H*O), 6.48 (t, *J* = 7.5 Hz, 2H, p-Ar*H*O), 5.76 (s, 1H, O*H*), 4.67 (d, *J* = 13.2 Hz, 2H, ArCH_{ax}HAr), 4.51 (d, *J* = 13.2 Hz, 2H, ArCHH_{ax}Ar), 4.30 – 4.20 (m, 2H, 26-O$CH_2CH_2OCH_2CH_3$), 4.16 - 4.00 (m, 6H, 25,27-O$CH_2CH_2OCH_2CH_3$, 26-$OCH_2CH_2OCH_2CH_3$), 3.88 (t, *J* = 4.7 Hz, 4H, 25,27-$OCH_2CH_2OCH_2CH_3$), 3.70 (q, *J* = 6.8 Hz, 2H, 26-$OCH_2CH_2OCH_2CH_3$), 3.67 (q, *J* = 6.8 Hz, 4H, 25,27-$OCH_2CH_2OCH_2CH_3$), 3.37 (d, *J* = 13.2 Hz, 2H, ArCHH_{eq}Ar), 3.31 (d, *J* = 13.2 Hz, 2H, ArCH_{eq}HAr), 1.32 – 1.24 (m, 9H, $OCH_2CH_2OCH_2CH_3$). The spectroscopic data obtained are in agreement with those ones reported in literature[34].

cone-25,26,27-tris(2-ethoxyethylether)-calix[4]arene-28-olo (45b) [direct trifunctionalization]: in a 2-necked round bottom flask compound **37** (4.10 mmol, 1.93 g), BaO (19.3 mmol, 3.29 g) and $Ba(OH)_2 \cdot 8H_2O$ (12.30 mmol, 3.88 g) was stirred in dry DMF (60 ml) for 2 h at room temperature. Then the mixture was heated up to 80°C, 2-bromo-ethoxyethylether (82.00 mmol, 9.247 ml) was added in and the mixture was kept stirring for 1 night, monitoring it by TLC (Hex/AcOEt 9:1). The reaction was quenched with 1N HCl (30 ml) and the mixture was re-extracted with DCM (3 x 30 ml). The combined organic phase were dried at rotavapor and the crude was purified by flash chromatography column (Hex/AcOEt 85:15→80:20) to get compound (?) as a white powder (1.80 g, 2.81 mmol, 62% yield). In the following characterization "tri-fz" is compound **45b** and "tetra-fz" is compound **50b**. On the basis of NMR peak relative intensities was determined the percentage composition of the mixture (tri-fz=80%, tetra-fz=20%). **^{1}H NMR** (400 MHz, Acetone) δ (ppm): 7.21 (d, *J* = 7.5 Hz, 2H, Ar*H* [tri-et]), 7.11 (d, *J* = 7.5 Hz, 2H, Ar*H* [tri-et])), 6.93 (t, *J* = 7.5 Hz, Ar*H* [tetra-et]), 6.70 (d, *J* = 7.4 Hz, Ar*H* [tetra-et]), 6.67 (d, *J* = 7.4 Hz, 2H, Ar*H* [tri-et]), 6.59 – 6.55 (m, Ar*H* [tetra-et]), 6.55 – 6.52 (m, 4H, Ar*H* [tri-et]), 6.44 (t, *J* = 7.4 Hz, 2H, Ar*H* [tri-et]), 5.79 (s, 1H, O*H* [tri-et]), 4.62 (d, *J* = 13.4 Hz, 2H, ArCHH_{ax}Ar [tri-et]), 4.60 (t, *J* = 13.2 Hz, axial ArCH_2Ar [tetra-et]), 4.46 (d, *J* = 13.4 Hz, 2H, ArCH_{ax}HAr [tri-et]), 4.25 – 4.18 (m, 6H, O$CH_2CH_2OCH_2CH_3$ [tri-et]), 4.15 (t, *J* = 5.6 Hz, O$CH_2CH_2OCH_2CH_3$ [tetra-et]), 4.11 – 3.99 (m, 6H, $OCH_2CH_2OCH_2CH_3$ [tri-et]), 3.92 (t, *J* = 5.5 Hz, $OCH_2CH_2OCH_2CH_3$ [tetra-et]), 3.85 (t, *J* = 4.7 Hz, 6H,), 3.64 (tt, *J* = 7.0, 3.5 Hz, 3H), 3.68 – 3.61 (m, 6H, $OCH_2CH_2OCH_2CH_3$ [tri-et]), 3.58 (q, *J* = 7.2 Hz, $OCH_2CH_2OCH_2CH_3$ [tetra-et]), 3.33 (d, *J* = 13.4 Hz, 2H, ArCHH_{ax}Ar [tri-et]), 3.27 (d, *J* = 13.4 Hz, 2H, ArCH_{ax}HAr [tri-et]), 3.17 (d, *J* = 13.2 Hz, equatorial ArCH_2Ar [tetra-et]), 1.26 – 1.17 (m, $OCH_2CH_2OCH_2CH_3$ [tri-et]/ [tetra-et]), 0.89 (t, *J* = 6.8 Hz, 3H, $OCH_2CH_2OCH_2CH_3$ [tri-et]). The spectroscopic data obtained are in agreement with those ones reported in literature[34].

cone-25-(3-N-phthalimido)propoxy-26,27,28-tripropoxy-calix[4]arene (46a): In a 2-necked round-bottom flask compound **45a** (0.32 mmol, 0.18 g) and 55% NaH (0.73 mmol, 31.00 mg)

were stirred in dry DMF (10 ml) for 30 minutes at 0°C. Then 3-N-bromopropylphthalimide (0.73 mmol, 0.20 g) was added in and the mixture was kept stirring for 1 night at room temperature, monitoring it by TLC (Hex/AcOEt 7:3). The reaction was quenched with 1N HCl (5 ml) and the mixture was re-extracted with DCM (2 x 30 ml). The combined organic phases were washed with H_2O (2 x 30 ml), brine (30 ml) and dried with anhydrous Na_2SO_4. Upon filtration, the solvent was removed by reduced pressure and the crude was purified by a flash chromatography column (Hex/AcOEt 8:2) to get compound **46a** as white powder (85.00 mg, 0.12 mmol, 36% yield). **^{1}H NMR** (300 MHz, $CDCl_3$) δ (ppm): 7.85 (dd, *J* = 7.1 Hz, 2H, Pht*H*), 7.72 (dd, *J* = 7.1 Hz, 2H, Pht*H*), 6.76 – 6.57 (m, 6H, ArH_{calix}), 6.57 – 6.42 (m, 6H, ArH_{calix}), 4.46 (d, *J* = 13.4 Hz, 2H, ArCHH_{ax}Ar), 4.42 (d, *J* = 13.4 Hz, 2H, ArCH_{ax}HAr), 4.02 (t, *J* = 7.5 Hz, 2H, NCH_2CH$_2$CH$_2$O), 3.88 (t, *J* = 7.5 Hz, 2H, NCH$_2$CH$_2$CH_2O), 3.86 – 3.75 (m, 6H, CH$_3$CH$_2$CH_2O), 3.16 (d, *J* = 13.4 Hz, 2H, ArCH_{eq}HAr), 3.13 (d, *J* = 13.4 Hz, 2H, ArCHH_{eq}Ar), 2.33 (p, *J* = 7.5 Hz, 2H, NCH$_2$CH_2CH$_2$O), 1.90 (hex, *J* = 7.5 Hz, 6H, CH$_3$CH_2CH$_2$O), 0.98 (t, *J* = 7.6 Hz, 6H, 26,28-CH_3CH$_2$CH$_2$O), 0.96 (t, *J* = 7.6 Hz, 3H, 27-CH_3CH$_2$CH$_2$O). The spectroscopic data obtained are in agreement with those ones reported in literature[35].

cone-25,26,27-tris(2-ethoxyethylether)-28-(3-N-phthalimido)propoxy-calix[4]arene (46b): In a 2-necked round bottom flask compound **45b** (1.78 mmol, 1.14 g, conc=80%) and 55% NaH (3.12 mmol, 0.14 g) were stirred in dry DMF (30 ml) for 30 minutes at 0°C. Then NaI (catalytic amount) and N-bromopropylphthalimide (3.12 mmol, 0.84 g) were added in and the mixture was kept stirring for 2 days at 80°C, monitoring it by TLC (Hex/AcOEt 7:3). The reaction was quenched with 1N HCl (20 ml) and the mixture was re-extracted with DCM (3 x 40 ml). The combined organic phases were hence washed with 0.5M $Na_2S_2O_3$ (1 x 20 ml), brine (3 x 40 ml), H_2O (1 x 30 ml) and eventually the solvent was removed by reduced pressure. The crude was purified by a flash chromatography column (Hex/AcOEt 75:25→70:30) to get compound **46b** as a white powder (0.89 g, 1.07 mmol, 75% yield). **^{1}H NMR** (400 MHz, $CDCl_3$) δ (ppm): 7.87 (dd, *J* = 5.4, 3.0 Hz, 2H, Pht*H*), 7.74 (dd, *J* = 5.4, 3.1 Hz, 2H, Pht*H*), 6.74 – 6.48 (m, 12H, Ar*H*), 4.53 (d, *J* = 13.3 Hz, 2H, ArCHH_{ax}Ar), 4.49 (d, *J* = 13.3 Hz, 2H, ArCH_{ax}HAr), 4.20 – 4.07 (m, 6H, OCH_2CH$_2$OCH$_2$CH$_3$), 4.04 (t, *J* = 7.2 Hz, 2H, OCH_2CH$_2$CH$_2$N), 3.86 (t, *J* = 7.2 Hz, 6H, OCH$_2$CH_2OCH$_2$CH$_3$), 3.84 (t, *J* = 7.2 Hz, 2H, OCH$_2$CH$_2$CH_2N), 3.54 (q, *J* = 7.0 Hz, 4H, 25,27-OCH$_2$CH$_2$OCH_2CH$_3$), 3.53 (q, *J* = 7.0 Hz, 2H, 26-OCH$_2$CH$_2$OCH_2CH$_3$), 3.18 (d, *J* = 13.4Hz, 2H, ArCH_{eq}HAr), 3.16 (d, *J* = 13.4 Hz, 2H, ArCHH_{eq}Ar), 2.35 (p, *J* = 7.2 Hz, 2H, OCH$_2$CH_2CH$_2$N), 1.22 – 1.16 (m, 9H, OCH$_2$CH$_2$OCH$_2$CH_3). **^{13}C NMR** (100 MHz, $CDCl_3$) δ (ppm): 168.2 (*C*=O), 156.6 (C_qAr), 156.2 (C_qAr), 135.2 (C_qAr), 135.0 (C_qAr), 134.9 (C_qAr), 133.9 (C_{Pht}), 132.2 (C_qAr), 128.3 (*C*Ar), 128.3 (*C*Ar), 128.1 (*C*Ar), 123.2 (C_{Pht}), 122.3 (*C*Ar), 122.2 (*C*Ar), 73.2 (OCH_2CH$_2$OCH$_2$CH$_3$), 72.5 (OCH_2CH$_2$CH$_2$N), 69.7 (OCH$_2$CH_2OCH$_2$CH$_3$), 66.3 (OCH$_2$CH$_2$OCH_2CH$_3$), 35.5 (OCH$_2$CH$_2$CH_2N), 31.0 (ArCH_2Ar), 30.9 (ArCH_2Ar), 29.6 (OCH$_2$CH_2CH$_2$N), 15.3 (OCH$_2$CH$_2$OCH$_2$CH_3). **ESI-MS (+)**: calcd. for $C_{51}H_{57}NO_9Na$ [(M+Na)$^+$] m/z 850.39, found m/z 850.69 (100%), calcd. for $C_{51}H_{57}NO_9K$ [(M+K)$^+$] m/z 866.37, found m/z 866.67 (25%).

cone-25-(3-N-amino)propoxy-26,27,28-tripropoxy-calix[4]arene (47a): In a 1-necked round-bottom flask compound **46a** (0.15 mmol, 85.00 mg) and $NH_2NH_2{\cdot}H_2O$ (2.30 mmol, 0.072 ml) were stirred in absolute EtOH (2 ml) for 1 night at reflux, monitoring the reaction by TLC (AcOEt/MeOH 8:2). The reaction was quenched with 1N HCl (1 ml) and the mixture was re-extracted with DCM (3 x 30 ml). The combined organic phases were washed with 1M NaOH (2 x 20 ml), H_2O (2 x 20 ml) and finally the solvent was removed by reduced pressure to get

compound **47a** as a white powder (38.00 mg, 62.56 umol, yield 54%). **^{1}H NMR** (300 MHz, $CDCl_3$) δ 6.74 – 6.43 (m, 10H, Ar*H*), 6.43 – 6.28 (m, 2H, Ar*H*), 5.39 (s, 2H, NH_2), 4.45 (d, *J* = 13.0 Hz, 2H, ArCH_{ax}HAr), 4.44 (d, *J* = 13.0 Hz, 2H, ArCHH_{ax}Ar), 3.95 (t, *J* = 6.9 Hz, 2H, NCH_2CH$_2$CH$_2$O), 3.86 (t, *J* = 6.9 Hz, 4H, 26,28-CH$_3$CH$_2$CH_2O), 3.83 (t, *J* = 6.9 Hz, 2H, 27-CH$_3$CH$_2$CH_2O), 3.74 (t, *J* = 6.9 Hz, 2H, NCH$_2$CH$_2$CH_2O), 3.16 (d, *J* = 13.0 Hz, 2H, ArCH_{eq}HAr), 3.15 (d, *J* = 13.0 Hz, 2H, ArCHH_{eq}Ar), 2.05 (p, *J* = 6.9 Hz, 2H, NCH$_2$CH_2CH$_2$O), 2.00 – 1.75 (m, 6H, CH$_3$CH_2CH$_2$O), 1.01 (t, *J* = 6.9 Hz, 3H, 27-CH_3CH$_2$CH$_2$O), 0.98 (t, *J* = 6.9 Hz, 6H, 26,28-CH_3CH$_2$CH$_2$O). The spectroscopic data obtained are in agreement with those ones reported in literature[35].

cone-25,26,27-tris(2-ethoxyethylether)-28-(3-N-amino)propoxy-calix[4]arene (47b): In a 1-necked round-bottom flask, compound **46b** (1.07 mmol, 0.89 g) and $NH_2NH_2{\cdot}H_2O$ (21.42 mmol, 0.667 ml) were stirred in absolute EtOH (8 ml) for 1 night at reflux, monitoring the reaction by TLC (AcOEt). The solvent was removed by reduced pressure and the mixture was extracted with DCM (4 x 30 ml). The combined organic phases were dried by reduced pressure to get compound **47b** as a colourless oil (0.71 g, 1.02 mmol, 95% yield). **^{1}H NMR** (400 MHz, MeOD) δ (ppm): 6.81 – 6.73 (m, 4H, Ar*H*), 6.71 – 6.61 (m, 6H, Ar*H*), 6.61 – 6.50 (m, 2H, Ar*H*), 4.54 (d, *J* = 13.2 Hz, 2H, ArCH_{ax}HAr), 4.54 (d, *J* = 13.2 Hz, 2H, ArCHH_{ax}Ar), 4.26 – 4.10 (m, 6H, OCH_2CH$_2$OCH$_2$CH$_3$), 4.04 (t, *J* = 6.9 Hz, 2H, OCH_2CH$_2$CH$_2$N), 3.89 (q, *J* = 5.6 Hz, 6H, OCH$_2$CH_2OCH$_2$CH$_3$), 3.65 (q, *J* = 7.2 Hz, 2H, 26-OCH$_2$CH$_2$OCH_2CH$_3$), 3.59 (q, *J* = 7.2 Hz, 4H, 25,27-OCH$_2$CH$_2$OCH_2CH$_3$), 3.22 (d, *J* = 13.2 Hz, 2H, ArCHH_{eq}Ar), 3.21 (d, *J* = 13.2 Hz, 2H, ArCH_{eq}HAr), 3.06 (t, *J* = 6.9 Hz, 2H, OCH$_2$CH$_2$CH_2N), 2.22 (p, *J* = 6.9 Hz, 2H, OCH$_2$CH_2CH$_2$N), 1.34 – 1.20 (m, 9H, OCH$_2$CH$_2$OCH$_2$CH_3). **^{13}C NMR** (100 MHz, MeOD) δ (ppm): 156.0 (C_qAr), 155.9 (C_qAr), 155.8 (C_qAr), 135.1 (C_qAr), 135.0 (C_qAr), 134.7 (C_qAr), 134.6 (C_qAr), 128.2 (*C*Ar), 128.1 (*C*Ar), 128.0 (*C*Ar), 128.0 (*C*Ar), 122.3 (*C*Ar), 122.25 (*C*Ar), 122.23 (*C*Ar), 73.6 (OCH_2CH$_2$OCH$_2$CH$_3$), 73.3 (OCH_2CH$_2$OCH$_2$CH$_3$), 73.0 (OCH_2CH$_2$CH$_2$N), 69.7 (OCH$_2$CH_2OCH$_2$CH$_3$), 69.5 (OCH$_2$CH_2OCH$_2$CH$_3$), 66.3 (OCH$_2$CH$_2$OCH_2CH$_3$), 66.1 (OCH$_2$CH$_2$OCH_2CH$_3$), 38.7 (OCH$_2$CH$_2$CH_2N), 32.0 (OCH$_2$CH_2CH$_2$N), 30.3 (Ar*C*H$_2$Ar), 14.3 (OCH$_2$CH$_2$OCH$_2$*C*H$_3$). **ESI-MS (+)**: calcd. for $C_{43}H_{56}NO_7$ [(M+H)$^+$]: m/z 698.40, found m/z 698.76 (100%), calcd. for $C_{43}H_{55}NO_7Na(H_2O)$ [(M+Na+H_2O)$^+$]: m/z 738.39, found m/z 738.66 (30%).

cone-25-(3-N-(amino))propoxy-26,27,28-tripropoxy-calix[4]arene hydrochloride (48a): In a 1-necked round-bottom flask, compound **47a** (0.30 mmol, 18.00 mg) was dissolved in MeOH (2 ml) and under magnetic stirring 1N HCl (2 ml) was dropped in as long as pH=1 was reached. The methanolic solution was evaporated under reduced pressure and the resulting aqueous phase was lyophilized to get compound **48a** as a white powder (19.00 mg, 29.64 umol, 99% yield). **^{1}H NMR** (300 MHz, MeOD) δ (ppm): 6.75 – 6.67 (m, 4H, Ar*H*), 6.65 – 6.55 (m, 2H, Ar*H*), 6.46 – 6.40 (m, 6H, Ar*H*), 4.43 (d, *J* = 13.2 Hz, 2H, ArCHH_{ax}Ar), 4.38 (d, *J* = 13.2 Hz, 2H, ArCH_{ax}HAr), 3.98 (t, *J* = 7.0 Hz, 2H, NCH_2CH$_2$CH$_2$O), 3.90 – 3.83 (m, 4H, 26,28-CH$_3$CH$_2$CH_2O), 3.76 (t, *J* = 7.0 Hz, 2H, NCH$_2$CH$_2$CH_2O), 3.19 – 3.07 (m, 6H, ArCH_{eq}HAr, ArCHH_{eq}Ar, 27-CH$_3$CH$_2$CH_2O), 2.28 – 2.16 (p, *J* = 7.0 Hz, 2H, NCH$_2$CH_2CH$_2$O), 1.91 (hex, *J* = 7.2 Hz, 6H, CH$_3$CH_2CH$_2$O), 0.92 – 0.89 (m, 9H, CH_3CH$_2$CH$_2$O). **^{13}C NMR** (75 MHz, MeOD) δ (ppm): 134.3, 133.9, 133.5, 133.3, 132.8, 132.8, 127.5, 127.5, 126.8, 126.7, 126.6, 126.5, 126.4, 126.2, 75.0, 51.9, 30.2 (Ar*C*H$_2$Ar), 29.1, 29.0, 27.8, 21.7, 21.5.

cone-25,26,27-tris(2-ethoxyethylether)-28-(3-N-amino)propoxy-calix[4]arene hydrochloride (48b): In a 1-necked round-bottom flask, compound **47b** (31.31 umol, 22.96 mg) was dissolved

in MeOH (2 ml) and under magnetic stirring 1N HCl (2 ml) was dropped in as long as pH=1 was reached. The methanolic solution was evaporated under reduced pressure and the resulting aqueous phase was lyophilized. Then it was suspended in DCM, filtered off and dried at rotavapor to get compound **48b** as a colourless oil (24.00 mg, 32.92 umol, 99% yield). ^{1}H NMR (400 MHz, MeOD) δ (ppm): 6.96 (dd, *J* = 7.4, 2.9 Hz, 4H, m-Ar*H*O), 6.89 (d, *J* = 7.4 Hz, 2H, m-Ar*H*O), 6.84 (d, *J* = 7.4 Hz, 2H, m-Ar*H*O), 6.75 (d, *J* = 7.7 Hz, 1H, p-Ar*H*O), 6.73 (t, *J* = 7.7 Hz, 1H, p-Ar*H*O), 6.66 (t, *J* = 7.7 Hz, 2H, p-Ar*H*O), 4.54 (d, *J* = 12.8 Hz, 2H, ArCH_{ax}HAr), 4.54 (d, *J* = 12.8 Hz, 2H, ArCHH_{ax}Ar), 4.31 – 4.20 (m, 4H, 25,27-OCH_2CH$_2$OCH$_2$CH$_3$), 4.19 – 4.08 (m, 4H, 26-OCH_2CH$_2$OCH$_2$CH$_3$, OCH_2CH$_2$CH$_2$N), 3.88 (t, *J* = 4.8 Hz, 2H, 26-OCH$_2$CH_2OCH$_2$CH$_3$), 3.81 (t, *J* = 4.8 Hz, 4H, 25,27-OCH$_2$CH_2OCH$_2$CH$_3$), 3.75 (q, *J* = 7.0 Hz, 2H, 26-OCH$_2$CH$_2$OCH_2CH$_3$), 3.67 (q, *J* = 7.0 Hz, 4H, 25,27-OCH$_2$CH$_2$OCH_2CH$_3$), 3.56 (t, *J* = 6.2 Hz, 2H, OCH$_2$CH$_2$CH_2N), 3.38 – 3.28 (m, 4H, equatorial ArCH_2Ar), 2.46 (p, *J* = 6.2 Hz, 2H, OCH$_2$CH_2CH$_2$N), 1.37 (t, *J* = 7.0 Hz, 3H, 26-OCH$_2$CH$_2$OCH$_2$CH_3), 1.30 (t, *J* = 7.0 Hz, 6H, 25,27-OCH$_2$CH$_2$OCH$_2$CH_3).

cone-25-(3-N-(sulfamoylbenzamido))propoxy-26,27,28-tripropoxy-calix[4]arene (49a): In a 2-necked round-bottom flask 4-sulfamoylbenzoic acid (33.00 umol, 7.00 mg) and DIPEA (8.40 umol, 0.015 ml) were stirred in dry DCM (10 ml). Then EDC (40.40 umol, 8.00 mg) and compound **47a** (3.40 umol, 20.00 mg) were added in and the mixture was kept stirring 1 night, monitoring the reaction by TLC (AcOEt/MeOH 8:2). The reaction was quenched with 1N HCl (5 ml) and the mixture was re-extracted with DCM (3 x 30 ml). The combined organic phases were washed with H_2O (2 x 20 ml) and finally the solvent was removed by reduced pressure to get compound **49a** as a white powder (11.00 mg, 13.92 umol, 41% yield). **^{1}H NMR** (400 MHz, MeOD) δ (ppm): 8.01 (d, *J* = 8.6 Hz, 2H, SO$_2$CC*H*), 7.97 (d, *J* = 8.6 Hz, 2H, SO$_2$CCHC*H*), 6.67 – 6.49 (m, 12H, Ar*H*), 4.50 (d, *J* = 13.2 Hz, 2H, ArCHH_{ax}Ar), 4.48 (d, *J* = 13.2 Hz, 2H, ArCH_{ax}HAr), 4.06 (t, *J* = 7.2 Hz, 2H, NCH_2CH$_2$CH$_2$O), 3.89 (t, *J* = 7.2 Hz, 2H, 27-CH$_3$CH$_2$CH_2O), 3.87 (t, *J* = 7.2 Hz, 4H, 26,28-CH$_3$CH$_2$CH_2O), 3.60 (t, *J* = 7.2 Hz, 2H, NCH$_2$CH$_2$CH_2O), 3.16 (d, *J* = 13.2 Hz, 2H, ArCH_{eq}HAr), 3.15 (d, *J* = 13.2 Hz, 2H, ArCHH_{eq}Ar), 2.02 (t, *J* = 7.2 Hz, 2H, NCH$_2$CH_2CH$_2$O), 1.97 (hex, *J* = 7.2 Hz, 6H, CH$_3$CH_2CH$_2$O), 1.05 (t, *J* = 7.2 Hz, 3H, 27-CH_3CH$_2$CH$_2$O), 1.03 (t, *J* = 7.2 Hz, 6H, 26,28-CH_3CH$_2$CH$_2$O). **^{13}C NMR** (100 MHz, MeOD) δ 208.7 (*C*ON), 156.8, 135.0, 135.0, 134.9, 134.8, 128.0, 127.9, 127.9, 127.9, 127.6, 76.9, 53.5, 30.6 (Ar*C*H$_2$Ar), 30.5 (Ar*C*H$_2$Ar), 29.9, 29.3, 29.3, 29.3, 23.1, 23.1, 22.8, 20.9. **ESI-MS (-)**: calcd. for $C_{47}H_{53}N_2O_7S$ [(M-H)$^-$] m/z 790.01, found m/z 790.40 (1%), calcd. for $C_{47}H_{54}N_2O_7SCl$ [(M+Cl)$^-$] m/z 825.33, found m/z 825.53 (2%).

cone-25,26,27-tris(2-ethoxyethylether)-28-(3-((4-benzensulfanamidyl)thioureido)propoxy)-calix[4]arene (49b): In a 2-necked round-bottom compound **47b** (0.14 mmol, 0.10 g) and 4-isothiocyanatebenzensolfonamide (96.72 mmol, 20.70 mg) were stirred in dry DMF/dry DCM (2 ml + 5 ml) for 1 day at room temperature, monitoring it by TLC (AcOEt/Hex 7:3). The reaction was quenched with 1N HCl (5 ml) and the mixture was extracted with DCM (3 x 30 ml). The combined organic phases were dried at rotavapor and the crude was purified by flash chromatography column (AcOEt/Hex 7:3) to get compound **49b** as a white powder (0.10 g, 0.11 mmol, 78% yield). **^{1}H NMR** (400 MHz, MeOD) δ (ppm): 7.86 (dt, *J* = 8.8, 1.6 Hz, 2H, ArH_{solf}), 7.66 (dt, *J* = 8.8, 1.6 Hz, 2H, ArH_{solf}), 6.63 (d, *J* = 7.2 Hz, 8H, Ar*H*), 6.60 – 6.51 (m, 4H, Ar*H*), 4.55 (d, *J* = 13.2 Hz, 2H, ArCH_{ax}HAr), 4.52 (d, *J* = 13.2 Hz, 2H, ArCHH_{ax}Ar), 4.20 – 4.07 (m, 6H, OCH_2CH$_2$OCH$_2$CH$_3$), 4.04 (t, *J* = 7.0 Hz, 2H, OCH_2CH$_2$CH$_2$N), 3.91 (t, *J* = 6.0 Hz, 2H, 26-OCH$_2$CH_2OCH$_2$CH$_3$), 3.89 (t, *J* = 6.0 Hz, 4H, 25,27-OCH$_2$CH_2OCH$_2$CH$_3$), 3.83 (t, *J* = 7.0 Hz, 2H, OCH$_2$CH$_2$CH_2N), 3.59 (q, *J* = 7.0 Hz, 2H, 26-OCH$_2$CH$_2$OCH_2CH$_3$), 3.58 (q, *J* = 7.0 Hz, 4H, 25,27-

$OCH_2CH_2OCH_2CH_3$), 3.18 (d, *J* = 13.2 Hz, 2H, ArCHH_{eq}Ar), 3.15 (d, *J* = 13.2 Hz, 2H, ArCH_{eq}HAr), 2.33 (p, *J* = 7.0 Hz, 2H, $OCH_2CH_2CH_2N$), 1.27 – 1.16 (m, 9H, $OCH_2CH_2OCH_2CH_3$). **^{13}C NMR** (100 MHz, MeOD) δ (ppm): 181.2 (*C*=O), 171.6 (C_qAr), 156.4 (C_qAr), 156.3 (C_qAr), 156.3 (C_qAr), 142.8 (C_qAr), 138.7 (C_qAr), 134.9 (C_qAr), 134.9 (C_qAr), 134.8 (C_qAr), 128.1 (*C*ArH), 128.0 (*C*ArH), 127.9 (*C*ArH), 126.7 (*C*Ar_{solf}), 121.9 (*C*Ar_{solf}), 121.9 (*C*ArH), 73.1 ($OCH_2CH_2OCH_2CH_3$), 73.0 ($OCH_2CH_2OCH_2CH_3$), 72.5 ($OCH_2CH_2CH_2N$), 69.9 ($OCH_2CH_2OCH_2CH_3$), 69.8 ($OCH_2CH_2OCH_2CH_3$), 66.1 ($OCH_2CH_2OCH_2CH_3$), 66.1 ($OCH_2CH_2OCH_2CH_3$), 41.8 ($OCH_2CH_2CH_2N$), 30.6 (ArCH_2Ar), 30.5 (ArCH_2Ar), 29.5 ($OCH_2CH_2CH_2N$), 14.4 $OCH_2CH_2OCH_2CH_3$), 14.4 ($OCH_2CH_2OCH_2CH_3$). **ESI-MS (-)**: calcd. for $C_{50}H_{60}N_3O_9S_2$ [(M-H)$^-$] m/z 910.38, found m/z 910.72 (38%), calcd. for $C_{50}H_{60}N_3O_9S_2Cl$ [(M+Cl)$^-$] m/z 946.35, found m/z 946.48 (13%), calcd. for $C_{100}H_{122}N_6O_{18}S_4$ [(2M-H)$^-$] m/z 1822.77, found m/z 1822.53 (95%).

cone-25,26,27-tris(2-ethoxyethylether)-28-(3-(4-sulfamoylbenzamido)propoxy)-calix[4]arene (49c): In a 10 ml microwave tube equipped with a magnetic stir bar, compound **47b** (0.14 mmol, 0.10 g), DIPEA (0.72 mmol, 0.125 ml) and EDC (0.34 mmol, 66.00 mg) were dissolved in dry DMF (6 ml). After 30 minutes of stirring, 4-sulfamoylbenzoic acid (0.32 mmol, 66.00 mg) was added in and the mixture was subjected to a first microwave cycle (T = 80°C, rampe time = 3 minutes, hold time = 1 h 30 minutes, P = 200 psi, Potenza = 200 W) at end of which it was monitored by TLC (AcOEt and AcOEt/MeOH 9:1). Due to incomplete conversion of compound (?), another portion of 4-sulfamoylbenzoic acid (0.32 mmol, 66.00 mg), EDC (0.34 mmol, 66.00 mg) and DIPEA (0.72 mmol, 0.125 ml) were added in and the mixture was subjected to a second microwave cycle with the same experimental parameters. Once assessed the reaction was almost finished, it was quenched with 1N HCl (5 ml). The mixture was extracted with DCM (4 x 20 ml), washed with brine (2 x 20 ml) and then H_2O (1 x 30 ml) and finally the solvent was removed by reduced pressure. The crude was purified by a flash chromatography column (AcOEt/Hex 1:1) to get compound **49c** as a white powder (59.9 mg, 68.04 umol, 48% yield). **^{1}H NMR** (400 MHz, MeOD) δ (ppm): 8.59 (t, *J* = 5.3 Hz, 1H, N*H*), 8.01 (d, *J* = 8.4 Hz, 2H, ArH_{solf}), 7.97 (d, *J* = 8.4 Hz, 2H, ArH_{solf}), 6.67 – 6.59 (m, 8H, Ar*H*), 6.59 – 6.51 (m, 4H, Ar*H*), 4.55 (d, *J* = 13.2 Hz, 2H, ArCH_{ax}HAr), 4.53 (d, *J* = 13.2 Hz, 2H, ArCHH_{ax}Ar), 4.20 – 4.09 (m, 6H, $OCH_2CH_2OCH_2CH_3$), 4.06 (t, *J* = 7.2 Hz, 2H, $OCH_2CH_2CH_2N$), 3.89 (t, *J* = 4.8 Hz, 4H, 25,27-$OCH_2CH_2OCH_2CH_3$), 3.88 (t, *J* = 4.8 Hz, 2H, 26-$OCH_2CH_2OCH_2CH_3$), 3.62 (t, *J* = 5.2 Hz, 2H, $OCH_2CH_2CH_2N$), 3.56 (q, *J* = 7.0 Hz, 6H, $OCH_2CH_2OCH_2CH_3$), 3.17 (d, *J* = 13.2 Hz, 2H, ArCHH_{eq}Ar), 3.12 (d, *J* = 13.2 Hz, 2H, ArCH_{eq}HAr), 2.32 (p, *J* = 13.2 Hz, 2H, $OCH_2CH_2CH_2N$), 1.19 (t, *J* = 6.0 Hz, 3H, 26-$OCH_2CH_2OCH_2CH_3$), 1.18 (t, *J* = 6.0 Hz, 6H, 25,27-$OCH_2CH_2OCH_2CH_3$). **^{13}C NMR** (100 MHz, MeOD) δ (ppm): 167.3 (*C*=O), 156.3 (C_qAr), 156.2 (C_qAr), 146.3 (C_qAr), 137.8 (C_qAr), 134.9 (C_qAr), 134.9 (C_qAr), 134.8 (C_qAr), 128.1 (*C*ArH), 128.0 (*C*ArH), 127.6 (*C*Ar_{solf}), 126.0 (*C*Ar_{solf}), 121.9 (*C*ArH), 73.1 ($OCH_2CH_2OCH_2CH_3$), 72.9 ($OCH_2CH_2OCH_2CH_3$), 72.7 ($OCH_2CH_2CH_2N$), 69.8 ($OCH_2CH_2OCH_2CH_3$), 69.7 ($OCH_2CH_2OCH_2CH_3$), 66.1 ($OCH_2CH_2OCH_2CH_3$), 66.0 ($OCH_2CH_2OCH_2CH_3$), 37.4 ($OCH_2CH_2CH_2N$), 30.6 (ArCH_2Ar), 30.5 (ArCH_2Ar), 29.9 ($OCH_2CH_2CH_2N$), 14.4 ($OCH_2CH_2OCH_2CH_3$). **ESI-MS (-)**: calcd. for $C_{50}H_{59}N_2O_{10}S$ [(M-H)$^-$] m/z 879.40, found m/z 879.10 (27%), calcd. for $C_{50}H_{60}N_2O_{10}SCl$ [(M+Cl)$^-$] m/z 915.37, found m/z 915.66 (27%).

mobile-25,26,27,28-tetramethoxycalix[4]arene (50a): in a 2-necked round-bottom flask compound **37** (2.82 mmol, 1.20 g) and 55% NaH (19.74 mmol, 0.95 g) were stirred in dry DMF (50 ml) for 30 minutes at 0°C. Then CH_3I (19.74 mmol, 1.23 mL) was added in and the mixture was kept stirring for 3 days at room temperature, monitoring it by TLC (Hex/AcOEt 7:3). The

reaction was quenched with 1N HCl (20 ml), extracted with DCM (3 x 30 ml) and then the combined organic phases were washed with H_2O (3 x 30 ml) and dried with anhydrous Na_2SO_4. Upon filtration, the solvent was removed by reduced pressure and the crude was recrystallized by DCM/MeOH to get compound **50a** as a white powder (1.07 g, 2.23 mmol, 79% yield). **^{1}H-NMR** (400 MHz, $CDCl_3$) δ (ppm): 7.40 – 6.30 (bs, Ar*H*), 6.75 (bs, cone Ar*H*), 6.36 (bs, cone Ar*H*), 4.39 (d, J = 13.0 Hz, cone axial ArCH_2Ar), 4.18 – 3.99 (bs, axial ArCH_2Ar), 3.85 (s, ArOCH_3), 3.79 – 3.35 (bs, ArOCH_3, ArCH_2Ar), 3.68 (bs, cone ArOCH_3), 3.22 (d, J = 13.0 Hz, cone equatorial ArCH_2Ar), 3.16 – 3.03 (bs, equatorial ArCH_2Ar). **^{13}C NMR** (100 MHz, CDCl3) δ (ppm): 163.3, 162.7, 158.2, 158.0, 157.7, 157.5, 157.3, 142.9, 142.5, 137.2, 136.5, 136.3, 136.2, 135.5, 135.1, 134.4, 134.1, 133.5, 133.2, 132.4, 131.6, 131.0, 129.8, 129.2, 129.0, 128.4, 128.2, 127.8, 125.9, 124.5, 123.5, 123.3, 123.0, 122.3, 121.8, 62.2, 61.9, 61.3, 60.9, 59.7, 59.2, 35.8, 35.5, 31.9, 30.6, 30.5, 29.7, 29.4, 22.7, 14.1. **ESI-MS** (+): calcd. for $C_{32}H_{33}O_4$ $[(M+H)^+]$: m/z 481.23, found m/z 481.46 (5%), calcd. for $C_{32}H_{32}O_4Na$ $[(M+Na)^+]$ m/z 503.22, found m/z 503.49 (82%), calcd. for $C_{32}H_{32}O_4K$ $[(M+K)^+]$ m/z 519.19, found m/z 519.40 (100%). The spectroscopic data obtained are in agreement with those ones reported in literature[36].

cone-25,26,27,28-(2-ethoxyethylether)calix[4]arene (50b): In a 2-necked round-bottom flask compound **37** (9.20 mmol, 3.91 g) and 55% NaH (39.01 mmol, 1.70 g) were stirred in dry DMF (110 ml) for 30 minutes at 40°C. Then 2-bromo ethylether (36.80 mmol, 4.149 ml) was added in and the mixture was kept stirring for 4 days at 40°C, monitoring it by TLC (Hex/AcOEt 8:2). As soon as the reaction was quenched with 1N HCl (70 ml), a precipitate was formed and hence was filtered and washed with H_2O (3 x 50 ml) to get compound **50b** as a yellow solid (6.54 g, 9.18 mmol, 99% yield). **^{1}H NMR** (300 MHz, Acetone-d_6) δ (ppm): 6.64 (d, *J* = 7.7 Hz, 8H, m-Ar*H*O), 6.53 (dd, *J* = 7.7, 6.7 Hz, 4H), 4.57 (d, *J* = 13.2 Hz, 4H, axial ArCH_2Ar), 4.12 (t, *J* = 5.5 Hz, 8H, O$CH_2CH_2OCH_2CH_3$), 3.89 (t, *J* = 5.5 Hz, 8H, $OCH_2CH_2OCH_2CH_3$), 3.55 (q, *J* = 7.0 Hz, 8H, $OCH_2CH_2OCH_2CH_3$), 3.14 (d, *J* = 13.2 Hz, 4H, equatorial ArCH_2Ar), 1.17 (t, *J* = 7.0 Hz, 12H, $OCH_2CH_2OCH_2CH_3$). The spectroscopic data obtained are in agreement with those ones reported in literature[34].

mobile-5-nitro-25,26,27,28-tetrametossicalix[4]arene (51a): in a 1-necked round-bottom flask compound **50a** (1.03 mmol, 0.50 g) and glacial CH_3COOH (45.32 mmol, 1.820 mL) were stirred in DCM (10 ml). Then 65% HNO_3 (13.71 mmol, 0.620 mL) was added in and the mixture was kept stirring for 40 minutes at room temperature, monitoring it by TLC (Hex/AcOEt 7:3). The reaction was quenched adding H_2O (10 mL) and sat. $NaHCO_3$ (10 ml) and stirring for 30 minutes. The mixture was extracted with DCM (3 x 30 ml) and the combined organic phases were subsequently washed with H_2O (3 x 30 ml) and dried with anhydrous Na_2SO_4. Upon filtration, the solvent was removed by reduced pressure and the crude was purified by a flash chromatography column (Hex/AcOEt 9:1) and subsequent precipitation of unreacted LFC by DCM/MeOH to get compound **51a** as a white powder (57.40 mg, 0.11 mmol, 10% yield). **^{1}H-NMR** (400 MHz, $CDCl_3$) δ (ppm): 8.23 (s, Ar*H*), 7.89 (s, Ar*H*), 7.30 – 7.07 (m, Ar-*H*), 6.96 (d, Ar*H*), 6.83 (t, Ar*H*), 6.56 (bs, Ar*H*), 6.45 (bd, Ar*H*), 6.40 (bd, Ar*H*), 6.30 (bs, Ar*H*), 4.41 (d, *J* = 13.6 Hz, cone axial ArCH_2Ar), 4.38 (d, *J* = 13.6 Hz, cone axial ArCH_2Ar), 4.08 (bs, axial ArCH_2Ar), 3.87 – 3.60 (m, ArOCH_3, ArCH_2Ar), 3.28 (d, *J* = 13.6 Hz, cone equatorial ArCH_2Ar), 3.23 (d, *J* = 13.6 Hz, cone equatorial ArCH_2Ar), 3.17 – 3.09 (m, equatorial ArCH_2Ar), 2.99 (s, ArOCH_3). **^{13}C-NMR** (100 MHz, $CDCl_3$): 163.0, 162.7, 158.2, 158.0, 157.7, 157.5, 157.3, 142.9, 142.5, 137.2, 136.5, 136.3, 136.2, 135.5, 135.1, 134.4, 134.1, 133.5, 133.2, 132.4, 131.6, 131.0, 129.8, 129.2, 129.0, 128.4,

128.2, 127.8, 125.9, 124.5, 123.5, 123.3, 123.0, 122.3, 121.8, 62.2, 61.9, 61.3, 60.9, 59.7, 59.2, 35.82, 35.5, 31.0, 30.6, 30.5, 29.72, 29.4, 22.7, 14.1. **ESI-MS (+)**: calcd. for $C_{32}H_{32}NO_6$ [$(M+H)^+$] m/z 526.22, found m/z 526.53 (2%), calcd. for $C_{32}H_{31}NO_6Na$ [$(M+Na)^+$] m/z 548.20, found m/z 548.41 (95%), calcd. for $C_{32}H_{31}NO_6K$ [$(M+K)^+$] m/z 564.18, found m/z 564.47 (95%).

cone-17-nitro-25,26,27,28-(2-ethoxyethylether)calix[4]arene (51b): In a 1-necked round-bottom flask, 65% HNO_3 (65.00 mmol, 2.940 ml) was slowly added into a solution of compound **50b** (7.22 mmol, 5.14 g) and glacial CH_3COOH (0.32 mol, 12.73 ml) in DCM (80 ml), meanwhile the mixture was kept stirring at room temperature. The mixture was left reacting for about 1 h 30 minutes till on TLC (Hex/AcOEt 6:4) di-nitro derivative spot showed up. The reaction was quenched with H_2O (80 ml) and the mixture was vigorously stirred for 30 minutes. The organic phase was then washed with sat. $NaHCO_3$ (80 ml) to remove all the acid remained. The organic phase was washed again with H_2O (3 x 80 ml) and brine (3 x 80 ml) and the solvent was removed by reduced pressure. The crude was purified by a flash chromatography column (Hex/AcOEt 7:3) to get compound **51b** as orange powder (0.70 g, 0.92 mmol, 16% yield). **^{1}H NMR** (400 MHz, $CDCl_3$) δ (ppm): 6.89 – 6.81 (m, 4H, Ar*H*), 6.76 (t, *J* = 7.4 Hz, 2H, p-Ar*H*), 6.43 – 6.29 (m, 3H, Ar*H*), 4.61 (d, *J* = 13.7 Hz, 2H, ArCH_{ax}HAr), 4.51 (d, *J* = 13.7 Hz, 2H, ArCHH_{ax}Ar), 4.31 – 4.08 (m, 8H, OCH_2CH$_2$OCH$_2$CH$_3$), 4.05 (t, *J* = 5.3 Hz, 2H, OCH$_2$CH$_2$OCH$_2$CH$_3$), 3.92 – 3.76 (m, 6H, OCH$_2$CH_2OCH$_2$CH$_3$), 3.63 – 3.49 (m, 8H, OCH$_2$CH$_2$OCH_2CH$_3$), 3.22 (d, *J* = 13.7 Hz, 2H, ArCH_{eq}HAr), 3.17 (d, *J* = 13.7 Hz, 2H, ArCHH_{eq}Ar), 1.34 – 1.15 (m, 12H, OCH$_2$CH$_2$OCH$_2$CH_3). The spectroscopic data obtained are in agreement with those ones reported in literature[34].

mobile-5-amino-25,26,27,28-methyl-calix[4]arene (52a): In a 1-necked round-bottom flask compound **51a** (0.25 mmol, 0.13 g) and $NH_2NH_2{\cdot}H_2O$ (4.95 mmol, 0.240 mL) were dissolved in absolute EtOH (30 ml) and DCM (5 ml). 10% Pd/C (catalytic amount) was added in and the mixture was stirred for 1 night at reflux, monitoring the reaction by TLC (Hex/AcOEt 7:3). The solvent was removed by reduced pressure and the crude was rinsed with DCM (20 ml). The catalyst was filtered off and washed with DCM (3 x 20 ml) and EtOH (3 x 20 ml). The solvent was removed again by reduced pressure to get compound **52a** as a yellow powder (crude 0.17 g). **^{1}H-NMR** (400 MHz, $CDCl_3$) δ (ppm): 7.12 – 6.38 (m, Ar*H)*, 4.41 – 4.31 (d, axial ArCH_2Ar), 4.10 – 3.39 (m, ArOCH_3, axial ArCH_2Ar), 3.30 – 3.00 (m, equatorial ArCH_2Ar). **^{13}C NMR** (100 MHz, MeOD) δ (ppm) [as ammonium species]: 158.5, 158.3, 158.0, 146.8, 136.4, 135.2, 133.5, 128.8, 128.3, 127.5, 122.7, 121.7, 61.6, 61.3, 60.2, 59.7, 59.1, 35.3, 30.1, 23.0. **ESI-MS** (+): calcd. for $C_{32}H_{34}NO_4$ [$(M+H)^+$] m/z 495.24, found m/z 496.35 (100%), calcd. for $C_{32}H_{33}NO_4Na$ [$(M+Na)^+$]: m/z 518.23, found m/z 518.40 (1%)., calcd. for $C_{32}H_{33}NO_4K$ [$(M+K)^+$] m/z 534.20, found m/z 534.39 (40%).

cone-5-amino-25,26,27,28-(2-ethoxyethylether)calix[4]arene (52b): In a 1-necked round-bottom flask compound **51b** (0.50 mmol, 0.38 g) and $NH_2NH_2{\cdot}H_2O$ (5.04 mmol, 0.240 ml) were dissolved in absolute EtOH (6 ml). 10% Pd/C (catalytic amount) was added in and the mixture was stirred for 5 h at reflux, monitoring the reaction by TLC (Hex/AcOEt 9:1). The solvent was removed by reduced pressure and the crude was rinsed with DCM (20 ml). The catalyst was filtered off and washed with DCM (3 x 20 ml) and EtOH (3 x 20 ml). The solvent was removed again by reduced pressure to get compound **52b** as a red powder (0.33 g, 0.45 mmol, 90% yield). **^{1}H NMR** (400 MHz, $CDCl_3$) δ (ppm): 6.76 – 6.60 (m, 11H, Ar*H*), 6.01 (s, 2H, C*H*CNH$_2$), 4.56 (d, *J* = 13.3 Hz, 2H, ArCHH_{ax}Ar), 4.47 (d, *J* = 13.3 Hz, 2H, ArCH_{ax}HAr), 4.17 (t, *J* = 5.9 Hz, 2H, 26-

OC*H*$_2$CH$_2$OCH$_2$CH$_3$), 4.16 (t, *J* = 5.9 Hz, 4H, 25,27-OC*H*$_2$CH$_2$OCH$_2$CH$_3$), 4.08 (t, *J* = 5.9 Hz, 2H, 28-OC*H*$_2$CH$_2$OCH$_2$CH$_3$), 3.94 – 3.85 (m, 8H, OCH$_2$C*H*$_2$OCH$_2$CH$_3$), 3.65 – 3.56 (m, 8H, OCH$_2$CH$_2$OC*H*$_2$CH$_3$), 3.29 (s, 2H, N*H*$_2$), 3.20 (d, *J* = 13.3 Hz, 2H, ArCH*H*$_{eq}$Ar), 3.08 (d, *J* = 13.3 Hz, 2H, ArC*H*$_{eq}$HAr), 1.33 – 1.18 (m, 12H, OCH$_2$CH$_2$OCH$_2$C*H*$_3$).

mobile-5-N-(4-Boc-aminobutanamido)-25,26,27,28-tetramethoxy-calix[4]arene (53a): In a 2-necked round-bottom flask EDC (0.85 mmol, 0.16 g) and Boc-Gaba-OH (0.78 mmol, 0.16 g) were stirred in dry DMF (10 ml) for 30 minutes at room temperature. Then compound **52a** (0.71 mmol, 0.35 g) was added in and the mixture was kept stirring for 3 days at room temperature, monitoring it by TLC (Hex/AcOEt 1:1). The solvent was removed by reduced pressure and the crude was suspended in H_2O (50 ml). The mixture was extracted with DCM (3 x 20 ml). The combined organic phases were washed again with H_2O (3 x 20 ml), dried at rotavapor and the crude was purified by a flash chromatography column (Hex/AcOEt 1:1) to get compound **53a** as a white powder (0.11 g 0.16 mmol, 23% yield). **^{1}H-NMR** (400 MHz, $CDCl_3$) δ (ppm): 8.69 (bs, N*H*), 8.27 (bs, N*H*), 8.03 (bs, N*H*), 7.60 – 6.30 (m, Ar*H*), 5.01 (s, 1H, N*H*Boc), 4.45 – 4.32 (m, axial ArC*H*$_2$Ar), 3.86 – 3.70 (m, ArOC*H*$_3$, axial ArC*H*$_2$Ar), 3.35 – 2.91 (m, equatorial ArC*H*$_2$Ar,NHCOC*H*$_2$), 2.32 (bs, 2H, C*H*$_2$NHCOO), 1.86 (bs, 2H, CH$_2$C*H*$_2$CH$_2$), 1.48 (s, 9H, C(C*H*$_3$)$_3$). **^{13}C-NMR** (400 MHz, $CDCl_3$) δ (ppm): 174.5, 171.2, 170.8, 157.7, 156.9, 154.4, 150.2, 135.6, 135.5, 134.6, 134.4, 133.8, 132.6, 130.3, 129.0, 128.2, 128.0, 122.4, 120.3, 82.8, 79.4, 61.7, 61.4, 60.4, 46.5, 39.5, 36.1, 34.5, 33.0, 32.0, 30.6, 28.4, 28.2, 28.1, 26.7, 21.1, 17.4, 14.2. **ESI-MS (+):** calcd. for $C_{33}H_{33}NO_5$ [(M-CH$_2$CH$_2$CH$_2$NHBoc)$^+$] m/z 546.23, found m/z 546.40 (10%), calcd. for $C_{32}H_{34}NO_4$ [(M-COCH$_2$CH$_2$CH$_2$NHBoc+H)$^+$] m/z 496.24, found m/z 496.36 (25%), calcd. for $C_{36}H_{41}N_2O_5$ [(M-Boc+H)$^+$] m/z 581.29, found m/z 581.47 (100%), calcd. for $C_{41}H_{48}N_2O_7Na$ [(M+Na)$^+$] m/z 703.34, found m/z 703.52 (40%), calcd. for $C_{41}H_{48}N_2O_7K$ [(M+K)$^+$] m/z 719.31, found m/z 719.50 (70%).

cone-5-N-(4-Boc-aminobutanamido)-25,26,27,28-(2-ethoxyethylether)calix[4]arene (53b): In a 2-necked round-bottom flask EDC (0.55 mmol, 0.11 g) and Boc-Gaba-OH (0.51 mmol, 0.10 g) were stirred in dry DMF (3 ml) for 30 minutes at room temperature. Then a solution of compound **52b** (0.50 mmol, 0.33 g) in dry DMF (4 ml) was added in and the mixture was kept stirring for 1 night at 50°C, monitoring it by TLC (AcOEt). The reaction was quenched with H_2O (20 ml) and the mixture was extracted with DCM (3 x 20 ml). The combined organic phases were dried at rotavapor and the crude was purified by a flash chromatography column (Hex/AcOEt 1:1) to get compound **53b** as a white powder (0.11 g, 0.12 mmol, 26% yield). **^{1}H NMR** (400 MHz, $CDCl_3$) δ (ppm): 8.02 (s, 1H, N*H*Boc), 6.85 (s, 2H, C*H*CNHCO), 6.71 – 6.53 (m, 15H), 4.86 (s, 1H, ArN*H*), 4.52 (d, *J* = 13.2 Hz, 2H, ArCH*H*$_{ax}$Ar), 4.48 (d, *J* = 13.2 Hz, 2H, ArC*H*$_{ax}$HAr), 4.18 – 4.07 (m, 8H, OC*H*$_2$CH$_2$OCH$_2$CH$_3$), 3.87 (t, *J* = 5.6 Hz, 2H, 28-OCH$_2$C*H*$_2$OCH$_2$CH$_3$), 3.84 (t, *J* = 5.6 Hz, 6H, 25,26,27-OCH$_2$C*H*$_2$OCH$_2$CH$_3$), 3.56 (q, *J* = 7.0 Hz, 8H, OCH$_2$CH$_2$OC*H*$_2$CH$_3$), 3.21 (t, *J* = 6.2 Hz, 2H, COCH$_2$CH$_2$C*H*$_2$NHBoc), 3.17 (d, *J* = 13.2 Hz, 2H, ArCH*H*$_{eq}$Ar), 3.13 (d, *J* = 13.2 Hz, 2H, ArC*H*$_{eq}$HAr), 2.30 (t, *J* = 6.2 Hz, 2H, COC*H*$_2$CH$_2$CH$_2$NHBoc), 1.84 (p, *J* = 6.2 Hz, 2H, COCH$_2$C*H*$_2$CH$_2$NHBoc), 1.47 (s, 9H, CH$_2$CH$_2$CH$_2$NH*Boc*), 1.22 (t, *J* = 6.2 Hz, 12H, OCH$_2$CH$_2$OCH$_2$C*H*$_3$). **^{13}C NMR** (100 MHz, $CDCl_3$) δ (ppm): 171.2 (O*C*NAr), 170.5 (*C*Ar), 156.9 (*C*Ar), 156.5 (*C*Ar), 156.3 (O*C*NBoc), 153.1 (*C*Ar), 135.5 (*C*Ar), 135.3 (*C*Ar), 134.9 (*C*Ar), 134.7 (*C*Ar), 132.4 (*C*Ar), 128.2 (*C*Ar), 122.3 (*C*Ar), 121.9 (*C*Ar), 120.1 (*C*Ar), 79.5 (Boc*C*(CH$_3$)$_3$), 73.2 (O*C*H$_2$CH$_2$OCH$_2$CH$_3$), 73.1 (O*C*H$_2$CH$_2$OCH$_2$CH$_3$), 73.1 (OCH$_2$CH$_2$OCH$_2$CH$_3$), 69.7 (OCH$_2$*C*H$_2$OCH$_2$CH$_3$), 69.6 (OCH$_2$*C*H$_2$OCH$_2$CH$_3$), 66.4 (OCH$_2$CH$_2$O*C*H$_2$CH$_3$), 60.4, 39.5 (COCH$_2$CH$_2$*C*H$_2$NHBoc), 34.5 (CO*C*H$_2$CH$_2$CH$_2$NHBoc), 30.9 (Ar*C*H$_2$Ar), 30.9 (Ar*C*H$_2$Ar), 29.7

($COCH_2CH_2CH_2NHBoc$), 28.4 ($BocC(CH_3)_3$), 26.9, 21.1, 15.3 ($OCH_2CH_2OCH_2CH_3$), 14.2 ($OCH_2CH_2OCH_2CH_3$). **ESI-MS (+)**: calcd. for $C_{53}H_{73}N_2O_{11}$ [$(M+H)^+$] m/z 913.51, found m/z 913.98 (5%), calcd. for $C_{53}H_{72}N_2O_{11}Na$ [$(M+Na)^+$] m/z 936.14, found m/z 936.16 (45%), calcd. for $C_{53}H_{72}N_2O_{11}K$ [$(M+K)^+$] m/z 952.24, found m/z 952.14 (100%), calcd. for $C_{49}H_{65}N_2O_{11}$ [(M-tBut+H)$^+$] m/z 857.81, found m/z 857.45 (5%), calcd. for $C_{48}H_{64}N_2O_9$ [$(M-Boc+H)^+$] m/z 814.04, found m/z 814.03 (1%).

mobile-5-N-(4-aminobutanamido)-25,26,27,28-tetramethoxy-calix[4]arene (54): In a 1-necked round-bottom flask compound **53a** (0.17 mmol, 0.11 g) was dissolved in dry DCM (10 ml). Then TES (3.35 mmol, 0.530 mL) and TFA (6.70 mmol, 0.510 mL) were added in and the mixture was kept stirring for 4 h at room temperature, monitoring it by TLC (AcOEt). The solvent was removed by reduced pressure and the crude was dissolved in DCM (15 ml), which was washed with 1N NaOH (2 x 10 ml). The solvent was removed by reduced pressure and the solid formed was triturated with hexane (2 ml) to get, upon filtration, compound **54** as a white powder (70.00 mg, 0.12 mmol, 72% yield). **^{1}H-NMR** (400 MHz, $CDCl_3$) δ (ppm): 8.76 (bs, N*H*), 8.54 (s, N*H*), 7.80 (s, N*H*), 7.35 – 6.49 (m, Ar*H*), 4.43 – 4.30 (bs, axial ArCH_2Ar), 4.18 – 3.42 (m, axial ArCH_2Ar, ArOCH_3), 3.34 – 3.07 (bs, equatorial ArCH_2Ar, $NHCOCH_2$), 2.79 (bs, NH_2), 2.56 – 2.32 (m, NH_2), 2.04 – 1.99 (m, 2H, CH_2NH_2), 1.87 (bs, 2H, $NHCOCH_2CH_2CH_2R$). **^{13}C-NMR** (100 MHz, $CDCl_3$) δ (ppm): 171.3, 170.7, 168.6, 157.9, 155.6, 154.5, 136.6, 135.3, 133.8, 133.2, 132.2, 131.0, 129.0, 128.1, 123.5, 123.4, 122.4, 122.2, 120.4, 119.2, 69.5, 62.9, 61.5, 60.7, 53.9, 53.4, 50.8, 42.0, 41.5, 36.1, 35.1, 32.1, 31.7, 31.6, 30.9, 30.9, 30.7, 29.7, 29.3, 29.2, 28.7, 26.4, 22.7, 20.9, 18.8, 14.1. **ESI-MS (+):** calcd. for $C_{32}H_{34}NO_4$ [$(M-COCH_2CH_2CH_2NH_2)^+$] m/z 496.24, found m/z 496.44 (75%), calcd. for $C_{36}H_{41}N_2O_5$ [$(M+H)^+$] m/z 581.29, found m/z 581.47 (100%), calcd. for $C_{36}H_{40}N_2O_5Na$ [$(M+Na)^+$] m/z 603.28, found m/z 603.43 (65%), calcd. for $C_{36}H_{40}N_2O_5K$ [$(M+K)^+$] m/z 619.26, found m/z 619.42 (40%).

cone-5-N-(4-aminobutanamido)-25,26,27,28-(2-ethoxyethylether)calix[4]arene hydrochloride (55): In a 1-necked round-bottom flask compound **53b** (81.00 umol, 74.00 mg) was dissolved in dry DCM (9.5 ml). Then TES (1.57 mmol, 0.250 ml) and TFA (3.26 mmol, 0.250 ml) were added in and the mixture was kept stirring for 1 night at room temperature, monitoring it by TLC (AcOEt). The solvent was removed by reduced pressure and the crude was stirred for 30 minutes into a mixture EtOH/37%HCl (10 ml + 1 ml). The solvent was removed by reduced pressure and two equal washes were reiterated onto the crude at the end of which compound **55** was obtained as a white powder (75.00 mg, 88.40 umol, 99% yield). **^{1}H NMR** (400 MHz, MeOD) δ (ppm): 6.81 (s, 2H, C*H*CNHCO), 6.72 (t, *J* = 8.1 Hz, 4H, Ar*H*), 6.61 (t, *J* = 7.4 Hz, 2H, Ar*H*), 6.56 (d, *J* = 6.8 Hz, 2H, Ar*H*), 6.53 - 6.45 (m, 1H, Ar*H*), 4.55 (d, *J* = 13.2 Hz, 4H, axial ArCH_2Ar), 4.15 (t, *J* = 5.3 Hz, 4H, $OCH_2CH_2OCH_2CH_3$), 4.10 (t, *J* = 5.3 Hz, 2H, $OCH_2CH_2OCH_2CH_3$), 4.10 (t, *J* = 5.3 Hz, 2H, $OCH_2CH_2OCH_2CH_3$), 3.94 – 3.85 (m, 8H, $OCH_2CH_2OCH_2CH_3$), 3.65 – 3.54 (m, 8H, $OCH_2CH_2OCH_2CH_3$), 3.15 (d, *J* = 13.2 Hz, 2H, ArCH_{eq}Ar), 3.12 (d, *J* = 13.2 Hz, 2H, ArCH_{eq}HAr), 2.99 (t, *J* = 7.0 Hz, 2H, $COCH_2CH_2CH_2NH_3^+$), 2.44 (t, *J* = 7.0 Hz, 2H, $COCH_2CH_2CH_2NH_3^+$), 1.96 (p, *J* = 7.0 Hz, 2H, $COCH_2CH_2CH_2NH_3^+$), 1.26 – 1.18 (m, 12H, $OCH_2CH_2OCH_2CH_3$). **^{13}C NMR** (100 MHz, MeOD) δ (ppm): 170.8 (O*C*NAr), 156.6 (*C*Ar), 156.1 (*C*Ar), 152.9 (*C*Ar), 135.2 (*C*Ar), 135.0 (*C*Ar), 134.8 (*C*Ar), 134.7 (*C*Ar), 132.3 (*C*Ar), 128.2 (*C*Ar), 128.0 (*C*Ar), 127.9 (*C*Ar), 122.0 (*C*Ar), 121.8 (*C*Ar), 120.2 (*C*Ar), 73.3 ($OCH_2CH_2OCH_2CH_3$), 73.2 ($OCH_2CH_2OCH_2CH_3$), 73.0 ($OCH_2CH_2OCH_2CH_3$), 69.8 ($OCH_2CH_2OCH_2CH_3$), 69.7 ($OCH_2CH_2OCH_2CH_3$), 69.7 ($OCH_2CH_2OCH_2CH_3$), 66.1 ($OCH_2CH_2OCH_2CH_3$), 66.0 ($OCH_2CH_2OCH_2CH_3$), 39.1 ($CH_2CH_2CH_2NH_3^+$), 33.0 ($CH_2CH_2CH_2NH_3^+$),

30.6 (Ar*C*H_2Ar), 30.5 (Ar*C*H_2Ar), 23.0 (CH_2*C*$H_2$$CH_2NH_3^+$), 14.4 ($OCH_2CH_2OCH_2$*C*$H_3$). **ESI-MS (+)**: calcd. for $C_{48}H_{65}N_2O_9$ [(M+H-Cl)$^+$] m/z 814.04, found m/z 814.03 (100%), calcd. for $C_{48}H_{64}N_2O_9Na$ [(M+Na-Cl)$^+$] m/z 836.02, found m/z 836.07 (20%), calcd. for $C_{48}H_{64}N_2O_9K$ [(M+K-Cl)$^+$] m/z 852.13, found m/z 852.06 (8%), calcd. for $C_{44}H_{57}NO_8$ [(M-Cl-$COCH_2CH_2CH_2NH_3$)$^+$] m/z 728.41, found m/z 728.85 (15%). **ESI-MS (-)**: calcd. for $C_{48}H_{64}N_2O_9Cl$ [(M-H)$^-$] m/z 47.44, found m/z 847.87 (100%).

Mobile-5-N-(4-(4-benzensolfonamidyl)thioureido-butanamido)-25,26,27,28-tetramethoxy-calix[4]arene (56a): in a 2-necked round-bottom flask compound **54** (0.12 mmol, 0.07 g) and DIPEA (0.60 mmol, 0.105 mL) were stirred in dry DCM/dry DMF (15 ml + 1 ml) for 10 minutes at room temperature. Then 4-isothiocyanatebenzensolfonamide (0.12 mmol, 25.00 mg) was added in and the mixture was kept stirring for 4 days at room temperature, monitoring it by TLC (DCM/MeOH 9:1). The solvent was removed by reduced pressure and then 1N HCl (25 ml) was added in. The precipitate was collected by filtration and it was purified by a flash chromatography column (DCM/MeOH 96:4) to get compound **56a** as a brown powder (25.00 mg, 31.48 umol, 26% yield). **^{1}H-NMR** (400 MHz, MeOD) δ (ppm): 7.85 (d, J = 8.6 Hz, 2H, solfonamide Ar*H*), 7.65 (bd, 2H, solfonamide Ar*H*), 7.31 – 6.35 (m, 11H, Ar*H*), 4.39 – 4.36 (bs, axial ArCH_2Ar), 4.18 – 3.36 (bs, axial ArCH_2Ar, ArOCH_3), 3.21 – 3.15 (m, 6H, equatorial ArCH_2Ar, NHCOCH_2R), 2.49 – 2.33 (bs, 2H, CH_2NHC=S), 2.00 (bs, 2H, CH_2C$H_2$$CH_2$). **^{13}C-NMR** (100 MHz, $CDCl_3$) δ (ppm): 180.3, 171.6, 157.8, 155.0, 135.4, 134.8, 128.2, 127.2, 122.8, 61.4, 32.0, 30.8, 30.6, 30.4, 30.2, 30.0, 29.8, 29.7, 29.4, 22.7, 14.2. **ESI-MS (-):** calcd. for $C_{43}H_{45}N_4O_7S_2$ [(M-H)$^-$] m/z 793.28, found m/z 793.36 (40%), calcd. for $C_{43}H_{46}N_4O_7S_2Cl$ [(M+Cl)$^-$] m/z 829.25, found m/z 829.33 (20%).

cone-5-N-((4-(4-benzensulfanamidyl)thioureido)butanamido)-25,26,27,28-(2-ethoxyethylether)calix[4]arene (56b): In a 2-necked round-bottom compound **55** (90.90 umol, 74.20 mg) and DIPEA (0.19 mmol, 0.032 ml) were stirred in dry DMF (3 ml) for 30 minutes at room temperature. Then 4-isothiocyanatebenzensolfonamide (90.90 umol, 19.50 mg) was added in and the mixture was kept stirring for 1 night at room temperature, monitoring it by TLC (AcOEt/Hex 9:1). The solvent was removed by reduced pressure and the crude was purified by a flash chromatography column (AcOEt/Hex 3:1) to get compound **56b** as a white powder (7.00 mg, 6.82 umol, 8% yield). **^{1}H NMR** (400 MHz, MeOD) δ (ppm): 7.85 (d, *J* = 8.6 Hz, 2H, CHC*H*CSO_2NH_2), 7.69 – 7.52 (m, 2H, CHC*H*CSO_2NH_2), 6.84 – 6.67 (m, 6H, Ar*H*), 6.62 (t, *J* = 7.4 Hz, 2H, Ar*H*), 6.58 – 6.47 (m, 3H, Ar*H*), 4.62 (bs, 2H, SO_2NH_2), 4.56 (d, *J* = 13.2 Hz, 2H, ArCH_{ax}HAr), 4.54 (d, *J* = 13.2 Hz, 2H, ArCHH_{ax}Ar), 4.16 (t, *J* = 5.3 Hz, 4H, OC$H_2$$CH_2OCH_2CH_3$), 4.10 (t, *J* = 5.3 Hz, 2H, OC$H_2$$CH_2OCH_2CH_3$), 4.07 (t, *J* = 5.3 Hz, 2H, OC$H_2$$CH_2OCH_2CH_3$), 3.92 (t, *J* = 5.3 Hz, 6H, OCH_2C$H_2$$OCH_2CH_3$), 3.89 (t, *J* = 5.3 Hz, 2H, OCH_2C$H_2$$OCH_2CH_3$), 3.61 (q, *J* = 7.2 Hz, 4H, $OCH_2CH_2OCH_2$C$H_2$$CH_3$), 3.59 (q, *J* = 7.2 Hz, 4H, $OCH_2CH_2OCH_2$C$H_2$$CH_3$), 3.20 – 3.07 (m, 6H, equatorial ArCH_2Ar, COC$H_2$$CH_2CH_2NH$), 2.36 (t, *J* = 7.2 Hz, 2H, $COCH_2CH_2$CH_2NH), 1.97 (p, *J* = 7.2 Hz, 2H, $COCH_2$C$H_2$$CH_2NH$), 1.23 (t, *J* = 7.2 Hz, 6H, $OCH_2CH_2OCH_2$CH_3), 1.22 (t, *J* = 7.2 Hz, 6H, $OCH_2CH_2OCH_2$CH_3). **^{13}C NMR** (75 MHz, MeOD) δ (ppm): 156.6 (*C*Ar), 156.1 (*C*Ar), 135.2 (*C*Ar), 134.9 (*C*Ar), 134.6 (*C*Ar), 132.4 (*C*Ar), 128.2 (*C*Ar_{sulf}), 128.1 (*C*Ar), 127.9 (*C*Ar), 127.6 (*C*Ar), 126.6 (*C*Ar), 122.0 (*C*Ar_{sulf}), 121.8 (*C*Ar), 120.3 (*C*Ar), 113.0 (*C*Ar), 109.2 (*C*Ar), 78.3, 77.9, 77.4, 73.3 (OC$H_2CH_2OCH_2CH_3$), 73.2 (OC$H_2CH_2OCH_2CH_3$), 72.9 (OC$H_2CH_2OCH_2CH_3$), 69.8 (OCH_2C$H_2$$OCH_2CH_3$), 66.0 ($OCH_2CH_2OCH_2CH_3$), 31.7 ($COCH_2CH_2CH_2$NH), 30.6 (ArC$H_2$Ar), 30.5 (Ar*C*$H_2$Ar), 29.4 (CO*C*$H_2CH_2CH_2NH$), 29.1 ($COCH_2CH_2CH_2NH$), 14.3 ($OCH_2CH_2OCH_2CH_3$). **ESI-MS (-**

): calcd. for $C_{55}H_{69}N_4O_{11}S_2$ $[(M-H)^-]$ m/z 1025.45, found m/z 1025.79 (48%), calcd. for $C_{55}H_{69}N_4O_{11}S_2Cl$ $[(M+Cl)^-]$ m/z 1061.42, found m/z 1061.67 (100%). **ESI-MS (+)**: calcd. for $C_{55}H_{70}N_4O_{11}S_2Na$ $[(M+Na)^+]$: m/z 1050.28, found m/z 1050.06 (100%), calcd. for $C_{55}H_{70}N_4O_{11}S_2K$ $[(M+K)^+]$: m/z 1066.39, found m/z 1066.11 (40%), calcd. for $C_{48}H_{65}N_2O_9$ $[(M\text{-}CSNHArSO_2NH_2)^+]$: m/z 814.03, found m/z 814.04 (55%), calcd. for $C_{44}H_{58}NO_8$ $[(M\text{-}CH_2CH_2CH_2HNCSNHArSO_2NH_2)^+]$: m/z 728.41, found m/z 728.92 (10%).

25,26,27-tribenzoyloxycalix[4]arene-28-olo (57) [tribenzylation strategy]: in a 1-necked round-bottom flask compound **37** (4.72 mmol, 2.0 g) and dry pyridine (25 ml) were stirred for 30 minutes at room temperature. Then benzoyl chloride (38.19 mmol, 4.440 mL) was added in at 0°C and the mixture was kept stirring for 1 h at room temperature, monitoring it by TLC (Hex/AcOEt 9:1). The reaction was quenched adding H_2O (150 ml) and the white precipitate formed was filtered and washed with MeOH (4 ml). The crude was recrystallized by $CHCl_3$/MeOH to get compound **57** as small white crystals (2.88 g, 3.91 mmol, 76% yield). **^{1}H NMR** (400 MHz, $CDCl_3$) δ (ppm): 8.10 (d, *J* = 7.4 Hz, 4H, benzoyl Ar-*H*), 7.75 (t, *J* = 7.4 Hz, 2H, benzoyl Ar-*H*), 7.58 – 7.50 (m, 1H, benzoyl Ar-*H*), 7.52 (t, *J* = 7.4 Hz, 4H, benzoyl Ar-*H*), 7.27 – 7.20 (m, 4H, benzoyl Ar-*H*), 7.06 (d, *J* = 7.5 Hz, 2H, Ar-*H*), 7.01 (dd, *J* = 7.0, 2,1 Hz, 2H, Ar-*H*), 6.90 (d, *J* = 7.5 Hz, 2H, Ar-*H*), 6.75 (t, *J* = 7.5 Hz, 2H, Ar-*H*), 6.72 (t, *J* = 7.5 Hz, 2H, Ar-*H*), 6.63– 6.56 (m, 4H, Ar-*H*), 5.46 (s, 1H, O*H*), 3.91 (d, *J* = 14.2 Hz, 2H, ArCHH_{ax}Ar), 3.84 (d, *J* = 15.4 Hz, 2H, ArCH_{ax}HAr), 3.72 (d, *J* = 15.4 Hz, 2H, ArCH_{eq}HAr), 3.52 (d, *J* = 14.2 Hz, 2H, ArCHH_{eq}Ar). The spectroscopic data obtained are in agreement with those ones reported in literature[34].

5-nitro-25,26,27-tribenzoyloxycalix[4]arene-28-olo (58) [tribenzylation strategy]: in a 1-necked round-bottom flask compound **57** (0.27 mmol, 0.20 g) and glacial CH_3COOH (33.4 mmol, 1.340 mL) were stirred in DCM (5 ml). Then 90% HNO_3 (0.78 mmol, 0.033 mL) was added in and the mixture was kept stirring for 40 minutes at room temperature, monitoring it by TLC (Hex/AcOEt 9:1). The reaction was quenched adding H_2O (20 mL) and the mixture was extracted with DCM (3 x 30 ml). The combined organic phases were subsequently washed with H_2O (3 x 30 ml) and dried with anhydrous Na_2SO_4. Upon filtration, the solvent was removed by reduced pressure to get compound **58** as a white powder (0.23 g crude), which wasn't characterized since it is subjected to a partial hydrolysis.

5-nitro-calix[4]arene-25,26,27,28-olo (59) [tribenzylation strategy]: in a 1-necked round-bottom flask 1N NaOH (21.620 ml) was added to a solution of compound **58** (0.29 mmol, 0.23 g) in THF/EtOH/H_2O (14.3 mL + 8.5 mL + 5.7 mL) stirring for 1 night at 85°C. The reaction was monitored by TLC (DCM) and upon completion, it was quenched with 1N HCl (60 ml). The precipitate was filtered and purified by flash chromatography column (DCM) to get compound **59** as a brown solid (0.36 g, 0.77 mmol, 37% yield). **^{1}H NMR** (400 MHz, $CDCl_3$) δ (ppm): 10.19 (s, 4H, O*H*), 8.00 (s, 2H, Ar*H*), 7.14 (d, *J* = 7.6 Hz, 4H, Ar*H*), 7.08 (d, *J* = 7.6 Hz, 2H, Ar*H*), 6.83 (t, *J* = 7.6 Hz, 2H, Ar*H*), 6.76 (t, *J* = 7.6 Hz, 1H, Ar*H*), 4.28 (bs, 4H, axial ArCH_2Ar), 3.66 (bs, 4H, equatorial ArCH_2Ar). **ESI-MS (-)**: calcd. for $C_{28}H_{22}NO_6$ $[(M-H)^-]$ m/z 468.15, found m/z 468.23 (100%). The spectroscopic data obtained are in agreement with those ones reported in literature[34].

5-nitro-25,26,27,28-methyl-calix[4]arene (51a) [tribenzylation strategy]: in a 2-necked round-bottom flask compound **59** (0.77 mmol, 0.36 g) and 55% NaH (5.37 mmol, 0.26 g) were stirred in dry DMF (15 ml) for 1 h at 0°C. Then CH_3I (5.37 mmol, 0.334 mL) was added in and the

mixture was kept stirring for 7 days, adding each day aliquots of 55% NaH (2.69 mmol, 0.13 g) and CH_3I (2.69 mmol, 0.167 mL). The reaction was monitored by TLC (Hex/AcOEt 7:3) and upon completion, it was quenched with 1N HCl (20 ml). The mixture was extracted with DCM (3 x 40 ml) and then the combined organic phases were washed with H_2O (3 x 40 ml) and dried with anhydrous Na_2SO_4. Upon filtration, the solvent was removed by reduced pressure to get compound **51a** as a yellow powder (crude 0.29 g, crude yield 71%)[34].

1,3-alternated-25,26,27,28-tetrakis(3-azidopropoxy)-calix[4]arene (60): In a 2-necked round-bottom compound **37** (1.88 mmol , 0.80 g) and Cs_2CO_3 (18.85 mmol, 6.14 g) were stirred in dry DMF (10 ml) for 1 h at room temperature. Then 1-iodo-3-azidopropane (9.42 mmol, 1.98 g) was added in and the mixture was kept stirring for 3 days at room temperature, monitoring the reaction by TLC (Hex/AcOEt 8:2 and 11:1). The reaction was quenched with 1N HCl/H_2O (10 ml + 10 ml) and the mixture was re-extracted with DCM (3 x 30 ml). The combined organic phases were washed with H_2O (3 x 30 ml), brine (3 x 30 ml) and eventually the solvent was removed by reduced pressure. The crude was recrystallized by DCM/Et_2O to get compound **60** as colourless crystals (0.46 g, 0.61 mmol, 33% yield). **^{1}H-NMR** (300 MHz, $CDCl_3$) δ (ppm): 7.08 (d, J = 7.4 Hz, 8H, m-Ar*H*O), 6.90 (t, J = 7.4 Hz, 4H,p-Ar*H*O), 3.86 (s, 8H, ArC*H*$_2$Ar), 3.57 (t, J = 6.9 Hz, 8H, $OCH_2CH_2CH_2N_3$), 2.99 (t, J = 6.9 Hz, 8H, $OCH_2CH_2CH_2N_3$), 1.50 (p, *J* = 6.9 Hz, 8H, $OCH_2CH_2CH_2N_3$). **^{13}C-NMR** (100 MHz, $CDCl_3$) δ (ppm): 156.6 (*C*Ar), 134.0 (*C*Ar), 129.4 (*C*Ar), 122.7 (*C*Ar), 66.9 ($OCH_2CH_2CH_2N_3$), 48.1 ($OCH_2CH_2CH_2N_3$), 38.2 (Ar*C*H$_2$Ar), 28.8 ($OCH_2CH_2CH_2N_3$). **ESI-MS** (+): calcd. for $C_{40}H_{46}N_{12}O_4Na$ [$(M+Na)^+$] m/z 781.37, found m/z 781.00 (100%), calcd. for $C_{40}H_{46}N_{12}O_4K$ [$(M+K)^+$] m/z 797.34, found m/z 797.00 (95%).

1,3-alternated-25,26,27,28-tetrakis(3-aminopropoxy)-calix[4]arene (61) [Staudinger strategy]: in a 2-necked round-bottom flask compound **60** (0.51 mmol, 0.39 g) and PPh_3 (4.08 mmol, 1.07 g) were stirred in dry $CHCl_3$ (20 ml) for 1 day at room temperature, monitoring it by TLC (AcOEt/MeOH + 1% NEt_3). Then H_2O (10 ml) was added in and the mixture was kept stirring for a further day at room temperature. The mixture was extracted with $CHCl_3$ (3 x 30 ml) and subsequently washed with H_2O (3 x 30 ml). To get rid of by-products it was extracted with 1N HCl (3 x 30 ml), the acqueous phase was neutralized with NaOH and then re-extracted with $CHCl_3$ (3 x 30 ml). The solvent was removed by reduced pressure to get compound **61** as a white powder (0.19 g, 0.29 mmol, 57% yield). **^{1}H-NMR** (400 MHz, MeOD) δ (ppm): 7.28 (d, *J* = 7.3 Hz, 8H, Ar*H*), 7.11 (t, *J* = 7.3 Hz, 4H, Ar*H*), 3.92 (s, 8H, ArC*H*$_2$Ar), 3.70 (t, *J* = 7.3 Hz, 8H, $OCH_2CH_2CH_2N$), 3.32 (t, J = 1.52, 8H, $OCH_2CH_2CH_2N$), 2.92 (d, J = 4.24 Hz, 4H, R-N*H*$_2$), 1.95 – 1.83 (m, 8H, $OCH_2CH_2CH_2NH_2$).

1,3-alternated-25,26,27,28-tetrakis(3-aminopropoxy)-calix[4]arene (61) [hydrogenation strategy]: In a Parr reactor 10% Pd/C (catalytic amount) was suspended into a solution of compound **60** (0.14 mmol, 0.11 g) in AcOEt (20 ml). H_2 was added in at 3.0 bar of pressure through a Parr apparatus and the mixture was left reacting for 7h at room temperature, monitoring the reaction by TLC (Hex/AcOEt 1:1). The catalyst was filtered off and the solvent was removed by reduced pressure to get compound **61** as a white powder (52.40 mg, 80.07 mmol, 57% yield). **^{1}H NMR** (300 MHz, MeOD) δ (ppm): 7.15 (d, *J* = 7.3 Hz, 8H, m-Ar*H*), 6.90 (t, *J* = 7.3 Hz, 4H, p-Ar*H*), 3.84 (s, 8H, ArC*H*$_2$Ar), 3.62 (t, *J* = 6.7 Hz, 8H, $OCH_2CH_2CH_2N$), 2.61 (t, *J* = 6.7 Hz, 8H, $OCH_2CH_2CH_2N$), 1.66 (t, *J* = 6.7 Hz, 8H, $OCH_2CH_2CH_2N$). **^{13}C-NMR** (100 MHz, MeOD) δ (ppm): 156.3 (*C*Ar), 134.7 (*C*Ar), 130.2 (*C*Ar), 128.6 (*C*Ar), 68.3 ($OCH_2CH_2CH_2N$), 37.6 (Ar*C*H$_2$Ar),

27.5 ($OCH_2CH_2CH_2N_3$), 20.7. **ESI-MS** (+): calcd. for $C_{40}H_{54}N_4O_4$ [$(M+H)^+$] m/z 653.41, found m/z 653.54 (30%), calcd. for $C_{40}H_{53}N_4O_4K$ [$(M+K)^+$] m/z 693.38, found m/z 693.57 (10%).

1,3-alternated-25,26,27,28-tetrakis(3-aminopropoxy)-calix[4]arene hydrochloride (62): In a round-bottom flask, compound **61** (10.70 umol, 7.00 mg) was dissolved in MeOH (1 ml) and under magnetic stirring 1N HCl (2 ml) was dropped in as long as pH=1 was reached. The methanolic solution was evaporated under reduced pressure and the resulting aqueous phase was lyophilized to get compound **62** as a white powder (8.45 mg, 10.59 umol, 99% yield). **^{1}H NMR** (300 MHz, MeOD) δ (ppm): 7.26 (d, *J* = 7.5 Hz, 8H, m-Ar*H*O), 7.01 (t, *J* = 7.5 Hz, 4H, p-Ar*H*O), 3.93 (s, 8H, ArCH_2Ar), 3.72 (t, *J* = 7.0 Hz, 8H, OC$H_2$$CH_2CH_2$N), 2.92 (t, *J* = 7.0 Hz, 8H, $OCH_2CH_2CH_2$N), 1.89 (t, *J* = 7.0 Hz, 8H, $OCH_2CH_2CH_2$N).

1,3-alternated-25,26,27,28-tetrakis(3-((4-benzensulfanamidyl)thioureido)propoxy)-calix[4]arene (63): in a 2-necked round-bottom flask compound **62** (0.29 mmol, 0.19 g) and DIPEA (2.91 mmol, 0.500 mL) were stirred in dry DMF (20 ml) for 10 minutes at room temperature. Then 4-isothiocyanatebenzensolfonamide (1.28 mmol, 0.27 g) was added in and the mixture was kept stirring for 1 day at room temperature, monitoring it by TLC (DCM/MeOH 9:1). The mixture was concentrated at rotavapor (10 ml) and then adding 1N HCl/H_2O (5 ml + 5 ml), a precipitate is formed. Upon filtration, the solid was recrystallized by acetone/Et_2O to get compound **63** as a brown powder (0.22 g, 0.15 mmol, 50% yield). **^{1}H-NMR** (400 MHz, Acetone-d_6) δ (ppm): 7.83 (m, *J* = 8.8 Hz, 8H, o-Ar*H*-SO_2NH_2), 7.76 (d, *J* = 8.8 Hz, 8H, m-Ar*H*-SO_2NH_2), 7.16 (d, *J* = 7.3 Hz, 8H, Ar*H*), 6.95 (t, *J* = 7.3 Hz, 4H, Ar*H*), 6.51 (s, 8H, SO_2NH_2), 3.92 (s, 8H, ArCH_2Ar), 3.48-3.44 (m, 8H, $OCH_2CH_2CH_2$N), 3.48-3.44 (m, 8H, OC$H_2$$CH_2CH_2$N), 1.67 – 1.61 (m, 8H, $OCH_2CH_2CH_2$N). **^{13}C-NMR** (100 MHz, Acetone-d_6) δ (ppm): 181.0, 156.7, 143.2, 142.6, 140.0, 138.6, 134.4, 129.8 (m-*C*Ar), 128.5, 127.4, 127.2 (m-*C*Ar-SO_2NH_2), 126.7, 126.6, 123.7, 123.2, 123.0 (p-*C*Ar), 122.8, 121.9 (o-*C*Ar-SO_2NH_2), 117.1, 68.0 ($OCH_2CH_2CH_2$N), 55.0, 54.1, 48.9, 43.0, 41.5 ($OCH_2CH_2CH_2$N), 37.7 (ArCH_2Ar), 28.0 ($OCH_2CH_2CH_2$N), 18.0, 16.6, 12.4, 0.5. **ESI-MS** (-): calcd. for $C_{68}H_{75}N_{12}O_{12}S_8Cl$ [$(M-3H+Cl)^{4-}$]: m/z 385.50, found m/z 385.00 (70%), calcd. for $C_{68}H_{77}N_{12}O_{12}S_8Cl$ [$(M-H+Cl)^{2-}$]: m/z 772.17, found m/z 772.17 (45%), calcd. for $C_{62}H_{72}N_{10}O_{10}S_7Cl$ [$(M+Cl-NHPhSO_2NH_2)^-$]: m/z 1373.60, found m/z 1373.58 (25%), calcd. for $C_{68}H_{78}N_{12}O_{12}S_8Cl$ [$(M+Cl)^-$]: m/z 1545.33, found m/z 1545.73 (18%).

Inhibition data.

Protocol. An Applied Photophysics stopped-flow instrument was used for assaying the CA catalyzed CO_2 hydration activity. Phenol red (at a concentration of 0.2 mM) was used as indicator, working at the absorbance maximum of 557 nm, with 20 mM Hepes (pH 7.5) as buffer, and 20 mM Na_2SO_4 (for maintaining a constant ionic strength), following the initial rates of the CA-catalyzed CO_2 hydration reaction for a period of 10-100 s. The CO_2 concentrations ranged from 1.7 to 17 mM for the determination of the kinetic parameters and inhibition constants. For each inhibitor, at least six traces of the initial 5-10% of the reaction were used for determining the initial velocity. The uncatalyzed rates were determined in the same manner and subtracted from the total observed rates. Stock solutions of inhibitor (0.1 mM) were prepared in distilled-deionized water, and dilutions up to 1 nM were done thereafter with distilled deionized water. Experiments were done using four different inhibitor concentrations, varying from 0.1 μM to 1 nM. Inhibitor and enzyme solutions were preincubated together for 6 h at room temperature (15 min just for AAZ) prior to assay, in order to allow for the formation

of the E-I complex. The inhibition constants were obtained by nonlinear least-squares methods using PRISM 3, as reported earlier and represent the mean from at least three different determinations.

Cocrystallization.

Crystallization and X-ray data collection for compound 56b-63. Crystals were obtained using the hanging drop vapour diffusion method using 24 well Linbro plate. 2 µl of 0.8 mM solution of hCA II in Tris-HCl pH=8.0 were mixed with of a solution of 1.5, 1.6 and 1.7 M sodium citrate, 50 mM Tris pH 8.0 and were equilibrated against 500 µl of the same solution at 296 K. Crystals of the protein grew in a few days. hCAII crystals were soaked in 5mM inhibitor solution for 2 days. The crystals were flash-frozen at 100K using a solution obtained by adding 25% (v/v) glycerol to the mother liquor solution as cryoprotectant. Data on crystals of the complexes hCAII/4b were collected using synchrotron radiation at the ID-11.2C beamline at Elettra (Trieste, Italy) with a wavelength of 1.000 Å and a Pilatus3_6M Dectris CCD detector. Data were integrated and scaled using the program XDS[37].

Structure determination for compound 56b-63. The crystal structure of hCA II (PDB accession code: 4FIK) without solvent molecules and other heteroatoms was used to obtain initial phases of the structures using Refmac5[38]. 5% of the unique reflections were selected randomly and excluded from the refinement data set for the purpose of Rfree calculations. The initial |Fo - Fc| difference electron density maps unambiguously showed the inhibitor molecules. Atomic models for inhibitors were calculated and energy minimized using the program JLigand 1.0.40[39]. Refinements proceeded using normal protocols of positional, anisotropic atomic displacement parameters alternating with manual building of the models using COOT[40]. Solvent molecules were introduced automatically using the program ARP[41]. The quality of the final models was assessed with COOT. Graphical representations were generated with Chimera[42].

Crystallization and X-ray data collection for compound 49b. Crystals of hCAII were obtained using the hanging drop vapour diffusion method using 24 well Linbro plate. 2 µl of 10 mg/ml solution of hCA II in Tris-HCl 20 mM pH 8.0 were mixed with 2 µl of a solution of 1.5 M sodium citrate, 0.1 M Tris pH 8.0 and were equilibrated against the same solution at 296 K. Crystals of the protein grew in one week. Afterwards hCAII crystals were soaked in 5mM inhibitor solution for 3 days. The crystals were flash-frozen at 100K using a solution obtained by adding 15% (v/v) glycerol to the mother liquor solution as cryoprotectant. Data on crystals of the complexes were collected using synchrotron radiation at the ID29 beamline at ESRF (Grenoble, France) with a wavelength of 0.827 Å and a PILATUS 6M Dectris CCD detector. Data were integrated and scaled using the program XDS[37].

Structure determination for compound 49b. The crystal structure of hCA II (PDB accession code: 4FIK) without solvent molecules and other heteroatoms was used to obtain initial phases of the structures using Refmac5[38]. 5% of the unique reflections were selected randomly and excluded from the refinement data set for the purpose of Rfree calculations. The initial |Fo - Fc| difference electron density maps unambiguously showed the inhibitor molecules. The inhibitor was introduced in the model with 0.5 occupancy. In the |Fo - Fc| difference electron density map a spheric density was present close to the benezensulphonamide moiety and was interpreted as a solvent molecule at 0.5 occupancy. Atomic models for inhibitors were

calculated and energy minimized using the program JLigand 1.0.40[39]. Refinements proceeded using normal protocols of positional, isotropic atomic displacement parameters alternating with manual building of the models using COOT[40]. Solvent molecules were introduced automatically using the program ARP[41]. The quality of the final models was assessed with COOT and RAMPAGE[41]. Crystal parameters and refinement data are summarized in **Table 3.5.1**. Atomic coordinates were deposited in the Protein Data Bank (PDB accession code: 6GOT). Graphical representations were generated with Chimera[42].

Table 3.5.1. Summary of Data Collection and Atomic Model Refinement Statistics. Values in parentheses are for the highest resolution shell.

HCAII/49b cocrystal XRD parameters	
PDB ID	6GOT
Wavelength (Å)	0.827
Space Group	P21
Unit cell (a, b, c, α, β, γ) (Å,°)	42.44 41.28 72.17 90.000 104.380 90.000
Limiting resolution (Å)	41.11-1.56
Unique reflections	33578 (6131)
Rsym (%)	17.1 (80.5)
Rmeas (%)	19.6 (91.6)
Redundancy	4.2 (4.3)
Completeness overall (%)	96.5 (96.1)
<I/σ(I)>	5.48 (1.26)
CC (1/2)	99.0 (53.6)
Refinement statistics	
Resolution range (Å)	41.11-1.56
Unique reflections, working/free	31883 / 1678
Rfactor (%)	19.88
Rfree(%)	22.33
r.m.s.d. bonds(Å)	0.015
r.m.s.d. angles (°)	1.7098
Ramachandran statistics (%)	
Most favored	98.0
additionally allowed	2.0
outlier regions	0.0
Average B factor (Å2)	
All atoms	15.83
inhibitors	16.70
solvent	21.22

3.6 References

1. Mammen, M., Choi, S.-K. & Whitesides, G. M. Polyvalent Interactions in Biological Systems: Implications for Design and Use of Multivalent Ligands and Inhibitors. *Angew. Chemie Int. Ed.* **37**, 2754–2794 (1998).

2. Baldini, L., Casnati, A., Sansone, F. & Ungaro, R. Calixarene-based multivalent ligands. *Chem. Soc. Rev.* **36**, 254–266 (2007).

3. Jencks, W. P. On the attribution and additivity of binding energies. *Proc. Natl. Acad. Sci. U. S. A.* **78**, 4046–4050 (1981).

4. Tomschy, A., Fauser, C., Landwehr, R. & Engel, J. Homophilic adhesion of E-cadherin occurs by a co-operative two-step interaction of N-terminal domains. *EMBO J.* **15**, 3507–14 (1996).

5. Brieher, W. M., Yap, A. S. & Gumbiner, B. M. Lateral dimerization is required for the homophilic binding activity of C-cadherin. *J. Cell Biol.* **135**, 487–496 (1996).

6. Ahrens, T. *et al.* Homoassociation of VE-cadherin follows a mechanism common to 'classical' cadherins. *J. Mol. Biol.* **325**, 733–42 (2003).

7. Leckband, D. & Sivasankar, S. Mechanism of homophilic cadherin adhesion. *Curr. Opin. Cell Biol.* **12**, 587–92 (2000).

8. Shapiro, L. *et al.* Structural basis of cell-cell adhesion by cadherins. *Nature* **374**, 327–337 (1995).

9. Harrison, O. J., Corps, E. M., Berge, T. & Kilshaw, P. J. The mechanism of cell adhesion by classical cadherins: The role of domain 1. *J. Cell Sci.* **118**, 711–721 (2005).

10. Posy, S., Shapiro, L. & Honig, B. Sequence and Structural Determinants of Strand Swapping in Cadherin Domains: Do All Cadherins Bind Through the Same Adhesive Interface? *J. Mol. Biol.* **378**, 954–968 (2008).

11. Baumgartner, W. *et al.* Cadherin interaction probed by atomic force microscopy. *Proc. Natl. Acad. Sci. U. S. A.* **97**, 4005–4010 (2000).

12. Jurriaan Huskens et al. *Multivalency Concepts, Research & Applications*. (2018).

13. Kolaczkowska, E. & Kubes, P. Neutrophil recruitment and function in health and inflammation. *Nature Reviews Immunology* **13**, 159–175 (2013).

14. Ley, K., Laudanna, C., Cybulsky, M. I. & Nourshargh, S. Getting to the site of inflammation: The leukocyte adhesion cascade updated. *Nature Reviews Immunology* **7**, 678–689 (2007).

15. McEver, R. P., Moore, K. L. & Cummings, R. D. Leukocyte trafficking mediated by selectin-carbohydrate interactions. *Journal of Biological Chemistry* **270**, 11025–11028 (1995).

16. Nimse, S. B. & Kim, T. Biological applications of functionalized calixarenes. *Chem. Soc. Rev.* **42**, 366–386 (2013).

17. Gutsche, C. D., Dhawan, B., No, K. H. & Muthukrishnan, R. Calixarenes. 4. The Synthesis, Characterization, and Properties of the Calixarenes from p-tert-Butylphenol. *J. Am. Chem. Soc.* **103**, 3782–3792 (1981).

18. Iwamoto, K., Araki, K. & Shinkai, S. Syntheses of all possible conformational isomers of O-alkyl-p-t-butylcalix[4]arenes. *Tetrahedron* **47**, 4325–4342 (1991).

19. Groenen, L. C. *et al.* syn-1,2-dialkylated calix[4]arenes : general intermediates in the NaH/DMF tetraalkylation of calix[4]arenes. *Tetrahedron Lett.* **32**, 2675–2678 (1991).

20. Rodger P. McEver. Selectins: lectins that initiate cell adhesion under flow. *Curr. Opin. Cell Biol.* **14**, 581–586 (2002).

21. Marshall, B. T. *et al.* Direct observation of catch bonds involving cell-adhesion molecules. *Nature* **423**, 190–193 (2003).

22. Sarangapani, K. K. *et al.* Low Force Decelerates L-selectin Dissociation from P-selectin Glycoprotein Ligand-1 and Endoglycan. *J. Biol. Chem.* **279**, 2291–2298 (2004).

23. Mak, R. H. & Kuo, H.-J. Pathogenesis of urinary tract infection: an update. *Curr. Opin. Pediatr.* **18**, 148–152 (2006).

24. Carta, F. *et al.* Poly(amidoamine) dendrimers with carbonic anhydrase inhibitory activity and antiglaucoma action. *J. Med. Chem.* **58**, 4039–4045 (2015).

25. Abellán-Flos, M., Tanç, M., Supuran, C. T. & Vincent, S. P. Organic & Biomolecular Chemistry Exploring carbonic anhydrase inhibition with multimeric coumarins displayed on a fullerene scaffold †. *Org. Biomol. Chem.* **13**, 7445 (2015).

26. Stiti, M., Cecchi, A., Rami, M., Abdaoui, M. & Biomole, I. the Tumor-Associated Isoform IX over the Cytosolic Isozymes I and II. *J. Am. Chem. Soc.* **130**, 16130–16131 (2008).

27. Chambers, J. M. *et al.* Cryptophane xenon-129 nuclear magnetic resonance biosensors targeting human carbonic anhydrase. *J. Am. Chem. Soc.* **131**, 563–569 (2009).

28. Ghosh, P., Judd, W. R., Ribelin, T. & Aubé, J. Asymmetrie total synthesis of alkaloids 223A and 6-epi-223A. *Org. Lett.* **11**, 4140–4142 (2009).

29. Genorio, B. The synthesis of diquinone and dihydroquinone derivatives of calix[4]arene and electrochemical characterization on Au(111) surface. *Acta Chim. Slov.* **63**, 496–508 (2016).

30. Arena, G. *et al.* Entropic origin of the sulfonate groups' electrostatic assistance in the complexation of quaternary ammonium cations by water soluble calix[4]arenes. *J. Chem. Soc. Perkin Trans. 2* 419–423 (2000). doi:10.1039/a909847j

31. Baldini, L. *et al.* CO2 capture by multivalent amino-functionalized calix[4]arenes: Self-assembly, absorption, and QCM detection studies. *J. Org. Chem.* **76**, 3720–3732 (2011).

32. Kuo, C. H. *et al.* 25,26-Dialkoxycalix[4]arenes. Part 2: 1-Alkoxy-3-benzoyloxy route. *Tetrahedron* **67**, 3936–3944 (2011).

33. Dondoni, A., Ghiglione, C., Marra, A. & Scoponi, M. Synthesis of Calix[4]arenylvinylene and Calix[4]arenylphenylene Oligomers by Stille and Suzuki Cross-Coupling Reactions. *J. Org. Chem.* **63**, 9535–9539 (1998).

34. Royappa, A. R. N. S. *et al.* Conformationally Selective Synthesis of Mononitrocalix[4]arene in *Cone* or *Partial Cone*. *Helv. Chim. Acta* **100**, (2017).

35. *Self-Assembly of a Threaded Molecular Loop*.

36. Priastomo, Y., Morisada, S., Kawakita, H., Ohto, K. & Jumina. Synthesis of macrocyclic polyphenol resin by methylene crosslinked calix[4]arene (MC-[4]H) for the adsorption of palladium and platinum ions. *New J. Chem.* **43**, 8015–8023 (2019).

37. Kabsch, W. <title>\n *XDS*\n</title>. *Acta Crystallogr. Sect. D Biol. Crystallogr.* **66**, 125–132 (2010).

38. Murshudov, G. N. *et al.* REFMAC5 for the refinement of macromolecular crystal structures. *Acta Crystallogr. Sect. D Biol. Crystallogr.* **67**, 355–367 (2011).

39. Lebedev, A. A. *et al.* JLigand: A graphical tool for the CCP4 template-restraint library. *Acta Crystallogr. Sect. D Biol. Crystallogr.* **68**, 431–440 (2012).

40. Emsley, P., Lohkamp, B., Scott, W. G. & Cowtan, K. Features and development of Coot. *Acta Crystallogr. Sect. D Biol. Crystallogr.* **66**, 486–501 (2010).

41. Langer, G., Cohen, S. X., Lamzin, V. S. & Perrakis, A. Automated macromolecular model building for X-ray crystallography using ARP/wARP version 7. *Nat. Protoc.* **3**, 1171–1179 (2008).

42. Pettersen, E. F. *et al.* UCSF Chimera - A visualization system for exploratory research and analysis. *J. Comput. Chem.* **25**, 1605–1612 (2004).

Chapter 4

Kinetic stabilizers of Transthyretin tetrameric structure against amyloidogenic diseases

4.1 Introduction

4.1.1 General

As already largely known, not all the proteins work in the monomeric form to exploit their functions such as some carbonic anhydrases. In fact, some of them self-assembles to create complex quaternary structures, which are essential for their functions, whereas monomeric building-blocks are partially or totally inactive. In this context loads of examples are present in biology. One of the most famous multimeric enzymes is ATP synthetase (**Figure 4.1.1.1A**), in which all the protein components cooperate together to transfer mechanical energy to active site, where ATP is really synthesized by clamping reactants together[1,2]. These components, since they are cooperating units with a particular geometry, shape and location, are totally useless taken singularly. Another example is Haemoglobin (**Figure 4.1.1.1B**), which is a plasmatic tetrameric complex involved in oxygen transport in biological fluids[3–5]. Also here the monomeric building blocks cooperate each other so much that when one oxygen molecule is bound to one Heme-monomer, the binding of the second oxygen molecule and, in turn, of the third and the fourth one is more and more favoured leading directly in a sort of cascade fashion to tetra adduct with oxygen. Nature developed several systems like these ones to increase enzymatic and storage properties useful for living beings. Among these proteins, the transport protein TTR (transthyretin) is a largely studied protein since it is implicated in the development of amyloid diseases following its quaternary structure destabilization.

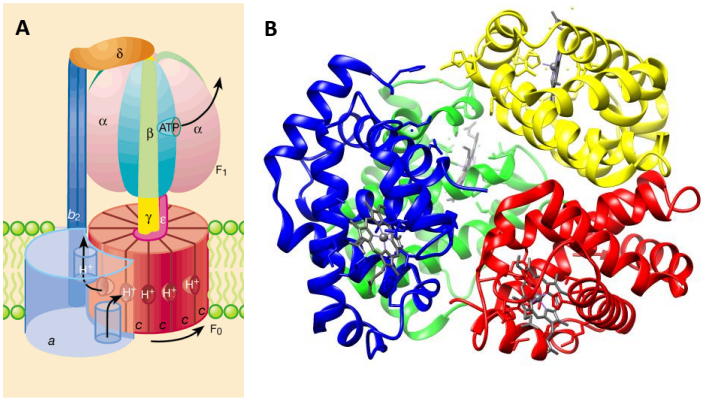

Figure 4.1.1.1. Examples of multicomponent proteins. In ATP synthase (**A**) the rotational motion generated in c wheel by transmembrane proton gradient is transferred mechanically to αβ unit, where ADP and Pi are clamped together to synthesize ATP. In **B** the four subunits are highlighted in blue, red, yellow and green, whereas heme prosthetic groups are highlighted in grey. The intermolecular interaction among these subunits is responsible for the positive feedback observed in oxygen complexation. Figure **A** has been adapted from reference[6], meanwhile figure B was elaborated with Chimera Software (PDB code: 2hhb)[7].

4.1.2 TTR: structure and physiological properties

Transthyretin (TTR) is one of the 26 proteins known to be responsible for amyloid disease[8–12]. The transthyretin gene (four exons and three introns spanning about 7 kbp) has been found in the long arm (q) of chromosome 18 in the region 18q11.2-q12.1[13]. TTR is mainly produced in

the liver but also in eyes and choroid plexus and it is secreted respectively in serum and cerebrospinal fluids, where carries out its transport function of thyroxine-based hormones (T4/T3)[14–18], thyroid-secreted molecules involved in metabolism and growth, and of retinol via plasma retinol-binding protein (RBP4)[19,20], vitamin essential for vision, immune functions and metabolism.

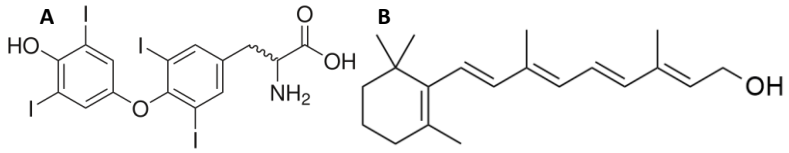

Figure 4.1.2.1. Molecular structures of T4-hormone (**A**) and Retinol (**B**).

TTR is a tetramer[21] (**Figure 4.1.2.2**), specifically a dimer of dimers (222 symmetry), with four identical monomers. Each monomer (127 residues each) is made of eight beta-strands, denoted A to H, and one short alpha helix. These eight β-strands form two β-sheets, that together create an immunoglobulin-like β-barrel structure. Two monomers dimerize mainly in an antiparallel fashion through strong interactions between the H-strands forming an eight stranded β-sheet.

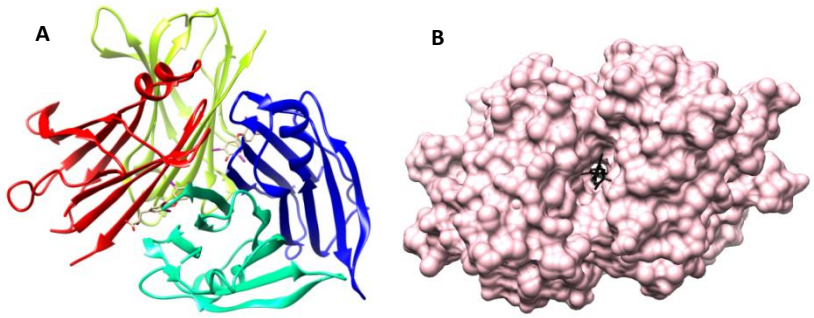

Figure 4.1.2.2. Human WT-TTR complex with T4 hormone (PDB code 1ICT): **A**) Ribbon-like representation (subunits are highlighted in blue, cyan, green and red), **B**) Surface-like representation (in black are highlighted T4 molecules located in the transversal channel active site). Figures were elaborated with Chimera software.

Moreover, some water molecules, as well, interact with side chains of F-strands in each monomer in order to facilitate dimerization. The functional tetramer is built up by hydrophobic contacts between the AB- and GH-loops at dimer-dimer interphase, which leads to the formation of a transversal funnel-shaped channel, along one of the two-fold axes of the protein. The two thyroid hormone binding sites, located at the two ends of the channel in between the two monomers belonging to the same dimer, are composed of three pairs of halogen-binding pockets (HBP), namely HBP1-HBP1', HBP2-HBP2', and HBP3-HBP3' (the apostrophe indicates the corresponding pocket of the symmetry-related dimer). HBP1 is located in the outermost part of the hydrophobic channel, which is covered with the side chains of Met13, Lys15 and Thr106. HBP2 is lined with the side chains of Lys15, Leu17, Ala109, Leu110, and the hydrophilic main chain carbonyl groups of Lys15, Ala108, and Ala109. The last and innermost pocket, HBP3, is surrounded by the side chains of Ala108, Ala109, Leu110, Ser117, Thr118 and Thr119[18]. In cocrystals of human-TTR and T4, the four iodine atoms are found oriented in HBP1 (I5), HBP2

(I3'), HBP2* (I3) and HBP3 (I5'), in which are stabilized by polar interactions along with the hydrogen bonds made at the entrance of channel between Lys15/Glu54 and amino group of T4 hormone[18]. Generally, in solid-state TTR is found in the saturated form, while in solution TTR binds just one hormone molecule because of a negative allosteric effect, which makes hard the second complexation[22,23]. *In vitro* solution studies demonstrated that this complexation, actually, is concentration-dependent, since, working in five-fold excess of T4, the equilibrium can be shifted towards double inclusion of the hormone inside the protein. Despite this low affinity, the bioavailability of these hormones for homeostasis is further guaranteed by other transport systems, in particular albumin (low affinity, high plasma concentration) and thyroxin-binding globulin (high affinity, low plasma concentration)[19].

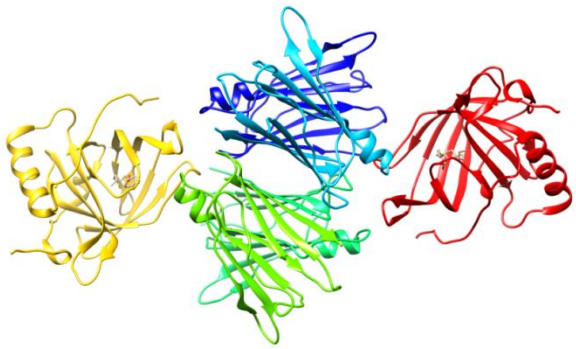

Figure 4.1.2.3. Human WT-TTR complex with oleic acid (PDB code 2WQA). The complex is presented in ribbon-like representation: TTR subunits are highlighted in blue, cyan, green and light green, whereas RBP units are highlighted in red and yellow, inside which oleic acid is complexed.

As far as retinol transport is concerned, it is realized in a different way. The molecule, in fact, is not bound directly to TTR, but it is complexed by plasma retinol-binding protein (RBP) and the complex, in turn, is bound to TTR (**Figure 4.1.2.3**). This method, beyond taking in solution hydrophobic molecules, as for T4, is exploited to avoid the loss of RBP by glomerular filtration in the kidneys[24,25]. In fact, when RBP/retinol-complex is associated with TTR in endoplasmic reticulum of hepatocytes, it cannot be extruded by Bowman's capsule because of its higher dimension. In this complex formation, as well as for T4-TTR complex, it has experimented negative cooperation, which makes very hard the binding of a second retinol molecule[26].
The monomeric retinol-binding protein is a 21 kDa molecule made of 183 residues. It is made of a short α-helix and nine β-strands where just six of them in each of the two orthogonal β-sheets build a β-barrel. This secondary structure is realized by sharing three strands (A, E and F) with the two sheets (strands A-B-C-D-E-F and E-F-G-H-A-I, respectively. The retinol is encapsulated in the hydrophobic core of binding cavity in a way that all contacts are maximized. In fact, the ring structure of the retinol inserts firstly so that just the alcohol moiety is exposed to solvent. Retinol is kept inside the cavity by hydrophobic amino acids located from the α-helix (residues 80-86) of TTR to the loop between β-strands 5 and 6 (residues 63-67), and the loop region between β-strands 7 and 8 in the RBP molecule. One TTR tetramer binds two molecules of RBP –retinol complex by means of hydrophobic residues localized in the carboxy-terminus domain[27,28]. Moreover, it has been demonstrated that this interaction is very sensitive to mutation or deletion. In fact, in urine it has been found a truncated form of RBP, lacking C-terminal lysine, which does not contain retinol and has no affinity for TTR[29].

TTR is largely studied for the significant impact which has on amyloidogenic pathologies. There are three TTR-related diseases: senile systemic amyloidosis (SSA)[30,31], familial amyloidotic polyneuropathy (FAP)[31–34] and familial amyloidotic cardiomyopathy (FAC)[35]. SSA is typically observed in older people because of formation of amyloid fibrils derived from Wild-type TTR, which undergoes some modifications still under investigation. Contrary, FAP and FAC are caused by an aggressive TTR mutant[35–37], which starts forming amyloid fibrils at much earlier age than Wild-type TTR. In this context, more than 80 single point mutations of TTR have been identified and defined to be responsible most of them of the disease. The mutations are spanned all over the transthyretin sequence but concentrated within a "hot spot" in the edge strand region (residues 45-58) from C-strand to D-strand and in a part of the DE-loop which is rich in amino acids prone to aggregation into amyloid fibrils (**Figure 4.1.2.4A**). TTR-Ile84Ser and TTR-Ile84Asn mutations occur naturally and they mainly are involved in FAP. These essentially prevent TTR-RBP complex formation, resulting in a lower RBP plasma concentration and consequent TTR aggregation into amyloid fibrils in affected patients[38]. The mechanism by which amyloid fibrils develop is still under investigation, in particular for WT-related ATTR. However, the guidelines, which drive this process, have been surely determined.

The pathological pathway starts from the destabilization of the TTR tetramer at dimer-dimer interface (**Figure 4.1.2.4B**). Some models have been recently proposed, but the most commonly used is the one reported in Yee et al.'s work[39].

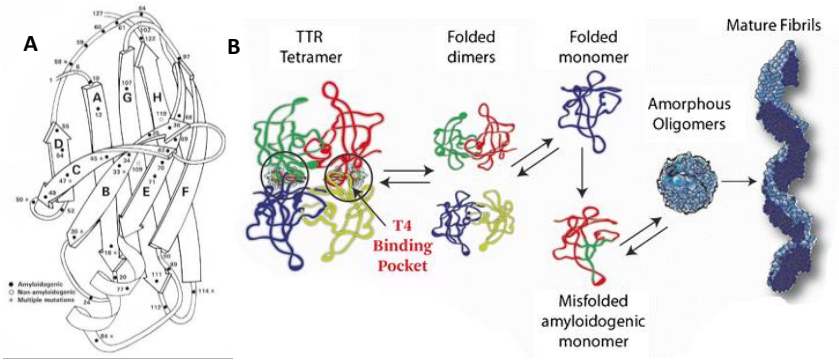

Figure 4.1.2.4. A) Cartoon representation of TTR with all mutations discovered so far. It can be seen that the hotspot from C to E sheet contributes for most of overall mutations. Figure adapted from reference[40]; **B**) TTR misfolding mechanism from tetramer destabilization to mature fibril generation. Figure adapted from reference[41].

By molecular dynamics[39], it has been demonstrated that the disease point mutations, whatever they are, trigger the dissociation of tetramer long dimer-dimer interphase releasing two dimers in solution. This step, which is known to be the rate-determining step of all process in WT-ATTR, here is totally fastened by this destabilizing modifications. At this point the two dimers, further destabilized by the dissociation, dissociate into monomers, which in cascade misfold and subsequently aggregate into amyloid fibrils. This represents a crude model of the process, but actually the exact destiny depends on the nature of mutation. In particular, it has been demonstrated that S52P-TTR mutant is more subjected to proteolytic cleavage between Lys48 and Thr49, which leads to a permanent misfolding favourite for aggregation. This is rationalized

by the higher propensity S52P-TTR mutant to misfold before dissociation, which exposes Lys48 in a less bulky area ready to be caught up by proteases[42,43].

Because of these diseases, amyloid aggregates were found in brain (FAP), heart (FAC), eye and kidney, which generally leads to several symptoms such as neuropathy, cardiac and gastrointestinal problems and muscles hypotonicity, which over times can lead to death[44–47]. Considering the dramatic impact of this life-threatening disease on human's life, a lot of research on this topic has been carried out. The first-ever gene therapy done in this context was liver transplantation[48,49], which represents nowadays a potent tool to slow or, in the luckiest cases, to halt the progression of FAP. Since TTR is mostly produced in liver, the transplantation indeed replaces effectively mutant gene with a WT gene resulting in a reduction of mutant TTR levels in body < 5% in respect to pretransplant levels[50]. Even if it is considered a useful strategy, this might not eliminate the problem since amyloid fibrils can grow on pre-existing deposits. In addition, some mutations cause CNS amyloidosis derived from production of choroid plexus-related TTR and so do not respond positively to gene therapy by liver transplantation. For these reasons, along with the high invasiveness, risk and cost of liver transplantation, the long-life immunosuppression and the limited organ availability, medicinal chemists are trying to develop new drugs to inhibit these pathological processes.

4.1.3 Inhibition strategies

Alternatively to liver and heart transplantation, over the past two decades have been developed three classes of pharmacological inhibitors, which had been grouped according to their inhibition strategy:

- Translation suppressor of TTR synthesis in hepatocytes[51,52]
- Kinetic stabilizers of the TTR tetramer[53,54]
- ATTR amyloid fibril clearers[55–57]

The first class is subdivided again into two different sub-groups: antisense oligonucleotide inhibitors (ASO)[41,52,58] and small interfering RNA inhibitors (siRNA)[59]. These approaches exploit the mRNA-binding properties of single-stranded oligonucleotides (around 20 nucleotides) to stop gene translation by steric effects or even by enzymatic degradation of the targeted mRNA. This is realized in three different ways: siRNA is bound to target mRNA, the complex, in turn, is bound to RNAse-H inducing the mRNA degradation; siRNA binds to mRNA preventing the translation on ribosome for steric hindrance; siRNA binds to pre-mRNA altering mRNA splicing[60,61]. In this context one of the most interesting drugs developed so far is Inotersen (IONIS-TTR_{Rx})[62], which, administered by weekly subcutaneous injections, is able to target a conserved region of TTR mRNA (**Figure 4.1.3.1**).

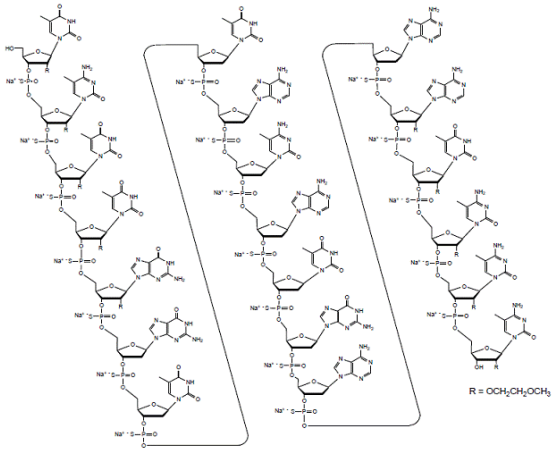

Figure 4.1.3.1. Inotersen (IONIS-TTR$_{Rx}$) chemical structure.

It has been tested on a small number of patients affected by FAP and what turned out, was that over 65 weeks a very good improvement of neuropathy progression was observed. Unfortunately though, since this conserved region is not generally mutated, these inhibitors, like patisiran and others[63], downregulate the mutant TTR expression, as well as WT-TTR expression. Inotersen has recently passed phase 2/3 clinical trial (NCT01737398) as drug for treatment of FAP and so for this reason, it is expected to be approved by FDA for neuropathic applications by the end of 2019[41,64–67].

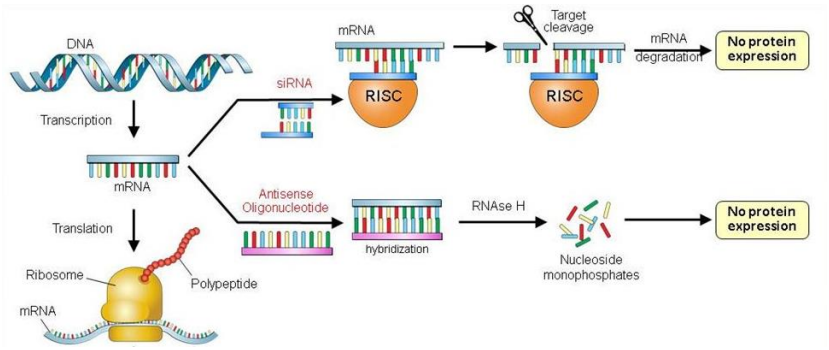

Figure 4.1.3.2. Schematic representation of protein expression regulation by antisense oligonucleotide and siRNAs. In both pathways mRNA strand is cut off by RISC complex or RNAase H by means of intermolecular pairing with a complementary strand. Figure adapted from reference[68].

siRNAs[51] are non-codifying short double-stranded oligonucleotides, which, packed in lipid nanoparticles to guarantee delivery to the liver, bind to a conserved regions of TTR mRNA activating their degradation and consequently reducing TTR expression. Their inhibition mechanism passes through endoribonuclease Dicer, a helicase enzyme, which unfolds the dsRNA and gives to RISC complex just one strand. Now RISC complex can recognize the complementary mRNA and degrade it (**Figure 4.1.3.2**)[69].

The kinetic stabilizers of TTR tetramer, differently from anti-translation drugs, play a stabilizing role in the dissociation of the tetramer. They, in fact, go into both thyroxine cavities acting essentially as a "supramolecular glue" (chaperones), which takes together the two dimers of dimers generally involved in the outbreak of the disease. Wide research has been doing in this field, since these synthetic molecules, smaller and more apolar than oligonucleotides, can be more easily internalized in cells. According to the sharp and very preorganized cavities, all the inhibitors synthesized so far are pretty rigid and flat. Most of them are polyaromatic molecules, such as diflunisal[70,71], tafamidis[72], tolcapone[73], and Thyrphorstin AG10 (**Figure 4.1.3.3**).

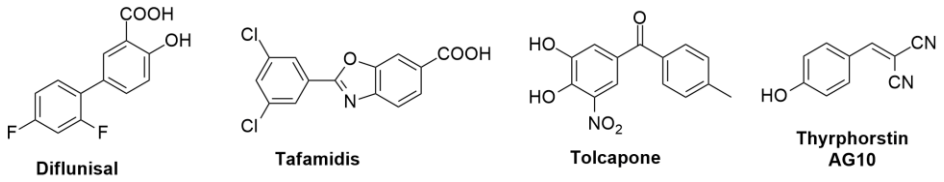

Figure 4.1.3.3. Chemical structure of most common drugs used as kinetic stabilizers in the treatment of ATTR.

Diflunisal is a nonacetylated salicylate nonsteroidal anti-inflammatory drug used for decades in the treatment of arthritis and musculoskeletal pain. In 2003 a randomized experimental study demonstrated that it is able to slow significantly the polyneuropathy progression[74–76]. In relative cocrystal two different binding modes have been observed: reverse and forward binding mode (**Figure 4.1.3.4 A,B**). The molecule can enter the channel in two opposite orientations because of the similar intermolecular interactions at stake. The reverse binding is stabilized by an electrostatic interaction between main chain oxygen atom of Ala 108 and its carboxyl group and the side chain oxygen atom of Thr 119, whereas the forward mode, on the contrary, is dominated by a halogen bond among one fluorine atom and the Thr 119 side chain oxygen atom. Moreover, after computational studies, it has been demonstrated that the binding, in this case, is increased by ionic interaction between Lys 15' and carboxyl group of diflunisal[70,72]. Recently, diflunisal has been taken as lead compound for the development of biphenyl-based inhibitors. According to Adamski-Werner[70], only small substitutions can be made on biphenyl scaffold like halogen groups. A large library was made and some derivatives have been shown as better inhibitors than diflunisal because of the better positions of groups involved in the binding. As well as Diflunisal, Tafamidis can enter TTR thyroxine-binding pocket and bind to tetramer (Kd_1 = 5.7 nM and Kd_2 = 260 nM towards WT-TTR). It stabilizes the TTR tetramer by hydrophobic interactions between 3,5-chloro groups of the inhibitor and HBPs. The whole binding is enhanced by water-mediated hydrogen bonds between the carboxylate of Tafamidis and Lys15/15' and Glu54/54' residues (**Figure 4.1.3.4C**).

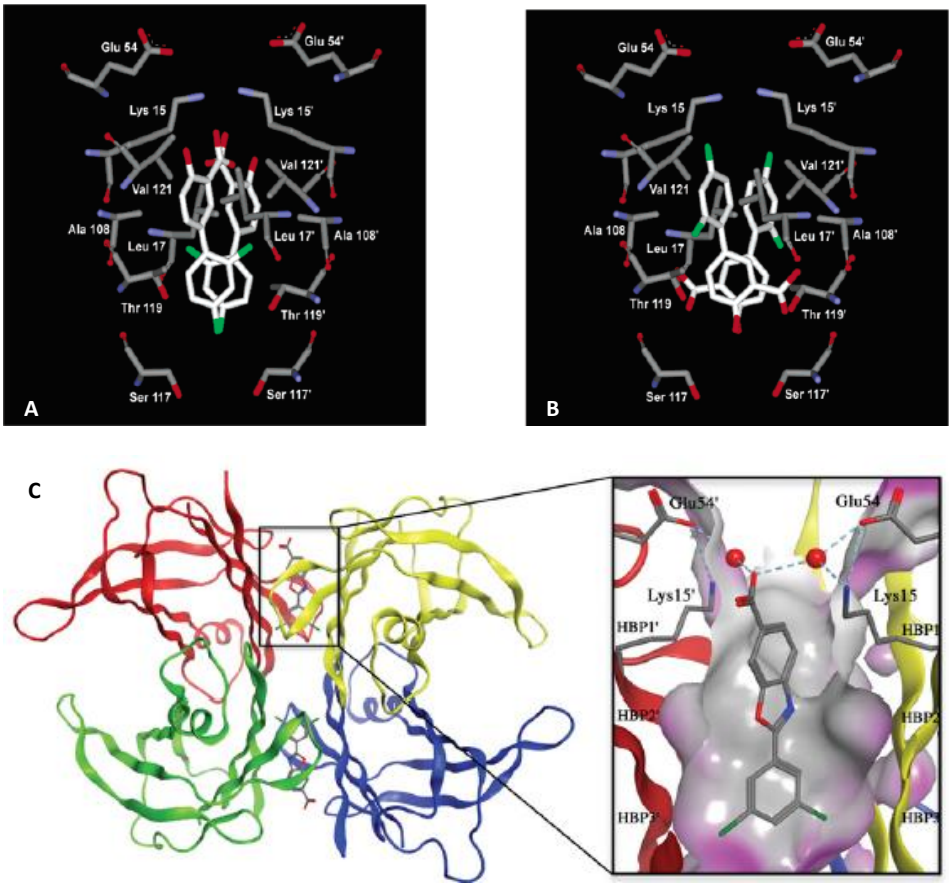

Figure 4.1.3.4. X-ray crystal structures of Diflunisal and Tafamidis bound to TTR. Diflunisal is shown bound to TTR in the forward binding mode (**A**) and in the reverse binding mode (**B**), meanwhile Tafamidis is just observed in the forward binding (**C**). In figure C it is shown that with Tafamidis the binding is enhanced by two water molecules involved in bridging hydrogen bonds with Glu54, Glu54'and Lys15. Figure adapted from references[70,72].

Tafamidis, for its high efficiency as chaperone and for the good results obtained in phase 3 clinical trial (NCT01994889), has been approved by European Medicinal Agency (EMA) for the treatment of FAP[72].

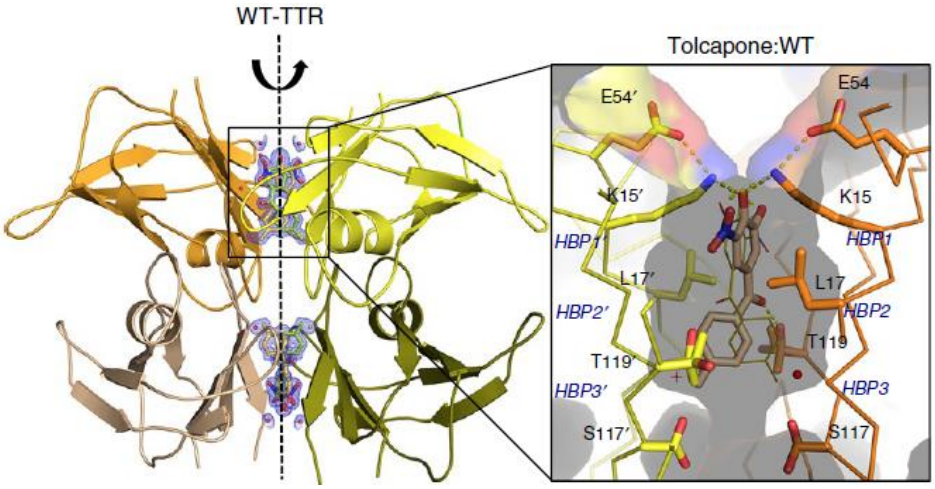

Figure 4.1.3.5. On the left-hand side WT-TTR/tolcapone complex is shown in ribbon representation. Dashed line indicates the twofold symmetry axis of the dimer–dimer interface. A magnification of one of the WT-TTR T4-binding sites is shown on the right-hand side (PDB code: 4D7B). Figure adapted from reference[73].

Recently, the Parkinson drug Tolcapone has been discovered to be a potent kinetic stabilizer for TTR tetramer through a simultaneous binding in both thyroxine-binding pockets (Kd_1 = 21 nM and Kd_2 = 58 nM towards WT-TTR)[73]. In cocrystal structure it has been seen that 4-methylphenyl ring of tolcapone makes hydrophobic interactions in HBP2–2′ and HBP3–3′ with Ala108, Leu110, Ser117 and Thr119, whereas a stabilizing hydrogen bond is established between the hydroxyl side chain of Thr119 and the central carbonyl group of the inhibitor. Contrary, the 3,4-dihydroxy-5-nitrophenyl ring is engaged into two different interactions: hydrophobic interactions with Lys15, Leu17, Thr106 and Ala108 in HBP2-2′ and HBP1 -1′ and electrostatic interactions between phenolic OHs and ε-amino group of Lys15, which, in turn, establishes polar contacts with the carboxylate group of Glu54. The polar interactions mediated by Lys15 represent a smart idea employed by Tolcapone to exclude solvent and preserve the protein/inhibitor complex. The slightly higher efficiency of Tafamidis over Tolcapone, beside the nature of interactions, can be explained by the entropic effect of a minor number of displaced water molecules upon binding. By a pharmacokinetic point of view, Tolcapone is characterized by rapid absorption properties (85% in gut) and good bioavailability (65%), because of its quantitative complexation in plasma protein, mainly by albumin.

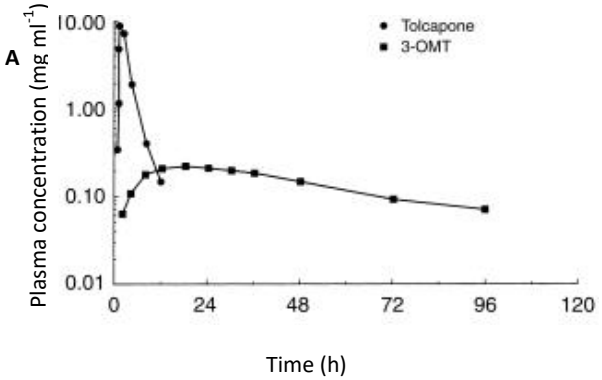

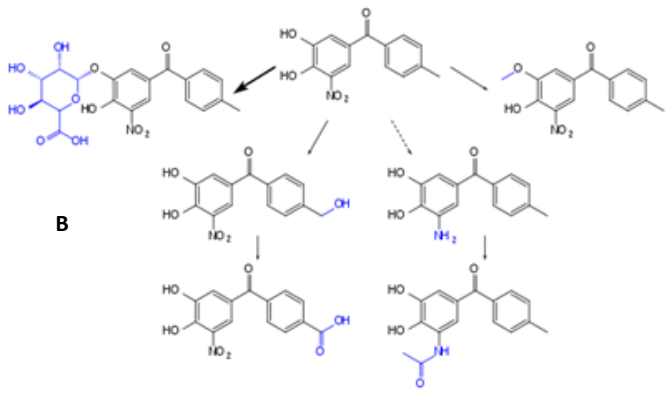

Figure 4.1.3.6. A) Plasma concentration of Tolcapone and 3-O-MethylTolcapone (3-OMT) over time. It is clear from the profile that Tolcapone reaches its maximum peak after 2-3 hours followed by a fast clearance. Figure adapted from reference[77]; **B**) Schematic representation of all reactions involved Tolcapone metabolism. From left to right: glucuronidation reaction, methyl oxidation to carboxylic acid, reduction of nitro group to amine and subsequent acyl capping, 3-O-methylation.

Tolcapone reaches its highest plasmatic concentration after 2 h, but unfortunately at the third hour its concentration is approximately equal to zero (**Figure 4.1.3.6**). This dramatic inactivation is due mainly to glucuronidation, after which the resulting molecule is rapidly excreted through biles via urine or via faeces. These reactions along with those reported in **Figure 4.1.3.6B**, are responsible for hepatic overstimulation, which limits tolcapone dosage[77]. For this reason, a lot of ongoing research is synthesizing and testing analogues, in which moieties responsible for pharmacokinetic clearance are combinatorially deleted. In parallel to these type of inhibitors, some researchers have employed some natural flavonoids as TTR tetramer stabilizers. Some of these, such luteolin, genistein and Biochanin A have been demonstrated good stabilizers[78,79]. The challenge now is to modify them to increase the binding and pharmacological properties.

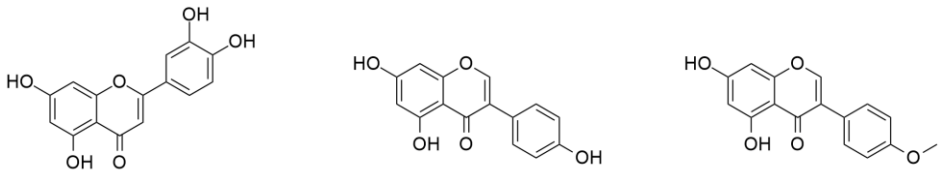

Figure 4.1.3.7: Chemical structure of natural molecules used as kinetic stabilizers in the treatment of ATTR.

Obviously, these inhibitors do not remove the pre-existing amyloid deposit, but they just prevent further deposition. With this need in mind, several are the molecules designed as sequestrants for disassembly. For example, Doxycycline (tetracycline antibiotic) and Tauroursodeoxycholic acid (bile acid) have been shown up as efficient tool for disruption of premature amyloid fibrils[80]. Also Epigallocatechin-3-gallate[81], a polyphenol extracted by green tea, is able to either stabilize TTR tetramer or disrupt fibrils, but binding in this case in a different site from that used by tafamidis and diflunisal. Also curcumin[82,83], binding to thyroxine-binding pocket, is able to act as tetramer stabilizer and fibril disruptor. Besides this "natural approach", recently, some examples of immunotherapy have been coming

up. One strategy consists in the synthesis of antibody specific to an amino acid sequence in TTR, which is buried in the tetramer, but exposed in the monomer[84,85]. This guarantees the possibility to target the dangerous monomer and trigger an immune response finalized to its elimination. Opposite to this, the second strategy exploits the heterogeneous composition of amyloid deposits. Among them, Serum amyloid P component (SAP) is found. Since this protein is a glycoprotein responsible for the resistance of amyloid deposits to proteases, SAP is a good target for amyloid disassembly. A few years ago, a monoclonal G1 anti-SAP antibody was used in this context with very good results[84]. 16 FAP-affected patients within a 6-weeks treatment period were subjected to significant reversal of the disease. By the way, these last systems are getting very interesting devices for the treatment of ATTR, but even if some have passed phase II of clinical trials, they still need to be studied more.

4.2 Aim of the project

In this project, we focused on the second class of inhibitors, the kinetic stabilizers of TTR tetrameric structure. We decided to choose two different well-known molecules as scaffolds: Tolcapone and Biochanin-A. The choice of these two molecules was driven by their known highly therapeutical properties, their rather easy chemical modification and the possibility to easily study them by Molecular Dynamics. Before the synthesis, in collaboration with prof. Berni of University of Parma, who is expert in TTR-related diseases, a preliminary computational study was carried out with the aim to understand which type of deletions/modifications on tolcapone and Biochain A scaffolds (known to be good kinetic stabilizers) can further stabilize the complex with TTR. For the synthesis of the related inhibitors we focused just on the modifications which gave promising results in binding energy stabilization. In particular, as far as Tolcapone is concerned, we focused on deletion of 3-OH, which is the hydroxy group mainly susceptible of glucuronidation that deactivates the molecule and triggers the clearance step. If confirmed the absence of negative effects by this deletion on the affinity of the inhibitor for TTR, this molecule could be a promising tool to overcome the hepatic overstimulation observed with Tolcapone. For the case of Biochanin A, we focused on 7-chlorination and 7-sulfation.

4.3 Results and discussion

4.3.1 Synthesis of 3-deoxy-tolcapone

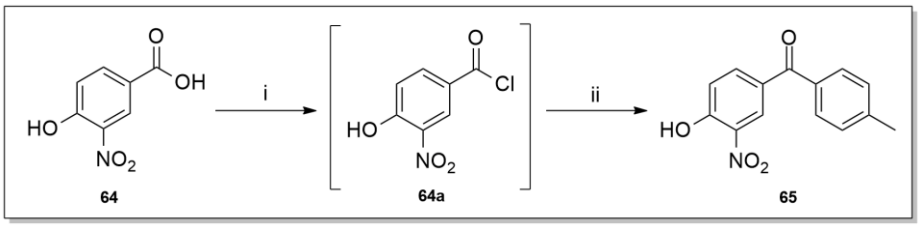

Figure 4.3.1.1: Synthesis of 3-deoxy-tolcapone. Reactions conditions: i) $SOCl_2$ (1.9 eq), dry DMF (0.2 eq), dry toluene, 65 °C, 4h; ii) dry $AlCl_3$ (2.2 eq), dry toluene, rt, on (55% overall yield).

The synthesis of 3-deoxytolcapone has been carried out through a one-pot strategy (**Figure 4.3.1.1**). Specifically, 4-hydroxy-5-nitrobenzoic acid was transformed into the corresponding acyl chloride by treatment with $SOCl_2$ and immediately used as reactant in the same round-bottomed flask. Toluene, which in the first step was merely a solvent, in the second step acted as the nucleophilic reagent of the Friedel-Craft acylation with 4-hydroxy-5-nitrobenzoyl chloride (not isolated). The large excess of toluene, together with the excess of $AlCl_3$ (2.20 eq), prevented side reactions such as the esterification between acyl chloride and phenolic hydroxyl group. In this context, in fact, 1 eq of $AlCl_3$ interacts with phenolic OH annihilating its reactivity. By-products such as the substitution at the less reactive ortho positions of toluene itself were not detected. By-products from $AlCl_3$, coming from unreacted and OH-protecting $AlCl_3$ upon acidic quenching, were easily filtered off and the resulting aqueous phase was re-extracted in toluene. Compound **65** was then subjected to basic extraction (30% NH_3) and subsequent acidic precipitation (1N HCl) and eventually purified by recrystallization from hot DCM at -4°C. Warming the solution at rt, before cooling it down to -4°C and using DCM enough to cover the bottom of the vial, very big rhombic crystals (range 0.5-1 cm) were obtained. Compound **65** was characterized by XRD, NMR, ESI-MS, elemental analysis and melting point. The achievement of target molecule was immediately confirmed through ^{1}H-NMR by the absence of signal related to free carboxylic OH and the presence of protons of toluene attached to nitrobenzene ring via carbonyl bond (respectively 7.70, 7.36 and 2.48 ppm) and through ^{13}C-NMR by the presence at 193.0 ppm the signal related to ketone group.

4.3.2 hTTR/3-deoxytolcapone and hTTR/3-O-methyltolcapone cocrystals

In collaboration with Prof. Michele Cianci of Department of Agricultural, Food and Environmental Sciences of Polytechnic University of Marche, hTTR cocrystals with 3-deoxytolcapone and 3-O-MethylTolcapone were obtained.

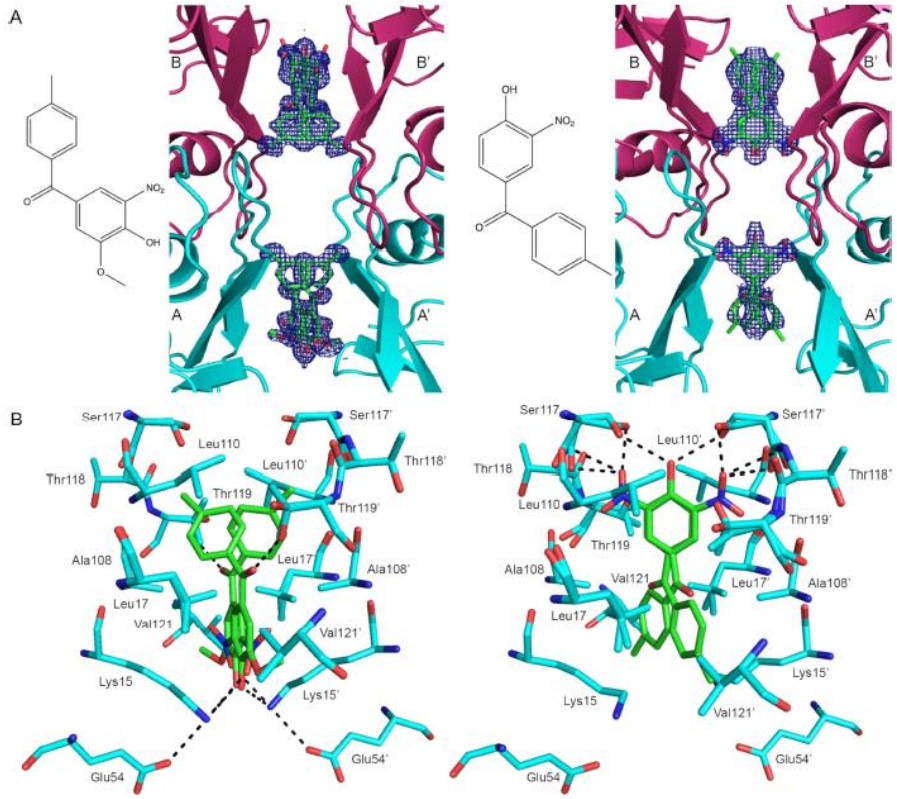

Figure 4.3.2.1: Crystal structure of the TTR-3-O-methyltolcapone (PDB code: 6SUH) and TTR-3-deoxytolcapone (PDB code: 6SUG) complexes. **A**) OMIT (Fo-Fc) electron density maps (blue), countered at 2.5 σ, of tolcapone analogues (left: 3-O-methyltolcapone; right: 3-deoxytolcapone) bound in the two cavities of the TTR tetramer. **B**) Detailed view of ligand interactions within the T4 binding cavity through residues present in HBP1 (Lys15, stabilized through the interaction with Glu54, and Thr106), HBP2 (Leu110, Leu17, Lys15), and HBP3 (Ser117, Leu110, Ala108, Thr118, and Thr119). The interacting residues are represented as sticks and reported only for the binding pocket AA'.

By X-ray analysis of hTTR cocrystal in complex with 3-O-methyltolcapone, determined at 1.26 Å resolution, the binding mode of 3-O-methyltolcapone was found to be the so-called 'direct binding mode', which is characterized by the position of the polar moiety of the 3-methoxy-4-hydroxy-5-nitrophenyl ring in the outermost part of the binding cavity (**Figure 4.3.2.1A**). The electron densities for both the 3-methoxy-4- hydroxy-5-nitrophenyl ring and the innermost apolar 4-methylphenyl ring are well defined. The overall electron density map is virtually identical to that of the TTR-tolcapone complex (PDB code: 4D7B 11). The r.m.s.d. between equivalent Cα atoms in the monomer of TTR in complex with 3-O-methyltolcapone and tolcapone is 0.484 Å and the two binding cavities are equally occupied (0.48/0.50). The 4-methyl-phenyl ring of 3-Omethyltolcapone is positioned near the inner hydrophobic binding sites HBP2 and HBP3, deeply into the TTR binding cavity, sitting between Leu110 and Thr119. The central carbonyl group of 3-O-methyltolcapone forms with the OH group of Thr119 at 2.67 Å away a relevant H-bond which is also established by tolcapone within a distance of 2.69 Å. 11 The 3-methoxy-4-hydroxy-5-nitrophenyl ring is also held in place by hydrophobic interactions with Leu17/Leu17', Ala108/Ala108', and Val121/Val121', in analogy with the TTR-tolcapone

complex. Moreover, the 3-methoxy group also participates in hydrophobic interactions, namely with Leu17, Val121' and Thr106'. The latter hydrophobic interactions at the dimer-dimer interface can thus enforce the dimer-dimer interactions that stabilize the TTR tetramer. At variance with the hydrophobic interactions established by the 3-methoxy group, in the TTR-tolcapone complex the 3-hydroxyl group can contribute to the stabilization of the TTR tetramer via polar interactions. The ε-amino group of Lys15' is sandwiched between the 4-hydroxy and 5-nitro groups of 3-O-methyltolcapone within H-bond distance (2.67 Å and 3.01 Å, respectively), and Glu54' at 3.00 Å away, in a fashion similar to that described for the TTR-tolcapone complex. However, in the case of the TTR-tolcapone complex Lys15 is sandwiched between the two hydroxyl groups of the 3-hydroxy 4-hydroxy-5-nitrophenyl ring, at distances of 2.97 Å, 2.55 Å, and the carboxyl group of Glu54 at 2.87 Å (**Figure 4.3.2.1B**). The presence of the 2-fold axis along the binding pocket creates two symmetrical binding modes of the ligand, related by a 180° rotation. This situation probably causes the presence of several alternate conformations of the residues in the proximity of 3-O-Methyltolcapone, namely Leu17, Thr19, Ser17, Ser 117, and Thr119, in analogy with previous observations reported for the TTR-tolcapone complex. Finally, a similar interaction pattern between TTR-bound 3-O-methyltolcapone and tolcapone is also confirmed by the presence of a well-conserved network of water molecules, mainly localized at the top and bottom gates of the binding cavity, which are sealed by the presence of Lys15/Glu54 and Ser117 residues, respectively.

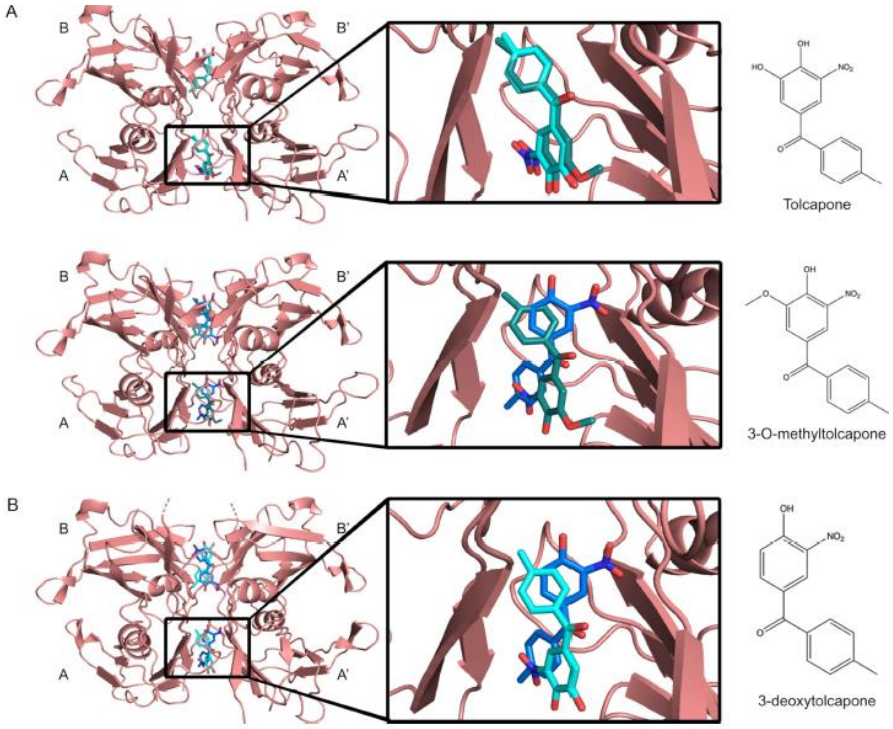

Figure 4.3.2.2: Close-up views of the superimposition of: **A**) TTR-3-O-methyltolcapone (dark green) with TTR-tolcapone (cyan) and TTR-3-deoxytolcapone (azure) complexes; **B**) TTR-3-deoxytolcapone with TTR-tolcapone complexes. The figure shows the displacement of the TTR-bound 3-deoxytolcapone relative to bound tolcapone and 3-O-methyltolcapone, and the rotation of the innermost phenyl ring, allowing the interaction of the ligand 3-hydroxyl group with the Ser117/Ser117' hydroxyl group.

Unexpectedly, the lack of the hydroxyl group at position 3 in the polar aryl ring causes a drastic change in the mode of binding of 3-deoxytolcapone. In fact, the structure of TTR /3-deoxytolcapone complex, determined at 1.21 Å resolution, reveals a 'reverse binding mode' of the ligand (**Figure 4.3.2.2A**), with the 4-hydroxy-5-nitrophenyl ring innermost. Nevertheless, the structure of protein moiety is not significantly affected by the change of bound ligand (r.m.s.d.: TTR-3-deoxytolcapone/TTR-3-O-methyltolcapone 0.079 Å; TTR-3-deoxy-tolcapone/TTR-tolcapone 0.503 Å). The electron densities for both the 4-hydroxy-5-nitrophenyl ring and the outermost apolar 4-methyl-phenyl ring are also well defined. 3-deoxytolcapone is bound to the two cavities of the TTR tetramer with nearly the same occupancy (0.47/0.50). The 4-hydroxyl group is within H-bond distance from Ser117 and Ser117' (2.89 Å for both residues), while the nitro group is tethered by H-bonds with the OH group of Ser117 at 2.25 Å and with the carbonyl and amide groups of the Thr118-Ser117 peptide bond at 2.89 Å and 3.17 Å, respectively. The 4-methyl-phenyl ring of 3-deoxytolcapone sits in the outer hydrophobic binding site HBP1, sandwiched between the aliphatic moieties of the side chains of Lys15/Lys15'and Thr106, and the side chains of Ala108/Ala108'and Val121. Several residues, namely Leu17, Thr19, Ser17, Ser117, Ser115, which are in the proximity of 3-deoxy-tolcapone, present alternate conformations. Differently from TTR-bound tolcapone and 3-O-methyltolcapone, the central carbonyl group of 3-deoxyltolcapone barely interacts with the OH group of Thr119 (**Figure 4.3.2.2B**). In fact, the estimated bond length of a hypothetical H-bond would be 4.22 Å. This behaviour is justified by the 'reverse binding mode', which induces a rotation of 33° and 29° for 3-deoxytolcapone as compared to tolcapone and 3-O-methyltolcapone, respectively, pulling the ligand further from the OH group on Thr119 (**Figure 4.3.2.2**). Moreover, the lack of the hydroxyl substituent in 3-deoxytolcapone allows for a slightly deeper penetration of the ligand of 5 1.42 Å, as compared to 3-O methyltolcapone, induced by the reduced steric hindrance and the different ligand binding orientation.

4.3.3 Attempts for the synthesis of 7-Cl Biochanin A derivative

For the synthesis of 7-Cl-7-deoxybiochanin A, we used as starting point a Nilsson's work in which it is showed a one-pot chlorination of 7-OH onto luteolin, a flavonoid regioisomer of biochanin A[86]. In this article, luteolin, an analogue of Biochanin A employed as nanomolar stabilizer of tetrameric TTR, was subjected to replacement of 7-OH with Cl and OMe groups in order to increase the binding affinities and overcome issues related to hepatic inactivation by glucuronidation on respective OH. Since Biochanin A is a regioisomer of luteolin and then theoretically the reactivity should be similar, we used the same chlorination protocol found in the article. Unfortunately, applying the same experimental conditions to Biochanin A, we were not able to get target molecule. On direct or inverse phase TLC just one non-running spot was observed. Neither ESI-MS analysis helped us in rationalizing the crude composition because of the high number of peaks, unfortunately not attributable to any kind of known fragmentation. Starting from this evidence, we tried to synthesize the target molecule varying the experimental parameters (e.g. time, inert gas, microwave potency, chlorinating agent), but unfortunately also in those cases the presence of the target molecule was not observed. Therefore a deeper literature research was carried out and what turned out, is that Biochanin A is easily subjected to degradation upon exposure of acid conditions.

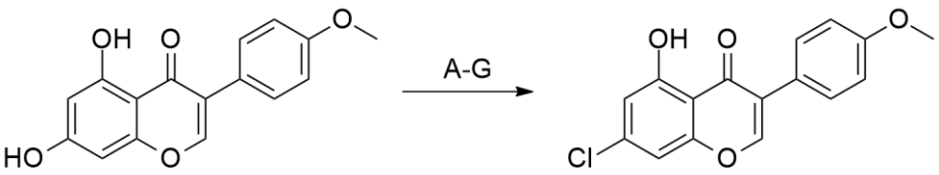

Biochanin A **7-Cl-Biochanin A**

	Experimental conditions	TLC
A	$POCl_3$ (3.3eq), 130°C, 200W, DMF dry (N_2), 5h	non-running spot
B	$POCl_3$ (3.3eq), 110°C, 100W, DMF dry (Ar), 1h	non-running spot
C	$POCl_3$, 80°C, DMF dry (Ar), overnight, round bottom flask	Biochanin A
D	$POCl_3$ (eq>100), 130°C, 150W, 4h	non-running spot
E	PCl_5, 160°C, 4h, fusione	Biochanin A + non-running spot
F	$POCl_3$ (eq>100), 130°C, 150W, 4h	non-running spot
G	$POCl_3$ (10 eq), pyridine (10 eq), 110°C, schlenk, 2h	4 spots

Figure 4.3.3.1: 7-Cl-BiochaninA one-pot reaction scheme and relative experimental conditions.

Considering the impossibility to synthesize 7-Cl-Biochanin A via Nilsson's protocol and the high number of peaks observed in ESI-MS trace, we thought that $POCl_3/PCl_5$ used for chlorination could be responsible for the acidic conditions causing the degradation. For these reasons, we decided to repeat the reaction at 110°C for 2h in a schlenk reactor with $POCl_3$ and pyridine, used as a sort of basic buffer to limit the possible acidic degradation. Even if in this case, differently from the other attempts, more than one spot was observed, chloro derivatives were observed neither by ESI-MS or by ^{1}H-NMR. Probably this very fragile scaffold makes unsuitable the post-synthesis functionalization strategy, so in future will be used the classical ex-novo synthesis strategy, which, starting from a suitable chlorinated building block, will allow to synthesize the modified molecule in more controlled and safer way by-passing acid-lability of Biochanin A itself.

4.3.4 Synthesis of 7-O-sulphate Biochanin A derivatives

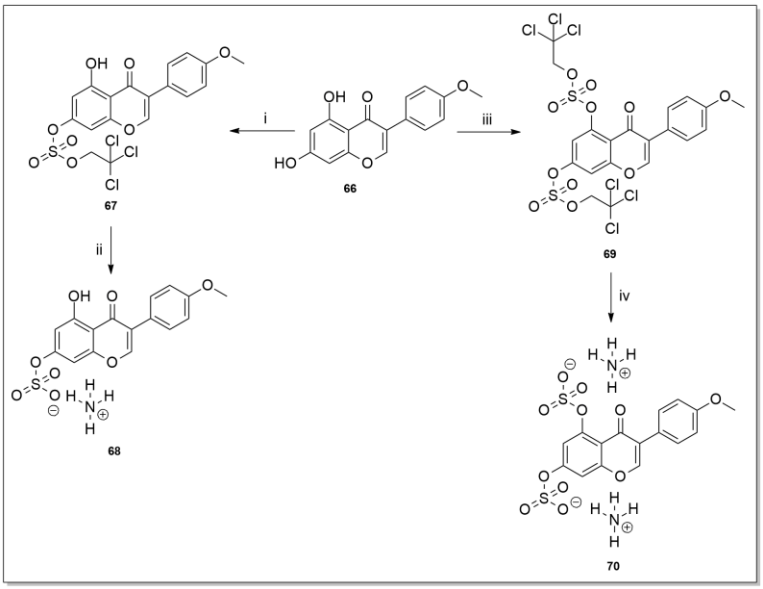

Figure 4.3.4.1: Synthesis of sulphated BiochaninA derivatives. Reactions conditions: i) NEt_3 (1.2 eq), DMAP (0.5 eq), 2,2,2-trichloroethyl sulphochloridate (1.2 eq), DCM, -10°C to rt, 5h (73% yield); ii) 10% Pd/C (catalytic amount), $HCOONH_4$ (6.0 eq), dry THF/dry MeOH, rt, 5 h (99% yield); iii) DMAP (2.0 eq), NEt_3 (7.8 eq), 2,2,2-trichloroethyl sulphochloridate (7.8 eq), dry THF, rt, 1 h (72% yield); iv) 10% Pd/C (catalytic amount), $HCOONH_4$ (12.1 eq), dry THF/dry MeOH, rt, 5 h (12% yield).

To obtain 7-sulfate Biochanin A **68**, it was taken inspiration by Mikula's work[87] on sulfation of β-resorcylic acid ester derivatives (**Figure 4.3.4.2**).

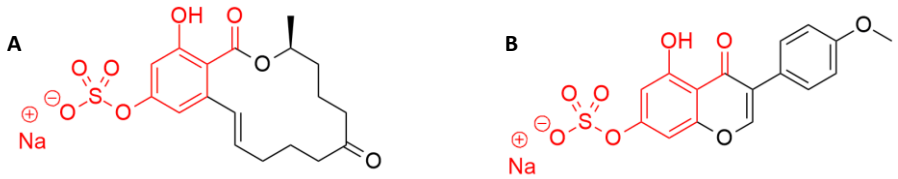

Figure 4.3.4.2: In **A** is represented the chemical structure of one of Mikula's derivatives synthesized. In red is highlighted the Biochanin A corresponding part (**B**), which makes Mikula's derivative a good model for Biochanin A scaffold.

As it can be seen in **Figure 4.3.4.2**, the β-resorcylic acid ester part of these molecules is a very reliable model of phenolic part of Biochanin A, since OHs and C=O are in the same geometry preserving, furthermore, the possibility of hydrogen bond between 5-OH and C=O. Considering the high similarity in structure with Biochanin A, which should guarantee an analogous reactivity, and the desired 7-O-sulfation the same sulfation protocol was employed for Biochanin A modification. Even if 5-OH is involved in a hydrogen bond with C=O and hence less reactive, to control monosubstitution on compound **66**, we decided to lower the temperature at -10°C with a $HOCH_2CH_2OH/N_2$(l) bath (kinetic control) and work in light excess (1.2 eq) of 2,2,2-trichloroethyl chlorosulphate TCE (stoichiometric control). The reaction was quenched in

acidic water and upon lyophilization, the crude was purified by semipreparative TLC with AcOEt/Hex 4:6 isolating the product in good yield (73%). The positive outcome of reaction was assessed by ^{1}H-NMR, having observed in the spectrum the presence of a singlet at 4.91 ppm for the two protons related to C*H*$_2$Cl$_3$ and the singlet at 13.01 ppm of 5-OH, which confirmed that the monosubstitution occurred. To confirm the nature of peak at 13.01 ppm, it was acquired the same spectrum adding 10 μl of pure MeOD into a $CDCl_3$ (500 μl) solution of compound **67**. As it can be seen in **Figure 4.3.4.3**, adding small aliquots of polar protic solvent, the peak at 13.01 ppm broadens and shifts to high fields, which is consistent with 5-OH proton involved in hydrogen bond with C=O.

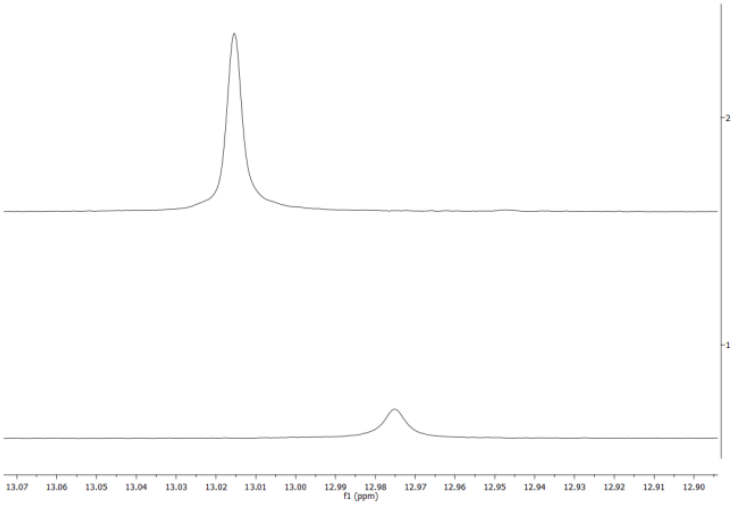

Figure 4.3.4.3: 1H-NMR spectra (25°C, 400MHz) of compound **67** in different solvents: **1**) solvent: MeOD/$CDCl_3$ 1:50; **2**) solvent: $CDCl_3$.

Moreover, as well, it was acquired a selective NOESY in $CDCl_3$ (d8=0.4, NS=64) irradiating the sample at 4.91 ppm in order to make resonate just C*H*$_2$Cl$_3$ protons. The resulting spectrum (**Figure 4.3.4.4**) shows that nuclear magnetization is transferred only to H_6 (7.01 ppm) and H_8 (6.84 ppm), which corresponds to aromatic ortho protons to 7-O-TCE. If the substitution was occurred in 5-OH, the nuclear magnetization would have been transferred to at most at H_6 and not to H_8, so this represents another evidence of the correct regioselectivity of the reaction.

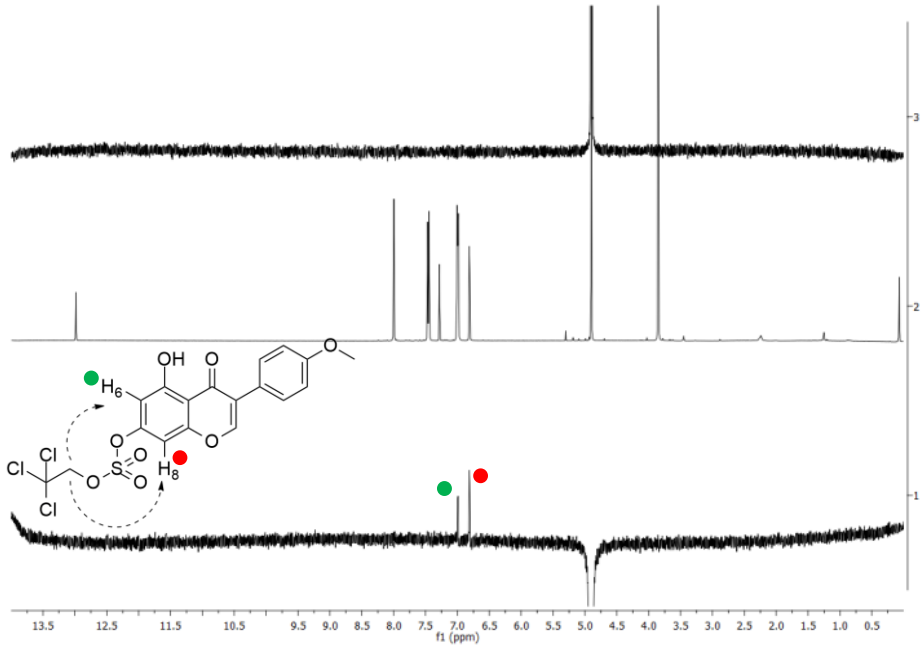

Figure 4.3.4.4: Selective ^{1}H-^{1}H NOESY (400MHz, 25 °C, $CDCl_3$) of compound **67**: **1**) final selective ^{1}H-^{1}H NOESY experiment after magnetization transfer; **2**) starting ^{1}H-NMR spectrum of compound **67**; **3**) selective pulse profile for selective ^{1}H-^{1}H NOESY experiment.

Compound **68** was obtained by quantitative catalytic hydrogenation of compound **67** with Pd/C as catalyst and $HCOONH_4$ as hydrogen source and, after filtration, it was simply recrystallized by EtOH. The obtaining of the target molecule was confirmed by the absence in the acquired ^{1}H-NMR spectrum in … of the singlet relative to CH_2Cl_3 protons and in ESI-MS by peak at 363.12 m/z related to (**68**-NH_4^+)$^-$. For the synthesis of disulfated derivative the procedure is similar to that used for monosulfated derivative. Differently from compound **67**, for the synthesis of compound **69** the reaction was carried out at room temperature for 1h and an excess of NEt_3 was employed. The presence of the two singlets at 5.21 ppm and 4.94 ppm, respectively for Cl_3CCH_2OSOC-7 and Cl_3CCH_2OSOC-5, were considered diagnostic for the target molecule. The deprotection of TCE groups to get compound **70** is analogous to synthesis protocol of compound **68**. In this very last case the yields are low (12%), but enough high to get sufficient amount to make biological assays.

4.3.5 Biological tests

As already said in **Paragraph 4.1.2**, when TTR is subjected to mutation, the tetrameric quaternary structure is destabilized and so the unfolding and the amyloid deposit formation is triggered. Since classical inhibitors usually stabilize the mutant TTR quaternary structure, the degree of oligomerization is a reliable index of stabilization efficiency and so, for this reason, separation techniques on molecular weight must be employed. One of the most famous is SDS-PAGE/Western-Blotting (or immunoblotting)[88], which consists in the immobilization on membrane and identification, with a specific antibody, of a specific antigene (or protein), present in a complex mixture of antigens (or proteins) upon a molecular weight-based

separation in polyacrylamide gel (alternatively dot blot or slot blot, not based on molecular weight separation, but just on antibody/antigene selectivity).

The method was created by George Stark at Standford University. The name comes ironically from “Southern blot”, technique for DNA detection previously invented by Edwin Southern. These techniques, along with Northern blot (for RNA detection), are very important and basilar techniques commonly used in biochemistry, immunogenetics and molecular biology.

The SDS-PAGE/Western-Blotting is made of four steps:

- Extraction and dosage of the proteins
- SDS-PAGE: protein separation by electrophoresis on polyacrylamide gel with sodium dodecylsulphate
- Western Blotting: transfer of proteins separated on gel onto a membrane, exposition of the membrane with antibody selective for the protein of interest (primary antibody), exposition of the membrane with labelled-antibody selective for primary antibody (secondary antibody), detection
- Densitometric analysis of pictures

The extraction step is composed of two phases: cellular lysis and protein isolation. The cellular lysis phase is essential to break biological membrane release macromolecules in buffer. Generally, upon appropriate preparation of tissues or cell culture by mechanical breaking with shaker (large volume), homogeneizator (small volume) or sonication, cytosolic proteins are collected as supernatant by centrifugation. To increase lysis and preserve the integrity of proteins by modification, degradation and unfolding, a buffer of salts, detergents and phosphatase and protease inhibitors is employed along with a working temperature of 4 °C, which limits side-reactions. If the target is a particular organelle protein, the supernatant is disposed and the pellet is treated with different biochemical and mechanical strategies using suitable cut-off filters. The protein supernatant is then quantified by spectrophotometric methods in order to determine the volume of protein solution to be used in the next analysis.

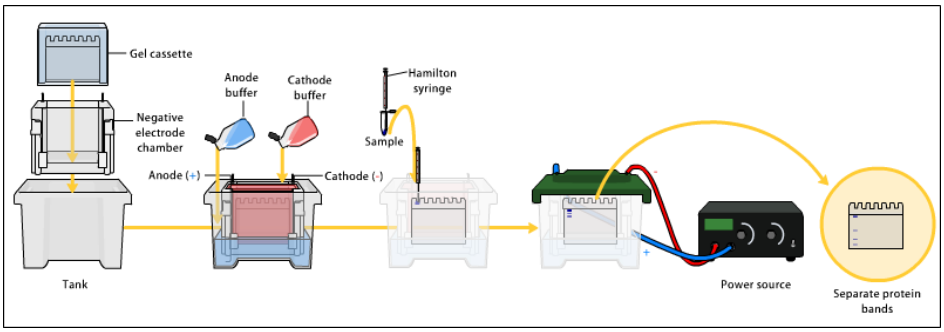

Figure 4.3.5.1: Schematic representation of an SDS-PAGE development

SDS-PAGE, because of its denaturing conditions, is the most favourite technique for protein purification just according to their molecular weight. In fact, here it is used sodium dodecyl sulphate, which coats proteins linearizing them. Since these aggregates are negatively-charged for sulphate groups, the actual protein charge is essentially shielded and so the separation can

be done just on molecular weight, where small proteins will run faster than the bigger ones. The electrophoretic run is done down to a polyacrylamide gel towards the positive anod inside a cassette prefilled with electrolytic buffer (generally TrisGly-pH 8.3). The gel is made in situ by polymerization of acrylamide and bis-acrylamide in Tris HCl buffer using APS (ammonium persulphate) as a cross-linking agent and TEMED (tetramethylenenediamine) as catalyst. Actually the generation of gel is made in a two-step process. In fact, first of all, a running gel is made taking the polymerization buffer at pH 8.8, which guarantees a type of gel with small pores appropriate for protein separation (the acrylamide percentage varies from 7.5% to 15% according to protein dimensions), meanwhile on the top of it is gelified a stacking gel with 4% acrylamide at pH 6.8, characterized by a very small cross-linking degree, appropriate for sample deposition. To facilitate the deposition, in sample buffer is added glycerol, which, being denser than buffer, drag the protein down to wells and prevents the mixing with the surrounding buffer. Beyond SDS, DTT and β-mercaptoethanol as denaturating agents, in sample buffer is present bromophenol blue, a negatively-charged dye, which, essentially behaving like the smallest protein in the sample, is used to track and monitor the electrophoretic run. Before loading into wells, lysate is heated up at 100 °C for 5 minutes into sample buffer to denaturate effectively the proteins to get them ready for electrophoresis. Once loaded the samples, proteins are firstly absorbed in stacking gel up to the interphase with running gel using low voltage (typically 60 V) and then it is raised up to 100V-200V to start the separation. The mass of protein bands can be easily compared with those coloured of first well ("protein ladder") which belongs generally to a standard of pre-stained proteins of known molecular weight. To enhance protein bands the gel is generally stained with different agents such as Coomassie blue or Zinc silver. This classical staining is employed generally when there is no problem of sensitivity and when the sample is not overcrowded, otherwise Western Blotting technique is required for satisfying results.

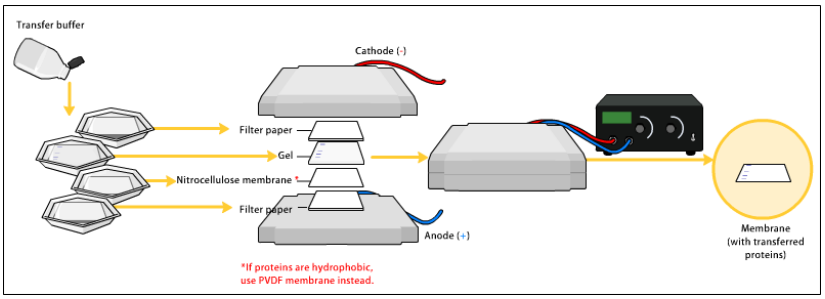

Figure 4.3.5.2: Schematic representation of Wester Blotting Transfer

Here, the gel is put in contact with an adsorbent membrane (Nitrocellulosa or Polivinilidenfluoruro), both of them enclosed between pairs of filter paper and sponges. The voltage polarity is negative to the gel and positive to the membrane. The power is switched on, the protein bands start to migrate to anod till they are captured by the membrane. This preliminary transfer is necessary to get proteins easily-accessible to next immunoassay. At the end of the blotting, since this membrane is sensible to all type of proteins, a blocking step with non-fat dry milk or purified BSA in Tris buffer is required to remove non-specific antibody background binding (0.5 - 5 ug/ml). Then the adsorbed proteins are rocked in a solution of antibody (primary antibody) specific to epitope present into protein of interest.

Upon repetitive washing with a mild detergent (TBST/PBST, tween 20 or triton x-100) in blocking solution, a further membrane wash is made with an antibody (secondary antibody) specific for the primary antibody used in the assay.

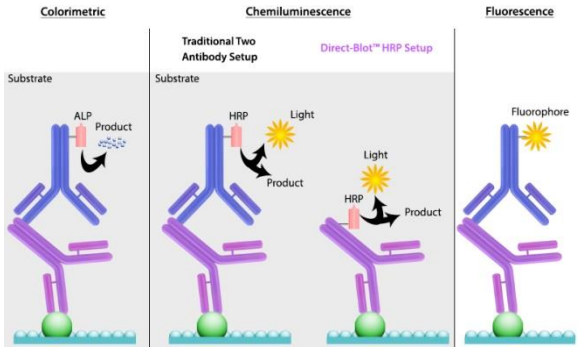

Figure 4.3.5.3: Examples of the most common types of immunorevelation.

This last antibody is generally labelled with different tags such as fluorophores, radioactive iodine atoms or reporter enzymes to get bands detected with UV/Vis light emission, X-ray emission or chemiluminescence (e.g horseradish peroxidases). In the case of UV-vis light, the detection is realized with CCD cameras, which capture the image of Western Blot, which in turn can be subjected to a densitometric analysis to assess the protein concentration for each band. In the common lab routine UVvis methods are preferred to X-ray methods since much safer.

In Berni's laboratory in the perspective of using 3-deoxytolcapone (**65**) as TTR stabilizer for ATTR pharmacological therapy, a Western Blotting method was optimized to qualitatively determine its affinity for TTR in plasma samples and at the same time give a proof of its stabilizing properties on the tetrameric TTR under partially denaturing conditions. In fact in order to replicate in plasma sample the high concentrations of monomer typical of FAP, plasmatic TTR was incubated with compound **65** in presence of 4M urea. These conditions provide the dissociation of the tetramer into monomers without affecting their folding, so the resulting monomer concentration was assumed representative of the fraction of denatured protein present in the sample. Operatively compound **65**, dissolved in DMSO, was incubated for 2h at 20°C in diluted plasma and then a volume of 8M urea was added in to get drug final concentrations of 15μM, 7.5μM, 4μM and 2μM. The mixture was finally left incubating for further 18 h at 20 °C. Upon SDS-PAGE and blotting, realized as described before, the immunodetection was realized with rabbit anti-human TTR polyclonal Ab (Dako) as primary Ab, and anti-rabbit Ab labelled with Dylight 680 (SERACARE) as secondary Ab, where the images were recorded using an Odyssey Image System (LI-COR).

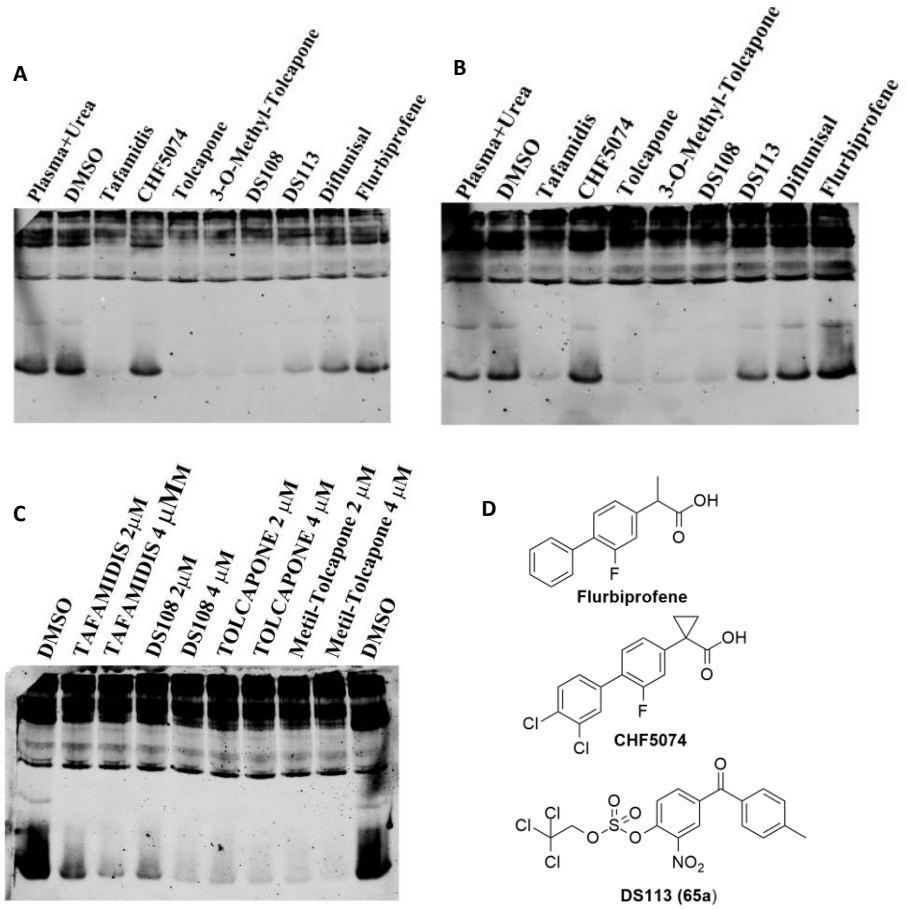

Figure 4.3.5.4. SDS-PAGE/Western Blotting of several drugs and potential inhibitors towards WT-TTR in plasma samples in denaturing conditions. In all SDS-PAGEs DMSO or PLASMA+UREA lanes were taken as negative controls, meanwhile Tafamidis and Tolcapone were taken as positive controls. DS108 corresponds to 3-deoxytolcapone **65**. Different concentrations of drugs were tested in the assay: 15μM (**A**), 7.5μM (**B**) and 2-4μM (**C**). In panel **D** molecular structures are illustrated of Flurbiprofene, CHF5074 and DS113, an intermediate for sulfation of 3-deoxytolcapone.

As it can be seen in **Figure 4.3.5.4**, all SDS-PAGE lanes are made of (from the bottom to the top): i) a first low band corresponding to the monomer, ii) an intermediate band, particularly evident upon treatment of TTR with DMSO and corresponding to the dimer and iii) a group of intense bands due to trimer, tetramer and other aggregates at higher MW of TTR. It is important to compare the monomer band in the different experiments, since its intensity represents a measurement of how much stabilizing is the molecule for the tetramer: the less intense, the better. As it can be seen by **Figure 4.3.5.4A**, compound **DS113** (precursor of sulphated 3-deoxytolcapone), diflunisal, flurbiprofene and CHF5074 are increasingly worse stabilizers (bands progressively more intense), while tafamidis, tolcapone, 3-O-methyl-tolcapone and compound **65** (**DS108**) showed to be very interesting stabilizers (bands faded), but at 15 μM concentration no difference among them is observed. Since neither at concentration of 7.5 μM our compound showed difference respect to tolcapone in stabilizing TTR tetramer (**Figure 4.3.5.4B**), we moved

to concentrations of 4 and 2 μM. Here (**Figure 4.3.5.4C**) discrimination is clearly seen in different band intensities. In fact, in plasma compound **65** (**DS108**) is clearly more selective to plasmatic WT-TTR than Tafamidis, which is the preferred drug used for the treatment of FAP nowadays. For this reason along with the fact that compound **65** includes deletion of the glucuronidation-affected OH, it represents a good alternative to Tafamidis. Unfortunately, compound **65** is less selective to WT-TTR than parent drugs tolcapone and methyltolcapone. Considering though that methyltolcapone is subjected to demethylation in hepatocytes being transformed in tolcapone (with all related problems inherent to hepatic overwork), our 3-deoxytolcapone is a promising tool for the treatment of FAP. In future this molecule will be studied in pharmacokinetic experiments in the hope to increase the half-life of the active substance circulating in blood.

In an analogous way to 3-deoxytolcapone, these BiochaninA derivatives were tested too in SDS-PAGE/Western Blotting. As it can be seen in **Figure 4.3.5.5**, compound **67** (DS114), **68** (DS120), **69** (DS121) and **70** (DS124) seem to be not selective to WT-TTR in serum samples.

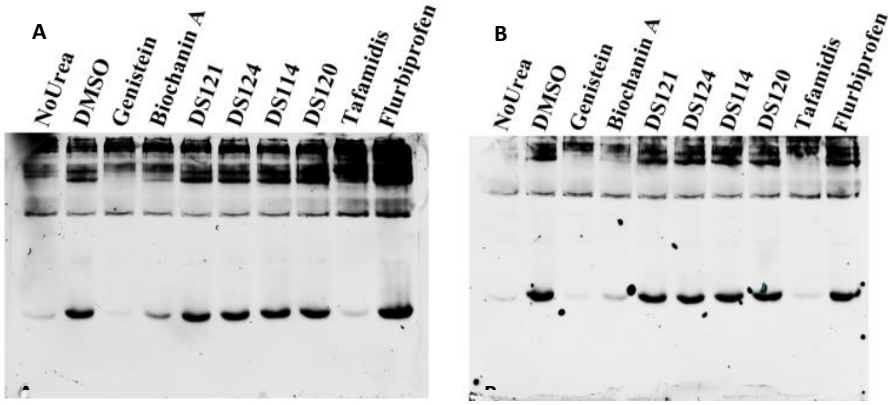

Figure 4.3.5.5: Western Blots of compound **67** (DS114), **68** (DS120), **69** (DS121) and **70** (DS124) with hTTR in plasma samples in denaturing conditions. Different drug concentrations were used in the assay: 7.5 μM (**A**) and 15 μM (**B**).

They, in fact, are characterized by a band corresponding to the monomer intense as much as for DMSO treatment, which is representative of actual monomeric TTR concentration observable in the disease. With this data, we cannot say anything about their affinities towards single TTR, but even if they were very efficient, they are totally useless for an actual therapy against amyloidogenic disease. Probably, the sulfate modification makes the molecule too bulky and non-electronically complementary to the active site.

In the whole discussion, we talked about selectivity and not affinity because the matrix is a complex mixture of several proteins. This means that these molecules in plasma can be either sequestrated or not by other targets so the bioavailability can be changed. In other words, Western Blot in plasma samples is representative of the effects of the molecules on the whole matrix without taking into account the single interaction.

4.4 Conclusions

Transthyretin TTR has been evidenced as one of the main etiological factors of amyloidogenic diseases. In fact, because of induced or spontaneous genetic mutations, it is expressed an unstable tetrameric TTR, which tends naturally to dissociate in monomers and unfold into the fibrils responsible of the diseases. In order to limit the initial dissociation of the tetrameric structure, a class of drugs called "kinetic stabilizers" has been developed to stabilize the tetrameric structure avoiding the formation of the harmful fibrils. Examples of these inhibitors are Tolcapone and the natural BiochainA, whose high efficiencies and specificities towards TTR have been largely studied in recent years. Despite their high potentialities as therapy in amyloidogenesis, they are rapidly glucuronidated in hepatocytes (in position 3 for tolcapone and in position 7 for BiochaninA) and excreted through biles via urine or via faeces. Due to the resulting hepatic overstimulation and the small concentration of drugs in bloodstream, the employment of these molecules in amyloidogenic therapy is definitely limited.

In order to improve the pharmacokinetic profile of Tolcapone and BiochaninA, in this project we synthetised analogues, in which phenolic OHs affected to glucuronidation were deleted or modified, in particular 3-deoxytolcapone and 7-O-sulphatebiochaninA. 3-deoxytolcapone was easily synthetised in good yield (55%) through a one-pot Friedel Craft acylation starting from 4-hydroxy-5-nitrobenzoic acid and toluene. The ease of synthesis along with the simple work-up procedures (acid-base extraction and recrystallization) makes this strategy very promising in possible future scale-up for pharmacokinetic studies. 7-O-sulphatebiochaninA, instead, was realized through the addition of 2,2,2-trichloroethyl sulphochloridate and subsequent catalytic hydrogenation in almost quantitative yields. In the optic to establish further stabilizing contacts with the protein, we proposed also the synthesis of 5,7-O-sulphatebiochaninA obtained by the introduction of a second sulphate group in position 7.

Western Blots obtained in collaboration with prof.Berni revealed that in plasmatic samples at a drug concentration of 2-4 μM 3-deoxytolcapone is more specific towards TTR than Diflunisal and Tafamidis, which are current drugs in the treatment of FAP disease. Moreover, it is can be seen in Western Blots that 3-deoxytolcapone is less specific than methyltolcapone, but is similar to tolcapone specificity. Considering, in addition, that methyltolcapone is more difficult to synthetise than tolcapone and in-vivo it is demethylated to tolcapone, 3-deoxytolcapone, being unaffected by glucuronidation, is an interesting alternative to common ATTR drugs. Contrarly to what observed with 3-deoxytolcapone, all sulphated biochaninA derivatives did not show stabilizing properties towards TTR in plasmatic samples. Considering that the assay is carried out in large excess of drug with respect to TTR, probably the bulk of these derivatives is too high preventing their entrance inside the channel.

Considering the good results obtained for 3-deoxytolcapone and the fact that 3-deoxytolcapone is smaller than BiochaninA derivatives, in future phenolic OH of 3-deoxytolcapone will be sulphated in the hope that in this case new stabilizing interaction will be established with TTR. Moreover, in particular with 3-deoxytolcapone, will be carried out Western Blot analysis towards mutant TTRs to determine if our compounds are still active towards these isoforms.

4.5 Experimental part

Synthesis

General information. All moisture-sensitive reactions were carried out under a nitrogen atmosphere. All dry solvents were prepared according to standard procedures and stored over 3 or 4 Å molecular sieves. All other reagents were commercial samples and used without further purification. TLC were performed using prepared plates of silica gel (Merck 60 F_{254} on aluminium) and revealed using UV light or staining reagents: $FeCl_3$ (1% in H_2O/MeOH 1:1), ninhydrin (5% in EtOH), basic solution of $KMnO_4$ (0.75% in H_2O). Flash chromatography was performed on 32-63 µm on 60 Å Merck silica gel. Melting points were determined on an electrothermal apparatus Gallenkamp, in capillaries sealed under nitrogen. ^{1}H NMR (300 or 400 MHz) and ^{13}C NMR spectra (75 or 100 MHz) were recorded on Bruker AV300 and AV400 spectrometers using partially deuterated solvents as internal standards. All ^{13}C NMR were performed with proton decoupling. Mass spectra were recorded in Electrospray Ionization (ESI) mode using a SQ Detector, Waters (capillary voltage = 2.40-3.50 kV, cone voltage = 40-100 V, extractor voltage = 2 V, source block temperature = 150 °C, desolvation temperature = 300 °C, cone gas (N_2) flow rates = 95 L/hr, desolvation gas (N_2) flow rates = 480 L/hr) in MeOH.

1-(4-hydroxy-5-nitrophenyl)-1-(4'-methylphenyl)methanone (65; 3-deoxy-tolcapone): 4-hydroxy-5-nitrobenzoic acid (5.46 mmol, 1.00 g) and dry DMF (1.31 mmol, 0.102 ml) were dissolved in dry toluene (15 ml) in a 2-necked round-bottom flask. Under magnetic stirring, $SOCl_2$ (10.10 mmol, 0.733 ml) was added to the yellow suspension and subsequently, using a condenser, heated up to 65 °C to get all the reactants more soluble in reaction solvent. After 4h the solution was quickly cooled down in an ice bath and then dry toluene (2 ml) and dry $AlCl_3$ (12.01 mmol, 1.60 g) were added in. The mixture was left reacting for 1 night at room temperature. The following morning the mixture showed up as a viscous brownish oil, which was analysed by TLC to assess total completion of the reaction (EtOAc/Hex 8:2). The oil was treated with 25 mN HCl (60 ml) leaving it stirring for 20 minutes. Once the oil was dissolved and the mixture turned orange, the suspension was filtered and the aqueous layer was extracted with toluene (2 x 50 ml). The organic layers were combined and basified with 30% NH_3 (5 ml). As the solution turned yellow, a solid precipitated which was filtered and suspended again in 1N HCl (20 ml). After 30 minutes, the solid was filtered and recrystallized at 0°C from hot DCM to give compound (?) as bright yellow crystals (0.78 g, 3.03 mmol, 55% yield). **^{1}H NMR** (300 MHz, $CDCl_3$) δ (ppm): 10.93 (s, 1H, O*H*), 8.59 (d, J = 2.0 Hz, 1H, H_6), 8.13 (dd, J = 8.7, 2.0 Hz, 1H, H_2), 7.70 (d, J = 8.1 Hz, 2H, H_2', H_6'), 7.34 (d, J = 8.1 Hz, 2H, H_3', H_5'), 7.32 (d, J = 8.7 Hz, 1H, H_3), 2.48 (s, 3H, C*H*$_3$). **^{13}C-NMR** (100 MHz, $CDCl_3$) δ (ppm): 193.0 (*C*=O), 157.8 (C_4), 143.9 (C_4'), 138.4 (C_2), 134.0 (C_5), 132.9 (C_1'), 130.3 (C_1), 130.0 (C_2', C_6'), 129.4 (C_3', C_5'), 127.7 (C_6), 120.3 (C_3), 21.7 (CH_3). **ESI-MS (-):** calc. for $C_{14}H_{11}NO_4$: 257.24; found m/z 256.07 [100%, $(M-H)^-$]. **Anal. CHNS:** calc. for $C_{14}H_{11}NO_4$: C (65.37%), H (4.31%), N (5.45%); found: C (64.99%), H (4.26%), N (5.32%). **Mp:** 124.8-125.2 °C.

2,2,2-trichloroethyl sulphochloridate: In 2-necked round-bottom flask, through a rubber sieve and syringes, dry Et_2O (100 ml), trichloroethanol (49.80 mmol, 4.800 ml) and pyridine (50.89 mmol, 4.100 ml) were stirred at -78°C with an AcOEt/N_2(l) bath. Once reached the temperature, sulfuryl chloride (49.49 mmol, 4.000 ml) was slowly dropped in over a period of 1 h. The

mixture was kept stirring for 3 h at room temperature and then it was filtered twice to remove completely the white side-product formed. The solution was purified by fractional distillation at reduced pressure (100°C, 18.5 mbar) to get target compound as transparent oil (quantitative yield).**^{1}H NMR** (300 MHz, $CDCl_3$) δ (ppm): 4.94 (s, 2H). **ESI-MS (+):** calc. for $C_2H_3Cl_4O_3S$: $[M+H]^+$: m/z 247.50, found m/z 247.99 (100%), calc. for $C_2H_2Cl_4O_3SNa$: $[M+Na]^+$: m/z 268.84, found m/z 268.10 (50%), calc. for $C_2H_2Cl_4O_3SK$: $[(M+K)^+]$: m/z 284.81, found m/z 284.17 (12%). Experimental procedure taken from reference[89].

1-(4-(2,2,2-trichloroethyl sulphate)-5-nitrophenyl)-1-(4'-methylphenyl)methanone (65a): In 2-necked round-bottom flask, 3-deoxy-tolcapone (0.12 mmol, 30.00 mg), 2,2,2-trichloroethyl sulphochloridate (0.14 mmol, 0.019 ml), DCM (1 ml), DMAP (58.35 umol, 7.13 mg) and NEt_3 (0.14 mmol, 0.016 ml) were stirred for 30 minutes at 0°C and then for 1 day at room temperature, monitoring the reaction by TLC (AcOEt/Hex 2:8, R_f=0.41). The reaction was quenched with 1N HCl (1 ml) and the solvent was then removed by reduced pressure. The crude was purified by semipreparative TLC (AcOEt) to get the target compound as a white powder (35.50 mg, 76.03 umol, 65% yield). **^{1}H NMR** (400 MHz, MeOD) δ (ppm): 8.46 (d, *J* = 2.0 Hz, 1H, H_6), 8.18 (dd, *J* = 8.5, 2.0 Hz, 1H, H_2), 7.91 (d, *J* = 8.5 Hz, 1H, H_3), 7.73 (d, *J* = 8.1 Hz, 2H, $H_{2'}$, $H_{6'}$), 7.39 (d, *J* = 8.1 Hz, 2H, $H_{3'}$, $H_{5'}$), 5.26 (s, 2H, C*H*$_2$), 2.47 (s, 3H, C*H*$_3$). **^{13}C NMR** (100 MHz, MeOD) δ (ppm): 192.6 (*C*=O), 144.7 (C_4), 143.7 ($C_{4'}$), 141.8 (C_2), 138.0 (C_5), 135.5 (C_1), 133.2 ($C_{1'}$), 130.0 ($C_{2'}$, $C_{6'}$), 129.2 ($C_{3'}$, $C_{5'}$), 127.2 (C_6), 124.0 (C_3), 92.3 (*C*Cl_3), 81.0 (*C*H_2), 20.3 (*C*H_3).

7-(2,2,2-trichloroethyl sulphate)-5-hydroxy-4'-methoxyisoflavone (67): A 2-necked round-bottom flask was firstly cooled down to -10°C with a $HOCH_2CH_2OH/N_2$(l) bath. Once reached the target temperature, 5,7-dihydroxy-4'-methoxyisoflavone (0.18 mmol, 50.00 mg), DCM (1 ml), NEt_3 (0.21 mmol, 29.40 ul), DMAP (87.95 umol, 10.75 mg) and 2,2,2-trichloroethyl sulphochloridate (0.21 mmol, 28.40 ul) were sequentially added in and stirred together for 5 h at room temperature, monitoring the reaction by TLC (AcOEt/Hex 1:1). The solvent was removed by reduced pressure and then the crude was suspended in acidic water (1 ml). The solvent was removed by lyophilization and the crude was purified by semipreparative TLC (Hex/AcOEt 6:4) to get compound **67** as a yellow powder (63.40 mg, 0.13 mmol, 73% yield). **^{1}H NMR** (400 MHz, $CDCl_3$) δ (ppm): 13.01 (s, 1H, 5-O*H*), 8.01 (s, 1H, H_2), 7.49 (d, *J* = 8.1 Hz, 2H, $H_{2'}$, $H_{6'}$), 7.02 (d, *J* = 8.1 Hz, 2H, $H_{3'}$, $H_{5'}$), 7.01 (d, *J* = 2.2 Hz, 1H, H_6), 6.84 (d, *J* = 2.2 Hz, 1H, H_8), 4.91 (s, 2H, CCl_3CH_2O), 3.88 (s, 3H, C*H*$_3$). **^{13}C NMR** (100 MHz, $CDCl_3$) δ (ppm): 181.3 (*C*=O), 163.1 (C_5), 160.2 ($C_{4'}$), 156.9 (C_8-*C*-O_1), 154.1 (C_7), 153.6 (C_2), 130.1 ($C_{2'}$, $C_{6'}$), 124.6 ($C_{1'}$), 122.0 (C_3), 114.3 ($C_{3'}$, $C_{5'}$), 110.6 (C_5-*C*-C_4), 104.4 (C_6), 100.1 (C_8), 92.1 (*C*Cl_3), 80.7 (CCl_3CH_2O), 55.4 (CH_3).

7-sulphate-5-hydroxy-4'-methoxyisoflavone ammonium (68): In a 2-necked round-bottom flask compound **67** (55.25 umol, 25.80 mg), 10% Pd/C (catalytic amount) and $HCOONH_4$ (0.33 mmol, 20.91 mg) were stirred in dry THF/dry MeOH (2 ml +2 ml) for 5 h at room temperature, monitoring the reaction by TLC (AcOEt/Hex 1:1, Rf=0.00). The suspension was centrifuged and the surnattant was dried at rotavapor. The crude was purified by recrystallization from hot EtOH to get compound **68** as a white powder (20.84 mg, 54.70 umol, 99% yield). **^{1}H NMR** (400 MHz, MeOD+D_2O) δ (ppm): 8.27 (s, 1H, H_2), 7.50 (d, *J* = 8.7 Hz, 2H, $H_{2'}$, $H_{6'}$), 7.08 (d, *J* = 8.7 Hz, 2H, $H_{3'}$, $H_{5'}$), 7.06 (d, *J* = 2.1 Hz, 1H, H_6), 6.77 (d, *J* = 2.1 Hz, 1H, H_8), 3.88 (s, 3H, C*H*$_3$). **^{13}C NMR** (100 MHz, MeOD+D_2O) δ (ppm): 181.6 (*C*=O), 161.1 (C_5), 159.6 ($C_{4'}$), 158.0 (C_8-*C*-O_1), 157.4 (C_7), 155.2 (C_2), 130.2 ($C_{2'}$, $C_{6'}$), 123.5 ($C_{1'}$), 122.9 (C_3), 114.0 ($C_{3'}$, $C_{5'}$), 108.1 (C_5-*C*-C_4), 103.5 (C_6), 99.5

(C_8), 55.0 (CH_3). ESI-MS (-): calc. for $C_{16}H_{11}O_8S$ [$(M\text{-}NH_4^+)^-$]: m/z 363.02; found m/z 363.12 (100%).

5,7-bis(2,2,2-trichloroethyl sulphate)-4'-methoxyisoflavone (69): In a 2-necked round-bottom flask, 5,7-dihydroxy-4'-methoxyisoflavone (0.18 mmol, 50.00 mg), DMAP (0.35 mmol, 42.99 mg), NEt_3 (1.41 mmol, 0.196 ml) and 2,2,2-trichloroethyl sulphochloridate (1.41 mmol, 0.189 ml) were added in sequentially and stirred in dry THF (1 ml) for 1 h at room temperature, monitoring the reaction by TLC (Hex/AcOEt 7:3). Under vigorous stirring, 0.5N HCl (1 ml) was added and subsequently the organic solvent was removed by reduced pressure. The yellow precipitate was filtered and purified by semipreparative TLC (AcOEt/petrol ether 2:8) to get compound **69** as a white powder (89.40 mg, 0.13 mmol, 72% yield). **^{1}H NMR** (400 MHz, $CDCl_3$) δ (ppm): 7.97 (s, 1H, H_2), 7.60 (d, *J* = 2.4 Hz, 1H, H_6), 7.54 (d, *J* = 2.4 Hz, 1H, H_8), 7.47 (d, *J* = 8.8 Hz, 2H, $H_{2'}$, $H_{6'}$), 7.00 (d, *J* = 8.8 Hz, 2H, $H_{3'}$, $H_{5'}$), 5.21 (s, 2H, Cl_3CCH_2OSOC-7), 4.94 (s, 2H, Cl_3CCH_2OSOC-5), 3.87 (s, 3H, CH_3). **^{13}C NMR** (100 MHz, $CDCl_3$) δ (ppm): 173.5 (*C*=O), 160.1 (C_5), 157.7 ($C_{4'}$), 151.7 (C_8-*C*-O_1), 151.6 (C_7), 148.7 (C_2), 130.3 ($C_{2'}$, $C_{6'}$), 126.9 ($C_{1'}$), 122.5 (C_3), 117.2 (C_5-*C*-C_4), 114.1 ($C_{3'}$, $C_{5'}$), 113.0 (C_6), 110.7 (C_8), 92.5 (7-$COSOCH_2CCl_3$), 91.9 (5-$COSOCH_2CCl_3$), 81.1 (7-$COSOCH_2CCl_3$), 81.0 (5-$COSOCH_2CCl_3$), 55.4 (CH_3).

5,7-disulphate-4'-methoxyisoflavone diammonium (70): In a 2-necked round-bottom flask compound **69** (35.52 umol, 25.00 mg), 10% Pd/C (catalytic amount) and $HCOONH_4$ (0.43 mmol, 26.88 mg) were stirred in dry THF/dry MeOH (2 ml +2 ml) for 5 h at room temperature, monitoring the reaction by TLC (AcOEt/Hex 3:7, Rf=0.00). The suspension was centrifuged and the surnattant was collected in a new round-bottom flask. The catalyst precipitated was washed with MeOH (2 ml), sonicated and centrifuged once again. The whole centrifuge procedure was reiterated once more. The solvent was removed by reduced pressure and the crude was purified by recrystallization from hot EtOH to get compound **70** as a white powder (2.00 mg, 4.18 umol, 12% yield). **^{1}H NMR** (300 MHz, MeOD) δ (ppm): 8.22 (s, 1H, H_2), 7.53 (d, *J* = 8.7 Hz, 2H, $H_{2'}$, $H_{6'}$), 7.02 (d, *J* = 8.7 Hz, 2H, $H_{3'}$, $H_{5'}$), 7.00 (d, *J* = 2.0 Hz, 1H, H_6), 6.74 (d, *J* = 2.0 Hz, 1H, H_8), 3.85 (s, 3H, CH_3). **^{13}C NMR** (100 MHz, MeOD) δ (ppm): 167.4 (*C*=O), 161.8 (7-*C*OS), 159.9 ($C_{4'}$), 158.7 (C_8-*C*-O_1), 157.3 (5-*C*OS), 154.4 (C_5), 130.00 ($C_{6'}$, $C_{2'}$), 123.6 ($C_{1'}$), 122.8 (C_3), 122.4 (C_5-*C*-C_4), 113.5 ($C_{3'}$, $C_{5'}$), 103.1 (C_6), 98.5 (C_8), 54.3 (CH_3).

Biological tests

General information and Western Blot. Recombinant wt human TTR was prepared and quantified essentially as described. 21. Tolcapone, 3-O-methyltolcapone and tafamidis were purchased from Carbosynth. TTR binding and stability assays in the presence of urea by TTR ligands were conducted for TTR present in human plasma by means of a Western Blot procedure carried out according to the protocol described by Nilsson et al.[90], with some modifications[91]. Aliquots of human plasma were diluted 16 folds in Na phosphate buffer (Na phosphate 40mM, NaCl 0.15M pH 7.4) and supplemented with increasing concentrations (4 and 8 μM) of each tested ligand (tolcapone, 3-O-methyltolcapone, 3-deoxy-tolcapone and tafamidis) dissolved in DMSO. One more plasma sample supplemented with DMSO was used as a negative control. After 2-hour incubation at 20° C, an equal volume of 8 M urea was added to each sample to obtain a final 4 M urea concentration (final ligand concentrations: 2 and 4 μM). The incubation was prolonged for 18 hours at 20° C, followed by nondenaturing SDS-PAGE,

using Tris-Glycine buffer containing 0.025% SDS in the running buffer and 0.2% SDS in the loading buffer. SDS at these concentrations does not denature TTR tetramers but does prevent re-association of monomers. The blotting step was accomplished by means of a Trans-Blot SD transfer apparatus (BIO-RAD), and the membrane after the blotting step was incubated overnight in blocking buffer containing 5% Skim Milk, at 25° C. Immunodetection of TTR monomers was performed by employing rabbit anti-human TTR polyclonal Ab (Dako) as primary Ab, and anti-rabbit Ab labeled with Dylight 680 (SERACARE) as secondary Ab. Western Blotting images were recorded by using an Odissey Image System (LI-COR). The employed rabbit anti-TTR antibody does not appear to specifically discriminate between the native fraction of tetrameric TTR distinct from other protein aggregates, and as a consequence only the change in TTR monomers, which reflects the level of tetrameric TTR dissociation, could be accurately monitored.

Cocrystallization

Crystals of wt human TTR in complex with 3-O-methyltolcapone and 3-deoxy- tolcapone were prepared by co-crystallization by using the hanging-drop vapor diffusion method essentially as described.[92] Human wt TTR (5 mg/ml) in 20 mM sodium phosphate, pH 7, was incubated with a 4-fold molar excess of each tolcapone derivative solubilized in DMSO. Drops (1.5 μl) were formed by mixing equal volumes of the solution containing the TTR ligand complexes and of the reservoir/precipitant solution (2.2M ammonium sulfate, 0.1M KCl, 30 mM sodium phosphate, pH 7.0). Single crystals were obtained in about one week of incubation at room temperature. Diffraction data were collected at 100 K using synchrotron radiation at the ID23-2 beamline of the ESRF storage ring, Grenoble (France). Data were processed using XDS[93] and AIMLESS[94]. The crystals of human TTR in complex with 3-O-methyltolcapone and 3-deoxytolcapone be longed to space group P21212, isomorphous with most previously determined crystal structures of human TTR, and diffracted to a resolution of 1.21 Å and 1.26 Å, respectively. The two structures were determined by rigid body refinement using REFMAC and, as a starting model, the crystal structure of TTR in complex with resveratrol-3-O-3-glucuronide (PDB ID: 5AKS)[92] devoid of solvent molecules and ligands, and randomized, to avoid any possible phase bias. Model building and water or ligand addition/inspection were manually conducted using COOT.[95] The structures were isotropically refined with REFMAC5[96], including the hydrogen atoms in the riding positions, and then, at the last round, anisotropically refined. Atomic coordinates of the ligand molecules and restraints were obtained through the Elbow software[97] within Phenix suite[98]. The ligand orientation was determined by inspecting the electron density map, calculated with (Fo-Fc) coefficients, and calculated with phases from the model, deprived of the ligand. The final Rfactor and Rfree values for TTR in complex with 3-O-methyltolcapone and 3-deoxytolcapone were 0.1589 and 0.1971, and 0.1515 and 0.1779 respectively. Models were checked with the PROCHECK[99] in the CCP4 suite[100]. Structure coordinates and structure factors were deposited in the Protein Data Bank with the accession codes 6SUH and 6SUG for the TTR-3-O-methyltolcapone and TTR-deoxy-tolcapone complexes, respectively.

4.6 References

1. Okuno, D., Iino, R. & Noji, H. Rotation and structure of FoF1-ATP synthase. *Journal of Biochemistry* **149**, 655–664 (2011).

2. Shirakihara, Y. ATP synthase. *Tanpakushitsu Kakusan Koso.* **44**, 538–545 (1999).

3. Hsia, C. C. W. Respiratory function of hemoglobin. *New England Journal of Medicine* **338**, 239–247 (1998).

4. Mihailescu, M. R. & Russu, I. M. A signature of the T → R transition in human hemoglobin. *Proc. Natl. Acad. Sci. U. S. A.* **98**, 3773–3777 (2001).

5. Perutz, M. F. *et al.* Structure of Hæmoglobin: A three-dimensional fourier synthesis at 5.5-. resolution, obtained by X-ray analysis. *Nature* **185**, 416–422 (1960).

6. Boyer, P. D. Molecular motors: What makes ATP synthase spin? *Nature* **402**, 247–249 (1999).

7. Fermi, G., Perutz, M. F., Shaanan, B. & Fourme, R. The crystal structure of human deoxyhaemoglobin at 1.74 A resolution. *J.Mol.Biol.* **175**, 159–174 (1984).

8. Amyloid Protein - an overview | ScienceDirect Topics. Available at: https://www.sciencedirect.com/topics/neuroscience/amyloid-protein. (Accessed: 6th November 2019)

9. Adams, D., Koike, H., Slama, M. & Coelho, T. Hereditary transthyretin amyloidosis: a model of medical progress for a fatal disease. *Nat. Rev. Neurol.* **15**, 387–404 (2019).

10. Chiti, F. & Dobson, C. Amyloid Formation, Protein Homeostasis, and Human Disease: A Summary of Progress Over the Last Decade. *Annu. Rev. Biochem.* **86**, 1–42 (2017).

11. Jin, M. *et al.* Soluble amyloid beta-protein dimers isolated from Alzheimer cortex directly induce Tau hyperphosphorylation and neuritic degeneration. *Proc. Natl. Acad. Sci. U. S. A.* **108**, 5819–24 (2011).

12. Knowles, T. P. J., Vendruscolo, M. & Dobson, C. M. The amyloid state and its association with protein misfolding diseases. *Nat. Rev. Mol. Cell Biol.* **15**, 384–96 (2014).

13. TTR transthyretin [Homo sapiens (human)] - Gene - NCBI. Available at: https://www.ncbi.nlm.nih.gov/gene/7276. (Accessed: 6th November 2019)

14. Braun, D. & Schweizer, U. Thyroid Hormone Transport and Transporters. *Vitam. Horm.* **106**, 19–44 (2018).

15. Richardson, S. J., Wijayagunaratne, R. C., D'Souza, D. G., Darras, V. M. & Van Herck, S. L. J. Transport of thyroid hormones via the choroid plexus into the brain: The roles of transthyretin and thyroid hormone transmembrane transporters. *Front. Neurosci.* **9**, 1–8 (2015).

16. Hennemann, G. *et al.* Plasma membrane transport of thyroid hormones and its role in thyroid hormone metabolism and bioavailability. *Endocrine Reviews* **22**, 451–476 (2001).

17. Stepien, B. K. & Huttner, W. B. Transport, metabolism, and function of thyroid hormones in the developing mammalian brain. *Front. Endocrinol. (Lausanne).* **10**, (2019).

18. Wojtczak, A., Cody, V., Luft, J. R. & Pangborn, W. Structures of human transthyretin complexed with thyroxine at 2.0 A resolution and 3',5'-dinitro-N-acetyl-L-thyronine at 2.2 A resolution. *Acta Crystallogr. D. Biol. Crystallogr.* **52**, 758–65 (1996).

19. Refetoff, S. *Thyroid Hormone Serum Transport Proteins*. *Endotext* (2000).

20. Zanotti, G. & Berni, R. Plasma retinol-binding protein: structure and interactions with retinol, retinoids, and transthyretin. *Vitam. Horm.* **69**, 271–95 (2004).

21. Power, D. M. *et al.* Evolution of the thyroid hormone-binding protein, transthyretin. *General and Comparative Endocrinology* (2000). doi:10.1006/gcen.2000.7520

22. Tomar, D. *et al.* Crystallographic Study of Novel Transthyretin Ligands Exhibiting Negative-Cooperativity between Two Thyroxine Binding Sites. *PLoS One* **7**, (2012).

23. Ferguson, R. N. & Edelhoch, H. Negative Cooperativity in the Binding of Thyroxine to Human Serum Prealbumin. *Biochemistry* **14**, 282–289 (1975).

24. Retinol Binding Protein 4 - an overview | ScienceDirect Topics. Available at: https://www.sciencedirect.com/topics/medicine-and-dentistry/retinol-binding-protein-4. (Accessed: 6th November 2019)

25. Kanai, M., Raz, A. & Goodman, D. S. Retinol-binding protein: the transport protein for vitamin A in human plasma. *J. Clin. Invest.* **47**, 2025–44 (1968).

26. Poodproh, R., Kaewmeechai, S., Leelawatwattana, L. & Prapunpoj, P. Increasing the length and hydrophobicity of the C-terminal sequence of transthyretin strengthens its binding affinity to retinol binding protein. *FEBS Open Bio* **7**, 1891–1898 (2017).

27. Newcomer, M. E. *et al.* The three-dimensional structure of retinol-binding protein. *EMBO J.* **3**, 1451–1454 (1984).

28. Naylor, H. M. & Newcomer, M. E. The structure of human retinol-binding protein (RBP) with its carrier protein transthyretin reveals an interaction with the carboxy terminus of RBP. *Biochemistry* **38**, 2647–2653 (1999).

29. Rask, L., Vahlquist, A. & Peterson, P. A. Studies on two physiological forms of the human retinol-binding protein differing in vitamin A and arginine content. *J. Biol. Chem.* **246**, 6638–46 (1971).

30. Westermark, P., Sletten, K., Johansson, B. & Cornwell, G. G. Fibril in senile systemic amyloidosis is derived from normal transthyretin. *Proc. Natl. Acad. Sci. U. S. A.* **87**, 2843–2845 (1990).

31. Zeldenrust, S. R. & Benson, M. D. Familial and Senile Amyloidosis Caused by Transthyretin. in *Protein Misfolding Diseases: Current and Emerging Principles and Therapies* 795–815 (John Wiley and Sons, 2010). doi:10.1002/9780470572702.ch36

32. Ando, Y. & Suhr, O. B. Autonomic dysfunction in familial amyloidotic polyneuropathy (FAP). *Amyloid* **5**, 288–300 (1998).

33. Coelho, T. Familial amyloid polyneuropathy: New developments in genetics and treatment. *Current Opinion in Neurology* **9**, 355–359 (1996).

34. João, M. & Saraiva, M. Transthyretin mutations in health and disease. *Hum. Mutat.* **5**, 191–196 (1995).

35. Jacobson, D. R. *et al.* Variant-sequence transthyretin (isoleucine 122) in late-onset cardiac amyloidosis in black americans. *N. Engl. J. Med.* **336**, 466–473 (1997).

36. Gertz, M. A. Hereditary ATTR amyloidosis: burden of illness and diagnostic challenges. *The American journal of managed care* **23**, S107–S112 (2017).

37. Kim, J. H., Oroz, J. & Zweckstetter, M. Structure of Monomeric Transthyretin Carrying the Clinically Important T119M Mutation. *Angew. Chemie - Int. Ed.* **55**, 16168–16171 (2016).

38. Monaco, H. L. The transthyretin-retinol-binding protein complex. *Recent Adv. Transthyretin Evol. Struct. Biol. Funct.* **1482**, 123–142 (2009).

39. Yee, A. W. *et al.* A molecular mechanism for transthyretin amyloidogenesis. *Nat. Commun.* **10**, 1–10 (2019).

40. Human Transthyretin. Available at: http://chemistry.berea.edu/~biochemistry/2008/db_td_kk/.

41. Hanna, M. Novel drugs targeting transthyretin amyloidosis. *Curr. Heart Fail. Rep.* **11**, 50–57 (2014).

42. Mangione, P. P. *et al.* Proteolytic cleavage of Ser52Pro variant transthyretin triggers its amyloid fibrillogenesis. *Proc. Natl. Acad. Sci. U. S. A.* **111**, 1539–1544 (2014).

43. Thylén, C. *et al.* Modifications of transthyretin in amyloid fibrils: analysis of amyloid from homozygous and heterozygous individuals with the Met30 mutation. *EMBO J.* **12**, 743–748 (1993).

44. Amyloid Neuropathy - an overview | ScienceDirect Topics. Available at: https://www.sciencedirect.com/topics/medicine-and-dentistry/amyloid-neuropathy. (Accessed: 6th November 2019)

45. Kapoor, M., Rossor, A. M., Jaunmuktane, Z., Lunn, M. P. T. & Reilly, M. M. Diagnosis of amyloid neuropathy. *Pract. Neurol.* **19**, 250–258 (2019).

46. Andrade, C. A peculiar form of peripheral neuropathy: Familiar atypical generalized amyloidosis with special involvement of the peripheral nerves. *Brain* **75**, 408–427 (1952).

47. Amyloidogenic transthyretin amyloidosis - Conditions - GTR - NCBI. Available at: https://www.ncbi.nlm.nih.gov/gtr/conditions/C2751492/. (Accessed: 6th November 2019)

48. Carvalho, A., Rocha, A. & Lobato, L. Liver transplantation in transthyretin amyloidosis: Issues and challenges. *Liver Transplantation* **21**, 282–292 (2015).

49. Suhr, O. B., Herlenius, G., Friman, S. & Ericzon, B. G. Liver transplantation for hereditary transthyretin amyloidosis. *Liver Transplantation* **6**, 263–276 (2000).

50. Kay, J., Menachem, J., O'Quinn, R. & Drachman, B. Progressive Cardiomyopathy in TTR

Amyloidosis after Liver Transplant. *J. Card. Fail.* **24**, S81 (2018).

51. Butler, J. S. *et al.* Preclinical evaluation of RNAi as a treatment for transthyretin-mediated amyloidosis. *Amyloid* **23**, 109–118 (2016).

52. Niemietz, C., Chandhok, G. & Schmidt, H. Therapeutic oligonucleotides targeting liver disease: TTR amyloidosis. *Molecules* **20**, 17944–17975 (2015).

53. Alhamadsheh, M. M. *et al.* Familial cardiac amyloidosis: Potent kinetic stabilizers that prevent transthyretin-mediated cardiomyocyte proteotoxicity. *Sci. Transl. Med.* **3**, (2011).

54. Adams, D. *et al.* TTR kinetic stabilizers and TTR gene silencing: a new era in therapy for familial amyloidotic polyneuropathies. *Expert Opin. Pharmacother.* **17**, 791–802 (2016).

55. Richards, D. B. *et al.* Therapeutic clearance of amyloid by antibodies to serum amyloid P component. *N. Engl. J. Med.* **373**, 1106–1114 (2015).

56. Richards, D. B. *et al.* Repeat doses of antibody to serum amyloid P component clear amyloid deposits in patients with systemic amyloidosis. *Sci. Transl. Med.* **10**, (2018).

57. A Study to Evaluate the Safety of GSK2398852 When Co-administered With GSK2315698 in Patients With Systemic Amyloidosis - Full Text View - ClinicalTrials.gov. Available at: https://www.clinicaltrials.gov/ct2/show/NCT01777243. (Accessed: 6th November 2019)

58. [Frontiers in Bioscience, 4, d782-786, November 1, 1999] ANTISENSE PROPERTIES OF PEPTIDE NUCLEIC ACIDS Ursel Soomets, Mattias Hällbrink and Ülo Langel. *Science (80-.).* 14–17 (1999).

59. Tan, F. L. & Yin, J. Q. RNAi, a new therapeutic strategy against viral infection. *Cell Research* **14**, 460–466 (2004).

60. Gene silencing by siRNAs and antisense oligonucleotides in the laboratory and the clinic. Available at: https://www.ncbi.nlm.nih.gov/pmc/articles/PMC3916955/. (Accessed: 6th November 2019)

61. Watts, J. K. & Corey, D. R. Silencing disease genes in the laboratory and the clinic. *Journal of Pathology* **226**, 365–379 (2012).

62. Mathew, V. & Wang, A. K. Inotersen: New promise for the treatment of hereditary transthyretin amyloidosis. *Drug Design, Development and Therapy* **13**, 1515–1525 (2019).

63. Kristen, A. V. *et al.* Patisiran, an RNAi therapeutic for the treatment of hereditary transthyretin-mediated amyloidosis. *Neurodegener. Dis. Manag.* **9**, 5–23 (2019).

64. Pinto, M. V. *et al.* Kind and distribution of cutaneous sensation loss in hereditary transthyretin amyloidosis with polyneuropathy. *J. Neurol. Sci.* **394**, 78–83 (2018).

65. Waddington-Cruz, M. *et al.* Hereditary transthyretin amyloidosis: baseline characteristics of patients in the NEURO-TTR trial. *Amyloid* **25**, 180–188 (2018).

66. Efficacy and Safety of Inotersen in Familial Amyloid Polyneuropathy - Full Text View -

ClinicalTrials.gov. Available at: https://clinicaltrials.gov/ct2/show/NCT01737398. (Accessed: 6th November 2019)

67. Alexander, K. M., Singh, A. & Falk, R. H. Novel pharmacotherapies for cardiac amyloidosis. *Pharmacol. Ther.* **180**, 129–138 (2017).

68. Sperry, B. W. & Tang, W. H. W. Amyloid heart disease: Genetics translated into disease-modifying therapy. *Heart* **103**, 812–817 (2017).

69. Dana, H. *et al.* Molecular Mechanisms and Biological Functions of siRNA. *Int. J. Biomed. Sci.* **13**, 48–57 (2017).

70. Adamski-Werner, S. L., Palaninathan, S. K., Sacchettini, J. C. & Kelly, J. W. Diflunisal Analogues Stabilize the Native State of Transthyretin. Potent Inhibition of Amyloidogenesis. *J. Med. Chem.* **47**, 355–374 (2004).

71. Sekijima, Y., Dendle, M. A. & Kelly, J. W. Orally administered diflunisal stabilizes transthyretin against dissociation required for amyloidogenesis. *Amyloid* **13**, 236–249 (2006).

72. Bulawa, C. E. *et al.* Tafamidis, a potent and selective transthyretin kinetic stabilizer that inhibits the amyloid cascade. *Proc. Natl. Acad. Sci. U. S. A.* **109**, 9629–9634 (2012).

73. Sant'Anna, R. *et al.* Repositioning tolcapone as a potent inhibitor of transthyretin amyloidogenesis and associated cellular toxicity. *Nat. Commun.* **7**, (2016).

74. Rybin, D. V. *et al.* Repurposing Diflunisal for Familial Amyloid Polyneuropathy. *Jama* **310**, 2658 (2015).

75. Castaño, A., Helmke, S., Alvarez, J., Delisle, S. & Maurer, M. S. Diflunisal for ATTR cardiac amyloidosis. *Congest. Heart Fail.* **18**, 315–9

76. Sekijima, Y., Tojo, K., Morita, H., Koyama, J. & Ikeda, S. Safety and efficacy of long-term diflunisal administration in hereditary transthyretin (ATTR) amyloidosis. *Amyloid* **22**, 79–83 (2015).

77. Jorga, K., Fotteler, B., Heizmann, P. & Gasser, R. Metabolism and excretion of tolcapone, a novel inhibitor of catechol-O-methyltransferase. *Br. J. Clin. Pharmacol.* **48**, 513–520 (1999).

78. Green, N. S., Foss, T. R. & Kelly, J. W. Genistein, a natural product from soy, is a potent inhibitor of transthyretin amyloidosis. *Proc. Natl. Acad. Sci. U. S. A.* **102**, 14545–14550 (2005).

79. Yokoyama, T. & Mizuguchi, M. Inhibition of the amyloidogenesis of transthyretin by natural products and synthetic compounds. *Biol. Pharm. Bull.* **41**, 979–984 (2018).

80. Cardoso, I., Martins, D., Ribeiro, T., Merlini, G. & Saraiva, M. J. Synergy of combined Doxycycline/TUDCA treatment in lowering Transthyretin deposition and associated biomarkers: Studies in FAP mouse models. *J. Transl. Med.* **8**, (2010).

81. Ferreira, N., Saraiva, M. J. & Almeida, M. R. Epigallocatechin-3-gallate as a potential therapeutic drug for TTR-related amyloidosis: 'in vivo' evidence from FAP mice models. *PLoS One* **7**, e29933 (2012).

82. Ferreira, N., Saraiva, M. J. & Almeida, M. R. Uncovering the Neuroprotective Mechanisms of Curcumin on Transthyretin Amyloidosis. *Int. J. Mol. Sci.* **20**, (2019).

83. Ferreira, N., Gonçalves, N. P., Saraiva, M. J. & Almeida, M. R. Curcumin: A multi-Target disease-modifying agent for late-stage transthyretin amyloidosis. *Sci. Rep.* **6**, (2016).

84. Higaki, J. N. *et al.* Novel conformation-specific monoclonal antibodies against amyloidogenic forms of transthyretin. *Amyloid* **23**, 86–97 (2016).

85. Galant, N. J. *et al.* Substoichiometric inhibition of transthyretin misfolding by immune-targeting sparsely populated misfolding intermediates: a potential diagnostic and therapeutic for TTR amyloidoses. *Sci. Rep.* **6**, 25080 (2016).

86. Nilsson, L. *et al.* Modifications of the 7-hydroxyl group of the transthyretin ligand luteolin provide mechanistic insights into its binding properties and high plasma specificity. *PLoS One* **11**, 1–19 (2016).

87. Mikula, H. *et al.* Synthesis of zearalenone-16-β,D-glucoside and zearalenone-16-sulfate: A tale of protecting resorcylic acid lactones for regiocontrolled conjugation. *Beilstein J. Org. Chem.* **10**, 1129–1134 (2014).

88. Mahmood, T. & Yang, P. C. Western blot: Technique, theory, and trouble shooting. *N. Am. J. Med. Sci.* **4**, 429–434 (2012).

89. Liu, Y., Lien, I. F. F., Ruttgaizer, S., Dove, P. & Taylor, S. D. Synthesis and Protection of Aryl Sulfates Using the 2,2,2-Trichloroethyl Moiety. *Org. Lett.* **6**, 209–212 (2004).

90. Nilsson, L. *et al.* Modifications of the 7-hydroxyl group of the transthyretin ligand luteolin provide mechanistic insights into its binding properties and high plasma specificity. *PLoS One* **11**, (2016).

91. Loconte, V. *et al.* Structure-activity relationships of flurbiprofen analogues as stabilizers of the amyloidogenic protein transthyretin. *J. Struct. Biol.* (2019). doi:10.1016/j.jsb.2019.08.011

92. Florio, P. *et al.* Transthyretin binding heterogeneity and antiamyloidogenic activity of natural polyphenols and their metabolites. *J. Biol. Chem.* **290**, 29769–29780 (2015).

93. Kabsch, W. <title>\n *XDS*\n</title>. *Acta Crystallogr. Sect. D Biol. Crystallogr.* **66**, 125–132 (2010).

94. Evans, P. Scaling and assessment of data quality. in *Acta Crystallographica Section D: Biological Crystallography* **62**, 72–82 (2006).

95. Emsley, P., Lohkamp, B., Scott, W. G. & Cowtan, K. Features and development of Coot. *Acta Crystallogr. Sect. D Biol. Crystallogr.* **66**, 486–501 (2010).

96. Murshudov, G. N. *et al.* REFMAC5 for the refinement of macromolecular crystal structures. *Acta Crystallogr. Sect. D Biol. Crystallogr.* **67**, 355–367 (2011).

97. Singharoy, A. *et al.* Macromolecular Crystallography for Synthetic Abiological Molecules: Combining xMDFF and PHENIX for Structure Determination of Cyanostar Macrocycles. *J. Am. Chem. Soc.* **137**, 8810–8818 (2015).

98. Adams, P. D. *et al.* PHENIX: A comprehensive Python-based system for macromolecular structure solution. *Acta Crystallogr. Sect. D Biol. Crystallogr.* **66**, 213–221 (2010).

99. Laskowski, R. A., MacArthur, M. W., Moss, D. S. & Thornton, J. M. PROCHECK: a program to check the stereochemical quality of protein structures. *J. Appl. Crystallogr.* **26**, 283–291 (1993).

100. Winn, M. D. *et al.* Overview of the CCP4 suite and current developments. *Acta Crystallographica Section D: Biological Crystallography* **67**, 235–242 (2011).

Chapter 5

Synthesis of amyloid models and potential calix[4]arene-based $A\beta_{16-22}$ sequestrants

5.1 Introduction

5.1.1 General: self-assembly

Self-assembly is at the base of several biological systems and it is responsible of the formation of highly organized and functional macroscale complexes/aggregates. By Nature it is exploited as a switcher for generation, quenching or modulation of biological activity. Unfortunately, moreover, in some diseases, such as Alzheimer and Parkinson[1–3], the failure of physiological proteins is the etiological cause of the disease itself, since are released peptides which are unable to fold correctly leading hence to amyloid species formation (for instance, as already described in the previous chapter for the case of TTR mutation and consequent destabilization of its physiological tetrameric form). Due to the dramatic and heavy impact of these pathologies on the public health, a new branch of research is hardly working to give effective answers in term of therapies. One of the strategies as potential therapy for amyloidogenic diseases is based on the development of peptide-based systems with modified structure with respect to the natural ones in terms of steric hindrance and hydrophobicity.

Peptide self-assembly is a spontaneous process driven by the cooperative action of simultaneous non-covalent interactions, such as π-π interactions, hydrogen bonds, hydrophobic, steric and electrostatic effects. If these interactions control the thermodynamics of the aggregates formed, by modulation of parameters such as concentrations, pH and temperature, kinetics can be modified with the possibility to trap the supramolecular assembly in a metastable state. The modulation of these parameters is a powerful tool to study peptide self-assembly, but since multi-factorial, most of the mechanisms are still unknown[4–6].

5.1.2 Diphenylalanine core

It has been demonstrated that diphenylalanine (FF) is the smallest recognition motif, mostly predominant in peptide self-assembly (**Figure 5.1.2.1**). According to Reches and Gazis[4,7], dipeptide H-Phe-Phe-OH, upon dilution in aqueous solution, rapidly assembles into distinct nanotubes. By a morphological point of view, six FF dipeptides interact sequentially each other by means of hydrogen bonds among the charged termini forming repeated hexagon rings: the inner part of these channels is covered by hydrophilic backbone, meanwhile the outer part is decorated by hydrophobic side-chains. By computational studies, it has been demonstrated that the major stabilization contribute is given by intermolecular π-π stacking and hydrophobic interactions between aromatic side-chains, rather than strong ionic pairing between backbone charged termini[1,8].

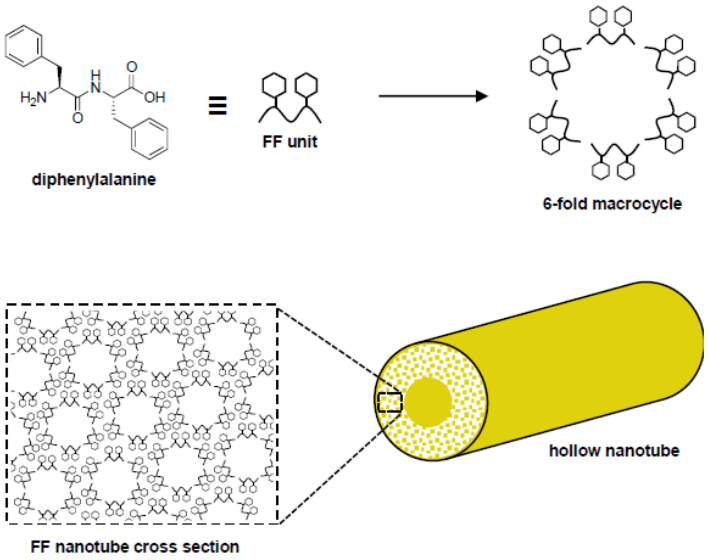

Figure 5.1.2.1: The chemical structure of diphenylalanine (FF) and the putative FF self-assembly within nanotubes. FF units build 6-fold macrocycles, which pair each other to form sheet structures by a hexagonal packing pattern. Figure adapted from references[1,8,9].

The FF motif is notoriously present in amyloidogenic peptides, such as the serum amyloid A, involved in pathogenesis of atherosclerosis, and the amyloid-β Aβ, responsible of outbreak of Alzeheimer's disease[10,11]. It has been demonstrated that the presence of this motif in central hydrophobic core of Aβ is the major driving-force of peptide aggregation[1,12–14]. A deeper insight of the topic was gained by Jeon et al. with MD studies on uncharged and zwitterionic FF peptides, which showed that electrostatic contacts promote the formation of small aggregates of zwitterionic FF, whereas hydrophobic interactions lead to larger aggregate structures[8]. All the information collected with studies on FF motif is the base of a deeper understanding of pathological pathway in amyloid aggregation.

5.1.3 β-amyloid

Aβ peptide is notably recognized as the etiological factor of several amyloidogenic diseases, such as Alzheimer's disease. In this pathology, a transmembrane protein called Amyloid Precursor Protein (APP)[15], whose the extracellular portion, in physiological conditions, is cleaved sequentially by α- and γ-secretases, in pathological conditions α-secretase is anticipated by β-secretase, which in cooperation with γ-secretase cuts the protein in a different position releasing the so-called $A\beta_{40}/A\beta_{42}/A\beta_{43}$ fragments responsible of the neurotoxic properties.

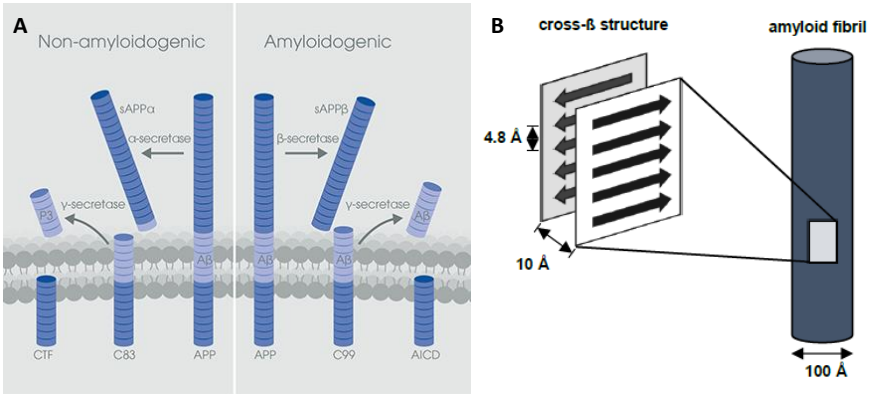

Figure 5.1.3.1: Schematic representation of non-amyloidogenic and amyloidogenic pathways in Alzheimer's disease (**A**) and fibril structure model (**B**). Figure adapted from references[16,17].

Once formed, these fragments tend to organize in highly-ordered fibrils (diameter = 7-10 nm) made of cross-β structures[16,18–20] packed together perpendicularly to the fibril axis (**Figure 5.1.3.1**).

Since it is not clear whether amyloid fibrils or metastable aggregates are the primary effectors of neurotoxicity and which are the factors for a neurotoxic response[21–25], it makes sense to study the aggregation process in the future optic to develop targeted therapeutics[26]. However, a lot of research is still ongoing in this field due to the polymorphic and the transient nature of these metastable aggregates (**Figure 5.1.3.2**)[25].

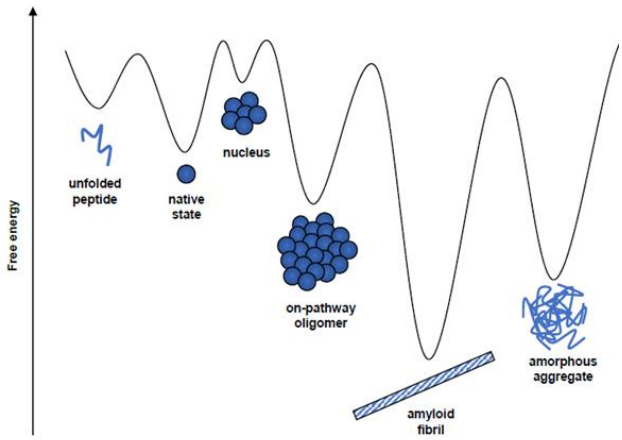

Figure 5.1.3.2: Free energy schematic graph of metastable intermediates encountered in self-assembly process. Figure adapted from reference[1].

5.1.4 Peptide models: $A\beta_{16-22}$ fragment

Dealing with full-length peptides, it is obviously uncomfortable, mainly for the long synthesis and hard purification. For these reasons, many experimental studies have been carried out for

the determination of short inner peptide fragments with self-aggregating properties similar to full-length ones. For instance, Tenedis et al.[27,28] have determined that the NFGAIL hexapeptide of islet amyloid peptide (IAPP) is a good model for the full-length peptide because of the similar cytotoxic and structural properties of the parent peptides. Due to their boosted kinetics in aggregation, short peptides are very convenient tools for drawing the basilar mechanisms in self-assembly. For amyloid-β peptide aggregation study, $A\beta_{16-22}$ has been denotated as a good reference model to study Alzeheimer's pathological pathways (**Figure 5.1.4.1**)[1,18]. In fact, it is well known that residues 17-21 represent a strong hydrophobic core essential for self-assembly of full-length peptide. So targeting this fragment with chemical modifications can be a way to alter this process by simply changing its polarity[12,18]. In addition, the compresence of polar Lys16 and Glu22 give the opportunity to change morphology to nanotubes at different pH conditions, which makes this peptide an interesting tool also in material sciences[1,18,29,30].

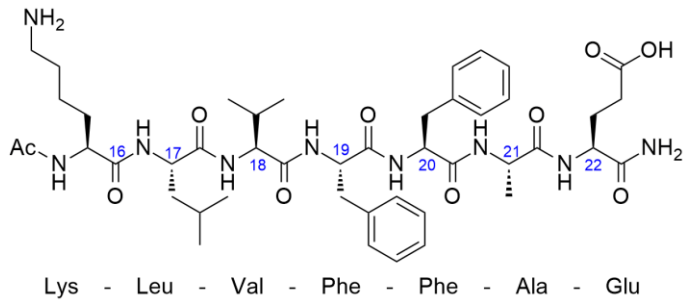

Figure 5.1.4.1: $A\beta_{16-22}$ chemical structure.

5.1.5 Amyloid-β aggregation

The mechanism of amyloid self-assembly is highly complex because of the high number of metastable aggregates involved. As evidenced in **Figure 5.1.5.1**, this process is characterized by a sigmoidal growth curve subdivided into three phases: lag phase, growth phase and plateau phase.

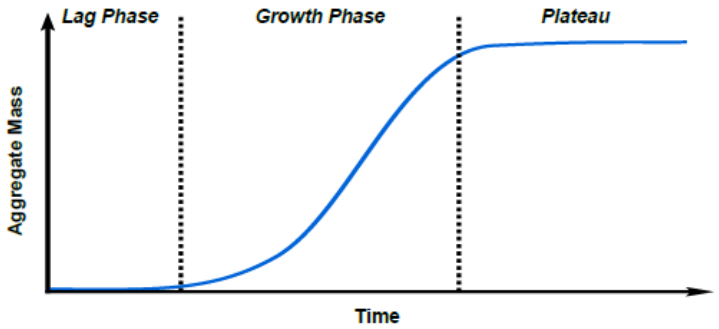

Figure 5.1.5.1: Growth curve of Amyloid-β: the sigmoidal pattern is evidence of the nucleation-dependent behaviour. The graph was obtained by Thioflavin T assay (ThT)[1,31–33]. Figure adapted from reference[1].

In the lag phase, it has been demonstrated by electron and atomic force microscopy studies that the low-molecular-aggregates formed have totally different structures to mature amyloid fibrils[31,34]. In fact, in this phase dominates the primary nucleation during which monomers spontaneously aggregate in a small nucleus stable enough to prefer further growth rather than the back-dissociation[1,35]. Since primary nucleation occurs without the involvement of pre-existing oligomers, the rate of this process depends only on monomeric concentration[35,36]. When a critical concentration of amyloid fibrils is reached, the growth phase is triggered and the aggregate masses increase exponentially. This is possible for the secondary nucleation mechanism, which dominates this phase. Here, in fact, new aggregates are formed on the surface of pre-existing fibrils as they were templates for their formation. Therefore, differently to the previous phase, here the rate is dependent on the concentration of pre-existing fibrils via positive feedback, which explains the rapid exponential growth[32]. The last plateau phase shows that the process is complete and no other aggregates are forming. This is a simplistic view of the entire process, but actually secondary pathways and further oligomerisation are involved adding more complexity to kinetic analysis[31,35,36].

5.1.6 Aggregation studies: Microscopy, Fluorescence Quenching and Photo-Induced Cross-Linking

For a qualitative study on amyloid aggregates are commonly used Electron and Atomic Force Microscopy[27,37]. One of the first experimental studies done on this topic was carried out by Hsieh et al.[38]. Taking TEM images in different time points over a range of 1h-14days, they discovered that WT-Aβ_{16-22} self-assemblies via a ribbon-like intermediate that, at neutral pH, rearranges into fibrils, while at acidic pH rearranges into nanotubes. Through CD experiments, then, by the β-sheet content demonstrated that under both conditions the self-assembly starts with the formation of anti-parallel out-of-register β-sheets, followed by a realignment at pH=6 into in-register fibrillary strands, which corresponds to ribbons observed with TEM (**Figure 5.1.6.1**).

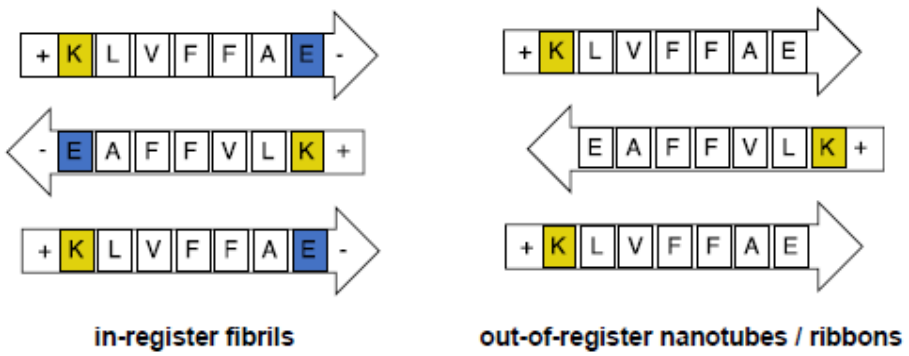

Figure 5.1.6.1: Aβ_{16-22} pairing modes in self-assembly: at physiological pH in-register fibrils are preferred by means of ionic interactions between K16 and E22, whereas at pH=2 out-of-register nanotubes/ribbons are favoured. Figure adapted from reference[38].

These interesting results, for the first time, proved, differently from what had been demonstrated in computational studies on FF self-assembly, that at neutral pH the intermolecular pairing of negatively charged E22 carboxylate and positively charged K16 does not drive the whole process but is just responsible of the thermodynamic stabilization of already-formed species[38].

Another way to study amyloid aggregation is the ThT fluorescence assay (**Figure 5.1.6.2**). This assay relies on the fluorescence increase due to the rotational immobilization of the central bond between the benzothiazole and aniline rings upon β-sheet-rich aggregates formation concomitant with the growth phase[21,26]. This rigidification and the subsequent conjugation extension makes fluorescence emission pathway the fastest process compared to the other non-radiative pathways[39]. Unfortunately, this assay is not suitable for the detection of the small β-sheet-free aggregates, which are implicated in Alzheimer's disease neurotoxicity[21,23,40–42].

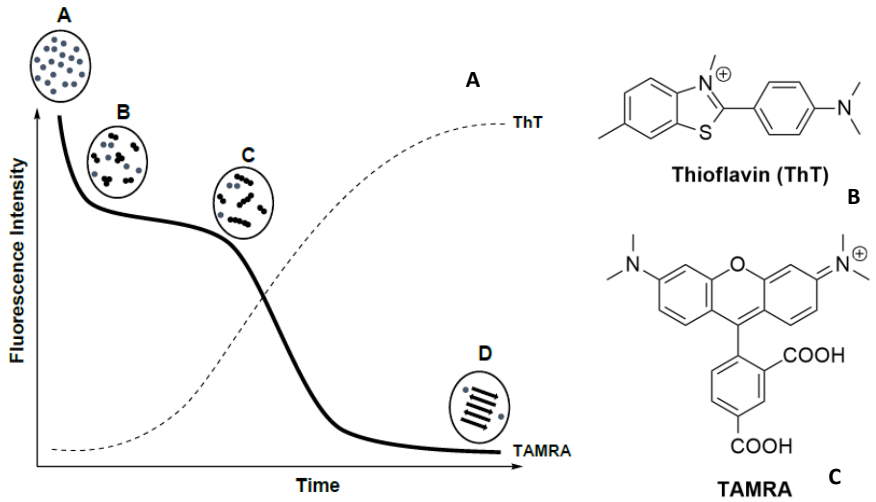

Figure 5.1.6.2: Fluorescence intensity profiles over aggregation time (**A**) through ThT (**B**) and TAMRA (**C**) assays. From A to B a lag phase is observed where primary nucleation dominates, followed by B-C phase where pre-existing nuclei reorganize themselves without further accumulation. The last C-D phase is the actual growth phase where β-sheet structures are formed. Figure adapted from references[21].

For a better understanding of β-amyloid aggregation, it is required the fluorescence self-quenching assay developed by Frieden and Garai[21], which can be useful also for a quantitative determination of the full-time course of β-amyloid aggregation. This assay essentially relies on the fluorescence quenching due to the proximity of two fluorescent tags in the aggregate state[43]. For $A\beta_{1-40}$ and $A\beta_{1-42}$ aggregation, the peptides are covalently labelled with tetramethylrhodamine (TAMRA). In **Figure 5.1.6.2** fluorescence emission in both assays (ThT/TAMRA) is represented as a function of time and shows how the information collected by both experiments are totally different because of the different mechanism of action[21]. For TAMRA-$A\beta_{1-42}$, an initial fast quenching is observed thanks to the first small aggregates formed. Simultaneously, in the ThT assay no variation in fluorescence intensity is observed for the absence of rigid β-sheet structures. During the subsequent lag phase, just a slight decrease in TAMRA fluorescence is observed, while in ThT assay it is observed a slight increase in

fluorescence. In this phase probably just a reorganization of pre-existing amorphous aggregates occurs and no monomers concur for accumulation. In the intermediate part of the graph in both experiments a fast change is observed because of the rapid $A\beta_{1-42}$ self-assembly. CD studies showed that this phase is mainly responsible of most of β-sheet content. The plateau observed at the end confirms that the self-assembly process is complete and no other growth is observed[21,44]. Even if ThT assays seem to be less accurate than TAMRA assays and not suitable for early-stage aggregates, they can discriminate the nature of aggregates in terms of β-sheet content[21,39].

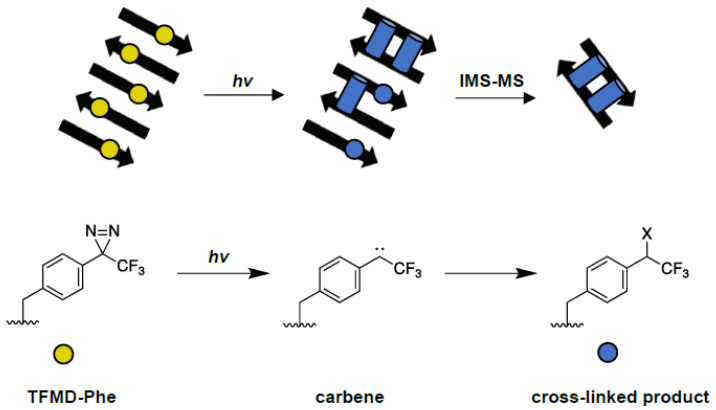

Figure 5.1.6.3: PIC strategy. Diazirines, upon activation by irradiation as carbenes, are directly involved in cross-linking. The cross-linked structures and relative cross-linking positions are easily detected by ion-mobility bidimensional mass spectrometry. Figure adapted from reference[45].

Photo-Induced Cross-Linking (PIC)[45,46] is a more accurate technique since by irradiation triggers covalent cross-linking useful to trap reversible and/or weak supramolecular interactions into stable irreversible bonds[47]. This is generally used in the lag phase where small aggregates are subjected to very fast changes in morphology so it is very important to freeze these intermediates to have a better understanding of the self-assembly process. As PIC group, nowadays, diazirines[45] are mainly employed thanks to the rapid carbene formation upon irradiation, which allows to use a very reliable temporal control in the technique. First examples in this context were made by Smith at al.[47], which incorporating 3-aryl-(trifluoromethyl)diazirine (TFMD) group in $A\beta_{16-22}$ observed in mass spectrometry, upon irradiation, several aggregates obtained by indiscriminate reactivity of TFMD[45,47]. A subsequent work of Preston et al.[46] demonstrated that it is possible to incorporate TFMD in $A\beta_{16-22}$ with solid-phase peptide synthesis (SPPS) and exploit it in amyloid aggregation at different pH conditions: the intermolecular cross-linking gave information about the reciprocal alignment of peptides, meanwhile intramolecular cross-linking gave information about monomer conformations. All the intermediates are generally analysed with electrospray ionisation-ion mobility spectrometry-mass spectrometry (ESI-IMS-MS)[45,46], which is able to discriminate high-mass fragments with equal molecular weight through collision-induced dissociation (CID) by means of tandem MS/MS techniques[46,47]. Specifically, MS-induced cleavage occurs onto amidic nitrogen easily protonated by ESI source[48,49]. After CID and second MS selection, an array of fragment

ions differing in mass by a single amino acid is obtained and through their analysis can easily deduct the cross-linking position and therefore the putative supramolecular contacts[46–49].

5.1.7 Aggregation effects on variant $A\beta_{16-22}$

Amyloid self-assembly, as can be simply deduced, is influenced by the nature of amino acids composing the $A\beta_{16-22}$ sequence, in particular by parameters such as steric hindrance, charge, aromaticity and hydrophobicity[5,44,50,51]. Senguen et al.[5,44], starting from the idea that the cross-strand pairing was driven by aromatic π-π interactions[29], proposed to synthesize by SPPS nine $A\beta_{16-22}$ variants of FF motifs using the more hydrophobic cyclohexylalanine (Cha) and pentafluorophenylalanine (F_5-Phe) and the less hydrophobic Ala or Tyr. What came out from HPLC sedimentation analysis, is that:

1) increasing hydrophobicity, the self-assembly is enhanced, whereas reducing hydrophobicity the self-assembly is inhibited;
2) removing π-π interactions by means of Cha, the related fibrils are not thermodynamically stable.

Considering that, besides hydrophobicity and π-π availability, steric hindrance is another parameter that influences amyloid stability[5], they decided to repeat the same synthesis with Val, Leu, Ile and hexafluoroleucine (Hfl). They discovered that:

1) replacement of Phe with Val (less hydrophobic) inhibits self-assembly, whereas replacement with Hfl (more hydrophobic) enhances self-assembly;
2) replacement of Phe wit Leu or Ile (similar in hydrophobicity, but smaller than Phe) leads to an increase in self-assembly tendency.

These preliminary data supported, hence, the idea that π-π interactions are not dominant factors in aggregation, while steric clashes are[44].

5.2 Aim of the work

Because of the relevance for $A\beta_{16-22}$ self-assembly of hydrophobicity and the steric issues, I decided to spend my secondment at University of Leeds in Wilson's laboratories, where are expert of amyloidogenic diseases and protein-protein interactions, in order to synthesize $A\beta_{16-22}$ variants in positions 19 and 20 with more hydrophobic phenylalanine-based residues (4-iodophenylalanine, 4-chlorophenylalanine, 4-methoxyphenylalanine) to study them in aggregation. These peptides, having the FF core modified, are supposed to behave in a different way in the self-assembly process with respect to WT peptides and they might be potential tools for aggregation study. Upon their synthesis through automatic SPPS, their aggregation properties were preliminary studied by TEM, checking at different pH the possible presence of aggregates in the incubation solution. Considering the ability of all synthesized peptides to be able to make some interesting structures, the same peptides were functionalized with TAMRA fluorescent probe in order to follow better the self-assembly process via fluorescence quenching assay.

The same sequences, considering their significant impact on human's life, were also thought for the synthesis of β-sheet mimetics as nucleation centre and sequestrants of $A\beta_{16-22}$, thus

employable as potential disaggregating agents of β-amyloids. In this perspective, as preorganized scaffold for their linkage mimicking a β-turn structure, was chosen the calix[4]arene, which can be exploited for upper- and/or lower difunctionalization (**Figure 5.2.1**).

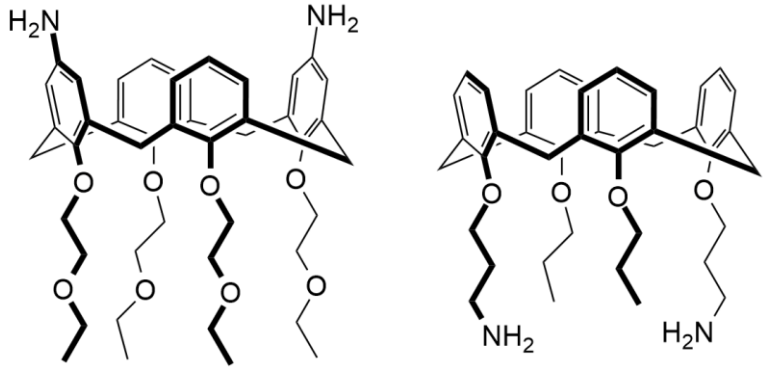

Figure 5.2.1: Scaffolds for the synthesis of calix[4]arene building blocks.

For the design of $A\beta_{16-22}$ sequestrants, 5,17-diaminocalix[4]arene and 25,27-dipropylamino calix[4]arene derivatives were used in the coupling of two parallel $A\beta_{16-22}$ sequences. Some attempts were done, but because of solubility and peptide synthesis issues, the target molecules were not obtained yet.

5.3 Results and discussion

5.3.1 Synthesis of TAMRA fluorescent-label

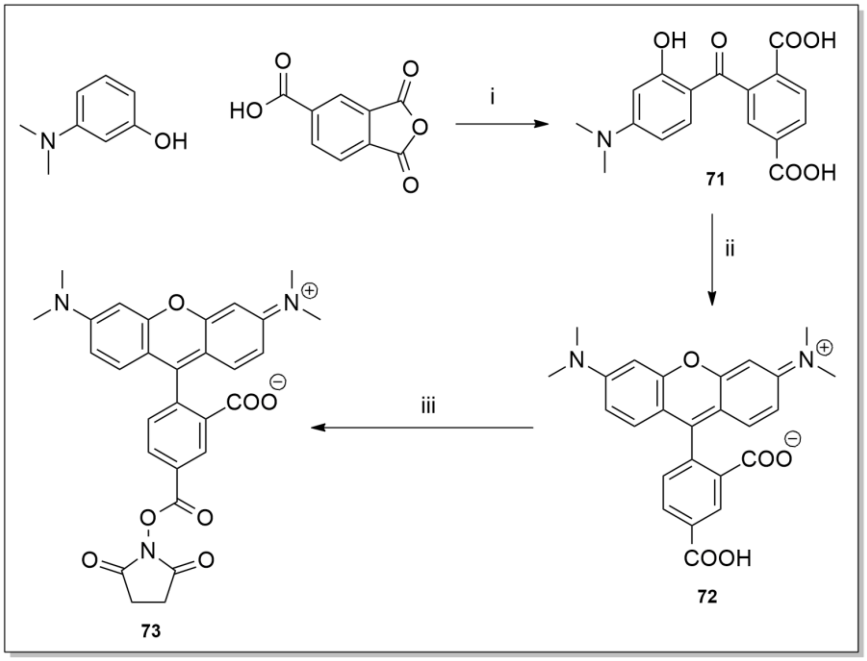

Figure 5.3.1.1: Synthesis of activated TAMRA. *Reactions conditions:* i) 3-dimethylaminophenol (1.0 eq), pounded benzene-1,2,4-tricarboxylic anhydride (1.2 eq), toluene, 60 °C to reflux, 1 day (27% yield); ii) 3-dimethylaminophenol (1.3 eq), trimethylsilylpolyphosphate solution in chloroform[52] (1.6 ml), DMF, reflux, 3h (98% yield); iii) 0.89 mmol DMAP (5.0 eq), NEt_3 (5.0 eq), N-disuccinimidyl carbonate (2.0 eq), DCM, rt, 1h (92% yield).

TAMRA label was synthesized through the protocol[53] showed in **Figure 5.3.1.1**. The synthesis of 4-dimethylamino-2-hydroxy-2',4'-dicarboxybenzophenone was characterized by low yield (27%), which can be rationalized by the poor solubility of reactants in hot toluene and the subsequent low conversion. Upon quenching in AcOH, compound **71** was recrystallized twice in MeOH to get rid of the undesired regioisomer produced in the reaction. In **Figure 5.3.1.2** it is showed by ^{1}H-NMR that recrystallizing more times, the crude gets a progressive purity.

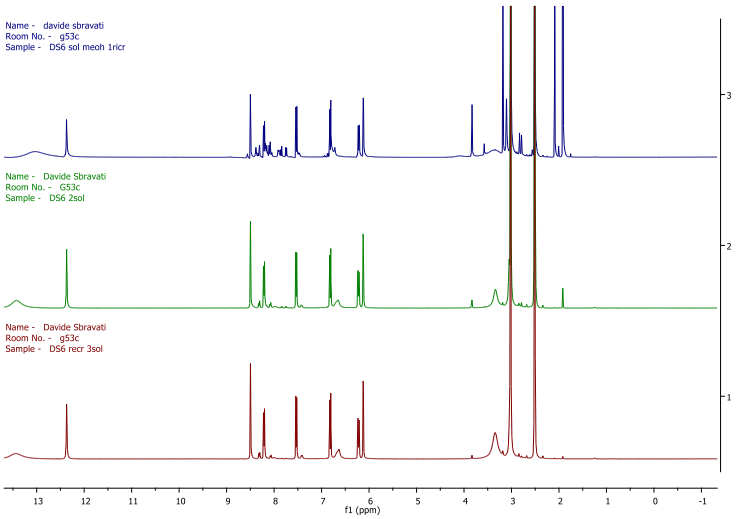

Figure 5.3.1.2: ^{1}H-NMR spectra (400 MHz, DMSO-d_6) of compound **71** after first (**3**), second (**2**) and third (**1**) recrystallization in MeOH.

Then compound **72** was synthesized by refluxing compound **71** in DMF for 3h with trimethylsilylpolyphosphate in the dark. The solvent was then removed by reduced pressure and the target compound **72**, upon dissolution in 5% NaOH, was reprecipitated with 37% HCl. The cyclization occurs pretty fast in quantitative yields with purity of 92% (calculated by ^{1}H-NMR).

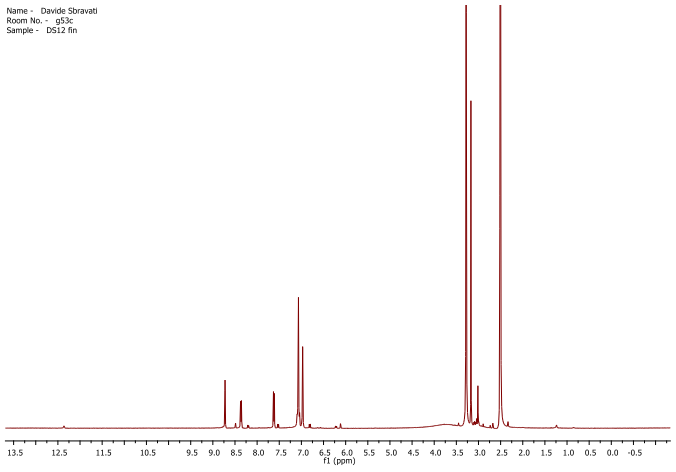

Figure 5.3.1.3: ^{1}H-NMR spectrum (400 MHz, DMSO-d_6) of compound **72**.

Then compound **72** was activated as N-succinimidyl ester with N-disuccinimidyl carbonate and purified by flash chromatography column and used subsequently in the coupling with peptides. Some attempts were made for the synthesis of the fluorophore via a one-pot strategy, as reported in **Figure 5.3.1.4**.

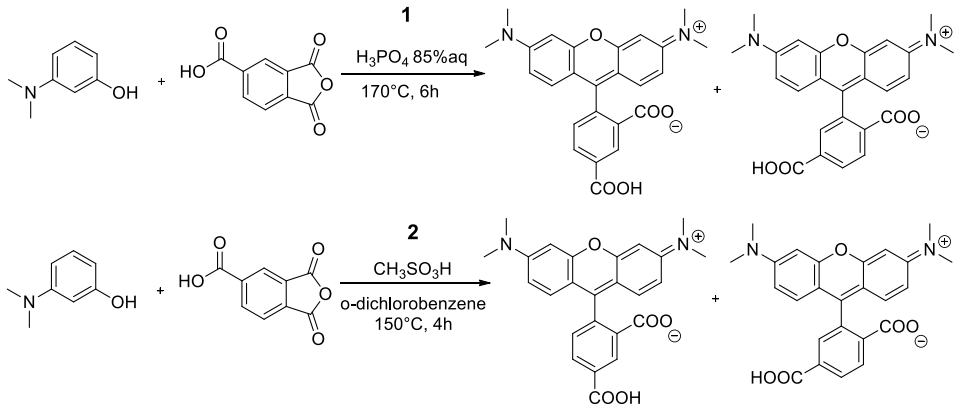

Figure 5.3.1.4: One-pot TAMRA synthesis attempts.

Unfortunately, the resulting crude was characterized by a complex mixture, in which the two TAMRA regioisomers run very close to each other on TLC. For this reason along with the fact that the crude tends to stick on silica gel, the regioisomers were not purified and so the strategy was rapidly abandoned.

5.3.2 SPPS of $A\beta_{16-22}$ iodo-variants

For the generation of halogen-based $A\beta_{16-22}$ library, I carried out the synthesis of iodo derivatives and WT, while in parallel Portia Rosemary Ye-Mae Hunt carried out the synthesis of chloro and methoxy derivatives[54]. WT-$A\beta_{16-22}$ and iodine-containing variants (reported in **Figure 5.3.2.1**) were synthesized on Rink Amide MBHA resin (100 - 200 mesh) through Liberty Blue Automated Microwave Peptide Synthesizer CEM using microwave conventional couplings (75°C; 4min) with DIC/Oxyma.

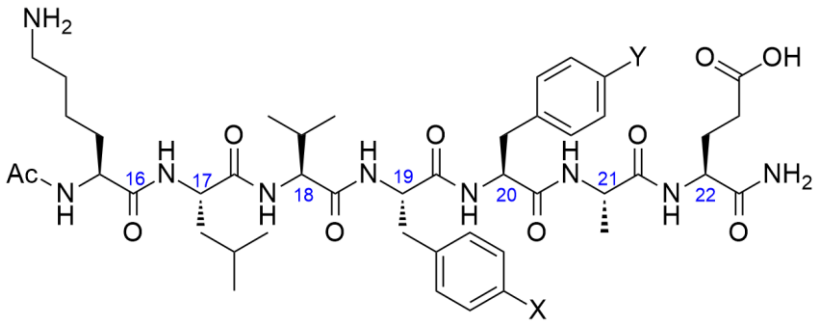

$A\beta_{16-22}$ peptide variants	Sequence	
	Acetylated	TAMRA-capped
WT (74)	Ac-KLVFFAE-NH_2 (X=H, Y=H)	*Purification issues*
F19 I (75a)	Ac-KLV**F***FAE-NH2 (X=I, Y=H)	*Purification issues*
F20 I (76a)	Ac-KLVF**F***AE-NH_2 (X=H, Y=I)	TAMRA-Ahx-KLVF**F***AE-NH2
F19, 20 I (77a)	Ac-KLV**F*F***AE-NH2 (X=I, Y=I)	*Purification issues*
F19 Cl (75b)	Ac-KLV**F***FAE-NH2 (X=Cl, Y=H)	TAMRA-Ahx-KLV**F***FAE-NH2
F20 Cl (76b)	Ac-KLVFF*AE-NH_2 (X=H, Y=Cl)	TAMRA-Ahx-KLVF**F***AE-NH2
F19, 20 Cl (77b)	Ac-KLV**F*F***AE-NH2 (X=Cl, Y=Cl)	TAMRA-Ahx-KLV**F*F***AE-NH2
F19 MeO (75c)	Ac-KLV**F****FAE-NH2 (X=OMe, Y=H)	TAMRA-Ahx-KLV**F****FAE-NH2
F20 MeO (76c)	Ac-KLVF**F****AE-NH2 (X=H, Y=OMe)	TAMRA-Ahx-KLVF**F****AE-NH2
F19, 20 MeO (77c)	Ac-KLV**F****F****AE-NH2 (X=OMe, Y=OMe)	TAMRA-Ahx-KLV**F****F****AE-NH2

Figure 5.3.2.1: $A\beta_{16-22}$ halogen variants synthesized so far either in the acetylated or TAMRA-capped form.

All the peptides were synthesized by a Fmoc/tBut strategy. After each coupling, the growing peptide chain was deprotected with two Fmoc deprotection cycles (75 °C and 3 min each). As a first preliminary study on the capacity of these variants to self-assemble into fibrils or nanotubes, the final Fmoc-deprotected peptides were capped on resin by acetic anhydride/DIPEA 1:1 solution and then cleaved in TFA/H_2O/TIS 950:25:25.

For the study of their aggregation kinetics by fluorescence, the final Fmoc-deprotected peptides were coupled to 6-aminohexanoic acid (Ahx), which showed to be in past a good linker to outdistance TAMRA enough far away from peptide structures limiting inappropriate interactions in the assay during aggregation. After their automatic deprotection from Fmoc, peptides were manually coupled to fluorophore using a solution of compound **73** (1.5 eq) in DMF which was left reacting on shaker at room temperature for 3 nights. Upon cleavage in TFA/H_2O/TIS 950:25:25, the HPLC traces of all TAMRA-labelled peptides synthesized showed a very complicated situation. In **Figure 5.3.2.2** is reported the HPLC chromatogram of **F_20_I** derivative representative for all TAMRA-labelled iodo derivatives. As it can be seen, a lot of peaks are present, which implies the hard work of numerous components collection and characterization via UPLC-MS. Because of this purification issue, just **F_20_I** derivative was purified and characterized by UPLC-MS and analytical HPLC. Since the peptides loaded with Ahx were synthesized months before their actual use in TAMRA coupling, we think that these precursor peptides are subjected to degradation over time.

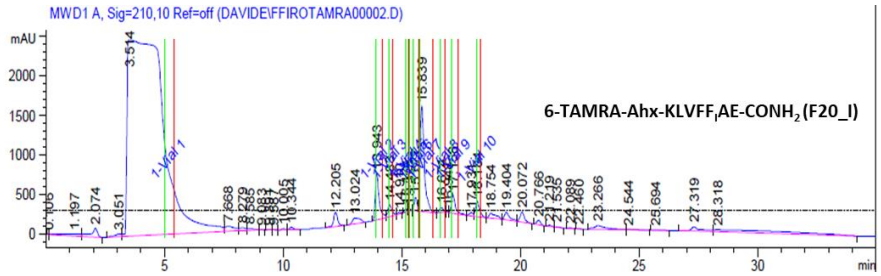

Figure 5.3.2.2: HPLC trace of 6-TAMRA-Ahx_KLVFF$_I$AE-CONH$_2$ (F20_I).

In fact, having this in mind, in parallel chloro- and OMe-derivatives were synthesized in the same way, as seen before for iodo-derivatives, but using them directly for TAMRA coupling. The HPLC traces looked less crowded than iodo those of derivatives, and it was possible purify all TAMRA-capped chloro- and methoxy-derivatives.

5.3.3 Amyloid morphology: Electron Microscopy experiments

In order to understand their possibility to self-assemble in fibrils or other organized structures, all halogen variants peptides at concentration of 300 μM were incubated either for 1 or 2 weeks in 100 mM NH_4HCO_3 buffer solution (pH=7) at room temperature and then the samples were analyzed by TEM.

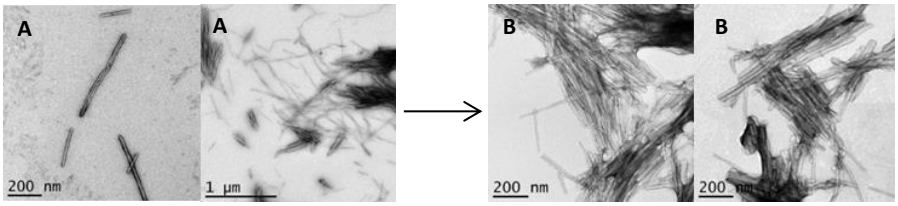

Figure 5.3.3.1: TEM images of **F19_I** aggregates. Acquisition was carried out after 1 week (**A**) and 2 weeks (**B**) at pH=7 (300 μM).

As it can be seen in **Figure 5.3.3.1**, for **F19_I** derivative it is crucial the incubation time. In fact, passing from 1 week to 2 weeks of incubation, we pass from a situation in which are present more fibrils isolated to a cluttered situation, in which fibrils are stacked together making big aggregates.

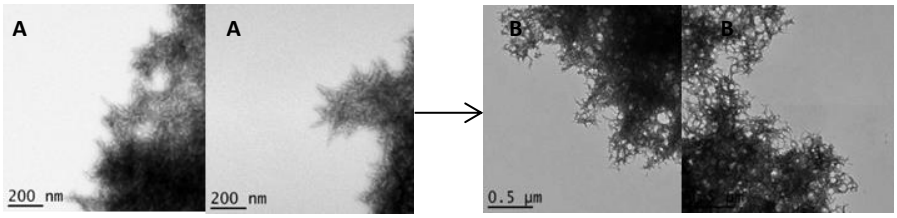

Figure 5.3.3.2: TEM images of **F19,20_I** aggregates. Acquisition was carried out after 1 week (**A**) and 2 weeks (**B**) at pH=7 (300 μM).

Differently from **F19_I**, **F19,20_I** shows no particular differences in self-assembly over time (**Figure 5.3.3.2**). Here, the peptide tends to form extremely stacked structures where all fibrils are totally glued each other in micrometer aggregates. The same behaviour is observed for **F20_I** derivative (**Figure 5.3.3.3**), except for the fact that after the first incubation week no aggregates were seen on grids. It is very strange that no aggregates after 1 week were present for this derivative considering that a very crowded situation is observed after 2 weeks; probably the grid used was faulty and so not able to adsorb the sample.

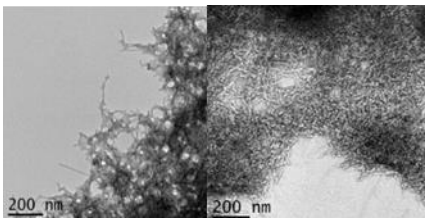

Figure 5.3.3.3: TEM images of **F20_I** aggregates. Aggregates were obtained after 2 weeks at pH=7 (300 μM). No aggregates were observed after an incubation time of 1 week.

Comparing these derivatives with Wild-Type peptide (**Figure 5.3.3.4**), we could see that even after 2 weeks the sample is characterized by the compresence of single fibrils distanced each from the other. In particular in **Figure 5.3.3.4** it can be seen how fibrils can roll around one another to make helical structures.

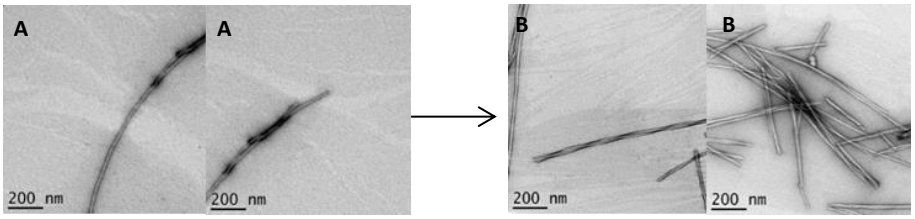

Figure 5.3.3.4: TEM images of WT peptide aggregates. Acquisition was carried out after 1 week (**A**) and 2 weeks (**B**) at pH=7 (300 μM).

Also, chloro- and OMe-derivatives were analysed by TEM. For chloro-derivatives we have large aggregates in which fibrils tend to stick laterally each other. For **F20_Cl** (**Figure 5.3.3.5**) are clearly shorter than the other variants and characterized by helical twist.

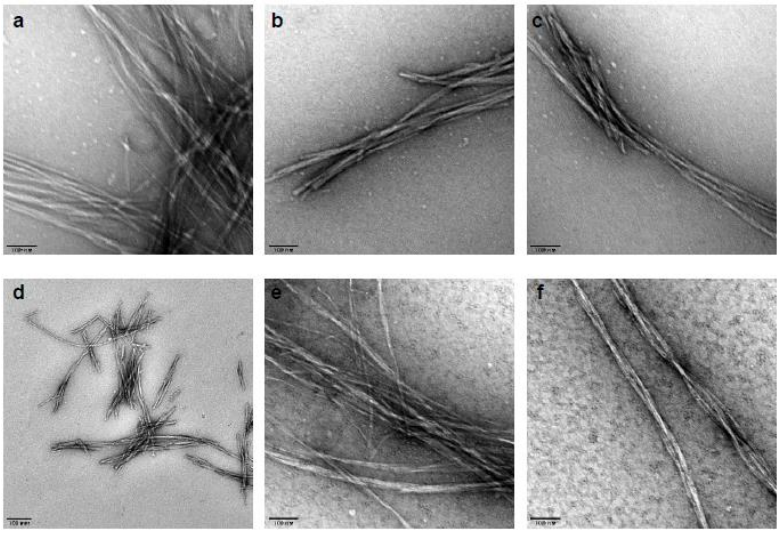

Figure 5.3.3.5: TEM images of **F19_Cl** (**a**, **b**, **c**), **F20_Cl** (**d**) and **F19,20_Cl** (**e**, **f**) aggregates. Acquisition was carried out after 1 week at pH=7 (300μM).

F19_MeO fibrils (**Figure 5.3.3.6**) show similar morphology to **F19,20_Cl** and **F19_Cl**. **F20_MeO** forms fibrils with a helicity more pronounced than **F19_MeO**. Wang et al.[55]using a ferrocene-modified FF dipeptide demonstrated that the helicity depends on hydrogen bonds, π-π stacking and molecule chirality as well as temperature, counterions and solvent. As observed for **F20_I**, also for **F19,20_MeO** no fibrils were observed. Besides likely faulty grid problems, in this case fibrils could have been too small to be seen in contrast to uranyl acetate aggregates.

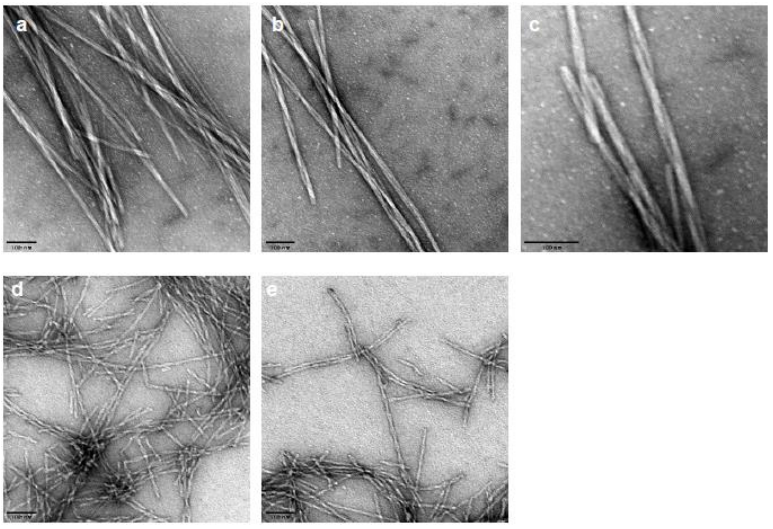

Figure 5.3.3.6: TEM images of **F19_MeO** (**a**, **b**, **c**) and **F20_MeO** (**d**, **e**) aggregates. Acquisition was carried out after 1 week incubation at pH=7 (300 μM).

The same experiments were carried out also at pH=2 dissolving chloro- and iodo-peptides in 40%ACN/H_2O+0.1%TFA at 1.3 mM concentration for 1 week. Starting from **F19_Cl**, we can observe a dense network of a mixture of ribbon (**Figure 5.3.3.7 b,e**), nanotube (**Figure 5.3.3.7 c,b,d**) and fibril (**Figure 5.3.3.7a**) structures. The relative ratio could not have been determined quantitatively, but qualitatively we can say that in **F19_Cl** more nanotubes than in the case of WT peptide are present. This suggests that the self-assembly process in **F19_Cl** is faster than for WT peptide. After 1 week, it is clear that nanotubes for WT peptide are not still mature since ribbon-like and sheet-like structures are present on the grid. What seen, is in agreement with Senguen et al.[5], which demonstrated that halogen atoms are responsible of an additional thermodynamic stabilization.

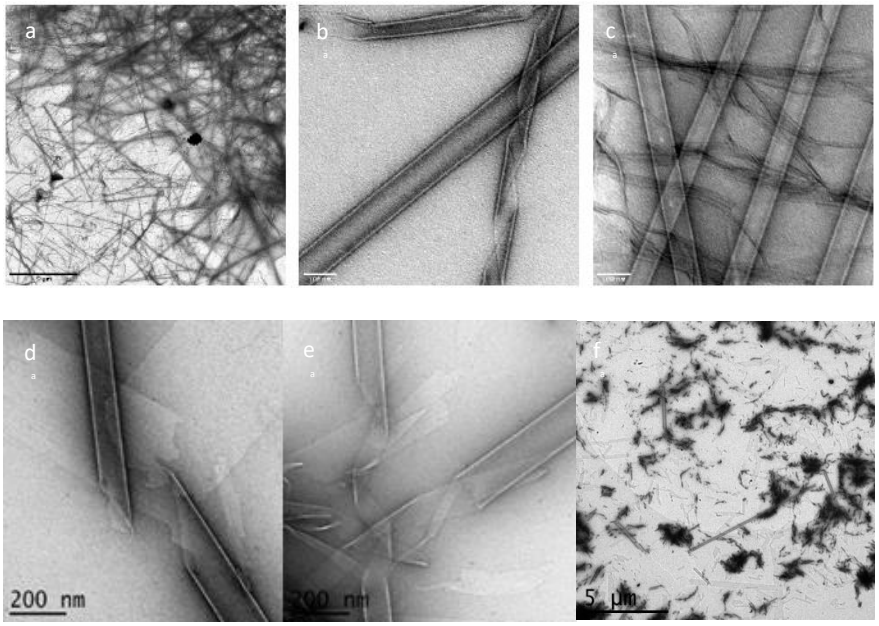

Figure 5.3.3.7: TEM images of **F19_Cl** (**a**, **b**, **c**) (scale 300 μm), WT peptide (**d**, **e**) and **F20_I** (**e**) aggregates after 1 week of incubation at pH=2).

On the contrary, **F20_Cl** produced at pH 2 a totally different situation (**Figure 5.3.3.8**), in which the peptide is assembled in very short nanofibrils with high tendency to align themselves in parallel wisps. Among these nanofibrils some ribbons are seen but no helical coiling is detected, differently from what observed for the same peptide in physiological pH conditions). The most remarkable information is that no nanotubes are present by the way.

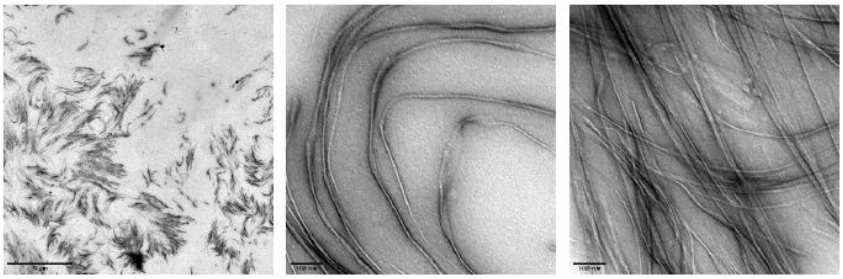

Figure 5.3.3.8: TEM images of **F20_Cl** (scale 300 μm) aggregates (incubation for 1 week at pH=2).

In the case of **F19,20_Cl** derivative, a wide network of ribbons is present (**Figure 5.3.3.9**). Obviously, in these conditions we don't know whether these peptides are able to assemble in nanotubes or not; maybe they might require more time to mature in nanotubes. So for this reason, in future it will be done a TEM time course in order to observe the time evolution of aggregates.

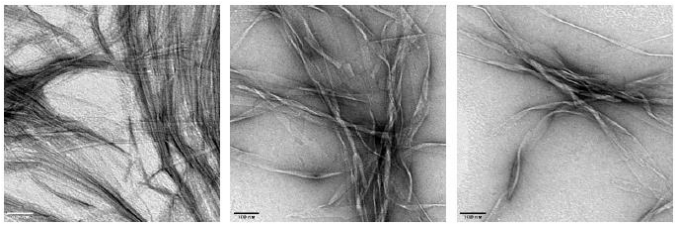

Figure 5.3.3.9: TEM images of **F19,20_Cl** (scale 300 μm) aggregates (incubated for 1 week at pH=2).

For all iodo derivatives, very nice nanotubes were observed. Due to the high number of nanotubes present seems that variants with iodo monosubstitution show a more predominant nanotube formation instead of **F19,20_I** for which the entire process seems slowed down (**Figure 5.3.3.10**).

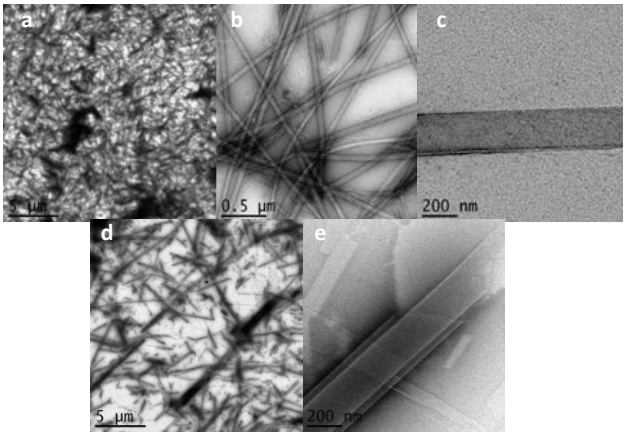

Figure 5.3.3.10: TEM images of **F19_I** (**a**, **b**), **F19,20_I** (**c**) and **F20_I** (**d**, **e**) aggregates (incubated for 1 week at pH=2).

To verify the reversibility of NTs into fibrils the same samples were treated with 1M NaOH to get a pH of 7. After 1 week, new acquisitions were done and what turned out, is that all iodo derivative nanotubes were converted into fibrils, while, the WT peptide nanotubes did not (**Figure 5.3.3.11**). Probably for iodo derivatives the interconversion is faster than the one observed with WT derivative.

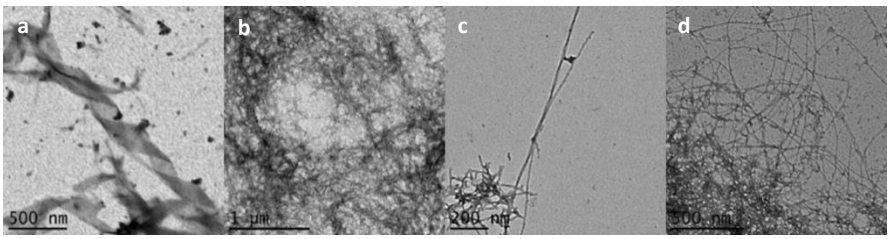

Figure 5.3.3.11: TEM images of (**a**) WT peptide, (**b**) **F19_I**, (**c**) **F19,20_I** and (**d**) **F20_I** aggregates after incubation of 1 week at pH=7. The analysis was applied to previous samples used for NT growth (at pH=2) after having taken them to pH=7.

5.3.4 Fluorescence quenching kinetic assays

The TAMRA fluorescence quenching assay to monitor the $A\beta_{16-22}$ aggregation was developed by Bunce[1], whose protocol was completely followed for our synthesized peptides with the exception of the sample incubation step. In fact, differently from Bunce, who had incubated the TAMRA-spiked peptide solution in ammonium bicarbonate before the introduction into the cuvette, the solution was dripped in it once already placed in the spectrofluorimeter and then the buffer jetted in with a micropipette in order to mix them rapidly. The acquisition was started just after few seconds of mixing. This improved protocol allowed us to monitor the initial seconds of the self-assembly process, which is crucial and very important over the employed timescale.

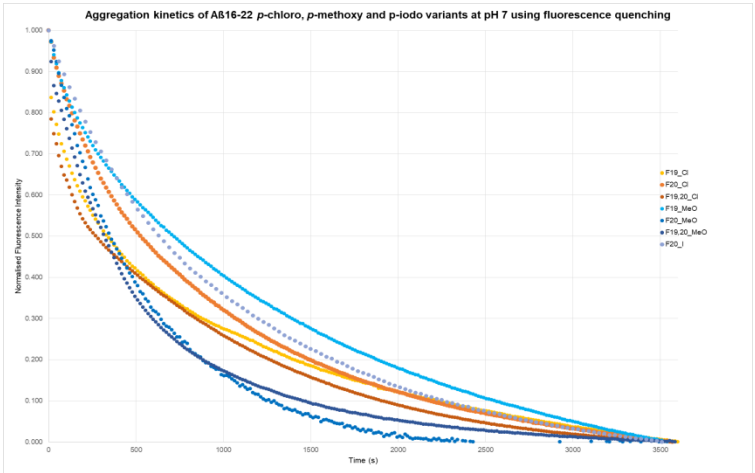

	WT	F19_Cl	F20_Cl	F19,20_Cl	F19_MeO	F20_MeO	F19,20_ MeO	F20_I
Kfast ($hour^{-1}$)	40.5	43.5	31.6	142.9	3.1	36.5	41.2	34.4
Kslow ($hour^{-1}$)	3.5	3.2	3.6	3.6	3.1	6.6	4.3	3.6

Figure 5.3.4.1: A) Normalized fluorescence intensity decay over time in TAMRA fluorescence quenching assay; **B**) Summary table kinetic constants obtained with Prism8 through two-decay fitting model[56].

Fluorescence intensity data were plotted with Prism8 with non-linear fit two-decay model, in which the plateau was constrained to zero[56]. In **Figure 5.3.4.1B** are illustrated calculated kinetic rate constants. As it can be seen in **Figure 5.3.4.1A**, all peptides tested shows a dramatic fast decrease in fluorescence intensity over 5 minutes, which is followed by a slower phase that plateaued after 1h. The initial phase, as anticipated in **paragraph 5.1.5**, is characterized by fast association of monomers in aggregates dominated by first nucleation, but as long as the monomer concentration decreases, first nucleation decreases as well and so a next slower phase is observed. This last phase essentially corresponds to intermediate/lag phase in which secondary nucleation and reorganization/aggregation of already formed oligomers occur without further significant fluorescence decrease[21]. This particular behaviour is clearly seen in **F19,20_Cl** variant since a break point is seen after the first three minutes and half, which is a real proof of the change in self-assembly mechanisms. Along this, the high value of **F19,20_Cl** variant Kfast is evidence, in comparison with WT peptide, **F19_Cl** and **F20_Cl**, of the cooperative effect of chloride atoms in fibrils aggregation kinetics.

Moreover, comparing chloro derivatives with OMe derivatives, **F19_Cl** substitution seems to increase the initial rate of $A\beta_{16-22}$ aggregation. Comparing **F20_Cl** and **F20_I** derivatives, no significant differences are observed in aggregation. Due to the higher steric hindrance of iodine atom, the overall effect is caused by a combination of hydrophobic and steric factors. In other words, probably **F20_I** derivative tends to aggregate faster than **F20_Cl**, but at the same time it is slowed down by the bulky iodide atom which prevents maximization of contacts. Of course, for the time being, no further considerations can be drawn onto iodo derivatives, since it could not have been possible to purify other variants yet.

Considering that electron-withdrawing substitutions decrease π-electron density favouring the π-π stacking configuration[57], the FF motif is the main driving factor of whole process and considering that dimer formation is considered the rate-determining step, it can be rationalized how fast is the first nucleation of **F19,20_Cl** variant. In addition, this behaviour can be interpreted by hydrophobic effect: in fact the more hydrophobic Cl moiety seems to increase aggregation, while the less hydrophobic OMe moiety seems to decrease it. All these findings are in agreement with Senguen et al.'s work[5], in which the initiation process is described as a desolvation/pairing phase of hydrophobic core, where the predominant effect even here is given by F19 contribute. Our study is just preliminary to confirm it, in future new variants will be synthesized.

The same experiment was carried out also at pH=2, whose assay theoretically could provide further information on the electrostatic contributions and mechanism onto nanotube self-assembly. In particular in these attempts chloro and **F20_I** derivatives were tested. During the first three minutes of acquisition it was observed a strange initial increase in fluorescence intensity, which could not be explained by light entering the fluorimeter before the closure of the sample compartment. After this experimental evidence, brief literature research has been

carried out on the topic and it has been found that TAMRA fluorophore at acidic pH shows a dramatic increase in fluorescence intensity[58]. So for this reason, probably the initial increase could be attributed to a sudden change in TAMRA protonation state and relative fluorescence properties. Following this initial step, a very complicated situation was observed. This non-exponential behaviour could be related to non-equilibrated TAMRA in solution or to compresence of fibrils and freshly-forming nanotubes by thermodynamic rearrangement of fibrils themselves. EM images of **F19_Cl** show some fibrils, which might support the theory previously explained.

5.3.5 Synthesis of amine-bearing calix[4]arenes

Since we have largely told about the high importance of hydrophobic interactions in amyloid aggregation, we thought that a way to enhance their contributes might be couple $A\beta_{16-22}$ sequence onto a preorganized scaffold such as calixarenes. Theoretically the scaffold in cone geometry should keep the sequences close together in aggregate-like disposition, which hence is much more inclined to sequestrate further amyloid. In this perspective, we propose the synthesis of two different scaffolds: a polar calix[4]arene functionalized in positions 5 and 17 with amino groups and fully functionalized at lower rim with ethoxyethyl chains and a more apolar calix[4]arene functionalized in positions 25 and 27 with propylamine chains and in positions 26 and 28 with propyl chains. In **Figure 5.3.5.1** the reaction scheme is reported of the synthesis of compound **80**. For the synthesis of compound **50b** see Chapter3.

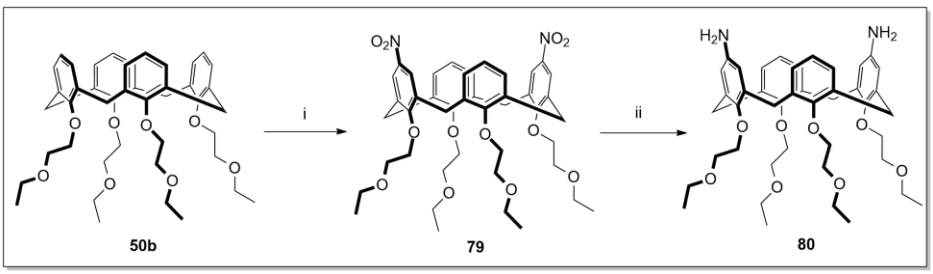

Figure 5.3.5.1: Synthesis of compound **80**. *Reaction conditions:* i) 90% HNO_3 (15.0 eq), glacial CH_3COOH (29.4 eq), DCM, rt , 1h (12% yield); ii) $NH_2NH_2 \cdot H_2O$ (10.4 eq), 10% Pd/C (catalytic amount), absolute EtOH, reflux, 3h (72% yield).

Compound **50b** was double nitrated with 90%HNO_3 in glacial CH_3COOH/DCM for 1h at room temperature. The reaction itself is very simple, except for the purification step. Two flash chromatography columns have been necessary (sequentially in Hex/AcOEt 6:4 and DCM/AcOEt 98:2→97:3) to remove impurities (mononitro and proximal 5,11-dinitro derivatives). Followed a recrystallization after solubilisation in hot MeOH and the bright white crystals obtained were characterized by ^{1}H-NMR. The difficult purification and the regioselectivity issues are factors responsible of the low yields of reaction. To obtain compound **80**, the nitro groups were classically reduced by hydrazine. Compound **80** was obtained in high yields and then characterized by ^{1}H-NMR.

5.3.6 Synthesis of fully-protected peptides and coupling attempts with amine-bearing calix[4]arenes

$A\beta_{16-22}$ sequence contains amino acids bearing amine and carboxy side chains, which would be available for oligomerization or coupling with calixarenes. Then this would result in a very complex mixture with a very small amount of the target molecule. For this reason, in our preliminary study, we proposed a fully-protected peptide strategy (**Figure 5.3.6.1**), which guarantees to have just the carboxy terminus free for the coupling, whereas all the other functions are kept protected, even after cleavage from resin.

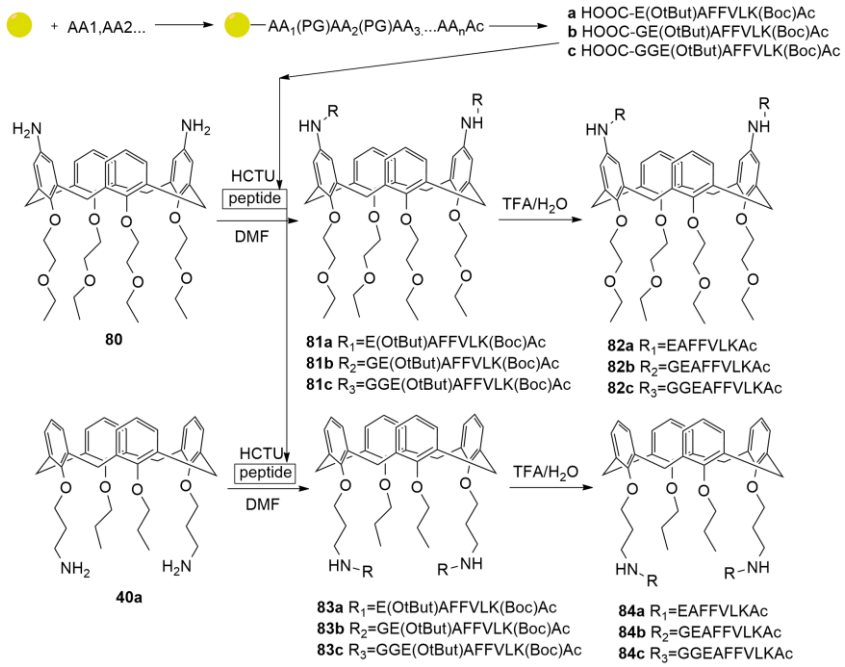

Figure 5.3.6.1: Synthesis strategy for Aβ16-22 calix[4]arene-based sequestrants.

For this aim, 2-chlorotrityl resin was employed, which has been widely used for these purposes in literature[59]. In past, in our laboratories, it was demonstrated that peptide chains at the upper rim of calixarene cannot interact entirely each other, if not outdistanced enough from the macrocycle scaffold. So for this reason, besides the synthesis of WT-$A\beta_{16-22}$ (**a**), we proposed the synthesis of the same sequence with 1 (**b**) or 2 glycine units (**c**) at C-terminus, which were manually added via Fmoc/tBut-Boc strategy through ex-novo synthesis. Since the employed resin is very sensitive to acid, capping step with Ac_2O after coupling was avoided and the terminal Lys was bought as Lys(Boc)Ac. All peptides were cleaved from the resin with 2 washes of 30 minutes each one with HFIP/DCM 1:4 solution, which produces light acidic conditions. The crude was obtained with a yield of 40% with good purity. As example, in **Figure 5.3.6.2** it is reported the UPLC-ESI-MS trace of compound **a**, which shows the purity of peptide itself.

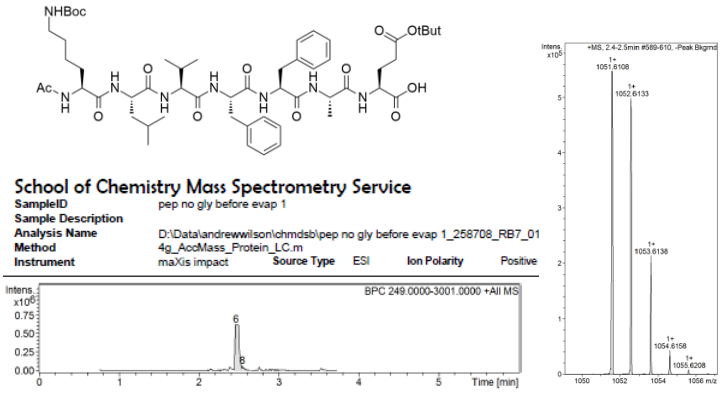

Figure 5.3.6.2: UPLC-MS traces for fully-protected peptide **a**.

The synthesis of these peptides was tried also onto Liberty Blue Automated Microwave Peptide Synthesizer CEM, but several issues were encountered, for example stacking of the resin inside the lines, temperature dependent couplings, unexpected low yields (2%), sensitivity of resin to coupling agent acidity (e.g. Oxyma). Using the manual line transfer, adding 0.1M DIPEA in coupling mixture and doing coupling at room temperature, an improvement in Fmoc deprotection UV traces was observed, but not in yields. Probably the residual acidity present inside the synthesizer, coming from in situ cleavage usage, makes this method not suitable for the synthesis of these peptides. Due to the high purity of the manually-synthetized peptides, some coupling attempts were done on calixarene scaffold directly using the crude.

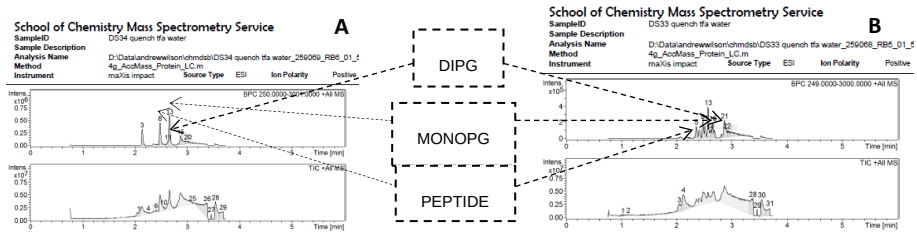

Figure 5.1.8.3: UPLC-MS traces of crudes, quenched with acid, related to coupling attempts between peptide **a** and compound **40a**. Two different coupling agents in DMF were tested: **A**) PyBop; **B**) HCTU. Signals for monofunctionalized (**DIPG**), difunctionalized (**MONOPG**) and compound **a** as fully-protected peptide were observed.

In particular, preliminary tests were made with the peptide **a** with calixarene **40a** and using PyBOP and HCTU as coupling agents and DMSO or DMF as solvents. In **Figure 5.1.8.3** are reported HighResolutionMass traces obtained after 1-week reaction and after quenching with water and TFA. The reactions were carried out in UPLC-MS vials and mixed on peptide shaker. As it can be seen, even if an excess of TFA was added in the remaining DMF, it does not seem to be able to deprotect all the side-chain protecting groups. Therefore, since the deprotection of the peptide did not occur, we proceeded with the purification. The crudes were injected in a preparative C18 HPLC column, but unfortunately, no signal was observed in UV chromatogram. This probably is related to the high hydrophobicity of the compound which was completely retained in column.

Actually also a coupling between compound **80** and peptide **a** with HCTU was tried, but unfortunately this reaction was even worse than the previous ones since no coupled products were observed, but only reactants. Probably here the problem is the fact that aromatic amines are poorly reactive and are not enough available for the coupling.

5.4 Conclusions

Fibrils aggregation has been defined as the cause of neuropathy in amyloidogenic diseases such as Alzeheimer's and Parkinson's diseases. In particular, in Alzeheimer's disease, $A\beta_{40}/A\beta_{42}/A\beta_{43}$ are the fragments, released by Amyloid Precursor Protein (APP), responsible of fibril aggregation in nerves. Considering that studying amyloid aggregation with these full-length peptides would be very unconfortable because of their difficult synthesis and fast degradation, recent studies aimed to identify model peptidic sequences able to behave in the same way as the full-length ones. Several computational studies have demonstrated that $A\beta_{16-22}$ is the smallest sequence that can be chosen to create reliable tools for understanding mechanisms underneath fibril formation. Taking into account that the whole process is driven by interstrand hydrophobic interactions, mainly by means of FF pairing, introducing proper chemical modifications onto FF core would be a very interesting method to study aggregation.

In this project it has been synthetised a combinatorial library of $A\beta_{16-22}$ peptides, in which FF core was functionalized with I, Cl and OMe groups in order to make derivatives progressively less hydrophobic. Starting from Rink Amide resin all the peptides were synthetized via automatic SPPS with acetylated N-terminus, cleaved and then purified through HPLC in good yields. In order to determine their aggregating properties at physiological pH, peptides were incubated in bicarbonate buffer for 1-2 weeks. From TEM analysis what came out is that iodo derivatives are responsible of formation of aggregates more cluttered than the fibrillary-like ones observed for WT, chloro- and methoxy-derivatives. The same peptides were grown also in acidic pH to generate nanotubes. Just in the case of iodo derivatives were observed mature nanotubes, whereas in other cases were observed only ribbon-like structures. These two evidence suggest that probably the increased hydrophobicity of iodo derivatives fasten the aggregation process. Moreover, for mature nanotubes obtained from iodo derivatives it was observed that going back to physiological pH after 1 week of incubation nanotubes are reconverted to fibrils.

To study the relative kinetics of aggregation the derivatives were synthetised again with a TAMRA fluorescent label linked to the peptidic scaffold with an aminohexanoic acid linker (AhX). TAMRA was synthetised ex-novo via two-step strategy and eventually activated as N-succinimide ester. Activated TAMRA was coupled to the peptides on resin through the free amino group released from Fmoc deprotection of AhX. Because of purification issues, were purified F20_I, chloro- and methoxy-TAMRA-labelled derivatives. The Quenching Fluorescence assays showed that $A\beta_{16-22}$ peptide variants exhibit two phase aggregation kinetics. The first phase is characterised by a rapid decrease in fluorescence within ~5 minutes. This is followed by a slower second phase, which plateaus around ~1 hour. Comparison of the aggregation kinetics for the $A\beta_{16-22}$ structural variants indicated that increasing sequence hydrophobicity enhances the initial rate of peptide self-assembly, which is in agreement with what observed with TEM

analysis. This effect is more pronounced with substitution at position 19 than at position 20, which suggests a dominant role for F19 in self-assembly.

In future will be concluded the synthesis of TAMRA-labelled iodo derivatives and tested in Fluorescence Quenching Assays in order to complete the library. In addition, a more rationale time-course TEM analysis along with Time-resolved anisotropy experiments at different pH will be done in order to study better the aggregation of all derivatives.

Considering the well-known potentiality of calixarenes as scaffolds for the synthesis of highly preorganized molecules, we proposed also to couple WT-$A\beta_{16-22}$ onto upper-rim- and lower-rim-difunctionalized calix[4]arenes with amine moieties in cone conformation to create potential $A\beta_{16-22}$ sequestrating tools. For the synthesis WT-$A\beta_{16-22}$, trityl resin was employed since gives the possibility to cleave the peptide in mild acidic conditions as carboxylic acid at C-terminus without deprotecting side chains. This is essential in the coupling with diaminocalixarenes since just terminal free-COOH must react. The fully-protected $A\beta_{16-22}$ was synthetized as WT sequence, but also with 1 or 2 Gly spacer in the optic to outdistance the recognition portion away from the calixarene scaffold. The synthesis was carried out manually with a Fmoc/tBut strategy after some failing attempts on automatic synthetiser. All the peptides were cleaved in mild conditions (HFIP/DCM 1:4) giving crudes characterized by high purity. Some preliminar coupling of WT-$A\beta_{16-22}$ onto calixarene **40a** and **80** were done. The presence of dipeptide- and monopeptide-calix[4]arene was confirmed by UPLC-MS. Unfortunately due to the complete retention in C18-HPLC, these derivatives could not be purified.

In future $A\beta_{16-22}$ will be coupled to calix[4]arene **40a** and **80** through polar spacers. This, theoretically, should increase the polarity of final derivatives making possible their purification with C18-HPLC.

5.5 Experimental part

General information. All chemical reagents were purchased from commercial suppliers and used without further purification. Thin layer chromatography was carried out on commercially available pre-coated aluminium plates (Merck silica 2 8 8 0 Kieselgel 60 F_{254}). Lyophilisation of compounds was performed using a Virtis Benchtop K freeze dryer. Preparative high performance liquid chromatography (HPLC) was performed on an Agilent 1260 Infinity Series equipped with a UV detector and Ascentis Express C_{18} reverse phase column using MeCN/water containing 0.1% formic acid. Analytical HPLC was performed on an Agilent 1290 Infinity Series equipped with a UV detector and a Hyperclone C_{18} reverse phase column using MeCN/water containing 0.1% formic acid, at either 0.5 mL min^{-1} over a period of five minutes or 1.0 mL min^{-1} over a period of 30 minutes. High resolution electrospray (ESI+) mass spectrometry was performed on a Bruker MaXis Impact QTOF mass spectrometer, and *m/z* values are reported in Daltons to four decimal places. LC-ESI-MS data were recorded on an Agilent Technologies 1200 series HPLC combined with a Bruker HCT Ultra ion trap using 50 × 20 mm C_{18} reverse phase columns using MeCN/water (5→95%) containing 0.1% formic acid. A flow rate of 1.5 mL min^{-1} was used and *m/z* values are given in Daltons to one decimal place. ^{1}H and ^{13}C NMR spectra were recorded in deuterated solvents on a Bruker Avance 500, Bruker Avance DPX 400 or Bruker Avance DPX 300. Chemical shifts are quoted in parts per million downfield of

tetramethylsilane and referenced to residual solvent peaks ($CDCl_3$: ^1H = 7.26 ppm, ^{13}C = 77.16 ppm, DMSO-d_6: ^1H = 2.50 ppm, ^{13}C = 39.52 ppm) and coupling constants (*J*) are reported to the nearest 0.1 Hz.

Fluorophore synthesis

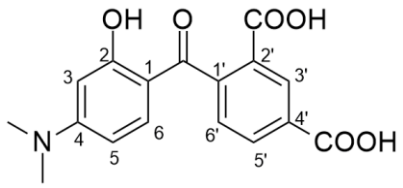

4-dimethylamino-2-hydroxy-2',4'-dicarboxy-benzophenone (71): To a solution of 3-dimethylaminophenol (0.50 g, 3.64 mmol) in toluene (11 mL), previously heated to 60 °C, pounded benzene-1,2,4-tricarboxylic anhydride (0.84 g, 4.37 mmol) was added in and the reaction mixture was stirred for 1 day at reflux. The reaction mixture was let cool to room temperature, then the residue was filtered, washed with toluene (3 × 5 mL), redissolved in MeOH (20 mL) and refluxed for 10 minutes. Then, acetic acid (6 mL) was added in and the mixture was evaporated to dryness. The solid was recrystallized from MeOH (10 mL) to get compound **71** as a purple crystalline powder (0.32 g, 0.97 mmol, 27% yield). **^{1}H NMR** (400 MHz, DMSO- d_6) δ (ppm): 13.40 (s, 1H, COO*H*), 12.37 (s, 1H, 2-O*H*), 8.49 (d, *J* = 1.6 Hz, 1H, 3'-C*H*), 8.21 (dd, *J* = 7.9, 1.6 Hz, 1H, 5'-C*H*), 7.53 (d, *J* = 7.9 Hz, 1H, 6'-C*H*), 6.81 (d, *J* = 9.1 Hz, 1H, 6-C*H*), 6.22 (dd, *J* = 9.1, 2.4 Hz, 1H, 5-C*H*), 6.12 (d, *J* = 2.4 Hz, 1H, 3-C*H*), 3.02 (s, 6H, N-CH_3). **^{13}C NMR** (125 MHz, DMSO-d_6) δ (ppm): 197.6 (*C*(O)-ketone), 166.1 (*C*(O)OH-2', *C*(O)OH-4'), 164.2 (*C*-2), 155.8 (*C*-4), 143.7 (*C*-1'), 133.8 (*C*H-6), 132.6 (*C*H-5'), 131.6 (*C*-2' or *C*-4'), 130.7 (*C*H-3'), 130.0 (*C*-2' or *C*-4'), 128.2 (*C*H-6'), 109.4 (*C*-1), 104.5 (*C*H-5), 97.0 (*C*H-3). **IR** (neat, ν_{max}/cm^{-1}) 2937, 1729 (C=O), 1633 (C=O), 1495, 1350, 1212. **ESI-HRMS (-):** calcd. for $C_{17}H_{14}NO_6$ [$(M-H)^-$]: m/z 328.0827, found m/z 328.0827. **M.p.:** 251.5 °C

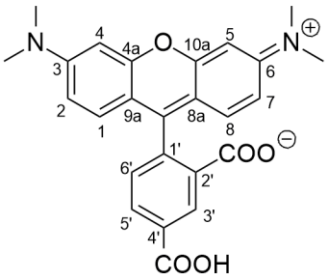

3,6-bis(dimethylamino)-9-[4-carboxy-2-carboxylatephenyl]xanthylium (72): To a solution of compound **71** (0.70 g, 2.13 mmol) in DMF (20 mL), 3-dimethylaminophenol (0.38 g, 2.77 mmol) and trimethylsilylpolyphosphate solution in chloroform (1.600 mL, prepared according to Yokoyama *et al.*[52]) were added in. The reaction mixture was stirred at reflux for 3 hours in the dark. The solvents were removed by reduced pressure, and the residue was dissolved in an aqueous solution of 5% NaOH (20 mL) and stirred at room temperature for 20 hours. The solution was diluted with H_2O (35 mL) and the rhodamine was precipitated with 37% HCl (2 mL).

The solid was filtered, washed with H_2O (20 mL) to get compound **72** as a dark purple solid (0.90 g, 2.09 mmol, 98% yield). **^{1}H NMR** (400 MHz, DMSO-d_6) δ (ppm): 8.51 (s, 1H, COO*H*), 8.35 (s, 1H, 3'-C*H*), 8.25 (d, *J* = 7.9 Hz, 1H, 5'-C*H*), 7.09 (d, *J* = 7.9 Hz, 1H, 6'-C*H*), 6.54 – 6.44 (m, 6H, 1,2,4,5,7,8-C*H*), 2.94 (s, 12H, N-CH_3). **^{13}C NMR** (125 MHz, d_4-MeOD) δ (ppm): 173.7 (*C*(O)OH-4'), 173.2 (*C*(O)OH-2'), 160.0 (*C*-9), 158.8 (*C*-4a, *C*-10a), 158.4 (*C*-3, *C*-6), 140.8 (*C* 1'), 136.4 (*C*-2', *C*-4'), 132.7 (*C*H-1, *C*H-8), 131.7 (*C*H-3'), 131.3 (*C*H-5'), 129.8 (*C*H-6'), 114.69, 114.65, (*C*H-2, *C*H-7, *C*-8a, *C*-9a), 97.3 (*C*H-4, *C*H-5), 47.5 (*C*H_3-N), 40.8 (*C*H_2-N), 9.2 (*C*H_3-CH_2). **IR** (neat, ν_{max}/cm^{-1}) 2978, 2604, 1745, 1633, 1344, 1246, 1118; . **ESI-HRMS (+):** calcd. for $C_{25}H_{22}N_2NaO_5$ [(M+Na)$^+$]: m/z 453.1421, found m/z 453.1426.

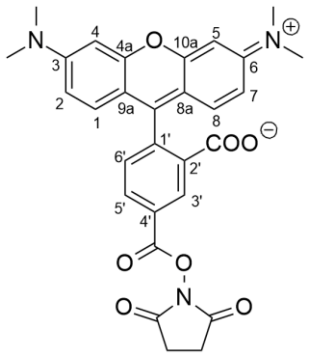

2,5-dioxopyrrolidin-1-yl 3',6'-bis(dimethylamino)-3-oxo-3H-spiro[isobenzofuran-1,9'-xanthene]-5-carboxylate (named as closed form) (73): To a solution of compound **72** (0.38 g, 0.89 mmol) in DCM (50 mL) was added DMAP (0.55 g, 4.46 mmol) and NEt_3 (622 µL, 4.47 mmol). N-disuccinimidyl carbonate (0.46 g, 1.79 mmol) was added and the reaction mixture was stirred for 1 hour at room temperature, monitoring it by TLC (AcOH-Acetone 1:100, R_f=0.10). The reaction was quenched with acetic acid (600 µL), reduced in volume *in vacuo* (to 2 mL), loaded onto an equilibrated flash chromatography column and eluted with AcOH-Acetone 1:100 to get compound **73** as a dark purple solid (0.43 g, 0.82 mmol, 92% yield). **^{1}H NMR** (500 MHz, $CDCl_3$) δ (ppm): 8.79 (d, *J* = 1.5 Hz, 1H, 3'-C*H*), 8.36 (dd, *J* = 8.1, 1.5 Hz, 1H, 5'-C*H*), 7.33 (d, *J* = 8.1 Hz, 1H, 6'-C*H*), 6.57 (d, *J* = 9.0 Hz, 2H, 1-C*H*, 8-C*H*), 6.49 (d, *J* = 2.5 Hz, 2H, 4-C*H,* 5-C*H*), 6.41 (dd, *J* = 8.9, 2.5 Hz, 2H, 2-C*H,* 7-C*H*), 3.09 (s, 4H), 3.01 (s, 12H, N-CH_3). **^{13}C NMR** (125 MHz, $CDCl_3$) δ (ppm): 176.6 (*C*(O)OH-2'), 169.1 (*C*(O)-NHS), 168.2 (*C*(O)O-4'), 161.0 (*C*-9), 153.5 (*C*-4a, *C*-10a), 153.0 (*C*-3, *C*-6), 135.7 (*C*-1'), 129.1 (*C*H-1, *C*H-8), 128.3 (*C*H-3'), 126.6 (*C*H-5'), 125.7 (*C*H-6'), 109.6 (*C*H-2, *C*H-7), 106.5 (*C*-8a, *C*-9a), 98.4 (*C*H-4, *C*H-5), 40.4 (*C*H_3-N), 25.8 (*C*H_2-NHS), *C*-2' and *C*-4' not observed. **IR** (neat, ν_{max}/cm^{-1}) 3392, 2924, 1703, 1588, 1340, 1182. **ESI-HRMS (+):** calcd. for $C_{29}H_{26}N_3O_7$ [(M+H)$^+$]: m/z 528.1765, found m/z 528.1764.

Peptide synthesis

General information. All amino acids and resins were purchased from either Novabiochem (Merck) or Sigma-Aldrich. All amino acids were *N*-Fmoc protected and side chains protected with Boc (Lys); ^{t}Bu (Glu); ^{t}Bu (Thr); Trt (Gln); Arg (Pbf). Synthesis of all peptides for fibrils and relative capping was performed using a microwave-assisted automated peptide synthesiser

(CEM, Liberty Blue). Synthesis of peptides for parallel β-sheet calixarene was performed manually. DMF, used in peptide synthesis, was of HPLC grade and bought from Sigma Aldrich. Lyophilisation was performed using a BenchTop Pro with Omnitronics^{TM} (VirTis SP Scientific). Preparative HPLC was performed on an Agilent Technologies 1260 infinity controller in conjunction with a diode array detector with eluents of HPLC grade. Water used for buffers and HPLC was ultrapure 18 MΩ prepared using an Elga PURELAB purification system. Analytical HPLC was performed on an Agilent Technologies 1260 infinity controller in conjunction with a diode array detector. Mass spectrometry data were obtained on a Bruker Daltonics microTOF using electrospray ionisation (ESI) MS instruments as appropriate. Liquid chromatography-mass spectrometry (LC-MS) was performed using an Agilent 1290 series HPLC system and Bruker HCT-Ultra mass spectrometer. HRMS was performed using a Bruker MicrOTOF mass spectrometer. 1H NMR spectroscopy was performed using a Bruker AVANCE III HD-400 (400 MHz) spectrometer.

Procedure for automated SPPS

Resin Loading: Clean reaction vessel; wash with DMF; transfer resin to reaction vessel; wash with DMF:DCM (1:1); vessel draining.

Deprotection and Coupling: Add 20% piperidine in DMF (4 mL); microwave method (30 sec); wash with DMF (4 × 4 mL); drain; add amino acid (2.5 mL); add coupling reagent DIC (1 mL); add Oxyma base (0.5 mL); microwave method (75°C, 4'); wash through manifold to waste (2 mL); drain. After the final acetylation capping, the resin was ejected from the reaction vessel and cleavage and deprotection were performed manually using method E.

Methods for manual solid phase *N*-terminal chain elongation and capping

Method A: Deprotection of N-Fmoc protecting groups

N-terminal Fmoc protecting groups were removed by the addition of 20% piperidine: DMF (2 × 2 mL × 8 min), followed by rinsing the resin with DMF (5 × 4 mL). Successful deprotection was determined by a positive colour test (Method C).

Method B: Activation and coupling

Dissolve HCTU (5eq) and aminoacid (5eq) in a Falcon tube with DMF (5 ml), add DIPEA (10eq), shake for 2', add to the resin.

Method C: Kaiser Test

The Kaiser test was used to determine successful coupling or deprotection of manually coupled residues. A few beads of resin were placed in a vial, two drops of each solution (1-3, see below) was added to the beads and the solution was heated to 100 °C for 1 minute. Successful coupling was indicated by no change in colour of the beads, whereas successful deprotection was indicated by bright blue beads.

1) Ninhydrin (5% w/v) in ethanol

2) Phenol (80% w/v) in ethanol

3) 1 mM KCN $_{(aq.)}$ in pyridine (2% v/v)

Method D: N-terminal acetylation

Acetic anhydride (10 equiv.) and DIPEA (10 equiv.) were dissolved in DMF (1 mL) and the solution was transferred to the resin. After 2 h, the resin was drained, washed with DMF (3 × 2 mL × 2 min) and successful capping determined by a negative colour test (Method B).

Method E: Cleavage and deprotection of Rink amide MBHA resin

After elongation and *N*-terminal capping were complete, the resin was washed with DMF (3 × 4 mL), DCM (3 × 4 mL), Et_2O (5 × 2 mL × 2 min) and dried under vacuum for 1 h. Peptides were simultaneously cleaved and side-chain deprotected using: TFA/H_2O/TIS 950:25:25 (1 × 2 mL × 3 h) for peptides synthesized on HMBA resin or HFIP/DCM 1:4 for peptides synthesized on preloaded 2-chlorotrityl resin. For peptides synthesized on HMBA resin it was operated as follows: the solution was precipitated in ice-cold Et_2O (50 mL), placed in a centrifuge (3000 rpm × 8 min), the supernatant was removed, the precipitate was washed with ice-cold Et_2O (3 × 30 mL) and finally the washed precipitate was dried under a stream of nitrogen (1 h), before being dissolved in DMSO ready for HPLC purification if needed. For peptides synthesized on preloaded 2-chlorotrityl resin it was operated as follows: the solvent was rapidly removed by reduced pressure and the solid was dissolved in DMSO ready for HPLC purification if needed.

Peptide synthesis procedure

Ac-KLVFFAE-COOH **a**
Ac-KLVFFAEG-COOH **b**
Ac-KLVFFAEGG-COOH **c**

Ac-KLVFFAE-$CONH_2$ **d**
Ac-KLV$_{\beta}$FAE-$CONH_2$ **e**
Ac-KLVFF$_{\beta}$AE-$CONH_2$ **f**
Ac-KLV$_{\beta}$F$_{\beta}$AE-$CONH_2$ **g**

TAMRA-Ahx-KLVFF$_{\beta}$AE-$CONH_2$ **h**

Peptides **a**-**c** were manually synthesised on a 0.9447 mol scale on 2-chlorotrityl resin (for G-preloaded resin, 0.79 $mmolg^{-1}$; for E-preloaded resin, 0.67 $mmolg^{-1}$) using procedures described before. As last aminoacid, a capped Lys was used (Ac-Lys-OH). At the end of the synthesis, the peptide was simultaneously cleaved and side-chain deprotected using Method E. Due to their high hydrophobicity, peptides **a**-**c** were not purified. **UPLC-ESI-TOF (+)** (**a**): calcd. for $C_{54}H_{83}N_8O_{13}$ $[(M+H)^+]$: m/z 1051.6000, found 1051.6108. **ESI-MS (+)** (**b**) as **fully deprotected**): calcd. for $C_{47}H_{70}N_9O_{12}$ $[(M+H)^+]$: m/z 952.51, found 952.77; calcd. for $C_{47}H_{71}N_9O_{12}$ $[(M+2H)^{2+}]$: m/z 476.76, found 476.82. **UPLC-ESI-TOF (+)** (**c**): calcd. for $C_{58}H_{89}N_{10}O_{15}$ $[(M\text{-}CH_3C{=}O{+}H)^+]$: m/z 1165.64, found 1165.6523; calcd. for $C_{47}H_{71}N_9O_{12}$ $[(M+2H)^{2+}]$: m/z 476.76, found 476.82. The purity wasn't assessed by analytical HPLC, so they were used in the calixarene coupling as themselves.

Peptides **d**-**g** were automatically synthesised on a 0.25 mmol scale on rink amide MBHA resin (0.810 $mmolg^{-1}$) using procedures described before, including in the automatic cycle the acetylation capping (Method D). The resin was transferred into SPPS Teflon reactors, drained, dried and then cleaved and side-chain deprotected using Method E. Peptides **d**-**g** were purified using UV-directed HPLC over a gradient of 10-40% acetonitrile in H_2O + 0.1% HCOOH to give **d** (30% yield), **e** (35% yield), **f** (28% yield) and **g** (29%yield). **ESI-MS (+)** (**1b**): calcd. for $C_{44}H_{64}N_9O_{11}$

$[(M+H)^+]$: m/z 894.46, found 894.67. **UPLC-ESI-TOF (+)** (**d**): calcd. for $C_{44}H_{64}N_9O_{11}$ $[(M+H)^+]$: m/z 894.46, found 894.5059. **ESI-MS (+)** (**e**): calcd. for $C_{44}H_{63}IN_9O_{11}$ $[(M+H)^+]$: m/z 1020.36, found 1020.58; calcd. for $C_{44}H_{64}IN_9O_{11}$ $[(M+2H)^{2+}]$: m/z 510.78, found 510.73. **UPLC-ESI-TOF (+)** (**e**): calcd. for $C_{44}H_{63}IN_9O_{11}$ $[(M+H)^+]$: m/z 1020.36, found 1020.4155. **ESI-MS (+)** (**f**): calcd. for $C_{44}H_{63}IN_9O_{11}$ $[(M+H)^+]$: m/z 1020.36, found 1020.58; calcd. for $C_{44}H_{64}IN_9O_{11}$ $[(M+2H)^{2+}]$: m/z 510.78, found 510.73. **UPLC-ESI-TOF (+)** (**f**): calcd. for $C_{44}H_{63}IN_9O_{11}$ $[(M+H)^+]$: m/z 1020.36, found 1020.3974; calcd. for $C_{44}H_{64}IN_9O_{11}$ $[(M+2H)^{2+}]$: m/z 510.78, found 510.7068. **ESI-MS (+)** (**g**): calcd. for $C_{44}H_{61}I_2N_9O_{11}$ $[(M+H)^+]$: m/z 1146.26, found 1146.46; calcd. for $C_{44}H_{62}I_2N_9O_{11}$ $[(M+2H)^{2+}]$: m/z 573.63, found 573.70. **UPLC-ESI-TOF (+)** (**g**): calcd. for $C_{44}H_{61}I_2N_9O_{11}$ $[(M+H)^+]$: m/z 1146.26, found 1146.2944; calcd. for $C_{44}H_{62}I_2N_9O_{11}$ $[(M+2H)^{2+}]$: m/z 573.63, found 573.6559. **Analytical HPLC**: purity≥95% (for all peptides).

Peptide **h** were synthesised on a 0.1 mmol scale on rink amide MBHA resin (0.810 $gmol^{-1}$) using procedures described before, including in the automatic cycle the spacer Fmoc-Ahx-OH too. TAMRA coupling was performed pouring a solution of compound **73** (1.5 eq) and NEt_3 (2 eq) in DMF (600 ul) onto the resin and shaking for 3 days. After removal of the reagents by filtration, the resin was washed with DMSO (3 × 4 mL), DMF (3 × 4 mL) and the success of coupling determined by a negative colour test (Method C). The peptide was simultaneously cleaved and side-chain deprotected using Method E. Peptide (series **c**) was purified using UV-directed HPLC over a gradient of 10-50% acetonitrile in H_2O + 0.1% HCOOH to give **h** (2% yield). **UPLC-ESI-TOF (+)** (**h**): calcd. for $C_{73}H_{92}IN_{12}O_{15}$ $[(M+H)^+]$: m/z 1502.58, found 1502.6127; calcd. for $C_{73}H_{93}IN_{12}O_{15}$ $[(M+2H)^{2+}]$: m/z 752.29, found 752.3140. **Analytical HPLC**: purity≥95%.

Peptide purification. Peptides **d**-**g** were purified by preparative UV-directed Gilson HPLC using an XBridge column preparative on an increasing gradient of acetonitrile in water + 0.1% HCOOH (v/v) at a flow rate of 10 $mLmin^{-1}$. Crude peptides were suspended in DMSO at an approximate concentration of 20 mg mL^{-1}. Purification runs injected a maximum of 0.4 mL of crude peptide solution and were allowed to run for 30 min, with acetonitrile increasing at a stated gradient. Fractions were collected by peak-based detection using fixed-wavelength UV detector scanning at 280 nm. To assess the presence of desired peptide tubes were checked with Bruker Daltonics microTOF Fractions containing purified peptide were combined, concentrated *in vacuo*, lyophilised and stored at -20°C. Peptide purity was analysed by Martin Huscroft (HPLC Technician, School of Chemistry) using an Ascentis Peptide C18 column.

General method for fluorescence quenching assays. Wild type $A\beta_{16-22}$ was spiked with TAMRA-Ahx-$A\beta_{16-22}$ at 5% and incubated in 100 mM ammonium bicarbonate, pH 7 with a final concentration of 2% DMSO (v/v). The total peptide concentration was 40 µM. Samples were placed in quartz cuvettes (Helma QS Quartz, 1 cm path length) and analysed using a temperature-controlled (Quantum Northwest PC425 Peltier controller) Quantamaster fluorimeter (Photon Technical Industries, Canada) at 37 °C. Kinetic measurements were taken every 30 s for the duration of the experiment (in triplicate). The TAMRA fluorophore was excited at 520 nm and emission recorded at 600 nm to reduce the inner filter effect. Slit widths were 0.3 nm for excitation and 5 nm for emission.

The following procedure was used for the analysis:

1. 2mM stock solution in DMSO was prepared for either peptide or TAMRA-labelled peptide

2. From stock solution a solution 5:95 TAMRA-labelled peptide:peptide in DMSO was made

3. 8ul of this solution were injected in the cuvette followed by 400ul of 100mM NH_4HCO_3 buffer solution (in the case of NTs, add 40% ACN/H_2O + 0.1%TFA)

Aggregation protocol for $A\beta_{16-22}$ phase diagram. $A\beta_{16-22}$ was diluted from a DMSO stock solution (30 mM) to the required concentration (10 – 300 µM) in 100 mM ammonium bicarbonate buffer (pH 7) into 1ml-ependorf tube at room temperature. Final DMSO concentration was kept at 1% (v/v) in all assays. After a week and two weeks, aliquots were taken for TEM analysis.

TEM analysis

Preparation protocol. TEM images were taken at the end of each experiment by removing 5 µL from the necessary eppendorf and incubated on carbon-formvar grids (previously glow-discharged using Pelco easiGlow) for 1 min prior to staining with 2% (w/v) uranyl acetate solution (5 ul) for an additional 30s. After having removed the excess of uranyl acetate, a second fast staining step was done in the same way (5 µL for 30 s). In the end the grids were rinsed with ddH_2O (2 x 5 ul) and dried under a halogen lamp. Images were taken on a JEM-1400 (JEOL Ltd., Toyko, Japan) transmission electron microscope. Images were taken using a Gatan Ultrascan 1000 XP (994) CCD camera (JEM-1400). Once taken, images were processed using ImageJ (NIH).

Calixarene synthesis

cone-5,17-dinitro-25,26,27,28-(2-ethoxyethylether)calix[4]arene (79): In a 1-necked round-bottom flask, 90% HNO_3 (50.98 mmol, 2.140 ml) was slowly added into a solution of compound **50b** (3.40 mmol, 2.42 g) and glacial CH_3COOH (0.10 mol, 5.831 ml) in DCM (85 ml), meanwhile the mixture was kept stirring at room temperature. The mixture was left reacting for about 1 h till on TLC (Hex/AcOEt 6:4) di-nitro derivative spot showed up and no reagent was present anymore. The reaction was quenched with H_2O (100 ml) and the mixture was vigorously stirred for 30 minutes. The organic phase was then washed with sat. $NaHCO_3$ (100 ml), brine (80 ml) and H_2O (50 ml) to remove all the acid remained. It was dried with anhydrous Na_2SO_4 and upon filtration, the solvent was removed by reduced pressure. The crude was purified by two subsequent flash chromatography: the first using Hex/AcOEt 6:4 as eluent to isolate dinitro derivatives, the second using DCM/AcOEt 98:2→97:3 as eluent to isolate 5,17-dinitro derivative. To obtain an higher purity the crude was recrystallized from hot MeOH to get compound **79** as bright white needle crystals (0.33 g, 0.41 mmol, 12% yield). **^{1}H NMR** (300 MHz, $CDCl_3$) δ (ppm): 7.69 (s, 4H, Ar*H*), 6.65 - 6.50 (m, 6H, Ar*H*), 4.60 (d, *J* = 13.6 Hz, 4H, ArCH_{ax}HAr), 4.32 (t, *J* = 4.8 Hz, 4H, OCH_2CH$_2$OCH$_2$CH$_3$), 4.09 (t, *J* = 4.9 Hz, 4H, OCH_2CH$_2$OCH$_2$CH$_3$), 3.85 (t, *J* = 4.8 Hz, 4H, OCH$_2$CH_2OCH$_2$CH$_3$), 3.80 (t, *J* = 4.8 Hz, 4H, OCH$_2$CH_2OCH$_2$CH$_3$), 3.56 (q, *J* = 6.8 Hz, 4H,

$OCH_2CH_2OCH_2CH_3$), 3.52 (q, *J* = 6.8 Hz, 4H, $OCH_2CH_2OCH_2CH_3$), 3.27 (d, *J* = 13.6 Hz, 4H, $ArCH_{eq}HAr$), 1.23 (t, *J* = 6.8 Hz, 6H, $OCH_2CH_2OCH_2CH_3$), 1.18 (t, *J* = 6.8 Hz, 6H, $OCH_2CH_2OCH_2CH_3$). The spectroscopic data obtained are in agreement with those ones reported in literature[60].

cone-5,17-diamino-25,26,27,28-(2-ethoxyethylether)calix[4]arene (80): In a 1-necked round bottom flask compound **79** (0.12 mmol, 0.10 g) and $NH_2NH_2 \cdot H_2O$ (1.25 mmol, 0.100 ml) were dissolved in absolute EtOH (3 ml). 10% Pd/C (catalytic amount) was added in and the mixture was stirred for 3 h at reflux, monitoring the reaction by TLC (Hex/AcOEt 1:1). The suspension was filtered off and the catalyst was washed with DCM (2 x 20 ml) and EtOH (2 x 20 ml). The solvent was removed by reduced pressure to get compound **80** as a white powder (66.13 mg, 89.07 umol, 72% yield). **^{1}H NMR** (400 MHz, MeOD) δ (ppm): 6.77 (d, *J* = 7.5 Hz, 4H, Ar*H*), 6.66 – 6.59 (m, 2H, Ar*H*), 6.06 (s, 4H, Ar*H*), 4.49 (d, *J* = 13.2 Hz, 4H, $ArCH_{ax}HAr$), 4.14 (t, *J* = 5.6 Hz, 4H, $OCH_2CH_2OCH_2CH_3$), 4.02 (t, *J* = 5.6 Hz, 4H, $OCH_2CH_2OCH_2CH_3$), 3.91 (t, *J* = 5.6 Hz, 4H, $OCH_2CH_2OCH_2CH_3$), 3.88 (t, *J* = 5.6 Hz, 4H, $OCH_2CH_2OCH_2CH_3$), 3.61 (q, *J* = 7.2 Hz, 4H, $OCH_2CH_2OCH_2CH_3$), 3.58 (q, *J* = 7.2 Hz, 4H, $OCH_2CH_2OCH_2CH_3$), 3.06 (d, *J* = 13.2 Hz, 4H, $ArCH_{eq}HAr$), 1.24 (t, *J* = 7.2 Hz, 6H, $OCH_2CH_2OCH_2CH_3$), 1.21 (t, *J* = 7.2 Hz, 6H, $OCH_2CH_2OCH_2CH_3$). **ESI-MS (+)**: calcd. for $C_{44}H_{58}N_2O_8$ $[M+H]^+$ m/z 743.42, found 743.75 (100%); calcd. for $C_{44}H_{58}N_2O_8Na$ $[(M+Na)^+]$ m/z 765.41, found 765.79 (20%). The spectroscopic data obtained are in agreement with those ones reported in literature[60].

For compound **40a** synthesis see **Chapter3**.

5.6 References

1. Bunce. Understanding the mechanism of peptide self-assembly. (University of Leeds, 2018).

2. Dobson, C. M. Protein folding and misfolding. *Nature* **426**, 884–890 (2003).

3. Cohen, S. I. A., Vendruscolo, M., Dobson, C. M. & Knowles, T. P. J. From macroscopic measurements to microscopic mechanisms of protein aggregation. *Journal of Molecular Biology* **421**, 160–171 (2012).

4. Wang, J., Liu, K., Xing, R. & Yan, X. Peptide self-assembly: Thermodynamics and kinetics. *Chemical Society Reviews* **45**, 5589–5604 (2016).

5. Senguen, F. T. *et al.* Probing aromatic, hydrophobic, and steric effects on the self-assembly of an amyloid-β fragment peptide. *Mol. Biosyst.* **7**, 486–496 (2011).

6. Ma, B. and Nussinov, R. Stabilities and conformations of Alzheimer's ß-amyloid peptide oligomers (Aß16-22, Aß16-35 and Aß10-35): Sequence effects. *Proc. Natl. Acad. Sci. U. S. A.* **99**, 14126–14131 (2002).

7. Reches, M. & Gazit, E. Casting metal nanowires within discrete self-assembled peptide nanotubes. *Science (80-.).* **300**, 625–627 (2003).

8. Jeon, J., Mills, C. E. & Shell, M. S. Molecular insights into diphenylalanine nanotube assembly: All-atom simulations of oligomerization. *J. Phys. Chem. B* **117**, 3935–3943 (2013).

9. Amaral, H.R., Kogikoski Jr., S., Silva, E.R., Souza, J.A. and Alves, W. A. Peptide nanostructures and their interplay with functionalizing agents. (2012). Available at: https://sites.google.com/site/dremersonsilva/research?tmpl=%2Fsystem%2Fapp%2Ftemplates%2Fprint%2F&showPrintDialog=1.

10. Makin, O. S., Atkins, E., Sikorski, P., Johansson, J. & Serpell, L. C. Molecular basis for amyloid fibril formation and stability. *Proc. Natl. Acad. Sci. U. S. A.* **102**, 315–320 (2005).

11. Yang, R. Z. *et al.* Acute-phase serum amyloid A: An inflammatory adipokine and potential link between obesity and its metabolic complications. *PLoS Med.* **3**, 0884–0894 (2006).

12. Hilbich, C., Kisters-Woike, B., Reed, J., Masters, C.L. and Beyreuther, K. Substitutions of Hydrophobic Amino Acids Reduce Amyloidogenicity of Alzheimer's Disease ßA4 Peptides. *J. Mol. Biol.* **228**, 460–473 (1992).

13. Wurth, C., Guimard, N.K. and Hecht, M. H. Mutations that Reduce Aggregation of the Alzheimer's Aß42 Peptide: an Unbiased Search for the Sequence Determinants of Aß Amyloidogenesis. *J. Mol. Biol.* **319**, 1279–1290 (2002).

14. Tjernberg, L. O. *et al.* A molecular model of Alzheimer amyloid β-peptide fibril formation. *J. Biol. Chem.* **274**, 12619–12625 (1999).

15. Serpell, L. C. Alzheimer's amyloid fibrils: Structure and assembly. *Biochimica et Biophysica Acta - Molecular Basis of Disease* **1502**, 16–30 (2000).

16. Eisenberg, D. & Jucker, M. The amyloid state of proteins in human diseases. *Cell* **148**, 1188–1203 (2012).

17. Beta-amyloid and tau in Alzheimer's disease. Available at: https://www.abcam.com/neuroscience/beta-amyloid-and-tau-in-alzheimers-disease.

18. Balbach, J. J. *et al.* Amyloid fibril formation by Aβ16-22, a seven-residue fragment of the Alzheimer's β-amyloid peptide, and structural characterization by solid state NMR. *Biochemistry* **39**, 13748–13759 (2000).

19. Gazit, E. Mechanisms of amyloid fibril self-assembly and inhibition: Model short peptides as a key research tool. *FEBS Journal* **272**, 5971–5978 (2005).

20. Makin, O. S. & Serpell, L. C. Structures for amyloid fibrils. *FEBS Journal* **272**, 5950–5961 (2005).

21. Garai, K. & Frieden, C. Quantitative analysis of the time course of Aβ oligomerization and subsequent growth steps using tetramethylrhodamine-labeled Aβ. *Proc. Natl. Acad. Sci. U. S. A.* **110**, 3321–3326 (2013).

22. Klein, W. L., Krafft, G. A. & Finch, C. E. Targeting small A β oligomers: The solution to an Alzheimer's disease conundrum? *Trends in Neurosciences* **24**, 219–224 (2001).

23. Marina, G. B. *et al.* Amyloid β-protein (Aβ) assembly: Aβ40 and Aβ42 oligomerize through distinct pathways. *Proc. Natl. Acad. Sci. U. S. A.* **100**, 330–335 (2003).

24. Haass, C. & Selkoe, D. J. Soluble protein oligomers in neurodegeneration: Lessons from

the Alzheimer's amyloid β-peptide. *Nature Reviews Molecular Cell Biology* **8**, 101–112 (2007).

25. Liu, C. *et al.* Out-of-register β-sheets suggest a pathway to toxic amyloid aggregates. *Proc. Natl. Acad. Sci. U. S. A.* **109**, 20913–20918 (2012).

26. Nilsson, M. R. Techniques to study amyloid fibril formation in vitro. *Methods* **34**, 151–160 (2004).

27. Gazit, E. Self Assembly of Short Aromatic Peptides into Amyloid Fibrils and Related Nanostructures. *Prion* **1**, 32 (2007).

28. Tenidis, K. *et al.* Identification of a penta- and hexapeptide of islet amyloid polypeptide (IAPP) with amyloidogenic and cytotoxic properties. *J. Mol. Biol.* **295**, 1055–1071 (2000).

29. Mehta, A. K. *et al.* Facial symmetry in protein self-assembly. *J. Am. Chem. Soc.* **130**, 9829–9835 (2008).

30. Lu, K., Jacob, J., Thiyagarajan, P., Conticello, V.P. and Lynn, D. G. Exploiting Amyloid Fibril Lamination for Nanotube Self-Assembly. *J. Am. Chem. Soc.* **125**, 6391–6393 (2003).

31. Kodali, R. & Wetzel, R. Polymorphism in the intermediates and products of amyloid assembly. *Current Opinion in Structural Biology* **17**, 48–57 (2007).

32. Hellstrand, E., Boland, B., Walsh, D. M. & Linse, S. Amyloid β-protein aggregation produces highly reproducible kinetic data and occurs by a two-phase process. *ACS Chem. Neurosci.* **1**, 13–18 (2010).

33. Mancini, O., Wellbrock, T., Rolinski, O. J., Kubiak-Ossowska, K. & Mulheran, P. A. Probing beta amyloid aggregation using fluorescence anisotropy: Experiments and simulation. *Phys. Chem. Chem. Phys.* **20**, 4216–4225 (2018).

34. Smith, A. M., Jahn, T. R., Ashcroft, A. E. & Radford, S. E. Direct Observation of Oligomeric Species formed in the Early Stages of Amyloid Fibril Formation using Electrospray Ionisation Mass Spectrometry. *J. Mol. Biol.* **364**, 9–19 (2006).

35. Cohen, S. I. A. *et al.* Proliferation of amyloid-β42 aggregates occurs through a secondary nucleation mechanism. *Proc. Natl. Acad. Sci. U. S. A.* **110**, 9758–9763 (2013).

36. Törnquist, M. *et al.* Secondary nucleation in amyloid formation. *Chem. Commun.* **54**, 8667–8684 (2018).

37. Murphy, R. M. Kinetics of amyloid formation and membrane interaction with amyloidogenic proteins. *Biochimica et Biophysica Acta - Biomembranes* **1768**, 1923–1934 (2007).

38. Hsieh, M. C., Liang, C., Mehta, A. K., Lynn, D. G. & Grover, M. A. Multistep Conformation Selection in Amyloid Assembly. *J. Am. Chem. Soc.* **139**, 17007–17010 (2017).

39. Xue, C., Lin, T. Y., Chang, D. & Guo, Z. Thioflavin T as an amyloid dye: Fibril quantification, optimal concentration and effect on aggregation. *R. Soc. Open Sci.* **4**,

(2017).

40. Jin, M. *et al.* Soluble amyloid beta-protein dimers isolated from Alzheimer cortex directly induce Tau hyperphosphorylation and neuritic degeneration. *Proc. Natl. Acad. Sci. U. S. A.* **108**, 5819–24 (2011).

41. Meisl, G. *et al.* Molecular mechanisms of protein aggregation from global fitting of kinetic models. *Nat. Protoc.* **11**, 252–272 (2016).

42. Klein, W. L., Stine, W. B. & Teplow, D. B. Small assemblies of unmodified amyloid beta-protein are the proximate neurotoxin in Alzheimer's disease. *Neurobiol. Aging* **25**, 569–80

43. Zhuang, X. *et al.* Fluorescence quenching: A tool for single-molecule protein-folding study. *Proc. Natl. Acad. Sci. U. S. A.* **97**, 14241–14244 (2000).

44. Senguen, F. T., Doran, T. M., Anderson, E. A. & Nilsson, B. L. Clarifying the influence of core amino acid hydrophobicity, secondary structure propensity, and molecular volume on amyloid-β 16-22 self-assembly. *Mol. Biosyst.* **7**, 497–510 (2011).

45. Preston, G. W. & Wilson, A. J. Photo-induced covalent cross-linking for the analysis of biomolecular interactions. *Chem. Soc. Rev.* **42**, 3289–3301 (2013).

46. Preston, G. W., Radford, S. E., Ashcroft, A. E. & Wilson, A. J. Covalent cross-linking within supramolecular peptide structures. *Anal. Chem.* **84**, 6790–6797 (2012).

47. Smith, D. P. *et al.* Trifluoromethyldiazirine: An effective photo-induced cross-linking probe for exploring amyloid formation. *Chem. Commun.* 5728–5730 (2008). doi:10.1039/b813504e

48. Biemann, K. Mass Spectrometry of Peptides and Proteins. *Annu. Rev. Biochem.* **61**, 977–1010 (1992).

49. Coon, J.J., Syka, J.E.P., Shabanowitz, J. and Hunt, D. F. Tandem Mass Spectrometry for Peptide and Protein Sequence Analysis. *Biotechniques* **38**, 519–523 (2005).

50. Williams, A. D., Shivaprasad, S. & Wetzel, R. Alanine scanning mutagenesis of Aβ(1-40) amyloid fibril stability. *J. Mol. Biol.* **357**, 1283–1294 (2006).

51. Bemporad, F. Assessing the role of aromatic residues in the amyloid aggregation of human muscle acylphosphatase. *Protein Sci.* **15**, 862–870 (2006).

52. Imamoto, T., Matsumoto, T., Yokoyama, H., Yokoyama, M. & Yamaguchi, K. Preparation and Synthetic Use of Trimethylsilyl Polyphosphate. A New Stereoselective Aldol-Type Reaction in the Presence of Trimethylsilyl Polyphosphate. *J. Org. Chem.* **49**, 1105–1110 (1984).

53. Kvach, M. V. *et al.* Practical synthesis of isomerically pure 5- and 6-carboxytetramethylrhodamines, useful dyes for DNA probes. *Bioconjug. Chem.* **20**, 1673–1682 (2009).

54. Hunt, P. R. Y.-M. Understanding the Mechanism of Peptide Self-Assembly Using the Amyloid-beta Peptide Fragment, Abeta16-22. (University of Leeds, 2019).

55. Wang, Y. *et al.* Rational Design of Chiral Nanostructures from Self-Assembly of a Ferrocene-Modified Dipeptide. *J. Am. Chem. Soc.* **137**, 7869–7880 (2015).

56. GraphPad Software. Two phase decay. Available at: https://www.graphpad.com/guides/prism/8/curvefitting/index.htm?reg_exponential_decay_2phase.html.

57. Hunter, C. A. & Sanders, J. K. M. The Nature of π-π Interactions. *J. Am. Chem. Soc.* **112**, 5525–5534 (1990).

58. Longmire, M. R. *et al.* Determination of optimal rhodamine fiuorophore for in vivo optical imaging. *Bioconjug. Chem.* **19**, 1735–1742 (2008).

59. Bollhagen, R., Schmiedberger, M., Barlos, K. & Grell, E. A new reagent for the cleavage of fully protected peptides synthesised on 2-chlorotrityl chloride resin. *J. Chem. Soc. Chem. Commun.* 2559–2560 (1994). doi:10.1039/C39940002559

60. Royappa, A. R. N. S. *et al.* Conformationally Selective Synthesis of Mononitrocalix[4]arene in *Cone* or *Partial Cone*. *Helv. Chim. Acta* **100**, (2017).

Chapter 6

α-helix mimics for hot spot recognition in protein-protein interaction

6.1 Introduction

6.1.1 General: protein-protein interaction

Protein-protein interaction (PPI) is an interesting way of communication and regulation largely exploited in biological world[1]. All these interactions are mediated by highly-specific physical contacts between two or more proteins by means of electrostatic and hydrophobic interactions. Thanks to this high specificity in recognition, the effect is fast and efficient, and for this reason it is employed in basilar physiological pathways such as electron transfer, signal transduction, membrane transport, cell metabolism and muscle contraction.

6.1.2 P300/HIF1α and Mcl-1/Bid complexes

As already said, many proteins exploit this mechanism to trigger the activation of several biological pathways. Among these, we have p300/HIF1α[2–5] and Mcl-1/Bid[6–12], which are very important in the regulation of genes involved in the generation of tumours. Considering the high impact of these proteic complexes in biology, a lot of research is ongoing nowadays to understand the real principles underneath genetic regulation in order to develop new systems able to stop genetic diseases.

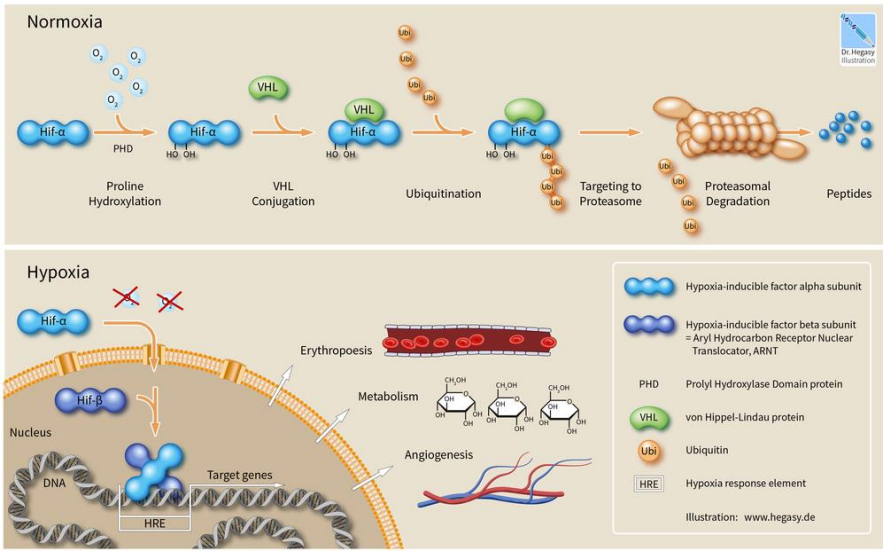

Figure 6.1.2.1. Schematic representation of HIF1α mechanism of action in normoxic and hypoxic conditions. Figure adapted from "Nobel Prize in Physiology or Medicine 2019: How Cells Sense and Adapt to Oxygen Availability".

HIF1α, is a subunit of Hypoxia-Inducible Factor (HIF)[13], often involved in hypoxic tumour growth. In normoxia conditions, PHD2 (Prolyl Hydroxylase Domain 2)[14] binds to HIF1α in correspondence of Pro-402 and Pro-564 (**Figure 6.1.2.1**). Considering the high oxygen partial pressure and the consequent high concentration of 2-oxoglutaric acid, derived from Krebbs

cycle, PHD2 can act as oxidase hydroxylating in position 4 Pro-402 and Pro-564 and producing succinic acid and CO_2 as by-products. When these OH groups are inserted, Von Hippel Lindau tumour suppressor (pVHL)[15] recognizes them and binds to HIF1α triggering its ubiquitylation[16] by relative enzymes (generally 4 ubiquitin molecules are added). This polyubiquitin tail in targeted HIF1α is hence easily recognized by proteasome and subsequently cleaved up to amino acid constituents. This target-to-death ubiquitylation represents, therefore, a system to control protein levels in normoxic conditions, mainly when unwanted overexpressions occur. Unfortunately, when oxygen levels go down reaching hypoxic conditions, HIF1α cannot be hydroxylated anymore by PHD2 and so HIF1α is readily accumulated in cytosol (upregulation)[2,5]. Consequently to this, HIF1α translocates in nucleus and associates to HIF1β building a dimer structure, which binds to Hypoxia Response Element (HRE) on DNA. This association recruits p300/CBP[17] activation complex, which, in turn, helps to recruit and orient RNA polymerase II into promoter region, where through its intrinsic histone acetyltransferase (HAT) activity the chromatin is unrolled and the target genes are processed. Generally, the translation regards proteins related to angiogenesis, erythropoiesis and anaerobic metabolism, which are exploited by growing tumour to recruit nutrients for survival[18]. Because of this very important process, new systems have been developed to avoid contact between proteins (e.g. HIF1α and p300) in order to stop this pathological pathway[3,4,6–8,10].

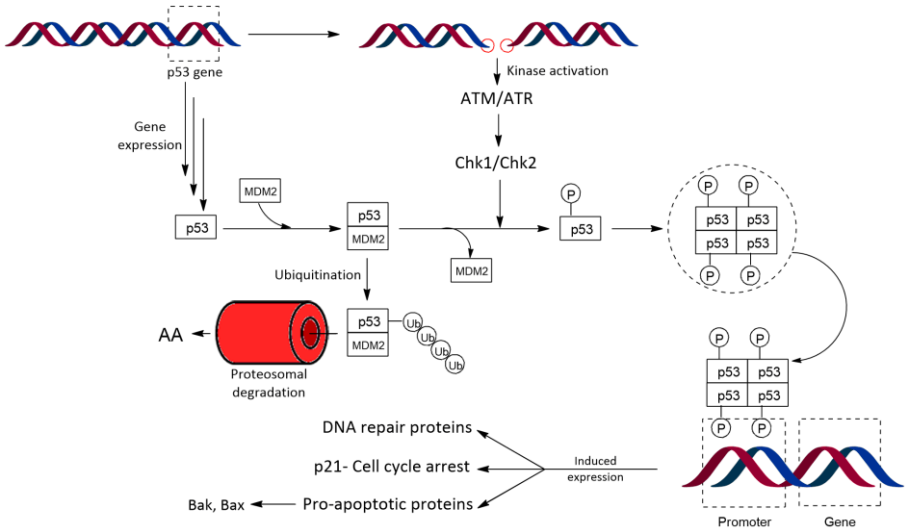

Figure 6.1.2.2. Schematic representation of p53 activation upon damage in genetic code.

To fully understand Mcl-1/Bid action, we have to make a little step back and talk rapidly about another important protein called p53, the so-called "guardian of the genome". Its concentration level is controlled by MDM2 pairing, which steadily takes to p53 ubiquitination and its subsequent death in proteasome (**Figure 6.1.2.2**)[19]. When some mutations prevent the p53-MDM2 stacking[20,21] or induce p53 overexpression or MDM2 downregulation, a consecutive free-p53 accumulation occurs[22–24]. This p53[25–27] excess is immediately phosphorylated by checkpoint kinase 1 and checkpoint kinase 2 (ChK1 and ChK2)[28], which, in turn, were phosphorylated by Ataxia Telangiectasia Mutated (ATM) or Ataxia Telangiectasia and RAD3 related proteins, which essentially are Serine/Threonine Kinases with the ability to be able to be

activated by damaged DNA. Once phosphorylated, p53 is prone to tetramerize and bind, as tetramer, in a promoter region typical for the activation of "self-defence" pathways. These classical pathways are essentially three: DNA repair protein expression[29], p21-cell cycle arrest[30] and pro-apoptotic protein expression[31]. Respectively, the pathways are activated progressively in order as long as the genetic error gets more crucial. In fact, when DNA repairing proteins or the arrest of p21 cell cycle are not enough to restore the damage in DNA, Bak and Bax proteins are expressed to induce apoptosis[32] (**Figure 6.1.2.3**). These proteins stack each other as a sort of proteic channel, which inserting itself within the mitochondrial outer membrane causes the total release of inner material, including the vital cytochrome c (CitC). CitC is captured by Apaf1 (Apoptotic Protease Activation Factor 1)[33], which along with Pro-Caspase-9[34] assemble in Apoptosome. This circular preorganized multiprotein complex put Cit c in the right position and distance to cleave Pro-Caspase-9 up into 2 large and 2 small subunits. These subunits can hence rearrange and be activated as Caspase-9, which exploit their protease properties onto Effector Pro-Caspases[34]. These ones, in turn, are cleaved up and rearrange again in a myriad of Effector Caspases, which degradate the most vital biological components such as chromatin, cellular membrane and so on. The cooperative effect mediated by Effector Caspases, but generated by just one type of Caspase (Pro-Caspase-9), is an example of amplification. Along with CitC, IAPs (anti-apoptosis inhibitors)[35,36] are released by mitochondria upon formation of Bak/Bax channel in order to modulate Caspase activity. A similar regulation mechanism is used in Bak/Bax channel formation. If it was not regulated, the all process it would be a non-sense suicide for the organism. So for this reason, AABPs (anti-apoptotic Bcl-2-like proteins)[37,38] tend to bind to Bax preventing the adhesion with Bak and subsequently stopping apoptosis. Also PABP (pro-apoptotic BH3-only proteins)[39] are expressed by cell as a secondary regulation system. These ones, since "pro-apoptotic", bind to the anti-apoptotic AABP releasing back Bax, making it available again for apoptotic pathway. The right balance of expression of all these proteins determines the cell response efficiency to genetic damages.

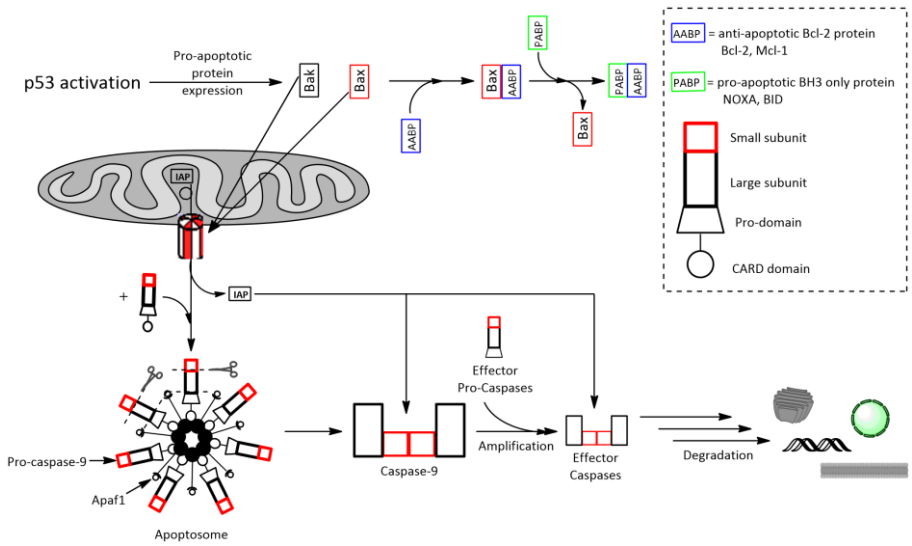

Figure 6.1.2.3. Apoptotic pathway mediated by Caspases.

In some tumours, AABPs, such as Mcl-1, are overexpressed[40,41] and thus the excess, not bound to PABPs, tends to bind directly to Bax stopping the apoptotic process. Considering that Mcl-1 interacts with either Bak/Bax or PABPs via the same BH_3 domain, a lot of research lines have been doing to develop new systems structurally complementary to BH_3 domain in order to exclude Mcl-1 from the pathway and so trigger cell death[8–10].

6.1.3 Hot spots: definition and structure

PPIs are very complex processes largely exploited by Nature to regulate and control subcellular proteic components[42–44]. Starting from X-Ray structures it has been demonstrated that in PPIs just a rather small patch of the whole protein is involved in the contact. Many experimental and theoretical studies have been carried out to localize inside these patches the areas responsible for most of the energy binding[45]. These protein-protein interfaces are differently characterized by size, shape and surface complementarity[46]. The average dimensions are around 1200 –2000 Å[47,48], but in some cases, larger or smaller interfaces can be observed (e.g. for proteases or G proteins can be observed contact patches up to 2000–4660 Å)[48,49]. Generally, all the contact interphases are larger than 600 Å, which through computational studies has been demonstrated to be the minimum area required to make a water-tight seal around the determinant amino acids involved in the most energetically favourable interactions[45,47,50]. These amino acid set is almost always hydrophobic and builds a large flat section of non-polar surface[51,52]. These exposed regions tend to pair each other by means of Van Der Waals interactions excluding steadily the water molecules from binding space. Considering that the number of these hydrophobic patches can vary from 1 to 15[53], the protein-protein complex is cooperatively stabilized by the simultaneous pairing and water expulsion. In other words, the free energy of the complex is the sum of the free energies related to all hydrophobic interactions, reinforced by the stabilizing entropic factor of water molecule displacement[46]. Besides this hydrophobic factor, the process is accompanied by electrostatic interactions, which help the complex formation and define the lifetime of the complexes. It has also been demonstrated that 76% of amino acid side-chains in the interphase is involved in the contact, whereas the remaining is involved in water complexation (one bond per each 100–200 Å)[54,55].
These patches, totally responsible for the overall binding energy, are still too large to be practically studied, so recently different methods are aiming at the identification of the key residues responsible for most of the binding energy. Nowadays, the favourite method is the alanine scanning mutagenesis. It essentially consists in single amino acid random substitution with alanine, which conserves chirality and minimizes the side-chain contribution. Gly would eliminate the side-chain contribution, but it would introduce flexibility, that could not be suitable for the investigation. Using this kind of technique surface areas, called “hot-spots”, can be defined in which are gathered the most influencing amino acids in the binding. Are defined “hot-spots”[43,47,56], those areas, which subjected to alanine mutations cause a free energy destabilization of at least 2.0 Kcal/mol[57]. To have a substantial structural change this energy gain should be of 4.0 Kcal/mol, but this is very uncommon in practice and the energetic threshold must be lowered to 2.0 Kcal/mol to be able to carry out a reliable statistical analysis. On Thorn’s and Bogan’s database[57] a brief analysis has demonstrated that only an average of 9.5% of contact interphase amino acids are hot spots. All hot spots are generally delimitated by a ring of amino acids not-relevant for the binding, whose role would be to shield hot spot residues from water[58]. This strategy is a smart way to reduce competition of water in hot spots

letting them free for the recognition of the other protein. This recognition process is highly specific since it occurs just when a perfect ‘‘complementarity’’ is reached: simultaneous shape and hydrophilic/hydrophobic matches are required for successful binding.

6.1.4 Methods for hot spot determination

A hot spot can be determined either by theoretical or experimental studies. Computational studies are ideal in the hot spots determination since they are fast, cheap and easy to perform screening tests. Unfortunately, the weak point of these methods is accuracy. In fact, a lot of researchers are trying to develop more reliable methods able to predict alanine scanning mutagenesis effect. They essentially have been creating different algorithms, characterized by increasing complexity, which can be classified into two categories: empirical or knowledge-based methods and fully atomistic methods[59]. In the optic of fast screening, generally are largely preferred the empirical/knowledge-based methods, since built on very simple statistical models rather than the fully atomistic ones in which more complex and time-consuming algorithms are required.
On the contrary, experimental systematic mutagenesis is time-consuming and very laborious since individual mutant proteins must be purified and analyzed separately but still remain the most reliable method to obtain accurate data[60]. Therefore, considering that there are drawbacks in both approaches, in PPI studies it is used a hybrid approach, in which computational results are starting guidelines for the experimental biosynthesis of alanine-mutated proteins. Alternatives to systematic mutagenesis are combinatorial and phage-display libraries of alanine substituted proteins[60]. These methods, differently from previous ones, guarantee high-throughput analysis, which can let optimize time and yields. Erlanson et al.[61] developed a new fascinating method to study directly the binding capacity of hotspots with a library of potential organic binding counterparts. This “covalent tethering” approach[62] exploits the disulphide equilibrium exchange to label potential binders at specific region nearby protein surface, which allows calculating easily relative binding affinities.

6.1.5 Inhibition strategies: mimicking α-helices

As largely discussed in previous paragraphs, a lot of diseases are still mediated by PPIs and frequently the interaction passes through the recognition of α-helix motifs.

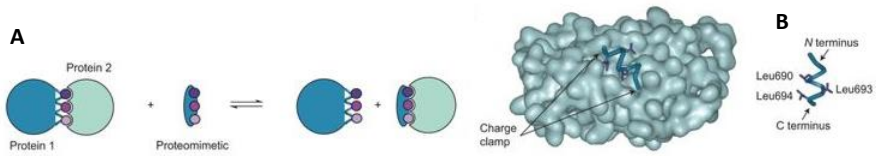

Figure 6.1.5.1. A) Schematic representation of proteomimetic approach; B) Mcl-1/NOXA B interaction (PDB code: 2JM6) along with NOXA B structure and the side-chains involved in binding. Figures adapted from reference[63].

Therefore this general pharmacophore (α-helix) is getting a central relevance in the design and synthesis of new inhibitors able to regulate the protein contacts in pathological conditions. In this context two main approaches have been developed so far: the helical folding mimics approach (**Figure 6.1.5.1B**), in which oligopeptides are employed to reproduce the local

topology of the helical fold and the proteomimetic approach (**Figure 6.1.5.1A**), where small molecule scaffolds can be used to orient active units in the same angular and spatial positions as observed in donor helix. In the helical folding mimics approach generally are used peptide-based derivatives, which have the advantage to conserve a lot of functions not reproducible by small molecules. Unfortunately, synthetic peptides tend to adopt in solution random conformations different from parent peptides/proteins, though. Recently several methods have been developed to constrain oligopeptides into the biological active α-helix conformation (**Figure 6.1.5.2A**). This, apart from giving to the peptide excellent transport properties and high resistance to proteases, guarantees peptides less mobile in the unbound state, which is required for an efficient binding with a minor loss of degree of freedom. Different are the ways with which this preorganization can be reached.

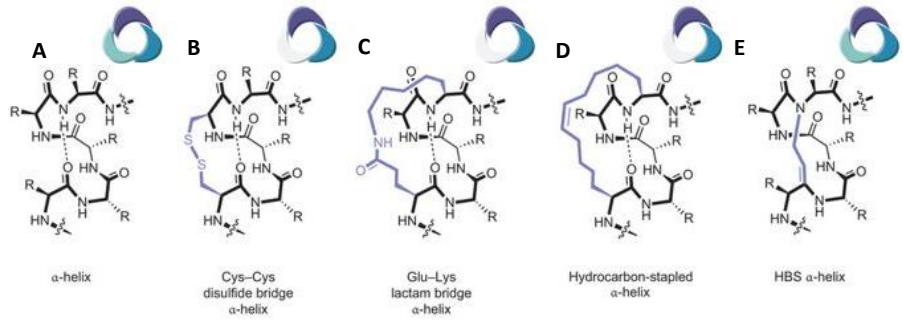

Figure 6.1.5.2. Representations of rigidification strategies commonly used. Figure adapted from reference[63].

One of these is making intramolecular disulphide bridges (**Figure 6.1.5.2B**). Mierke and Spatola groups[64,65] developed a disulphide-linked peptide as inhibitor of nuclear-receptor co-activator interactions. Another study was carried out on another disulphide-bridge nonapeptide as inhibitor of oestrogen receptor α (ERα)/co-activator interaction and what turned out was that circular dichroism spectra in water confirmed its small helical character, meanwhile X-ray cocrystal structure (PDB code: 3ERD) confirmed the expected conformation in the binding[66]. An evidence of high potency of this method is the low inhibition constant (Ki=25nM), much lower than other common inhibitors towards this target. In substitution to disulphide bonds, lactam bridges are often used in cross-linking (**Figure 6.1.5.2C**). On the basis on McDowell's work[67], Kim group[68] developed a method to stabilize in an α-helix structure a 14-residue peptide, rich indeed in helix-favouring amino acids, via chemical cross-linking in order to target the hydrophobic pocket of HIV-1 gp41. The cross-linking in correspondence of two glutamic acid residues in position i and i+7 with α,ω-diaminoalkane group gives to the peptide high inhibition properties (Kd=1.2 μM). Considering that the above mentioned modifications are susceptible to cellular degradation, Grubbs and Blackwell[69] developed the so-called "hydrocarbon stampling method" (**Figure 6.1.5.2D**), which consists in the incorporation in the peptide sequence of O-allyl serine α,α-disubstituted unnatural amino acids exploitable for ring-closing metathesis. Korsmeyer et al.[70] incorporated in BID sequence in i and i+4 positions olefin-modified residues and just upon cyclization, the peptide in question showed to be a very potent tumour suppressor. Moreover, Walensky and co-workers[71] have demonstrated that a double stampling on peptide backbone can increase the bio-lifetime thanks to the enhanced protease resistance. Another way to increase stability in helical folding is making covalent bonds wherein the natural

backbone are present hydrogen bonds. This hydrogen-bonding surrogate (HBS) motif (**Figure 6.1.5.2E**) was used by Arora and co-workers[72–75] to link residues in i and i+4 positions to make a Bak BH3 α-helix mimic for the inhibition of Bcl-xL. This peptide showed to be a nanomolar inhibitor (Kd=69nM) and 60-fold more resistant to proteases than the linear analogue. Loads of linkers have been tested in this perspective, but azobenzene-based crosslinkers showed to be the most interesting ones. In fact, since they are photoactive, the binding activity of the peptide can be reversibly controlled by an external stimulus. Alleman and co-workers[76] developed BH3 domain peptides of Bak and BID mimics for the targeting of anti-apoptotic Bcl-xL, which upon light stimulus could undergo cis/trans isomerization, switching among a random coil-like and α-helix conformations. Also the use of β-peptides[77] and mixed α-/β-peptides[77–79] have been used for the inhibition of Bcl-2 family. Different systems were studied such as BIM-BH3 peptide, PUMA, Mcl-1 for which in some cases inhibition constants of 1 nM were even observed.

In the proteomimetic approach, instead, it is copied the original topography in helix meaning the spatial orientation of hot spot residues rather than the helical conformation coiling, as seen in peptide approach. Here the helix pharmacophore is simplified to a rod-shaped object, in which intramolecular hydrogen bonds required for helix stabilization are eliminated. With this simplification these binders are more synthetically accessible and at the same time can be exploited as lead-like scaffolds. On the basis of Willems' and Rees' previous work[80] on trisubstituted indanes as inhibitors of tachykinin receptors, Hamilton group[81] for the first time synthesized a library of 3,2',2''-terphenyl derivatives, which because of their staggered aromatic core orient ortho substituents in i, i+3(4), i+7 α-helix-like positions. These compounds, which are the first real α-helix mimics, showed to be very efficient nanomolar inhibitors in PPIs in systems like calmodulin/phosphodiesterase, Bcl-xL/Bak and gp41 interactions[82,83]. Considering their difficult synthesis Hamilton developed terephthalamide and 4,4-dicarboxamide scaffolds more synthetically accessible and druggable[84]. To get longer mimics, a 4,4-dicarboxamide subclass was created in which every second aromatic ring was substituted with the more hydrophilic acylurea isostere[85,86]. All these derivatives showed very interesting inhibition properties in Bcl-xL/Bak PPI within the micromolar range. Rebek group synthesized a oxazole-pyridazine-piperazine scaffold able to mimic i, i+4 and i+7 positions[87]. Here the heterocycle rings, besides the hydrophobic properties given by side-chains, give to the backbone the so-called "wet edge", on which donor and acceptor atoms can increase solubility in aqueous environment by hydrogen bonds. An interesting alternative to these last derivatives have been developed by Hamilton and coworkers. They prepared compounds characterized by 5-6-5-imidazole-phenyl-thiazole scaffold, in which terminal aromatic rings are replaced with more hydrophilic five-membered heterocycles[88]. Considering the inapplicability of these compounds in library synthesis for their multi-step synthesis, Hamilton developed a trispyridylamide scaffold[89–91], which is much more accessible via amide bond formation. By means of modelling and X-Ray studies it has been demonstrated that these molecules, besides keeping their properties of projecting ortho substituents in classical i, i+4, i+7 orientations, are almost planar because the high preorganization induced by hydrogen bonds between amide NH and pyridyl and ortho alkoxy moieties. These molecules showed to be very interesting inhibitors (micromolar range) thanks to the high preorganization exploitable in induced fit. By several groups analogous derivatives were then realized[92–95], modifying the curvature of the molecule by mixing in suitable ratio benzene and pyridine rings and so altering the rigidity induced by intramolecular hydrogen bonds. Recently in Wilson's laboratories were synthesized 2-O-

alkylated (less curvated for the higher planarity) and 3-O-alkylated (more curvated) aromatic oligoamides as inhibitors of p53/hDM2 interactions[96,97]. A large library of these compounds with several side chains was synthesised and in some cases even IC50=1.0μM were observed totally comparable to the potency of native peptide (IC50=1.2μM). Craik and co-workers[98] synthesized also mixed benzamide/pyridyl dimers as inhibitors of active dimer found in Kaposi's sarcoma-associated herpesvirus protease. For these type of compounds the first solid-phase synthesis was realized by Wilson's group in 2010 with N-alkylated oligobenzamides towards p53/hDM2 interaction[99,100]. Similarly to these ones, Lim and co-workers[101] synthesised new pyrrolopyrimidine-based α-helix mimetics, which have the advantage to be rigid and preorganized and present at the same time the wet edge to increase water solubility. All the above-mentioned derivatives have the limitation that can mimic the α-helix just by one face. So just recently have been designed molecules that are able to exploit both sides. In this context, Hamilton and coworkers modified his previous terphenyl scaffold with an indane ring in central localization to mimic i+5 position[102]. Ahn and co-workers[103] instead proposed to modify the O-alkylated oligobenzamide scaffold by placing a new second alkoxy moiety on the opposite side of aromatic ring. Recently Hamilton proposed new bis aryl-pyridyl-pyridone scaffold to inhibit the ER/co-activator interaction[104]. These compounds are still under investigation and large libraries have been developing in order to understand their overall properties.

6.2 Aim of the work

Since a wide research has been carried out on the synthesis of new α-helix mimetics, in this context, in collaboration with prof. A.J.Wilson of University of Leeds we proposed to use upper-functionalized calix[4]arene in cone geometry as scaffold for α-helix targeting. This idea came out from a preliminary topology study onto trialkylcalix[4]arene and NOXA B-BID/Mcl-1.

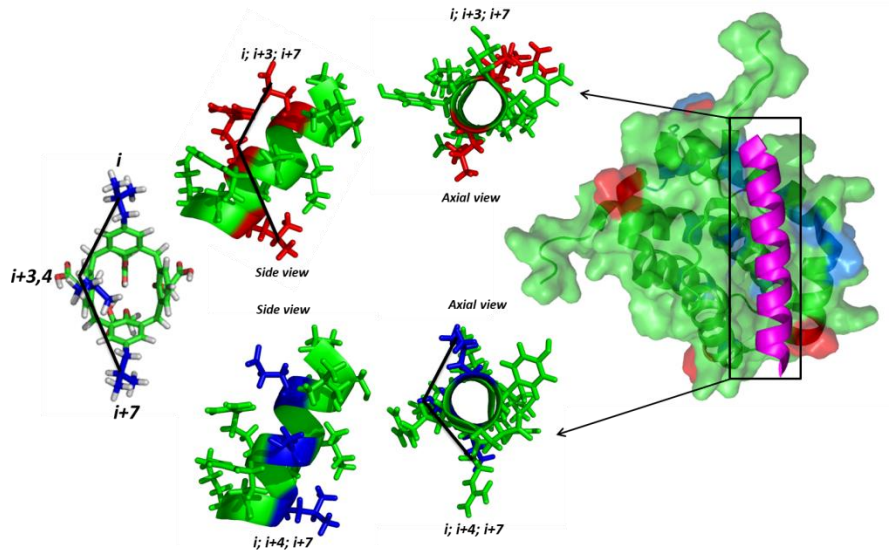

Figure 6.2.1. Spatial orientation of classical I, i+3(4) and i+7 residues onto NOXA B (highlighted in violet). Comparing these positions with positions 5,11,17 onto calix[4]arene scaffold, it can be seen how calixarene can fit this disposition. Figures obtained with PyMol software (PDB code: 2JM6).

It can be seen in **Figure 6.2.1** that positions i, i+3(4) and i+7 onto natural α-helix are totally superimposable to positions 5,11,17 of the calix[4]arene scaffold blocked in cone geometry. For these reasons, we proposed the synthesis of tetraethoxycalix[4]arenes in cone conformation trifunctionalized at the upper rim with methylene-O-trisopropyl (**88a**), methylene-O-trisobutyl (**88b**) and trisobutyl moieties (**91**, **92b**, **94**), which represent good mimics of aliphatic amino acids observed on hot spots localized in HIF1α (Leu819-Leu822-Val825) and NOXA-Bid (Leu690-Leu693-Leu694). Trisobutyl calixarenes (**91**, **92b**, **94**) were synthetised with different groups at lower rim to furthermore understand the contribute of macrocycle rigidity and polarity in the recognition event. During my secondment in Wilson's labs at University of Leeds, these derivatives were tested in Fluorescence Anisotrophy and NMR studies to determine their ability as PPI inhibitors. Moreover, at the end of my secondment some crystals were obtained with methylenecarboxylate derivative **94** and Mcl-1, but their nature is still under investigation to assess if suitable for X-ray shooting.

6.3 Results and discussion

6.3.1 Synthesis of upper-rim-trifunctionalized calix[4]arenes

The synthesis of calix[4]arene derivatives trifunctionalized at upper rim with isopropyl and isobutyl chains through CH_2O spacer is represented in **Figure 6.3.1.1**.

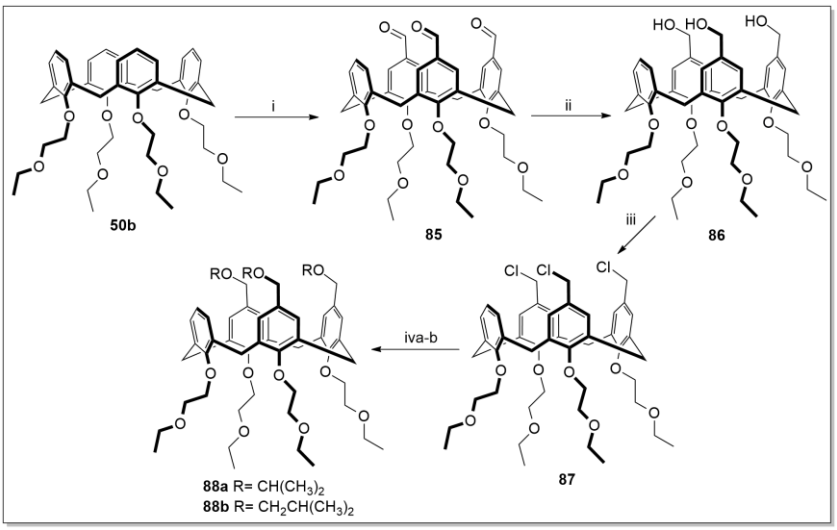

Figure 6.3.1.1: Synthesis of calix[4]arene derivatives trifunctionalized at upper rim with aliphatic chains through CH_2O spacer. *Reaction conditions:* i) 1,1-dichloromethyl methyl ether (49.9 eq), $TiCl_4$ (40.4 eq), dry DCM, rt, 1h (44% yield); ii) $NaBH_4$ (3.1 eq), absolute EtOH, rt, 1 day (99% yield); iii) $SOCl_2$ (14.7 eq), dry DCM, rt, 1h 30 minutes (99% yield); iva) NaH (4.3 eq) in isopropanol (10 ml), toluene, rt to reflux, 30 minutes+2 days (18% yield); v) NaH (5.7 eq) in isopropanol (3 ml), toluene, rt to reflux, 30 minutes+1 days (48% yield).

The synthesis of compound **50b** won't be discussed here since already done in **Chapter 3**. Compound **50b** was triformylated at upper rim with 1,1-dichloromethyl methyl ether, as formylating agent, and $TiCl_4$, as catalyst, in dry DCM. The reaction was rapidly quenched after

1h due to the sudden appearance on TLC of the tetraformyl derivative. The target molecule was purified by a flash chromatography column with a slow eluent gradient (AcOEt/Hex 1:1→8:2) to get rid of the unwanted di-formyl and tetra-formyl derivatives, derived from the absence of regioselectivity in the reaction. Compound **85** was characterized by ^{1}H-NMR and the two singlets at 9.51 and 9.49 ppm respectively of 11-C*H*O and 5,17-C*H*O were considered diagnostic for the well-occurrence of reaction. Compound **85** was subjected then to a reduction of all formyl groups by $NaBH_4$ in absolute ethanol for 1 day at room temperature. The target molecule was characterized by ^{1}H-NMR.

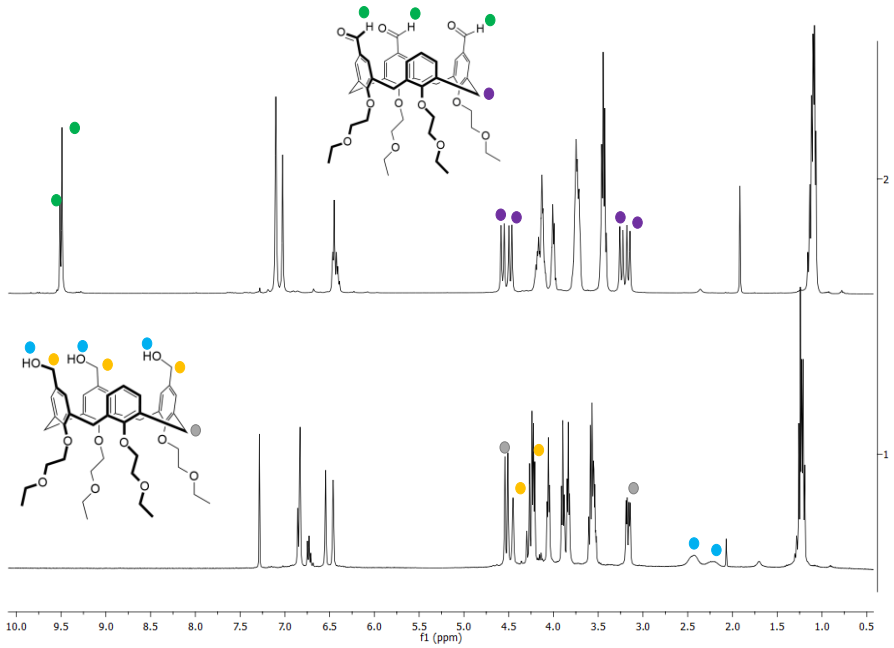

Figure 6.3.1.2: ^{1}H-NMR spectra ($CDCl_3$, 400 MHz) of (**1**) compound **86** and (**2**) compound **85**

As it can be seen in **Figure 6.3.1.2**, in the ^{1}H-NMR spectrum in $CDCl_3$ of compound **86** the two singlets at around 9.5 ppm are absent, while two broad singlets at 2.43 and 2.24 ppm appear for 5,17-OH and 11-OH, respectively and two signals at 4.45 and 4.25 ppm for 11-CH_2OH and 5,17-CH_2OH, respectively. It is interesting also highlight that introduction of methylene spacer with the reduction reaction outdistances more the functional group from calix[4]arene scaffold and this seems to reduce the asymmetry in the trifunctionalized calix[4]arene. In fact, passing from compound **85** to compound **86** in ^{1}H-NMR the signals related to equatorial protons of methylene bridges are less away from the axial protons. Compound **86** was then subjected to chlorination of OHs with $SOCl_2$ at room temperature for around 1h. The disappearing of OH signals at 4.45 and 4.25 was taken diagnostic in ^{1}H-NMR spectrum for compound **87**. For the synthesis of compound **88a** and **88b** was initially formed in situ the alkoxide ion stirring NaH in the respective alcohol (isopropanol for compound **88a** and isobutanol for compound **88b**) and subsequently, once dried out, compound **87** was added in and stirred in toluene at reflux for 1-2 days. Upon purification by means of chromatographic techniques, both compounds were characterized with ^{1}H-, ^{13}C-NMR and ESI-MS.

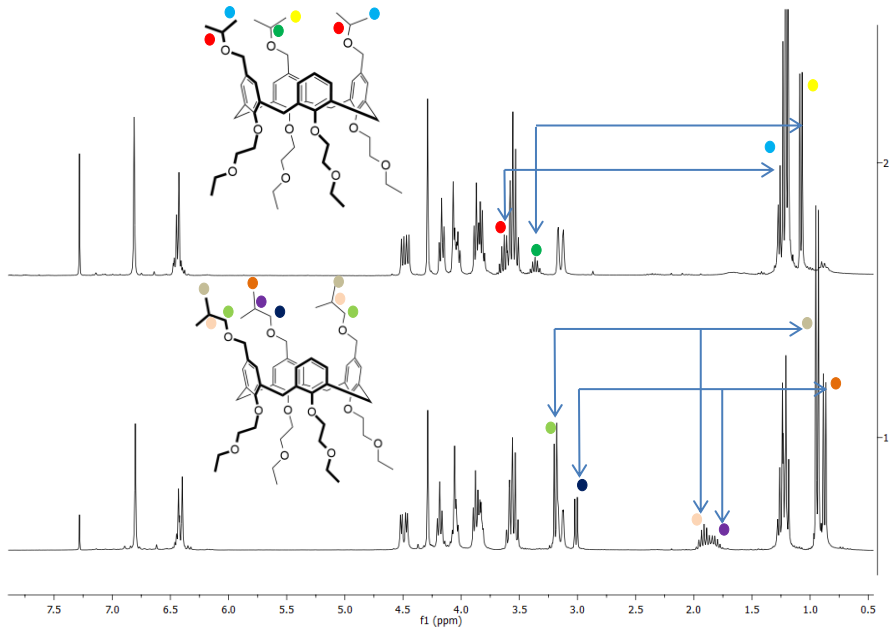

Figure 6.3.1.3: ^{1}H-NMR spectra ($CDCl_3$, 300MHz) of compound **88b** (**1**) and compound **88a** (**2**). The blue arrows show the ^{1}H-^{1}H COSY correlations.

The assignment of alkyl protons in ^{1}H-NMR was driven by comparison with compound **87** and by identification in COSY spectrum of isolated spin systems.

As regards the synthesis of calix[4]arene upper-trifunctionalized with triisobutyl moieties, the strategy employed is pretty different than the previous one.

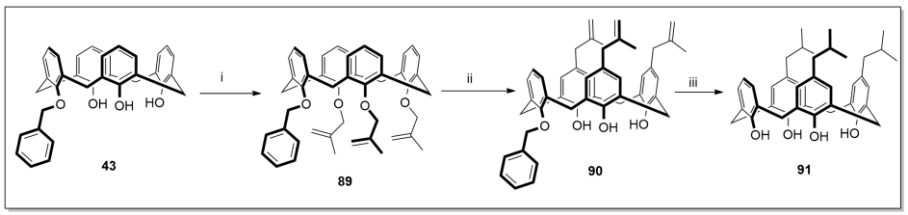

Figure 6.3.1.4: Synthesis of compound **91**. *Reaction conditions:* i) NaH (5.0 eq), 3-chloro-2-methylprop-1-ene (5.0 eq), dry DMF, rt to 50°C, 30 minutes+1 day (81% yield); ii) N,N-dimethylaniline (15 ml), 210°C, 1h (46% yield); iii) 10% Pd/C (catalytic amount), H_2 (2.5 bar), AcOEt/EtOH, rt, on (99% yield).

As it can be seen in **Figure 6.3.1.4**, instead of introducing the isopropyl moieities directly at the calixarenes upper rim, we proposed a lower-rim trifunctionalization, followed by Michael transposition, which allows the migration of the alkylic groups to the right position at the upper rim. Compound **43**, whose synthesis was already discussed in **Chapter 3**, was subjected to a trialkylation at lower rim with NaH as base and 3-chloro-2-methylprop-1-ene as alkylating agent at 50 °C for 1 day. The successful outcome of reaction was assessed by ^{1}H-NMR. In the spectrum in $CDCl_3$ it is observed the disappearing of free OHs singlets at 9.55 and 9.20 ppm and the presence of alkenyl protons at 5.29 (OCH_2C=CH*H*), 5.09 (OCH_2C=CH*H*), 4.80 (27-OCH_2C=CH_2),

4.40 (26,28-OCH_2C=CH_2) and 2.05 ppm (CH_3). Compound **89** was then subjected to Michael transposition in N,N-dimethylaniline at 210 °C for 1h. After acidic quenching, the crude was purified by flash chromatography column in toluene/Hex 1:1.

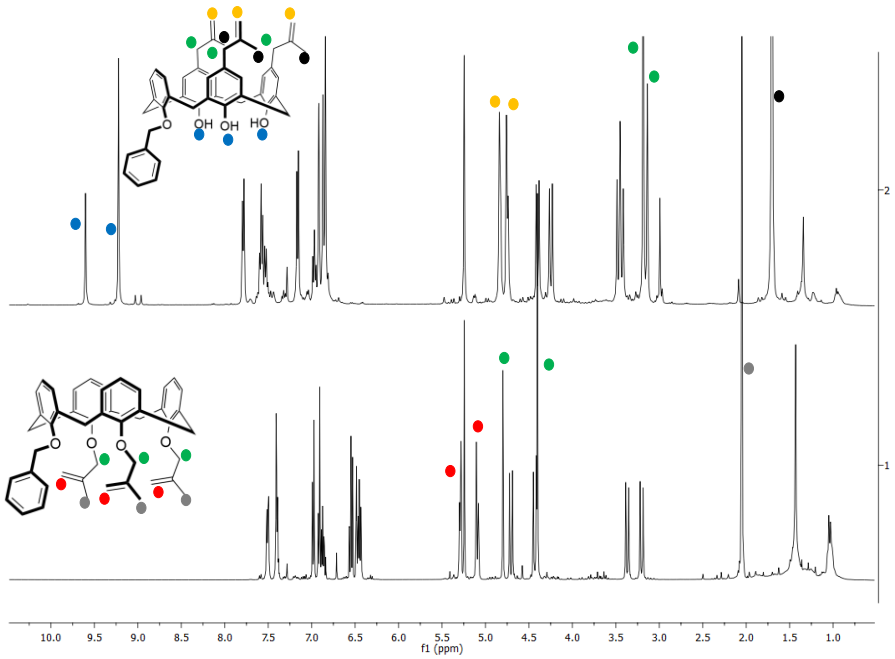

Figure 6.3.1.5: ^{1}H-NMR ($CDCl_3$, 300MHz) spectra of (**1**) compound **89** and (**2**) compound **90**.

From relative ^{1}H-NMR spectrum in $CDCl_3$ (**Figure 6.3.1.5**), a proof of migration of alkenyl groups was obtained from the presence of the OH singlets at 9.56 and 9.18 ppm and the systematic down-field shift experienced by alkenyl protons at the upper rim.

A following quantitative catalytic hydrogenation onto compound **90** led to total reduction of alkenes and benzyl removal. The successful outcome of reaction was confirmed through ^{1}H-NMR by 1) a singlet at 10.22 ppm related to unfunctionalized phenolic OHs; 2) the loss of the signals related to methylenebenzene moiety; 3) the shielding of isopropyl protons to 2.28, 1.78 and 0.89 ppm, characteristic of a saturated system.

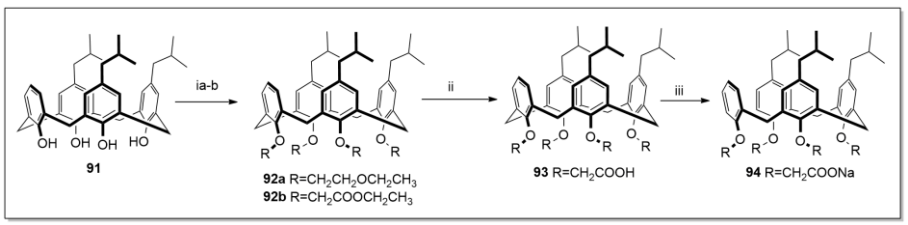

Figure 6.3.1.6: Synthesis of compound **92a** and **94**. *Reaction conditions:* ia) 55% NaH (5.1 eq), 0.76 mmol, 2-bromoethyl ethyl ether (5.1 eq), dry DMF, rt, 30min+1 day (74% yield); ib) Na_2CO_3 (19.9 eq), 2-bromo ethylacetate (10.0 eq), NaI (4.0 eq), dry ACN, reflux, 3 days (80% yield); ii) 1M NaOH (24.9 eq), THF, reflux, 1h (56% yield); iii) 1M NaOH (4.0 eq), rt, 1h (99% yield).

Compound **92a** and **92b** were obtained by nucleophilic substitution between compound **91** and relative alkylating agent (respectively 2-bromoethyl ethyl ether and 2-bromo ethylacetate). In order to deprotonate OHs of compound **91**, for compound **92a** NaH was suspended in dry DMF, while for compound **92b** was used a suspension of Na_2CO_3 in dry ACN. The yields for both processes are very good, but the synthesis of compound **92b** required longer time even with the addition of NaI as catalyst.

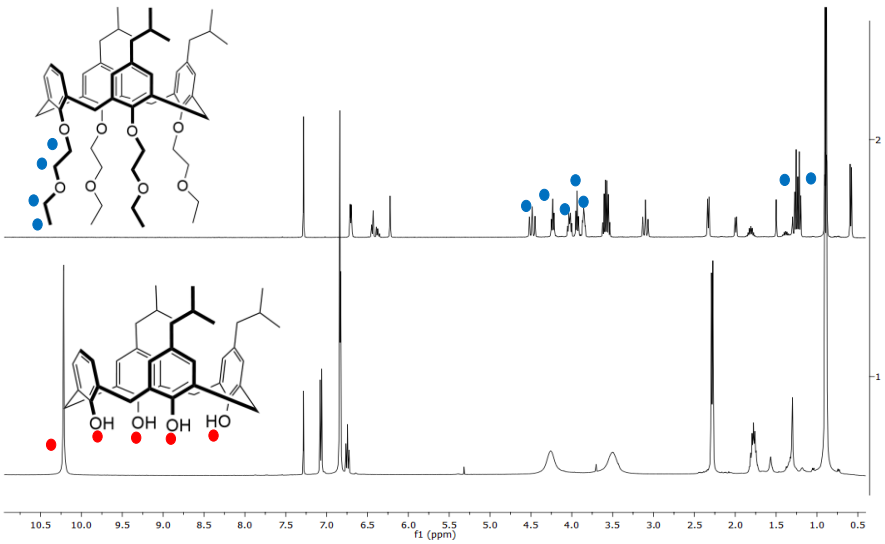

Figure 6.3.1.7: ^{1}H-NMR spectra (400 MHz, $CDCl_3$) of compound **91** (**1**) and **92a** (**2**).

The successful outcome of synthesis of compound **92a** was confirmed through ^{1}H-NMR by the loss of OH singlet at 10.2 ppm and the appearing of signals related to ethoxyethyl chain protons (highlighted in blue in **Figure 6.3.1.7**). It can be seen also that the two broad singlets of methylene bridges in compound **92a**, upon functionalization, are transformed into four sharp doublets, which demonstrates that the expected rigidification of the scaffold occurred. Compound **92b** was then hydrolized for 1h at reflux using an excess of 1M NaOH and upon acidic quenching, it was isolated and characterized as carboxylic acid derivative. To increase its solubility in aqueous media it was made reacted with stoichiometric quantity of NaOH to produce the sodium carboxylate salt.

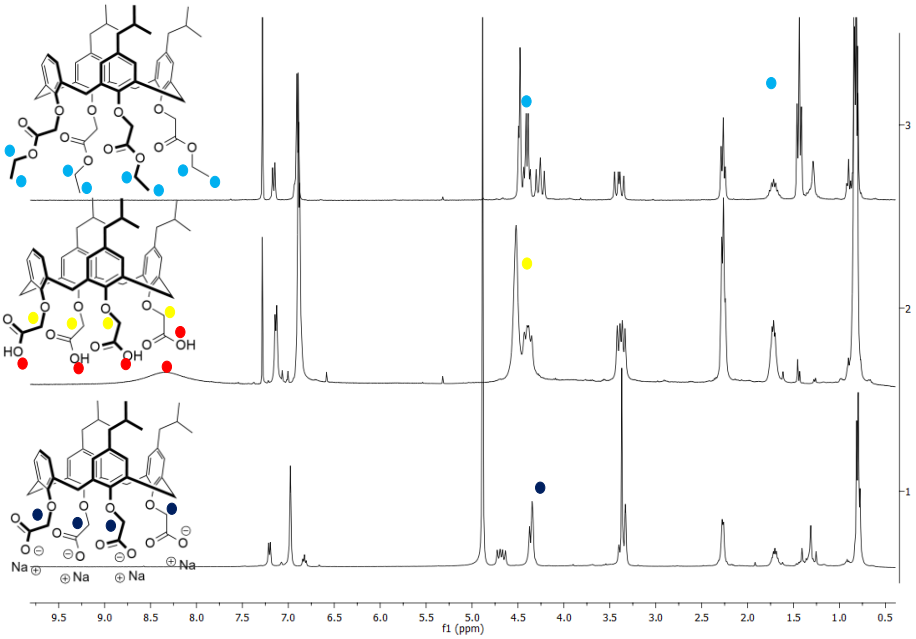

Figure 6.3.1.8: 1H-NMR spectrum of **1**) compound **94** (400 MHz, MeOD), **2**) of compound **93** (400 MHz, $CDCl_3$), **3**) of compound **92b** (300 MHz, $CDCl_3$).

The good development of the strategy was controlled in these last intermediates with ^{1}H-NMR spectroscopy, thanks to which for the hydrolysis step was checked the loss of ethyl protons (highlighted in light blue in **Figure 6.3.1.8**) and the appearing of the broad singlet related to carboxylic acid at 8.30 ppm, while the deprotonation step was confirmed by the slight shielding effect observed for methylene protons of carboxy moiety (**Figure 6.3.1.8**). Compounds **89**-**94**, since not present in literature, were fully characterized with additional ^{13}C-NMR and ESI-MS spectra.

6.3.2 Fluorescence Anisotropy Assays

To understand their inhibition efficiency towards p300 and Mcl-1, compounds **88a**, **88b**, **91** and **94** were tested in Fluorescence Anisotropy Assays. In this type of assays the protein is titrated with the potential inhibitor keeping constant the concentration of the fluorescent-labelled biological counterpart of the protein in question. This procedure is simply realized with 384-well Optiplates, which allows preparing in parallel two different triplicates (testing and control lanes), characterized by 1:1 dilution concentration gradient, just by pipetting the same amount from a column to another one. The analysis of each well was performed with Perkin Elmer EnVision™ 2103 MultiLabel plate reader, whose excitation and emission wavelength were set up to 480 nm (30 nm bandwidth) and 535 nm (40 nm bandwidth), respectively, which correspond to absorption and emission wavelengths of fluorescein-based FITC and FAM used for HIF-1α and BID tagging (see experimental part for more information about). This assay is essentially a competitive assay, which measures the ability of the new potential inhibitor to displace the fluorescent-tagged biological counterpart bound to the protein. The displacement

experimentally showed as a sigmoidal decrease of fluorescence anisotropy due to the faster tumbling of the fluorescent tag in solution rather than when stuck to protein walls.
To assess the good state of the p300 and Mcl-1, the fluorescent-labelled biological counterpart (FITC-HIF1α for p300 and FAM-Bid for Mcl-1) was titrated with the protein (p300 or Mcl-1). The clear increase in fluorescence anisotropy shows that at increasing concentrations of p300 or Mcl-1 the binding occurs as the fluorophore tumbling is reduced. As it can be seen in **Figure 6.3.2.1**, for p300/FITC-HIF direct titration acquisitions were taken at different time, which shows that stability is reached at least after 3h. However, for both systems the error onto EC50 is very small and the EC50 obtained are in agreement with literature data (0.02±0.01μM for p300 and 0.14±0.01μM for Mcl-1).

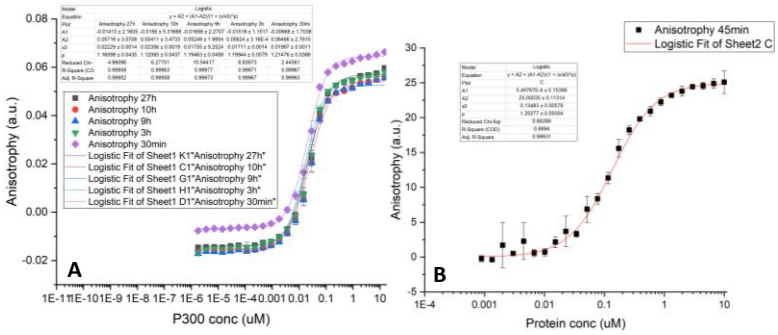

Figure 6.3.2.1: A) Direct titration of p300/FITC-HIF. *Experimental conditions:* 15 μM p300 (final concentration), 50 nM FITC-Hif1α, 0.02M Tris, 0.15M NaCl, 0.01% Triton, pH 7.55, 1mM DTT; **B**) Direct titration of Mcl-1/FAM-Bid. *Experimental conditions:* 15 μM Mcl-1 (final concentration), 50 nM Fam-Bid, 20 mM Tris, 100 mM NaCl, 1mM DTT, pH 7.46. Data are plotted with XOrigin through a sigmoidal logistic fitting.

At this point, competition assays with our derivatives were run. As it can be seen in **Figure 6.3.2.2**, just DS102 (**94**) has an effective inhibitory properties. For other compounds LVC6 (**88a**), LVC5 (**88b**), DS47 (**92a**) and DS46 (**91**), no sigmoidal decrease was observed. Considering that for these last compounds the addition of buffer to inhibitor stock solution resulted in an immediate visible precipitation, the respective data were not considered, since not reliable. Evidently ethoxyethyl chains are not enough to dissolve the calixarene derivatives in buffer, whereas, as already anticipated, methylencarboxylate chains are. Obviously nothing excludes that they would have been active if they had been soluble. For active compound **94**, it has been calculated an IC50 of 1.98±0.86μM, which in comparison with the reference AcHIF (0.06±0.01μM) is less active of two orders of magnitude.

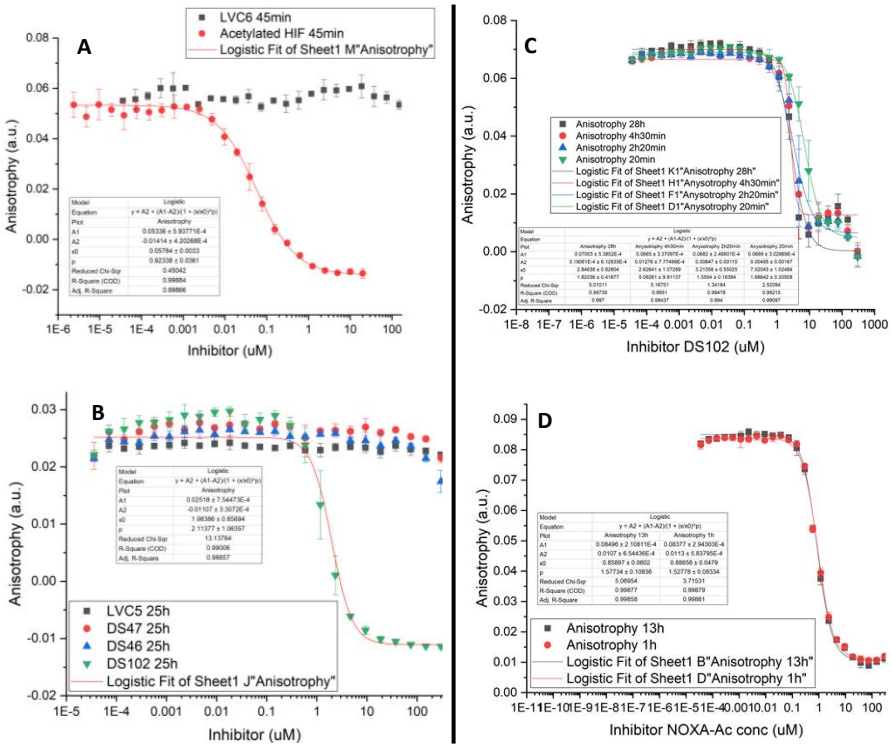

Figure 6.3.2.2: A) Competitive titration of p300/FITC-HIF-Inhibitor. *Experimental conditions:* 100 nM p300, 300 μM LVC6 (**88a**) or 20 μM AcHIF-1α, 50 nM Fitc HIF-1α, 20 mM Tris, 100 mM NaCl 1mM DTT, pH 7.4; **B**) Competitive titration of p300/FITC-HIF-Inhibitor. *Experimental conditions:* 300μM LVC5 (**88b**) or DS47 (**92a**) or DS46 (**91**) or DS102 (**94**) (final concentration), 15 μM P300, 50 nM FITC-HIF, 0.02M Tris, 0.15M NaCl, 0.01% Triton, pH 7.55, 1mM DTT; **C**) Competitive titration of Mcl-1/FAM-Bid-Inhibitor. *Experimental conditions:* 300μM DS102 (**94**) (final concentration), 15 μM P300, 50 nM FITC-HIF, 0.02M Tris, 0.15M NaCl, 0.01% Triton, pH 7.55, 1mM DTT; **D**) Competitive titration of Mcl-1/FAM-Bid-Inhibitor. *Experimental conditions:* 300μM NOXA-Ac (final concentration), 200 μM Mcl-1, 25 nM FAM-BID, 0.02M Tris, 0.15M NaCl, 0.01% Triton, pH 7.55, 1mM DTT. Data are plotted with OriginPro through a sigmoidal logistic fitting.

Since NOXA and BID, as well, owns the same hot spot triad Val-Val-Leu, compound **94** was tested in competition with them. For compound **94** was calculated an IC_{50}=(2.85±0.83)μM, while towards NoxaAc, another protein involved in Mcl-1 regulation, was calculated an IC_{50}=(0.86±0.06)μM. Here, differently from p300, there is just one order of magnitude in difference, which makes this compound a very interesting device for Mcl-1/NOXA-Bid regulation. Moreover in **Figure 6.3.2.2C** it can be seen that the curve profile is totally different from the other graphs. Here it is clearly observed a second bulge at high concentration of inhibitor. Probably this could be related to the involvement of a second new active site (e.g. allosteric site), but more studies are required to shed light on this. In future, besides studying more deeply this behaviour, the same compound will be tested with BidAc.

6.3.3 ^{1}H-^{15}N HSQC-NMR Mcl-1 titration with compound and cocrystallization attempts

To better understand which kind of amino acids were involved in the binding, a Mcl-1 titration with compound **94** was monitored by bidimensional ^{1}H-^{15}N HSQC-NMR. Operatively ^{15}N-enriched Mcl-1 solution was realized adding buffer components and a mixture of D_2O/H_2O 1:9 in a NMR tube provided with a Shigemi tube. From a stock solution of compound **94** 3 aliquots were taken and added to NMR tube in order to get 1:1, 1:2 and 1:4 ^{15}N-Mcl-1\DS102 molar ratios and acquiring ^{1}H-^{15}N HSQC spectra (HSQCETFPF3GPSI) after each addition. The same spectrum was acquired for free Mcl-1. By these acquisitions the 2D spectrum showed in **Figure 6.3.3.1** was obtained.

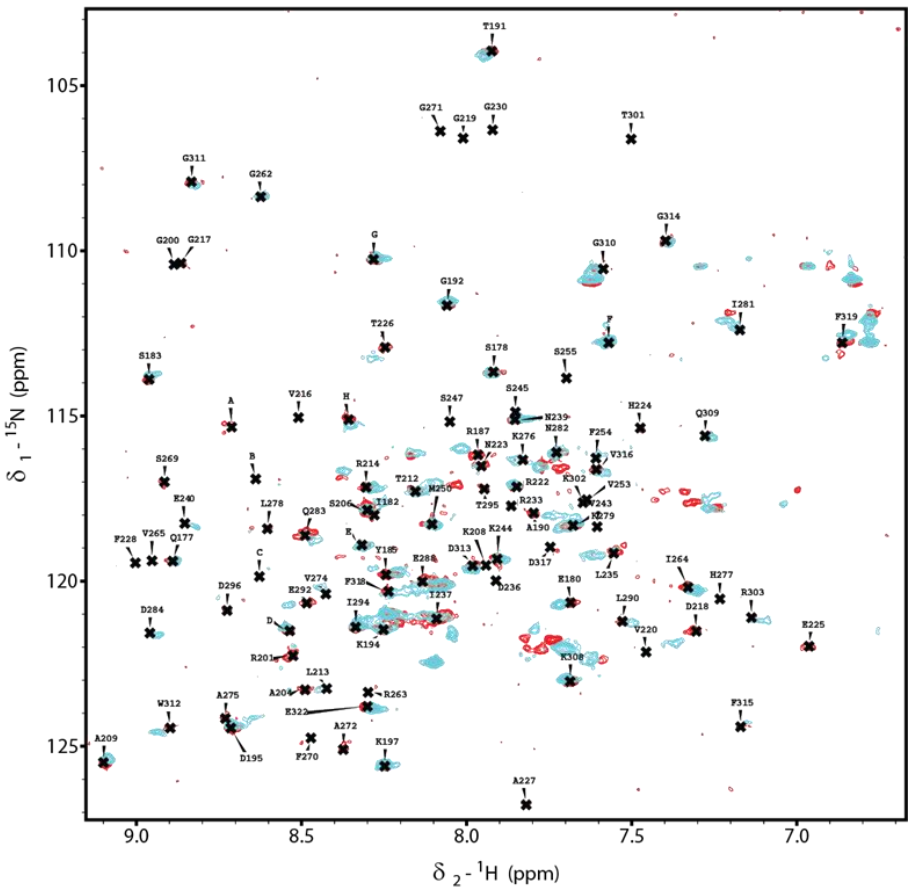

Figure 6.3.3.1: ^{1}H-^{15}N HSQC 2D spectrum of Mcl-1 titraton: red spots are related to free Mcl-1, blue spots are related to Mcl-1/x 1:4 titration point. The loss of resolution in these conditions, perhaps, is justified by the precipitation observed in the NMR tube of a white solid.

Each spot was assigned to each peptide NH of the relative amino acids undergoing linear deviation with respect to free Mcl-1 1H-15N HSQC. These amino acids perturbated upon

titration were plotted in red (for Lys) or blue (for general amino acids) on protein structure model, obtained by PyMol software.

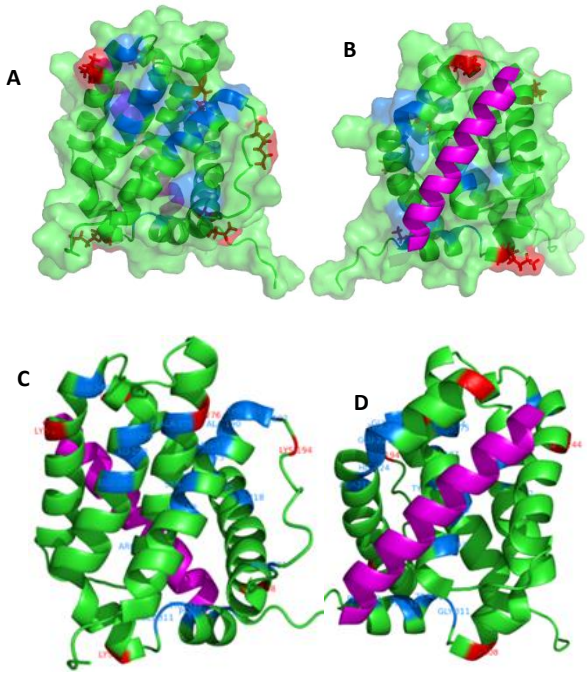

Figure 6.3.3.2: Front and back views of Mcl-1 with BID superimposition (violet): **A**-**B**) transparent surface representation; **C**-**D**) ribbon representation. On the green protein (Mcl-1) amino acids involved in the titration are highlighted in red (Lys) or blue (other aminoacids, not Lys). Figures obtained with PyMol software (PDB code: 2JM6).

The list of perturbated amino acids is: I182, S183, Y185, R187, A190, T191, G192, K194, R201, K208, D218, H224, E225, T226, K234, E240, K244, R263, V274, A275, K276, E288, L290, E292, K308, G311, W312, F315, F319. As it can be immediately seen in **Figure 6.3.3.2**, blue amino acids are mostly concentrated onto the back of the protein with respect to NOXA/BID recognition site. This suggests that probably compound **94** might inhibit through an allosteric site located in the back of the protein, as predicted by Fluorescence Anisotropy Assays. We have also to take into account that an aspecific binding of lysines is observed. Probably they are bound to calixarene via carboxylates or cavity through an inclusion event, which has been widely reported in literature[105,106]. Unfortunately for the high number of variables and the low number of information collected by 1H-15N HSQC, we cannot draw definitive conclusions. For these reasons a preliminary cocrystallization screening was carried out with different ratio of Mcl-1 or p300 over compound **94** (free protein, 1 and 1.5) with Formulatrix Robot. From stock solutions were taken aliquots mixed together in microcentrifuge tubes and left one day of incubation to let the formation of the complex protein/inhibitor. The solutions were loaded on automatic robot and set up in order to have a protein final concentration of 300 μM.

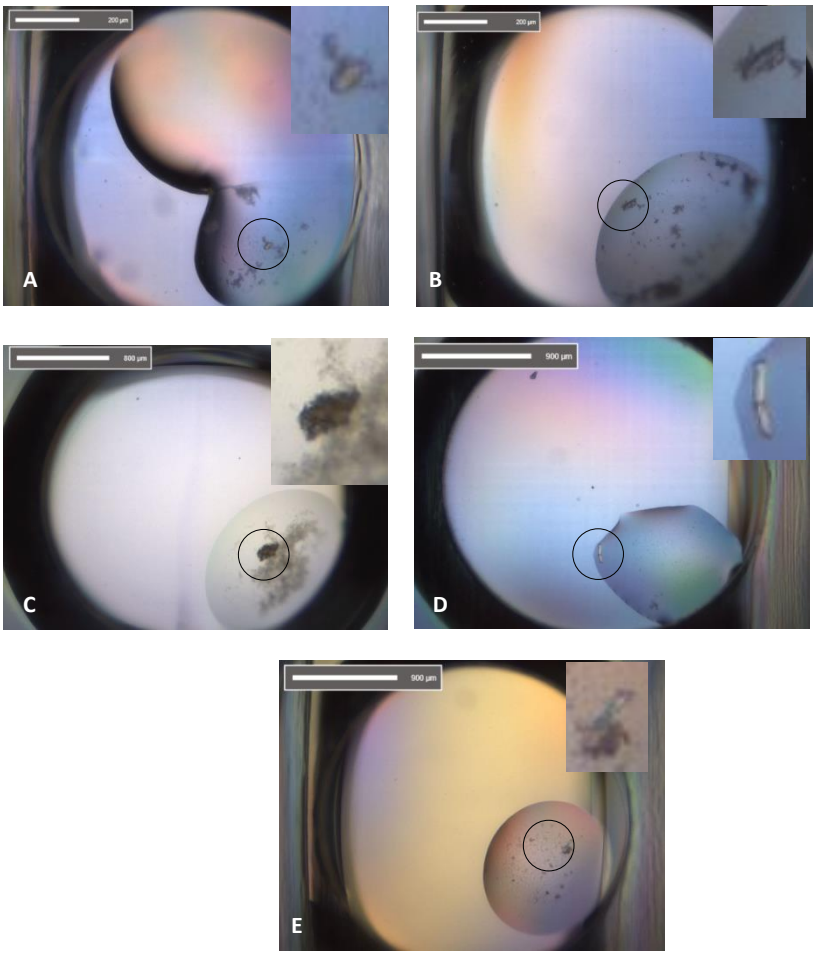

Figure 6.3.3.3: Cocrystallization plate wells. A) Free Mcl-1 (experimental conditions: 35% v/v dioxane; total volume 7.5µl; image scale 200µm); B) **94**/Mcl-1 ratio 1.5 (experimental conditions: 0.1M Tris 8.5 pH, 20% w/v PEG 6K; total volume 12.5µl; image scale 200µm); C) **94**/Mcl-1 ratio 2 (experimental conditions: 0.085M Hepes 7.5 pH, 1.7%v/v PEG 400, 1.7M $(NH_4)_2SO_4$, 15%v/v glycerol; total volume 8.075µl, image scale 800µm); D) **94**/Mcl-1 ratio 1.5 (experimental conditions: 0.2M MgCl2, 0.09M Hepes 7.5 pH, 27%v/v PEG 400, 10%v/v glycerol; total volume 11.5µl; image scale 900µm); E) **94**/Mcl-1 ratio 1.5 (experimental conditions: 0.17M CH_3COONH_4, 0.085M Na_3Citrate 5.6 pH, 25.5%w/w PEG 4K, 15% v/v glycerol; total volume 2.125µl; image scale 900µm).

In **Figure 6.3.3.3** are reported the most promising drops, in which some crystals were seen. For the time being it is still under investigation if these crystals are suitable for X-ray shooting (or for soaking with solution of compound **94**) or they must be optimized around crystallization conditions used. Unfortunately all other conditions tested showed a general precipitation where no crystals were observed.

6.3.4 Aggregation studies in water

Considering, up to now, the poor information collected by HSQC-NMR and cocrystallization, we actually do not know which kind of structure of compound **94** (aggregate or single molecule)

binds to the protein in question. With this in mind we proposed a new fluorescence assay focused on the determination of minimum micellar concentration (m.m.c). The method was firstly optimized on widely-used detergent Triton X-100 in the same buffer used for Mcl-1 fluorescence anisotropy assays. As fluorescent probe was used NileRed (NR), which is known to increase its fluorescence intensity when excluded by water molecules in apolar environment such as in micelles.

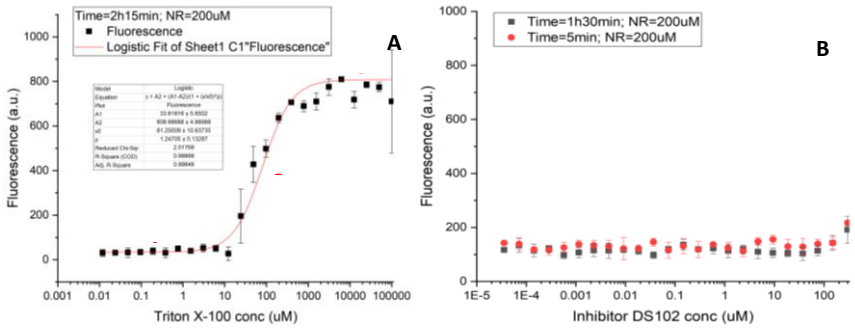

Figure 6.3.4.1: Fluorescence assay for m.m.c determination. **A**) Triton X-100 test assay. Experimental conditions: 0.1 M Triton X-100 (final concentration), 200 nM NileRed, 0.02 M Tris, 0.15 M NaCl, 0.01% Triton, pH 7.55, 1 mM DTT; **B**) Compound X assay. Experimental conditions: 300 μM DS102 (**94**) (final concentration), 200nM NileRed, 0.02 M Tris, 0.15 M NaCl, 0.01% Triton, pH 7.55, 1 mM DTT.

Before the actual assay, a sort of calibration curve was done for NileRed over a range concentration of 1 μM-1 mM with a constant concentration of Triton X-100 of 1mM. Considering the linear response over all the range, a NR concentration of 200 nM was set up, which guarantees a good sensitivity to the method limiting possible interferences related to NR aggregation observed in higher concentrations. The test Triton X-100 assay was performed in 384-well Optiplates in the same way as done for Fluorescence Anisotropy assays (see **Paragraph 6.3.2**), setting the monochromator slits onto excitation and emission wavelengths of NR, namely respectively 550 nm and 633 nm. As it can be seen in **Figure 6.3.4.1**, in the first plateau step no fluorescence enhancement is observed, because this concentration range is still too low for the generation of micelles able to include and desolvate NR. Increasing detergent concentration, at the inflexion point Triton X-100 tails orient around NR molecules, which, thanks to them, the water molecules are excluded and the fluorescence is switched on till is reached the maximum fluorescence intensity at concentration higher than 1mM, where all NR molecules are included in micelles. Data were plotted with a sigmoidal logistic fitting in OriginPro software, with which was possible to determine m.m.c. at the inflection point (0.08±0.01) mM. Considering the presence in the buffer analysis of 0.01%Triton X-100, the experimental value was corrected with an additional factor, which took into account the detergent concentration before the analysis (0.155 mM). The final corrected experimental m.m.c. is (0.24±0.01) mM, which is totally in agreement with m.m.c. determined by viscosimetry (0.23 mM).

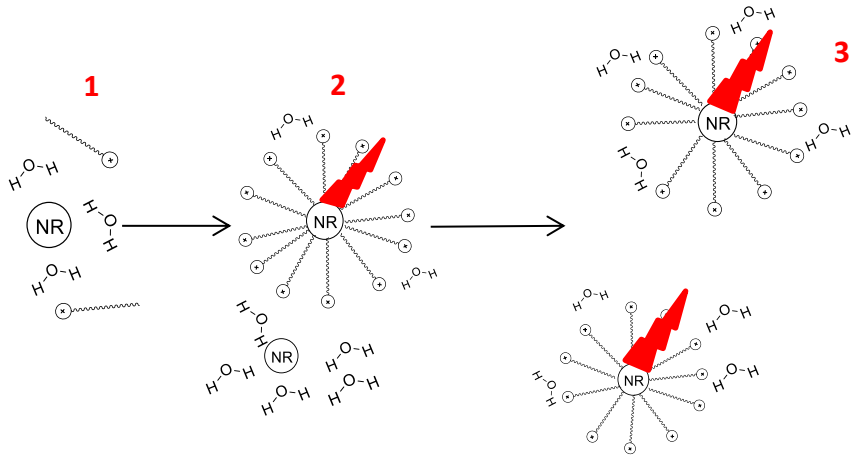

Figure 6.3.4.2: Microscopic schematic representation of Triton X-100 assay. Red numbers are referred to the same steps highlighted in **Figure 6.3.4.1A**.

Considering the successful outcome of Triton X-100 m.m.c. determination, the same assay was repeated in the same way with compound **94**, used as detergent, in the same concentration conditions employed in Mcl-1 FA (300 μM-10 nM). A flat line is observed with a weak fluorescence increase at 100 μM. Since we did not have further compound to span the concentration range, we can just say that for almost all concentration range compound **94** seems to behave as a single-molecule binder. If the terminal slow increase was attributable to an initial formation of micelles, the micelle binding could be another reason for the second bulge observed in **Figure 6.3.2.2**, beyond the hypothetical additional allosteric binding.

6.4 Conclusions

Protein-protein interactions (PPIs) are common strategies exploited by cell to carry out several physiological functions such as cell-cell communication, DNA translation and replication, cellular respiration and so on (**Paragraph 6.1**). When genes encoding for these proteins are effectively mutated in hot spot region (protein surface areas, which contribute mostly in the recognition event), the resulting proteins carry structural modifications, which unable them to recognize each other. This, obviously, triggers a series of events aimed to activate several pathological pathways for the development of the associated disease. Taking into account that almost all PPIs are mediated by α-helix recognition in the hot spots, recently a lot of researchers are trying to design α-helix mimetics able to inhibit PPIs and limit as well the progression of the disease.

In this project, we proposed the use of upper-rim trifunctionalized calix[4]arenes in cone conformation as a suitable scaffold for mimicking i, i+3 (4) and i+7 positions in α-helices. In particular, we synthetised analogues with methylene-O-trisopropyl (**88a**), methylene-O-trisobutyl (**88b**) and trisobutyl moieties (**91**, **92b**, **94**). During my secondment at University of Leeds, our derivatives, structural mimetics of hot spots of HIF1α (Leu819-Leu822-Val825) and NOXA-Bid (Leu690-Leu693-Leu694), were tested in the competition Fluorescence Anysotrophy Assays with p300/HIF1α and Mcl-1/NOXA-Bid. What turned out is that just derivative **94**,

characterized by carboxy moieties at lower rim, showed to be active in the inhibition of both complexes. In particular, for p300/HIF1α was calculated an IC50=(1.98±0.86)μM, whereas for Mcl-1/Bid was calculated an IC50=(2.85±0.83)μM. Even if they are respectively two and one order of magnitude less active than the references HIF1α-Ac (0.06±0.01)μM and NOXA-Ac (0.86±0.06)μM, compound 94 is an interesting inhibitor that must be studied more deeply in this field. So to understand more about the inhibition mechanism a Mcl-1 1H-15N HSQC titration was carried out with compound **94**. What we obtained is that a huge number of amminoacids in the back of Mcl-1 (with respect to NOXA-Bid recognition site) are involved in the binding. This evidences the fact that Mcl-1 might be inhibited by 94 through an allosteric site as suggested in the two-bulge Fluorescence Quenching Assay profile. In order to understand more about this binding, in future the cocrystals obtained will be shooted with X-Rays or will be setup new cocrystallization conditions to optimize their morphology. Considering the amphiphilic nature of compound **94**, a fluorescence assay for the determination of minimum micellar concentration was setup. From respective experimental data, it is clear that at inhibition concentrations no micelles are formed and so compound 94 behaves like a single-molecule binder.

6.5 Experimental part

Calixarene synthesis

General information. All moisture-sensitive reactions were carried out under a nitrogen atmosphere. All dry solvents were prepared according to standard procedures and stored over 3 or 4 Å molecular sieves. All other reagents were commercial samples and used without further purification. TLC were performed using prepared plates of silica gel (Merck 60 F_{254} on aluminium) and revealed using UV light or staining reagents: $FeCl_3$ (1% in H_2O/MeOH 1:1) and basic solution of $KMnO_4$ (0.75% in H_2O). Flash chromatography was performed on 32-63 μm on 60 Å Merck silica gel. Melting points were determined on an electrothermal apparatus Gallenkamp, in capillaries sealed under nitrogen. ^1H NMR (300 or 400 MHz) and ^{13}C NMR spectra (75 or 100 MHz) were recorded on Bruker AV300 and AV400 spectrometers using partially deuterated solvents as internal standards. All ^{13}C NMR were performed with proton decoupling. Mass spectra were recorded in Electrospray Ionization (ESI) mode using a SQ Detector, Waters (capillary voltage = 2.40-3.50 kV, cone voltage = 40-100 V, extractor voltage = 2 V, source block temperature = 150 °C, desolvation temperature = 300 °C, cone gas (N_2) flow rates = 95 L/hr, desolvation gas (N_2) flow rates = 480 L/hr) in MeOH.

cone-5,11,17-tris(formyl)-25,26,27,28-(2-ethoxyethylether)calix[4]arene (85): In a 2-necked round-bottom flask compound **50b** (4.21 mmol, 3.00 g) and dichloromethyl methyl ether (0.21 mol, 19.000 ml) were dissolved in dry DCM (150 ml) and then $TiCl_4$ (0.17 mol, 18.500 ml) was added in. The brown mixture was kept stirring for about 1h at room temperature, monitoring it very carefully each 10 minutes by TLC (AcOEt/Hex 6:4, R_f=0.51). The mixture was quenched pouring it in a flask containing H_2O (400 ml), meanwhile a vigorous stirring was kept. The organic phase was washed again with H_2O (200 ml) and eventually the organic solvent was removed by reduced pressure. The crude was purified by a flash chromatography column (AcOEt/Hex 1:1→6:4→7:3→8:2) to get compound **85** as a yellow oil (1.48 g, 1.86 mmol, 44%

yield). **^{1}H NMR** (400 MHz, $CDCl_3$) δ (ppm): 9.51 (s, 1H, 11-C*H*O), 9.49 (s, 2H, 5,17-C*H*O), 7.10 (s, 4H, Ar*H*), 7.03 (s, 2H, Ar*H*), 6.51 – 6.36 (m, 3H, Ar*H*), 4.57 (d, *J* = 13.8 Hz, 2H, ArCH_{ax}HAr), 4.48 (d, *J* = 13.8 Hz, 2H, ArCHH_{ax}Ar), 4.26 – 4.06 (m, 6H, OCH_2CH$_2$OCH$_2$CH$_3$), 4.06 – 3.96 (m, 2H, OCH_2CH$_2$OCH$_2$CH$_3$), 3.80 – 3.65 (m, 8H, OCH$_2$CH_2OCH$_2$CH$_3$), 3.52 – 3.38 (m, 8H, OCH$_2$CH$_2$OCH_2CH$_3$), 3.24 (d, *J* = 13.8 Hz, 2H, ArCH_{eq}HAr), 3.16 (d, *J* = 13.8 Hz, 2H, ArCHH_{eq}Ar), 1.21 – 0.99 (m, 12H, OCH$_2$CH$_2$OCH$_2$CH_3). The spectroscopic data obtained are in agreement with those ones reported in literature[107].

cone-5,11,17-tris(methylen-1-olo)-25,26,27,28-(2-ethoxyethylether)calix[4]arene (86): In a 2-necked round-bottom flask compound **85** (1.86 mmol, 1.48 g) and $NaBH_4$ (5.76 mmol, 0.22 g) were stirred in absolute EtOH (15 ml) for 1 day at room temperature, monitoring the reaction by TLC (Hex/AcOEt 4:6). The reaction was quenched with 1N HCl (15 ml) and EtOH was subsequently removed by reduced pressure. The aqueous phase was extracted with AcOEt (3 x 20 ml) and then the combined organic phases were washed with H_2O (20 ml), sat. $NaHCO_3$ (20 ml) and finally H_2O again (20 ml). The organic phase was dried with anhydrous Na_2SO_4 and upon filtration, the solvent was removed by reduced pressure to get compound **86** as a colourless oil (1.49 g, 1.86 mmol, 99% yield). **^{1}H NMR** (400 MHz, $CDCl_3$) δ (ppm): 6.85 (d, *J* = 7.5 Hz, 2H, m-Ar*H*), 6.83 (s, 1H, Ar*H*), 6.73 (t, *J* = 7.5 Hz, 1H, p-Ar*H*), 6.55 (s, 2H, Ar*H*), 6.46 (s, 2H, Ar*H*), 4.52 (d, *J* = 13.3 Hz, 4H, axial ArCH_2Ar), 4.45 (s, 2H, 11-CH_2OH), 4.31 – 4.19 (m, 8H, 5,17- CH_2OH, OCH_2CH$_2$OCH$_2$CH$_3$), 4.06 (t, *J* = 5.5 Hz, 4H, OCH_2CH$_2$OCH$_2$CH$_3$), 3.89 (t, *J* = 5.5 Hz, 4H, OCH$_2$CH_2OCH$_2$CH$_3$), 3.83 (t, *J* = 5.5 Hz, 4H, OCH$_2$CH_2OCH$_2$CH$_3$), 3.62 – 3.50 (m, 8H, OCH$_2$CH$_2$OCH_2CH$_3$), 3.17 (d, *J* = 13.3 Hz, 2H, ArCH_{eq}HAr), 3.16 (d, *J* = 13.3 Hz, 2H, ArCHH_{eq}Ar), 2.43 (s, 2H, 5,17-O*H*), 2.24 (s, 1H, 11-O*H*), 1.32 – 1.17 (m, 12H, OCH$_2$CH$_2$OCH$_2$CH_3). The spectroscopic data obtained are in agreement with those ones reported in literature[108].

cone-5,11,17-tris(methylen-1-chloro)-25,26,27,28-(2-ethoxyethylether)calix[4]arene (87): In a 2-necked round-bottom flask compound **86** (0.31 mmol, 0.21 g) and $SOCl_2$ (4.56 mmol, 0.332 ml) were stirred in dry DCM (2 ml) for 1 h 30 minutes at room temperature, monitoring the reaction by TLC (Hex/AcOEt 7:3). The mixture was simply dried out at rotavapor to get compound **87** as a yellow oil (0.25 g, 0.29 mmol, 99% yield). **^{1}H NMR** (300 MHz, $CDCl_3$) δ (ppm): 6.70 (d, *J* = 3.0 Hz, 4H, Ar*H*), 6.53 (s, 5H, Ar*H*), 4.47 (d, *J* = 13.5 Hz, 4H, axial ArCH_2Ar), 4.32 (s, 4H, 5,17-CH_2Cl), 4.25 (s, 2H, 11-CH_2Cl), 4.11 (t, *J* = 5.1 Hz, 8H, OCH_2CH$_2$OCH$_2$CH$_3$), 4.07 (t, *J* = 5.1 Hz, 8H, OCH_2CH$_2$OCH$_2$CH$_3$), 3.80 (t, *J* = 6.4 Hz, 8H, OCH$_2$CH_2OCH$_2$CH$_3$), 3.52 (q, *J* = 6.4 Hz, 4H, OCH$_2$CH$_2$OCH_2CH$_3$), 3.51 (q, *J* = 6.4 Hz, 4H, OCH$_2$CH$_2$OCH_2CH$_3$), 3.13 (d, *J* = 13.5 Hz, 2H, ArCH_{eq}HAr), 3.12 (d, *J* = 13.5 Hz, 2H, ArCHH_{eq}Ar), 1.19 (t, *J* = 6.4 Hz, 6H, OCH$_2$CH$_2$OCH$_2$CH_3), 1.18 (t, *J* = 6.4 Hz, 6H, OCH$_2$CH$_2$OCH$_2$CH_3). The spectroscopic data obtained are in agreement with those ones reported in literature[107].

cone-5,11,17-tris(methylen-1-(2-propoxy)-25,26,27,28-(2-ethoxyethylether)calix[4]arene (88a): In a 2-necked round-bottom flask NaH (0.52 mmol, 20.93 mg) was stirred in isopropanol (10 ml) for about 30 minutes at room temperature. The solvent was totally removed by reduced pressure and the salt was hence suspended in toluene (11 ml). Then a solution of compound **87** (0.12 mmol, 0.1 g) in toluene (4 ml) was added in and the mixture was kept stirring for 2 days at reflux, monitoring the reaction by TLC (DCM/MeOH 99:1). The mixture was washed with 1N HCl (5 ml), with H_2O (10 ml) and eventually with sat. $NaHCO_3$ (10 ml). The organic phase was dried with anhydrous Na_2SO_4 and upon filtration, the solvent was removed by reduced pressure. An

impure fraction of the title compound was isolated by a first purification with a flash chromatography column (Hex/AcOEt 76:24) and finally it was totally purified by a second purification with semipreparative TLC to get compound **88a** as a white solid (19.10 mg, 20.57 umol, 18% yield). **^{1}H NMR** (300 MHz, $CDCl_3$) δ (ppm): 6.81 (s, 4H, Ar*H*), 6.50 – 6.38 (m, 5H, Ar*H*), 4.49 (d, *J* = 13.3, 2H, ArCH_{ax}HAr), 4.47 (d, *J* = 13.3, 2H, ArCHH_{ax}Ar), 4.29 (s, 4H, 5,17-CH_2OCH$(CH_3)_2$), 4.17 (t, *J* = 6.2 Hz, 4H, OCH_2CH$_2$OCH$_2$CH$_3$), 4.07 (s, 2H, 11-CH_2OCH$(CH_3)_2$), 4.06 – 3.99 (m, 4H, OCH_2CH$_2$OCH$_2$CH$_3$), 3.87 (t, *J* = 6.2 Hz, 4H, OCH$_2$CH_2OCH$_2$CH$_3$), 3.83 (t, *J* = 6.2 Hz, 4H, OCH$_2$CH_2OCH$_2$CH$_3$), 3.62 (hept, *J* = 6.2 Hz, 2H, 5,17-CH$_2$OC*H*$(CH_3)_2$), 3.58 (q, *J* = 6.2 Hz, 4H, OCH$_2$CH$_2$OCH_2CH$_3$), 3.56 (q, *J* = 6.2 Hz, 4H, OCH$_2$CH$_2$OCH_2CH$_3$), 3.36 (hept, *J* = 6.2 Hz, 1H, 11-CH$_2$OC*H*$(CH_3)_2$), 3.14 (d, *J* = 13.3 Hz, 2H, ArCH_{eq}HAr), 3.14 (d, *J* = 13.3 Hz, 2H, ArCHH_{eq}Ar), 1.33 – 1.15 (m, 30H, CH$_2$OCH$(CH_3)_2$, OCH$_2$CH$_2$OCH$_2$CH_3), 1.08 (d, *J* = 6.2 Hz, 6H, CH$_2$OCH$(CH_3)_2$). **^{13}C NMR** (75 MHz, $CDCl_3$) δ (ppm): 171.1 (*C*-O), 156.4 (*C*-O), 155.7 (*C*-O), 155.1 (*C*-O), 135.5, 135.5, 134.3, 134.1, 132.3, 132.3, 128.2, 128.0, 127.9 (*C*Ar), 127.4 (*C*Ar), 121.9, 73.4, 73.4 (O*C*H$_2$CH$_2$OCH$_2$CH$_3$), 72.8 (O*C*H$_2$CH$_2$OCH$_2$CH$_3$), 70.6 (11-CH$_2$O*C*H$(CH_3)_2$), 70.2, 70.0, 69.8, 69.6 (5,17-*C*H$_2$OCH$(CH_3)_2$), 69.6, 66.4 (11-*C*H$_2$OCH$(CH_3)_2$), 66.3 (OCH$_2$CH_2OCH$_2$CH$_3$), 60.4 (OCH$_2$CH$_2$OCH$_2$CH$_3$), 31.9, 31.6, 30.8 (ArC_{ax}H$_2$Ar), 29.7 (ArC_{eq}H$_2$Ar), 29.4, 22.7, 22.2, 22.1, 21.0 (OCH$_2$CH$_2$OCH$_2$*C*H$_3$), 15.3 (CH$_2$OCH$(CH_3)_2$), 15.3, 14.2, 14.1. **ESI-MS (+):** calc. for $C_{56}H_{80}O_{11}Na$ $[(M+Na)^+]$: m/z 951.56, found m/z 951.64 (100%); calc. for $C_{56}H_{80}O_{11}K$ $[(M+K)^+]$: m/z 967.53, found m/z 967.63 (100%).

cone-5,11,17-tris(methylen-1-(isobutoxy))-25,26,27,28-(2-ethoxyethylether)calix[4]arene (88b): In a 2-necked round-bottom flask NaH (0.70 mmol, 27.92 mg) was stirred in isopropanol (3 ml) for about 30 minutes at room temperature. The solvent was totally removed by reduced pressure and the salt was hence suspended in toluene (5 ml). Then a solution of compound **87** (0.12 mmol, 0.10 g) in toluene (2 ml) was added in and the mixture was kept stirring for 1 day at reflux, monitoring the reaction by TLC (Hex/AcOEt 7:3). The mixture was washed with 1N HCl (5 ml), with H_2O (10 ml) and eventually with sat. $NaHCO_3$ (10 ml). The organic phase was dried with anhydrous Na_2SO_4 and upon filtration, the solvent was removed by reduced pressure. The crude was eventually purified by semipreparative TLC (DCM/acetone 9:1) to get compound **88b** as a yellow oil (53.90 mg, 55.53 umol, 48% yield). **^{1}H NMR** (300 MHz, $CDCl_3$) δ (ppm): 6.80 (s, 4H, Ar*H*), 6.48 – 6.36 (m, 5H, Ar*H*), 4.50 (d, *J* = 13.3 Hz, 2H, ArCH_{ax}HAr), 4.48 (d, *J* = 13.3 Hz, 2H, ArCHH_{ax}Ar), 4.29 (s, 4H, 5,17-CH_2OCH$_2$CH$(CH_3)_2$), 4.18 (t, *J* = 6.1 Hz, 4H, OCH_2CH$_2$OCH$_2$CH$_3$), 4.10 – 4.00 (m, 4H, OCH_2CH$_2$OCH$_2$CH$_3$), 4.06 (s, 2H, 11-CH_2OCH$_2$CH$(CH_3)_2$), 3.88 (t, *J* = 6.1 Hz, 4H, OCH$_2$CH_2OCH$_2$CH$_3$), 3.85 – 3.78 (m, 4H, OCH$_2$CH_2OCH$_2$CH$_3$), 3.56 (q, *J* = 6.1 Hz, 4H, OCH$_2$CH$_2$OCH_2CH$_3$), 3.56 (q, *J* = 6.1 Hz, 4H, OCH$_2$CH$_2$OCH_2CH$_3$), 3.19 (d, *J* = 6.7 Hz, 4H, 5,17-CH$_2$OCH_2CH$(CH_3)_2$), 3.15 (d, *J* = 13.3 Hz, 2H, ArCH_{eq}HAr), 3.14 (d, *J* = 13.3 Hz, 2H, ArCHH_{eq}Ar), 3.01 (d, *J* = 6.7 Hz, 2H, 11-CH$_2$OCH_2CH$(CH_3)_2$), 1.91 (hept, *J* = 6.7 Hz, 2H, 5,17-CH$_2$OCH$_2$C*H*$(CH_3)_2$), 1.82 (hept, *J* = 6.7 Hz, 1H, 11-CH$_2$OCH$_2$C*H*$(CH_3)_2$), 1.32 – 1.15 (m, 12H, OCH$_2$CH$_2$OCH$_2$CH_3), 0.94 (d, *J* = 6.7 Hz, 12H, 5,17-CH$_2$OCH$_2$CH(CH_3)$_2$), 0.88 (d, *J* = 6.7 Hz, 6H, 11-CH$_2$OCH$_2$CH(CH_3)$_2$). **^{13}C NMR** (75 MHz, $CDCl_3$) δ (ppm): 156.5, 155.7, 155.1, 135.5, 134.3, 134.1, 132.0, 132.0, 128.1 (*C*Ar), 128.0 (*C*Ar), 127.9 (*C*Ar), 127.3 (*C*Ar), 121.9 (*C*Ar), 77.0 (CH$_2$OCH$_2$CH$(CH_3)_2$), 76.8 (CH$_2$OCH$_2$CH$(CH_3)_2$), 73.4, 73.4, 72.9 (*C*H$_2$OCH$_2$CH$(CH_3)_2$), 72.8 (O*C*H$_2$CH$_2$OCH$_2$CH$_3$), 72.8 (O*C*H$_2$CH$_2$OCH$_2$CH$_3$), 69.7 (OCH$_2$*C*H$_2$OCH$_2$CH$_3$), 66.4 (OCH$_2$CH$_2$O*C*H$_2$CH$_3$), 66.3 (OCH$_2$CH$_2$O*C*H$_2$CH$_3$), 30.9 (Ar*C*H$_2$Ar), 28.5 (CH$_2$OCH$_2$*C*H$(CH_3)_2$), 28.4 (CH$_2$OCH$_2$*C*H$(CH_3)_2$), 19.5 (CH$_2$OCH$_2$CH(*C*H$_3$)$_2$), 19.5 (CH$_2$OCH$_2$CH(*C*H$_3$)$_2$), 15.3 (OCH$_2$CH$_2$OCH$_2$*C*H$_3$), 15.3

($OCH_2CH_2OCH_2CH_3$). **ESI-MS (+):** calc. for $C_{59}H_{86}O_{11}Na$ [$(M+Na)^+$]: m/z 993.61, found m/z 993.77 (100%); calc. for $C_{59}H_{86}O_{11}K$ [$(M+K)^+$]: m/z 1109.58, found m/z 1009.76 (40%).

cone-25-(benzyloxy)-26,27,28-tris((2-methyl-3-ene)propoxy)calix[4]arene (89): In a 3-necked round-bottom flask compound **43** (1.13 mmol, 0.58 g) and NaH (5.64 mmol, 0.25 g) were stirred in dry DMF (5 ml) for 30 minutes at room temperature. Then, once the mixture had been heated up to 50°C, 3-chloro-2-methylprop-1-ene (5.64 mmol, 0.549 ml) was added in and the mixture was kept stirring for 1 day at 50°C, monitoring the reaction by TLC (toluene/Hex 7:3, Rf=0.63). The reaction was quenched with 1N HCl (5 ml) and then the mixture was extracted with AcOEt (3 x 100 ml). The combined organic phases were washed with brine (3 x 100 ml), dried with anhydrous Na_2SO_4 and upon filtration, the solvent was removed by reduced pressure. The solid was reprecipitated in DCM/MeOH gaining beige needle crystals, which were purified by flash chromatography column (toluene/Hex 2:8→1:1) to get compound **89** as a white powder (0.61 g, 0.91 mmol, 81% yield). **^{1}H NMR** (400 MHz, $CDCl_3$) δ (ppm): 7.51 (m, 2H, m-Bn*H*), 7.43 – 7.38 (m, 3H, o,p-Bn*H*), 6.98 (d, *J* = 7.4 Hz, 2H, m-Ar*H*O), 6.95 – 6.83 (m, 4H, Ar*H*), 6.55 (t, *J* = 7.4 Hz, 2H, p-Ar*H*O), 6.51 – 6.40 (m, 4H, Ar*H*), 5.29 (dt, *J* = 9.2, 1.6 Hz, 3H, OCH_2C=CH*H*), 5.24 (s, 2H, 25-OCH_2Ar), 5.09 (dt, *J* = 9.2, 1.6 Hz, 3H, OCH_2C=CH*H*), 4.80 (s, 2H, 27-OCH_2C=CH_2), 4.71 (d, *J* = 13.7 Hz, 2H, ArCH_{ax}HAr), 4.43 (d, *J* = 13.7 Hz, 2H, ArCH_{ax}HAr), 4.40 (s, 4H, 26,28-OCH_2C=CH_2), 3.37 (d, *J* = 13.7 Hz, 2H, ArCH_{eq}HAr), 3.20 (d, *J* = 13.7 Hz, 2H, ArCH_{eq}HAr), 2.05 (s, 9H, CH_3). **^{13}C NMR** (100 MHz, $CDCl_3$) δ (ppm): 156.9, 155.7, 155.5, 142.6, 142.3, 137.9, 136.6, 135.7, 134.3, 133.9, 130.3 (m-CAr_{Bn}), 128.9 (m-CAr_{calix}), 128.7 (*C*Ar_{calix}), 128.1, 128.1, 128.0 (*C*Ar_{calix}), 127.9 (o,p-*C*Ar_{Bn}), 122.3, 122.3, 121.9, 114.6, 113.6 (OCH_2C=CH_2), 78.7 (26,28-OCH_2C=CH_2), 78.3 (27-OCH_2C=CH_2), 77.5, 77.2, 76.9, 75.6 (27-OCH_2Ar), 31.6 (ArCH_2Ar), 31.5 (ArCH_2Ar), 29.9, 21.0, 20.7 (CH_3). **ESI-MS (+):** calc. for $C_{47}H_{48}O_4Na$ [$(M+Na)^+$]: m/z 699.35; found m/z 699.56 (100%); calc. for $C_{47}H_{48}O_4K$ [$(M+K)^+$]: m/z 715.32; found m/z 715.47 (65%).

cone-25-(benzyloxy)-5,11,17-tris((2-methyl-3-ene)propyl)-calix[4]arene-26,27,28-triolo (90): In a 2-necked round-bottom flask compound **89** (0.97 mmol, 0.66 g) and N,N-dimethylaniline (15 ml) were stirred for 1 h at 210°C with a sand bath monitoring the reaction by TLC (toluene/Hex 1:1). The mixture was cooled down at 0°C for 10 minutes and then quenched with 1N HCl (50 ml). After having stirred for 1 h, the mixture was extracted with DCM (3 x 30 ml) and the combined organic phases were dried with anhydrous Na_2SO_4. Upon filtration, the solvent was removed by reduced pressure and the crude was purified by a flash chromatography column (toluene/Hex 1:1) to get compound **90** as a white powder (0.30 g, 0.45 mmol, 46% yield). **^{1}H NMR** (400 MHz, $CDCl_3$) δ (ppm): 9.56 (s, 1H, 27-O*H*), 9.18 (s, 2H, 26,28-O*H*), 7.78 – 7.72 (m, 2H, m-Bn*H*), 7.59 – 7.47 (m, 3H, o,p-Bn*H*), 7.12 (d, *J* = 7.6 Hz, 2H, m-Ar*H*O), 6.93 (t, *J* = 7.6 Hz, 1H, p-Ar*H*O), 6.88 (d, *J* = 1.9 Hz, 2H, o-Ar*H*CH_2C=CH_2), 6.83 (d, *J* = 1.9 Hz, 2H, o-Ar*H*CH_2C=CH_2), 6.80 (s, 2H, o-Ar*H*CH_2C=CH_2), 5.21 (s, 2H, 25-OCH_2Ar), 4.80 (d, *J* = 7.3 Hz, 3H, ArCH_2C=CH*H*), 4.71 (d, *J* = 7.3 Hz, 3H, ArCH_2C=C*H*H), 4.36 (d, *J* = 13.3 Hz, 2H, ArCH_{ax}HAr), 4.21 (d, *J* = 13.3 Hz, 2H, ArCH_{ax}HAr), 3.44 (d, *J* = 13.3 Hz, 2H, ArCH_{eq}HAr), 3.39 (d, *J* = 13.3 Hz, 2H, ArCH_{eq}HAr), 3.15 (s, 4H, 5,17-CH_2C=CH_2), 3.10 (s, 2H, 11-OCH_2C=CH_2), 1.68 (s, 9H, CH_3). **^{13}C NMR** (100 MHz, $CDCl_3$) δ (ppm): 151.4, 149.2, 147.5 (m-*C*ArO), 145.6, 145.5, 135.6, 134.6, 132.7, 131.8, 129.4 (o-*C*ArCH_2C=CH_2), 129.3 (o-*C*ArCH_2C=CH_2), 129.2 (p-*C*ArO), 129.1 (o,p-*C*Bn), 129.0 (m-*C*Bn), 129.0 (o,p-*C*Bn), 128.7, 128.6, 128.3, 128.1, 126.3, 111.6 (ArCH_2C=*C*H_2), 111.6 (ArCH_2C=*C*H_2), 79.3 (OCH_2Ar), 43.8 (ArCH_2C=CH_2), 32.1 (ArCH_2Ar), 31.7 (ArCH_2Ar), 22.2 (CH_3), 22.2 (CH_3). **ESI-MS (-):** calc. for $C_{47}H_{47}O_4$ [$(M-H)^-$]: m/z 675.87; found m/z 675.72 (100%).

cone-5,11,17-tris((2-methyl)propyl)-calix[4]arene-25,26,27,28-tetraolo (91): In a Parr reactor 10% Pd/C (catalytic amount) was suspended into a solution of compound **90** (0.39 mmol, 0.27 g) in AcOEt/EtOH (100 + 25 ml). H_2 was added in at 2.5 bar of pressure through a Parr apparatus and the mixture was left reacting for 1 night at room temperature, monitoring the reaction by TLC (Hex/AcOEt 8:2, Rf=0.67). The catalyst was filtered off and the solvent was removed by reduced pressure to get compound **91** as a white powder (0.25 g, 0.37 mmol, 99% yield). **^{1}H NMR** (400 MHz, $CDCl_3$) δ (ppm): 10.22 (s, 4H, O*H*), 7.07 (d, *J* = 7.6 Hz, 2H, m-Ar*H*O), 6.85 – 6.82 (m, 6H, Ar*H*), 6.74 (t, *J* = 7.6 Hz, 1H, p-Ar*H*), 4.26 (bs, 4H, axial ArC*H*$_2$Ar), 3.50 (bs, 4H, equatorial ArC*H*$_2$Ar), 2.28 (d, *J* = 6.9 Hz, 6H, C*H*$_2$CH(CH$_3$)$_2$), 1.86 – 1.70 (m, 3H, C*H*), 0.89 (d, *J* = 6.9 Hz, 18H, C*H*$_3$). **^{13}C NMR** (100 MHz, $CDCl_3$) δ (ppm): 149.0, 146.8, 146.7, 135.2, 129.6, 129.6, 129.5 (*C*Ar$_{calix}$), 128.9 (m-*C*ArO), 128.5, 128.0, 127.9, 127.7, 122.1 (p-*C*ArO), 44.7 (*C*H$_2$CH(CH$_3$)$_2$), 31.9 (Ar*C*H$_2$Ar), 31.9 (Ar*C*H$_2$Ar), 30.2 (*C*H), 22.4 (*C*H$_3$). **ESI-MS (-):** calc. for $C_{40}H_{47}O_4$ [(M-H)$^-$]: m/z 591.36; found m/z 591.59 (100%).

cone-5,11,17-tris((2-methyl)propyl)-25,26,27,28-tetrakis(2-ethoxyethylether)calix[4]arene (92a): In a 2-necked round-bottom flask compound **91** (0.15 mmol, 86.80 mg) and 55% NaH (0.76 mmol, 33.15 mg) were stirred in dry DMF (5 ml) for 1 h at room temperature. Then 2-bromoethyl ethyl ether (0.60 mmol, 100 μl) was added in and the mixture was kept stirring for 1 day at room temperature, monitoring the reaction by TLC (Hex/AcOEt 8:2, R_f=0.39). The mixture was diluted with EtOAc (50 ml) and then washed with 1N HCl (50 ml). The organic phase was dried out at rotavapor and the title compound was separated by most of the impurities through semipreparative TLC (Hex/AcOEt 8:2). The oil obtained was recrystallized with DCM/MeOH at -4°C to get compound **92a** as white bright crystals (95.00 mg, 0.11 mmol, 74% yield). **^{1}H NMR** (400 MHz, $CDCl_3$) δ (ppm): 6.70 (d, *J* = 4.6 Hz, 4H, m-Ar*H*OCH$_2$CH$_2$), 6.44 (d, *J* = 7.2 Hz, 2H, m-Ar*H*OH), 6.37 (dd, *J* = 8.4, 6.4 Hz, 1H, p-Ar*H*OH), 6.22 (s, 2H, m-Ar*H*OCH$_2$CH$_2$), 4.50 (d, *J* = 13.3 Hz, 2H, ArC*H*$_{ax}$HAr), 4.47 (d, *J* = 13.3 Hz, 2H, ArC*H*$_{ax}$HAr), 4.23 (t, *J* = 6.0 Hz, 4H, OC*H*$_2$CH$_2$OCH$_2$CH$_3$), 4.04 (t, *J* = 6.0 Hz, 2H, OC*H*$_2$CH$_2$OCH$_2$CH$_3$), 4.02 (t, *J* = 6.0 Hz, 2H, OC*H*$_2$CH$_2$OCH$_2$CH$_3$), 3.94 (t, *J* = 6.0 Hz, 4H, OCH$_2$C*H*$_2$OCH$_2$CH$_3$), 3.85 (td, *J* = 6.0, 2.6 Hz, 1H, OCH$_2$C*H*$_2$OCH$_2$CH$_3$), 3.63 – 3.52 (m, 8H, OCH$_2$CH$_2$OC*H*$_2$CH$_3$), 3.12 (d, *J* = 13.3 Hz, 2H, ArC*H*$_{eq}$HAr), 3.08 (d, *J* = 13.3 Hz, 2H, ArC*H*$_{eq}$HAr), 2.33 (d, *J* = 7.0 Hz, 4H, 5,17-C*H*$_2$CH(CH$_3$)$_2$), 1.99 (d, *J* = 7.0 Hz, 2H, 11-C*H*$_2$CH(CH$_3$)$_2$), 1.81 (hept, *J* = 7.0 Hz, 2H, 5,17-CH$_2$C*H*(CH$_3$)$_2$), 1.37 (hept, *J* = 7.0 Hz, 1H, 11-CH$_2$C*H*(CH$_3$)$_2$), 1.25 (t , *J* = 7.0 Hz, 6H, OCH$_2$CH$_2$OCH$_2$C*H*$_3$), 1.22 (t, *J* = 7.0 Hz, 6H, OCH$_2$CH$_2$OCH$_2$C*H*$_3$), 0.90 (d, *J* = 7.0, 3.1 Hz, 12H, 5,17-CH$_2$CH(C*H*$_3$)$_2$), 0.88 (), 0.59 (d, *J* = 6.6 Hz, 6H, 11-CH$_2$CH(C*H*$_3$)$_2$). **^{13}C NMR** (100 MHz, $CDCl_3$) δ (ppm): 155.0 (*C*-O), 153.1 (*C*-O), 135.4 (*C*Ar$_{calix}$), 135.2 (*C*Ar$_{calix}$), 135.1 (*C*Ar$_{calix}$), 134.8 (*C*Ar$_{calix}$), 134.6 (*C*Ar$_{calix}$), 133.9 (*C*Ar$_{calix}$), 133.2 (*C*Ar$_{calix}$), 129.3 (*C*Ar$_{calix}$), 129.1 (*C*Ar$_{calix}$), 128.6 (*C*Ar$_{calix}$), 127.7 (*C*Ar$_{calix}$), 122.5 (*C*Ar$_{calix}$), 73.7 (O*C*H$_2$CH$_2$OCH$_2$CH$_3$), 72.6 (O*C*H$_2$CH$_2$OCH$_2$CH$_3$), 69.7 (OCH$_2$*C*H$_2$O*C*H$_2$CH$_3$), 66.5 (OCH$_2$CH$_2$OCH$_2$*C*H$_3$), 66.3 (OCH$_2$CH$_2$OCH$_2$*C*H$_3$), 44.8 (*C*H$_2$CH(CH$_3$)$_2$), 44.6 (*C*H$_2$CH(CH$_3$)$_2$), 30.8 (Ar*C*H$_2$Ar), 30.5 (CH$_2$*C*H(CH$_3$)$_2$), 29.8 (CH$_2$*C*H(CH$_3$)$_2$), 22.4 (CH$_2$CH(*C*H$_3$)$_2$), 22.4 (CH$_2$CH(*C*H$_3$)$_2$), 22.3 (CH$_2$CH(*C*H$_3$)$_2$), 15.4 (OCH$_2$CH$_2$OCH$_2$*C*H$_3$), 15.3 (OCH$_2$CH$_2$OCH$_2$*C*H$_3$). **ESI-MS (+):** calc. for $C_{56}H_{80}O_8Na$ [(M+Na)$^+$]: m/z 903.58, found m/z 903.83 (100%); calc. for $C_{56}H_{80}O_8K$ [(M+K)$^+$]: m/z 919.55, found m/z 919.89 (13%).

cone-5,11,17-tris((2-methyl)propyl)-25,26,27,28-(2-ethoxyacetate)calix[4]arene (92b): In a 2-necked round-bottom flask compound **91** (0.21 mmol, 0.12 g) and Na_2CO_3 (4.18 mmol, 0.58 g)

were stirred in dry ACN (10 ml) for 30 minutes at reflux. Then 2-bromo ethylacetate (2.09 mmol, 0.232 ml) and NaI (0.84 mmol, 0.13 g) were added in and the mixture was left reacting for 3 days, monitoring it by TLC (Hex/AcOEt 8:2). The reaction was quenched with 1N HCl (10 ml) and so the mixture was extracted with DCM (3 x 20 ml). The combined organic phases were dried out at rotavapor and the crude was recrystallized with DCM/Hex to get compound **92b** as a yellow powder (0.16 g, 0.17 mmol, 80% yield). **^{1}H NMR** (300 MHz, $CDCl_3$) δ (ppm): 7.16 (d, *J* = 8.0 Hz, 2H, m-Ar*H*O), 6.90 (t, *J* = 8.0 Hz, 6H, Ar*H*), 4.49 (s, 2H, CH_2COOCH_2CH_3), 4.48 (s, 6H, CH_2COOCH_2CH_3), 4.40 (q, *J* = 7.0 Hz, 8H, CH_2COOCH_2CH_3), 4.28 (d, *J* = 12.9 Hz, 2H, ArCH_{ax}HAr), 4.24 (d, *J* = 12.9 Hz, 2H, ArCHH_{ax}Ar), 3.43 (d, *J* = 12.9 Hz, 2H, ArCH_{eq}HAr), 3.37 (d, *J* = 12.9 Hz, 2H, ArCHH_{eq}Ar), 2.27 (t, *J* = 6.6 Hz, 6H, CH_2CH(CH_3)$_2$), 1.72 (hept, *J* = 6.6 Hz, 3H, CH_2CH(CH_3)$_2$), 1.44 (t, *J* = 7.0 Hz, 12H, CH_2COOCH_2CH_3), 0.83 (t, *J* = 7.0 Hz, 18H, CH_2CH(CH_3)$_2$). **^{13}C NMR** (100 MHz, $CDCl_3$) δ (ppm): 171.3 (*C*=O), 152.2 (*C*=O), 150.2 (*C*-O), 150.1 (*C*Ar), 139.7 (*C*Ar), 135.0 (*C*Ar), 134.4 (*C*Ar), 134.2 (*C*Ar), 134.1 (*C*Ar), 130.0 (*C*Ar), 129.9 (*C*Ar), 129.9 (*C*Ar), 129.2 (*C*Ar), 126.5 (*C*Ar), 73.3 (*C*H_2COOCH_2CH_3), 62.1 (CH_2COO*C*H_2CH_3), 44.9 (*C*H_2CH(CH_3)$_2$), 31.6 (CH_2*C*H(CH_3)$_2$), 30.1 (Ar*C*H_2Ar), 29.8 (Ar*C*H_2Ar), 22.4 (CH_2CH(*C*H_3)$_2$), 22.3 (CH_2CH(*C*H_3)$_2$), 22.3 (CH_2CH(*C*H_3)$_2$), 14.3 (CH_2COOCH_2*C*H_3).

cone-5,11,17-tris((2-methyl)propyl)-25,26,27,28-(2-ethoxycarboxylic acid)calix[4]arene (93): In a 1-necked round-bottom flask compound **92b** (30.90 umol, 31.60 mg) and 1M NaOH (0.77 mmol, 1.000 ml) were stirred in THF (2 ml) for 1 h at room temperature, monitoring the reaction by TLC (Hex/AcOEt 1:1). The reaction was quenched with 1N HCl (2 ml) and then the suspension was dried out at rotavapor. The crude was suspended in DCM (20 ml) and the white precipitate formed was filtered out. The solvent was removed by reduced pressure to get compound **93** as a yellow powder (21.20 mg, 25.72 umol, 56% yield). **^{1}H NMR** (400 MHz, $CDCl_3$) δ (ppm): 8.34 (s, 4H, COO*H*), 7.14 (d, *J* = 7.3 Hz, 2H, m-Ar*H*O), 6.95 – 6.83 (m, 7H, Ar*H*), 4.52 (s, 8H, CH_2COOH), 4.42 (d, *J* = 12.3 Hz, 2H, ArCH_{ax}HAr), 4.37 (d, *J* = 12.3 Hz, 2H, ArCH_{ax}HAr), 3.40 (d, *J* = 12.3 Hz, 2H, ArCH_{eq}HAr), 3.35 (d, *J* = 12.3 Hz, 2H, ArCH_{eq}HAr), 2.26 (t, *J* = 7.9 Hz, 6H, CH_2CH(CH_3)$_2$), 1.72 (m, 3H, *J* = 6.9 Hz, CH_2CH(CH_3)$_2$), 0.82 (t, *J* = 6.9 Hz, 18H, CH_2CH(CH_3)$_2$).

cone-5,11,17-tris((2-methyl)propyl)-25,26,27,28-(2-ethoxysodiumcarboxylate)calix[4]arene (94): In a 1-necked round-bottom flask compound **93** (27.42 umol, 22.60 mg) and 1M NaOH (0.11 mmol, 0.110 ml) were stirred in H_2O (1 ml) for 1 h at room temperature. Once a yellow-green solution is obtained, the solution was lyophilized to get compound **94** as a green powder (25.00 mg, 27.40 umol, 99% yield). **^{1}H NMR** (400 MHz, MeOD) δ (ppm): 7.20 (d, *J* = 7.5 Hz, 2H, m-Ar*H*O), 6.98 (s, 6H, Ar*H*), 6.82 (t, *J* = 7.5 Hz, 1H, p-Ar*H*O), 4.71 (d, *J* = 12.1 Hz, 2H, ArCH_{ax}HAr), 4.65 (d, *J* = 12.1 Hz, 2H, ArCHH_{ax}Ar), 4.37 (s, 2H,), 4.35 (s, 6H, CH_2COOH), 3.39 (d, *J* = 12.1 Hz, 2H, ArCH_{eq}HAr), 3.34 (d, *J* = 12.1 Hz, 2H, ArCHH_{eq}Ar), 2.27 (d, *J* = 6.8 Hz, 6H, CH_2CH(CH_3)$_2$), 1.70 (hept, *J* = 6.8 Hz, 3H, CH_2CH(CH_3)$_2$), 0.79 (t, *J* = 6.8 Hz, 18H, CH_2CH(CH_3)$_2$). **^{13}C NMR** (100 MHz, MeOD) δ (ppm): 175.2 (*C*=O), 160.1 (*C*-O), 153.2 (*C*-O), 151.0 (*C*=O), 137.8 (*C*Ar), 137.8 (*C*Ar), 135.8 (*C*Ar), 135.1 (*C*Ar), 135.1 (*C*Ar), 134.9 (*C*Ar), 129.3 (*C*Ar), 128.6 (m-*C*ArO), 124.5 (p-*C*ArO), 75.8 (*C*H_2COO), 44.4 (*C*H_2CH(CH_3)$_2$), 29.9 (CH_2*C*H(CH_3)$_2$), 29.5 (Ar*C*H_2Ar), 29.4 (Ar*C*H_2Ar), 21.3 (CH_2CH(*C*H_3)$_2$).

Fluorescence anisotropy assays: general remarks

Fluorescence anisotropy assays were run in 384 well Optiplates and scanned using a Perkin Elmer EnVision™ 2103 MultiLabel plate reader. Fluorescein labelled peptides used an excitation and emission wavelength of 480 nm (30 nm bandwidth) and 535 nm (40 nm bandwidth) respectively.

Direct binding assays

General remarks

All competition assays were performed in 384 well plates with the concentration of protein serially diluted over 24 points in a 1:2 regime with [tracer] fixed at 50 nM. The assays consisted of three test rows (containing protein and tracer), and three control rows (tracer peptide was replaced with buffer). The intensity, *I*, and anisotropy, *r*, were calculated using eq. 1 and 2, respectively. A plot of anisotropy against competitor concentration was plotted in OriginPro 8.5 and fitted using Eq. 4 to determine an IC_{50} value.

Processing of fluorescence anisotropy data

The data obtained for both the *P* (perpendicular intensity) and *S* (parallel intensity) channels were corrected by subtracting the corresponding control wells, and the resulting values were used to calculate intensity (Eq. 1) and anisotropy (Eq. 2) for each well (using Microsoft Excel). These data were transferred into OriginPro 8.5, where a plot of anisotropy against protein concentration was fitted using a logistic model (Eq. 3) to obtain the minimum (r_{min}) and maximum (r_{max}) values of anisotropy. These values were used to determine the fraction of labelled peptide bound to the protein (fraction ligand bound, L_b, Eq. 4), and fitted (Eq. 5) in OriginPro 8.5 to determine the dissociation constant, K_d.

$$\mathrm{I} = 2\mathrm{PG} + \mathrm{S} \qquad \text{Eq. 1}$$

Where *I* is the total intensity, *G* is an instrument factor which was set to 1, and *r* is the anisotropy.

$$r = \frac{S - PG}{I} \qquad \text{Eq. 2}$$

$$y = r_{max} + \frac{r_{min} - r_{max}}{1 + \left({}^{x}/_{x_0}\right)^{p}} \qquad \text{Eq. 3}$$

$$Lb = \frac{r - r_{min}}{(\lambda(r_{max} - r) + r - r_{min})} \qquad \text{Eq. 4}$$

Where x_0 is the midpoint, *p* is the power and λ is the ratio of $I_{bound}/I_{unbound}$ and is equal to 1.

$$y = \frac{(K_d + x + [FL]) - \sqrt{((K_d + x + [FL])^2 - 4x[FL])}}{2} \qquad \text{Eq. 5}$$

Where *Lb* is the fraction ligand bound, [FL] is the concentration of fluorescent ligand, y is Lb*[FL], *x* = [added titrant].

p300/FITC-HIF direct titration

Titration of p300 into FITC-HIF was performed in a 384 well plate in Tris Buffer (20 mM Tris, 150 mM NaCl, 0.01% Triton X-100, pH 7.55) + 1 mM DTT with the concentration of p300 starting at 15 µM, diluted over 24 points in a 1:2 regime with [FITC-HIF] fixed at 50 nM. Plates were read after 30', 3h, 9h, 10h and 27 h incubation. Assays were run in triplicate (both test wells and control wells).

Mcl-1/FAM-BID direct titration

Titration of Mcl-1 into FAM-BID was performed in a 384 well plate in Tris Buffer (20 mM Tris, 100 mM NaCl, pH 7.46) + 1 mM DTT with the concentration of Mcl-1 starting from 15 µM, diluted over 24 points in a 1:2 regime with [FAM-BID] fixed at 50 nM. Plates were read after 45' and 20 hours incubation (data don't change significantly after 45'). Assays were run in triplicate (both test wells and control wells).

Competition assays

General remarks

All competition assays were performed in 384 well plates with the concentration of competitor serially diluted over 24 points in a 1:2 regime with [tracer] fixed at 50 nM (except in Mcl-1 titration with NOXA-Ac, fixed at 25 nm). The assays consisted of three test rows (containing protein, tracer and competitor), and three control rows (tracer peptide was replaced with buffer). As said before, the intensity, *I*, and anisotropy, *r*, were calculated using equations 1 and 2, respectively. A plot of anisotropy against competitor concentration was plotted in OriginPro 8.5 and fitted using Eq. 4 to determine an IC_{50} value.

Competition of p300/FITC-HIF interaction by 88b-88a-91-92a-94-AcHIF

p300/FITC-HIF competition assays were performed in Tris Buffer (20 mM Tris, 150 mM NaCl, 0.01% Triton X-100, pH 7.55) + 1 mM DTT. Inhibitor and p300 starting concentration as shown in the table below. Assays were run in triplicate (both test wells and control wells). Plates were read after 1 h and 25 h incubation.

	p300						Mcl-1	
	88b	**88a**	**91**	**92a**	**94**	**AcHIF**	**94**	**NOXAAc**
Protein conc. (μM)	15	100000	15	15	15	100000	15	200
Competitor conc. (μM)	300	300	300	300	300	20	300	300

Competition of Mcl-1/FAM-BID interaction by DS102-NOXAAc

Mcl-1/FAM-BID competition assays were performed in Tris Buffer (20 mM Tris, 100 mM NaCl, pH 7.46) + 1 mM DTT. Inhibitor and p300 starting concentration as shown in the previous table. Both control wells and test wells were run in triplicate. Plates were read after 45' and 25 h incubation.

Titration results

	p300						Mcl-1	
	88b	**88a**	**91**	**92a**	**94**	**AcHIF**	**94**	**NOXAAc**
IC50 (μM)	n.d.	n.d.	n.d.	n.d.	1.98	0.06	2.85	0.86
Error (μM)	n.d.	n.d.	n.d.	n.d.	0.86	0.01	0.83	0.06

Minimum Micellar Concentration determination (Fluorescence assay)

Fluorescence assays: general remarks

Fluorescence assays were run in 384 well Optiplates and scanned using a Perkin Elmer EnVision™ 2103 MultiLabel plate reader. Nile Red used an excitation wavelength of 550 nm and emission wavelength of 633 nm with a slit of 5 nm.

All mcm fluorescence assays were performed in 384 well plates with the concentration of surfattant serially diluted over 24 points in a 1:2 regime with [Nile Red] fixed at 200 nM. The assays consisted of three test rows (containing surfattant and Nile Red), and three control rows (Nile Red was replaced with buffer). Fluorescence data were just corrected with control fluorescence and plotted over Triton X-100 (test) or DS102 concentration through OriginPro 8.5 and fitted using a logistic fitting to determine an mcm value. Eventually, mcm values were corrected with an adding factor of 0.155mM, which represents the exact concentration of Triton X-100 in each well exclusively from the buffer.

Triton X-100 mcm fluorescence assay

Triton X-100 mcm fluorescence assay was performed in Tris Buffer (20 mM Tris, 150 mM NaCl, 0.01% Triton X-100, pH 7.55) + 1 mM DTT with the concentration of Triton X-100 starting at 0.1 M diluted over 24 points in a 1:2 regime with [Nile Red] fixed at 200 nM. Plates were read after 2h 15' incubation. Assays were run in triplicate (both test wells and control wells).

DS102 mcm fluorescence assay

DS102 mcm fluorescence assay was performed in Tris Buffer (20 mM Tris, 150 mM NaCl, 0.01% Triton X-100, pH 7.55) + 1 mM DTT with the concentration of DS102 starting at 300 µM diluted over 24 points in a 1:2 regime with [Nile Red] fixed at 200 nM. Plates were read after 30' and 1h 30' incubation. Assays were run in triplicate (both test wells and control wells).

Titration results

	94	Triton X-100 (exp.)	Triton X-100 (lit.)
Mcm (mM)	n.d.	0.08±0.01	0.23
Corrected mcm (mM)	n.d.	0.24±0.01	

NMR-assisted Mcl-1/DS102 titration (^{1}H-^{15}N HSQC)

The ^{15}N-enriched protein solution (100mM phosphate, 1mM DTT, 2% glycerol, pH 7.5 and ^{15}N-Mcl-1) was made dissolving each single component in D_2O/H_2O 1:9 in an NMR tube provided with a shigemi tube. A DS102 stock solution (C=10 mM in DMSO) was added in 3 aliquots in order to get 1:1, 1:2 and 1:4 ^{15}N-Mcl-1\DS102 molar ratios acquiring ^{1}H-^{15}N HSQC (HSQCETFPF3GPSI) after each addition. Each signal was assigned to each peptidic NH of the relative aminoacids and the signals subjected to linear deviation with respect to free Mcl-1 ^{1}H-^{15}N HSQC were plotted in red (for Lys) or blue (for general aminoacids) on PyMol protein structure.

6.6 References

1. Waksman, G. & Sansom, C. Introduction: Proteomics and Protein-Protein Interactions: Biology, Chemistry, Bioinformatics, and Drug Design. in *Proteomics and Protein-Protein Interactions* 1–18 (Springer US). doi:10.1007/0-387-24532-4_1

2. Gu, J., Milligan, J. & Huang, L. E. Molecular mechanism of hypoxia-inducible factor 1α-p300 interaction. A leucine-rich interface regulated by a single cysteine. *J. Biol. Chem.* **276**, 3550–3554 (2001).

3. Jayatunga, M. K. P. *et al.* Inhibition of the HIF1α-p300 interaction by quinone- and indandione-mediated ejection of structural Zn(II). *Eur. J. Med. Chem.* **94**, 509–516 (2015).

4. Wu, D. *et al.* A Novel Function of Novobiocin: Disrupting the Interaction of HIF 1α and p300/CBP through Direct Binding to the HIF1α C-Terminal Activation Domain. *PLoS One* **8**, (2013).

5. Masoud, G. N. & Li, W. HIF-1α pathway: Role, regulation and intervention for cancer therapy. *Acta Pharmaceutica Sinica B* **5**, 378–389 (2015).

6. Clohessy, J. G., Zhuang, J., De Boer, J., Gil-Gómez, G. & Brady, H. J. M. Mcl-1 interacts with truncated bid and inhibits its induction of cytochrome c release and its role in receptor-mediated apoptosis. *J. Biol. Chem.* **281**, 5750–5759 (2006).

7. Akçay, G. *et al.* Inhibition of Mcl-1 through covalent modification of a noncatalytic lysine side chain. *Nat. Chem. Biol.* **12**, 931–936 (2016).

8. Hird, A. W. & Tron, A. E. Recent advances in the development of Mcl-1 inhibitors for cancer therapy. *Pharmacol. Ther.* **198**, 59–67 (2019).

9. Akgul, C. Mcl-1 is a potential therapeutic target in multiple types of cancer. *Cellular and Molecular Life Sciences* **66**, 1326–1336 (2009).

10. Xiang, W., Yang, C. Y. & Bai, L. MCL-1 inhibition in cancer treatment. *OncoTargets and Therapy* **11**, 7301–7314 (2018).

11. Arbour, N. *et al.* Mcl-1 is a key regulator of apoptosis during CNS development and after DNA damage. *J. Neurosci.* **28**, 6068–6078 (2008).

12. Thomas, L. W., Lam, C. & Edwards, S. W. Mcl-1; the molecular regulation of protein function. *FEBS Letters* **584**, 2981–2989 (2010).

13. Li, H. L. *et al.* Characterization and functional analysis of hypoxia-inducible factor HIF1α and its inhibitor HIF1αn in tilapia. *PLoS One* **12**, e0173478 (2017).

14. Fong, G. H. & Takeda, K. Role and regulation of prolyl hydroxylase domain proteins. *Cell Death and Differentiation* **15**, 635–641 (2008).

15. Kaelin, W. G. The von Hippel-Lindau tumor suppressor protein: Roles in cancer and oxygen sensing. in *Cold Spring Harbor Symposia on Quantitative Biology* **70**, 159–166 (2005).

16. Haglund, K. & Dikic, I. Ubiquitylation and cell signaling. *EMBO Journal* **24**, 3353–3359 (2005).

17. Iyer, N. G., Özdag, H. & Caldas, C. p300/CBP and cancer. *Oncogene* **23**, 4225–4231 (2004).

18. Goodman, R. H. & Smolik, S. CBP/p300 in cell growth, transformation, and development. *Genes and Development* **14**, 1553–1577 (2000).

19. Harris, S. L. & Levine, A. J. The p53 pathway: Positive and negative feedback loops. *Oncogene* **24**, 2899–2908 (2005).

20. Brooks, C. L. & Gu, W. p53 ubiquitination: Mdm2 and beyond. *Molecular Cell* **21**, 307–315 (2006).

21. Kubbutat, M. H. G., Jones, S. N. & Vousden, K. H. Regulation of p53 stability by Mdm2. *Nature* **387**, 299–303 (1997).

22. Stark, L. A. *et al.* Accumulation of p53 is associated with tumour progression in cutaneous lesions of renal allograft recipients. *Br. J. Cancer* **70**, 662–667 (1994).

23. Mantovani, F., Collavin, L. & Del Sal, G. Mutant p53 as a guardian of the cancer cell. *Cell Death and Differentiation* **26**, 199–212 (2019).

24. Yue, X. *et al.* Mutant p53 in Cancer: Accumulation, Gain-of-Function, and Therapy. *Journal of Molecular Biology* **429**, 1595–1606 (2017).

25. Meek, D. W. The p53 response to DNA damage. *DNA Repair* **3**, 1049–1056 (2004).

26. Brooks, C. L. & Gu, W. New insights into p53 activation. *Cell Research* **20**, 614–621 (2010).

27. Bensaad, K. & Vousden, K. H. p53: new roles in metabolism. *Trends in Cell Biology* **17**, 286–291 (2007).

28. Walworth, N. C. Cell-cycle checkpoint kinases: checking in on the cell cycle. *Curr. Opin. Cell Biol.* **12**, 697–704 (2000).

29. Kelley, M. R. & Fishel, M. L. DNA repair proteins as molecular targets for cancer therapeutics. *Anticancer. Agents Med. Chem.* **8**, 417–25 (2008).

30. Karimian, A., Ahmadi, Y. & Yousefi, B. Multiple functions of p21 in cell cycle, apoptosis and transcriptional regulation after DNA damage. *DNA Repair* **42**, 63–71 (2016).

31. Elmore, S. Apoptosis: A Review of Programmed Cell Death. *Toxicologic Pathology* **35**, 495–516 (2007).

32. Westphal, D., Dewson, G., Czabotar, P. E. & Kluck, R. M. Molecular biology of Bax and Bak activation and action. *Biochimica et Biophysica Acta - Molecular Cell Research* **1813**, 521–531 (2011).

33. Shakeri, R., Kheirollahi, A. & Davoodi, J. Apaf-1: Regulation and function in cell death. *Biochimie* **135**, 111–125 (2017).

34. McIlwain, D. R., Berger, T. & Mak, T. W. Caspase functions in cell death and disease. *Cold Spring Harb. Perspect. Biol.* **5**, 1–28 (2013).

35. Berthelet, J. & Dubrez, L. Regulation of Apoptosis by Inhibitors of Apoptosis (IAPs). *Cells* **2**, 163–187 (2013).

36. Silke, J. & Meier, P. Inhibitorofapoptosis(IAP)proteins-modulators of cell death and inflammation. *Cold Spring Harb. Perspect. Biol.* **5**, (2013).

37. Portt, L., Norman, G., Clapp, C., Greenwood, M. & Greenwood, M. T. Anti-apoptosis and cell survival: A review. *Biochimica et Biophysica Acta - Molecular Cell Research* **1813**, 238–259 (2011).

38. Campbell, K. J. & Tait, S. W. G. Targeting BCL-2 regulated apoptosis in cancer. *Open Biology* **8**, (2018).

39. L.Omonosova, E. & C.Hinnadurai, G. BH3-only proteins in apoptosis and beyond: An overview. *Oncogene* **27**, S2–S19 (2008).

40. Sieghart, W. *et al.* Mcl-1 overexpression in hepatocellular carcinoma: A potential target for antisense therapy. *J. Hepatol.* **44**, 151–157 (2006).

41. Pfeil, K. *et al.* The anti-apoptotic protein Mcl-1 is overexpressed in prostate cancer. *Cancer Res.* **64**, (2004).

42. Janin, J. Elusive affinities. *Proteins Struct. Funct. Genet.* **21**, 30–39 (1995).

43. Janin, J. Protein-protein recognition. *Prog. Biophys. Mol. Biol.* **64**, 145–66 (1995).

44. Russell, R. B. *et al.* A structural perspective on protein-protein interactions. *Current Opinion in Structural Biology* **14**, 313–324 (2004).

45. Jones, S. & Thornton, J. M. Principles of protein-protein interactions. *Proceedings of the National Academy of Sciences of the United States of America* **93**, 13–20 (1996).

46. Fernández, A. & Scheraga, H. A. Insufficiently dehydrated hydrogen bonds as determinants of protein interactions. *Proc. Natl. Acad. Sci. U. S. A.* **100**, 113–118 (2003).

47. Conte, L. Lo, Chothia, C. & Janin, J. The atomic structure of protein-protein recognition sites. *J. Mol. Biol.* **285**, 2177–2198 (1999).

48. Horton, N. & Lewis, M. Calculation of the free energy of association for protein complexes. *Protein Sci.* **1**, 169–181 (1992).

49. Keskin, O., Ma, B. & Nussinov, R. Hot regions in protein-protein interactions: The organization and contribution of structurally conserved hot spot residues. *J. Mol. Biol.* **345**, 1281–1294 (2005).

50. Privalov, P. L. Stability of proteins: Small Globular Proteins. *Adv. Protein Chem.* **33**, 167–241 (1979).

51. Young, L., Jernigan, R. L. & Covell, D. G. A role for surface hydrophobicity in protein-protein recognition. *Protein Sci.* **3**, 717–729 (1994).

52. Korn, A. P. & Burnett, R. M. Distribution and complementarity of hydropathy in mutisunit proteins. *Proteins Struct. Funct. Bioinforma.* **9**, 37–55 (1991).

53. Lijnzaad, P. & Argos, P. Hydrophobic patches on protein subunit interfaces: Characteristics and prediction. *Proteins Struct. Funct. Genet.* **28**, 333–343 (1997).

54. Jones, S. & Thornton, J. M. Analysis of protein-protein interaction sites using surface patches. *J. Mol. Biol.* **272**, 121–132 (1997).

55. Jones, S. & Thornton, J. M. Prediction of protein-protein interaction sites using patch analysis. *J. Mol. Biol.* **272**, 133–143 (1997).

56. Wells, J. A. Systematic mutational analyses of protein-protein interfaces. *Methods Enzymol.* **202**, 390–411 (1991).

57. Thorn, K. S. & Bogan, A. A. ASEdb: A database of alanine mutations and their effects on the free energy of binding in protein interactions. *Bioinformatics* **17**, 284–285 (2001).

58. Li, J. & Liu, Q. 'Double water exclusion': A hypothesis refining the O-ring theory for the hot spots at protein interfaces. *Bioinformatics* **25**, 743–750 (2009).

59. Kollman, P. Free Energy Calculations: Applications to Chemical and Biochemical Phenomena. *Chem. Rev.* **93**, 2395–2417 (1993).

60. Morrison, K. L. & Weiss, G. A. Combinatorial alanine-scanning. *Curr. Opin. Chem. Biol.* **5**, 302–7 (2001).

61. Erlanson, D. A. *et al.* Site-directed ligand discovery. *Proc. Natl. Acad. Sci. U. S. A.* **97**, 9367–9372 (2000).

62. Lodge, J. M., Justin Rettenmaier, T., Wells, J. A., Pomerantz, W. C. & Mapp, A. K. FP tethering: A screening technique to rapidly identify compounds that disrupt protein-protein interactions. *Medchemcomm* **5**, 370–375 (2014).

63. Azzarito, V., Long, K., Murphy, N. S. & Wilson, A. J. Inhibition of α-helix-mediated protein-protein interactions using designed molecules. *Nat. Chem.* **5**, 161–173 (2013).

64. Galande, A. K. *et al.* Potent inhibitors of LXXLL-based protein-protein interactions. *ChemBioChem* **6**, 1991–1998 (2005).

65. PELLEGRINI, M., ROYO, M., CHOREV, M. & MIERKE, D. F. Conformational consequences of i, i + 3 cystine linkages: nucleation for α-helicity? *J. Pept. Res.* **49**, 404–414 (2009).

66. Leduc, A. M. *et al.* Helix-stabilized cyclic peptides as selective inhibitors of steroid receptor - Coactivator interactions. *Proc. Natl. Acad. Sci. U. S. A.* **100**, 11273–11278 (2003).

67. Judice, J. K. *et al.* Inhibition of HIV type 1 infectivity by constrained α-helical peptides: Implications for the viral fusion mechanism. *Proc. Natl. Acad. Sci. U. S. A.* **94**, 13426–13430 (1997).

68. Sia, S. K., Carr, P. A., Cochran, A. G., Malashkevich, V. N. & Kim, P. S. Short constrained peptides that inhibit HIV-1 entry. *Proc. Natl. Acad. Sci. U. S. A.* **99**, 14664–14669 (2002).

69. Blackwell, H. E. & Grubbs, R. H. Highly efficient synthesis of covalently cross-linked peptide helices by ring-closing metathesis. *Angew. Chemie - Int. Ed.* **37**, 3281–3284 (1998).

70. Walensky, L. D. *et al.* Activation of apoptosis in vivo by a hydrocarbon-stapled BH3 helix. *Science (80-.).* **305**, 1466–1470 (2004).

71. Walensky, L. D. *et al.* A Stapled BID BH3 Helix Directly Binds and Activates BAX. *Mol. Cell* **24**, 199–210 (2006).

72. Patgiri, A., Jochim, A. L. & Arora, P. S. A hydrogen bond surrogate approach for stabilization of short peptide sequences in α-helical conformation. *Acc. Chem. Res.* **41**, 1289–1300 (2008).

73. Chapman, R. N., Dimartino, G. & Arora, P. S. A highly stable short α-helix constrained

by a main-chain hydrogen-bond surrogate. *J. Am. Chem. Soc.* **126**, 12252–12253 (2004).

74. Wang, D., Liao, W. & Arora, P. S. Enhanced metabolic stability and protein-binding properties of artificial α helices derived from a hydrogen-bond surrogate: Application to Bcl-xL. *Angew. Chemie - Int. Ed.* **44**, 6525–6529 (2005).

75. Wang, D., Lu, M. & Arora, P. S. Inhibition of HIV-1 fusion by hydrogen-bond-surrogate-based α helices. *Angew. Chemie - Int. Ed.* **47**, 1879–1882 (2008).

76. Wysoczanski, P. *et al.* NMR solution structure of a photoswitchable apoptosis activating bak peptide bound to Bcl-x L. *J. Am. Chem. Soc.* **134**, 7644–7647 (2012).

77. Lee, E. F. *et al.* High-resolution structural characterization of a helical α/β-peptide foldamer bound to the anti-apoptotic protein Bcl-x L. *Angew. Chemie - Int. Ed.* **48**, 4318–4322 (2009).

78. Lee, E. F. *et al.* Structural basis of Bcl-x L recognition by a BH3-mimetic α/β-peptide generated by sequence-based design. *ChemBioChem* **12**, 2025–2032 (2011).

79. Horne, W. S., Boersma, M. D., Windsor, M. A. & Gellman, S. H. Sequence-based design of α/β-peptide foldamers that mimic BH3 domains. *Angew. Chemie - Int. Ed.* **47**, 2853–2856 (2008).

80. Horwell, D. C., Howson, W., Ratcliffe, G. S. & Willems, H. M. G. The design of dipeptide helical mimetics: The synthesis, tachykinin receptor affinity and conformational analysis of 1,1,6-trisubstituted indanes. *Bioorganic Med. Chem.* **4**, 33–42 (1996).

81. Orner, B. P., Ernst, J. T. & Hamilton, A. D. Toward proteomimetics: Terphenyl derivatives as structural and functional mimics of extended regions of an α-helix [18]. *Journal of the American Chemical Society* **123**, 5382–5383 (2001).

82. Ernst, J. T. *et al.* Design of a protein surface antagonist based on alpha-helix mimicry: inhibition of gp41 assembly and viral fusion. *Angew. Chem. Int. Ed. Engl.* **41**, 278–81 (2002).

83. Kutzki, O. *et al.* Development of a potent Bcl-xL antagonist based on α-helix mimicry. *J. Am. Chem. Soc.* **124**, 11838–11839 (2002).

84. Yin, H. *et al.* Terephthalamide derivatives as mimetics of helical peptides: Disruption of the Bcl-xL/Bak interaction. *J. Am. Chem. Soc.* **127**, 5463–5468 (2005).

85. Rodriguez, J. M. *et al.* Structure and function of benzoy lurea-derived A-helix mimetics targeting the Bcl-x L /bak binding interface. *ChemMedChem* **4**, 649–656 (2009).

86. Rodriguez, J. M. & Hamilton, A. D. Benzoylurea oligomers: Synthetic foldamers that mimic extended α helices. *Angew. Chemie - Int. Ed.* **46**, 8614–8617 (2007).

87. Biros, S. M. *et al.* Heterocyclic α-helix mimetics for targeting protein-protein interactions. *Bioorganic Med. Chem. Lett.* **17**, 4641–4645 (2007).

88. Cummings, C. G., Ross, N. T., Katt, W. P. & Hamilton, A. D. Synthesis and biological evaluation of a 5-6-5 imidazole-phenyl-thiazole based α-helix mimetic. *Org. Lett.* **11**, 25–28 (2009).

89. Saraogi, I. *et al.* Synthetic α-helix mimetics as agonists and antagonists of islet amyloid polypeptide aggregation. *Angew. Chemie - Int. Ed.* **49**, 736–739 (2010).

90. Rodger P. McEver. Selectins: lectins that initiate cell adhesion under flow. *Curr. Opin. Cell Biol.* **14**, 581–586 (2002).

91. Ernst, J. T., Becerril, J., Park, H. S., Yin, H. & Hamilton, A. D. Design and application of an α-helix-mimetic scaffold based on an oligoamide-foldamer strategy: Antagonism of the Bak BH3/Bcl-xL complex. *Angew. Chemie - Int. Ed.* **42**, 535–539 (2003).

92. Saraogi, I., Incarvito, C. D. & Hamilton, A. D. Controlling curvature in a family of oligoamide α-helix mimetics. *Angew. Chemie - Int. Ed.* **47**, 9691–9694 (2008).

93. Yin, H., Frederick, K. K., Liu, D., Wand, A. J. & DeGrado, W. F. Arylamide derivatives as peptidomimetic inhibitors of calmodulin. *Org. Lett.* **8**, 223–225 (2006).

94. Ahn, J.-M. & Han, S.-Y. Facile synthesis of benzamides to mimic an α-helix. *Tetrahedron Lett.* **48**, 3543–3547 (2007).

95. Plante, J. *et al.* Synthesis of functionalised aromatic oligamide rods. *Org. Biomol. Chem.* **6**, 138–146 (2008).

96. Shaginian, A. *et al.* Design, Synthesis, and Evaluation of an α-Helix Mimetic Library Targeting Protein−Protein Interactions. *J. Am. Chem. Soc.* **131**, 5564–5572 (2009).

97. Plante, J. P. *et al.* Oligobenzamide proteomimetic inhibitors of the p53-hDM2 protein-protein interaction. *Chem. Commun.* 5091–5093 (2009). doi:10.1039/b908207g

98. Shahian, T. *et al.* Inhibition of a viral enzyme by a small-molecule dimer disruptor. *Nat. Chem. Biol.* **5**, 640–646 (2009).

99. Campbell, F., Plante, J. P., Edwards, T. A., Warriner, S. L. & Wilson, A. J. N-alkylated oligoamide α-helical proteomimetics. *Org. Biomol. Chem.* **8**, 2344–2351 (2010).

100. Long, K., Edwards, T. A. & Wilson, A. J. Microwave assisted solid phase synthesis of highly functionalized N-alkylated oligobenzamide α-helix mimetics. *Bioorganic Med. Chem.* **21**, 4034–4040 (2013).

101. Lee, J. H. *et al.* Novel pyrrolopyrimidine-based α-helix mimetics: Cell-permeable inhibitors of protein-protein interactions. *J. Am. Chem. Soc.* **133**, 676–679 (2011).

102. Kim, I. C. & Hamilton, A. D. Diphenylindane-Based Proteomimetics Reproduce the Projection of the *i* , *i* +3, *i* +4, and *i* +7 Residues on an α-Helix. *Org. Lett.* **8**, 1751–1754 (2006).

103. Marimgantl, S., Cheemala, M. N. & Ahn, J. M. Novel amphiphilic α-helix mimetics based on a bis-benzamide scaffold. *Org. Lett.* **11**, 4418–4421 (2009).

104. Becerril, J. & Hamilton, A. D. Helix mimetics as inhibitors of the interaction of the estrogen receptor with coactivator peptides. *Angew. Chemie - Int. Ed.* **46**, 4471–4473 (2007).

105. Masci, B. Homooxacalixarenes. 3. Complexation of quaternary ammonium ions by parent homooxacalixarenes in CDCl3 solution. *Tetrahedron* **51**, 5459–5464 (1995).

106. Harrowfield, J. M., Richmond, W. R. & Sobolev, A. N. Inclusion of quaternary ammonium compounds by calixarenes. *J. Incl. Phenom. Mol. Recognit. Chem.* **19**, 257–276 (1994).

107. Arduini, A. *et al.* Direct Regioselective Formylation of Tetraalkoxycalix[4]arenes Fixed in the Cone Conformation and Synthesis of New Cavitands. *J. Org. Chem.* **60**, 1448–1453 (1995).

108. Spencer, D. J. E., Johnson, B. J., Johnson, B. J. & Tolman, W. B. Calix[4]arenes Linked to Multiple Bidentate N-Donors: Potential Ligands for Synthetic Modeling of Multinuclear Metalloenzymes. *Org. Lett.* **4**, 1391–1393 (2002).